WOODHEAD PUBLISHING SERIES IN BIOMATERIALS

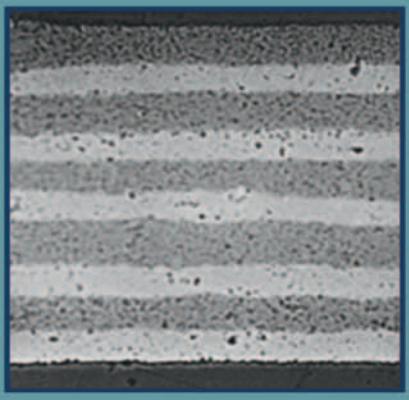

Thin Film Coatings for Biomaterials and Biomedical Applications

Edited by Hans J Griesser

WP
WOODHEAD PUBLISHING

Thin Film Coatings for Biomaterials and Biomedical Applications

Related titles

Surface Modification of Magnesium and Its Alloys for Biomedical Applications Vol 1
(ISBN 978-1-78242-077-4)
Surface Modification of Magnesium and Its Alloys for Biomedical Applications Vol 2
(ISBN 978-1-78242-078-1)
Surface Modification of Metallic Biomaterials
(ISBN 978-1-78242-303-4)
Switchable Surfaces for Biomedical Applications
(ISBN 978-0-85709-713-2)

Woodhead Publishing Series in Biomaterials: Number 110

Thin Film Coatings for Biomaterials and Biomedical Applications

Edited by

Hans J Griesser

AMSTERDAM • BOSTON • CAMBRIDGE • HEIDELBERG
LONDON • NEW YORK • OXFORD • PARIS • SAN DIEGO
SAN FRANCISCO • SINGAPORE • SYDNEY • TOKYO
Woodhead Publishing is an imprint of Elsevier

Woodhead Publishing is an imprint of Elsevier
The Officers' Mess Business Centre, Royston Road, Duxford, CB22 4QH, UK
50 Hampshire Street, 5th Floor, Cambridge, MA 02139, USA
The Boulevard, Langford Lane, Kidlington, OX5 1GB, UK

Notices
Knowledge and best practice in this field are constantly changing. As new research and experience broaden our understanding, changes in research methods, professional practices, or medical treatment may become necessary.

Practitioners and researchers must always rely on their own experience and knowledge in evaluating and using any information, methods, compounds, or experiments described herein. In using such information or methods they should be mindful of their own safety and the safety of others, including parties for whom they have a professional responsibility.

To the fullest extent of the law, neither the Publisher nor the authors, contributors, or editors, assume any liability for any injury and/or damage to persons or property as a matter of products liability, negligence or otherwise, or from any use or operation of any methods, products, instructions, or ideas contained in the material herein.

British Library Cataloguing-in-Publication Data
A catalogue record for this book is available from the British Library

Library of Congress Cataloging-in-Publication Data
A catalog record for this book is available from the Library of Congress

ISBN: 978-1-78242-453-6 (print)
ISBN: 978-1-78242-476-5 (online)

Publisher: Matthew Deans
Acquisition Editor: Laura Overend
Editorial Project Manager: Lucy Beg
Production Project Manager: Poulouse Joseph
Designer: Maria Ines Cruz

Typeset by TNQ Books and Journals

Contents

This page intentionally left blank

List of contributors

B. Ben-Nissan University of Technology, Sydney, NSW, Australia

A. Bendavid Commonwealth Scientific and Industrial Research Organisation, Lindfield, NSW, Australia

J. Chen Newcastle University, Newcastle upon Tyne, United Kingdom

A.H. Choi University of Technology, Sydney, NSW, Australia

P.K. Chu City University of Hong Kong, Kowloon, Hong Kong, China

V.B. Damodaran Rutgers University, New Brunswick, NJ, United States

T. Fernandez University of South Australia, Adelaide, SA, Australia

A.S. Hwang Vanderbilt University, Nashville, TN, United States

J. Kiwi Ecole Polytechnique Fédérale de Lausanne, EPFL-SB-ISIC-GPAO, Lausanne, Switzerland

B. Latella Commonwealth Scientific and Industrial Research Organisation, Perth, WA, Australia

S.H. Lee Vanderbilt University, Nashville, TN, United States

P.H. Li City University of Hong Kong, Kowloon, Hong Kong, China

J.S.C. Loo Nanyang Technological University, Singapore

M. Malmsten Uppsala University, Uppsala, Sweden

A. Michelmore University of South Australia, Mawson Lakes, SA, Australia

D.K. Mills Louisiana Tech University, Ruston, LA, United States

M. Mozafari Materials and Energy Research Center (MERC), Tehran, Iran

N.S. Murthy Rutgers University, New Brunswick, NJ, United States

A.A. Ogwu University of the West of Scotland, Paisley, Scotland, United Kingdom

T.I.T. Okpalugo University of the West of Scotland, Paisley, Scotland, United Kingdom

C. Pulgarin Ecole Polytechnique Fédérale de Lausanne, EPFL-SB-ISIC-GPAO, Lausanne, Switzerland

A. Ramedani Sharif University of Technology, Tehran, Iran

N. Rogers University of South Australia, Adelaide, SA, Australia

S. Rtimi Ecole Polytechnique Fédérale de Lausanne, EPFL-SB-ISIC-GPAO, Lausanne, Switzerland

T.W.J. Steele Nanyang Technological University, Singapore

H.-J. Sung Vanderbilt University, Nashville, TN, United States

S.S. Venkatraman Nanyang Technological University, Singapore

J.D. Whittle University of South Australia, Adelaide, SA, Australia

Y.N. Zhang University of Toronto, Toronto, ON, Canada

Woodhead Publishing Series in Biomaterials

1 **Sterilisation of tissues using ionising radiations**
Edited by J. F. Kennedy, G. O. Phillips and P. A. Williams
2 **Surfaces and interfaces for biomaterials**
Edited by P. Vadgama
3 **Molecular interfacial phenomena of polymers and biopolymers**
Edited by C. Chen
4 **Biomaterials, artificial organs and tissue engineering**
Edited by L. Hench and J. Jones
5 **Medical modelling**
R. Bibb
6 **Artificial cells, cell engineering and therapy**
Edited by S. Prakash
7 **Biomedical polymers**
Edited by M. Jenkins
8 **Tissue engineering using ceramics and polymers**
Edited by A. R. Boccaccini and J. Gough
9 **Bioceramics and their clinical applications**
Edited by T. Kokubo
10 **Dental biomaterials**
Edited by R. V. Curtis and T. F. Watson
11 **Joint replacement technology**
Edited by P. A. Revell
12 **Natural-based polymers for biomedical applications**
Edited by R. L. Reiss et al.
13 **Degradation rate of bioresorbable materials**
Edited by F. J. Buchanan
14 **Orthopaedic bone cements**
Edited by S. Deb
15 **Shape memory alloys for biomedical applications**
Edited by T. Yoneyama and S.Miyazaki
16 **Cellular response to biomaterials**
Edited by L. Di Silvio
17 **Biomaterials for treating skin loss**
Edited by D. P. Orgill and C. Blanco
18 **Biomaterials and tissue engineering in urology**
Edited by J. Denstedt and A. Atala
19 **Materials science for dentistry**
B. W. Darvell

20 **Bone repair biomaterials**
Edited by J. A. Planell, S. M. Best, D. Lacroix and A. Merolli
21 **Biomedical composites**
Edited by L. Ambrosio
22 **Drug–device combination products**
Edited by A. Lewis
23 **Biomaterials and regenerative medicine in ophthalmology**
Edited by T. V. Chirila
24 **Regenerative medicine and biomaterials for the repair of connective tissues**
Edited by C. Archer and J. Ralphs
25 **Metals for biomedical devices**
Edited by M. Niinomi
26 **Biointegration of medical implant materials: Science and design**
Edited by C. P. Sharma
27 **Biomaterials and devices for the circulatory system**
Edited by T. Gourlay and R. Black
28 **Surface modification of biomaterials: Methods analysis and applications**
Edited by R. Williams
29 **Biomaterials for artificial organs**
Edited by M. Lysaght and T. Webster
30 **Injectable biomaterials: Science and applications**
Edited by B. Vernon
31 **Biomedical hydrogels: Biochemistry, manufacture and medical applications**
Edited by S. Rimmer
32 **Preprosthetic and maxillofacial surgery: Biomaterials, bone grafting and tissue engineering**
Edited by J. Ferri and E. Hunziker
33 **Bioactive materials in medicine: Design and applications**
Edited by X. Zhao, J. M. Courtney and H. Qian
34 **Advanced wound repair therapies**
Edited by D. Farrar
35 **Electrospinning for tissue regeneration**
Edited by L. Bosworth and S. Downes
36 **Bioactive glasses: Materials, properties and applications**
Edited by H. O. Ylänen
37 **Coatings for biomedical applications**
Edited by M. Driver
38 **Progenitor and stem cell technologies and therapies**
Edited by A. Atala
39 **Biomaterials for spinal surgery**
Edited by L. Ambrosio and E. Tanner
40 **Minimized cardiopulmonary bypass techniques and technologies**
Edited by T. Gourlay and S. Gunaydin
41 **Wear of orthopaedic implants and artificial joints**
Edited by S. Affatato
42 **Biomaterials in plastic surgery: Breast implants**
Edited by W. Peters, H. Brandon, K. L. Jerina, C. Wolf and V. L. Young
43 **MEMS for biomedical applications**
Edited by S. Bhansali and A. Vasudev

44 **Durability and reliability of medical polymers**
Edited by M. Jenkins and A. Stamboulis
45 **Biosensors for medical applications**
Edited by S. Higson
46 **Sterilisation of biomaterials and medical devices**
Edited by S. Lerouge and A. Simmons
47 **The hip resurfacing handbook: A practical guide to the use and management of modern hip resurfacings**
Edited by K. De Smet, P. Campbell and C. Van Der Straeten
48 **Developments in tissue engineered and regenerative medicine products**
J. Basu and J. W. Ludlow
49 **Nanomedicine: Technologies and applications**
Edited by T. J. Webster
50 **Biocompatibility and performance of medical devices**
Edited by J-P. Boutrand
51 **Medical robotics: Minimally invasive surgery**
Edited by P. Gomes
52 **Implantable sensor systems for medical applications**
Edited by A. Inmann and D. Hodgins
53 **Non-metallic biomaterials for tooth repair and replacement**
Edited by P. Vallittu
54 **Joining and assembly of medical materials and devices**
Edited by Y. (Norman) Zhou and M. D. Breyen
55 **Diamond-based materials for biomedical applications**
Edited by R. Narayan
56 **Nanomaterials in tissue engineering: Fabrication and applications**
Edited by A. K. Gaharwar, S. Sant, M. J. Hancock and S. A. Hacking
57 **Biomimetic biomaterials: Structure and applications**
Edited by A. J. Ruys
58 **Standardisation in cell and tissue engineering: Methods and protocols**
Edited by V. Salih
59 **Inhaler devices: Fundamentals, design and drug delivery**
Edited by P. Prokopovich
60 **Bio-tribocorrosion in biomaterials and medical implants**
Edited by Y. Yan
61 **Microfluidic devices for biomedical applications**
Edited by X-J. James Li and Y. Zhou
62 **Decontamination in hospitals and healthcare**
Edited by J. T. Walker
63 **Biomedical imaging: Applications and advances**
Edited by P. Morris
64 **Characterization of biomaterials**
Edited by M. Jaffe, W. Hammond, P. Tolias and T. Arinzeh
65 **Biomaterials and medical tribology**
Edited by J. Paolo Davim
66 **Biomaterials for cancer therapeutics: Diagnosis, prevention and therapy**
Edited by K. Park
67 **New functional biomaterials for medicine and healthcare**
E. P. Ivanova, K. Bazaka and R. J. Crawford

68 **Porous silicon for biomedical applications**
Edited by H. A. Santos
69 **A practical approach to spinal trauma**
Edited by H. N. Bajaj and S. Katoch
70 **Rapid prototyping of biomaterials: Principles and applications**
Edited by R. Narayan
71 **Cardiac regeneration and repair Volume 1: Pathology and therapies**
Edited by R-K. Li and R. D. Weisel
72 **Cardiac regeneration and repair Volume 2: Biomaterials and tissue engineering**
Edited by R-K. Li and R. D. Weisel
73 **Semiconducting silicon nanowires for biomedical applications**
Edited by J. L. Coffer
74 **Silk biomaterials for tissue engineering and regenerative medicine**
Edited by S. Kundu
75 **Biomaterials for bone regeneration: Novel techniques and applications**
Edited by P. Dubruel and S. Van Vlierberghe
76 **Biomedical foams for tissue engineering applications**
Edited by P. Netti
77 **Precious metals for biomedical applications**
Edited by N. Baltzer and T. Copponnex
78 **Bone substitute biomaterials**
Edited by K. Mallick
79 **Regulatory affairs for biomaterials and medical devices**
Edited by S. F. Amato and R. Ezzell
80 **Joint replacement technology Second edition**
Edited by P. A. Revell
81 **Computational modelling of biomechanics and biotribology in the musculoskeletal system: Biomaterials and tissues**
Edited by Z. Jin
82 **Biophotonics for medical applications**
Edited by I. Meglinski
83 **Modelling degradation of bioresorbable polymeric medical devices**
Edited by J. Pan
84 **Perspectives in total hip arthroplasty: Advances in biomaterials and their tribological interactions**
S. Affatato
85 **Tissue engineering using ceramics and polymers Second edition**
Edited by A. R. Boccaccini and P. X. Ma
86 **Biomaterials and medical-device associated infections**
Edited by L. Barnes and I. R. Cooper
87 **Surgical techniques in total knee arthroplasty (TKA) and alternative procedures**
Edited by S. Affatato
88 **Lanthanide oxide nanoparticles for molecular imaging and therapeutics**
G. H. Lee
89 **Surface modification of magnesium and its alloys for biomedical applications Volume 1: Biological interactions, mechanical properties and testing**
Edited by T. S. N. Sankara Narayanan, I. S. Park and M. H. Lee

90 **Surface modification of magnesium and its alloys for biomedical applications Volume 2: Modification and coating techniques**
Edited by T. S. N. Sankara Narayanan, I. S. Park and M. H. Lee
91 **Medical modelling: The application of advanced design and rapid prototyping techniques in medicine Second Edition**
Edited by R. Bibb, D. Eggbeer and A. Paterson
92 **Switchable and responsive surfaces and materials for biomedical applications**
Edited by Z. Zhang
93 **Biomedical textiles for orthopaedic and surgical applications: fundamentals, applications and tissue engineering**
Edited by T. Blair
94 **Surface coating and modification of metallic biomaterials**
Edited by C. Wen
95 **Hydroxyapatite (HAP) for biomedical applications**
Edited by M. Mucalo
96 **Implantable neuroprostheses for restoring function**
Edited by K. Kilgore
97 **Shape memory polymers for biomedical applications**
Edited by L. Yahia
98 **Regenerative engineering of musculoskeletal tissues and interfaces**
Edited by S. P. Nukavarapu, J. W. Freeman and C. T. Laurencin
99 **Advanced cardiac imaging**
Edited by K. Nieman, O. Gaemperli, P. Lancellotti and S. Plein
100 **Functional marine biomaterials: Properties and applications**
Edited by SK. Kim
101 **Shoulder and elbow trauma and its complications: Volume 1: The shoulder**
Edited by R. M. Greiwe
102 **Nanotechnology-enhanced orthopedic materials: Fabrications, applications and future trends**
Edited by L. Yang
103 **Medical devices: Regulations, standards and practices**
Edited by S. Ramakrishna, L. Tian, C. Wang, S. L. and T. Wee Eong
104 **Biomineralisation and biomaterials: fundamentals and applications**
Edited by C. Aparicio and M. Ginebra
105 **Shoulder and elbow trauma and its complications Volume 2: The elbow**
Edited by R. M. Greiwe
106 **Characterisation and design of tissue scaffolds**
Edited by P. Tomlins
107 **Biosynthetic polymers for medical applications**
Edited by L. Poole-Warren, P. Martens & R. Green
108 **Advances in polyurethane biomaterials**
Edited by S. L. Cooper
109 **Nanocomposites for musculoskeletal tissue regeneration**
Edited by H. Liu
110 **Thin film coatings for biomaterials and biomedical applications**
Edited by H. J. Griesser

This page intentionally left blank

Part One

Fundamentals of thin film technologies for biomedical applications

This page intentionally left blank

Thin film deposition technologies and processing of biomaterials

1

P.H. Li, P.K. Chu
City University of Hong Kong, Kowloon, Hong Kong, China

1.1 Introduction

On the heels of continuous biomedical and clinical research and development, high demand is placed on the processing and engineering of biomaterials. Besides the rigorous selection of materials based on their bulk properties, the surface properties of biomaterials are crucial to clinical success. Compared with the development of new biomaterials, modification of selected surface biological and mechanical properties of existing biomaterials to cater to specific needs and applications tends to be more economical and less time-consuming. In particular, deposition of thin films or coatings is a common and effective technique in surface modification and engineering. Methods for thin film deposition can be divided into two groups based on the nature of the deposition process, chemical or physical. Basically, chemical methods such as chemical vapor deposition (CVD) and sol-gel involve gas-phase or liquid-phase chemical reactions whereas physical methods typically include evaporation, sputtering (ejection of materials from a target followed by condensation to form films), and spraying. This chapter presents an overview of the fundamentals of thin film deposition and pertinent instrumentation with an emphasis on applications to biomaterials.

1.2 Chemical vapor deposition

1.2.1 Plasma-enhanced chemical vapor deposition

CVD is a well-understood thin film deposition method that uses chemical reactions of vapor-phase precursors. CVD processes have traditionally been initiated and controlled by heat as the source of energy. An elevated deposition temperature is normally required, which restricts the types of substrates that can be used and coating materials that can be deposited, especially thermally sensitive ones (Jones and Hitchman, 2009). However, thermal energy is not the only energy supplied to the system; plasmas and photons are widely used in CVD processes. Plasma-enhanced chemical vapor deposition (PECVD), or plasma-assisted CVD, is a CVD technique in which plasma in lieu of thermal energy is used primarily to activate ions and radicals in the chemical reactions leading to layer formation on the substrate. One major advantage of PECVD over

Thin Film Coatings for Biomaterials and Biomedical Applications. http://dx.doi.org/10.1016/B978-1-78242-453-6.00001-8

conventional thermal CVD is that the lower temperature in PECVD allows the deposition of layers that cannot tolerate a high temperature, and temperature-sensitive substrates can be used. Moreover, the deposition rate in PECVD is typically higher and more easily controlled because the precursors activated by the plasma are more reactive and a biased voltage can be applied to control the arrival rate of the ionized precursors (Chu et al., 2004).

The plasma in PECVD is usually triggered and sustained by radio frequency (RF), microwave (MW), and a combination of these. RF PECVD systems use either internal electrodes or external plasma excitation employing a coil or rings, as illustrated in Fig. 1.1(a) and (b). The frequency used in RF PECVD is commonly between 50 kHz and 13.56 MHz, and operation pressure is between 0.1 and 2.0 Torr. Plasma density is typically between 10^8 and 10^{12} cm^{-3}, and the fastest electrons may possess energy as high as 10−30 eV (Kern, 1991; Chu et al., 2004). MW discharge (Fig. 1.1(c)) typically takes place at a MW frequency of 2.54 GHz. Plasma density in the surface wave discharge can be as low as 10^8 cm^{-3} in the low-pressure and low-frequency range and can be as large as 10^{15} cm^{-3} at atmospheric pressure (Anders, 2000; Chu et al., 2004). There are also dual-mode PECVD systems that apply RF-biased voltage to the substrate holder (Fig. 1.1(d) and (e)).

PECVD has been used industrially for several decades to deposit oxides and nitrides of silicon, polycrystalline silicon, and epitaxial silicon (Tedrow and Reif, 1994) for microelectronics. There are also many applications in the automotive,

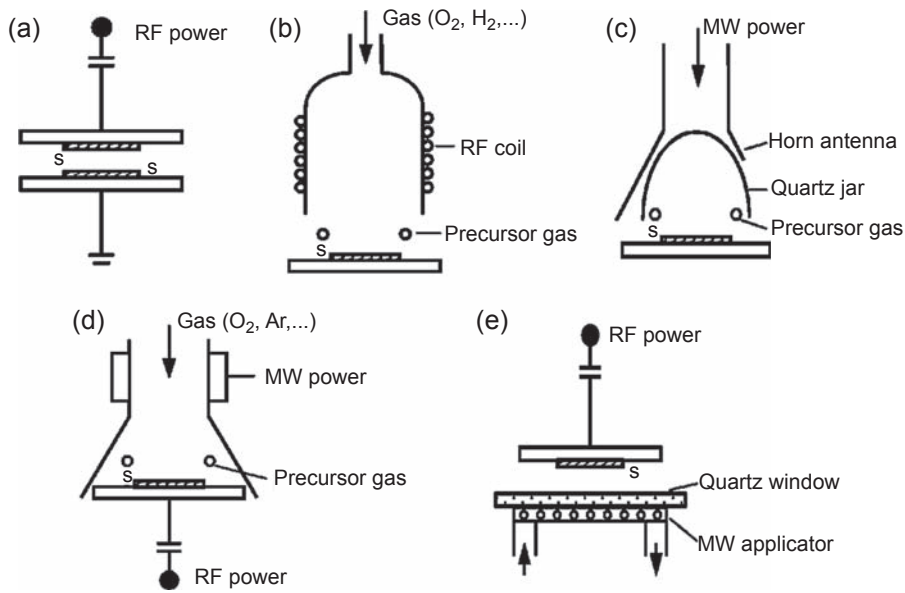

Figure 1.1 Typical PECVD reactor systems: (a) parallel plate RF PECVD; (b) remote RF PECVD; (c) MW PECVD; (d) remote MW/RF PECVD; (e) dual-mode MW/RF PECVD. Reprinted with permission from Martinu, L., Poitras, D., 2000. Plasma deposition of optical films and coatings: a review. J. Vac. Sci. Technol. A Vac. Surf. Films 18, 2619−2645.

biomedical, and manufacturing fields (Martinu et al., 2009). Here, the deposition of inorganic or metallic films by PECVD for biomaterials applications is discussed. The PECVD process of polymer films or coatings with organic precursors, termed plasma polymerization, will be discussed in Section 1.2.2.

PECVD films have received much attention in the biomedical field, especially silicon-based films such as amorphous silicon (Persheyev et al., 2011), silicon carbide (Bolz and Schaldach, 1990; Daves et al., 2011), and silicon nitride (Wei et al., 2008; Wan et al., 2005). Owing to the wide use of silane (SiH_4), these films are typically hydrogenated; for instance, a-Si:H, a-SiC:H, and a-SiN:H. Liu et al. (2007) fabricated hydrogenated amorphous silicon (a-Si:H) films on silicon by PECVD and examined the formation of hydroxyapatite on the surface. The presence of surface Si−H bonds is believed to induce apatite formation, and surface bioactivity is crucial to the development of bioactive silicon-based implants. SiN_x:H films with different N/Si ratios have been synthesized and their surface hemocompatibility has been investigated. Improved hemocompatibility is observed in SiN_x:H films compared with low-temperature isotropic carbon (LTI-C), and films with more Si−N bonds show less platelet activation, which makes them potentially more blood-compatible than LTI-C and SiN_x:H films with fewer Si−N bonds (Wan et al., 2005). Carbon-based films such as diamond-like carbon (DLC) and carbon nitride deposited by PECVD are attracting increasing interest as biomaterials. DLC films are deposited onto silicon by PECVD with methane (CH_4) as the precursor; osteoblast adhesion and proliferation tests conducted in vitro reveal that the DLC coating has better surface stability and exhibits improved cellular response (Chai et al., 2008). Ahmed et al. (2012) incorporated fluorine into DLC using acetylene (C_2H_2) and carbon tetrafluoride (CF_4) to control protein adsorption. Their results indicate that adsorption of amino acids is enhanced at low fluorine doping, but a larger fluorine concentration results in reduced adsorption compared with undoped DLC. Fluorine doping of DLC is thus a feasible approach to tailor protein adsorption.

1.2.2 Plasma polymerization

Plasma polymerization, or glow discharge polymerization (Yasuda, 1981), is the process of forming plasma-polymerized thin films based on PECVD using organic or organometallic precursors. Briefly, plasma polymerization involves the fragmentation and subsequent deposition of organic precursors or monomers (Siow et al., 2006). The organic monomer gas is fed into the reaction chamber alone or combined with a carrier gas such as argon or helium, forming the plasma and recombining on the substrate to realize film deposition (Förch et al., 2005). Plasma chemistry is normally complex and nonspecific in nature, and so plasma polymerization cannot be explicated without considering the fragmentation of molecules in both the gas and solid phases. That is, the reactive species in the plasma phase do not all originate from the monomer gas, but may be mixed with reactive species from competitive ablation of the already deposited materials. The polymerization and ablation mechanisms occur simultaneously on the substrate; these complicated processes have been described by Yasuda as competitive ablation polymerization (Yasuda and Yasuda, 2000).

The chemical reactions leading to polymer fabrication in plasma polymerization are generally complex, and the mechanisms of plasma polymerization have been extensively studied but are also controversial. Friedrich (2011) reviewed the mechanism from a chemical point of view and concluded that there are two predominant mechanisms: plasma-induced radical chain-growth polymerization and atomic fragmentation−recombination. Plasma-induced radical chain-growth polymerization is similar to classical radical polymerization involving initiation, chain-growth, and termination processes. Radicals or radical fragments (fragments•) are produced in the plasma and initiate the reaction. The polymer chain grows by addition of monomer molecules (M) and chain growth is predominately terminated by radical recombination, thus forming a polymer:

$$\mathrm{M} + \mathrm{plasma} \rightarrow \mathrm{fragments}^{\bullet} \ (\mathrm{initiation})$$

$$\mathrm{fragments}^{\bullet} + \mathrm{M} \rightarrow \mathrm{fragment} - \mathrm{M}^{\bullet} \ldots \rightarrow \mathrm{fragment} - \mathrm{M}^{\bullet} + \mathrm{M} \rightarrow \mathrm{P_n}^{\bullet} \ (\mathrm{chain\text{-}growth})$$

$$2\mathrm{P_n}^{\bullet} \rightarrow \mathrm{P_n} - \mathrm{P_n} \ (\mathrm{termination})$$

Plasma-induced ionic chain-growth polymerization may also occur similar to that of radicals: $\mathrm{fragment}^{+} + \mathrm{M} \rightarrow \mathrm{P_n^{+}}, \mathrm{P_n^{+}} + \mathrm{M} \rightarrow \mathrm{P_{n+1}^{+}}$.

The monomer molecules are extensively fragmented into single atoms or atomic fragments in high-power plasma. The polymerization process obeys the atomic fragmentation−recombination mechanism. The atoms and fragments bombard the substrate surface, forming plasma polymers with a high degree of irregularity by random recombination (Friedrich, 2011):

$$\mathrm{n(ABCDEF)} + \mathrm{plasma} \rightarrow \mathrm{n(A + B + CD + E + F)}$$

$$\mathrm{n(A + B + CD + E + F)} \rightarrow \mathrm{[FCDBAE]_n}$$

The mechanism differs greatly from conventional polymerization. Plasma polymers do not contain chains with regular repeating units, but tend to form a branched or cross-linked network. Thus, plasma polymers can have exceptional mechanical properties and good adhesion to most substrates (Stamm, 2008). Monomers in plasma polymerization are not restricted to unsaturated organics used in conventional polymerization and can be unpolymerizable saturated organic molecules. The diversity of organic monomers makes plasma polymerization a versatile tool for the deposition of polymeric thin films in a variety of applications.

The biomedical application of plasma polymerization mainly relies on changing the surface chemistry and tailoring the surface to be either bioreactive or nonreactive (Förch et al., 2007). Plasma polymerization can be implemented with a high retention of functional groups from the organic monomers. Amine or carboxyl groups are of particular interest to form a bioreactive surface to effect the binding of biomolecules and the adhesion of cells (Carton et al., 2012; Yang et al., 2014; Zhao et al., 2011). Finke et al. (2007) coated a very thin, adherent, cross-linked, pinhole- and additive-free allylamine plasma polymer layer (PPAAm) on polished

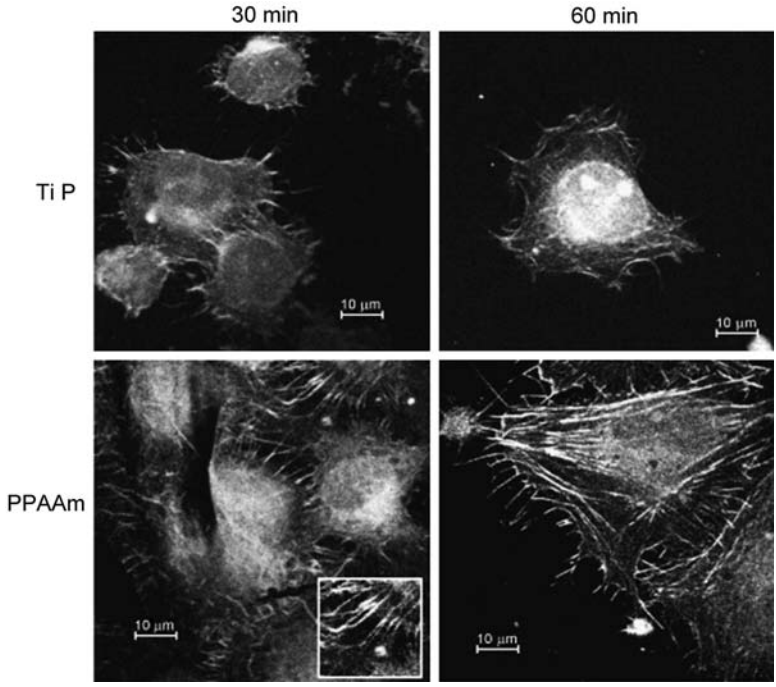

Figure 1.2 Time-dependent actin development in MG-63 osteoblasts.
Reprinted with permission from Finke, B., Luethen, F., Schroeder, K., Mueller, P.D., Bergemann, C., Frant, M., Ohl, A., Nebe, B.J., 2007. The effect of positively charged plasma polymerization on initial osteoblastic focal adhesion on titanium surfaces. Biomaterials 28, 4521−4534.

titanium. Time-dependent actin development of human MG-63 osteoblast cells after short attachment for 30 and 60 min was pronounced on the PPAAm surface (Fig. 1.2), indicating enhanced initial osteoblastic focal adhesion formation. In addition to the interactive surface, sometimes antifouling surfaces with bio-nonreactive properties are needed to prevent adhesion of proteins, platelets, or any other biological entities. Plasma polymers with polyethylene glycol-like groups or similar structures rich in ether functional groups have particular protein resistance properties. Plasma-polymerized fluorinated coatings are good candidates for bio-nonreactive surfaces (Kumar et al., 2010; Favia, 2012).

1.2.3 Atomic layer deposition

Atomic layer deposition (ALD), originally termed atomic layer epitaxy, was pioneered and patented by T. Suntola and coworkers for growing ZnS (Suntola and Antson, 1977). Initial motivation for the development of ALD came from thin film electroluminescent displays. After extensive research advances in the past 40 years, ALD, which allows deposition at the atomic or molecular level, can be used for a variety of thin films such as metal oxides and nitrides, polymers, and inorganic−organic

hybrid materials with control at the atomic or molecular level (George, 2010). This versatile technique has been adopted by the microelectronics industry but is also used to produce plasmonics materials, medical devices, and biomaterials (Im et al., 2012; Knez et al., 2007; Skoog et al., 2013).

ALD is conducted in cycles. In one cycle, alternating chemical reactions of two precursors, "a" and "b," occur with purging with an inert gas in between. Precursor "a" is first saturated and chemisorbed on the surface of the substrate. After excessive precursor "a" in the gas phase is removed by purging with the inert gas, the precursor gas "b" then reacts with the chemisorbed precursor "a" on the substrate, producing a layer of the desired materials. The excess precursor "b" and by-products are removed by a second purging and the growth cycle is repeated until the desired film thickness is obtained. As an example, the growth cycle to deposit a TiO_2 thin film employing gaseous precursors $TiCl_4$ and H_2O is presented in Fig. 1.3. The sequential and saturating surface reactions ensure self-limitation of the film growth. Thus, the film thickness depends only on the number of reactions cycles, thereby enabling precise and simple control of the thickness. The small deposition rate in ALD is also desirable in some applications (Ritala and Niinisto, 2009).

Thin films prepared by ALD possess biologically relevant surface properties enabling many biomedical applications. For instance, hard CrN coatings on steel have been sealed with 50-nm-thick $Al_2O_3-Ta_2O_5$ nano-laminates prepared by ALD (Härkönen et al., 2014). The ALD layer smoothes the CrN surface because it

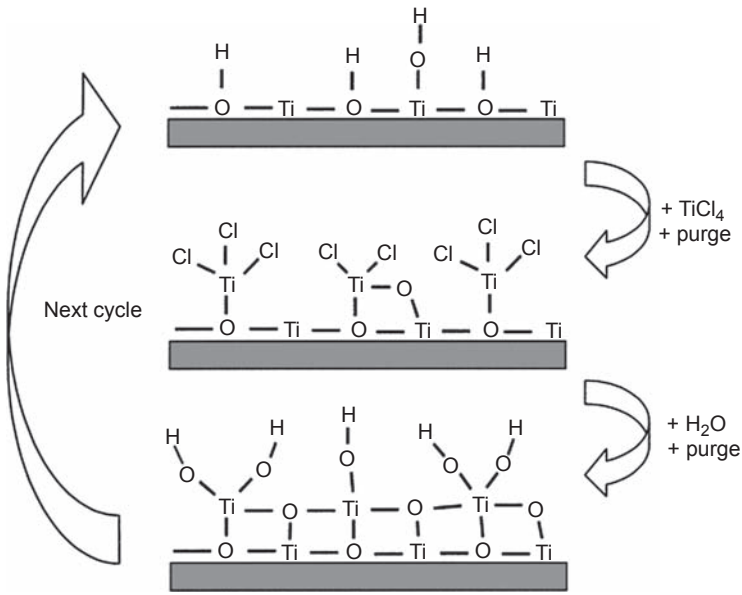

Figure 1.3 Schematic illustration of ALD deposition of TiO_2 films using $TiCl_4$ and H_2O. Reprinted with permission from Leskelä, M., Ritala, M., 2003. Atomic layer deposition chemistry: recent developments and future challenges. Angew. Chem. 42, 5548–5554.

penetrates the pinhole defects. Effective sealing by ALD improves corrosion protection of the CrN coatings. Slaney et al. (2011) used ALD to produce a 15-nm-thick conformal silica film with superior electrochemical properties. Trialkoxysilane derivatives of two monosaccharides are then attached to the hydroxyl groups of silica, enabling straightforward functionalization of the silica-coated stainless-steel surface. The presence and biological function of the monosaccharides on the functionalized surfaces are confirmed by an enzyme-linked lectin assay, which suggests that ALD can functionalize stainless-steel stents and other implants. Putkonen et al. (2009) conducted ALD to prepare hydroxyapatite on Si (100) and Corning (0211) substrates. Postdeposition annealing at 500°C produces partially crystalline hydroxyapatite films and the degree of crystallinity increases with annealing temperature. In vitro studies reveal that mouse MC3T3-E1 osteoblast cells attach better on the annealed hydroxyapatite surface and indicate that the ALD-deposited hydroxyapatite film has enhanced biocompatibility.

Compared with conventional CVD methods, the saturation/reaction/purging cycles in ALD allow the longer lifetime of the precursor molecules to transport and diffuse to the cavities in complicated three-dimensional substrates. As a result, one can expect better uniformity and conformity on complex substrates for ALD compared with conventional CVD (Lee et al., 2011). Hence, ALD is practical for substrates with a complex surface morphology. Hyde et al. (2009) deposited conformal and uniform $TiNO_x$ films on cellulose fiber substrates at 100°C. In vitro studies involving human adipose-derived adult stem cells are carried out on films with different thicknesses. The 20-Å-thick $TiNO_x$ film has the largest amount of adhered cells, and by altering the film thickness it is possible to control the quantities of adhered cells. The results suggest that ALD is useful in the surface modification of biocompatible implant materials. Skoog et al. (2012) used ALD to produce nanoporous alumina membranes with zinc oxide. In vitro agar diffusion assays show that zinc oxide—coated nanoporous alumina membranes inhibit the growth of several bacteria found on skin, including *Bacillus subtilis*, *Escherichia coli*, *Staphylococcus aureus*, and *Staphylococcus epidermidis*. Im et al. (2010) deposited thin alumina dielectric layers by ALD to form vertical nanogap structures for surface-enhanced Raman scattering (SERS) (Fig. 1.4). By decreasing the gap size to 5 nm, local SERS enhancement of up to 10^9 can be accomplished. With state-of-the-art ALD protocols, it is possible to push the limits of this scheme to make well-defined 1- to 2-nm nanogaps, and the technique can be applied to nonlinear optics and biosensing.

1.3 Physical vapor deposition

1.3.1 Evaporation

Evaporation, or vacuum deposition, is a simple physical vapor deposition (PVD) process in which atoms or molecules are evaporated from the source thermally, travel without collisions with residual gas molecules in the deposition chamber, and condense on the substrate. Two heating mechanisms are commonly used in

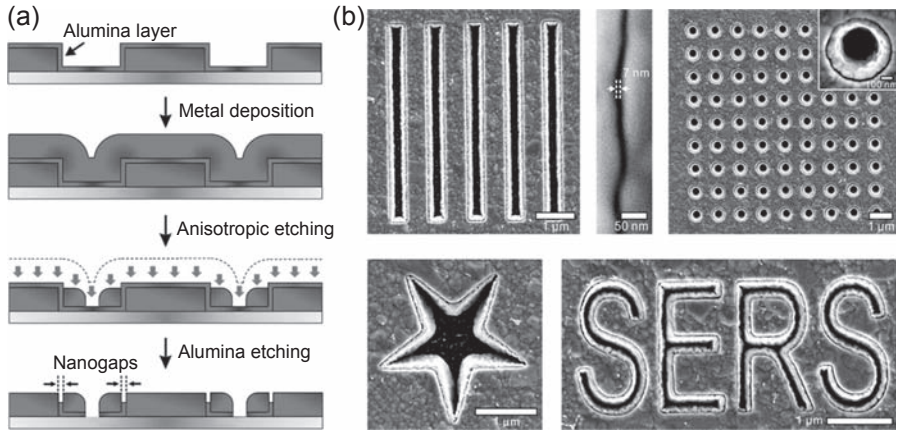

Figure 1.4 (a) Schematic showing the fabrication process of nanogap arrays using ALD. The nanogap size is determined by the thickness of the alumina layer. (b) Scanning electron microscopy images of various nanogap structures.
Reprinted with permission from Im, H., Bantz, K.C., Lindquist, N.C., Haynes, C.L., Oh, S.-H., 2010. Vertically oriented sub-10-nm plasmonic nanogap arrays. Nano Lett. 10, 2231−2236.

evaporation: resistive heating and electron beam heating, as illustrated in Fig. 1.5. In resistive heating, the materials in a boat of crucible are evaporated by heating with a filament. Common materials are W, Ta, Mo, C, and BN/TiB_2 composite ceramics. Resistive heating is the most common technique to vaporize materials at temperatures below about 1500°C (Mattox, 2010; Adachi and Wasa, 2012). In comparison, high-energy electron beams are used (commonly referred to as e-beam heating) for refractory materials. The electron beam from an e-beam gun is accelerated to a high voltage (10−20 kV),

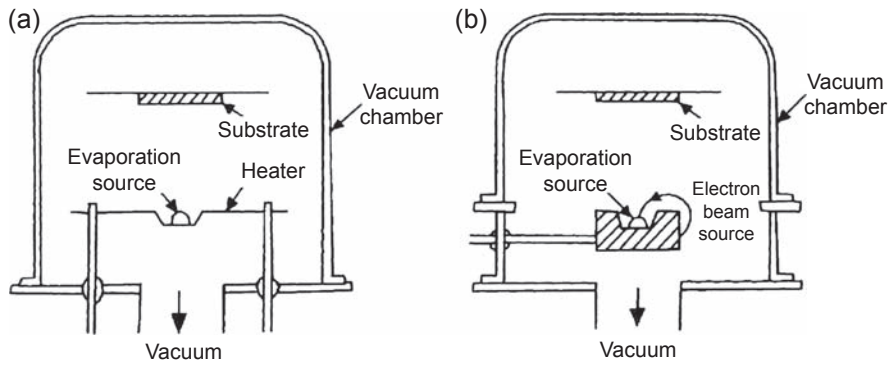

Figure 1.5 (a) Typical thermal evaporation system and (b) electron beam evaporation system.
Reprinted with permission from Adachi, H., Wasa, K., 2012. Thin films and nanomaterials. In: Wasa, K., Kanno, I., Kotera, H. (Eds.), Handbook of Sputtering Technology, second ed. William Andrew Publishing, Oxford, pp. 3−39.

electrostatically or magnetically collimated and focused, and impinged onto the surface of the materials to be evaporated (Mattox, 2010). One advantage of e-beam evaporation over resistive heating is that the energy is transferred as heat only to melt the source locally instead of the entire crucible, and consequently there is less contamination from the crucible.

The evaporation process requires a relatively good vacuum to ensure collision-less trajectories of evaporated atoms before condensation. Evaporation is normally carried out in a vacuum more than 10^{-5} Torr. To minimize residual gases that can contaminate the film, a high (10^{-7} Torr) or ultrahigh ($<10^{-9}$ Torr) vacuum may be needed to produce films with the desired purity (Hung et al., 1992). The pumping system is usually based on a diffusion pump with a liquid nitrogen—cooled anticreep-type baffle backed by a mechanical pump or a Roots blower/mechanical pump combination in large systems. For high-purity film deposition in which a base pressure of 10^{-9} to 10^{-10} Torr is needed, ion pumps backed by cryosorption pumps are commonly used (Martin, 2009).

Evaporation is widely used for a variety of materials including metals, elemental semiconductors, alloys, intermetallic compounds, and refractory compounds (oxides, carbides, nitrides, borides, etc.). Shah et al. (2010) reviewed materials deposited by evaporation as well as different evaporation processes such as multiple-source evaporation, reactive evaporation, and activated reactive evaporation. For instance, evaporated films of titanium (Ti), titanium oxide (TiO_2), and calcium phosphate are commonly used to tailor surface chemistry and topography for a better biological response (Hacking et al., 2007; Han et al., 2010; Chen et al., 2010). Han et al. (2010) deposited a pure titanium (Ti) layer on polyetheretherketone (PEEK) to enhance biocompatibility and adhesion to bone tissues. The Ti layer adheres firmly to the substrate and enhances wettability. The initial cell adhesion images shown in Fig. 1.6(c) and (d) indicate better cell attachment and biocompatibility. In vivo animal tests show that the Ti-coated PEEK implants have a larger bone-in-contact ratio than pure PEEK implants. Lin et al. (2009) deposited titanium oxide films by electron beam evaporation. The surface contact angle decreased and biological tests revealed substantial cell adhesion and little platelet adhesion, indicating that the e-beam—deposited Ti has good potential in cardiovascular stents.

1.3.2 Sputtering deposition

Sputtering refers to the basic and well-known process involving backward scattering of the solid surface atoms to the surface upon bombardment by energetic ions, as illustrated in Fig. 1.7 (Rautray et al., 2011). Sputtering is an etching process suitable for surface cleaning, micromachining, depth profiling, and so on. Deposition of the ejected vapor products, known as sputtering deposition, is a common film deposition technique.

Although the deposition rate is typically smaller than that of evaporation, sputtering deposition possesses several advantages compared with other PVD methods. In the sputtering system, sputtered species are generally composed of neutrals of the target materials with only a small fraction of ions when the target is bombarded ions with energies of several hundreds to thousands of electron volts. Clusters of atoms may be formed as well (Wasa, 2012a). Deposition of films by sputtering is predictable

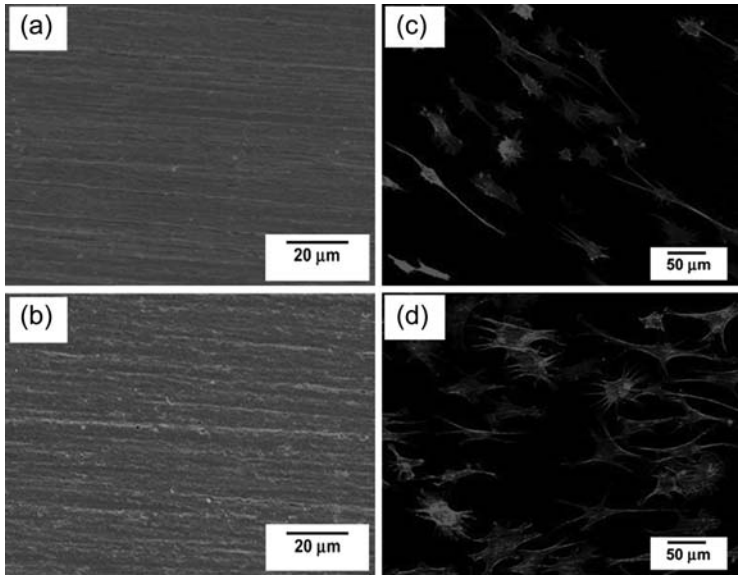

Figure 1.6 Scanning electron microscopy images of the surface of (a) as-machined and (b) Ti-coated PEEK. Confocal laser scanning microscopy images of MC3T3-E1 cells cultured on (c) as-machined and (d) Ti-coated PEEK for 3 h.
Reprinted with permission from Han, C.-M., Lee, E.-J., Kim, H.-E., Koh, Y.-H., Kim, K.N., Ha, Y., Kuh, S.-U., 2010. The electron beam deposition of titanium on polyetheretherketone (PEEK) and the resulting enhanced biological properties. Biomaterials 31, 3465−3470.

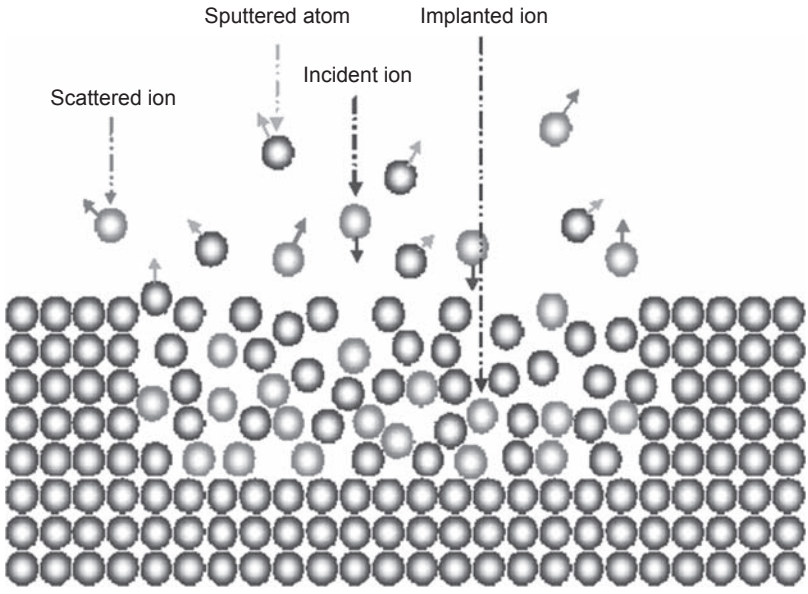

Figure 1.7 Illustration of various processes in ion−solid interactions.
Reprinted with permission from Rautray, T.R., Narayanan, R., Kim, K.-H., 2011. Ion implantation of titanium based biomaterials. Prog. Mater. Sci. 56, 1137−1177.

and stable. The energy distribution of the sputtered species usually has a maximum of about 4−7 eV with a long tail of over 50 eV. These energies are more than an order of magnitude higher than those of the evaporated species and allow the depositing species to penetrate more deeply into the substrate and enhance the surface mobility to form dense, well-bonded films (Suryanarayana, 1999). Moreover, sputtering is essentially a kinetic process involving momentum transfer in lieu of chemical and/or thermal processes; therefore, virtually any materials can be introduced into a gas phase by sputtered a solid target (Kern, 1991).

There are two primary ways to generate energetic ions by sputtering by means of a plasma and ion beam; common sputtering systems adopt a DC diode, RF diode, magnetron diode, and ion beam sputtering (Seshan, 2002; Wasa, 2012b). Typical systems are depicted in Fig. 1.8. DC diode sputtering constitutes a simplest sputtering system in which two planar electrodes are positioned opposite each other in a vacuum chamber. The chamber is filled with a noble gas, typically argon at 1−5 Pa. When high voltage in the range of 2000 V is applied between the cathode and anode, a glow discharge is ignited. Argon ions in the glow discharge are accelerated and sputter the cathode target, resulting in the deposition of materials sputtered from the target onto the substrate. Diode plasma cannot be operated on insulators because the sputtering discharge cannot be sustained owing to the immediate buildup of surface-positive charges on the front side of the insulators. Hence, RF-diode sputtering is commonly used to sputter insulators. The difference is that the power supply is at a high frequency, commonly 13.56 MHz. In addition to the ability to sputter insulators, the RF in the discharge chamber increases the collision probability between secondary electrons and gas molecules, thereby producing higher plasma density, larger ion currents, and faster sputtering than the DC process (Wasa, 2012b).

Magnetron sputtering is a promising low-pressure method used in most sputtering applications. Two common types of magnetron sputtering systems, cylindrical and planar, are shown in Fig. 1.8. The magnetic field is located parallel to the cathode surface, and electrons in the glow discharge experience the $E \times B$ (E cross B) drift, in which E and B denote the electric field in the discharge and superposed transverse magnetic field, respectively. By setting up the magnetic field properly, a close current loop of drifting secondary electrons is formed. This electron trapping effect increases the collision rates between the electrons and sputtering gas molecules. The working pressure in the magnetron sputtering system is 10^{-5} to 10^{-3} Torr, and so the sputtered particles traverse the discharge space without collisions, consequently yielding high deposition rates. In the ion beam sputtering system, the incident ions are generated by an ion source separated from the sputtering chamber. The pressure in the sputtering chamber is typically 10^{-5} to 10^{-4} Torr range. Ion beam sputtering systems are used in sputter etching of semiconducting devices and have gained interest in thin film deposition.

1.3.3 Plasma immersion ion implantation and deposition

Plasma immersion ion implantation and deposition (PIII&D) is a versatile technique that can conduct simultaneous and sequential ion implantation and deposition, owing to a combination of the advantages offered by conventional plasma and ion beam technologies (Lu et al., 2012). The uniqueness of PIII&D over conventional ion

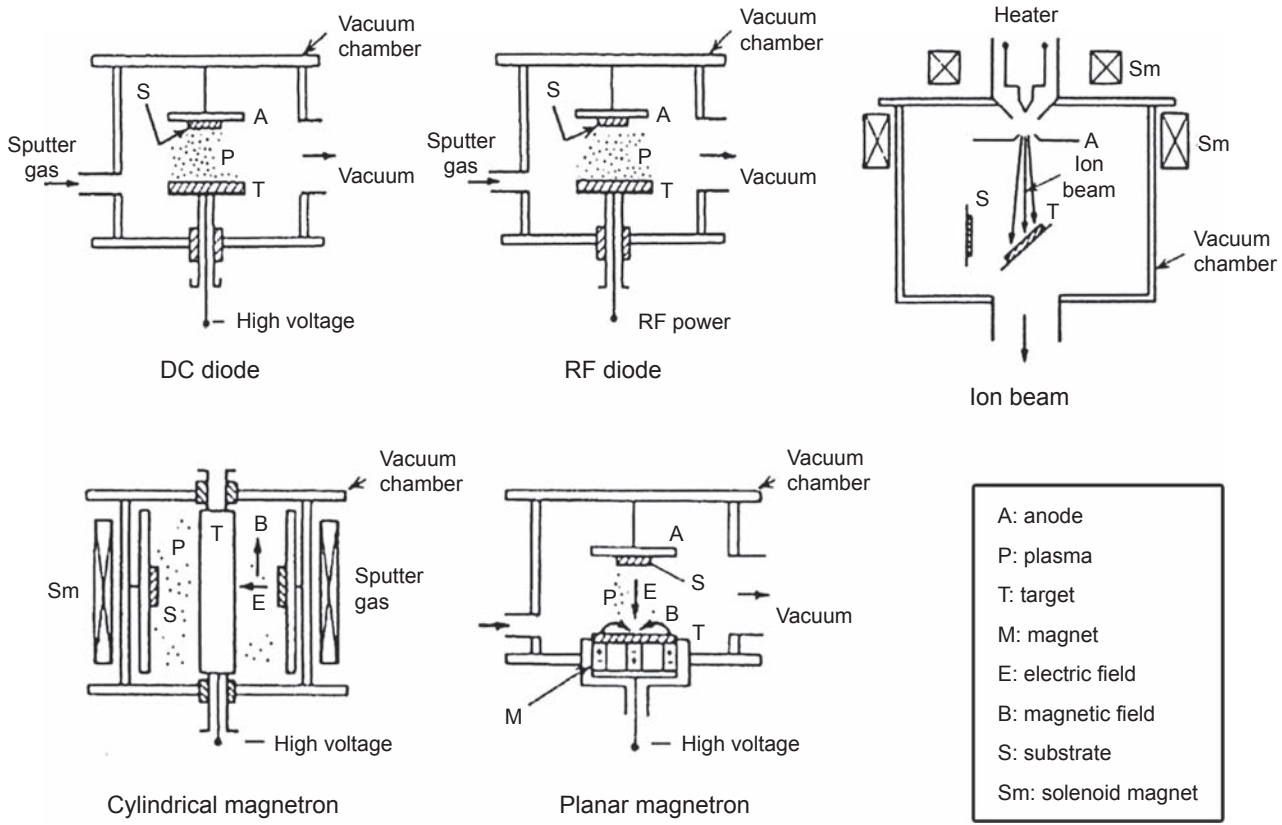

Figure 1.8 Sputtering deposition systems.
Reprinted with permission from Wasa, K., 2012b. Sputtering systems. In: Wasa, K., Kanno, I., Kotera, H. (Eds.), Handbook of Sputtering Technology, second ed. William Andrew Publishing, Oxford, pp. 77−139; Adachi, H., Wasa, K., 2012. Thin films and nanomaterials. In: Wasa, K., Kanno, I., Kotera, H. (Eds.), Handbook of Sputtering Technology, second ed. William Andrew Publishing, Oxford, pp. 3−39.

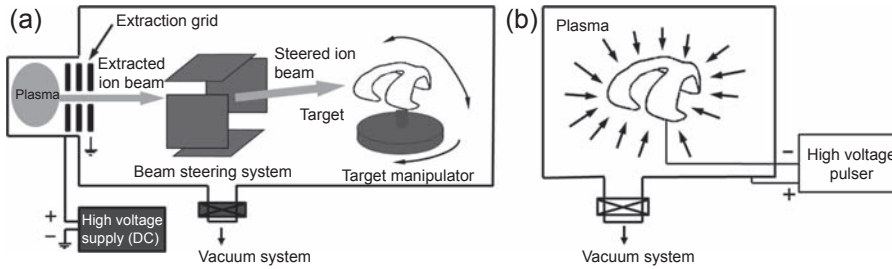

Figure 1.9 Schematic illustrations: (a) Conventional beam line ion implantation and (b) plasma immersion ion implantation.
Reprinted with permission from Anders, A., 2000. Handbook of Plasma Immersion Ion Implantation and Deposition. Wiley, New York.

implantation stems from the separation of the ion source and target. Conventional ion implantation (Fig. 1.9(a)) is a line-of-sight process in which ions are extracted from plasma in an extraction system, accelerated as a beam to high energy, and then bombard the sample. Owing to the small cross-sectional area of the ion beam, either beam or sample rotating must be performed to achieve uniform implantation into a large sample. Ion implantation is suitable for planar substrates such as silicon wafers, but for complicated surfaces, sample rotation is required for uniform implantation, which adds complexity and limits the size of the samples (Liu et al., 2008).

In the PIII&D system, rather than using conventional ion extraction, the sample is immersed in plasma normally sustained by an external plasma source (Fig. 1.9(b)). The plasma can be generated by a number of plasma sources, including hot filament, RF, and electron cyclotron resonance. The negative high voltage applied to the sample accelerates electrons away from the sample surface while positive ions are accelerated from the plasma to bombard the sample surface. Under the sample bias, a plasma sheath through which ion implantation takes place forms around the sample (Anders, 2000). The plasma sheath, which dictates the implantation process, thus has an important role in PIII&D and can be used to predict the processing parameters and results, including the implantation current, implantation fluency, and depth profile. Because the sample is enshrouded by the plasma sheath, PIII&D can be used to process nonplanar ones. PIII&D has many advantages over conventional implantation; for example, high ion current density, relatively short processing time (eg, minutes), high dose rates (eg, 10^{14} cm^{-2} s^{-1}), wide ion energy range ($10-10^5$ eV), large implantation areas (hundreds square centimeters), and treatment of devices with complex shapes without special target manipulation (Pelletier and Anders, 2005; Chu et al., 1996).

Since its inception in the late 1980s, PIII&D has spurred many significant applications, particularly semiconductor and microelectronics processing (Chu et al., 1996; Anders, 2002; Chu, 2004). PIII&D has also gained great attention in biomedical engineering related to the surface modification of biomedical implants to enhance mechanical properties, bioactivity, biocompatibility, blood compatibility, and antibacterial activity (Huang et al., 2004; Chu, 2013). For example, magnesium alloys, which

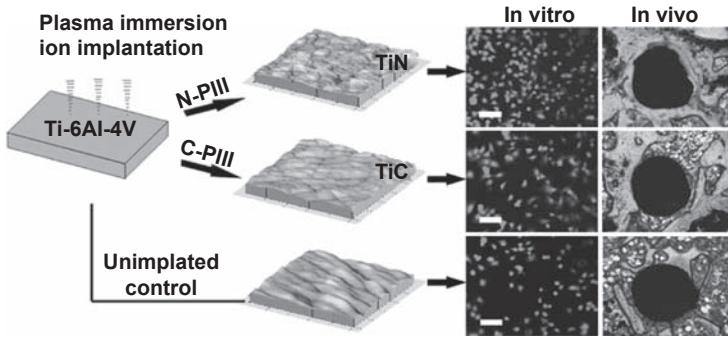

Figure 1.10 Schematic illustration of enhanced cell adhesion and early bone formation on Ti-6Al-4V after nitrogen and carbon plasma immersion ion implantation.
Reprinted with permission from Zhao, Y., Wong, S.M., Wong, H.M., Wu, S., Hu, T., Yeung, K.W.K., Chu, P.K., 2013. Effects of carbon and nitrogen plasma immersion ion implantation on in vitro and in vivo biocompatibility of titanium alloy. ACS Appl. Mater. Interfaces 5, 1510−1516.

possess unique properties such as natural biodegradability, experience fast corrosion in the physiological environment. The corrosion resistance of the magnesium alloys can be enhanced by PIII of gaseous or metallic elements such as oxygen (Wu et al., 2012a), chromium (Xu et al., 2012), aluminum (Wu et al., 2012b), zirconium (Zhao et al., 2014), and so on. PIII&D has also been carried out on titanium and titanium alloys to improve bioactivity and biocompatibility (Maitz et al., 2005; Xie et al., 2005; Zhao et al., 2013). Zhao et al. (2013) conducted nitrogen and carbon plasma immersion ion implantation on Ti-6Al-4V to form surface layers of TiN and TiC (Fig. 1.10). In vitro studies reveal improved cell adhesion and proliferation, and early bone formation is enhanced by in vivo tests. Moreover, there has been considerable research on the treatment of biomedical and degradable polymers such as poly(butylene succinate) (Wang et al., 2009) and polytetrafluoroethylene (Wang et al., 2010, 2012) by PIII&D to enhance surface bioactivity and biocompatibility.

1.4 Electrophoretic deposition

Thin film deposition methods based on gas-phase processes such as CVD, evaporation, and sputtering are straightforward and thin films with good purity and structural properties can be produced. However, there are some drawbacks, such as the strict instrumentation requirement, relatively high processing cost, as well as gaseous waste treatment. In comparison, chemical and electrochemical solution methods are cost-effective and waste is confined to the solution.

Electrophoretic deposition (EPD) is a wet electrolytic deposition technology for thin films. EPD employs the electrophoresis mechanism, as illustrated schematically in Fig. 1.11. The electric field is applied between two electrodes and charged particles dispersed or suspended in a liquid medium move toward the oppositely charged

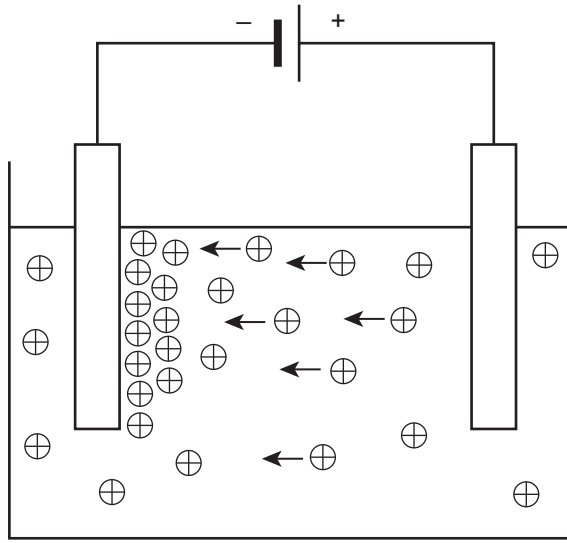

Figure 1.11 Two-electrode cell for electrophoretic deposition showing positively charged particles in the suspension migrating toward the negative electrode.
Reprinted with permission from Corni, I., Ryan, M.P., Boccaccini, A.R., 2008. Electrophoretic deposition: from traditional ceramics to nanotechnology. J. Eur. Ceram. Soc. 28, 1353−1367.

electrode (electrophoresis), followed by accumulation of particles on the deposition electrode in an ordered manner, producing a relatively compact and homogeneous film (deposition) (Corni et al., 2008). Stability of the suspension is critical to EPD to allow free movement of the charged particles in the solution. The charged particles can be fine powders, colloids, or macromolecules, and EPD is a versatile method to fabricate films composed of ceramics, metals, polymers, and even organic/inorganic hybrid materials.

On the heels of major development of EPD in the deposition of bulk materials and coatings, the application of EPD to biomaterials starts with the preparation of hydroxyapatite (HA) $Ca_{10}(PO_4)_6(OH)_2$ coatings on Ti (Boccaccini et al., 2010; Ducheyne et al., 1986). In a typical process involving the EPD of HA coatings, HA powders are homogenously dispersed in ethanol to obtain a colloidal suspension and electrophoretically deposited on stainless steel. Results show that a long deposition time (more than 90 s) results in spalling owing to shrinkage from drying, but a repetitive deposition method instead of single deposition can be employed to overcome the spalling problem (Wang et al., 2002). EPD has also found success in the production of other bioceramic coatings or metallic films. Zhang et al. (2010) prepared TiO_2 films on nickel with low-temperature EPD. The photocatalytic activity of the TiO_2 film is evaluated by monitoring the degradation rate of methyl orange (MO), and the degradation rate of MO increases with the amount of TiO_2. Zhu et al. (2012) reported an EPD method for the fabrication of gold nanoparticle thin films on indium tin oxide as sensitive SERS substrates.

Biomedical applications of EPD have been extended to the deposition of functional composite coatings and multilayer films (Fig. 1.12). Jiang et al. (2010) prepared pure chitosan and CS/G coatings on titanium substrates via EPD. The coatings possess a similar macroporous structure and the shear bonding strength of the CS/G coatings increases with the gelatin contents. In vitro biological tests demonstrate that human MG63 osteoblast-like cells have better affinity on the coatings with larger gelatin contents. Pang et al. (2009) prepared hydroxyapatite (HA)−$CaSiO_3$(CS)−chitosan coatings by cathodic EPD. The EPD HA−CS−chitosan composite coatings have monolayered or laminated structures containing different layers, as shown in Fig. 1.12(a). Potentiodynamic polarization studies coupled with electrochemical impedance spectroscopy indicate that the composite coatings enhance the corrosion protection of the stainless-steel substrate. EPD has also been used to codeposit other

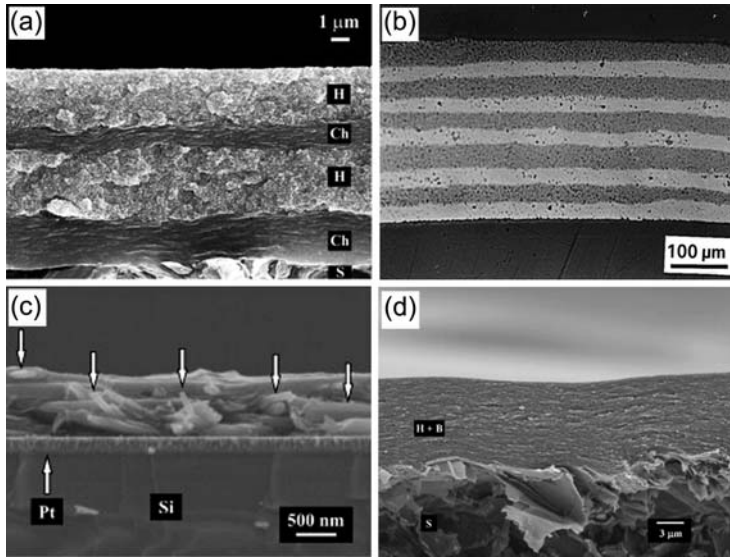

Figure 1.12 Cross-sectional scanning electron microscopy images of EPD-fabricated composites or multilayered coatings: (a) Laminate coatings of chitosan (Ch) and HA (H) with different layers on a graphite substrate (S); (b) 10 alternating layers of Al_2O_3 and ZrO_2; (c) polyacrylic acid films containing halloysite nanotubes (white arrows) on the platinized silicon wafer substrate; (d) sodium hyaluronate and bovine serum albumin composite films (H + B) on a graphite substrate (S).
Reprinted with permission from Pang, X., Casagrande, T., Zhitomirsky, I., 2009. EPD of hydroxyapatite-$CaSiO_3$-chitosan composite coatings. J. Colloid Interface Sci. 330, 323−329; Ferrari, B., Sánchez-Herencia, A.J., Moreno, R., 1998. Aqueous EPD of Al_2O_3/ZrO_2 layered ceramics. Mater. Lett. 35, 370−374; Wang, Y., Deen, I., Zhitomirsky, I., 2011. EPD of polyacrylic acid and composite films containing nanotubes and oxide particles. J. Colloid Interface Sci. 362, 367−374; Ma, R., Epand, R.F., Zhitomirsky, I., 2010. Electrodeposition of hyaluronic acid and hyaluronic acidebovine serum albumin films from aqueous solutions. Colloids Surf. B Biointerfaces 77, 279−285, respectively.

materials and realize further functionalization of composite coatings such as Al_2O_3–ZrO_2-layered ceramics (Ferrari et al., 1998), polyacrylic acid films containing nanotubes and oxide particles (Wang et al., 2011), and hyaluronic acid–bovine serum albumin films (Ma et al., 2010).

1.5 Sol-gel method

The sol-gel technique has emerged as a versatile method for the preparation of oxide thin films and oxide-containing composite films. The sol-gel process consists of three parts: preparation of the precursor solution, deposition of the sol onto the substrate, and heat treatment for densification. The precursors are commonly metal alkoxides in organic solvents or metal salts in aqueous solutions, depending on the nature of the molecular precursors (Livage and Ganguli, 2001). Sol deposition is normally performed by means of spin- or dip-coating techniques, and the thickness of the thin film can be controlled at the submicrometer level by varying the withdrawal or spinning rate in the case of dip and spin coatings (Brinker et al., 1992). The abundance of choice in each step endows the sol-gel method with versatility and renders the controllability of thin film structural properties. In a review of sol-gel deposition of zinc oxide thin films, Znaidi (2010) summarized the chemical and physical parameters influencing the structural properties of thin films in the sol-gel process.

In addition to better control of the chemical composition and microstructure of the films, the sol-gel method offers advantages over other thin film processes including the preparation of homogeneous films, reduced densification temperature, simpler equipment, and lower cost (Liu et al., 2010). There has been extensive research on the use of sol-gel deposition to improve the bioactivity, blood compatibility, and antibacterial properties of biomaterials. Table 1.1 lists common thin films fabricated by the sol-gel method, including the chemical systems used and biomedical applications.

1.6 Spraying processes

Thermal spraying refers to the spraying of molten or semimolten particles onto a substrate at a high speed to prepare coatings (0.5–2 mm thick). According to the different heating sources to melt the particles, thermal spraying can be divided into flame, electrical arc, plasma, and detonation-gun spraying (Pawlowski, 2008). Plasma spraying is the most common method, typically composed of atmospheric plasma spraying and vacuum plasma spraying. In plasma spraying, illustrated in Fig. 1.13(a), the high energy of the high-frequency electrical arc ignited between the anode and cathode with the aid of the plasma-forming gas (Ar, He, H_2, N_2, or mixtures) melts and sprays the particles onto a substrate at a high velocity. The melted or partially melted particles undergo splat formation, splat layering, and coating formation before they flatten and solidify on the substrate (Fauchais, 2004). Currently, DC plasma arc devices dominate the commercial market, whereas RF or inductively coupled plasma devices have a few commercial applications in plasma spraying (Liu et al., 2004).

Table 1.1 Thin films fabricated by the sol-gel process and their biomedical applications

Films	Substrate	Coating technique	Pre-heat treatment (°C)	Post-heat treatment (°C)	Application	References
Carbon nanotube/ hydroxyapatite	Ti-6Al-4V	Dip coating	50	500	Biocompatibility	Abrishamchian et al. (2013)
TEOS−MTES−SiO_2	Stainless steel	Dip coating	r.t.	450	Bioactivity	Ballarre et al. (2010)
TiO_2, Nb_2O_5, SiO_2, SiO_2-TiO_2	Pure titanium	Spin coating	150	450	Osteoblast responses	Ochsenbein et al. (2008)
Ag-TiO_2	Silicon	Spin coating	100	500	Antibacterial	Yu et al. (2011)
Ag-SiO_2	Glass	Dip coating	100	200−600	Antibacterial	Jeon et al. (2003)
Silica	Ti-6Al-4V	Dip coating	–	r.t.	Controlled release of vancomycin	Radin and Ducheyne (2007)
TiO_2/$SrFe_{12}O_{19}$ composite	316L stainless steel, NiTi alloy	Spin coating	–	500	Blood compatibility	Liu et al. (2011)

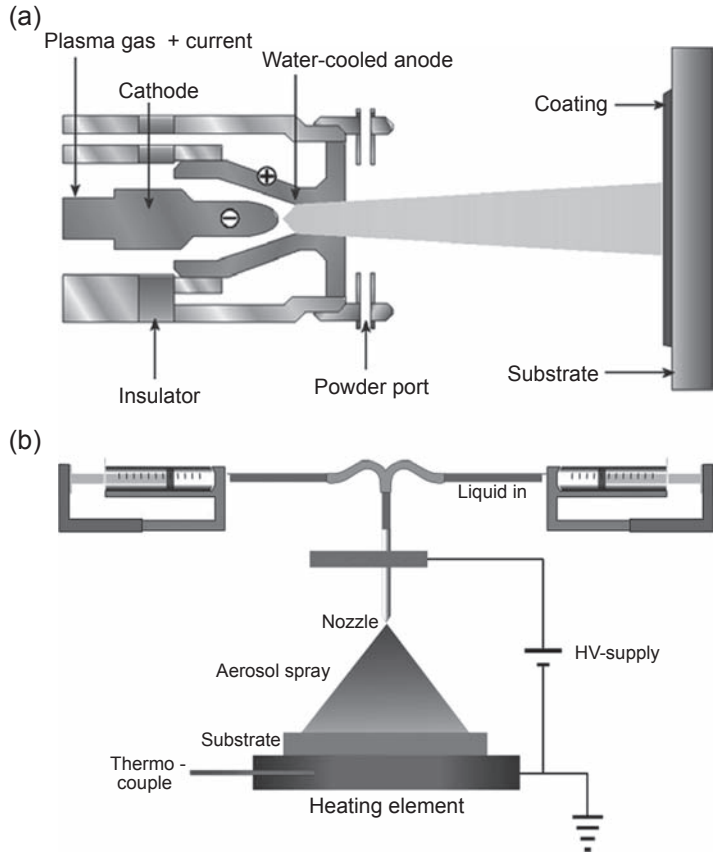

Figure 1.13 (a) Schematic diagram of the plasma spray process and (b) experimental setup of the electrostatic spray deposition technique.
Reprinted with permission from Vencl, A., Mrdak, M., Cvijovic, I., 2006. Microstructures and tribological properties of ferrous coatings deposited by APS (Atmospheric Plasma Spraying) on Al-alloy substrate. FME Trans. 34, 151−157; Leeuwenburgh, S., Wolke, J., Schoonman, J., Jansen, J., 2005. Influence of deposition parameters on chemical properties of calcium phosphate coatings prepared by using electrostatic spray deposition. J. Biomed. Mater. Res. A 74, 275−284.

As a surface modification technique for biomaterials, plasma spraying is a favorable method to deposit bioceramic coatings. Hydroxyapatite coatings provide orthopedic implants with a mineral phase similar to natural hard tissues and improve bioactivity and osteoconductivity. Considerable research efforts have been devoted to producing plasma-sprayed HA coatings on metallic implants and resulting applications to dentistry and orthopedics (Sun et al., 2001). In addition, other coatings such as $CaSiO_3$ and TiO_2 have been plasma sprayed and confirmed to reinforce apatite formation on the surface (Chen et al., 2008; Liu et al., 2001, 2005).

Electrostatic spray deposition (ESD) has been developed to prepare bioactive calcium phosphate coatings. The basic principle of ESD encompasses the

generation and spraying of an aerosol and dispersion of charged particles or droplets by means of electrostatic atomization of the inorganic or organometallic precursors (Leeuwenburgh et al., 2003). As shown in Fig. 1.13(b), high voltage between the nozzle and grounded substrate (typically between 6 and 15 kV) produces droplets at the tip of the nozzle, forming a spray of highly charged droplets. These spray droplets impinge onto the heated substrate as a result of the applied potential and lose their charge. Consequently, a thin inorganic layer is formed by complete solvent evaporation (Leeuwenburgh et al., 2005).

1.7 Conclusion

In summary, common thin film deposition technologies for surface modification and the engineering of biomaterials have been reviewed with an emphasis on the fundamentals and technology of each method. Examples of fabricated films and their applications in the biomedical fields are described. Properties such as film thickness, mechanical properties, and surface chemistry produced by different techniques can differ greatly and the choice requires systematic study and comparison. From the perspective of the development of thin film deposition techniques, the combination of the different techniques, chemical and physical, can realistically enable the exploration and expansion of existing techniques for the fabrication of future films and coatings.

References

Abrishamchian, A., Hooshmand, T., Mohammadi, M., Najafi, F., 2013. Preparation and characterization of multi-walled carbon nanotube/hydroxyapatite nanocomposite film dip coated on Ti-6Al-4V by sol-gel method for biomedical applications: an in vitro study. Mater. Sci. Eng. C 33, 2002–2010. http://dx.doi.org/10.1016/j.msec.2013.01.014.

Adachi, H., Wasa, K., 2012. Thin films and nanomaterials. In: Wasa, K., Kanno, I., Kotera, H. (Eds.), Handbook of Sputtering Technology, second ed. William Andrew Publishing, Oxford, pp. 3–39.

Ahmed, M.H., Byrne, J.A., Mclaughlin, J., 2012. Evaluation of glycine adsorption on diamond like carbon (DLC) and fluorinated DLC deposited by plasma-enhanced chemical vapour deposition (PECVD). Surf. Coat. Technol. 209, 8–14. http://dx.doi.org/10.1016/j.surfcoat.2012.07.011.

Anders, A., 2000. Handbook of Plasma Immersion Ion Implantation and Deposition. Wiley, New York.

Anders, A., 2002. From plasma immersion ion implantation to deposition: a historical perspective on principles and trends. Surf. Coat. Technol. 156, 3–12. http://dx.doi.org/10.1016/S0257-8972(02)00066-X.

Ballarre, J., Manjubala, I., Schreiner, W., Orellano, J., Fratzl, P., Ceré, S., 2010. Improving the osteointegration and bone-implant interface by incorporation of bioactive particles in sol-gel coatings of stainless steel implants. Acta Biomater. 6, 1601–1609. http://dx.doi.org/10.1016/j.actbio.2009.10.015.

Boccaccini, A., Keim, S., Ma, R., Li, Y., Zhitomirsky, I., 2010. Electrophoretic deposition of biomaterials. J. R. Soc. Interface 7, S581–S613. http://dx.doi.org/10.1098/rsif.2010.0156.focus.

Bolz, A., Schaldach, M., 1990. Artificial heart valves: improved blood compatibility by PECVD a-SiC: H coating. Artif. Organs 14, 260–269. http://dx.doi.org/10.1111/j.1525-1594.1990.tb02967.x.

Brinker, C.J., Hurd, A.J., Schunk, P.R., Frye, G.C., Ashley, C.S., 1992. Review of sol-gel thin film formation. J. Non-Cryst. Solids 147–148. http://dx.doi.org/10.1016/S0022-3093(05)80653-2.

Carton, O., Ben Salem, D., Bhatt, S., Pulpytel, J., Arefi-Khonsari, F., 2012. Plasma polymerization of acrylic acid by atmospheric pressure nitrogen plasma jet for biomedical applications. Plasma Processes Polym. 9, 984–993. http://dx.doi.org/10.1002/ppap.201200044.

Chai, F., Mathis, N., Blanchemain, N., Meunier, C., Hildebrand, H.F., 2008. Osteoblast interaction with DLC-coated Si substrates. Acta Biomater. 4, 1369–1381. http://dx.doi.org/10.1016/j.actbio.2008.04.011.

Chen, C., Lee, I.-S., Zhang, S.-M., Yang, H.C., 2010. Biomimetic apatite formation on calcium phosphate-coated titanium in Dulbecco's phosphate-buffered saline solution containing $CaCl_2$ with and without fibronectin. Acta Biomater. 6, 2274–2281. http://dx.doi.org/10.1016/j.actbio.2009.11.033.

Chen, D., Jordan, E., Gell, M., Wei, M., 2008. Apatite formation on alkaline-treated dense TiO_2 coatings deposited using the solution precursor plasma spray process. Acta Biomater. 4, 553–559. http://dx.doi.org/10.1016/j.actbio.2007.11.008.

Chu, P.K., 2004. Recent developments and applications of plasma immersion ion implantation. J. Vac. Sci. Technol. B 22, 289–296. http://dx.doi.org/10.1116/1.1632920.

Chu, P.K., 2013. Progress in direct-current plasma immersion ion implantation and recent applications of plasma immersion ion implantation and deposition. Surf. Coat. Technol. 229, 2–11. http://dx.doi.org/10.1016/j.surfcoat.2012.03.073.

Chu, P.K., Qin, S., Chan, C., Cheung, N.W., Larson, L.A., 1996. Plasma immersion ion implantation—a fledgling technique for semiconductor processing. Mater. Sci. Eng. R Rep. 17, 207–280. http://dx.doi.org/10.1016/S0927-796X(96)00194-5.

Chu, P.K., Tian, X., Li, L., 2004. Surface engineering methods. In: Totten, G.E., Funatani, K., Xie, L. (Eds.), Handbook of Metallurgical Process Design. CRC Press.

Corni, I., Ryan, M.P., Boccaccini, A.R., 2008. Electrophoretic deposition: from traditional ceramics to nanotechnology. J. Eur. Ceram. Soc. 28, 1353–1367. http://dx.doi.org/10.1016/j.jeurceramsoc.2007.12.011.

Daves, W., Krauss, A., Behnel, N., Häublein, V., Bauer, A., Frey, L., 2011. Amorphous silicon carbide thin films (a-SiC:H) deposited by plasma-enhanced chemical vapor deposition as protective coatings for harsh environment applications. Thin Solid Films 519, 5892–5898. http://dx.doi.org/10.1016/j.tsf.2011.02.089.

Ducheyne, P., Van Raemdonck, W., Heughebaert, J.C., Heughebaert, M., 1986. Structural analysis of hydroxyapatite coatings on titanium. Biomaterials 7, 97–103. http://dx.doi.org/10.1016/0142-9612(86)90063-3.

Fauchais, P., 2004. Understanding plasma spraying. J. Phys. D Appl. Phys. 37, R86. http://dx.doi.org/10.1088/0022-3727/37/9/R02.

Favia, P., 2012. Plasma deposited coatings for biomedical materials and devices: fluorocarbon and PEO-like coatings. Surf. Coat. Technol. 211, 50–56. http://dx.doi.org/10.1016/j.surfcoat.2012.01.032.

Ferrari, B., Sánchez-Herencia, A.J., Moreno, R., 1998. Aqueous electrophoretic deposition of Al_2O_3/ZrO_2 layered ceramics. Mater. Lett. 35, 370–374. http://dx.doi.org/10.1016/S0167-577X(97)00280-2.

Finke, B., Luethen, F., Schroeder, K., Mueller, P.D., Bergemann, C., Frant, M., Ohl, A., Nebe, B.J., 2007. The effect of positively charged plasma polymerization on initial osteoblastic focal adhesion on titanium surfaces. Biomaterials 28, 4521–4534. http://dx.doi.org/10.1016/j.biomaterials.2007.06.028.

Förch, R., Chifen, A.N., Bousquet, A., Khor, H.L., Jungblut, M., Chu, L.Q., Zhang, Z., Osey-Mensah, I., Sinner, E.K., Knoll, W., 2007. Recent and expected roles of plasma-polymerized films for biomedical applications. Chem. Vap. Depos. 13, 280–294.

Förch, R., Zhang, Z., Knoll, W., 2005. Soft plasma treated surfaces: tailoring of structure and properties for biomaterial applications. Plasma Processes Polym. 2, 351–372. http://dx.doi.org/10.1002/ppap.200400083.

Friedrich, J., 2011. Mechanisms of plasma polymerization – reviewed from a chemical point of view. Plasma Processes Polym. 8, 783–802. http://dx.doi.org/10.1002/ppap.201100038.

George, S.M., 2010. Atomic layer deposition: an overview. Chem. Rev. 110, 111–131. http://dx.doi.org/10.1021/cr900056b.

Hacking, S.A., Zuraw, M., Harvey, E.J., Tanzer, M., Krygier, J.J., Bobyn, J.D., 2007. A physical vapor deposition method for controlled evaluation of biological response to biomaterial chemistry and topography. J. Biomed. Mater. Res. A 82A, 179–187. http://dx.doi.org/10.1002/jbm.a.31131.

Han, C.-M., Lee, E.-J., Kim, H.-E., Koh, Y.-H., Kim, K.N., Ha, Y., Kuh, S.-U., 2010. The electron beam deposition of titanium on polyetheretherketone (PEEK) and the resulting enhanced biological properties. Biomaterials 31, 3465–3470. http://dx.doi.org/10.1016/j.biomaterials.2009.12.030.

Härkönen, E., Kolev, I., Diaz, B., Swiatowska, J., Maurice, V., Seyeux, A., Marcus, P., Fenker, M., Toth, L., Radnoczi, G., Vehkamäki, M., Ritala, M., 2014. Sealing of hard CrN and DLC coatings with atomic layer deposition. ACS Appl. Mater. Interfaces 6, 1893–1901. http://dx.doi.org/10.1021/am404906x.

Huang, N., Yang, P., Leng, Y.X., Wang, J., Sun, H., Chen, J.Y., Wan, G.J., 2004. Surface modification of biomaterials by plasma immersion ion implantation. Surf. Coat. Technol. 186, 218–226. http://dx.doi.org/10.1016/j.surfcoat.2004.04.041.

Hung, L.S., Zheng, L.R., Blanton, T.N., 1992. Epitaxial growth of MgO on (100)GaAs using ultrahigh vacuum electron-beam evaporation. Appl. Phys. Lett. 60, 3129–3131. http://dx.doi.org/10.1063/1.106745.

Hyde, G.K., Mccullen, S.D., Jeon, S., Stewart, S.M., Jeon, H., Loboa, E.G., Parsons, G.N., 2009. Atomic layer deposition and biocompatibility of titanium nitride nano-coatings on cellulose fiber substrates. Biomed. Mater. 4, 25001. http://dx.doi.org/10.1088/1748-6041/4/2/025001.

Im, H., Bantz, K.C., Lindquist, N.C., Haynes, C.L., Oh, S.-H., 2010. Vertically oriented sub-10-nm plasmonic nanogap arrays. Nano Lett. 10, 2231–2236. http://dx.doi.org/10.1021/nl1012085.

Im, H., Wittenberg, N.J., Lindquist, N.C., Oh, S.-H., 2012. Atomic layer deposition (ALD): a versatile technique for plasmonics and nanobiotechnology. J. Mater. Res. 27, 663–671. http://dx.doi.org/10.1557/jmr.2011.434.

Jeon, H.-J., Yi, S.-C., Oh, S.-G., 2003. Preparation and antibacterial effects of Ag-SiO_2 thin films by sol-gel method. Biomaterials 24, 4921–4928. http://dx.doi.org/10.1016/S0142-9612(03)00415-0.

Jiang, T., Zhang, Z., Zhou, Y., Liu, Y., Wang, Z., Tong, H., Shen, X., Wang, Y., 2010. Surface functionalization of titanium with chitosan/gelatin via electrophoretic deposition: characterization and cell behavior. Biomacromolecules 11, 1254–1260. http://dx.doi.org/10.1021/bm100050d.

Jones, A.C., Hitchman, M.L., 2009. Chemical Vapour Deposition: Precursors, Processes and Applications. Royal Society of Chemistry.

Kern, W., 1991. Thin Film Processes II. Academic Press.

Knez, M., Nielsch, K., Niinistö, L., 2007. Synthesis and surface engineering of complex nanostructures by atomic layer deposition. Adv. Mater. 19, 3425−3438. http://dx.doi.org/10.1002/adma.200700079.

Kumar, V., Pulpytel, J., Rauscher, H., Mannelli, I., Rossi, F., Arefi-Khonsari, F., 2010. Fluorocarbon coatings via plasma enhanced chemical vapor deposition of 1H,1H,2H,2H-perfluorodecyl acrylate - 2, morphology, wettability and antifouling characterization. Plasma Processes Polym. 7, 926−938. http://dx.doi.org/10.1002/ppap.201000038.

Lee, S.-M., Pippel, E., Knez, M., 2011. Metal infiltration into biomaterials by ALD and CVD: a comparative study. ChemPhysChem 12, 791−798. http://dx.doi.org/10.1002/cphc.201000923.

Leeuwenburgh, S., Wolke, J., Schoonman, J., Jansen, J., 2003. Electrostatic spray deposition (ESD) of calcium phosphate coatings. J. Biomed. Mater. Res. A 66A, 330−334. http://dx.doi.org/10.1002/jbm.a.10590.

Leeuwenburgh, S., Wolke, J., Schoonman, J., Jansen, J., 2005. Influence of deposition parameters on chemical properties of calcium phosphate coatings prepared by using electrostatic spray deposition. J. Biomed. Mater. Res. A 74, 275−284. http://dx.doi.org/10.1002/jbm.a.30420.

Leskelä, M., Ritala, M., 2003. Atomic layer deposition chemistry: recent developments and future challenges. Angew. Chem. 42, 5548−5554. http://dx.doi.org/10.1002/anie.200301652.

Lin, Z., Lee, I.-S., Choi, Y.-J., Noh, I.-S., Chung, S.-M., 2009. Characterizations of the TiO_{2-x} films synthesized by e-beam evaporation for endovascular applications. Biomed. Mater. 4, 15013. http://dx.doi.org/10.1088/1748-6041/4/1/015013.

Liu, Q., Cheng, X.N., Fei, H.X., 2011. Effects of micro-magnetic field at the surface of 316L and NiTi alloy on blood compatibility. Med. Biol. Eng. Comput. 49, 359−364. http://dx.doi.org/10.1007/s11517-010-0685-z.

Liu, X., Chu, P.K., Ding, C., 2004. Surface modification of titanium, titanium alloys, and related materials for biomedical applications. Mater. Sci. Eng. R Rep. 47, 49−121. http://dx.doi.org/10.1016/j.mser.2004.11.001.

Liu, X., Chu, P.K., Ding, C., 2007. Formation of apatite on hydrogenated amorphous silicon (a-Si:H) film deposited by plasma-enhanced chemical vapor deposition. Mater. Chem. Phys. 101, 124−128. http://dx.doi.org/10.1016/j.matchemphys.2005.10.035.

Liu, X., Ding, C., Wang, Z., 2001. Apatite formed on the surface of plasma-sprayed wollastonite coating immersed in simulated body fluid. Biomaterials 22, 2007−2012. http://dx.doi.org/10.1016/S0142-9612(00)00386-0.

Liu, X., Fu, R.K.Y., Chu, P.K., 2008. Surface modification of biomaterials using plasma immersion ion implantation and deposition. In: Chu, P.K., Liu, X. (Eds.), Biomaterials Fabrication and Processing Handbook. CRC Press, Boca Raton.

Liu, X., Xu, Y., Chu, P.K., 2010. Preparation, characterization, and potential biomedical applications of nanostructured zirconia coatings and films. In: Kumar, C.S.S.R. (Ed.), Nanostructured Thin Films and Surfaces. Wiley-VCH, Weinheim, pp. 251−275.

Liu, X., Zhao, X., Fu, R.K.Y., Ho, J.P.Y., Ding, C., Chu, P.K., 2005. Plasma-treated nanostructured TiO_2 surface supporting biomimetic growth of apatite. Biomaterials 26, 6143−6150. http://dx.doi.org/10.1016/j.biomaterials.2005.04.035.

Livage, J., Ganguli, D., 2001. Sol−gel electrochromic coatings and devices: a review. Sol. Energy Mater. Sol. Cells 68, 365−381. http://dx.doi.org/10.1016/S0927-0248(00)00369-X.

Lu, T., Qiao, Y., Liu, X., 2012. Surface modification of biomaterials using plasma immersion ion implantation and deposition. Interface Focus 2, 325−336. http://dx.doi.org/10.1098/rsfs.2012.0003.

Ma, R., Epand, R.F., Zhitomirsky, I., 2010. Electrodeposition of hyaluronic acid and hyaluronic acid−bovine serum albumin films from aqueous solutions. Colloids Surf. B Biointerfaces 77, 279−285. http://dx.doi.org/10.1016/j.colsurfb.2010.02.002.

Maitz, M.F., Poon, R.W.Y., Liu, X.Y., Pham, M.T., Chu, P.K., 2005. Bioactivity of titanium following sodium plasma immersion ion implantation and deposition. Biomaterials 26, 5465−5473. http://dx.doi.org/10.1016/j.biomaterials.2005.02.006.

Martin, P.M., 2009. Handbook of Deposition Technologies for Films and Coatings: Science, Applications and Technology. William Andrew.

Martinu, L., Poitras, D., 2000. Plasma deposition of optical films and coatings: a review. J. Vac. Sci. Technol A Vac. Surf. Films 18, 2619−2645. http://dx.doi.org/10.1116/1.1314395.

Martinu, L., Zabeida, O., Klemberg-Sapieha, J., 2009. Plasma-enhanced chemical vapor deposition of functional coatings. In: Martin, P.M. (Ed.), Handbook of Deposition Technologies for Films and Coatings, third ed. Elsevier.

Mattox, D.M., 2010. Handbook of Physical Vapor Deposition (PVD) Processing. Noyes Publications, New Jersey.

Ochsenbein, A., Chai, F., Winter, S., Traisnel, M., Breme, J., Hildebrand, H., 2008. Osteoblast responses to different oxide coatings produced by the sol-gel process on titanium substrates. Acta Biomater. 4, 1506−1517. http://dx.doi.org/10.1016/j.actbio.2008.03.012.

Pang, X., Casagrande, T., Zhitomirsky, I., 2009. Electrophoretic deposition of hydroxyapatite-$CaSiO_3$-chitosan composite coatings. J. Colloid Interface Sci. 330, 323−329. http://dx.doi.org/10.1016/j.jcis.2008.10.070.

Pawlowski, L., 2008. Thermal spraying techniques. In: Pawlowski, L. (Ed.), The Science and Engineering of Thermal Spray Coatings, second ed. John Wiley & Sons, Ltd., Chichester, pp. 67−113.

Pelletier, J., Anders, A., 2005. Plasma-based ion implantation and deposition: a review of physics, technology, and applications. IEEE Trans. Plasma Sci. 33, 1944−1959. http://dx.doi.org/10.1109/TPS.2005.860079.

Persheyev, S., Fan, Y., Irving, A., Rose, M.J., 2011. BV-2 microglial cells sense micro-nanotextured silicon surface topology. J. Biomed. Mater. Res. A 99A, 135−140. http://dx.doi.org/10.1002/jbm.a.33159.

Putkonen, M., Sajavaara, T., Rahkila, P., Xu, L., Cheng, S., Niinistö, L., Whitlow, H.J., 2009. Atomic layer deposition and characterization of biocompatible hydroxyapatite thin films. Thin Solid Films 517, 5819−5824. http://dx.doi.org/10.1016/j.tsf.2009.03.013.

Radin, S., Ducheyne, P., 2007. Controlled release of vancomycin from thin sol−gel films on titanium alloy fracture plate material. Biomaterials 28, 1721−1729. http://dx.doi.org/10.1016/j.biomaterials.2006.11.035.

Rautray, T.R., Narayanan, R., Kim, K.-H., 2011. Ion implantation of titanium based biomaterials. Prog. Mater. Sci. 56, 1137−1177. http://dx.doi.org/10.1016/j.pmatsci.2011.03.002.

Ritala, M., Niinisto, J., 2009. Atomic layer deposition. In: Jones, A.C., Hitchman, M.L. (Eds.), Chemical Vapour Deposition: Precursors, Processes and Applications. Royal Society of Chemistry, pp. 158−206.

Seshan, K., 2002. Handbook of Thin Film Deposition Processes and Techniques, second ed. Noyes Publications, New York.

Shah, S.I., Jaffari, G.H., Yassitepe, E., Ali, B., 2010. Evaporation: processes, bulk microstructures, and mechanical properties. In: Martin, P.M. (Ed.), Handbook of Deposition Technologies for Films and Coatings, third ed. William Andrew Publishing, Boston, pp. 135−252.

Siow, K.S., Britcher, L., Kumar, S., Griesser, H.J., 2006. Plasma methods for the generation of chemically reactive surfaces for biomolecule immobilization and cell colonization − a review. Plasma Processes Polym. 3, 329−418. http://dx.doi.org/10.1002/ppap.200600021.

Skoog, S.A., Bayati, M.R., Petrochenko, P.E., Stafslien, S., Daniels, J., Cilz, N., Comstock, D.J., Elam, J.W., Narayan, R.J., 2012. Antibacterial activity of zinc oxide-coated nanoporous alumina. Mater. Sci. Eng. B 177, 992–998. http://dx.doi.org/10.1016/j.mseb.2012.04.024.

Skoog, S.A., Elam, J.W., Narayan, R.J., 2013. Atomic layer deposition: medical and biological applications. Int. Mater. Rev. 58, 113–129. http://dx.doi.org/10.1179/1743280412y.0000000009.

Slaney, A.M., Wright, V.A., Meloncelli, P.J, Harris, K.D., West, L.J., Lowary, T.L., Buriak, J.M., 2011. Biocompatible carbohydrate-functionalized stainless steel surfaces: a new method for passivating biomedical implants. ACS Appl. Mater. Interfaces 3, 1601–1612. http://dx.doi.org/10.1021/am200158y.

Stamm, M., 2008. Polymer Surfaces and Interfaces – Characterization, Modification and Applications. Springer.

Sun, L., Berndt, C.C., Gross, K.A., Kucuk, A., 2001. Material fundamentals and clinical performance of plasma-sprayed hydroxyapatite coatings: a review. J. Biomed. Mater. Res. 58, 570–592. http://dx.doi.org/10.1002/jbm.1056.

Suntola, T., Antson, J., 1977. Method for Producing Compound Thin Films. US Patent 4058430.

Suryanarayana, C., 1999. Non-equilibrium Processing of Materials. Elsevier.

Tedrow, P.K., Reif, R., 1994. Plasma-enhanced chemical vapor deposition. In: Cotell, C.M., Sprague, J.A., Smidt Jr., F.A. (Eds.), ASM Handbook. ASM International, pp. 1524–1536.

Vencl, A., Mrdak, M., Cvijović, I., 2006. Microstructures and tribological properties of ferrous coatings deposited by APS (Atmospheric Plasma Spraying) on Al-alloy substrate. FME Trans. 34, 151–157.

Wan, G.J., Yang, P., Shi, X.J., Wong, M., Zhou, H.F., Huang, N., Chu, P.K., 2005. In vitro investigation of hemocompatibility of hydrophilic SiN_x:H films fabricated by plasma-enhanced chemical vapor deposition. Surf. Coat. Technol. 200, 1945–1949. http://dx.doi.org/10.1016/j.surfcoat.2005.08.068.

Wang, C., Ma, J., Cheng, W., Zhang, R., 2002. Thick hydroxyapatite coatings by electrophoretic deposition. Mater. Lett. 57, 99–105. http://dx.doi.org/10.1016/S0167-577X(02)00706-1.

Wang, H., Ji, J., Zhang, W., Zhang, Y., Jiang, J., Wu, Z., Pu, S., Chu, P.K., 2009. Biocompatibility and bioactivity of plasma-treated biodegradable poly(butylene succinate). Acta Biomater. 5, 279–287. http://dx.doi.org/10.1016/j.actbio.2008.07.017.

Wang, H., Kwok, D.T.K., Wang, W., Wu, Z., Tong, L., Zhang, Y., Chu, P.K., 2010. Osteoblast behavior on polytetrafluoroethylene modified by long pulse, high frequency oxygen plasma immersion ion implantation. Biomaterials 31, 413–419. http://dx.doi.org/10.1016/j.biomaterials.2009.09.066.

Wang, H., Kwok, D.T.K., Xu, M., Shi, H., Wu, Z., Zhang, W., Chu, P.K., 2012. Tailoring of mesenchymal stem cells behavior on plasma-modified polytetrafluoroethylene. Adv. Mater. 24, 3315–3324. http://dx.doi.org/10.1002/adma.201104967.

Wang, Y., Deen, I., Zhitomirsky, I., 2011. Electrophoretic deposition of polyacrylic acid and composite films containing nanotubes and oxide particles. J. Colloid Interface Sci. 362, 367–374. http://dx.doi.org/10.1016/j.jcis.2011.07.007.

Wasa, K., 2012a. Sputtering phenomena. In: Wasa, K., Kanno, I., Kotera, H. (Eds.), Handbook of Sputtering Technology, second ed. William Andrew Publishing, Oxford, pp. 41–75.

Wasa, K., 2012b. Sputtering systems. In: Wasa, K., Kanno, I., Kotera, H. (Eds.), Handbook of Sputtering Technology, second ed. William Andrew Publishing, Oxford, pp. 77–139.

Wei, J., Ong, P.L., Tay, F.E.H., Iliescu, C., 2008. A new fabrication method of low stress PECVD SiN_x layers for biomedical applications. Thin Solid Films 516, 5181–5188. http://dx.doi.org/10.1016/j.tsf.2007.07.051.

Wu, G., Feng, K., Shanaghi, A., Zhao, Y., Xu, R., Yuan, G., Chu, P.K., 2012a. Effects of surface alloying on electrochemical corrosion behavior of oxygen-plasma-modified biomedical magnesium alloy. Surf. Coat. Technol. 206, 3186−3195. http://dx.doi.org/10.1016/j.surfcoat.2012.01.001.

Wu, G., Xu, R., Feng, K., Wu, S., Wu, Z., Sun, G., Zheng, G., Li, G., Chu, P.K., 2012b. Retardation of surface corrosion of biodegradable magnesium-based materials by aluminum ion implantation. Appl. Surf. Sci. 258, 7651−7657. http://dx.doi.org/10.1016/j.apsusc.2012.04.112.

Xie, Y., Liu, X., Huang, A., Ding, C., Chu, P.K., 2005. Improvement of surface bioactivity on titanium by water and hydrogen plasma immersion ion implantation. Biomaterials 26, 6129−6135. http://dx.doi.org/10.1016/j.biomaterials.2005.03.032.

Xu, R., Wu, G., Yang, X., Zhang, X., Wu, Z., Sun, G., Li, G., Chu, P.K., 2012. Corrosion behavior of chromium and oxygen plasma-modified magnesium in sulfate solution and simulated body fluid. Appl. Surf. Sci. 258, 8273−8278. http://dx.doi.org/10.1016/j.apsusc.2012.05.036.

Yang, Z., Xiong, K., Qi, P., Yang, Y., Tu, Q., Wang, J., Huang, N., 2014. Gallic acid tailoring surface functionalities of plasma-polymerized allylamine-coated 316L SS to selectively direct vascular endothelial and smooth muscle cell fate for enhanced endothelialization. ACS Appl. Mater. Interfaces 6, 2647−2656. http://dx.doi.org/10.1021/am405124z.

Yasuda, H., 1981. Glow discharge polymerization. J. Polym. Sci. Macromol. Rev. 16, 199−293. http://dx.doi.org/10.1002/pol.1981.230160104.

Yasuda, H., Yasuda, T., 2000. The competitive ablation and polymerization (CAP) principle and the plasma sensitivity of elements in plasma polymerization and treatment. J. Polym. Sci. A Polym. Chem. 38, 943−953. http://dx.doi.org/10.1002/(SICI)1099-0518(20000315)38:6<943::AID-POLA3>3.0.CO;2-3.

Yu, B., Leung, K.M., Guo, Q., Lau, W.M., Yang, J., 2011. Synthesis of Ag-TiO_2 composite nano thin film for antimicrobial application. Nanotechnology 22, 115603. http://dx.doi.org/10.1088/0957-4484/22/11/115603.

Zhang, Y., Wan, J., Ke, Y., 2010. A novel approach of preparing TiO_2 films at low temperature and its application in photocatalytic degradation of methyl orange. J. Hazard. Mater. 177, 750−754. http://dx.doi.org/10.1016/j.jhazmat.2009.12.095.

Zhao, J.H., Michalski, W.P., Williams, C., Li, L., Xu, H.-S., Lamb, P.R., Jones, S., Zhou, Y.M., Dai, X.J., 2011. Controlling cell growth on titanium by surface functionalization of heptylamine using a novel combined plasma polymerization mode. J. Biomed. Mater. Res. A 97, 127−134. http://dx.doi.org/10.1002/jbm.a.33035.

Zhao, Y., Jamesh, M.I., Li, W.K., Wu, G., Wang, C., Zheng, Y., Yeung, K.W.K., Chu, P.K., 2014. Enhanced antimicrobial properties, cytocompatibility, and corrosion resistance of plasma-modified biodegradable magnesium alloys. Acta Biomater. 10, 544−556. http://dx.doi.org/10.1016/j.actbio.2013.10.012.

Zhao, Y., Wong, S.M., Wong, H.M., Wu, S., Hu, T., Yeung, K.W.K., Chu, P.K., 2013. Effects of carbon and nitrogen plasma immersion ion implantation on in vitro and in vivo biocompatibility of titanium alloy. ACS Appl. Mater. Interfaces 5, 1510−1516. http://dx.doi.org/10.1021/am302961h.

Zhu, S.-Q., Zhang, T., Guo, X.-L., Wang, Q.-L., Liu, X., Zhang, X.-Y., 2012. Gold nanoparticle thin films fabricated by electrophoretic deposition method for highly sensitive SERS application. Nanoscale Res. Lett. 7, 613. http://dx.doi.org/10.1186/1556-276X-7-613.

Znaidi, L., 2010. Sol−gel-deposited ZnO thin films: a review. Mater. Sci. Eng. B 174, 18−30. http://dx.doi.org/10.1016/j.mseb.2010.07.001.

Thin film growth on biomaterial surfaces

2

A. Michelmore
University of South Australia, Mawson Lakes, SA, Australia

2.1 Introduction

Surface engineering has rapidly expanded in recent years as the demand for improved materials has increased. In 2004 it was estimated that the value of products which incorporated surface engineering being produced per annum was about $A50 trillion (Matthews et al., 2004). The desire for materials to exhibit favourable bulk properties (elasticity, optical transparency/opaqueness, toughness, etc.) as well as interact with external systems in a specific way has driven this expansion. In addition, the ever-decreasing size of many devices necessarily involves an increase in the surface area−volume ratio, which makes surface engineering even more important.

There are two generalized methods to engineer a surface for a desired outcome: chemically modifying the existing surface − for example, by exposing the surface to high-energy ions (Chan et al., 1996; Oehr, 2003), such as in the plasma treatment of tissue culture polystyrene (Amstein and Hartman, 1975; Doherty et al., 2013) − or depositing a thin film with the desired properties onto the existing surface. The first method has been used extensively (Variola et al., 2009) because it is relatively simple, but its application is limited by the initial properties of the surface. The second method offers increased flexibility because a wide range of thin film properties are possible which can be tuned using different chemistries, film thicknesses and processing conditions (Ratner et al., 1990). This latter method will be the focus of the following discussion.

Biomaterials offer an interesting and important challenge in relation to surface engineering (Langer and Tirrell, 2004; Pashuck and Stevens, 2012). Biomaterials were used early on as dental implants around AD 200 (Crubezy et al., 1998); criteria were that they had to be biocompatible (even if the term had yet to be coined) and relatively hard-wearing (perhaps over a few years). With an ageing population, biomaterial surfaces which are placed in contact with biological systems must be biocompatible (Busscher et al., 2012) and free from infectious agents (MacNeil, 2007) in the short term, but properties such as long-term corrosion (Dobbs, 1982) and toxicity (Skinner and Kay, 2011) must also be addressed. Often modern biomaterials are not designed to be “passive” prosthetic implants, but “active” implants which incorporate some biological therapy (eg, drug delivery) (Burns, 2009). This not only increases the number of functions that the surface must satisfy but also requires a deeper knowledge of how the biomaterial surface interacts with cells and molecules in biological systems. An important consideration in the 21st century is also the increase in regulatory

Thin Film Coatings for Biomaterials and Biomedical Applications. http://dx.doi.org/10.1016/B978-1-78242-453-6.00002-X

hurdles before a biomaterial can be introduced commercially, which necessitates even greater understanding of surfaces, their properties and their interactions (Prestwich et al., 2012).

2.2 Some examples of applications

There are numerous examples of biomaterials which incorporate thin films currently in use or under development. Therefore, a comprehensive review would be prohibitive. Here, we will discuss a few examples aimed at giving the reader an appreciation of the breadth of possible applications.

2.2.1 Bone mineralization

Natural bone repair is limited to small defects, and thus in cases where large sections of bone need to be repaired or replaced, implants are required to assist the natural bone mineralization process. This may be performed using autograft or allograft bone tissue, but this is often painful and increases the chance of infections. An alternative approach is to use engineered bone tissue scaffolds (Laurencin et al., 2006). This has usually been achieved with titanium/titanium alloy implants; however, titanium has poor biocompatibility and forms a fibrous layer between the titanium and the native bone (Sommerdijk et al., 2007). It has been shown that coatings such as calcium carbonate or hydroxyapatite (Bigi et al., 2008) films may be used to improve osteoconductivity while also being degraded during osteoclast activity, thus improving bone healing.

2.2.2 Cell screening, delivery and stem cell maintenance

Biomaterials are currently being used for diagnostic technologies such as cell screening. For example, gradients of chemistry (Michelmore et al., 2012), nanotopography (Goreham et al., 2011) and elasticity (Hopp et al., 2013; Tse and Engler, 2011) have been used to determine the optimum surface conditions for various cell types. These surfaces allow high-throughput assaying of cell−substrate interactions because a range of test conditions are present on a single sample. In the early stages of development of thin films for biomaterial applications, emphasis was placed on determining the optimum surface chemistry. More recently, it has been found that elastic modulus (Hopp et al., 2013) and nanotopography (Goreham et al., 2013) can also have a profound effect on cells. Furthermore, two-dimensional (2D) gradients of both chemistry and nanotopography have been developed to determine the optimum surface properties in a single experiment (Yang et al., 2009). Biomaterials have also been used successfully as a vehicle to grow and deliver cells to wounds such as burns (Haddow et al., 2006).

In addition, it has been shown that polymeric thin films can be used to maintain the phenotype and pluripotency of stem cells (McMurray et al., 2011). Factors such as the elastic modulus, contact angle and nanoroughness were found to be important parameters, which can be controlled through the judicious choice of polymer structure (Mei et al., 2010).

2.2.3 Nonfouling and antibacterial surfaces

For many devices, fouling of surfaces with proteins, cells or bacteria is an important consideration. Fouling with proteins and cells is particularly relevant for devices incorporating micro- or nanochannels (Salim et al., 2007), but also for applications in which optical transparency is critical, such as intraocular lenses (Mateo and Ratner, 1989). The most widely chosen family of films for these applications is based on polyethylene glycol (Johnston et al., 2005), which shows remarkable ability to resist protein adsorption (Menzies et al., 2010). Endowing surfaces with antibacterial films is obviously important for biomaterials which come into contact with the body (Arciola et al., 2005). For this purpose, surfaces which release silver ions have been known to resist bacterial growth for thousands of years (Vasilev et al., 2010a,b); however, at high doses, silver may become toxic to mammalian cells as well. More recently, polymer substrates have been identified which possess antibacterial properties by resisting bacterial attachment rather than killing microorganisms (Hook et al., 2012).

2.2.4 Biosensors

Biosensors are devices which combine a biological component to detect an analyte and a physicochemical component to produce a signal which is measurable. An early example of biosensor was introduced in 1962 to monitor blood gas levels during surgery (Clark and Lyons, 1962). The most common biosensors today are home pregnancy tests and glucose detectors; however, there is a drive to produce new biosensors for a wide range of applications including food analysis, deoxyribonucleic acid testing and drug detection. Thin films offer the promise for these sensors to be increasingly small and with decreased detection limits (Zeng et al., 2014).

2.3 Materials and technologies

There are a wide range of substrates and films which can be produced as biomaterials. Metals such as titanium alloys are often used where high strength or toughness is required, such as hip implants. Their mechanical properties can be somewhat similar to bone, which makes them ideal candidates as "structural" bioimplants. However, as outlined by Skinner and Kay (2011), metal erosion can be a potentially dangerous problem. Ceramic films such as TiO_2, SiO_2 or hydroxyapatite $Ca_{10}(PO_4)_6(OH)_2$ are often added to the surface to reduce wear of the implant and improve biocompatibility.

Although synthetic polymers are a relatively recent invention (Andrady and Neal, 2009), polymers and polymeric materials are increasingly being used as bioimplants because they often exhibit good biocompatibility. Indeed, an early example of "accidental" biomaterial implantation was during World War II, when plane canopies were damaged and shards of polymers were lodged in aviators' eyes (Ratner, 2013). It was observed that even years later, shards remained in the eye without causing inflammation. The major advantage with polymeric thin films is that chemical functionality may be incorporated into the surface. It is well-known that certain functional groups will

increase cell adhesion depending on the cell type, but in addition, these functional groups may be used to immobilize biologically active molecules (Siow et al., 2006) such as heparin (Robinson et al., 2008). Functional groups which can be incorporated into these surfaces include acids, alcohol, amines, ethers and aromatic groups.

Between metals/ceramics and polymers are a class of hybrid materials. Films composed of these materials are often useful when weak adhesion between the substrate and film is observed because the organic and metal oxide components facilitate good adhesion to many substrate types. Consequently, these films are sometimes used as an intermediate layer to decrease the likelihood of the top layer delaminating. Examples of this type of thin film are plasma polymers formed from hexamethyldisiloxane−oxygen mixtures in which the ratio of the two components can be varied to produce a "glassy" or organic layer (Hegemann et al., 1999) and "bioactive glasses" (Floroian et al., 2012).

A wide range of techniques are also available to produce thin films. These include films fabricated from the liquid phase (eg, self-assembled monolayers) (Hwang et al., 2002) and the gas phase. Deposition from the gas phase offers a number of advantages because the process does not require (potentially hazardous) solvents or any finishing drying stages. Most gas phase deposition techniques also operate under high vacuum, which may assist in minimizing contamination of the substrate during sample preparation and processing (Forrest, 1997). Here, we will discuss a few of the major techniques currently in use for depositing thin films from the gas phase and point out their major advantages and weaknesses.

2.3.1 Atomic layer deposition

Atomic layer deposition (ALD) is an elegant technique which involves sequential deposition of atomic layers of two precursors (George, 2010). One major advantage of this technique is that the reactions are self-limiting, meaning that at each step the reaction proceeds until the surface is completely covered with the precursor and then stops because no reactive sites remain. This enables precise control of the surface chemistry. In addition, adhesion of the film to the substrate is strong because atoms are sequentially bonded to the substrate covalently. For example, $TiCl_4$ can be deposited on surfaces containing hydroxyl groups by reacting surface OH groups with a chloride ion releasing HCl, resulting in $TiCl_3$ being bound to the surface through the remaining oxygen (Fig. 2.1). This reaction may repeat until all of the surface hydroxyls are

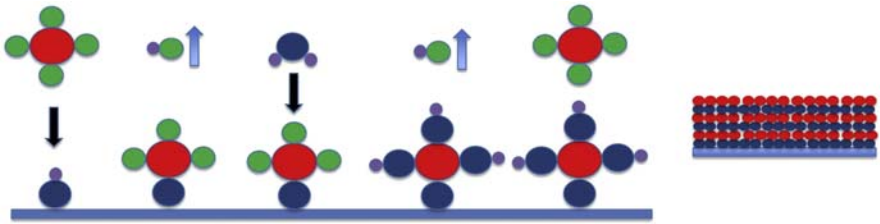

Figure 2.1 Schematic of ALD steps resulting in an atomic layer-by-layer sandwich.

consumed. Once this process is complete, water molecules can be added to the system which react with the O−$TiCl_3$, releasing HCl and leaving a regenerated hydroxyl-containing surface. In this manner, thin films may be built one atomic layer at a time. In theory, then, ALD should produce epitaxial, smooth films; however, this has not always been shown to be the case (Sammelselg et al., 1998). This technique is usually applied in the microelectronics industry, but it can be used to produce functionalized surfaces for use as biosensors (Purniawan et al., 2010) and may be applied to nanoporous materials (Detavernier et al., 2011). Disadvantages of this technique are that it is slow because the deposition must be performed layer by layer, and surface contamination results in surface defects in the growing film which cannot be repaired.

2.3.2 Plasma-based techniques

The vast majority of the universe is composed of plasma (Alfven, 1990), but on earth natural plasmas are limited to localized events such as lightning. Typically these plasmas exist at very high temperatures, greater than 10,000 K. However, man-made, nonthermal plasmas have become useful tools in surface engineering because they provide a method of delivering high-energy species to surfaces while maintaining the bulk gas, substrate and reactor close to ambient temperature. For nonthermal plasmas, electrical energy in the form of electrical fields provides kinetic energy to charged species within the gas phase (electrons and ions) whereas neutral species (which compose the vast majority of the mass) remain at or near ambient temperature. The electrical circuit may be direct current, but more often microwave or radio frequency generators are used. The charged energetic particles in the gas phase then provide the energy required to propagate film growth. This enables films to be grown from species which ordinarily do not have the chemical energy required to grow films because the energy to form the film is provided as kinetic energy. The physics of enclosed plasma systems are complicated; for a more comprehensive description, the reader is directed to Lieberman and Lichtenberg (1994). Several techniques are capable of depositing thin films using plasma.

2.3.2.1 Sputter deposition

Probably the simplest plasma-based technique is sputter deposition. A target surface (usually a metal) is placed in a chamber. The gas is often a noble gas such as argon, to reduce oxidation. A plasma is then ignited, resulting in ions with energies >10 eV impacting the target surface. The ions can then ablate atoms from the target surface, which are then transported through the gas phase to the substrate to be coated (Fig. 2.2). The film can then grow on the substrate almost atom by atom, depending on the parameters used. The rate of deposition can be controlled using a range of parameters including the distance between the target and the substrate, gas flow rate and applied plasma power (Ishii, 1989).

2.3.2.2 Pulsed laser deposition

Pulsed laser deposition uses energy from a laser source to excite the target surface (Chrisey et al., 2003). This energy results in electronic excitation, heating and physical

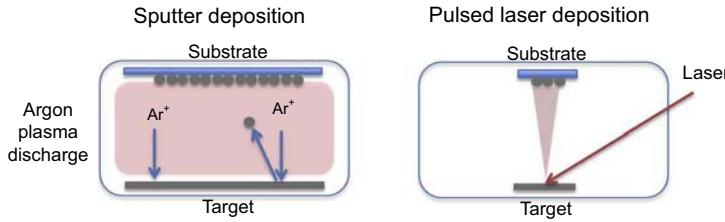

Figure 2.2 Schematics of sputter deposition and pulsed laser deposition.

ablation of the surface atoms/molecules. The atoms/molecules which are ablated from the surface then form a plasma plume which is directed to the substrate where deposition may occur. The physical and chemical processes which occur at both the target and substrate surface are complex and depend on the target chemistry, laser energy, laser intensity, distance from the target to substrate and the carrier gas in the chamber (often PLD is performed under vacuum but may deliberately contain oxygen if oxidized surfaces are desired). By controlling these parameters, the species arriving at the substrate may vary between individual atoms, small molecules and molten globular clusters. The topography of the resulting thin film may then vary between relatively smooth and micro-roughened surfaces exhibiting "island" formations (Ferguson et al., 2009).

2.3.2.3 *Plasma polymer deposition*

Deposition of polymer-like films directly from plasmas of organic vapour was first reported in 1960 (Goodman). Initially this technique was used for barrier coatings (Williams and Hayes, 1966), but around 1980 it was discovered that this method could produce films which are chemically functional. High-energy electrons (>3 eV) in the plasma phase collide with neutral gas molecules and either break bonds homolytically, resulting in gas phase radical formation, or cause ionization and the release of another electron. Although the mechanisms of polymer growth have been well characterized (Flory, 1953), the growth of plasma polymers is less well understood because many random processes occur in the plasma phase and the species which contribute to film growth may be neutral, radical, ionic or even metastable (Michelmore et al., 2013a). Indeed, the term "plasma polymer" is a misnomer because the monomer undergoes fragmentation and oligomerization in the plasma phase before depositing on the substrate, and then the growing film is subjected to etching by high-energy ions. Thus, the resulting film is a highly cross-linked organic layer, which may retain some functional groups from the monomer. Probably the most studied plasma polymer films are those derived from acrylic acid, in which a percentage of the functional carboxylic acid group can be retained on the plasma polymer surface. Retention of these acid groups can be controlled simply by adjusting either the power being supplied to the reactor or the flow rate of monomer. Other classes of functionalized plasma polymers which are routinely produced using this method include amines (Choukourov et al., 2005), alcohols (Rinsch et al., 1996), siloxanes (Hegemann et al., 1999) and halogenated surfaces (Coad et al., 2014).

2.4 Mechanisms of deposition

An important consideration in designing biomaterial thin films is how the film deposits and grows in the first place. This can affect the performance of the films because it determines the film surface chemistry, topography, mechanical properties, stability, solubility and so forth. The energy with which adsorbing particles (adparticles) arrive at the interface (both kinetic energy and chemical potential) and their interaction with other atoms determine many properties of the film. For example, polymeric films formed from ions with high energy can form highly cross-linked films which exhibit high elastic modulus and low solubility; similar films formed from lower-energy processes can be soft and soluble (Michelmore et al., 2013b). It is possible to produce films which appear identical chemically but exhibit different mechanical and stability performance.

With the drive for films to become thinner, interactions between the substrate and the adsorbing layer become more important. For example, for thick layers (>100 nm, say), adsorbing atoms or molecules interact with previously adsorbed molecules with the same or similar chemistry. Substrate–adparticle interactions thus may influence the adherence of the thin film to the substrate and control whether the film delaminates, but they are unlikely to affect the chemistry and function of the top surface of the film significantly. However, in the initial stages of adsorption, adparticles arrive at the surface and interact with the substrate directly. This can result in the chemistry at the substrate interface being different to that on the top layer of the thin film (Vasilev et al., 2010a,b). Because many modern applications require ultra-thin films (<10 nm), it is vital to understand the interactions between the substrate, the top surface of the growing film and adsorbing particles.

An important thermodynamic distinction can be made between homogeneous nucleation and film growth on a substrate. If we consider the nucleation of a homogeneous spherical particle, a change in free energy occurs as the particle grows owing to the change in the surface area and volume (Ohring, 1992). The total free energy of the particle, ΔG, can then be written as:

$$\Delta G = 4/3\ \pi\ r^3 \Delta G_{\mathrm{v}} + 4\ \pi\ r^2 \gamma \qquad [2.1]$$

where r is the radius of the growing particle, ΔG_{v} is the volume free energy and γ is the surface free energy. Taking the derivative of this equation yields the critical radius, r^*, below which the nucleus is unstable and shrinks.

$$r* = -2\gamma/\Delta G_{\mathrm{v}} \qquad [2.2]$$

For film growth on a planar surface, however, adparticles adhere to the surface and then may aggregate with other adparticles forming islands, or remain separate, forming a layer-by-layer film. These processes are governed by the homogeneous interaction forces between the adparticles and the heterogeneous interaction forces between the adparticles and the substrate. We can consider an aggregate of adparticles on a surface

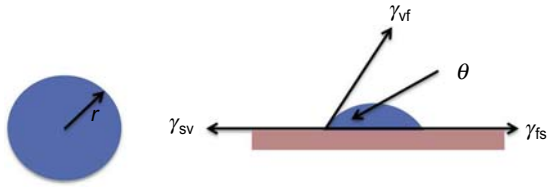

Figure 2.3 Free energy forces on a growing homogeneous particle (left) and a thin film growing on a planar substrate (right).

as a spherical cap, as shown in Fig. 2.3, and the forces acting at the three-phase interface are the interfacial tensions, γ_{fs}, γ_{sv} and γ_{fv}, where f, s and v represent the film, substrate and vapour phase, respectively. A force balance at the three-phase line yields Young's equation:

$$\gamma_{sv} = \gamma_{fs} + \gamma_{fv} \cos\theta \qquad [2.3]$$

There are then three general growth modes to describe how thin films form based on the relative interaction strengths between the adparticles and the substrate, as shown in Fig. 2.4 (Ohring, 1992).

Volmer–Weber: For the Volmer–Weber model, the interaction between adparticles is stronger than those between the adparticles and the substrate. Therefore, adparticles approaching the substrate are more likely to adhere to other adparticles already on the surface. This leads to the formation of atomic/molecular clusters which grow into 3D islands on the surface. For very thin layers, the surface can look patchy with discrete areas covered by the adsorbate, with areas of bare substrate. If these islands are allowed to grow, they can coalesce on the surface, resulting in a chemically homogeneous but roughened surface. After sufficient thickness has been achieved, the surface may become smooth.

Frank–van der Merwe: When the interaction strength between the adparticles and the substrate is strongest, adparticles will tend to deposit in layers rather than islands. This results in smoother layers which are generally strongly adhered to the substrate. This is the case for ALD described previously, in which the interaction between the adparticles is essentially zero, but the substrate–adparticle interactions are strong.

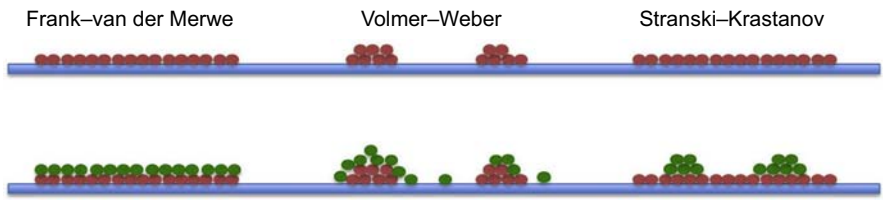

Figure 2.4 Models of deposition showing layer-by-layer deposition (Frank–van der Merwe), island growth (Volmer–Weber) and mixed (Stranski–Krastanov).

Stranski–Krastanov: Often, growth of thin films occurs in the regime between the Volmer–Weber and Frank–van der Merwe mechanisms, in which an initial layer is formed on the substrate, but then 3D island structures form.

The parameter which separates these modes is the thermodynamic interaction between the substrate and the adparticles, which physically manifests as the contact angle (if it can be measured) (Venables et al., 1984). For the Frank–van der Merwe growth mode, the interaction between the substrate and the adparticles is strong, and adhesion between the substrate and the forming layer is energetically favourable. Thus, the contact angle approaches zero. When the substrate–adparticle interaction is weaker than the adparticle–adparticle interaction, the contact angle will be greater than zero and there will be a tendency for the film to grow as islands.

These models are generalized, however, and do not take into account how the energy required to grow the film is delivered. For example, ALD uses chemical energy to deposit small molecules to specific sites on the substrate. In plasma deposition, some species arrive at the surface with very high kinetic energy (>10 eV), enough to cause bond cleavage, which enables deposition to occur; other species in the plasma (neutrals and radicals) arrive with very little kinetic energy and rely on chemical energy to deposit on the substrate. We might expect that the way these species deposit may be different, both chemically and topographically (Hegemann et al., 2012). In addition, the mechanism of deposition can greatly affect the kinetics. For example, gas or plasma phase deposition, which uses chemical energy in the form of double bonds, can be extremely fast; deposition of high-energy species is generally slower because the sticking probability is lower, and these species may also etch the surface physically. In many cases, detailed knowledge regarding the growth mechanisms is not currently understood; this information would greatly assist in tailoring thin films in the future.

2.5 Monitoring thin film growth

A wide range of parameters may be required to be controlled when considering thin films, including film thickness, topography, density, mechanical properties and chemical functionality. There is similarly a range of techniques available to measure these parameters. In situ methods are preferred because they allow growth of the film to be monitored in real time; however, this is not always possible, and so ex situ methods are often employed. Here, we will briefly describe some of the major techniques in use and discuss their advantages and shortcomings.

2.5.1 Ex situ techniques

2.5.1.1 Atomic force microscopy

Atomic force microscopy (AFM) is a high-resolution 3D imaging technique capable of measuring topographical features to less than 1 nm (Binning et al., 1986). A cantilever with a sharp tip is brought into contact with the surface, in which the force between the tip and the surface results in deflection of the cantilever. The cantilever is rastered over

the surface, typically over areas of 100 × 100 μm for microscopic features, but it can be less than 1 × 1 μm for nanoscale or even atomic scale features. Deflections of the cantilever as it scans over features on the surface are measured by reflecting a laser off the back of the cantilever onto a four-quadrant photodiode. Usually, to avoid the tip hitting large features and being damaged, the cantilever is mounted on a piezoelectric tube and a feedback mechanism is used to maintain constant force between the tip and the surface. Resolution of the technique is limited by the sharpness of the tip, which is typically less than 10 nm radius. For higher resolution, tips featuring carbon nanotubes can be used.

AFM can be used to follow the deposition of thin films over time. Simple thickness measurements can be performed by either scoring the film with a scalpel after deposition or masking part of the substrate before deposition of the film, and measuring the height of the step created. In Fig. 2.5, plasma polymer films grown from acrylic acid monomer are shown to grow initially as discrete islands, which then coalesce and eventually form a flat, pinhole-free film after approximately 240 s. This result is contrary to the often-stated view of plasma deposition that films always grow as a conformal layer.

Other measurements to assess film quality are also possible using AFM. The mechanical properties of films can be quantified by applying a force to the surface through the tip and measuring the depth of the indent created on the surface. Experimental data of indentation depth (δ) versus force (F) can be applied to the Hertz equation (Eq. [2.4]) using the fitting parameter α, which is related to Young's modulus (E), as shown in Eq. [2.5] (Choukourov et al., 2012).

$$\delta = \alpha F^{2/3} \quad [2.4]$$

$$E = \frac{3\left(1-\mu^2\right)}{4\alpha^{3/2}R^{1/2}} \quad [2.5]$$

With developments in instrumentation, AFM has become a relatively inexpensive and simple tool for assessing thin films. Its major disadvantage is that it cannot be performed in situ, so measurement is performed after processing.

Figure 2.5 Atomic force microscopy images (2 × 2 μm) of acrylic acid plasma polymers after 60 s (left), 90 s (middle) and 240 s (right), showing initial island formation followed by island intergrowth, eventually resulting in a smooth film. The height scale is the same for each image, with a maximum peak height of 10.9 nm.

2.5.1.2 Chemical characterization

Surface chemical analytical techniques may also be interesting when monitoring film growth, particularly for films below about 10 nm. There are many techniques available for this purpose, each with their own attributes and disadvantages. For films in which retention of chemical functionality is important, techniques which probe the top surface layers are particularly relevant.

2.5.1.3 Infrared spectroscopy

For thick films, infrared (IR) spectroscopy may be used to probe film chemistry (Kazarian and Chan, 2013). The sample is exposed to IR radiation, typically between 1000 and 4000 cm^{-1}, and molecules absorb energy at resonant frequencies that are characteristic of their chemical structure. The depth of analysis is >1 μm, meaning that the bulk properties of the film may be determined rather than just the surface chemistry. The advantage of IR spectroscopy is that differences between functional groups which are chemically similar may be obtained because the absorption peaks can generally be distinguished easily. The obvious disadvantage is the depth resolution.

2.5.1.4 X-ray photoelectron spectroscopy

Information regarding the chemistry of the film with greater surface resolution can be obtained using X-ray photoelectron spectroscopy (XPS) (Beamson and Briggs, 1992). Here, the surface is irradiated with soft X-rays which interact with atoms in the film and eject photoelectrons. The kinetic energy of these photoelectrons is then measured using a hemispherical analyser, and their binding energy is calculated using:

$$E_B = h\nu - E_K - \phi \qquad [2.6]$$

where E_B is the binding energy, E_K is the measured kinetic energy of the photoelectron, $h\nu$ is the X-ray energy and ϕ is the work function (usually around 4 eV).

Each binding energy peak can be attributed to a core level or valence level particular to each element. X-ray photoelectron spectroscopy can then provide an elemental analysis of the surface. In addition, small shifts in the core-level photoelectron peaks may be used to determine the bonding of the atoms in the sample. These shifts result from changes in the electronegativity of the bonded atom(s). The disadvantage of XPS is that functional groups which have similar electronegativity (for example, C−O and C−N) give rise to overlapping peaks, which makes deconvolution of the spectra, and therefore assessment of the chemical environment, difficult.

Whereas the X-rays may penetrate many microns into the sample, the photoelectrons which are generated must escape the sample to be measured. Thus, XPS generally has a sampling depth of around 5−10 nm because the signal from photoelectrons generated deeper in the surface is attenuated due to scattering. Even greater surface resolution may be obtained by angle-resolved XPS, in which the sample is placed at an angle to the entrance of the hemispherical analyser. This can be important because

it has been shown that the chemical composition of films at the top surface can be different to that at the substrate (Chen et al., 2011). This can affect the performance of the film, because films which are too thin may not perform as desired; for example, it has been shown that for nonfouling polyethylene glycol coatings, below about 4 nm the functionality of the surface is impaired (Chu et al., 2006).

2.5.1.5 Secondary ion mass spectrometry

Secondary ion mass spectrometry (SIMS) involves bombarding the sample film with heavy high-energy ions (Briggs, 1998). The primary ions may be noble gases (typically Ar or Xe) or heavy metal ions such as gold or gallium, with ion energies usually around 10−40 keV. For samples which are particularly sensitive to damage, such as polymeric films, C60 ion sources may be used (Fletcher et al., 2006). These high-energy ions then impact the sample surface and eject secondary ions, which may be positively or negatively charged. To keep the secondary ions relatively intact, the primary ion dose is kept low ($<10^{12}$ ions cm^{-2}). The secondary ions are then sorted and counted based on their mass-to-charge ratio (m/z) using either a quadrupole mass spectrometer or a time-of-flight mass spectrometer.

SIMS gives information about atoms which are present on the surface, and particularly for a polymeric surface, it can provide an indication of bonding and potentially whether the film structure is linear or highly cross-linked. The sampling depth for SIMS is also extremely low ($\sim$1 nm), which makes it highly surface sensitive. Depth profiling can be achieved by controlled etching the surface (Magee et al., 1978). The weaknesses of SIMS are that the method is expensive and destructive to the surface, and analysis can be complex because the measured signal represents fragments of the film and the mass of these fragments often changes with the energy of the sputtering ions.

2.5.2 In situ techniques

Although ex situ assessment of thin films is useful, monitoring the growth of thin films as they form can be critical both from a process control standpoint and to understand the fundamental mechanisms involved. Unfortunately, this is not always trivial because often it is not possible to incorporate surface analysis equipment into the apparatus used for deposition of thin films. Other techniques may also interfere with the deposition process and are therefore inappropriate. For example, imaging of thin films in real time at the atomic scale or nanoscale using AFM would affect the film being formed.

2.5.2.1 Direct mass deposition and quartz crystal microbalance

A critical measure of thin film deposition industrially is the deposition rate. It is possible to measure the rate of deposition simply by weighing a very thin substrate over time using a mass balance. This becomes difficult for very thin films only a few atoms thick. This also gives the mass deposited, rather than the film thickness;

to calculate the film thickness, a density value must be assumed, which is not always reliable. Also, direct measurement by traditional mass balance may not always be possible in situ.

An alternative method is quartz crystal microbalance (QCM), which may be used to measure the deposition rate during film deposition (King, 1964). The collecting surface consists of a quartz crystal typically coated with gold or silver electrodes. The crystal is then biased with alternating current and driven at its resonance frequency. The adsorption (or removal) of mass to the surface is then measured as a shift in the resonance frequency. The mass resolution of a QCM is usually below 10 $\mu g/m^2$ per second, which makes it suitable for very thin films. It should be noted that QCM also measures deposited mass, not film thickness directly. Limitations include sensitivity to temperature changes and the fact that the electrode is gold or silver, which may not be a suitable proxy for the test substrate.

2.5.2.2 Ellipsometry and surface plasmon resonance

Developed by Alexandre Rothen in 1945, ellipsometry measures the change in reflected polarized light to calculate the thickness and optical properties of films on surfaces. A polarized light source is passed through the thin film and then reflected off the substrate. When the light is reflected, the elliptical polarization of the light changes, and this is measured by a detector. The ratio (r) of the plane (p) and perpendicular (s) polarized light can then be used to calculate the thickness of the thin film:

$$r = r_p/r_s \qquad [2.7]$$

It is claimed to be able to measure thicknesses with an accuracy of about 0.3 A, approximately the thickness of an atomic layer. Because the method relies on polarized light, ellipsometry is a nondestructive technique, which makes it suitable for in situ measurements in some cases. One disadvantage is that the substrate must be reflective, so gold or silicon wafer is often used. However, a major disadvantage with the technique is interpretinging the data, which is not trivial; models of the air−thin film−substrate must be used. The dielectric and optical properties of the thin film must be known accurately to calculate the thickness of the film, and even then the modelling usually assumes a homogeneous layer which may not always be justified.

Surface plasmon resonance is a related technique which measures the change in intensity of the reflected light with the angle of incidence. When the light reflects off the surface of a metal, a surface plasmon wave is generated. The intensity of the surface plasmon wave depends on the refractive indexes of the metal and thin film and the angle of incidence of the light. The intensity of the reflected light is then the intensity of the incident light minus the intensity of the surface plasmon wave. When the reflected intensity versus the incident angle is plotted, a minimum in intensity is observed corresponding to the optimum angle for surface plasmon resonance. The presence of a thin film on the substrate changes the angle at which this occurs, and the shift in angle can be related to the thickness of the film. Again, though, accurate optical data and modelling are required.

Both ellipsometry and surface plasmon resonance can be performed ex situ, but they may also be incorporated into deposition experiments to measure film thickness in real time in some cases.

2.6 Challenges and future trends

As outlined previously, controlling the properties of thin films for biomedical applications is crucial to their performance in terms of both short-term function and long-term safety. Parameters such as chemical functionality, solubility, topography and mechanical properties all have a significant role. Currently, optimizing the conditions for a thin film may involve a compromise between two mutually exclusive conditions. For example, if a plasma polymer film is required to be highly chemically functionalized and with low elastic modulus, it may be difficult to produce such a film without being highly soluble. For many bioapplications, there is a desire to fabricate thinner films with controlled nanostructures and/or increased density of functional groups. At the same time, there is a need to provide biomaterials at reduced cost with improved efficacy and ultimately improved outcomes. On top of all this is the ever-present requirement for reliability and safety particular to biomaterials and biomedical devices. Further fundamental understanding of how thin films grow at the molecular level will help in discovering new methods to control the deposition process.

There are areas in which other thin film applications may be able to lead the way. For example, the solar energy industry is working on surfaces which have very low reflectivity by controlling the topography of silicon wafers (Ravipati et al., 2013), and nanofabrication is used in many different applications (Zheng et al., 2010). Researchers can now fabricate batteries from foldable paper, reducing not only their cost but also their energy footprint (Cheng et al., 2013). Knowledge gained regarding substrate selection and fabrication methods in these areas may assist in designing improved biomaterials in the future.

In the context of biomaterials and biomedical devices, there is significant overlap among biology, chemistry and physics. The examples mentioned in this chapter demonstrate that while considerable collaboration has already occurred, further "blurring" of the lines between these fields of research will result in improved devices in the future.

2.7 Further reading

For a detailed thermodynamic description of thin film growth processes, Milton Ohring's *The Materials Science of Thin Films* is a great place to start. For information on gas and plasma phase processes, the reader is directed to Brian Chapman's *Glow Discharge Processes*, or for the more intrepid reader, Lieberman and Lichtenberg's *Principles of Plasma Discharges and Materials Processing*.

References

Alfven, H., 1990. Cosmology in the plasma universe: an introductory exposition. IEEE Trans. Plasma Sci. 18, 5.

Amstein, C.F., Hartman, P.A., 1975. Adaptation of plastic surfaces for tissue culture by glow discharge. J. Clin. Microbiol. 2, 46−54.

Andrady, A.L., Neal, M.A., 2009. Applications and societal benefits of plastics. Phil. Trans. R. Soc. B 364, 1977−1984.

Arciola, C.R., Alvi, F.I., An, Y.H., Campoccia, D., Montanaro, L., 2005. Implant infection and infection resistant materials: a mini review. Int. J. Artif. Organs 28, 1119.

Beamson, G., Briggs, D., 1992. High Resolution XPS of Organic Polymers: The Scienta ESCA300 Database. Wiley and Sons, Chichester.

Bigi, A., Fini, M., Bracci, B., Boanini, E., Torricelli, P., Giavaresi, G., Aldini, N.N., Facchini, A., Sbaiz, F., Giardino, R., 2008. The response of bone to nanocrystalline hydroxyapatite-coated Ti13Nb11Zr alloy in an animal model. Biomaterials 29, 1730−1736.

Binning, G., Quate, C.F., Gerber, C., 1986. Atomic force microscope. Phys. Rev. Lett. 56, 930.

Briggs, D., 1998. Surface Analysis of Polymers by XPS and Static SIMS. Cambridge University Press, Cambridge.

Burns, J.W., 2009. Biology takes centre stage. Nat. Mater. 8, 441−443.

Busscher, H.J., van der Mei, H.C., Subbiahdoss, G., Jutte, P.C., van den Dungen, J.J., Zaat, S.A., Schultz, M.J., Grainger, D.W., 2012. Biomaterial-associated infection: locating the finish line in the race for the surface. Sci. Transl. Med. 4, 153rv10.

Chan, C.-M., Ko, T.M., Hiraoka, H., 1996. Polymer surface modification by plasmas and photons. Surf. Sci. Rep. 24, 1−54.

Chen, R.T., Muir, B.W., Thomsen, L., Tadich, A., Cowie, B.C.C., Such, G.K., Postma, A., McLean, K.M., Caruso, F., 2011. New insight into the substrate-plasma polymer interface. J. Phys. Chem. B 115, 6495−6502.

Cheng, Q., Song, Z., Ma, T., Smith, B.B., Tang, R., Yu, H., Jiang, H., Chan, C.K., 2013. Folding paper-based lithium-ion batteries for higher areal energy densities. Nano Lett. 13, 4969−4974.

Choukourov, A., Biederman, H., Slavinska, D., Hanley, L., Grinevich, A., Boldyryeva, H., Mackova, A., 2005. Mechanistic studies of plasma polymerization of allylamine. J. Phys. Chem. B 109, 23086−23095.

Choukourov, A., Gordeev, I., Arzhakov, D., Artemenko, A., Kousal, J., Kylián, O., Slavínská, D., Biederman, H., 2012. Does cross-link density of PEO-like plasma polymers influence their resistance to adsorption of fibrinogen? Plasma Processes Polym. 9, 48.

Chrisey, D.B., Pique, A., McGill, R.A., Horwitz, J.S., Ringeisen, B.R., 2003. Laser deposition of polymer and biomaterial films. Chem. Soc. Rev. 103, 553−576.

Chu, L.-Q., Knoll, W., Forch, R., 2006. Pulsed plasma polymerized di(ethylene glycol) monovinyl ether coatings for nonfouling surfaces. Chem. Mater. 18, 4840−4844.

Clark, L.C., Lyons, C., 1962. Electrode systems for continuous monitoring in cardiovascular surgery. Ann. N. Y. Acad. Sci. 102, 29−45.

Coad, B.R., Styan, K.E., Meagher, L., 2014. One step ATRP initiator immobilization on surfaces leading to gradient-grafted polymer brushes. ACS Appl. Mater. Interfaces 6, 7782−7789.

Crubezy, E., Murail, P., Girard, L., Bernadou, J.-P., 1998. False teeth of the Roman world. Nature 391, 29.

Detavernier, C., Dendooven, J., Sree, S.P., Ludwig, K.F., Martens, J.A., 2011. Tailoring nanoporous materials by atomic layer deposition. Chem. Soc. Rev. 40, 5242–5253.

Dobbs, H.S., 1982. Fracture of titanium orthopaedic implants. J. Mater. Sci. 17, 2398–2404.

Doherty, K.G., Oh, J.-S., Unsworth, P., Bowfield, A., Sheridan, C.M., Weightman, P., Bradley, J.W., Williams, R.L., 2013. Polystyrene surface modification for localized cell culture using a capillary dielectric barrier discharge atmospheric-pressure microplasma jet. Plasma Processes Polym. 10, 978–989.

Ferguson, J.D., Arikan, G., Dale, D.S., Woll, A.R., Brock, J.D., 2009. Measurements of surface diffusivity and coarsening during pulsed laser deposition. PRL 103, 256103.

Fletcher, J.S., Conlan, X.A., Jones, E.A., Biddulph, G., Lockyer, N.P., Vickerman, J.C., 2006. Tof-sims analysis using C60. Effect of impact energy on yield and damage. Anal. Chem. 78, 1827–1831.

Floroian, L., Florescu, M., Sima, F., Popescu-Pelin, G., Ristoscu, C., Mihailescu, I.N., 2012. Synthesis of biomaterial thin films by pulsed laser technologies: electrochemical evaluation of bioactive glass-based nanocomposite coatings for biomedical applications. Mater. Sci. Eng. C 32, 1152–1157.

Flory, P.J., 1953. Principles of Polymer Chemistry. Cornell University Press, New York.

Forrest, S.R., 1997. Ultrathin organic films grown by organic molecular beam deposition and related techniques. Chem. Rev. 97, 1793–1896.

George, S.M., 2010. Atomic layer deposition: an overview. Chem. Rev. 110, 111–131.

Goodman, J., 1960. The formation of thin polymer films in the gas discharge. J. Polym. Sci. 44, 551–552.

Goreham, R.V., Short, R.D., Vasilev, K., 2011. Method for the generation of surface-bound nanoparticle density gradients. J. Phys. Chem. C 115, 3429–3433.

Goreham, R.V., Mierczynska, A., Smith, L.E., Sedev, R., Vasilev, K., 2013. Small surface nanotopography encourages fibroblast and osteoblast cell adhesion. RSC Adv. 3, 10309–10317.

Haddow, D.B., MacNeil, S., Short, R.D., 2006. A cell therapy for chronic wounds based upon a plasma polymer delivery surface. Plasma Processes Polym. 3, 419–430.

Hegemann, D., Korner, E., Blanchard, N., Drabik, M., Guimond, S., 2012. Densification of functional plasma polymers by momentum transfer during film growth. Appl. Phys. Lett. 101, 211603.

Hegemann, D., Vohrer, U., Oehr, C., Riedel, R., 1999. Deposition of SiOx films from O_2/HMDSO plasmas. Surf. Coat. Technol. 116–119, 1033–1036.

Hook, A.L., Chang, C.-Y., Yang, J., Luckett, J., Cockayne, A., Atkinson, S., Mei, Y., Bayston, R., Irvine, D.J., Langer, R., Anderson, D.G., Williams, P., Davies, M.C., Alexander, M.R., 2012. Combinatorial discovery of polymers resistant to bacterial attachment. Nat. Biotechnol. 30, 868–877.

Hopp, I., Michelmore, A., Smith, L.E., Robinson, D.E., Bachhuka, A., Mierczynska, A., Vasilev, K., 2013. The influence of substrate stiffness gradients on primary human dermal fibroblasts. Biomaterials 34, 5070–5077.

Hwang, J.J., Iyer, S.N., Li, L.-S., Claussen, R., Harrington, D.A., Stupp, S.I., 2002. Self-assembling biomaterials: liquid crystal phases of cholesteryl oligo(L-lactic acid) and their interactions with cells. PNAS 99, 9662–9667.

Ishii, K., 1989. High-rate low kinetic energy gas-flow-sputtering system. J. Vac. Sci. Technol. A 7, 256–258.

Johnston, E.E., Beyers, J.D., Ratner, B.D., 2005. Plasma deposition and surface characterization of oligoglyme, dioxane and crown ether nonfouling films. Langmuir 21, 870.

Kazarian, S.G., Chan, K.L.A., 2013. ATR-FTIR spectroscopic imaging: recent advances and applications to biological systems. Analyst 138, 1940−1951.

King, W.H., 1964. Piezoelectric sorption detector. Anal. Chem. 36, 1735−1739.

Langer, R., Tirrell, D.A., 2004. Designing materials for biology and medicine. Nature 428, 487−492.

Laurencin, C., Khan, Y., El-Amin, S.F., 2006. Bone graft substitutes. Expert Rev. Med. Devices 3, 49−57.

Lieberman, M.A., Lichtenberg, A.J., 1994. Principles of Plasma Discharges and Materials Processing. John Wiley and Sons, New York.

MacNeil, S., 2007. Progress and opportunities for tissue-engineered skin. Nature 445, 874−880.

Magee, C.W., Harrington, W.L., Honig, R.E., 1978. Secondary ion quadrupole mass spectrometer for depth profiling—design and performance evaluation. Rev. Sci. Instrum. 49, 477.

Mateo, N.D., Ratner, B.D., 1989. Relating the surface properties of intraocular lens materials to endothelial cell adhesion damage. Invest. Ophthalmol. Vis. Sci. 30, 853−860.

Matthews, A., Artley, R.J., Holiday, P., 2004. 2005 Revisited: The UK Engineering Coatings Industry to 2010. NASURF/DERA, 1998.

Mei, Y., Saha, K., Bogatyrev, S.R., Yang, J., Hook, A.L., Kalcioglu, Z.I., Cho, S.-W., Mitalipova, M., Pyzocha, N., Rojas, F., Van Vliet, K.J., Davies, M.C., Alexander, M.R., Langer, R., Jaenisch, R., Anderson, D.G., 2010. Combinatorial development of biomaterials for clonal growth of human pluripotent stem cells. Nat. Mater. 2010 (9), 768−778.

Menzies, D.J., Cowie, B., Fong, C., Forsythe, J.S., Gengenbach, T.R., McLean, K.M., Puskar, L., Textor, M., Thomsen, L., Tobin, M., Muir, B.W., 2010. One-step method for generating PEG-like plasma polymer gradients: chemical characterization and analysis of protein interactions. Langmuir 26, 13987.

Michelmore, A., Clements, L., Steele, D.A., Voelcker, N.H., Szili, E.J., 2012. Gradient technology for high-throughput screening of interactions between cells and nanostructured materials. J. Nanomater. 2012, 839053.

Michelmore, A., Steele, D.A., Whittle, J.D., Bradley, J.W., Short, R.D., 2013a. Nanoscale deposition of chemically functionalised films via plasma polymerisation. RSC Adv. 3, 13540−13557.

Michelmore, A., Steele, D.A., Robinson, D.E., Whittle, J.D., Short, R.D., 2013b. The link between mechanisms of deposition and the physico-chemical properties of plasma polymer films. Soft Matter 9, 6167−6175.

McMurray, R.J., Gadegaard, N., Tsimbouri, P.M., Burgess, K.V., McNamara, L.E., Tare, R., Murawski, K., Kingham, E., Oreffo, R.O.C., Dalby, M.J., 2011. Nanoscale surfaces for the long-term maintenance of mesenchymal stem cell phenotype and multipotency. Nat. Mater. 10, 637−644.

Oehr, C., 2003. Plasma surface modification of polymers for biomedical use. Nucl. Instrum. Methods Phys. Res. B 208, 40−47.

Ohring, M., 1992. Materials Science of Thin Films, second ed. Academic Press, New Jersey.

Pashuck, E.T., Stevens, M.M., 2012. Designing regenerative biomaterial therapies for the clinic. Sci. Transl. Med. 4, 160sr4.

Prestwich, G.D., Bhatia, S., Breuer, C.K., Dahl, S.L.M., Mason, C., McFarland, R., McQuillan, D.J., Sackner-Bernstein, J., Schox, J., Tente, W.E., Trounson, A., 2012. What is the greatest regulatory challenge in the translation of biomaterials to the clinic? Sci. Transl. Med. 4, 160cm14.

Purniawan, A., Frencha, P.J., Pandraudb, G., Sarro, P.M., 2010. TiO_2 ALD nanolayer as evanescent waveguide for biomedical sensor applications. Procedia Eng. 5, 1131−1135.

Ratner, B.D., 2013. A history of biomaterials. In: Ratner, B.D., Hoffman, A.S., Schoen, F.J., Lemons, J.E. (Eds.), Biomaterials Science: An Introduction to Materials in Medicine, third ed.

Ratner, B.D., Chilkoti, A., Lopez, G.P., 1990. Plasma deposition and treatment for biomaterial applications. In: d'Agostino, R. (Ed.), Plasma Deposition, Treatment and Etching of Polymers. Academic Press, San Diego, pp. 463−516.

Ravipati, S., Shieh, J., Ko, F.-H., Yu, C.-C., Chen, H.-L., 2013. Ultralow reflection from a -Si nanograss/Si nanofrustum double layers. Adv. Mater. 25, 1724−1728.

Rinsch, C.L., Chen, X., Panchalingam, V., Eberhart, R.C., Wang, J.-H., Timmons, R.B., 1996. Pulsed radio frequency plasma polymerization of allyl alcohol: controlled deposition of surface hydroxyl groups. Langmuir 12, 2995−3002.

Robinson, D.E., Marson, A., Short, R.D., Buttle, D.J., Day, A.J., Parry, K.L., Wiles, M., Highfield, P., Mistry, A., Whittle, J.D., 2008. Surface gradient of functional heparin. Adv. Mater. 20, 1166−1169.

Rothen, A., 1945. The ellipsometer, an apparatus to measure thicknesses of thin surface films. Rev. Sci. Instrum. 16, 26.

Salim, M., Mishra, G., Fowler, G., O'Sullivan, G.J.S., Wright, B., McArthur, S.L., 2007. Non-fouling microfluidic chip produced by radio frequency tetraglyme plasma deposition. Lab Chip 7, 523.

Sammelselg, A., Rosental, A., Tarre, L., Niinisto, K., Heiskanen, K., Ilmonen, L.-S., Johansson, T., Uustare, V., 1998. TiO thin films by atomic layer deposition: a case of uneven growth at low temperature. Appl. Surf. Sci. 134, 78−86.

Siow, K.S., Britcher, L., Kumar, S., Griesser, H.J., 2006. Plasma methods for the generation of chemically reactive surfaces for biomolecule immobilization and cell colonization − a review. Plasma Processes Polym. 3, 392−418.

Skinner, J., Kay, P., 2011. Metal on metal hips. BMJ 342, d3009.

Sommerdijk, N.A.J.M., van Leeuwen, E.N.M., Vos, M.R.J., Jansen, J.A., 2007. Calcium carbonate thin films as biomaterial coatings using DNA as crystallization inhibitor. CrystEngComm 9, 1209−1214.

Tse, J.R., Engler, A.J., 2011. Stiffness gradients mimicking in vivo tissue variation regulate mesenchymal stem cell fate. PLoS One 6, e15978.

Variola, F., Vetrone, F., Richert, L., Jedrzejowski, P., Yi, J.-H., Zalzal, S., Clair, S., Sarkissian, A., Perepichka, D.F., Wuest, J.D., Rosei, F., Nanci, A., 2009. Improving biocompatibility of implantable metals by nanoscale modification of surfaces: an overview of strategies, fabrication methods and challenges. Small 5, 996−1006.

Vasilev, K., Sah, V., Anselme, K., Ndi, C., Mateescu, M., Dollmann, B., Martinek, P., Ys, H., Ploux, L., Griesser, H.J., 2010a. Tunable antibacterial coatings that support mammalian cell growth. Nano Lett. 10, 202−207.

Vasilev, K., Michelmore, A., Martinek, P., Chan, J., Sah, V., Griesser, H.J., Short, R.D., 2010b. Early stages of growth of plasma polymer coatings deposited from nitrogen and oxygen containing monomers. Plasma Processes Polym. 7, 824−835.

Venables, J.A., Spiller, G.D.T., Hanbucken, M., 1984. Nucleation and growth of thin films. Rep. Prog. Phys. 47, 399−459.

Williams, T., Hayes, M.W., 1966. Polymerization in a glow discharge. Nature 209, 769−773.

Yang, J., Rose, F., Gadegaard, N., Alexander, M.R., 2009. A High-Throughput Assay of Cell-Surface Interactions using Topographical and Chemical Gradients. Adv. Mater. 21, 300−304.

Zeng, S., Baillargeat, D., Ho, H.-P., Yong, K.-T., 2014. Nanomaterials enhanced surface plasmon resonance for biological and chemical sensing applications. Chem. Soc. Rev. 43, 3426−3452.

Zheng, J., Yang, R., Xie, L., Qu, J., Liu, Y., Li, X., 2010. Plasma-assisted approaches in inorganic nanostructure fabrication. Adv. Mater. 22, 1451−1473.

This page intentionally left blank

Tailoring thin films for implant-specific applications

3

T.W.J. Steele, J.S.C. Loo, S.S. Venkatraman
Nanyang Technological University, Singapore

3.1 Introduction

3.1.1 High-throughput assessment of drug delivery

Hydrophobic drugs are prime candidates for encapsulation and controlled release in bioresorbable thin films. The common biodegradable matrices of polyesters and polyanhydrides offer an ideal environment for hydrophobic drugs to disperse molecularly with little phase separation. However, screening thin formulations is a tedious task; formulation parameters are diverse and often include thin film thickness, various grades and molecular weights of the polymer matrix, the specific drug and its encapsulation percentage, additives to modulate drug release and material properties, etc. Optimizing several parameters can lead to several hundred formulations. Considering replicates and multiple sampling that comes with characterizing drug release kinetics, an efficient method must be found to characterize hundreds if not thousands of samples that can be generated per day.

When undergoing a high-throughput screening of thousands of samples, a global perspective is often necessary that divides the standard operating procedures (SOPs) from formulation synthesis to data analysis. SOPs need to be designed for every stage of the drug release, with common SOPs covering the following drug release operations: (1) synthesis of the encapsulated thin films; (2) characterization of thin film formulation constituents; (3) sampling and replacement of the release medium to prevent drug sink effects; (4) sample quantitation of drug, polymer, additive or a combination of them; (5) data analysis and storage; and (6) post-drug release polymer matrix characterization.

3.2 Materials and technologies

3.2.1 Quantitation of release kinetics

Pertaining to sample quantitation, high-performance liquid chromatography (HPLC) is the reference standard for drug quantitation, but it is slow when considering the inherent sample preparation procedures (ie, filtering and capping). Quantitation by microplate-based fluorescence spectroscopy is a faster methodology that avoids much of the laborious preparation of HPLC SOPs while maintaining similar levels of sensitivity. Microplates in plate readers shorten the instrument analysis time to

Thin Film Coatings for Biomaterials and Biomedical Applications. http://dx.doi.org/10.1016/B978-1-78242-453-6.00003-1

seconds per sample, and in our experience they speed analysis through automated Excel macros or algorithms. Several pharmacophores readily fluoresce under certain conditions, including coumarins, nucleosides, dienones and amido-pyridines.[1,2] The downside of this approach is there are many more nonfluorescent pharmacophores than fluorescent ones. Two alternative strategies may be beneficial. First, most pharmacophores can be readily derivatized with a fluorophore such as dansyl chloride. The drawback is that the derivatized pharmacophore must have sufficiently different fluorescent properties from the reagent so that separation or cleanup procedures are avoided. Fluorescent readings can then be rapidly recorded after the protocol.

Take, for example, the hydrophobic drug paclitaxel, a powerful drug employed in antitumour and heart disease therapies. Paclitaxel is not fluorescent, but fluorescent analogues exist toward various life science protocols in which minute quantities suffice.[3] In the amounts required for encapsulation into thin films and subsequent drug release protocols, they are prohibitively expensive. The next best method is to employ a fluorescent economical mimic of the hydrophobic drug of interest to narrow release formulations that fit the delivery profile desired. Once the formulations are focused, the more laborious HPLC quantitation procedures can be verified with the original drug of interest.

Fig. 3.1 displays the end results for screening various hydrophobic fluorescent mimics against paclitaxel in a variety of thin film formulations.[4] Of various fluorescent molecules that had similar log *P* values as paclitaxel, fluorescein diacetate (FDAc) mimicked paclitaxel drug release as long as additive ratios were kept low within a polyester poly(lactic-*co*-glycolic acid) (PLGA) matrix, as seen in Fig. 3.1. Inclusion of large amounts of polyethylene glycol (PEG) additive, a common plasticizer and drug release enhancer,[5] caused phase partitioning within the PLGA matrix, ultimately shifting the mechanism of release between FDAc and paclitaxel. As the ratio of PEG increased, greater deviations in drug release were apparent.

The encapsulation of FDAc into drug release films has other advantages, as well; by itself, FDAc is not fluorescent and is activated into fluorescein only after base treatment or enzyme (esterase) activation.[6] Thus, FDAc will not photobleach (unlike fluorescein) and is a good candidate for investigations into photo-induced drug delivery.[7] FDAc is also colourless when mixed into thin film formulations, whereas fluorescein is a highly coloured green-orange dye and is easily discerned by the naked eye. In this regard, FDAc acts as a visual sensor toward thin film damage, especially for polymers that have a significant percentage of polyester backbone. For example, our laboratory once explored various polyamines as additives into PLGA films, but found the films quickly turning orange under dry storage conditions. Inherent amines (eg, polyethylenimine) quickly catalyse the hydrolysis of the polyester backbone and FDAc. Polyamine-based additives were quickly abandoned as drug release modifiers (unpublished data).

3.2.2 Synthesis of thin-film gradients

Thin films specified for medical applications often go through many rounds of optimization, considering a generic film constituent of one or more polymer matrices,

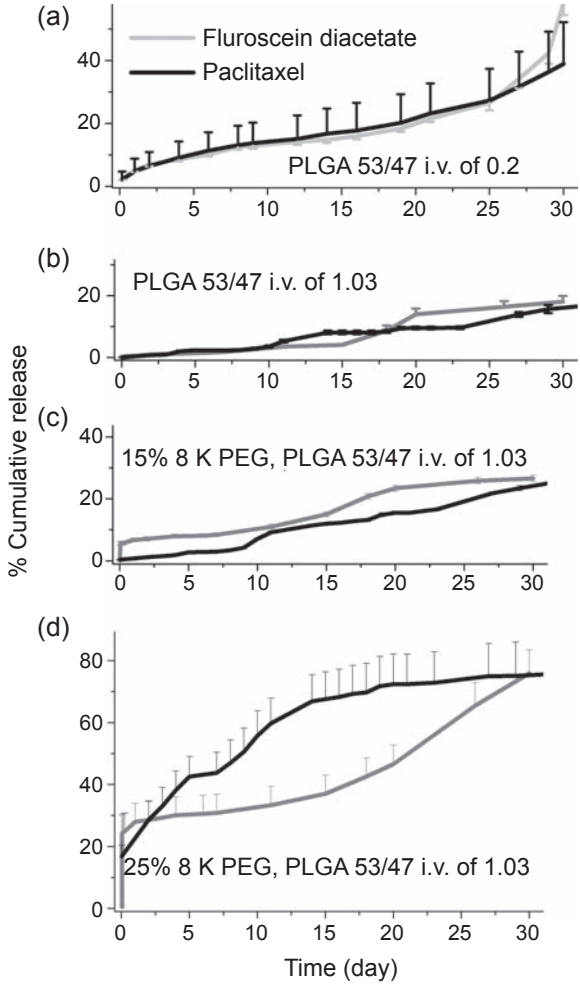

Figure 3.1 Drug flux comparison of fluorescein diacetate (FDAc) and paclitaxel in poly(lactic-*co*-glycolic acid) (PLGA) 53/47: (a) intrinsic viscosity (i.v.) of 0.2 ester terminated (Purac PDLG 5002), (b) i.v. of 1.03 ester terminated (Purac PDLG 5010), (c) PLGA 53/47 i.v. of 1.03 with 15% w/w 8 kDa polyethylene glycol (PEG) and (d) with 25% w/w 8 kDa PEG.

encapsulated drugs(s) and the inclusion of modifying additives. Each formulation needs to be assessed empirically, often generating tens if not hundreds of films even when limiting the investigation to just a few parameters. We find the most important parameters to be the amount and method of encapsulated drug, and inclusion of modifying additive toward drug release, material properties or both. This assumes that a formulation scientist can limit the matrix to a single commercially available (medical grade) polymer matrix and an agreed-upon pharmaceutical suitable for the polymer matrix of choice.

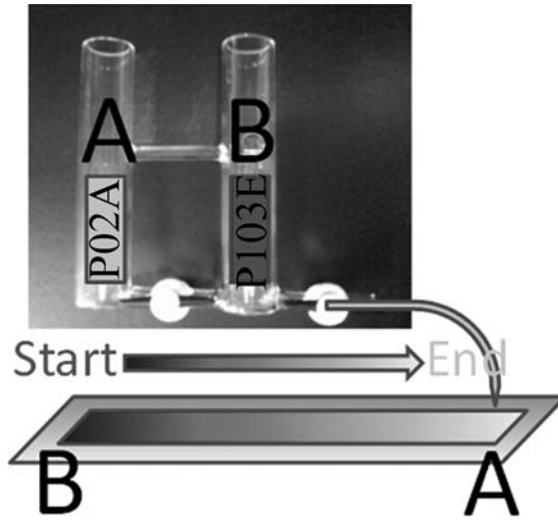

Figure 3.2 Scheme of a theoretical gradient of two constituents of solution A and solution B. Solution A flows into solution B as both valves are opened. A gradient mixture of B to A is then flowed onto a glass plate for knife casting.

To speed product development, ideally one can make a single film that addresses the minimum and maximum variants under a single parameter. For example, specific rates of release are often sought from the surfaces of thin films (henceforth drug flux, with typical units of $\mu g/cm^2$ d), based on known clearance rates, therapeutic levels desired, or tissue absorption characteristics. Thus, by synthesizing a horizontal gradient of drug concentrations within a single thin film, various rates of drug flux could be assessed. Simple techniques exist for gradient-casting thin films by knife casting (as seen in Fig. 3.2) or through film extrusion. Knife casting is a simple and inexpensive procedure but it has residual solvent encapsulation. This is a problem only when direct in vivo investigations are planned. Modern research and development (R&D) extruders have the capability of using only 2 g polymer toward filament or film extrusion, with no solvent required (eg, Xplore twin screw compounder from Xplore Instruments, The Netherlands). Both methods have the advantage of minimal materials needed, work staff and faster return of results.

In our experience, drug flux based on polymer additive concentration or polymer matrix blending tends to yield more worthwhile information (in terms of drug flux), whereas exploring levels of drug encapsulation within the thin films is one of the last parameters that should be assessed. In the sections that follow, we will describe how a combination of high-throughput quantitation and gradient film casting was employed to assess and predict drug flux, material properties and phase separation.

3.3 Challenges and examples

3.3.1 Tailoring drug delivery without additives through polyester acidic end groups

Depending on the medical application, tailoring the drug flux from a resorbable thin film is a first priority and depends on the therapeutic of choice and the pathology under treatment. Additives are the most common method for modifying drug flux from biodegradable thin films. PEG is a common additive employed in various thin film formulations. PEG is known to increase drug flux because it readily dissolves in both organic and aqueous solvents, increasing matrix water penetration, or because it acts as a solubility enhancer toward sparingly soluble drugs.[5,8] However, the addition of PEG or other additives often has far-reaching effects on more than drug flux: It can act as a plasticizer, induce phase separation, alter surface wetting or all of these.[5,9] To avoid these detrimental shifts in material properties, modulation of drug flux without additives has been attempted with varying success by blending molecular weight, using polymer blends, or including various functional groups.[10–16] We have found acidic end groups particularly adept at tuning drug release from polyester matrices.[11,17]

Fig. 3.3 displays typical results obtained with the high-throughput assessment methods described above. Thin films (about 20 μm thick) of medical grade PLGA 53/47 obtained from Purac (The Netherlands) were synthesized through gradient knife casting. Fig. 3.3(a)–(c) shows the drug flux of FDAc with respect to composition (ester or acid terminal end groups) and time. Various compositions are present at different lengths of the gradient-cast film (Fig. 3.3(d) and (e)). Fig. 3.3(a) displays a relatively flat drug flux with little to no dependence on the amount of the ester-terminated P02E over 30 days. This is in sharp contrast to the acid-terminated P02A composition, in which a high Pearson R correlation (>0.9) was assessed between drug flux and the concentration for the acidic groups. The wide range of total drug release that could be selected was most useful for the formulation scientist. For example, at day 20 the compositions in Fig. 3.3(b) could be predicted to give a total drug release of 40–90%. The FDAc fluxes of 1–2, 2–6 and 5–30 $\mu g/cm^2$ d were observed in the formulations observed in Fig. 3.3(a)–(c), respectively.

These investigational studies encapsulated a relatively small amount of drug (2.5% w/w FDAc/P103E) to limit drug release from diffusion or burst release–based processes. As one increases the FDAc concentration fivefold, higher linear correlations of drug flux are observed, as seen in Fig. 3.3(c). This results from the balance of burst release and polymer degradation within the thin film. Burst release allows fast drug flux at the start of the medium incubation by diffusion whereas polymer degradation processes allow high drug flux only after an initial incubation period. The encapsulation of the terminal acidic groups catalyses polyester hydrolysis and shortens the incubation period whereas degraded oligomer fragments become soluble in aqueous media.[18,19]

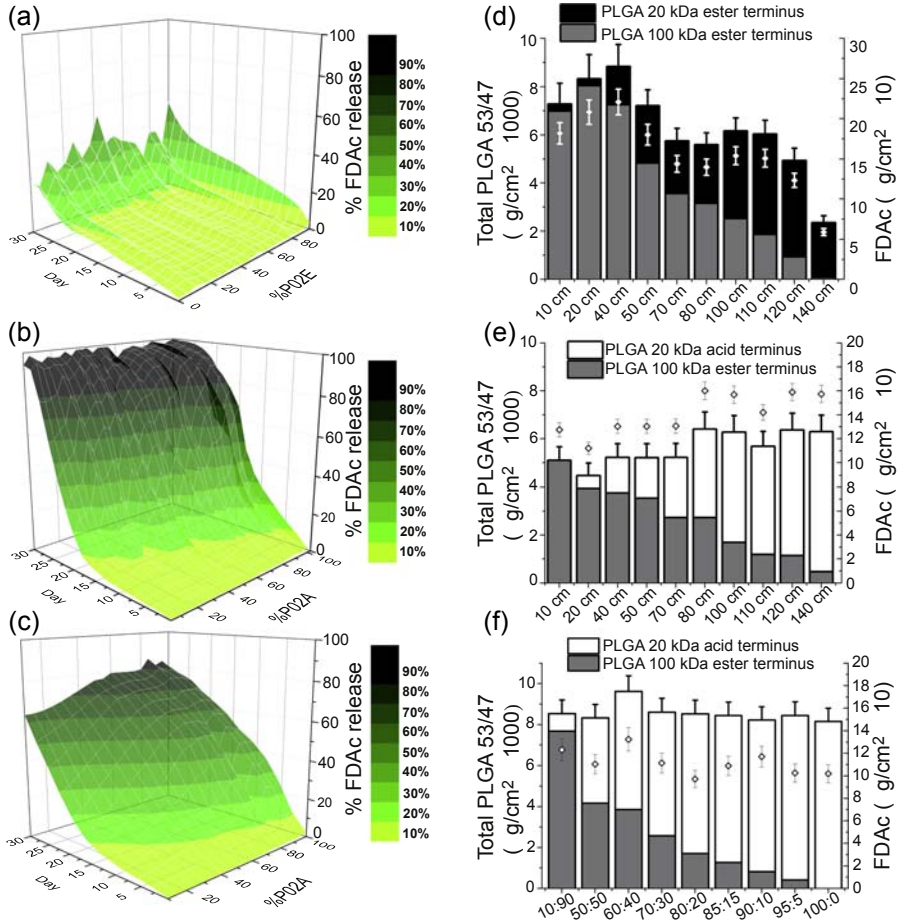

Figure 3.3 Drug flux of fluorescein diacetate (FDAc; *z* axis) with respect to time (*x* axis) and (a) gradient-cast P02E; (b) gradient-cast P02A; (c) fixed-cast P02A; (d) gradient composition of P02E/P103E, 2.5% w/w FDAc/P103E; (e) gradient composition of P02A/P103E, 2.5% w/w FDAc/P103E; (f) fixed composition of P02A/P103E, 10% w/w FDAc/P103E. **P103E**: PLGA 53/47 i.v. of 1.03 ester-terminated Purac PDLG 5010, **P02E**: PLGA 53/47 i.v. of 0.2 ester-terminated Purac PDLG 5002. **P02A**: PLGA 53/47 i.v. of 0.2 acid-terminated Purac PDLG 5002A.

The corresponding surface compositions of total PLGA, PLGA ratio and FDAc concentration are given in Fig. 3.3(d)−(f). These data are easily generated through nuclear magnetic resonance (NMR) and gel permeation chromatography (GPC) instruments equipped with appropriate autosamplers. Gradient casting gives many formulations for assessment but the technique has drawbacks. Most notable is the large variance in total PLGA across gradient-cast films (Fig. 3.3(d)) compared with fixed formulations (Fig. 3.3(f)). This is caused by changes in viscosity during gradient casting. Variations in viscosity lead to disparities in film thickness and constituent surface

concentrations. Another drawback is the additional analysis required: A fixed formulation requires minimal characterization of the constituents, but gradient casting requires a dedicated approach (NMR or GPC). However, this analysis can be subject to the film surpassing certain milestone requirements before labour is invested. If the films do not display the required drug flux, they can be discarded and R&D can quickly move on to the next phase.

3.3.2 Tailoring material properties through oligomer additives while maintaining drug flux

The previous section focused on altering drug flux while minimizing changes in material properties and the use of additives. In this section, we focus on the challenge of shifting material properties such as modulus while minimizing changes in drug flux. PEG and its more hydrophobic variant, polypropylene glycol (PPG), affect both drug flux and modulus in concentration-dependent ways. PEG, which is amphiphilic, has a small shift in drug flux, with 15% w/w additive concentration in PLGA 53/47. However, much more PPG is required to observe a significant increase in drug flux: about 25% w/w, as shown in Fig. 3.4(a). Below the stated w/w ratios, few to no changes in drug flux are observed within the 30-day measurement window. The modulus has a drastic change within these stated w/w ratios, however. Mechanical properties of PEG and PPG additives in PLGA 53/47 are assessed according to ASTM standard D882 from 0% to 15% w/w additive/PLGA. PEG additives of 2, 4 and 8 kDa decrease the neat PLGA 53/47 sample modulus from about 13 MPa to less than 0.05 MPa at 15% w/w additive, as displayed in Fig. 3.4(b). Elongation was only slightly affected with changes of 50% or less. PPG 4000 has the opposite effect: The modulus was seen to increase PLGA 53/47 thin films linearly to about 19 MPa at 15% w/w PPG additive, but elongation decreased by more than 10 times; the films effectively became more brittle. The modulus characterized in these studies was from dry thin films and the mechanical properties will dramatically shift in wet conditions. For example, the wet modulus of neat PLGA 53/47 samples decreases to about 3.7 MPa in phosphate-buffered saline at 37°C.[11] Thus, the PEG- and PPG-containing films will have completely different properties in wet environments.

3.3.3 Example of how oligomer additives can achieve controlled drug flux

Films loaded with anticancer drugs may find applications in managing localized tumours while avoiding the route of systemic administration. Oftentimes, such an approach is ideal for tumours that have been excised for biopsy, and a film can be locally implanted as a device to release drugs to the surrounding tissues. For example, a drug such as vemurafenib (VF) can be loaded into biodegradable PLGA film using the gradient-casting solvent evaporation method as outlined above. To accelerate the release of this hydrophobic drug from the film, PEG was introduced into the PLGA solution to act as a plasticizer. Similarly, a film applicator was used to cast the film under atmospheric conditions. These films were left to dry in a vacuum oven for up to a week.

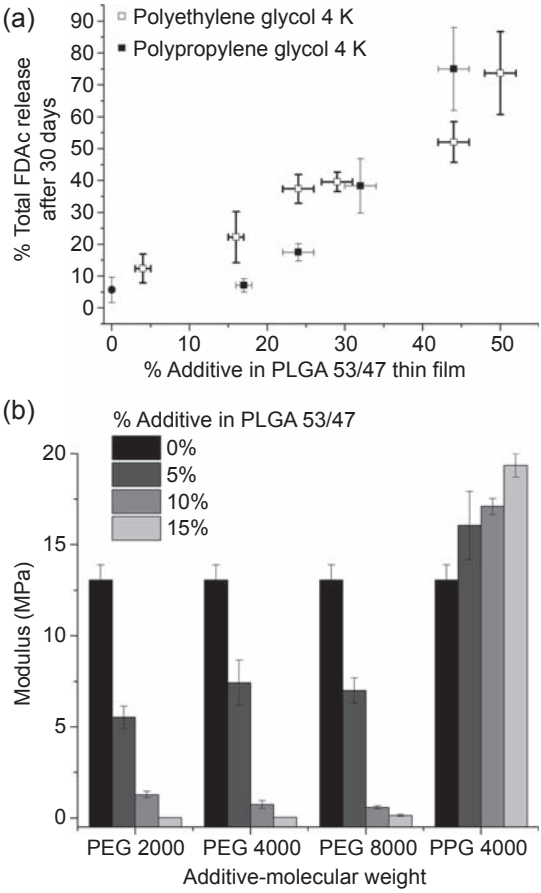

Figure 3.4 (a) Fluorescein diacetate flux from PLGA 53/47 i.v. of 1.03 ester-terminated Purac PDLG 5010 with a range of PEG 4000 and PPG 4000 additives. (b) Modulus of PLGA 53/47 i.v. of 1.03 ester-terminated thin films with 5, 10 and 15% PEG and PPG additives.
Some data points have been redrawn from Steele TW, Huang CL, Kumar S, Irvine S, Boey FY, Loo JS, et al. Novel gradient casting method provides high-throughput assessment of blended polyester poly(lactic-*co*-glycolic acid) thin films for parameter optimization. *Acta Biomater* 2012;**8**(6):2263−2270.

These films were subsequently investigated for the release profile of the VF drug. For this study, the drug-loaded films were punched out into 6-mm-diameter discs. The discs were placed individually into wells of a 96-well plate and immersed in 200 μL PBS, pH 7.4, at 37°C. The medium was removed at predetermined time points and replaced, maintaining sink conditions throughout. The withdrawn medium was filtered through a 0.2-μm PTFE syringe filter directly into HPLC vials and immediately capped. The VF was quantified with an Agilent Series 1100 HPLC (Santa Clara, CA) equipped with a UV/vis detector, autosampler and column heater set to 35°C. A ZORBAX Eclipse XDB-C18 (5-μm) column of acetonitrile/water 60/40 (vol. %) served as the mobile buffer, eluting the VF peak at 5.4 min at a flow rate of 1.0 mL/min, with the UV/vis detector recording at 227 nm. The results showed that VF can be released in a controlled

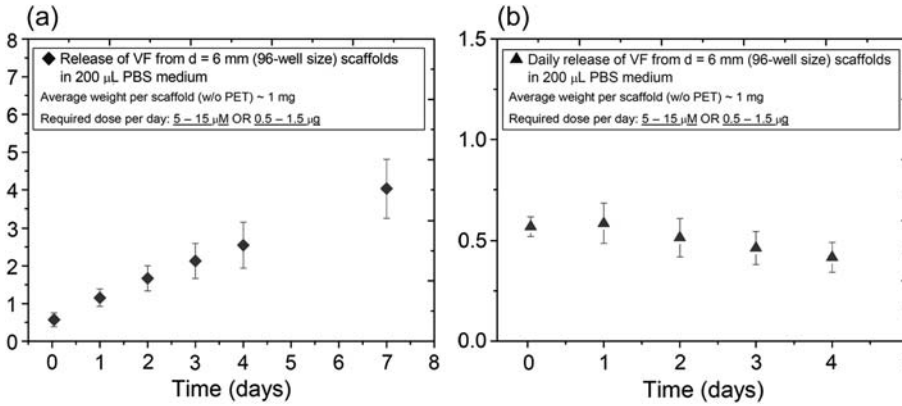

Figure 3.5 (a) Cumulative release of VF from PEG-PLGA polymer blend films. Linear release from in vitro studies was obtained for up to a week. (b) Release of VF per day from the blended films, giving a release amount of approximately 0.5 µg/d.

linear fashion (Fig. 3.5(a)), in which release each day was consistent at about 0.5 µg/d (Fig. 3.5(b)). Such a release profile was made possible because of the introduction of an additive, ie, PEG, into an otherwise hydrophobic PLGA film, which generally inhibits the release of a hydrophobic drug. This shows the key contribution of another polymer in creating a blend to achieve a profile that is ideal for a particular application. The continuous release of drugs will be useful to deliver drugs locally to surrounding tissues and inhibit the growth of local tumours in cancer therapy.

3.4 Future trends

3.4.1 Tailoring surface properties, drug flux and mechanical properties through plasma post-treatment

The formulations described here necessitate the design and manufacture of myriad formulations to optimize drug flux and material properties. The properties are generally fixed and cannot be changed once the synthesized films are prepared, or so conventional thinking goes. If a post-treatment method were developed, a fixed manufactured film could be optimized after it has been manufactured. Treatment of PLGA 53/47 thin films with oxygen and argon plasma has been shown to have this unique post-treatment flexibility. Fig. 3.6 displays how contact angle, surface roughness and drug flux could be shifted with specific treatments of radio frequency (RF) vacuum plasma.[20] A brief 1-min treatment is all that is required to change the surface energy using 1:1 argon:oxygen plasma. Longer treatments will not necessarily change the contact angle more, but more intense treatments of 5 min or longer display the ability to etch the PLGA 53/47 surface in the tens of nanometres, as seen in Fig. 3.6(a). Surprisingly, little effect on the PLGA molar mass is seen, because the etching process is believed to degrade the polyesters chains through a terminal end group induced thermal oxidative pathway. Drug flux of plasma-treated PLGA thin films is found to increase to 65% versus that of the untreated PLGA control under 1:1 argon:oxygen plasma. However, pure argon plasma initially

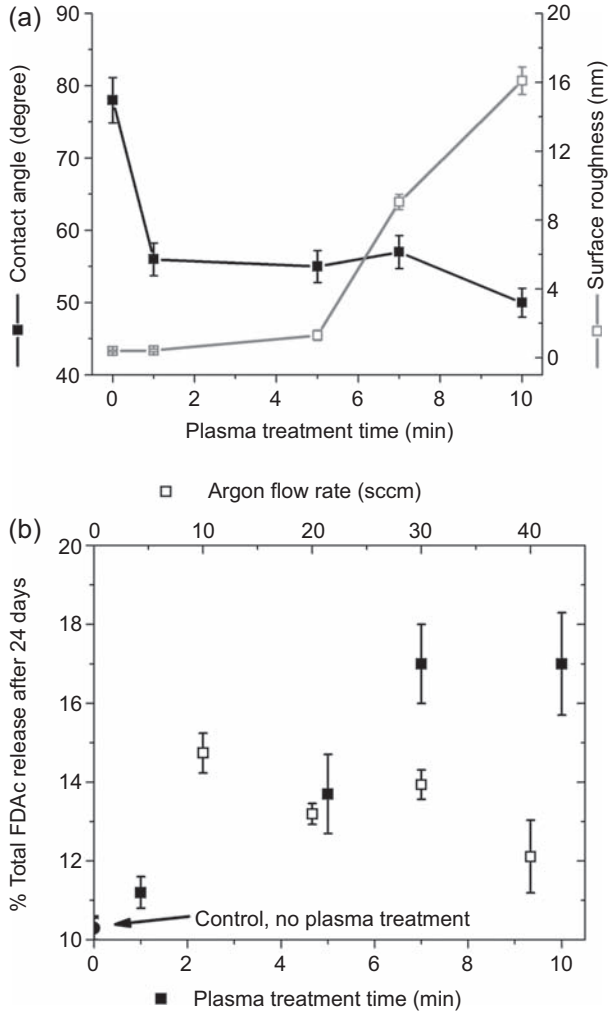

Figure 3.6 Plasma post-treatment of PLGA 53/47. (a) Contact angle (left *y*-axis) and surface roughness (right *y*-axis), plotted against treatment time of 1:1 argon:oxygen RF vacuum plasma. (b) Drug flux plotted against argon plasma flow rate (top *x*-axis) or treatment time of 1:1 argon: oxygen RF vacuum plasma (bottom *x*-axis).
Data points have been redrawn from Mogal VT, Yin CS, O'Rorke R, Boujday S, Methivier C, Venkatraman SS, et al. Tuning model drug release and soft-tissue bioadhesion of polyester films by plasma post-treatment. *ACS Appl Mater Interfaces* 2014;**6**(8):5749−5758.

increases drug flux, but higher flow intensities subsequently decrease the drug elution almost to that of the untreated PLGA control, as displayed in Fig. 3.6(b). This is likely because of radical-induced polymer chain cross-linking. Plasma post-treatment can also be used to tune the mechanical properties of polyester films. Savoji et al. showed that fibre mats synthesized from poly(ethylene terephthalate) gave a substantial reduction in Young's modulus within 5 min of oxygen plasma treatment with no apparent damage to the nanofibres.[21]

Plasma-based post-treatment processing of thin films is still in its infancy because high-throughput and scaled-up manufacturing are relatively difficult for the current generation of vacuum-based RF plasma instruments. However, as atmospheric pressure−based plasma instruments become cheaper and simpler to operate, more laboratory and commercial application will ensue.

References

1. Burchak ON, Mugherli L, Ostuni M, Lacapere JJ, Balakirev MY. Combinatorial discovery of fluorescent pharmacophores by multicomponent reactions in droplet arrays. *J Am Chem Soc* 2011;**133**(26):10058−61.
2. Makarov MV, Leonova ES, Rybalkina EY, Khrustalev VN, Shepel NE, Roschenthaler GV, et al. Methylenebisphosphonates with dienone pharmacophore: synthesis, structure, antitumor and fluorescent properties. *Arch Pharm* 2012;**345**(5):349−59.
3. Han Y, Chaudhary AG, Chordia MD, Sackett DL, Perez-Ramirez B, Kingston DG, et al. Interaction of a fluorescent derivative of paclitaxel (Taxol) with microtubules and tubulin-colchicine. *Biochemistry* 1996;**35**(45):14173−83.
4. Steele TW, Huang CL, Kumar S, Widjaja E, Chiang Boey FY, Loo JS, et al. High-throughput screening of PLGA thin films utilizing hydrophobic fluorescent dyes for hydrophobic drug compounds. *J Pharm Sci* 2011;**100**(10):4317−29.
5. Steele TW, Huang CL, Widjaja E, Boey FY, Loo JS, Venkatraman SS. The effect of polyethylene glycol structure on paclitaxel drug release and mechanical properties of PLGA thin films. *Acta Biomater* 2011;**7**(5):1973−83.
6. Lim AM, Steele TWJ. *Study of esterase activity from drug (FDAc) loaded nanoparticles*. Singapore: NTU; 2012.
7. Cheng T, Ortiz RF, Vedantham K, Naccache R, Vetrone F, Marks RS, et al. Tunable chemical release from polyester thin film by photocatalytic zinc oxide and doped $LiYF_4$ upconverting nanoparticles. *Biomacromolecules* 2014;**16**(1).
8. Vlachou M, Hani N, Efentakis M, Tarantili PA, Andreopoulos AG. Polymers for use in controlled release systems: the effect of surfactants on their swelling properties. *J Biomater Appl* 2000;**15**(1):65−77.
9. Steele TW, Huang CL, Kumar S, Irvine S, Boey FY, Loo JS, et al. Novel gradient casting method provides high-throughput assessment of blended polyester poly(lactic-*co*-glycolic acid) thin films for parameter optimization. *Acta Biomater* 2012;**8**(6):2263−70.
10. Huang CL, Steele TWJ, Widjaja E, Boey FYC, Venkatraman SS, Loo JSC. The influence of additives in modulating drug delivery and degradation of PLGA thin films. *NPG Asia Mater* 2013;**5**:e54.
11. Huang CL, Kumar S, Tan JJZ, Boey FYC, Venkatraman SS, Steele TWJ, et al. Modulating drug release from poly(lactic-*co*-glycolic acid) thin films through terminal end-groups and molecular weight. *Polym Degrad Stab* 2013;**98**(2):619−26.
12. Duvvuri S, Gaurav Janoria K, Mitra AK. Effect of polymer blending on the release of ganciclovir from PLGA microspheres. *Pharm Res* 2006;**23**(1):215−23.
13. Ishihara T, Kubota T, Choi T, Takahashi M, Ayano E, Kanazawa H, et al. Polymeric nanoparticles encapsulating betamethasone phosphate with different release profiles and stealthiness. *Int J Pharm* 2009;**375**(1−2):148−54.
14. Raiche AT, Puleo DA. Modulated release of bioactive protein from multilayered blended PLGA coatings. *Int J Pharm* 2006;**311**(1−2):40−9.
15. Tang ZG, Hunt JA. The effect of PLGA doping of polycaprolactone films on the control of osteoblast adhesion and proliferation in vitro. *Biomaterials* 2006;**27**(25):4409−18.

16. Nguyen J, Steele TW, Merkel O, Reul R, Kissel T. Fast degrading polyesters as siRNA nano-carriers for pulmonary gene therapy. *J Control Release* 2008;**132**(3):243−51.
17. Steele TWJ, Huang CL, Kumar S, Iskandar A, Baoxin A, Boey FYC, et al. Tuning drug release in polyester thin films: terminal end-groups determine specific rates of additive-free controlled drug release. *NPG Asia Mater* 2013;**5**.
18. Korber M. PLGA erosion: solubility- or diffusion-controlled? *Pharm Res* 2010;**27**(11): 2414−20.
19. Glaessl B, Siepmann F, Tucker I, Rades T, Siepmann J. Deeper insight into the drug release mechanisms in Eudragit RL-based delivery systems. *Int J Pharm* 2010;**389**(1−2): 139−46.
20. Mogal VT, Yin CS, O'Rorke R, Boujday S, Methivier C, Venkatraman SS, et al. Tuning model drug release and soft-tissue bioadhesion of polyester films by plasma post-treatment. *ACS Appl Mater Interfaces* 2014;**6**(8):5749−58.
21. Savoji H, Lerouge S, Ajji A, Wertheimer MR. Plasma-etching for controlled modification of structural and mechanical properties of electrospun PET scaffolds. *Plasma Processes Polym* 2014;**12**(4): n/a-n/a.

Protein and peptide interactions with phospholipid membranes and surfaces

4

M. Malmsten
Uppsala University, Uppsala, Sweden

4.1 Introduction

Compared with simpler homopolymers, in which adsorption is largely driven by homogeneous enthalpic interactions and opposed by conformational and translational entropy restrictions, the driving force for protein, and to some extent also peptide, adsorption is more complex. Hence, adsorption is generally driven by a combination of van der Waals interactions, hydrophobic interactions, hydration effects, and electrostatic interactions between surfaces and proteins/peptides, or domains of these. In addition, adsorption may be promoted by entropy gains coupled to adsorption-induced conformational changes, as well as to the release of counterions and/or solvation water, and it also depends sensitively on protein−protein interactions in the adsorbed layer.[1−3] In relation to protein/peptide−surface interactions, adsorption depends on a range of factors, including the protein/peptide and surface net charge and charge distribution, the occurrence of hydrophobic domains in the protein/peptide or the surface, and the size of the protein/peptide, to mention a few. Although there are numerous exceptions, most proteins tend to adsorb more extensively at hydrophobic than at hydrophilic surfaces. Shorter peptides, on the other hand, have less capacity to expose buried hydrophobic residues on adsorption-induced conformational changes and display a similar dependence on surface hydrophobicity primarily for peptides containing hydrophobic residues. Regarding electrostatic interactions, proteins may somewhat simplistically be divided into two classes. For proteins displaying large conformational changes on adsorption ("soft" proteins), nonelectrostatic driving forces contribute significantly; hence, adsorption is not solely dictated by electrostatics. For proteins undergoing limited conformational changes ("hard" proteins), in contrast, adsorption tends to follow expectations from electrostatic considerations more closely. These and other general aspects of protein and peptide adsorption have been extensively discussed previously in the literature.[1−3]

Interest in protein and peptide interactions with phospholipid membranes and surfaces originates from its importance for both key biophysical processes (eg, atherosclerosis, Alzheimer's, and other plaque-related diseases) and a wide range of biomedical applications. For example, control of protein/peptide adsorption allows reduction of inflammation and other unwanted biopharmaceutical effects in phospholipid-based biomaterials and drug delivery but also improved signal-to-noise in biosensors and

Thin Film Coatings for Biomaterials and Biomedical Applications. http://dx.doi.org/10.1016/B978-1-78242-453-6.00004-3

solid-phase diagnostics, to mention a few areas of interest. In addition, interactions between amphiphilic peptides and phospholipid membranes have a key role in the performance of these as antimicrobial, antiinflammatory, anticancer, and cell-penetrating peptides.[4,5] Examples of factors affecting protein/peptide interactions with phospholipid membranes and surfaces are provided below, with particular focus on applications for parenteral drug delivery and antimicrobial peptides (AMPs).

4.2 Protein interactions with phospholipid membranes and surfaces

After intravenous administration of nanoparticulate drug carriers, these are generally cleared rapidly from bloodstream circulation by macrophages of the reticuloendothelial system (RES) and accumulated in tissues such as liver, spleen, and marrow.[6,7] With the exception of cases when targeting of these tissues is needed, fast RES uptake is unwanted. Thus, short bloodstream circulation time results in low bioavailability in non-RES tissues, whereas drug accumulation in RES-related tissues results in dose-limiting local toxicity. Therefore, extended bloodstream circulation and a more even tissue distribution are generally advantageous from a therapeutic point of view. RES uptake of nanoparticulate drug carriers depends on a range of factors, including nanoparticle size and surface properties (hydrophobicity, charge, chemical functionality, etc.). Generally, macrophage uptake increases with particle size, hydrophobicity, and charge (contrast) but also depends in a complex manner on the precise chemical functionalities of the nanoparticles.[6–8] The uptake is triggered by adsorption of certain serum proteins, the so-called opsonins, at the carrier surface. These include, for instance, immunoglobulins, complement proteins, adhesion proteins, the Hageman factor, and C-reactive protein. The detailed adsorption pattern of these and many other serum proteins affects macrophage uptake and RES clearance in a complex way, in which the composition of the adsorbed layer, interfacial exchange phenomena, as well as surface-induced activation have key roles.[9,10] Having said that, adsorption of serum proteins is frequently similarly dependent on phospholipid membrane composition.[11–13] As a result of this, RES clearance depends strongly on the total amount of serum proteins adsorbed at the drug carrier surface.[6,14] More precisely, there is an inverse correlation between the total serum protein adsorption on the one hand and the bloodstream circulation time on the other (Fig. 4.1). Thus, by reducing overall serum protein adsorption to a nanoparticulate drug carrier, its bloodstream circulation can be prolonged.

Adsorption of (serum) proteins at phospholipid membranes and surfaces depends sensitively on membrane properties, including headgroup charge and structure, acyl group length, saturation, and symmetry, as well as the presence of cholesterol and other membrane components. In relation to headgroup properties, phospholipids with close to zero net surface charge (eg, phosphatidylcholine (PC) or sphingomyelin (SM)), or for which its charge is shielded by an outer uncharged group (eg, ganglioside GM1 or phosphatidylinositol (PI)), serum protein adsorption is generally low[12,13] and bloodstream circulation correspondingly long.[6,14] For phospholipids displaying bare charges (eg, phosphatidic acid (PA) or cardiolipin (DPG)), on the other hand, serum protein adsorption is substantial, and clearance from bloodstream circulation is swift.

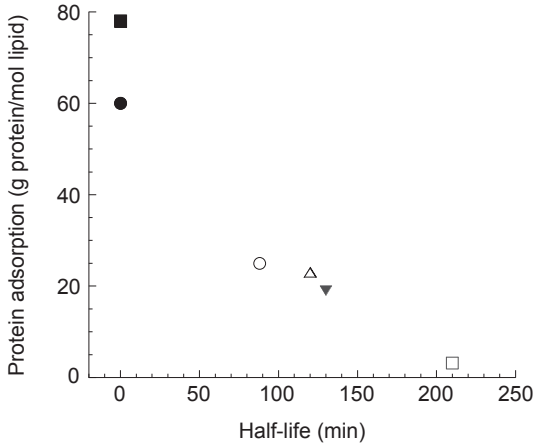

Figure 4.1 Correlation between total amount protein adsorbed and circulation half-life before plasma clearance of liposomes administered intravenously in mice. Results are shown for liposomes containing SM:PC:GM1 (72:18:10) (*open square*), PC:CH (55:45) (*open triangle*), PC:CH:plant PI (35:45:20) (*open circle*), SM:PC (4:1) (*filled triangle*), PC:CH:DOPA (35:45:20) (*filled square*), and PC:CH:DPG (35:45:20) (*filled circle*).
Adapted from Chonn A, Semple SC, Cullis PR. Association of blood proteins with large unilamellar liposomes in vivo. *J Biol Chem* 1992;**267**:18759−18765.

Apart from polar headgroup properties, serum protein adsorption depends on membrane cohesion, stability, and ordering, in turn resulting in a dependence on acyl group length, saturation, and symmetry, as well as the presence of cholesterol and other membrane components. For example, Semple et al. demonstrated low overall serum adsorption to cholesterol-containing PC-based vesicles, thereby resulting in low serum protein adsorption.[15] In the absence of cholesterol, on the other hand, serum protein adsorption to the lipid membranes increased drastically as a result of increased membrane insertion (see subsequent discussion on antimicrobial peptides), causing a pronounced shortening of bloodstream circulation time. Analogously, increasing acyl chain length precludes serum protein insertion into the membrane and results in decreased protein adsorption. For long and saturated acyl chains, however, adsorption increases once again, and circulation time decreases, effects associated with membrane defects related to domain formation, resulting in exposure of hydrophobic regions, in turn facilitating protein binding.

An alternative way to reduce serum protein adsorption to phospholipid-based and other drug carriers is through surface modifications with poly(ethylene glycol) (PEG) derivatives, eg, through PEG-conjugated lipids or PEG-containing block copolymers.[16−18] This, in turn, results in a drastically prolonged bloodstream circulation, and in a correspondingly decreased accumulation in RES-related tissues and increased accumulation in non-RES tissues.[6−8] To understand the origin of these observations, it is instructive to consider the effect of PEG-based coatings on serum protein adsorption. As mentioned earlier, protein adsorption generally occurs as a result of several different driving forces, the most important of which are electrostatic, hydrophobic, and van der Waals interactions. Because PEG-based surface coatings are uncharged and hydrophilic, and contain a lot of water, all of these driving forces for

protein adsorption are reduced. In addition, through a repulsive steric interaction, tethered PEG chains efficiently oppose protein adsorption. Together, this results in low serum protein adsorption. Critical to this, however, is that the PEG chain density is sufficiently high to avoid small serum proteins to slip through the PEG layer and to ensure that the steric interactions are sufficient to withstand strongly attractive protein−surface interactions. In addition, for the attractive interactions between the serum proteins and the underlying nanoparticle surface to be fully screened, and the repulsive steric interactions resulting from the PEG chains maximized, the PEG layer needs to be sufficiently thick. Hence, PEG molecular weights in the range 1000−2000 Da are generally required, unless exceedingly high PEG grafting densities are used (eg, as in PEG-modified thiol-based self-assembled monolayers).[16]

4.3 Peptide interactions with phospholipid membranes and surfaces

As a result of accelerating problems with multidrug resistance, there is much current interest in AMPs.[5] Many AMPs have distinct amphiphilic characteristics with a sizeable fraction of hydrophobic residues. Furthermore, AMPs are frequently rich in arginine and lysine and thus carry a net positive charge. Electrostatic interactions therefore facilitate peptide binding to anionic bacterial membranes and lysis of these. In addition, peptide amphiphilicity through the presence of hydrophobic residues is important for many AMPs to adsorb to and disrupt membrane bilayers, particularly at high ionic strength, in the presence of serum, and for low-charged pathogens.[4,5]

Several mechanisms have been proposed for AMP-induced membrane disruption, including the formation of toroidal pores and membrane disruption by detergent-like effects[4,19,20] (Fig. 4.2). For pore formation, the peptide initially adsorbs parallel to the membrane surface. Once a sufficient concentration is reached, it subsequently inserts into the membrane or induces a positive curvature strain in the membrane. Complete membrane disruption and micellization may ultimately result at sufficiently high peptide densities. Alternatively, membrane destabilization may occur through chemical potential gradients, which may drive translocation of peptides initially adsorbed at the outer membrane leaflet. In addition, peptide binding to the polar headgroup region of membranes causes lateral expansion, allowing alkyl chain relaxation and resulting in membrane thinning. Also peptide-induced phase transitions or lipid segregation may cause membrane rupture.

4.3.1 Effects of lipid membrane composition

It is important to the performance of AMPs that they be efficient in killing bacteria and other pathogens but leave human cells unaffected. The basis for such selectivity is that membranes of bacteria and human cells have different compositions. For example, cholesterol is rich (up to about 45%) in human cell membranes, while it is replaced by ergosterol in fungi and absent in bacteria.[21] There are also differences in phospholipid composition. For example, PC and SM are abundant in the outer layer of erythrocytes, which renders these essentially uncharged. In contrast, the outer membrane of bacteria is rich in anionic lipids, such as phosphatidylglycerol (PG), cardiolipin,

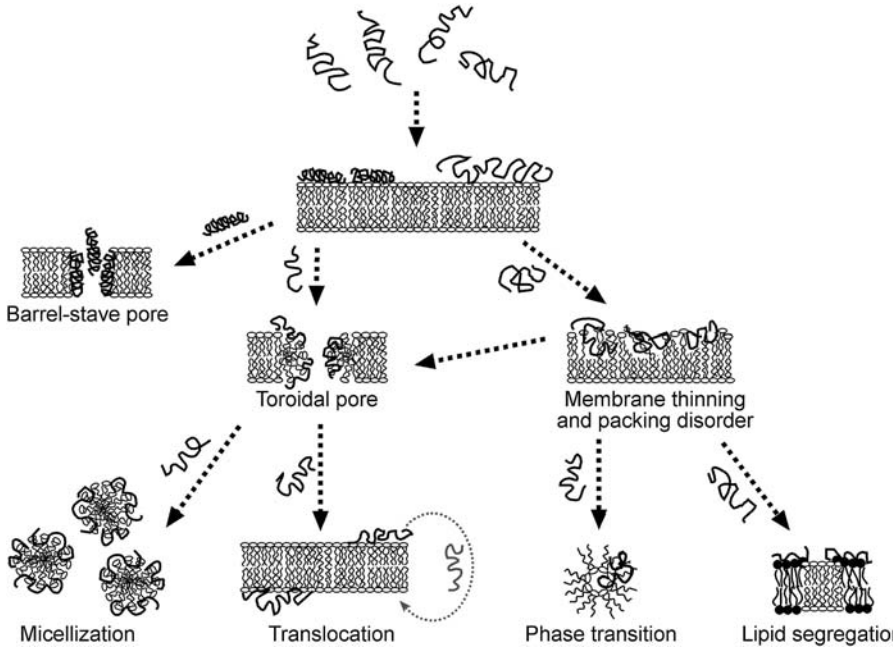

Figure 4.2 Schematic illustration of different mechanisms for AMP-induced membrane destabilization.
Adapted from Strömstedt A, Ringstad L, Schmidtchen A, Malmsten M. Interaction between amphiphilic peptides and phospholipid membranes. *Curr Opin Colloid Interface Sci* 2010;**15**: 467−478.

and lysylPG.[22,23] In addition, the outer membrane of gram-negative bacteria is rich in negatively charged lipopolysaccharide (LPS), whereas gram-positive bacteria contain lipoteichoic acid.[24] Together, these differences in membrane composition provide opportunities for reaching AMP selectivity.

4.3.1.1 Membrane charge

For AMPs displaying selectivity between bacteria and human cells, bacteria-mimicking liposomes formed by anionic phospholipids frequently display larger sensitivity to peptide-induced rupture than liposomes formed by zwitterionic ones (mimicking human cells). For example, the peptides GKH17-WWW and GRR10W4N were both found to be efficient against a range of gram-positive and gram-negative bacteria, but at the same time low toxic to erythrocytes and keratinocytes. In parallel, both peptides potently caused leakage of anionic 1,2-dioleoyl-sn-glycero-3-phosphoethanolamine (DOP)E/DOPG liposomes ($z \approx -35$ mV), whereas peptide-induced liposome leakage was much lower for zwitterionic DOPC liposomes ($z \approx -9$ mV). In parallel, DOPC membranes displayed substantially lower adsorption of these peptides.[25,26] Similarly, Ringstad et al. investigated peptide binding to zwitterionic DOPC-based and anionic DOPC/DOPA-based membranes and reported higher adsorption and enhanced membrane disruption for the anionic membrane, effects observed both for CNY21 variants,[27] repeat consensus peptides,[28] and HKH20.[29] Thus, membrane charge density is an important

determinant for peptide-induced membrane rupture. Having said that, electrostatic interactions can be so strong for highly charged membranes that peptide insertion and membrane destabilization are precluded owing to arrest of the peptide in the polar headgroup region. For example, Strömstedt et al. investigated membrane binding and resulting membrane rupture for bee venom peptide melittin,[30] a peptide displaying reversed selectivity, targeting mammalian cell membranes rather than those of bacteria.[31] In parallel, anionic lipids (eg, PI and PA) provide higher resistance to liposomes against melittin-induced leakage than zwitterionic ones. Quenching of the single melittin tryptophan residue by depth-specific doxyl groups showed that melittin penetrates deeper into the bilayer in the case of zwitterionic PC liposome compared with anionic PA- and PI-containing ones. Together, these findings show that in some special cases, strongly increasing the membrane negative charge may lead to increased membrane tolerance through electrostatic arrest in the headgroup region.

4.3.1.2 Presence of cholesterol and other sterols

Sterols are found in membranes from a wide range of species. For example, ergosterol and lanosterol are present in fungi and protozoa membranes, whereas cholesterol is an abundant membrane component for animals, and bacteria lack sterols altogether.[32] Among sterols, cholesterol is particularly potent in providing mechanical strength to membranes.[33] Because cholesterol condenses phospholipid bilayers, its presence in membranes precludes peptide adsorption and insertion, particularly for peptides containing bulky aromatic groups such as W and F.[34] For example, lower liposome leakage, as well as lower peptide adsorption, for DOPC/cholesterol than for DOPC was demonstrated for GRR10W4N[26] (Fig. 4.3). In addition, this peptide inserts into monolayers and destabilizes liposomes to a much larger extent for ergosterol-containing membranes than for cholesterol-containing ones, analogous to its potent antifungal properties but simultaneously low toxicity against human cells.

4.3.2 Effect of peptide properties

4.3.2.1 Charge

Analogous to lipid headgroup effects discussed earlier, increasing the AMP-positive charge constitutes a way to increase peptide binding to negatively charged lipid membranes. For example, Ringstad et al. found both peptide binding and membrane rupture by CNY21 variants to increase with increasing peptide positive charge, whereas elimination of the positive charge drastically reduced membrane binding, liposome lysis, and antibacterial effects.[27] In addition, replacement of lysine and arginine in $(AKKARA)_4$ and $(ARKAAKKA)_3$ by histidine completely abrogates their antimicrobial activities at neutral pH,[35] ie, above the pKa of histidine ($\approx$6.0), whereas these activities are restored at acidic conditions (pH 5.5). In parallel, peptide binding was significantly enhanced at pH 5.5, and membrane rupture was observed only at this acidic pH. Similar pH dependence was also reported for the histidine-rich peptide histatin 5 and peptides derived from histidine-rich glycoprotein and high-molecular weight kininogen. Makovitzki and Shai investigated the pH dependence of dodecanoic acid-modified peptides of the type LXXLLXXLLXXL, in which X is H, K, or R.[36] Whereas the (permanently charged) K- and R-containing peptides displayed little pH dependence,

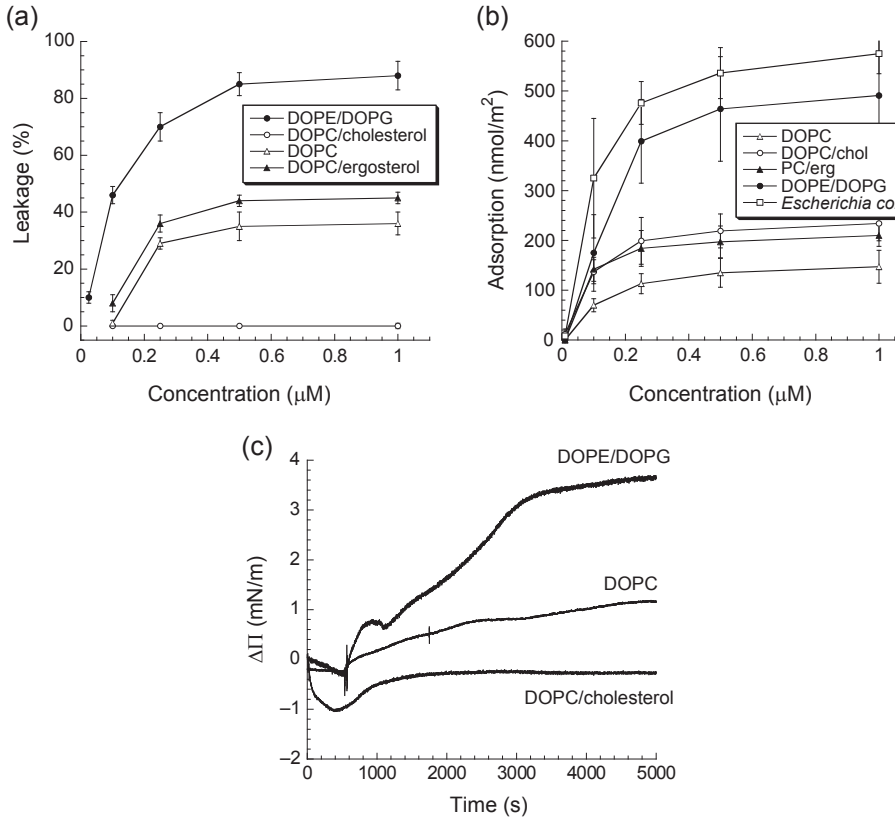

Figure 4.3 (a) Peptide-induced liposome leakage for GRR10W4N at 10 mM Tris, pH 7.4. Shown in (b) and (c) is the adsorption of the same peptide to supported lipid bilayers, as well as the change in surface pressure ($\Delta\Pi$) resulting from insertion of GRR10W4N to zwitterionic DOPC and DOPC/cholesterol, as well as anionic DOPE/DOPG monolayers from Tris buffer, pH 7.4. Adapted from Schmidtchen A, Ringstad L, Kasetty G, Mizuno H, Rutland MW, Malmsten M. Membrane selectivity by W-tagging of antimicrobial peptides. *Biochim Biophys Acta* 2011;**1808**: 1081−1091.

an H-containing one showed pronounced pH dependence, displaying antifungal activity at pH 5.5 but not at pH 7. The H-containing peptide induced liposome leakage at pH 5.5 but not at 7.4, an effect related to higher peptide adsorption at the lower pH.

4.3.2.2 Hydrophobicity

Complementary to increasing peptide positive charge, membrane binding and disruption can be enhanced by increasing peptide hydrophobicity. This approach offers opportunities to lyse and kill pathogens with low electrostatic surface potential, and for applications in which the antimicrobial effect must be retained at high ionic strength.[37] Importantly, however, such increased potency generally comes at the price of decreased selectivity. Because membrane binding of hydrophobic peptides is driven by poor solvency, peptide accumulation is largely insensitive to membrane composition, causing lysis of bacteria and human cell membranes alike. For example,

hydrophobic L/K peptides are even more hemolytic than the bee venom melittin.[34] Thus, increased hydrophobicity can only be used to a limit for boosting peptide potency. Remaining within the regime of modestly increased hydrophobicity, Ringstad et al. demonstrated positive effects of increasing peptide hydrophobicity for the C3a-derived peptide CNY21.[27,38] Thus, substituting the two histidine residues in this peptide with leucines, thereby increasing its hydrophobicity, promoted peptide binding and deeper penetration into the hydrophobic region of DOPC monolayers, in turn resulting in increased membrane disruption and an antimicrobial effect. By comparing electrochemical results for monolayers and bilayers, it was furthermore demonstrated that transmembrane structures do not have a role in membrane destabilization in these systems, but that this instead relies on transient defects in the subnanomolar range.

At the other extreme, acyl conjugation has been used to maximize the antimicrobial effects of AMPs, even at the price of toxicity, for challenging infections.[39] For example, Makovitzki et al. investigated a series of acylated peptides and found a clear correlation between an antibacterial effect and liposome leakage.[36] Investigating related effects for $C_{14}K_n$ peptides, Jia et al. found the adsorption of these peptides to increase with peptide hydrophobicity.[40] Because of their long acyl chains, most lipopeptides are able to insert extensively into lipid membranes of a wide range of compositions. For example, Eeman et al. found fengomycin to display very high expulsion pressure also for cholesterol-containing (mammalian-mimicking) and cholesterol/fatty acid-containing (stratum corneum-mimicking) membranes.[41] Such a lack of selectivity has restricted the use of lipopeptides to local applications and to severe indications for which other antibiotics are ineffective, eg, multiresistant *Pseudomonas aeruginosa* infections in cystic fibrosis.[39]

Alternatively, AMPs can be end-tagged with hydrophobic amino acids to achieve high but selective AMP-induced membrane destabilization. For example, W tagging has been found to promote binding of GKH17 to bacteria and subsequent lysis.[25] In parallel, peptide binding to anionic DOPE/DOPG membranes, as well as liposome leakage, was dramatically enhanced for GKH17-WWW compared with GKH17, also at physiological ionic strength. In contrast, zwitterionic DOPC/cholesterol membranes displayed lower peptide binding and liposome leakage. Similarly, the peptide GRR10W5N displays potent antimicrobial potency but simultaneous low eukaryotic cell toxicity; this is illustrated, for example, by a striking ability to kill bacteria and fungi in blood selectively. Analogously, GRR10W5N displays potent destabilization of DOPE/DOPG, but not DOPC/cholesterol, liposomes.[26] In parallel, ellipsometry showed higher peptide binding to the anionic membranes, whereas monolayer studies showed that cholesterol content and low membrane charge density both reduce membrane insertion in the case of DOPC/cholesterol (Fig. 4.3).

4.3.2.3 Length

As for polyelectrolytes, peptide binding to phospholipid membranes and surfaces is expected to decrease with decreasing peptide length as a result of the increased entropy penalty (per amino acid) on adsorption. For peptides displaying adsorption-induced conformational changes, there is also a decreased tendency to form ordered

(amphiphilic) secondary structures with decreasing peptide length. Therefore, peptide binding, membrane lysis, and antimicrobial effect all decrease with decreasing peptide length, as demonstrated, eg, for $(AKKARA)_n$ and $(ARKAAKKA)_n$ peptides[28] (Fig. 4.4). However, there may also be considerable room for selective truncations without losing activity, in some cases even resulting in improved performance. For example, by judicious truncations, it is possible to truncate LL-37 to less than half its length without losing antimicrobial and several other functions.[42,43] When truncated to become sufficiently short, however, specific membrane-rupturing capacity is eventually lost for all peptides.

4.3.2.4 Secondary structure

The formation of amphiphilic ordered structures (notably α-helices) by some AMPs on membrane binding has been found to correlate to the ability of AMPs to disrupt lipid

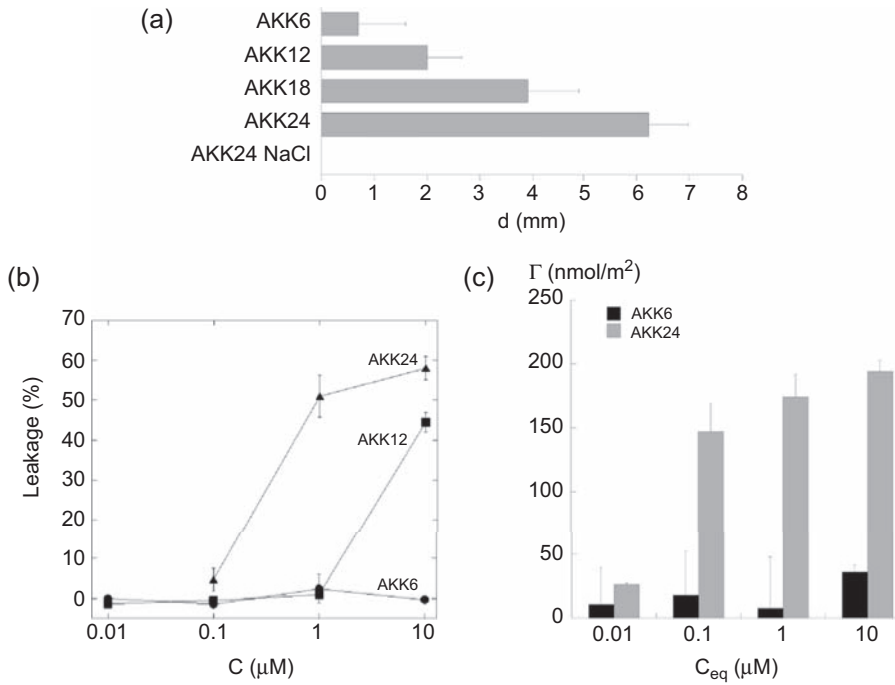

Figure 4.4 (a) Antimicrobial activity of $(AKKARA)_n$ ($1 \leq n \leq 4$) peptides against *Bacillus subtilis* determined by radial diffusion assay (RDA) at a peptide concentration of 100 μM. In RDA, peptides are placed in wells in agar gels containing confluent microbes. On radial diffusion, the peptide will kill bacteria and result in a clearance zone containing disintegrated microbes. Thus, the higher the diameter (d), the more potent the peptide. Also shown is length-dependent, peptide-induced leakage in anionic DOPA-containing liposomes (b) and peptide adsorption to the corresponding lipid membrane (c), all in 10 mM Tris, pH 7.4. Adapted from Ringstad L, Schmidtchen A, Malmsten M. Effect of peptide length on the interaction between consensus peptides and DOPC/DOPA bilayers. *Langmuir* 2006;**22**: 5042−5050.

membranes and kill bacteria.[4,5] A widely investigated peptide undergoing such binding-induced helix induction is LL-37.[44] Challenges with nonnegligible cytotoxicity and susceptibility to proteolytic degradation have fueled research in variants that are proteolytically more stable and/or less toxic than the native peptide. For example, Sigurdadottir et al. found that the truncated 21-mer GKE21 maintains the bactericidal potency of LL-37 but displays lower toxicity.[42] Similar effects were reported for the truncated 17-mer EFK17. The latter peptide forms an essentially perfect amphiphilic helix with all polar/charged residues on one side and all nonpolar/hydrophobic residues on the other.[43] Consequently, helix formation induces amphiphilicity in this peptide. Whereas selected D-enantiomer substitutions rendered the peptide indigestible by proteases, this comes at the cost of suppressed (conformation-dependent) amphiphilicity, resulting in decreased membrane binding and an antimicrobial effect. In contrast, peptide variants proteolytically stabilized by W-substitutions displayed increased antimicrobial effects owing to the increase in peptide amphiphilicity. In parallel, the latter variant displayed increased membrane adsorption and peptide-induced liposome leakage. Also proline substitutions and other means for reducing helicity have been found to reduce peptide interaction with phospholipids membranes and have been correlated with decreased toxicity.[45] As demonstrated for EFK17, however, helix destabilization may ultimately result in elimination of peptide adsorption and membrane lysis for peptides forming strongly amphiphilic helices.

4.3.3 PEGylation

Similar to larger serum proteins, peptide adsorption is dramatically affected by the presence of tethered PEG chains. As with larger proteins, peptide adsorption generally decreases with increasing density of tethered PEG chains. For smaller peptides, however, requirements on reaching high chain densities are generally higher, because these may slip through PEG coatings and adsorb at the underlying surface. For example, in a series of studies, McGuire et al. investigated the effects of PEG-containing block copolymer coatings for surface interactions of nisin.[46,47] For such block copolymers containing a small hydrophobic moiety, nisin binding was effectively suppressed. For block copolymers containing a large hydrophobic block, however, nisin is able to bind to hydrophobic domains in the PEG-modified surface, although with decreased affinity compared with the uncoated surface. Interestingly, the latter depends on the density of tethered PEG chains and is facilitated at intermediate chain densities, possibly a consequence of block copolymer self-assembly. At sufficiently high PEG chain densities, however, nisin adsorption is again suppressed in a density-dependent manner. Furthermore, nisin adsorbed at Pluronic F108 surface coatings at intermediate chain densities retained its antimicrobial effect and was found to be more efficient in this respect than the underlying surface in the presence of serum proteins, an effect resulting from suppressed serum protein adsorption at the PEG-modified surfaces. Likewise PEGylation of AMPs generally reduces peptide adsorption at phospholipid membranes and surfaces, suppressing both its antimicrobial effect and toxicity. For example, Singh et al. investigated the effects of PEGylation on peptide interactions with lipid membranes

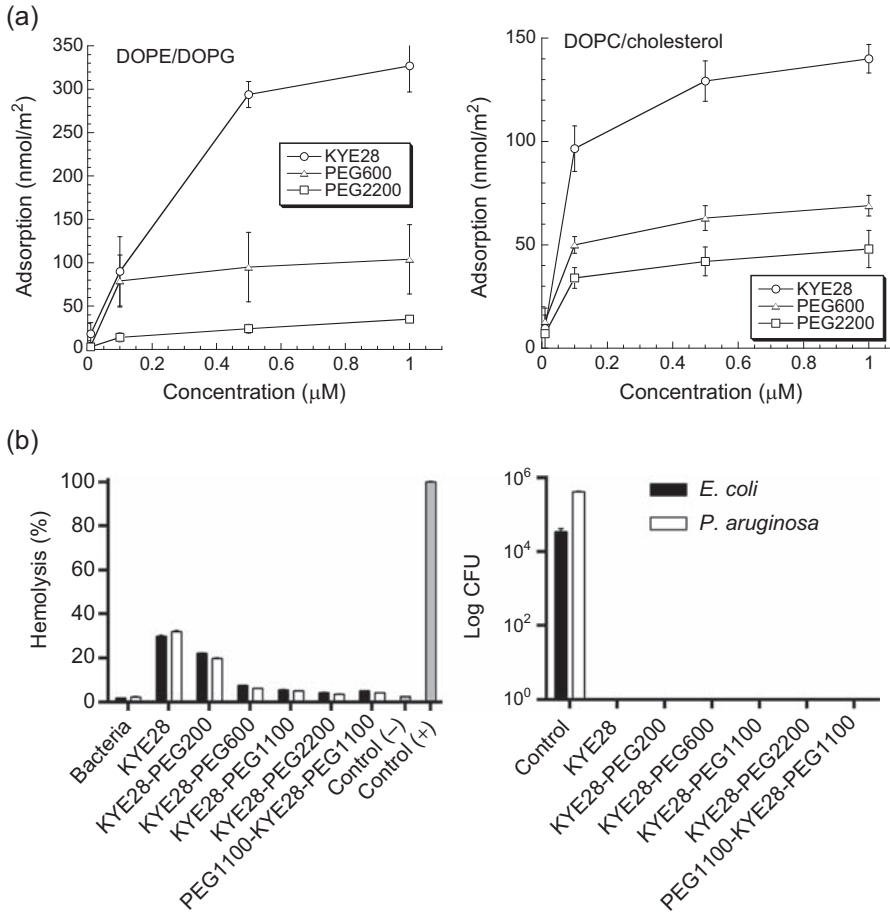

Figure 4.5 (a) Peptide binding to DOPE/DOPG (75/25 mol/mol) or DOPC/cholesterol (60/40 mol/mol) bilayers. Measurements were performed in 10 mM Tris, pH 7.4. (PEGMw refers to KYE28PEGMw throughout.) (b) Combined hemolysis (left) and antibacterial assay (right) for *Escherichia coli* and *Pseudomonas aeruginosa* (both 2×10^8 colony-forming units/mL) added to 50% citrate blood, for the indicated peptides at a concentration of 120 μM. For the PEGylated peptides, the bacterial count was not detectable.
Adapted from Singh S, Papareddy P, Mörgelin M, Schmidtchen A, Malmsten M. Effects of PEGylation on membrane and lipopolysaccharide interactions of host defense peptides. *Biomacromolecules* 2014;**15**:1337−1345.

and LPS for KYE28 and found PEGylation to reduce peptide binding to lipid membranes, an effect that increased with PEG length[48] (Fig. 4.5). The antimicrobial effects of KYE28 were partially lost with increasing PEG length, but hemolysis also strongly suppressed and selectivity improved. Through this, conditions could be identified at which the PEGylated peptide displays simultaneously efficient antimicrobial effects and low hemolysis in blood.

4.4 Phospholipid-mimicking polymers

Because phospholipid self-assemblies are inherently complex, efforts have been made to reach the positive effects of such systems regarding reduced protein adsorption and cell adhesion, with approaches not requiring controlled self-assembly. In particular, phosphorylcholine-containing and related polymers have been investigated as non-fouling or biocompatible surface coatings, in which the polymer is either physically adsorbed at the surface or covalently attached to this.[49] As with phospholipids, such polymer coatings have been found to result in decreased serum protein adsorption, as demonstrated, eg, by Murphy et al.,[50] Ishihara et al.,[51] and Nederberg et al.[52,53] More detailed investigations of the role of the structure of such polymers (charge density, nature of the charged group, interplay between electrostatic and hydrophobic interactions, etc.) and their surface coatings (thickness, adsorbed layer density, functional group density, etc.) for determining protein and peptide adsorption are largely still lacking, however.

4.5 Future trends

As exemplified earlier, lipid composition has a pivotal role for protein/peptide binding to phospholipid membranes and surfaces, as well as its consequences, eg, for bloodstream circulation and tissue distribution of parentally administered, phospholipid-based drug delivery systems, or the function of AMPs. Effects of headgroup charge, acyl chain length, and saturation, as well as the presence of sterols and other functional cosolutes (eg, PEG derivatives), are all becoming increasingly understood, as are the effects of size, charge, hydrophobicity, and secondary structures for protein/peptide interaction with phospholipid membranes and surfaces. Indeed, this has resulted in a couple of substances already either on the market (lipopeptide) or in late clinical trials (AMPs). Similarly, long-circulating PEGylated liposomes have been successfully employed for years as cancer therapeutics. Thus, it is fair to say that simpler aspects of protein/peptide interactions with phospholipid membranes are becoming an increasingly mature research area. Having said that, important issues remain in this context, including detailed molecular mechanisms of membrane translocation and cell internalization of biomacromolecular drugs for cell-penetrating peptides (still poorly understood despite decades of intense research),[54] and factors affecting membrane selectivity between different human cell types. The latter is particularly interesting for anticancer peptides, either killing cancer cells selectively through outer membrane lysis or lysing mitochondria membranes and restoring apoptosis, hence reducing problems with chemoresistance.[55]

Although issues thus remain with simpler aspects of protein/peptide interactions with phospholipid membranes, there has been a clear shift in the past few years to more complex membranes, notably those containing key nonlipid membrane components such as LPS, lipoteichoic acid, and proteoglycans. Protein/peptide interactions with such LPSs are important in various biological contexts, including lipoprotein deposition at proteoglycan-covered endothelial surfaces in atherosclerosis, lectin

functionality, and potential effects for selective attack on cancer cells and other therapeutic targets, and the function of antiinflammatory peptides.

For example, the use of AMPs to combat not only infections but also their consequences for immune responses, inflammation, cytokine generation, coagulation, etc., has attracted considerable interest during the past few years. A striking example in this context is sepsis, which remains the leading cause of death in intensive care units (with 30−40% overall mortality, and about 70% for chronically ill and elderly patients), accounting for 40% of total intensive care unit expenditures.[56] Despite massive efforts from the pharmaceutical industry, there are currently no safe and efficient drugs on the market. The main reason for this is that sepsis is a complex syndrome characterized by the simultaneous occurrence of proinflammatory and antiinflammatory effects, alternatively predominating over time. Here, some AMPs have shown promising effects and therefore have attracted considerable interest. However, AMP antiendotoxic effects are complex, with multiple mechanisms, including direct prevention of LPS binding to LPS-binding protein (a key step in the cascade resulting in nuclear factor-κB generation) through its lipid A epitope, peptide-triggered phagocytosis, and membrane-localized LPS scavenging.[57] Despite emerging understanding of these processes, there is considerable uncertainty regarding the relative importance of these effects and how this may be used in therapeutic peptide design. Indeed, a holistic approach is most likely needed, covering not only effects on cytokines but also less understood effects on complement activation and coagulation.

Another area attracting increasing attention in relation to protein/peptide interactions with phospholipid membranes, and their LPS components in particular, is atherosclerosis and related cardiovascular diseases. Whereas these are complex pathologies involving not only the endothelium but also connective tissue, the initial step of these is binding of lipoproteins to the endothelial membrane, including its proteoglycan components.[58] Consequently, studies of the adsorption of lipoproteins involved in atherosclerosis at either supported endothelial cells or surfaces coated with proteoglycans provide accelerated information on initial atherosclerotic plaque formation. Importantly, correlations have also been found between lipoprotein adsorption and well-known clinical effects of lipoprotein composition and of treatment with antiatherosclerotic drugs, including, eg, lipoprotein profiles and relevant enzyme (superoxide dismutase) levels in individuals, with concentrations of vasodilating substances, and with results obtained on contraction/dilatation of human blood vessels. Considering this, studies of lipoprotein interactions with proteoglycan-containing membranes and surfaces seem to offer biosensor opportunities, eg, for monitoring cardiovascular risk in the general population or as support in the development of novel cardiovascular therapeutics.

In these and other areas, studies of protein/peptide interactions with complex membranes need to build on a foundation of careful biophysical model investigations, but also on progression to increasingly complex systems, including studies on protein/peptide binding, internalization, and trafficking in supported and suspended cells of different types. Such studies, in turn, form the starting point for investigations of pharmacokinetic aspects and for in experiments in vivo. Indeed, translation from

fundamental biophysical studies all the way to the complex in vivo situation is a prerequisite for the development of any novel therapeutic, which ultimately motivates much of the research in the area.

Acknowledgments

This work was financed by the Swedish Research Council.

References

1. Norde W. Adsorption of proteins from solution at the solid-liquid interface. *Adv Colloid Interface Sci* 1984;**25**:267−340.
2. Malmsten M. Formation of adsorbed protein layers. *J Colloid Interface Sci* 1998;**207**: 186−99.
3. Malmsten M, editor. *Biopolymers at interfaces*. New York: Marcel Dekker; 2003.
4. Strömstedt A, Ringstad L, Schmidtchen A, Malmsten M. Interaction between amphiphilic peptides and phospholipid membranes. *Curr Opin Colloid Interface Sci* 2010;**15**: 467−78.
5. Pasupuleti M, Schmidtchen A, Malmsten M. Antimicrobial peptides: key components of the innate immune system. *Crit Rev Biotechnol* 2012;**32**:143−71.
6. Semple SC, Chonn A, Cullis PR. Interactions of liposomes and lipid-based carrier systems with blood proteins: relation to clearance behavior in vivo. *Adv Drug Deliv Rev* 1998;**32**: 3−17.
7. Sahay G, Alakhova DY, Kabanov AV. Endocytosis of nanomedicines. *J Control Release* 2010;**145**:182−95.
8. Malmsten M. In: Malmsten M, editor. *Biopolymers at interfaces*. New York: Marcel Dekker; 2003.
9. Malmsten M, Muller D, Lassen B. Sequential adsorption of human serum albumin (HSA), immunoglobulin G (IgG) and fibrinogen (Fgn) at HMDSO plasma polymer surfaces. *J Colloid Interface Sci* 1997;**193**:88−95.
10. Cedervall T, Lynch I, Lindman S, Berggard T, Thulin E, Nilsson H, et al. Understanding the nanoparticle-protein corona using methods to quantify exchange rates and affinities of proteins for nanoparticles. *Proc Natl Acad Sci USA* 2007;**104**:2050−5.
11. Steinem C, Janshoff A. Multicomponent membranes on solid surfaces: interfaces for protein binding. *Curr Opin Colloid Interface Sci* 2010;**15**:479−88.
12. Malmsten M. Protein adsorption at phospholipid surfaces. *J Colloid Interface Sci* 1995; **172**:106−15.
13. Malmsten M. Ellipsometry studies of protein adsorption at phospholipid surfaces. *J Colloid Interface Sci* 1994;**168**:247−54.
14. Chonn A, Semple SC, Cullis PR. Association of blood proteins with large unilamellar liposomes in vivo. *J Biol Chem* 1992;**267**:18759−65.
15. Semple SC, Chonn A, Cullis PR. Influence of cholesterol on the association of plasma proteins with liposomes. *Biochemistry* 1995;**35**:2521−5.
16. Kingshott P, Griesser HJ. Surfaces that resist bioadhesion. *Curr Opin Solid State Mater Sci* 1999;**4**:403−12.

17. Malmsten M, Emoto K, Van Alstine JM. Effect of chain density on protein adsorption by poly(ethylene glycol) based coatings. *J Colloid Interface Sci* 1998;**202**:507−17.
18. Malmsten M, Van Alstine JM. Adsorption of poly(ethylene glycol) amphiphiles which inhibit protein adsorption. *J Colloid Interface Sci* 1996;**177**:502−12.
19. Huang HW. Molecular mechanism of antimicrobial peptides: the origin of cooperativity. *Biochim Biophys Acta* 2006;**1758**:1292−302.
20. Brogden KA. Antimicrobial peptides: pore formers or metabolic inhibitors in bacteria? *Nat Rev Microbiol* 2005;**3**:238−50.
21. Boesze-Battaglia K, Schimmel RJ. Cell membrane lipid composition and distribution: implications for cell function and lessons learned from photoreceptors and platelets. *J Exp Biol* 1997;**200**:2927−36.
22. Lugtenberg EJJ, Peters R. Distribution of lipids in cytoplasmic and outer membranes of *Escerichia coli* K12. *Biochim Biophys Acta* 1976;**441**:38−47.
23. Haest CW, de Gier J, den Kamp JA, Bartels P, van Deenen LL. Changes in permeability of *Staphylococcus aureus* and derived liposomes with varying lipid composition. *Biochim Biophys Acta* 1972;**255**:720−33.
24. Snyder DS, McIntosh TJ. The lipopolysaccharide barrier: correlation of antibiotic susceptibility with antibiotic permeability and fluorescent probe binding kinetics. *Biochemistry* 2000;**39**:11777−87.
25. Schmidtchen A, Pasupuleti M, Mörgelin M, Davoudi M, Alenfall J, Chalupka A, et al. Boosting antimicrobial peptides by hydrophobic oligopeptide end-tags. *J Biol Chem* 2009; **284**:17584−94.
26. Schmidtchen A, Ringstad L, Kasetty G, Mizuno H, Rutland MW, Malmsten M. Membrane selectivity by W-tagging of antimicrobial peptides. *Biochim Biophys Acta* 2011;**1808**: 1081−91.
27. Ringstad L, Andersson Nordahl E, Schmidtchen A, Malmsten M. Composition effect on peptide interaction with lipids and bacteria: variants of C3a peptide CNY21. *Biophys J* 2007;**92**:87−98.
28. Ringstad L, Schmidtchen A, Malmsten M. Effect of peptide length on the interaction between consensus peptides and DOPC/DOPA bilayers. *Langmuir* 2006;**22**:5042−50.
29. Ringstad L, Kacprzyk L, Schmidtchen A, Malmsten M. Effects of topology, length, and charge on the activity of a kininogen-derived peptide on lipid membranes and bacteria. *Biochim Biophys Acta* 2007;**1768**:715−27.
30. Strömstedt AA, Wessman P, Ringstad L, Edwards K, Malmsten M. Effect of lipid headgroup composition on the interaction between melittin and lipid bilayers. *J Colloid Interface Sci* 2007;**311**:56−69.
31. Raghuraman H, Chattopadhyay A. Melittin: a membrane-active peptide with diverse functions. *Biosci Rep* 2007;**27**:189−223.
32. Henriksen J, Rowat AC, Brief E, Hsueh YW, Thewalt JL, Zuckermann MJ, et al. Universal behavior of membranes with sterols. *Biophys J* 2006;**90**:1639−49.
33. Mouritsen OG, Zuckermann MJ. What's so special about cholesterol? *Lipids* 2004;**39**: 1101−13.
34. Schmidtchen A, Pasupuleti M, Malmsten M. Effect of hydrophobic modifications in antimicrobial peptides. *Adv Colloid Interface Sci* 2014;**205**:265−74.
35. Kacprzyk L, Rydengård V, Mörgelin M, Davoudi M, Pasupuleti M, Malmsten M, et al. Antimicrobial activity of histidine-rich peptides is dependent on acidic conditions. *Biophys Biochim Acta* 2007;**1768**:2667−80.
36. Makovitzki A, Shai Y. pH-dependent antifungal lipopeptides and their plausible mode of action. *Biochemistry* 2005;**44**:9775−84.

37. Nizet V. Antimicrobial peptide resistance mechanisms of human bacterial pathogens. *Curr Issues Mol Biol* 2006;**8**:11−26.
38. Ringstad L, Protopapa E, Lindholm-Sethson B, Schmidtchen A, Nelson A, Malmsten M. An electrochemical study into the interaction between complement-derived peptides and DOPC mono- and bilayers. *Langmuir* 2008;**24**:208−16.
39. Jerala R. Synthetic lipopeptides: a novel class of anti-infectives. *Expert Opin Investig Drugs* 2007;**16**:1159−69.
40. Jia D, Tao K, Wang J, Wang C, Zhao W, Yaseen M, et al. Dynamic adsorption and structure of interfacial bilayers adsorbed from lipopeptide surfactants at the hydrophilic silicon/water interface: effects of the headgroup length. *Langmuir* 2011;**27**:8798−809.
41. Eeman M, Francius G, Dufrene YF, Nott K, Paquot M, Deleu M. Effect of cholesterol and fatty acids on the molecular interactions of fengycin with stratum corneum mimicking lipid monolayers. *Langmuir* 2009;**25**:3029−39.
42. Sigurdadottir T, Andersson P, Davoudi M, Malmsten M, Schmidtchen A, Bodelsson M. In silico identification and biological evaluation of antimicrobial peptides based on human cathelicidin LL-37. *Antimicrob Agents Chemother* 2006;**50**:2983−9.
43. Strömstedt AA, Pasupuleti M, Schmidtchen A, Malmsten M. Evaluation of strategies for improving proteolytic resistance of antimicrobial peptides by using variants of EFK17, an internal segment of LL-37. *Antimicrob Agents Chemother* 2009;**53**:593−602.
44. Durr UH, Sudheendra US, Ramamoorthy A. LL-37, the only human member of the cathelicidin family of antimicrobial peptides. *Biochim Biophys Acta* 2006;**1758**: 1408−25.
45. Andrushchenko VV, Vogel HJ, Prenner EJ. Interactions of tryptophan-rich cathelicidin antimicrobial peptides with model membranes studied by differential scanning calorimetry. *Biochim Biophys Acta* 2007;**1768**:2447−58.
46. Dill JK, Auxier JA, Schilke KF, McGuire J. Quantifying nisin adsorption behavior at pendant PEO layers. *J Colloid Interface Sci* 2013;**395**:300−5.
47. Tai YC, McGuire J, Neff JA. Nisin antimicrobial activity and structural characteristics at hydrophobic surfaces coated with the PEO-PPO-PEO triblock surfactant Pluronic® F108. *J Colloid Interface Sci* 2008;**322**:104−11.
48. Singh S, Papareddy P, Mörgelin M, Schmidtchen A, Malmsten M. Effects of PEGylation on membrane and lipopolysaccharide interactions of host defense peptides. *Biomacromolecules* 2014;**15**:1337−45.
49. Lewis AL. Phosphorylcholine-based polymers and their use in prevention of biofouling. *Colloids Surf B Biointerfaces* 2000;**18**:261−75.
50. Murphy EF, Lu JR, Brewer J, Russel J, Penfold J. The reduced adsorption of proteins at the phosphoryl choline incorporated polymer-water interface. *Langmuir* 1999;**15**:1313−22.
51. Ishihara K, Nomura H, Mihara T, Kurita K, Iwasaki Y, Nakabayashi N. Why do phospholipid polymers reduce protein adsorption? *J Biomed Mater Res* 1998;**39**:323−30.
52. Nederberg F, Watanabe J, Ishihara K, Hilborn J, Bowden J. Biocompatible and biodegradable phosphorylcholine ionomers with reduced protein adsorption and cell adhesion. *J Biomater Sci Polym Ed* 2006;**17**:605−14.
53. Nederberg F, Bowden T, Hilborn J. Synthesis, characterization, and properties of phosphoryl choline functionalized poly ε-caprolactone and charged phospholipid analogues. *Macromolecules* 2004;**37**:954−65.
54. Zorko M, Langel U. Cell-penetrating peptides: mechanism and kinetics of cargo delivery. *Adv Drug Deliv Rev* 2005;**57**:529−45.
55. Gaspar D, Veiga AS, Castanho MARB. From antimicrobial to anticancer peptides. A review. *Front Microbiol* 2013;**4**:1−16.

56. Martin GS, Mannino DM, Moss M. The epidemiology of sepsis in the United States from 1979 to 2000. *N Engl J Med* 2003;**348**:1546−54.
57. Schmidtchen A, Malmsten M. Peptide interactions with bacterial lipopolysaccharides. *Curr Opin Colloid Interface Sci* 2013;**18**:381−92.
58. Siegel G, Malmsten M, Ermilov E. Anionic biopolyelectrolytes of the syndecan/perlecan superfamily: physicochemical properties and medical significance. *Adv Colloid Interface Sci* 2014;**205**:275−318.

This page intentionally left blank

Part Two

Properties of thin films for biomedical applications

This page intentionally left blank

Characterization of thin films for biomedical applications

5

N.S. Murthy, V.B. Damodaran
Rutgers University, New Brunswick, NJ, United States

S.H. Lee, A.S. Hwang, H.-J. Sung
Vanderbilt University, Nashville, TN, United States

5.1 Introduction

Synthetic biomaterials are designed to be biocompatible or biologically acceptable; they are meant to cause no harm to the host, and the material itself is not to be rendered nonfunctional by the host. In addition to this minimal requirement, the surfaces of implantable medical devices are modified to improve the functionality of the materials, such as promoting the osteointegration of orthopedic implants and preventing unfavorable physiological reactions such as thrombosis formation. The biological response of surface coatings is determined by their structure, chemical composition, and functionalities. Changing the surface characteristics is the most obvious way to control cell attachment, proliferation, and differentiation. This can be accomplished by a thin film coating that could be in the form of a layer deposited on the substrate (eg, chemical vapor deposition and Langmuir–Blodgett (LB) film) or in the form of biomolecules adsorbed onto the surface of an implanted device. In addition to these physical means, the surface film can be formed chemically by chemisorption, plasma, or ozone treatments and by radiation such as γ, electron beam, or ion beam. Performance of these surface layers depends highly on their interaction with the host medium, which is initiated and mediated by host proteins adsorbing onto the thin-film surface immediately upon implantation (Anderson, 2001; Latour, 2008; Ratner et al., 1997). For example, hemocompatibility and thrombogenicity of thin-film coatings on medical devices depend largely on proteins adsorbed at the blood–thin-film interface (Gorbet and Sefton, 2004).

Tissue response is determined by a sequence of events that occurs at several different time and length scales. After hydration of the implanted surface, which occurs on a microsecond timescale, small molecules migrate toward the surface in milliseconds, and protein over a timescale of minutes. Subsequent cell attachment that occurs over the adsorbed protein layers determines the long term tissue response of the implanted material. Each of these processes needs to be characterized and understood when designing the surface to elicit the required tissue response. Some features of the surface layer that are typically monitored include macroscopic characteristics such as the thickness and the surface energy of the layer, the hydration state of the surface layer, the structure and conformation of

Thin Film Coatings for Biomaterials and Biomedical Applications. http://dx.doi.org/10.1016/B978-1-78242-453-6.00005-5

the molecules in the surface layer, their chemical composition, and the nature of the biological interactions between the surface layer and the surrounding biological environment. The techniques described in this chapter will span the timescale on the scale of protein and cell attachment, but not the water or the ions interacting with the substrate.

Areas in which such measurements are useful are tissue scaffolds, regenerative medicine, drug discovery, biosensors, and biofouling. For the most part, study of the adsorption of proteins is amenable to detailed investigation and is often used as a proxy to predict cell response to substrates. In vitro measurements do not always correlate with in vivo results. Nevertheless, an understanding of the fundamental biophysical chemistry of the protein adsorption can provide useful insight into tissue response. These measurements are useful in applications such as drug discovery, food science, and generally any material development effort.

The topics discussed in this chapter are divided into three sections: physical characterization, chemical analysis, and the characterization of biointerfacial events. In each section, the principles behind the most commonly used characterization methods are presented, the techniques are described, and typical measurements are illustrated with examples. The emphasis is on methods to quantify and characterize protein adsorption on thin films, which precedes host biological responses.

5.2 Physical characterization

Physical characteristics of surface coatings that influence the performance of a biomedical device include the thickness and adhesivity of the coating, surface topography, mechanical characteristics, and phase compositions or inhomogeneity of the surface layers. The thickness of surface layers, a primary consideration in studying the adsorption of cells and proteins onto substrates, can be studied by one of four main techniques: ellipsometry (ELM), surface plasmon resonance (SPR), quartz crystal microbalance (QCM), and X-ray reflectivity (XRR). In some instance, X-ray photoelectron spectroscopy (XPS) and time-of-flight mass spectrometry (ToF MS) can also be used to obtain the film thickness (see Section 5.3.1). X-ray scattering provides additional information about the structural features of the adsorbed layers. These measurements can be used to understand the mechanism and strength of interactions between host molecules and the substrate, as well how much and how quickly they are adsorbed.

5.2.1 Ellipsometry

ELM is an optical method widely used to measure the thickness and surface roughness of ultrathin films in the semiconductor industry. It measures changes in the polarization of a light beam reflected from a surface, which can be related to the characteristics of the surface layer, such as an adsorbed protein layer or a layer of cells attached to a surface (Elwing, 1998; Theeten, 1981; Tompkins and Irene, 2005). When a linearly

polarized light is incident on a surface, the surface will alter the intensity of the E-field perpendicular and parallel to the plane of incidence (labelled as s- and p- polarizations, respectively). As a result, the polarization state will change, and this change is measured by the relative attenuation of the *p*- and *s*-polarized light, r_p and r_s, respectively. This is expressed in Eq. [5.1] in terms of the ratio of the magnitude ($\tan \psi$) and phase shift (Δ), as

$$\frac{r_p}{r_s} = \tan(\psi)e^{i\Delta} \qquad [5.1]$$

This change in the polarization state of the reflected light can be graphically expressed as elliptical polarization. ELM is an indirect method because in most cases an iterative procedure is used to calculate the optical constants and the thickness of the films to fit the observed $\tan \psi$ and Δ values at various wavelengths.

A schematic of an ELM instrument is shown in Fig. 5.1(a). A beam of laser light is directed onto the sample surface and the reflected light is captured by a detector. Data are collected at several angles of incidence. A typical ellipsometric result is illustrated in Fig. 5.1(b); the data were obtained from mussel adhesive protein (Höök et al., 2001), which is a glue (*Mytilus edulis* foot protein (*Mefp*-1)) that mussels use to anchor to a solid surface, such as the hull of a ship. It is made of repeating units of almost identical decapeptides that have an open flexible conformation in solution. Cross-linking using, for instance, sodium periodate ($NaIO_4$) can dramatically change this conformation as well as the mechanical properties of the protein. The data show that as the proteins are attached to the surface, there is an increase in mass. Upon rinsing and cross-linking, there is no change or perhaps only a small decrease in mass. As will be discussed in Section 5.2.3 on QCM-D, this mass is the dry mass of the protein and contains no information about the coupled water.

The advantages of ELM are that it is a simple technique sensitive to small changes in mass, thickness, and surface roughness (Elwing, 1998; Theeten, 1981; Tompkins and Irene, 2005), and it can be used in real time and in situ. Because a ratio of two attenuations, r_p and r_s, are measured, it is a precise measurement independent of source fluctuations. As a contact-free, nondestructive method, ELM also allows for real-time data collection to study the kinetics of protein binding. Disadvantages are that the technique requires thick samples with flat and reflective surfaces. Polymers with low refractive indices that cannot be tested in this modality are spin-coated onto a suitable substrate for ELM measurements (Gölander and Kiss, 1988). Details of the material characteristics that can be derived depend on the model used to interpret the data. Therefore, the choice of the appropriate models and the parameters for protein adsorption measurement, such as the refractive indices and extinction coefficients of proteins and buffers (Mora et al., 2009; Nilsson and Nilsson, 1982; Unsworth et al., 2005), becomes critical. Although samples are label-free, sample preparation can be tedious and needs to be done with special care.

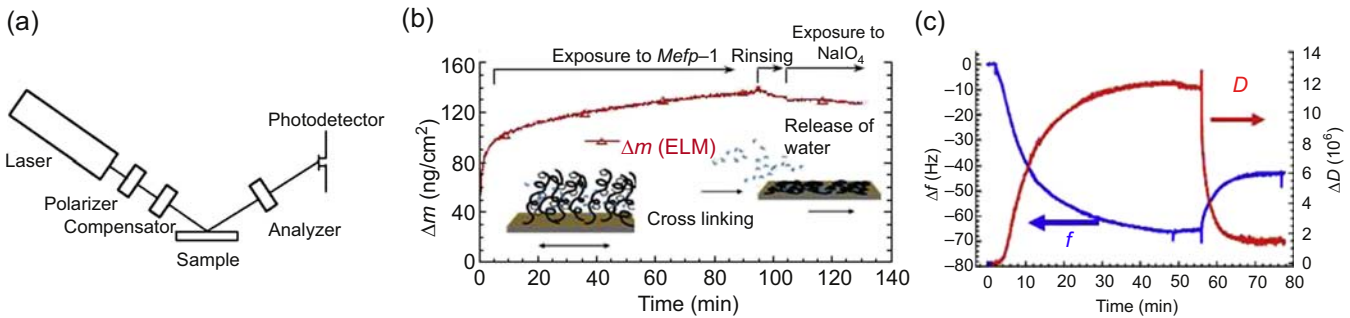

Figure 5.1 (a) Schematic of instrumentation used in ellipsometry. (b) Ellipsometry data plotted as adsorbed mass versus time for exposure of methyl-terminated surface to a buffer solution containing 25 mg/mL *Mefp*-1 in 0.1 M acetate buffer (0.75 M NaCl, pH 5.5) followed by exchange of protein solution for a pure buffer solution, which interrupts exposure of the surface to the protein solution. The adsorption of *Mefp*-1 was subsequently followed by addition of the same buffer solution containing 1 mM $NaIO_4$. (Reproduced with permission from QCM-D Basic Training Course, © 2007 Biolin Scientific.) (c) QCM data in the form of changes in the frequency (*blue curve*) and dissipation (*red curve*) for the third harmonic versus time for *Mefp*-1 adsorption and subsequent rinsing and cross-linking using $NaIO_4$ (Höök et al., 2001). (Reproduced with permission from QCM-D Basic Training Course, © 2007 Biolin Scientific.)

5.2.2 Surface plasmon resonance

Oscillations in the electron cloud in a lattice of positive charges that occur in some metals are called plasma oscillations. Collective oscillations of this electron cloud create a plasma wave, which when quantized is referred to as a plasmon. Surface plasmons occur at the interfaces between a metal and a dielectric such as water or buffer or air. Because as a whole, the surface is neutral, the electron oscillations create compensating oscillations of positive charges at the surface. The periodicities of these oscillations are on the order of 1000−5000 Å, and therefore can absorb visible light. Consider a beam of light that is incident on a glass surface, usually the bottom of a prism, at such an angle so that light undergoes total internal reflection. Not all of the other energy is reflected at the surface and a wave (evanescent wave) of decreasing intensity propagates into the surface layer. If the wavelength of this light is equal to that of the plasma waves at the interface, there is a resonance between the evanescent wave and the plasmon. As a result, at this particular angle the intensity of the light wave is reduced. In SPR, resonance enhancement is achieved by evaporating a thin metal (gold or silver) layer at the base of the prism. At the metal−liquid interface, there is a change in the refractive index (n) that changes the intensity and angle of the reflected light. The changes in intensity as a function of the incident angle are monitored using a photodiode array. As the surface layer changes, it changes n, causing SPR to occur at a different angle. This shift in the angle corresponds to the change in the n, or the change in the thickness (Brockman et al., 2000). For SPR to occur, the incident light has to be p-polarized, ie, the E-vector has to be in the incident plane. In practice, a flow cell is used on the undersurface of the prism.

A schematic of an SPR instrument is shown in Fig. 5.2(a) (Giebel et al., 1999). Also shown in this figure is an SPR spectrum, which is a record of the reflected light intensity versus the angle of incidence. In the case of plasmon resonance, a dip in the reflected spectrum is observed. When the evanescent field is altered by adding a liquid or a protein layer, the angle at which the SPR occurs shifts to larger angles, from θ_1 to θ_2. The shift in the position of the peak that occurs with an increase in the thickness of the film can be used to monitor the deposition. By calibrating the magnitude of the change with some other technique, it is possible to ascertain the thickness of the adsorbed protein layer, as shown in Fig. 5.2(b) for bovine serum albumin (BSA), fibrinogen (FIB), and immunoglobulin G (IgG) (Anand et al., 2010). It is also possible to simulate the shapes of the resonance curves shown in Fig. 5.2(a) and obtain the thickness by comparing the simulated data with the observed data. The SPR signal also depends on the distance, so that it can be used as a microscope.

Many of the comments made with respect to ELM apply to SPR as well. Another advantage of SPR is that because a cell membrane has different components with different n, the kinetics of cell membrane formation in the form of a thin film can be studied.

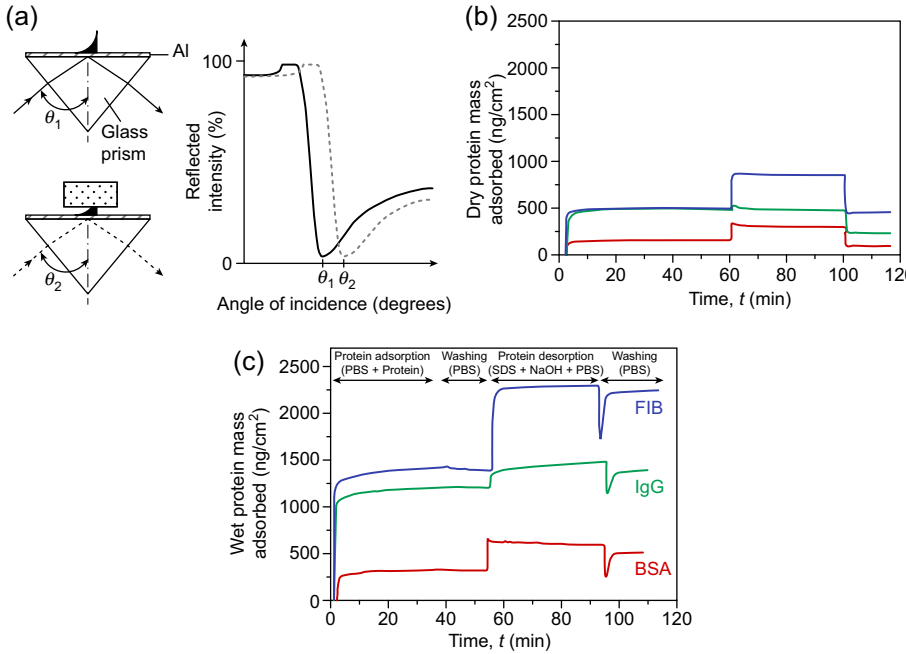

Figure 5.2 (a) Schematic of SPR instrumentation. (Reproduced with permission from Giebel, K.F., Bechinger, C., Herminghaus, S., Riedel, M., Leiderer, P., Weiland, U., Bastmeyer, M., 1999. Imaging of cell/substrate contacts of living cells with surface plasmon resonance microscopy. Biophys. J. 76, 509–516, © 1999 Elsevier.) (b) Dry mass of protein adsorbed onto a gold substrate as a function of time as measured by SPR (lowest, BSA; intermediate, IgG; highest, FIB) (Reproduced with permission from Anand, G., Zhang, F., Linhardt, R.J., Belfort, G., 2010. Protein-associated water and secondary structure effect removal of blood proteins from metallic substrates. Langmuir 27, 1830–1836, © 2011 American Chemical Society.) (c) Mass of proteins adsorbed versus time on a gold substrate measured by QCM-D. Protein adsorption period from 0 to 40 min, washing with PBS buffer for 40–55 min, cleaning with NaOH plus SDS at pH 11 for 55–95 min, and washing with PBS for 95–110 min at pH 7.40. (Reproduced with permission from Anand, G., Zhang, F., Linhardt, R.J., Belfort, G., 2010. Protein-associated water and secondary structure effect removal of blood proteins from metallic substrates. Langmuir 27, 1830–1836, © 2011 American Chemical Society.)

5.2.3 Quartz crystal microbalance

QCM is essentially an extremely sensitive balance that can measure changes in the mass of micrograms of films deposited onto a substrate with nanogram sensitivity (Marx, 2003; Rodahl et al., 1995; Reviakine et al., 2011). The mass change can be followed in real time, for example, as the protein is being adsorbed onto the substrate over which the medium is flowed. Adsorption of protein can be monitored at sub-microgram amounts, along with the binding kinetics and the rigidity of the protein layer. In addition by monitoring dissipation, viscous properties of the protein layer can be determined.

Measurement relies on the piezoelectric properties of quartz (Fig. 5.3). The quartz crystal that is used is cut so that it undergoes shear deformation when external electric voltage is applied (Fig. 5.3(a)). The resonant frequency of this deformation, typically 5 MHz, depends on the mass of the crystal (Fig. 5.3(b)). The change in the frequency (Δf) resulting from a change in the mass of the crystal (Δm) is given by the Sauerbrey equation (Eq. [5.2]):

$$\Delta f = -C \cdot \Delta m \qquad [5.2]$$

where C is the mass sensitivity of the crystal ($C = 17.7$ ng/cm^2 s). This equation assumes that the adsorbed layer is rigid. If the adsorbed mass is not rigid, the decay in the oscillations that occurs once the excitation is turned off (Fig. 5.3(c)) can be used to calculate a dissipation factor, D; D is the ratio of the energy lost per oscillation to the energy stored in the system that can be related to the viscosity (η) and the shear modulus (μ) of the adsorbed layer. Thus, QCM can measure both the areal mass density $\Delta m/A$ of the adsorbed layer and the viscoelastic properties of the film deposited onto the crystal if $\Delta D > 10\%\ \Delta f$).

In a typical experiment, the decay characteristics of several overtones are measured, usually up to 13. The instruments pings sequentially at fundamental thirds, fifths, and on up to thirteen harmonics, and the output of the frequency shift and the dissipation at each harmonic as a function of time. All the 13 measurements are repeated in about

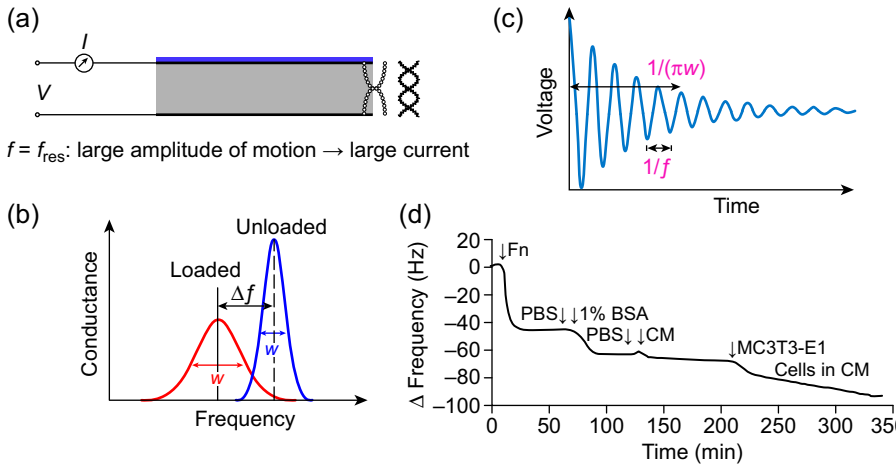

Figure 5.3 (a) Principle of QCM instrumentation. (b) Shift in resonance owing to increased mass. (c) Decay of signal used to measure the dissipation component. (d) Plot of change in frequency (drop in frequency corresponding to an increase in mass) in a sequence of adsorption events ending with the attachment of MC3T3-E1 cells onto gold sensors. The sequence as shown in the figure is fibronectin (Fn), PBS wash (PBS), BSA (1% BSA), PBS wash (PBS), cell media (CM), and the cells (MC3T3-E1 Cells in CM). (CM, complete medium or minimal essential medium-alpha supplemented with 10% fetal bovine serum). (Reproduced with permission from Felgueiras, H.P., Sommerfeld, S.D., Murthy, N.S., Kohn, J., Migonney, V., 2014. Poly(NaSS) functionalization modulates the conformation of fibronectin and collagen type I to enhance osteoblastic cell attachment onto Ti6Al4V. Langmuir 30 (31), 9477−9483.)

~0.2 s. Only the odd harmonics are observed because when the crystal oscillates, the node at the midplane of the crystal and the antinodes are at the surface.

Fig. 5.3(d) shows the change in frequency at various stages of adsorption of proteins and cells (Felgueiras et al., 2014). These frequency shifts can be converted into a mass change using the Sauerbrey Eq. (5.2) and if the density of the deposited layer is known, they can be converted into thicknesses. The results show that the formation of a thin layer of fibronectin (Fn) and the BSA that follows Fn covers the area not covered by Fn. BSA serves to block the adsorption of additional proteins that are present in the culture medium used to deposit cells onto the surface. The eventual goal of this experiment was to follow the formation of the layer of MC3T3 cells on a Fn-coated substrate.

To interpret these data fully, it is necessary to model the frequency and dissipation plots using an appropriate model. The Voigt model is generally used (Voinova et al., 1999). In this model, the elastic component of the coating is represented by a spring, and the viscous component by a dash pot. Modeling consists of calculating the frequency and dissipation curves for at least two overtones, refining the parameters until the results are meaningful, and reproducing the observed data. Alternate models are also being investigated (Eisele et al., 2012).

QCM is extremely sensitive and accurate. Data can be collected in real time to follow the kinetics of adsorption, reaction, and film growth. In addition to measuring the mass, the technique can also measure the mechanical properties, eg, changes in the stiffness and viscosity of the material, in real time. However, these viscoelastic effects can complicate interpretation of the data. Attachment of cells and the formation of biofilms can also be monitored. Drawbacks are that the measurement can be time-consuming. Automation using robots may be necessary to increase the otherwise low throughput.

Comparison of different techniques: Fig. 5.1(b) and (c) show the ELM and QCM data, respectively, during the adsorption of the protein onto a hydrophobic surface, and subsequent cross-linking using sodium per iodate, as discussed in Section 5.2.1. In the QCM data, the large decrease in frequency when the polymer attached to the substrate resulted from to the expected increase in mass that occurs during this step. However, the frequency increases upon cross-linking, which suggests a large decrease in mass compared with a small decrease seen in ELM. This discrepancy between QCM and ELM results can be interpreted as follows. The film that forms when the protein is adsorbed onto the surface contains a significant amount of water. When the film is cross-linked with sodium periodate, some of this water is expelled from the film; therefore, the total mass as well as the thickness decreases. Sodium periodate does not bind significantly to the protein film. Calculations show that 91% of the coupled mass before cross-linking and 82% after cross-linking result from water. Cross-linking radically increases the shear modulus and shear viscosity. The film becomes rigid and dissipation decreases. These effects on the mechanical properties are not captured by ELM or by SPR.

Fig. 5.2 (b) and (c) shows adsorption−desorption of the same proteins, BSA, IgG, and FIB, by SPR and QCM, respectively, as discussed in Section 5.2.2. The three steps in the figure correspond to the adsorption of proteins and washing the unbound protein,

cleaning with a detergent (sodium dodecyl sulfate (SDS)), and rinsing with phosphate-buffered saline (PBS). As in the case of ELM, there are differences between QCM and SPR data. In particular, upon washing with the detergent and PBS, all proteins show an increase in mass in QCM. However, the SPR plot shows a decrease in mass, which is least in FIB and most in IgG. This decrease in SPR reflects the different percentages of the proteins that are removed with the SDS−PBS wash. The increase in QCM seen after the SDS−PBS wash is the result of the adsorbed water, which depends on the protein.

The conclusion from these comparisons is that QCM differs from the other two techniques because whereas ELM and SPR measure changes in dry mass, QCM measures changes in the hydrated mass and viscoelastic properties. Specifically, ELM and SPR do not measure the coupled water because the changes in n due to coupled and free water are not much different. However, it affects the viscoelastic properties of the surface, and thus the QCM signal.

The advantage of ELM, SPR, and QCM, and the XRR technique described in Section 5.2.4 over other techniques such as XPS and fluorescence microscopy is that they require no labeling and measure in real time. In all of these instances, a preprepared surface can be used to immobilize different types of molecules. In all of these techniques, with the exception of QCM and rigid surface layers, some modeling is required to simulate the observed data before parameters such as sample thickness can be obtained.

5.2.4 Structural analysis by X-ray measurements

Whereas the technique described thus far can provide the thickness-related characteristics of the coatings, the X-ray scattering methods discussed in this section can provide information about density distribution, surface roughness, and the atomic structure in thin films (Birkholz, 2006). These measurements can also be performed with neutrons instead of X-rays, but this will not be discussed here. In an X-ray experiment, the sample is exposed to a collimated beam of X-rays, and intensity scattered by the sample, which is measured as a function of the scattering angle, 2θ, is plotted as a function of the scattering vector, q, where $q = (4\pi \sin\theta)/\lambda$, in which λ is the wavelength of the X-ray radiation. Two scattering techniques will be discussed in this section. In XRR, the intensity distribution of the specularly reflected X-rays is analyzed to study surface roughness and electron density distributions in the surface in addition to the layer thickness. In grazing incidence diffraction (GID), scattering intensity from the surface layers is enhanced relative to the substrate. In GID, the X-rays are incident on the surface at a very shallow angle to attenuate the scattering signal from the underlying structures. These experiments are typically done at a synchrotron source, although in-house measurements are possible.

Reflectivity: When an X-ray beam is incident from air onto a solid surface, because the X-ray refractive index of solids is less than that of air, X-rays are reflected back into air by total internal reflection. Because of the small difference in the refractive indices of solids and air, the critical angle at which total internal reflection occurs is very small, $\sim 0.1^\circ$. In XRR, the intensity profile of this reflected beam is measured to study the

characteristics of the films deposited onto substrates (Gibaud and Hazra, 2000). When such a film is exposed to a highly collimated beam of X-rays below the critical angle, the X-rays reflected from the bottom of the film (top of the substrate) and the top of the film interfere at the detector (Fig. 5.4(a)). As the angles of incidence and reflection are systematically changed, there is a sequence of constructive and destructive interference events. As a result, the intensity shows periodic oscillations. These changes in the reflected intensity are used to characterize the surface film.

Fig. 5.4(b) shows typical reflectivity data from a thin polymer film on an aqueous surface (Wang et al., 2013). A thick poly(D,L-lactic acid) (PDLLA) film that is formed at higher pressures (21 mN/m) causes multiple oscillations. These oscillations are absent in the diffuse polymer layer at lower pressures (15 mN/m). The spacing between ripples corresponds to the thickness of the layer. The rate of fall of the overall profile is determined by the surface roughness, and the height of the ripples depends on the density contrast between the substrate and the deposited film. The total XRR curve can also be used to model the density variation across the depth. This is shown by the electron density distributions derived from the data (Fig. 5.4(c)).

Grazing incidence diffraction: When the coating is from an inorganic material such as bioceramics (eg, hydroxyapatite, tricalcium phosphate, and bioglass) (Dorozhkin, 2012) and metal coating (eg, TiN) (Paschoal et al., 2003), their atomic structural data

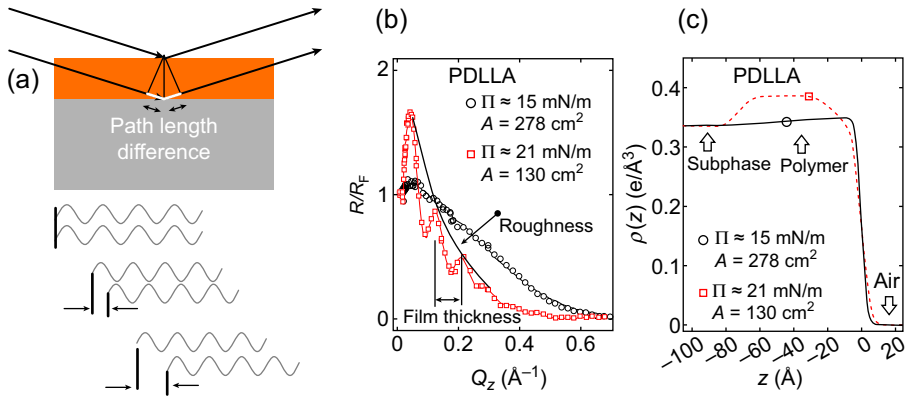

Figure 5.4 (a) The scattering geometry with incoming and reflected X-rays. The wave forms show the phase-angle between the waves reflected from the top and the bottom surface of the deposited film as the path difference between the incident and the reflected angles is increased. The top and the bottom pair show constructive interference, while the middle pair shows destructive interference. (b) X-ray measurements of PDLLA polymer film on the aqueous surface at different surface pressures and with different amounts of spread, as indicated in the figure. Data are presented in the form of R/R_F versus q. (Reproduced with permission from Wang, W., Murthy, N.S., Kuzmenko, I., Anderson, N.A., Vaknin, D., 2013. Structure of biodegradable films at aqueous surfaces: X-ray diffraction and spectroscopy studies of polyactides and tyrosine-derived polycarbonates. Langmuir 29, 11420−11430.) (c) The electron density profile of PDLLA polymer film generated by best-fit parameters to the data shown in Figure (b). (Reproduced with permission from Wang, W., Murthy, N.S., Kuzmenko, I., Anderson, N.A., Vaknin, D., 2013. Structure of biodegradable films at aqueous surfaces: X-ray diffraction and spectroscopy studies of polyactides and tyrosine-derived polycarbonates. Langmuir 29, 11420−11430.)

can be derived from the diffraction pattern obtained from the widely used Bragg–Brentano ($\theta-2\theta$) mode. When the coating is not a strong scatterer, either because it is extremely thin or because it is an organic coating, in the commonly used diffraction geometry, the signal from the coating will be swamped by the scattering from the substrate. In such instances, GID can be used to enhance the surface contribution. Such a diffraction pattern is similar to the powder diffraction pattern obtained from the bulk materials. An example is shown in Fig. 5.5(a) (Ueda et al., 2007). Such patterns are useful for identifying compounds using standard ICDD databases (Icdd, 2014). The atomic structure can also be obtained from such powder diffraction patterns by methods such as Rietveld refinement (Izumi and Young, 1993; Wilson et al., 1999).

Fig. 5.5(b) shows GID data corresponding to the XRR experiment shown in Fig. 5.4(b). These data were obtained from PDLLA film spread on an aqueous surface (Wang et al., 2013). The large q values in these figures compared with Fig. 5.4(b) show that these are wide-angle X-ray scattering (WAXS) scans. These WAXS data reveal the molecular arrangement of the polymer chains in the thin film. At low pressure, the signal from the polymer is weak, consistent with the diffuse layer seen in XRR data. At high pressure, there is strong scattering from the polymer, which is again consistent with the ~80-nm film seen in the XRR data. These WAXS data are consistent with those seen in bulk films, with some small differences.

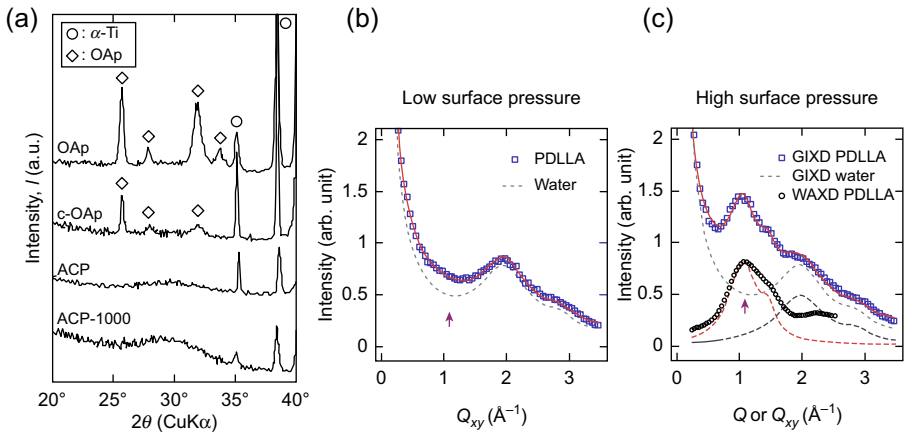

Figure 5.5 (a) XRD patterns of calcium phosphate films on titanium plate. (Reproduced with permission from Ueda, K., Narushima, T., Goto, T., Katsube, T., Nakagawa, H., Kawamura, H., Taira, M., 2007. Evaluation of calcium phosphate coating films on titanium fabricated using RF magnetron sputtering. Mater. Trans. 48, 307–312.), © 2007 The Japan Institute of Metals and Materials. (b) Grazing incidence diffraction data from PDLLA polymer film spread on an aqueous surface under low surface pressure. (Reproduced with permission from Wang, W., Murthy, N.S., Kuzmenko, I., Anderson, N.A., Vaknin, D., 2013. Structure of biodegradable films at aqueous surfaces: X-ray diffraction and spectroscopy studies of polyactides and tyrosine-derived polycarbonates. Langmuir 29, 11420–11430.) (c) Grazing incidence diffraction data from PDLLA polymer film spread on an aqueous surface under high surface pressure. (Reproduced with permission from Wang, W., Murthy, N.S., Kuzmenko, I., Anderson, N.A., Vaknin, D., 2013. Structure of biodegradable films at aqueous surfaces: X-ray diffraction and spectroscopy studies of polyactides and tyrosine-derived polycarbonates. Langmuir 29, 11420–11430.)

5.2.5 Surface energy and morphology

Two other characteristics that are relevant to an understanding of surface coatings are morphology changes in surface energy as a result of surface coating. These methods are not specific to thin-film coating and are described in detail in books and reviews that deal with a characterization of surfaces in general (Williams, 2010). Therefore, only a few key points will be summarized below.

Several microscopic techniques need to be employed to characterize the surface of coatings at different length scales. These include optical microscopy (millimeter to micrometer), scanning electron microscopy ($\sim$0.1 μm), and atomic force microscopy (AFM) (nanometer). AFM has the further advantage of quantitative mapping of surface roughness at atomic resolutions. Surface roughness can also be inferred from XRR, which provides the same information as an AFM-like technique, but with one important difference: XRR provides details about surface features averaged over a large area (order of square centimeters), whereas the microscopic technique provides information over an area on the order square micrometers that is actually being seen in the microscope.

Another key parameter that characterizes film coatings is the surface energy. This is usually done by contact angle measurements.

5.3 Chemical characterization

The performance of thin films is determined by the physical attributes described in Section 5.2, as well as by the chemical composition of the film. These include the elemental composition, the chemical species, and the structure of the molecules that are present in the thin film. These attributes can be determined by the methods described in this section.

5.3.1 X-ray photoelectron spectroscopy

XPS, also known as electron microscopy for chemical analysis, is a powerful tool for elemental detection, chemical state identification, and quantification of various atomic species at the surface (Devries, 1998; Fadley, 2010). XPS uses photoelectrons that are emitted after the absorption of X-rays (Fig. 5.6). In XPS, samples are irradiated with a monochromatic beam of X-rays with a known energy (usually Mg Kα (1253.5 eV) or Al Kα (1486.6 eV)), which penetrates deeply into the sample; the depth varies from micrometers to millimeters, resulting in the emission of electrons. Because electrons are readily absorbed, only the electrons emitted from the few top atomic layers escape the material and are detected. Consequently, the information depth of XPS is less than 10 nm, depending on the nature of the material under evaluation and the kinetic energy (E_k) of the emitted electrons. The kinetic energy of the emitted electrons will be

$$E_k = h\nu - E_B - \phi_{spec} \quad [5.3]$$

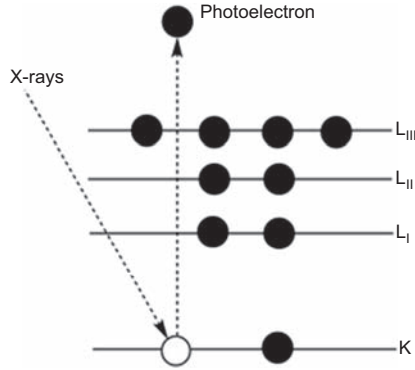

Figure 5.6 Schematic illustration of XPS principle.

where $h\nu$ is the energy of interacting photon, E_B is the binding energy of electron in the atomic orbital from which it originates, and ϕ_{spec} is the work function of the spectrometer. Binding energy can be interpreted as the ionization energy of a particular atom, and hence it is characteristic of the atom in a particular orbital with a specific bonding environment. This results in a distinctive energy distribution, peak position, and intensity that are characteristic of a particular atom (except hydrogen and helium), which enable its identification and quantification with a sensitivity of up to 0.1 atm%.

Typically, low-resolution survey scans are used to identify the surface elemental composition and high-resolution scans evaluate the chemical environment of a particular atomic species. In high-resolution scans, core level peaks show a characteristic shift in binding energies (ranging from 0.2 eV upward), depending on the specific environment of the functional groups associated with the emitting element and thereby enabling identification of various functional moieties (Ratner and Castner, 2009). Although XPS is generally considered to be a nondestructive analytical technique, overexposure to X-rays can result in an altered surface chemistry (Ratner, 1995). Coexistence of certain functional groups can make it difficult to identify them directly and quantify them during normal XPS analysis. For example, identification and estimation of amine on an aminated surface is often tedious when it is present with other nitrogen-containing functional groups with similar binding energies (Oran et al., 2006; Girard-Lauriault et al., 2008). In such cases, specific identification and quantification of the functional groups can be achieved using chemical derivatization XPS (Batich, 1988).

In addition to its ability to quantify both elemental and chemical state information, XPS can be used to obtain additional film features such as thickness, growth mechanisms, and interface properties with relative simplicity from a single analysis (Hartmann and Lamb, 1997). Assuming the overlayer thin film is homogeneous in nature, the thickness (t) of the film can be calculated from the peak intensity of a particular peak from the thin film (I_f) and the substrate (I_s^0), usually from a high-resolution

scan, using a standard uniform overlayer model (Petrovykh et al., 2003; Popat et al., 2004), which is given by Eq. [5.4]:

$$I_f = I_s^0 \exp\left(-\frac{t}{E_L}\right) \quad [5.4]$$

where E_L is the electron attenuation length of the peak under evaluation. In general, the E_L of a particular peak is characteristic of its electron energy (Damodaran et al., 2010b); this overlayer model provides greater accuracy in determining film thickness in the nanometer range, provided the film thickness is less than nearly three times the mean escape depth (λ) (Cumpson and Seah, 1997). Alternatively, the film thickness can be expressed as a function of λ and the electron takeoff angle (θ), as given by Eq. [5.5] (Bhaskar et al., 2006):

$$t = 3\lambda \sin\theta \quad [5.5]$$

The overlayer model (Eq. [5.4]) has been used successfully to quantify the thickness of various surface films including those made from silica (Joong Kim et al., 2006; Van Der Marel et al., 2005), nickel (Jablonski and Zemek, 2009), polyethylene glycol (Popat et al., 2004; Damodaran et al., 2010a,b), and DNA (Petrovykh et al., 2003). XPS intensities can be used to determine film thickness irrespective of the geometry of the surface, such as arbitrarily shaped rough and curved substrates (Chatelier et al., 1997) and small particles such as catalysts (Fulghum and Linton, 1988; Mohai and Bertóti, 2004).

In many cases, thin-film measurements using XPS at a single electron takeoff angle can result in significant errors caused by the geometry of the instrument and the nature of the overlayer and its thickness. This can be overcome using angle-resolved X-ray photoelectron spectroscopy (AR-XPS), in which photoemission spectra are measured as a function of θ. (Opila and Eng, 2002; Oswald et al., 2006; Bhaskar et al., 2006; Cumpson, 1999). The distance traveled by the photoelectron through the material increases at low θ (Fig. 5.7). Consequently, at lower θ, the sensitivity of the measurement will be higher because of increased inelastic photoelectron scattering. In addition, AR-XPS provides a useful tool for constructing concentration−depth profiles for various thin films (Champaneria et al., 2003; Chang et al., 2000) and it allows nondestructive depth profiling on buried interfaces without sputtering the sample surfaces.

5.3.2 Time-of-flight secondary ion mass spectrometry

ToF-secondary ion mass spectrometry (ToF-SIMS) is a versatile surface analytical technique that provides detailed information about molecular composition and imaging of surface monolayers with high sensitivity and resolution. In a typical SIMS sample, surfaces are exposed to a beam of energetic primary ions or atoms (5−25 keV), which results in the emission of secondary ions including quasimolecular ions, atoms, and molecules (Benninghoven, 1994). The secondary ions formed as a result of this

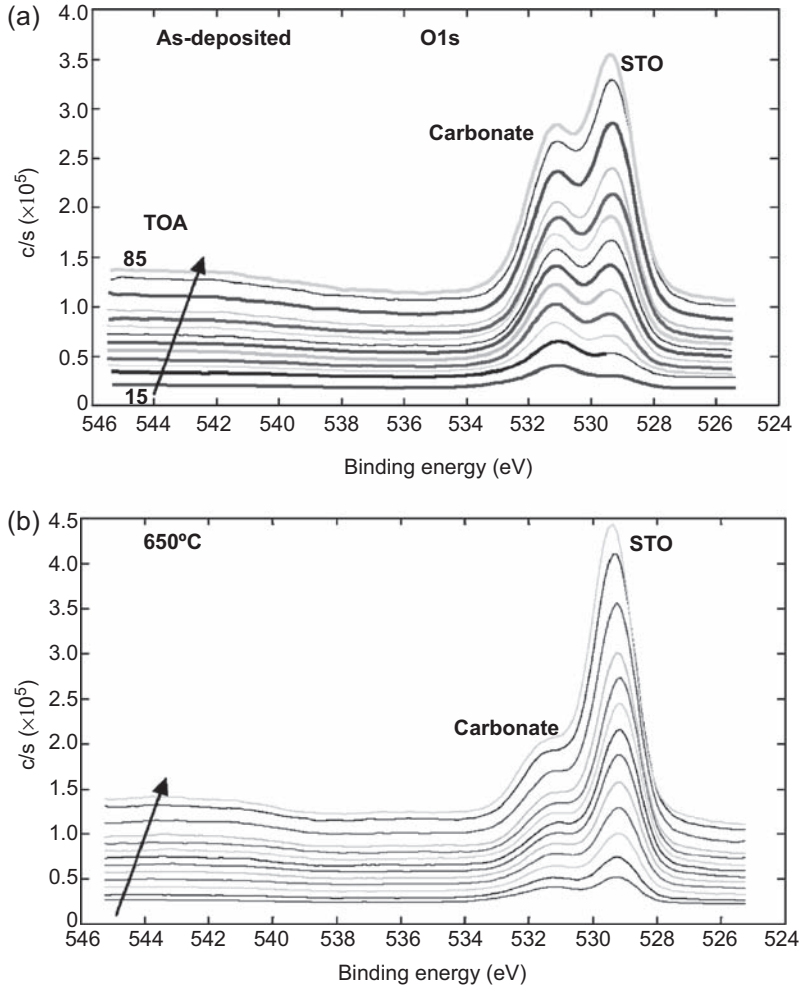

Figure 5.7 Slow scan of 1 s spectra acquired for various takeoff angles of 15 to 85 degrees for (a) as deposited and (b) 650°C annealed $SrTiO_3$ (STO) thin films.
Reproduced with permission from Bhaskar, S., Allgeyer, D., Smythe, J.A., 2006. Depth profiling of dielectric $SrTiO_3$ thin films by angle-resolved X-ray photoelectron spectroscopy. Appl. Phys. Lett. 89, 254103/1−254103/3, © 2006 American Institute of Physics.

sputtering process are analyzed as a function of the mass over charge ratio (*m/z*) using any conventional mass spectrometric technique. In static SIMS (S-SIMS), very low primary ion fluxes are used to achieve a small sputtering rate so that less than 10% of surface atoms erode away from the sample surface. Consequently, S-SIMS causes minimal damage to the sample surface and secondary ions produced during this process have close resemblance to surface structures. This technique was used by Benninghoven et al. in the early 1970s to characterize surface thin films made from chromium

oxide and various amino acids including alanine, phenylalanine, cysteine, and arginine (Benninghoven and Müller, 1973; Benninghoven et al., 1976).

In contrast to S-SIMS, in dynamic SIMS, high-flux continuous etching of the surface is used to determine the surface composition as a function of depth. The development of a highly sensitive ToF-SIMS analyzer significantly improved the capabilities of this surface characterization technique with exceptional mass resolution, range, transmission, and sensitivity, and molecular imaging capabilities (Benninghoven, 1994).

In ToF-SIMS analysis, secondary ions generated during analysis have to enter the flight path simultaneously or within the shortest possible time interval to allow the simultaneous extraction of secondary ions by the analyzer. This simultaneous extraction of secondary ions is achieved by bombarding the area of the surface to be analyzed with primary ions with very short pulse durations (Δt_p). The secondary ions generated from one single pulse are then accelerated by a constant accelerating voltage (V_{ac}, ~3 keV) over a short distance before entering the flight path of length L (Fig. 5.8) with a constant kinetic energy, E_{kin} given by Eq. [5.6]:

$$E_{kin} = zV_{ac} = \frac{mv^2}{2} \quad [5.6]$$

where z is the secondary ion charge, m is the mass, and v is its velocity. Because of differences in velocities, which can be attributed to variations in their mass, mass separation will occur as a function of flight time t (Eq. [5.7]) and enable calculation of m/z (Eq. [5.8]):

$$t = \frac{L}{v} = L\sqrt{\frac{m}{2zV_{ac}}} \quad [5.7]$$

$$\frac{m}{z} = \frac{2V_{ac}\,t^2}{L^2} \quad [5.8]$$

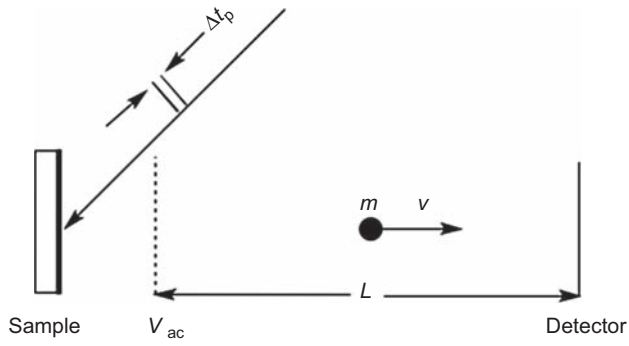

Figure 5.8 Schematic illustration of the principle of a linear ToF mass spectrometer.

In general, ToF-SIMS can operate in four different modes: large-area surface analysis, surface imaging and micro-area analysis, depth profiling, and trace analysis. Large-area surface analysis can provide information about a wide range of surface characteristics including chemical and physical surface modifications (Léonard et al., 1998), molecular layer structures (Pérez-Luna et al., 1997), surface defects (Darmstadt and Roy, 2001), and adhesion properties (Idla et al., 2000). High-resolution surface imaging capabilities of SIMS are used extensively in various microelectronics and micromechanics, nanotechnology, and biomolecular surface imaging applications (Altelaar et al., 2005; Lamberti, 2005; Brison et al., 2011). Beyond complementing other depth-profiling techniques such as XPS, ToF-SIMS offers superior spatial and depth resolution, high molecular specificity, and better mass resolution. Consequently, this technique is widely used for depth-profiling applications in many areas ranging from materials to biological sciences (Brison et al., 2010; Fletcher et al., 2006; Wagner, 2004). The ability of SIMS to detect and identify even minute quantities of unknown substances from surface monolayers, particularly for materials that cannot be vaporized, makes this technique extremely useful for trace analysis applications (Galuska, 2001; Grasserbauer et al., 1983; Douglas and Chen, 1998). In brief, ToF-SIMS, in any of the four modes or in combination, is routinely used to characterize thin films.

5.3.3 Vibrational spectroscopy

Although optical vibrational techniques are less sensitive than electron-based spectrometric methods, these techniques are employed extensively for thin-film characterization because of the specific and characteristic vibrational spectrum shown by various functional groups and molecules present in the film. The most commonly used vibrational spectroscopic techniques are infrared (IR) and Raman spectroscopy. Because of the interference caused by absorption of IR by the underlying substrate, IR reflection-adsorption spectroscopy (IRRAS) and its polarization modulation (PM) analog, PM-IRRAS, which uses the polarization selectivity of surface adsorption, are typically employed to characterize thin films (Gregoriou and Rodman, 2006).

In IRRAS spectroscopic analysis of thin films, a well-defined *p*- or *s*-polarized light is directed onto the sample surface at a grazing angle. The vibrations of molecules from surface layers of the films (that are adsorbed on IR nontransparent planar surfaces, particularly metal surfaces characterized with high reflectivity) are recorded in reflection mode at an angle equal to the angle of incidence. Theoretical interpretation of the spectra is based on measuring the wavelength dependence of reflectance R, which can be defined as (Schnabel, 2014):

$$R = \frac{I_{\text{reflected}}}{I_{\text{incident}}} \qquad [5.9]$$

where $I_{\text{reflected}}$ and I_{incident} are the intensity of the reflected and the corresponding incident light beams on the sample surface at a grazing angle. Because of the

absorption of light by the thin film, a change in reflection will occur, as given by Eq. [5.10]:

$$\frac{\Delta R}{R_0} = \frac{R_0 - R}{R_0} = \frac{4n_1^3 \sin^2\psi_0}{n_2^3 \cos\psi_0} at \qquad [5.10]$$

where R and R_0 are the reflectance with and without the thin film, n_1 and n_2 are the refractive indices of the ambient medium and the film, ψ_0 is the incident angle, a is the absorption coefficient, and t is the film thickness. Consequently, measuring the change in reflection in IRRAS analysis will enable direct measurements of thin-film thickness.

IRRAS spectroscopy has been used to characterize chain conformational changes in Langmuir monolayer and lipid films since the late 1980s (Hunt et al., 1989; Mendelsohn et al., 2010). This technique allowed extensive and detailed characterization and structural analysis of monolayers and thin films on various surfaces and interfaces over the past decade (Cumpston and Jensen, 1995; Liao and Du, 2009; Rodriguez-Llorente et al., 1998). However, the sensitivity of the IRRAS technique is often limited by weak signals in the thin layer sample and noise in the spectra owing to background adsorptions caused by atmospheric water vapor and CO_2. Using the advantage of the polarization selectivity of surface absorption, PM-IRRAS offers a convenient option to reduce these background noises and provides a surface-selective and sensitive method for characterizing very thin surface films (Frey et al., 2006).

In a PM-IRRAS experiment (Fig. 5.9), an IR beam is directed to the sample surface after passing through a polarizer and a photoelastic modulator (PEM). The reflected

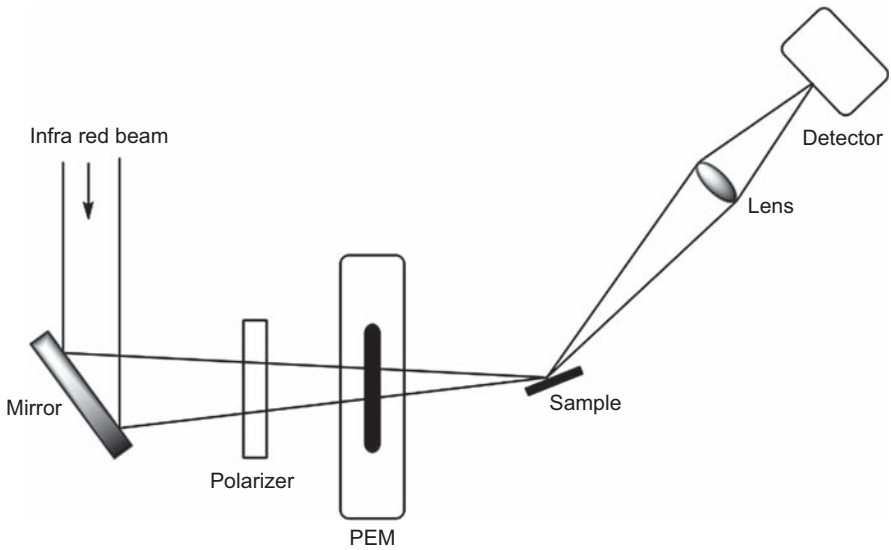

Figure 5.9 Schematic illustration of PM-IRRAS setup.

beam from the sample is collected with an IR lens (BaF_2) into a detector. The entire instrumentation can be evacuated to avoid background atmospheric adsorptions. The intensity differences between the *s*- and *p*-polarized lights using the PEM and the sum of their intensities are used as reference, and hence there is no requirement for additional reference substances (Eq. [5.11]):

$$I_{(t)} = \left[I_p + I_s + (I_p - I_s) \cos\left(\frac{V_m}{\lambda} \cos(\gamma t) \right) \right] \Big/ 2 \qquad [5.11]$$

where $I_{(t)}$ is the intensity of the output light at time t; I_p and I_s are the intensities of *p*- and *s*-polarized lights, respectively; γ is the modulation frequency; V_m is the modulation voltage; and λ is the wavelength of the IR light.

PM-IRRAS spectroscopy has been used extensively to characterize self-assembled monolayers (SAMs) on various reflective metal substrates, particularly gold surfaces (Ramin et al., 2011; Zorn et al., 2010; Meiners et al., 2013). For example, Vanderah et al. (2003) used PM-IRRAS spectroscopy to investigate the conformation, organization, and phase of isostructural SAMs of a series of octadecyl 1-thiaoligo(ethylene oxide) disulfide adsorbed onto a gold surface. In particular, they evaluated the detailed conformational behavior of 1-thiaoligo(ethylene oxide), polyethylene oxide, and hydrocarbon segments present in the SAMs of these long-chain alkanethiols. PM-IRRAS spectroscopy has been employed routinely to follow surface monolayer reaction, including carbodiimide-mediated amine conjugation (Bedford et al., 2014) and electrochemical reactions (Cheng and Corn, 1999) commonly used for protein and polypeptide immobilization. Brand et al. (2009) successfully evaluated the structural features of the D-alkane and oligoethylene glycol (OEG) parts of perdeuterated hexaethylene glycol-terminated alkanethiol, $HS(CD_2)_{12}(O{-}CH_2{-}CH_2)_6OCH_3$, (D-OEG) SAMs on gold. The progress of OEG SAM oxidation by bromine was monitored by PM-IRRAS spectra after exposing the SAMs to a Br_2 solution (Fig. 5.10(a) and (b)) and in a galvanic cell Au|D-OEG SAM| 25 μM Br_2 + 0.1 M Na_2SO_4|| 50 μM KBr + 0.1 M Na_2SO_4|Au (Fig. 5.10(c) and (d)). Reaction with Br_2 resulted in reduced surface coverage of OEG and consequently reduced the intensities of IR bands over time (Fig. 5.10(a) and (b)). However, in the galvanic cell the oxidant is scavenged by a heterogeneous electron transfer reaction and results in slower removal of the OEG chains. Moreover, the initial increase in the integrated intensities of γ_s (OCH_2) at 2880 cm^{-1}, γ_s (COC) at 1110 cm^{-1}, and CH_2 wagging mode at 1357 cm^{-1} confirms an increase in disorder in the SAM followed by a gradual inclination of the OEG chains (Fig. 5.10(c) and (d)).

Surface-enhanced Raman scattering (SERS) is another important vibrational spectroscopic technique commonly employed for thin-layer characterization. This technique provides enhanced Raman signals with an enhancement factor as high as 10^{14} to 10^{15} for Raman-active surface thin layers adsorbed onto certain specially prepared metal surfaces (Moskovits, 2005, 2006). The SERS technique provides both surface sensitivity and selectivity, and thus extends the use of Raman scattering to a wide variety of interfacial surface characterizations. Because the primary

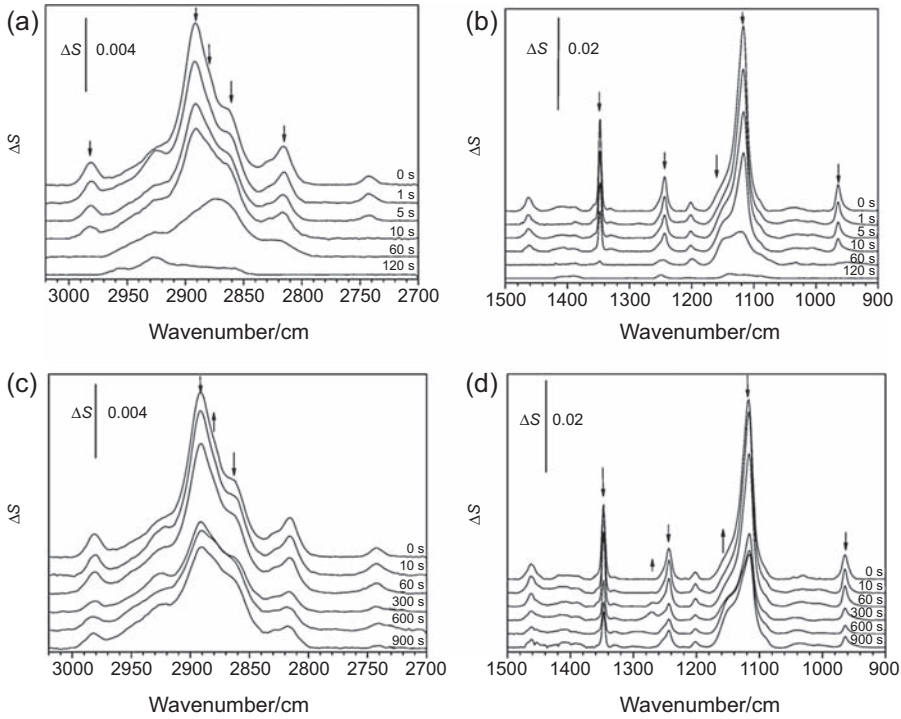

Figure 5.10 PM-IRRAS spectra of D-OEG monolayers on Au after different reaction times with 25-μM Br_2 solution (times are given in the figure) (a and b) and in the galvanic cell Au|D-OEG SAM| 25 μM Br_2 + 0.1 M Na_2SO_4|| 50 μM KBr + 0.1 M Na_2SO_4|Au (c and d) in CH stretching (a and c) and CH_2 deformation and COC stretching modes region (b and d). Reproduced with permission from Brand, I., Nullmeier, M., KlüNer, T., Jogireddy, R., Christoffers, J., Wittstock, G., 2009. Structural analysis of $HS(CD_2)_{12}(O{-}CH_2{-}CH_2)_6OCH_3$ monolayers on gold by means of polarization modulation infrared reflection absorption spectroscopy. Progress of the reaction with bromine. Langmuir 26, 362−370, © 2010 American Chemical Society.

enhancement in the SERS technique results from an electromagnetic process, the technique depends on distance and the theoretical SERS surface enhancement factor, G, that is defined as:

$$G \approx \left[\frac{r}{(r + d)}\right]^{12} \qquad [5.12]$$

where r is the radius of the spherical metal roughness feature and d is the distance of the analyte to that feature (Kneipp et al., 2002). This equation clearly indicates the decay of the enhancement factor over a distance, and the experimental values suggest a 10-fold decrease at a distance of 20−30 Å or a monolayer or two (Kneipp et al., 1999). The SERS technique is commonly employed to characterize thin layers adsorbed onto

coinage (Au, Ag, or Cu) or alkali (Li, Na, or K) metal surfaces using an excitation wavelength near the visible region (Garrell, 1989).

Choi et al. (2010) successfully demonstrated the use of this technique to determine adenine concentrations as low as 10 nM on SERS-active Ag-deposited silica magnetic particles ($Fe_3O_4/SiO_2/Ag$) and to measure the film thickness of rhodamine B isothiocyanate−poly(allylamine hydrochloride) film on a glass slide by doping with the same magnetic particles. A series of SERS spectra of adenine in various concentrations ranging from 10^{-4} to 10^{-8} M was recorded, and the intensity of the characteristic adenine peak at 734 cm^{-1} was used to plot the intensity−concentration standard curve to determine the unknown concentration (Fig. 5.11). Similarly, this technique has been routinely used to characterize various surface thin films, including those made from synthetic (Hariprasad and Radhakrishnan, 2013; Mura et al., 2013) as well as natural origin (Gullekson et al., 2011). In addition, SERS studies provided details on the structural and stability features of various SAMs (Orendorff et al., 2005) and LB films (Aoki et al., 2013).

5.3.4 Other surface characterization techniques

In addition to these characterization tools, surface analytical techniques such as surface matrix-assisted laser desorption ionization (Surface MALDI) mass spectrometry, Rutherford backscattering spectroscopy (RBS), and near-edge X-ray absorption fine structure spectroscopy (NEXAFS) are used to obtain structural and chemical details about surface thin films. Surface MALDI, also known as MALDI-ToF MS (see Section 5.4.2), offers high mass resolution for analyzing surface films and molecular layers using the *m*/*z* of various ions generated from the sample surface (mixed with an

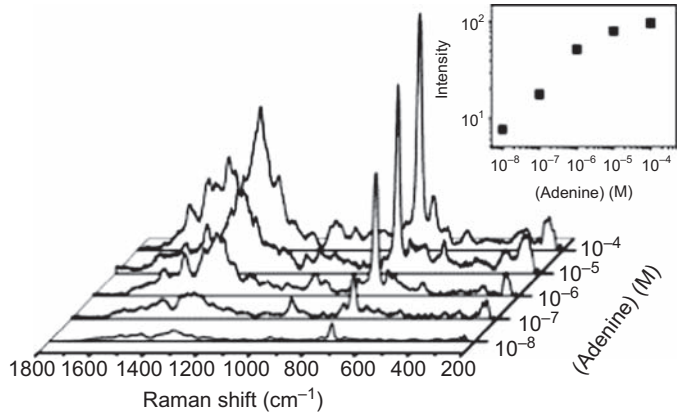

Figure 5.11 SERS spectra of adenine on $Fe_3O_4/SiO_2/Ag$ gathered by varying the concentration from 10^{-4} to 10^{-8} M.

Reproduced with permission from Choi, J.-Y., Kim, K., Shin, K.S., 2010. Surface-enhanced Raman scattering inducible by recyclable Ag-coated magnetic particles. Vib. Spectrosc. 53, 117−120, 2010 © Elsevier.

excess of small ultraviolet (UV)-absorbing molecules, the matrix) caused by pulsed-UV laser irradiation. The matrix molecules ionize and volatilize the analyte molecules by rapidly converting the absorbed UV energy into heat, finally detected by the ToF analyzer (Griesser et al., 2004). Typical examples include quantification of surface concentrations of multicomponent polymer films (Wang et al., 2012) and biomolecular layers (Kingshott et al., 2000).

RBS is a nondestructive nuclear method for characterizing thin films by analyzing the energy of backscattered ions such as H^+ or He^+ from the surface (Perrière, 1987; Kimura, 2006). RBS allows quantification of the surface composition without the need for reference standards and it provides depth profiling of individual elements (Haireche et al., 2013; Jeynes et al., 2012).

NEXAFS is a synchrotron-based spectroscopic tool routinely used as a complementary technique with XPS for surface characterizations. This method probes the adsorption of X-rays by the excitation of core (K-shell) electrons into unoccupied electronic states near the ionization limit. Subsequent emission of Auger electrons results in the formation of an NEXAFS electron yield the observed spectrum. Because the source of Auger electrons can extend only up to 10 nm and the spectral peak positions and intensities are directly related to the nature of unoccupied electronic states, NEXAFS spectroscopy provides an important tool for studying structural and chemical features of various surface thin films and coatings (Hemraj-Benny et al., 2006; Hahner, 2006).

5.4 Characterization of initial biological interactions

Some examples of biologically relevant thin films are layers made by adsorbed proteins that are the precursors for cell attachment, bacterial films or biofilms, and coatings of minerals such as hydroxyapatite to enhance integration of the implants to bones. This section describes the evaluation of some of the biological attributes of such surface coatings.

5.4.1 Quantification of adsorbed proteins

The mass or the thickness of adsorbed proteins can be determined by one of four techniques, ELM, SPR, QCM, and XRR, described in Section 5.2. Here, we will discuss radiolabeling, which has an advantage over other nonlabeled techniques because of its unparalleled sensitivity (in the range of picomolar concentrations, depending on the specific application) and a large linear range of detection by γ-ray detectors. For these reasons, despite the hazardous nature of radioactive material, radiolabeling remains a powerful and commonly used method.

Radiolabeling or isotopic labeling of molecules has been widely used in biology and medicine for several decades. Here, one or more atoms in the molecules of interest are replaced with radioactive isotopes whose decay produces γ-radiation that can easily be detected or imaged even on a very small scale. Positron emission tomography or single-photon emission computed tomography scans for medical diagnosis are

based on this principle. γ-rays, whose energy exceeds 100 keV per photon, even higher than that of X-rays, can penetrate deep into the sample. Combined with the rare occurrence of radioactive elements in the normal settings, γ-radiation can easily be detected in biological samples.

Detailed protocols for analyzing proteins adsorbed on a thin-film surface through radiolabeling proteins can be found in Martins et al. (2012) and Caplan and Baniyash (2002). Quantifying the amount of adsorbed proteins through radiolabeling first involves labeling the proteins of interest with γ-emitting radioisotopes, most commonly ^{125}I and ^{131}I because of their relatively longer half-lives of about 59 and 8 days, respectively, and owing to the relative ease of the labeling process compared with other radionuclides (Lane and Richardson, 2011). Currently, radioiodination of proteins is usually achieved through indirect addition of ^{125}I-labeled acrylating reagent, also called the Bolton–Hunter reagent, to the free amines of proteins in a reaction shown in Fig. 5.12 (Lane and Richardson, 2011). Solutions containing radiolabeled proteins are allowed to interact with thin-film samples. After a few washes to remove free proteins, the amount of adsorbed proteins can be inferred by measuring the γ-radiation emitting directly from the thin-film surface using a γ-counter against known standards (Martins et al., 2003; Unsworth et al., 2005; Benesch et al., 2000). Rapid and large-scale measurements are possible because each measurement in small vials typically lasts from a few seconds to a few minutes, and automated γ-counters can usually analyze hundreds of samples.

Radiolabeling is a well-established technique that is widely used and can be performed using commercially available reagents for radiolabeling. (eg, Pierce and PerkinElmer). However, precise control on a labeling site is largely lacking. As a result, the functionality of labeled proteins may be compromised during

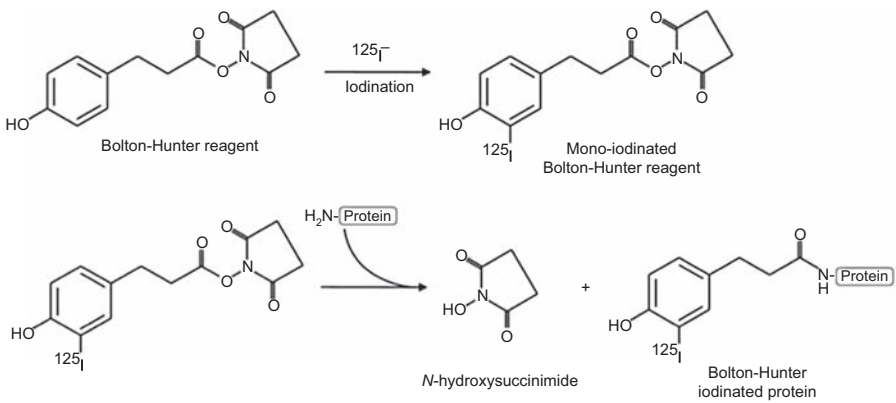

Figure 5.12 Mechanism of Bolton–Hunter reagent in radioiodination of free amines of proteins.

Reprinted with permission from Lane, D.J.R., Richardson, D.R., 2011. William Hunter and radioiodination: revolutions in the labelling of proteins with radionuclides of iodine. Biochem. J. 2011, c1–4, © 2011 Portland Press.

modification. The technique can achieve high sensitivity and direct measurements are possible on thin films. Special precautions are required for the storage and handling of radioactive materials, and there is a potential for compromising the functionality of the proteins.

5.4.2 Identification of adsorbed proteins

In general, MS offers a powerful way to identify one or more molecules that are present in sufficient amounts in the sample by their unique mass. Many researchers have used MS in biomedical studies, including identifying adsorbed proteins on a biomaterial surface. For identifying adsorbed proteins, the general process involves isolating adsorbed proteins from the test surface, followed by separating proteins by molecular weight via electrophoresis, and submitting them to various modes of MS for identification. Based on the peaks in the resulting mass spectra, the adsorbed proteins can be identified by comparing them with the published literature on the molecular masses of many relevant proteins, in addition to newly obtained genomic sequence data that predict molecular weights of most proteins.

Sodium dodecyl sulfate–polyacrylamide gel electrophoresis: SDS-polyacrylamide gel electrophoresis (PAGE) is used to separate proteins by their mass in a polyacrylamide gel, which is required for some types of MS, and it is one of the most commonly used processes in biochemistry because it serves as the starting point for many different biochemical assays. SDS is an anionic detergent that binds to proteins and linearizes them from their bulky three-dimensional conformations while giving them an even distribution of negative charge per unit mass. In this linearized and negatively charged form, when an electric field is applied across the polyacrylamide gel, proteins can pass through the fine mesh of polyacrylamide gel with differing mobility, depending on their molecular size. When a voltage is applied, the negatively charged proteins will move toward the positively charged anode at the opposite end of the gel. The end result is a polyacrylamide gel with proteins separated by their molecular weight (Shapiro et al., 1967; Weber and Osborn, 1969).

After SDS-PAGE, the gel may be stained with a protein dye such as Coomassie Blue or silver stain to visualize the separated proteins (Candiano et al., 2004). Staining the separated proteins in the gel itself may provide valuable information on the profile of adsorbed proteins. For example, Faucheux et al. (2004) used SDS-PAGE to separate desorbed serum proteins from cell substrates made of alkyl silanes with various terminating groups, and silver-stained the proteins (Fig. 5.13). Clearly, each substrate tends to bind different sets of proteins in differing amounts. This information could then be used as a starting point to investigate and explain the differences in biocompatibility or bioactivity of a certain biomaterial surface. In addition, selected protein bands on the gel may be processed further for MS (Cohen and Chait, 1997; Faucheux et al., 2004).

Matrix-assisted laser desorption/ionization–time-of-flight mass spectrometry: MALDI-ToF MS is a variant of mass spectroscopy with the advantage of avoiding molecule fragmentation, especially with large organic molecules such as proteins,

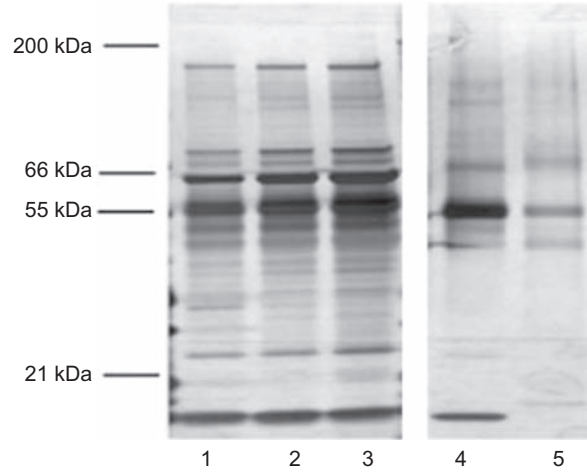

Figure 5.13 SDS-PAGE of desorbed serum proteins after 45 min incubation from COOH (lane 1), NH_2 C_{11} (lane 2), CH_3 (lane 3), OH (lane 4), and PEG (lane 5) terminated alkyl silane-coated cell substrates.
Reprinted with permission from Faucheux, N., Schweiss, R., Lützow, K., Werner, C., Groth, T., 2004. Self-assembled monolayers with different terminating groups as model substrates for cell adhesion studies. Biomaterials 25, 2721−2730, © 2004 Elsevier.

DNA, and other polymers. The ability to measure the mass of the intact, full-length molecules makes the interpretation of the spectra more easy and straightforward. MALDI-ToF MS avoids molecule fragmentation through the use of an UV-absorbing matrix that encases large organic molecules in crystals when dried. When irradiated with a UV laser, the matrix crystals are heated to high temperatures, causing the encased molecules to vaporize. The matrix molecule compounds are ionized and accelerated through a chamber, and the ToF mass spectrometer determines the mass-to-charge ratio of the large organic molecules (Vickerman and Briggs, 2013; Oleschuk et al., 2000). Because the method does not fragment the molecules, it is widely used in proteomics and organic/polymer chemistry to identify large molecules, and it is becoming more popular in biomaterials research.

Surface layer-MALDI-MS has been developed specifically to identify proteins adsorbed onto biomaterial surfaces. Although the experimental approach for this technique is analogous to traditional MALDI-ToF MS, surface layer-MALDI-MS does not require protein isolation from the biomaterial surface, because the protein-adsorbed surface is submerged directly in a matrix solvent for crystallization (Griesser et al., 2004). For example, surface-MALDI-MS can be used to identify which proteins from blood plasma adsorb onto a biomaterial surface directly off the original material surface, such as polyurethane, as shown in Fig. 5.14 (Oleschuk et al., 2000). The acquired spectra show clear peaks, indicating different proteins with a distinct mass. Each of these proteins can be identified by comparing the experimentally determined masses with those in the literature.

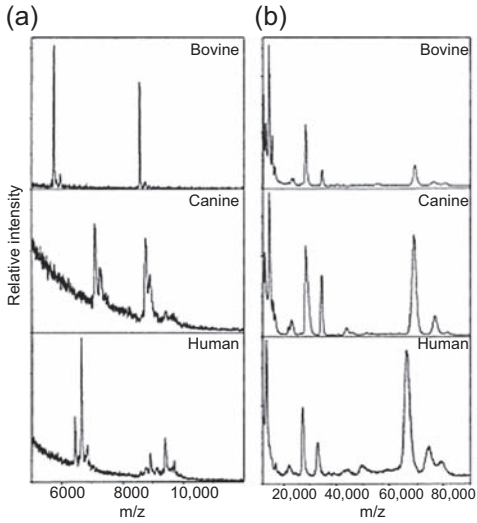

(c)

Protein	Molecular weight (Da)	
	Literature	Experimental
Immunoglobulin G	150,000	148,361
Transferrin	79,754	78,513
Comp C3-β	75,000	73,953
Albumin	66,472	66,463[c]
α_2-HS glycoprotein	49,000	49,575
Apo A–4	43,400	44,175
Apo E	34,236	33,109
Apo A–1	28,000	27,502
Apo D	22,500	22,174
Apo H-III (HDL)	17,000	16,327
Transthyretin	13,761	13,555
Apo C-II	8914	8946
Apo C-III	8764	8783
Apo C-I	6630	6631

Figure 5.14 MALDI-ToF MS of three different plasma standards: bovine, canine, and human on polyurethane membrane. (a) Low-molecular weight region. (b) High-molecular weight region. (c) Identification of adsorbed proteins in mass spectra compared with the literature values of proteins.
Reprinted with permission from Oleschuk, R.D., Mccomb, M.E., Chow, A., Ens, W., Standing, K.G., Perreault, H., Marois, Y., King, M., 2000. Characterization of plasma proteins adsorbed onto biomaterials by MALDI-TOF MS. Biomaterials 21, 1701−1710, © 2000 Elsevier.

An advantage of MALDI-MS is its nonfragmenting nature for large molecules. The detection limits are low and comparable to those of chromatographic techniques. The technique is tolerant toward contaminants such as buffer salts and detergents. Surface-MALDI-MS bypasses time- and labor-consuming protein isolation from samples, which may be cumbersome and miss strongly adsorbed proteins. However, MALDI-MS shares similar shortcomings common to various MS modalities: shot-to-shot reproducibility is typically low and detecting irreversibly adsorbed or cross-linked proteins remains difficult.

5.4.3 Characterization of material interactions with blood

For applications involving direct contact with blood (eg, vascular grafts, dialysis membrane, blood storage, and collection devices), ensuring hemocompatibility of the interfacing material surface is of paramount importance, and in fact the International Standardization Organization mandates several types of hemocompatibility tests on such devices (USDHHS, 2013). Hemocompatibility is a broad term that includes several requirements such as low hemolysis (rupture of oxygen-carrying red blood cells) and low adsorption tendency for coagulating agents and molecules involved in the complement activation pathway, which could lead to a severe immune response. Both hemolysis and adsorption of molecules can have life-threatening consequences

(hemolytic anemia and thrombosis, thromboembolism, or severe inflammation); hence, these tendencies must be characterized as much as possible in vitro. Accordingly, various assays have been developed to carry out this task (Autian, 1975; Belanger and Marois, 2001).

Hemolysis assay: To assess the hemolytic tendency of a new material surface, blood diluted in anticoagulant acid citrate dextrose (ACD) solution is most commonly used. The test surface is allowed to interact with an ACD blood solution for a few hours in a static condition, after which the blood solution is collected and spun down to separate the intact blood cells. The cell-free supernatant is then collected and its absorbance measured at about 540 nm. In this process, free hemoglobin is released from rupturing red blood cells which results in a noticeable change in the absorptive spectrum. Such change can then be measured by a spectrophotometer. From the absorption value, the percentage of hemolysis can be determined using known positive and negative standards (Singhal and Ray, 2002; Nan et al., 1998; Li et al., 2011). Only a marginal level of hemolysis, less than about 5%, is permissible for in vivo use (Autian, 1975). Further modifications to the material would be required until this condition is met for clinical success and safety. This method closely mimics in vivo conditions and is simple, fast, reproducible, and affordable. This makes it the single major method for assessing the hemolytic potential of a biomaterial surface.

It is also important to characterize protein adsorption on blood-contacting medical devices. Fatal thrombosis and severe inflammation can potentially occur as a result of complement activation initiated and mediated by initial adsorption of certain proteins onto the blood-contacting surface. For example, FIB, thrombin, and platelets, among others involved in the coagulation process, can adhere onto a biomaterial surface, whereas several complement component proteins and anaphylatoxins that circulate in human blood plasma are known to bind to nonself elements including the biomaterial surface, whereby the complement system is then activated and results in an intense inflammatory response. Thrombosis and complement activation are complicated, interconnected physiological processes involving hundreds of proteins and cells. Gorbet and Sefton, (2004) wrote a comprehensive review on this topic. The following describes several common methods for investigating the thrombogenicity and complement activation of biomaterial surfaces; naturally, many of them use previously introduced assays to quantify adsorbed proteins.

Various assays exist to gauge the thrombogenicity of a surface by investigating the adsorption of a number of different molecules on a thin-film surface. The first type aims to measure the adsorption of specific proteins or cells associated with thrombosis or a complement system. For example, radiolabeling, discussed earlier, is often used to label such proteins (FIB, thrombin, or complement component proteins) or platelets to measure the degree of adsorption of a specific molecule or cell on a biomaterial surface. Labeled molecules are mixed back into whole blood for the test. Radiolabeled component-containing blood is then allowed to interact with the thin-film surface typically for a few minutes, because protein adsorption takes place in a few seconds to minutes. Adsorption of the labeled proteins onto the thin-film surface can be measured on a γ-counter, as mentioned earlier (Gappa-Fahlenkamp and Lewis, 2005; Maechling-Strasser et al., 1989; Suggs et al., 1999).

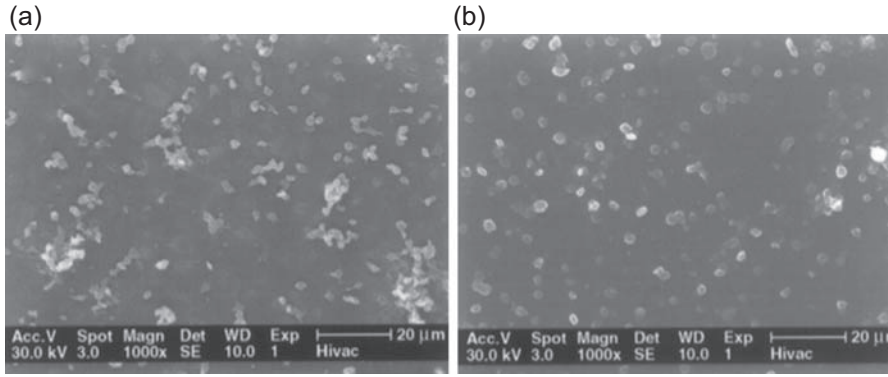

Figure 5.15 Scanning electron microscopic images of platelet surface coverage on (a) glass and (b) silicone rubber under static conditions at ×1000 magnification.
Reprinted with permission from Suggs, L.J., West, J.L., Mikos, A.G., 1999. Platelet adhesion on a bioresorbable poly(propylene fumarate-*co*-ethylene glycol) copolymer. Biomaterials 20, 683−690, © 1999 Elsevier.

In the case of platelet adhesion measurement to assess the thrombogenicity of thin films, two other commonly used alternative methods include (1) directly counting the number of platelets in the blood before and after interacting with the thin-film surface to determine the amount of adhering or missing platelets; and (2) using light microscopy, or in the case of opaque materials, scanning electron microscopy to visualize platelet adhesion directly on a surface, as shown in Fig. 5.15 (Huang et al., 2003; Mao et al., 2004; Suggs et al., 1999; Damodaran et al., 2013).

5.5 Concluding remarks

The characterization of thin-film coatings is a prerequisite for optimization of the coating process and the performance of thin films. The techniques discussed here encompass physical (ELM, SPR, and QCM) and structural (X-ray scattering) characteristics and chemical (XPS, MS, and spectroscopy) and biological (radiolabeling, MS, and SDS-PAGE) attributes of thin films. The goal was to describe them in sufficient detail so that the information can be useful for a beginning practitioner. While the data collection techniques and analysis software continue to evolve, the basic principles and the instrumentation described here will remain useful.

Whereas ELM and SPR provide us with the dry mass, QCM provides information about the coupled water. Thus, a combination of techniques can reveal much about the interaction of protein with the substrates as well as the surrounding medium. XRR provides another dimension by providing structural detail in the form of electron density distribution normal to the surface. Further information about the surface can be obtained by using GID. Thus, each method described here provides details about a particular aspect of thin-film coatings and, more important, about the adsorption process that

leads to the formation of a surface layer. Most of these methods can be used in real time so that the kinetics of the formation of thin films can be observed. In all of these techniques, it is critical to use a proper model to analyze the data. Results obtained using improper models would lead to erroneous conclusions that might continue to be cited in the literature. Advances in understanding the mechanism of adsorption and the formation of thin layers will lead to better experimental protocols and robust methods of analyzing the data. The significance of such advances will be reliable coatings and consistent performance, which will lead to further advances in thin-film coatings.

For the relatively nascent field of characterizing biological interactions on thin films interfacing material/device and host, much development is still needed to investigate the suitability of thin films efficiently for specific applications. Various analytical tools are available to study events taking place at the interface; difficulties lie in the inherent complexities that come with biology (for example, the same type of thin film could have vastly different responses from the host upon implantation, depending on the implantation site). Hence, development of application-specific in vitro models could significantly expedite the process of identifying suitable thin films and allow for the rapid translation of thin-film applications into the clinic.

References

Altelaar, A.F.M., Klinkert, I., Jalink, K., De Lange, R.P.J., Adan, R.A.H., Heeren, R.M.A., Piersma, S.R., 2005. Gold-enhanced biomolecular surface imaging of cells and tissue by SIMS and MALDI mass spectrometry. Anal. Chem. 78, 734−742.

Anand, G., Zhang, F., Linhardt, R.J., Belfort, G., 2010. Protein-associated water and secondary structure effect removal of blood proteins from metallic substrates. Langmuir 27, 1830−1836.

Anderson, J.M., 2001. Biological responses to materials. Annu. Rev. Mater. Res. 31, 81−110.

Aoki, P.H.B., Carreon, E.G.E., Volpati, D., Shimabukuro, M.H., Constantino, C.J.L., Aroca, R.F., Oliveira, O.N., Paulovich, F.V., 2013. SERS mapping in Langmuir−Blodgett films and single-molecule detection. Appl. Spectrosc. 67, 563−569.

Autian, J., 1975. Biological Model Systems for the Testing of the Toxicity of Biomaterials. Plenum Press, NY.

Batich, C.D., 1988. Chemical derivatization and surface analysis. Appl. Surf. Sci. 32, 57−73.

Bedford, E.E., Boujday, S., Humblot, V., Gu, F.X., Pradier, C.-M., 2014. Effect of SAM chain length and binding functions on protein adsorption: β-lactoglobulin and apo-transferrin on gold. Colloids Surf. B Biointerfaces 116, 489−496.

Belanger, M.C., Marois, Y., 2001. Hemocompatibility, biocompatibility, inflammatory and in vivo studies of primary reference materials low-density polyethylene and polydimethylsiloxane: a review. J. Biomed. Mater. Res. 58, 467−477.

Benesch, J., Askendal, A., Tengvall, P., 2000. Quantification of adsorbed human serum albumin at solid interfaces: a comparison between radioimmunoassay and simple null ellipsometry. Colloids Surf. B Biointerfaces 18, 71−81.

Benninghoven, A., Müller, A., 1973. Investigation of surface reactions by the static method of secondary ion mass spectrometry: II. The oxidation of chromium in the monolayer range. Surf. Sci. 39, 416−426.

Benninghoven, A., Jaspers, D., Sichtermann, W., 1976. Secondary-ion emission of amino acids. Appl. Phys. 11, 35–39.

Benninghoven, A., 1994. Chemical analysis of inorganic and organic surfaces and thin films by static time-of-flight secondary ion mass spectrometry (TOF-SIMS). Angew. Chem. Int. Ed. Engl. 33, 1023–1043.

Bhaskar, S., Allgeyer, D., Smythe, J.A., 2006. Depth profiling of dielectric $SrTiO_3$ thin films by angle-resolved X-ray photoelectron spectroscopy. Appl. Phys. Lett. 89, 254103/1–254103/3.

Birkholz, M., 2006. Thin Film Analysis by X-ray Scattering. John Wiley & Sons.

Brand, I., Nullmeier, M., KlüNer, T., Jogireddy, R., Christoffers, J., Wittstock, G., 2009. Structural analysis of $HS(CD_2)_{12}(O{-}CH_2{-}CH_2)_6OCH_3$ monolayers on gold by means of polarization modulation infrared reflection absorption spectroscopy. Progress of the reaction with bromine. Langmuir 26, 362–370.

Brison, J., Muramoto, S., Castner, D.G., 2010. ToF-sims depth profiling of organic films: a comparison between single-beam and dual-beam analysis. J. Phys. Chem. C 114, 5565–5573.

Brison, J., Benoit, D.S.W., Muramoto, S., Robinson, M., Stayton, P.S., Castner, D.G., 2011. ToF-SIMS imaging and depth profiling of HeLa cells treated with bromodeoxyuridine. Surf. Interface Anal. 43, 354–357.

Brockman, J.M., Nelson, B.P., Corn, R.M., 2000. Surface plasmon resonance imaging measurements of ultrathin organic films. Annu. Rev. Phys. Chem. 51, 41–63.

Candiano, G., Bruschi, M., Musante, L., Santucci, L., Ghiggeri, G.M., Carnemolla, B., Orecchia, P., Zardi, L., Righetti, P.G., 2004. Blue silver: a very sensitive colloidal Coomassie G-250 staining for proteome analysis. Electrophoresis 25, 1327–1333.

Caplan, S., Baniyash, M., 2002. Radioiodination of cellular proteins. Curr. Protoc. Cell Biol. John Wiley & Sons, Inc.

Champaneria, R., Mack, P., White, R., Wolstenholme, J., 2003. Non-destructive analysis of ultrathin dielectric films. Surf. Interface Anal. 35, 1028–1033.

Chang, J.P., Green, M.L., Donnelly, V.M., Opila, R.L., Eng, J., Sapjeta, J., Silverman, P.J., Weir, B., Lu, H.C., Gustafsson, T., Garfunkel, E., 2000. Profiling nitrogen in ultrathin silicon oxynitrides with angle-resolved X-ray photoelectron spectroscopy. J. Appl. Phys. 87, 4449–4455.

Chatelier, R.C., St John, H.A.W., Gengenbach, T.R., Kingshott, P., Griesser, H.J., 1997. Incorporation of surface topography in the XPS analysis of curved or rough samples covered by thin multilayers. Surf. Interface Anal. 25, 741–746.

Cheng, Y., Corn, R.M., 1999. Ultrathin polypeptide multilayer films for the fabrication of model liquid/liquid electrochemical interfaces. J. Phys. Chem. B 103, 8726–8731.

Choi, J.-Y., Kim, K., Shin, K.S., 2010. Surface-enhanced Raman scattering inducible by recyclable Ag-coated magnetic particles. Vib. Spectrosc. 53, 117–120.

Cohen, S.L., Chait, B.T., 1997. Mass spectrometry of whole proteins eluted from sodium dodecyl sulfate–polyacrylamide gel electrophoresis gels. Anal. Biochem. 247, 257–267.

Cumpson, P.J., Seah, M.P., 1997. Elastic scattering corrections in AES and XPS. II. Estimating attenuation lengths and conditions required for their valid use in overlayer/substrate experiments. Surf. Interface Anal. 25, 430–446.

Cumpson, P.J., 1999. Angle-resolved XPS depth-profiling strategies. Appl. Surf. Sci. 144–145, 16–20.

Cumpston, B.H., Jensen, K.F., 1995. Photo-oxidation of polymers used in electroluminescent devices. Synth. Met. 73, 195–199.

Damodaran, V.B., Fee, C.J., Popat, K.C., 2010a. Prediction of protein interaction behaviour with PEG-grafted matrices using X-ray photoelectron spectroscopy. Appl. Surf. Sci. 256, 4894–4901.

Damodaran, V.B., Fee, C.J., Ruckh, T., Popat, K.C., 2010b. Conformational studies of covalently grafted poly(ethylene glycol) on modified solid matrices using X-ray photoelectron spectroscopy. Langmuir 26, 7299–7306.

Damodaran, V.B., Leszczak, V., Wold, K.A., Lantvit, S.M., Popat, K.C., Reynolds, M.M., 2013. Antithrombogenic properties of a nitric oxide-releasing dextran derivative: evaluation of platelet activation and whole blood clotting kinetics. RSC Adv. 3, 24406–24414.

Darmstadt, H., Roy, C., 2001. Comparative investigation of defects on carbon black surfaces by nitrogen adsorption and SIMS. Carbon 39, 841–848.

Devries, J.E., 1998. Surface characterization methods—XPS,TOF-SIMS, and SAM a complimentary ensemble of tools. J. Mater. Eng. Perform. 7, 303–311.

Dorozhkin, S.V., 2012. Calcium orthophosphate coatings, films and layers. Prog. Biomater. 1, 1–40.

Douglas, M.A., Chen, P.J., 1998. Quantitative trace metal analysis of silicon surfaces by ToF-SIMS. Surf. Interface Anal. 26, 984–994.

Eisele, N.B., Andersson, F.I., Frey, S., Richter, R.P., 2012. Viscoelasticity of thin biomolecular films: a case study on nucleoporin phenylalanine-glycine repeats grafted to a histidine-tag capturing QCM-D sensor. Biomacromolecules 13, 2322–2332.

Elwing, H., 1998. Protein absorption and ellipsometry in biomaterial research. Biomaterials 19, 397–406.

Fadley, C.S., 2010. X-ray photoelectron spectroscopy: progress and perspectives. J. Electron Spectrosc. Relat. Phenom. 178–179, 2–32.

Faucheux, N., Schweiss, R., Lützow, K., Werner, C., Groth, T., 2004. Self-assembled monolayers with different terminating groups as model substrates for cell adhesion studies. Biomaterials 25, 2721–2730.

Felgueiras, H.P., Sommerfeld, S.D., Murthy, N.S., Kohn, J., Migonney, V., 2014. Poly(NaSS) functionalization modulates the conformation of fibronectin and collagen type I to enhance osteoblastic cell attachment onto Ti6Al4V. Langmuir 30 (31), 9477–9483.

Fletcher, J.S., Lockyer, N.P., Vickerman, J.C., 2006. C60, Buckminsterfullerene: its impact on biological ToF-SIMS analysis. Surf. Interface Anal. 38, 1393–1400.

Frey, B.L., Corn, R.M., Weibel, S.C., 2006. Polarization-Modulation Approaches to Reflection–Absorption Spectroscopy. Handbook of Vibrational Spectroscopy. John Wiley & Sons, Ltd.

Fulghum, J.E., Linton, R.W., 1988. Quantitation of coverages on rough surfaces by XPS: an overview. Surf. Interface Anal. 13, 186–192.

Galuska, A.A., 2001. Quantitative ToF-SIMS analysis of monomers, oxidation and trace elements in EPDM gels. Surf. Interface Anal. 31, 177–184.

Gappa-Fahlenkamp, H., Lewis, R.S., 2005. Improved hemocompatibility of poly(ethylene terephthalate) modified with various thiol-containing groups. Biomaterials 26, 3479–3485.

Garrell, R.L., 1989. Surface-enhanced Raman spectroscopy. Anal. Chem. 61, 401A–411A.

Gibaud, A., Hazra, S., 2000. X-ray reflectivity and diffuse scattering. Curr. Sci. 78, 1467–1477.

Giebel, K.F., Bechinger, C., Herminghaus, S., Riedel, M., Leiderer, P., Weiland, U., Bastmeyer, M., 1999. Imaging of cell/substrate contacts of living cells with surface plasmon resonance microscopy. Biophys. J. 76, 509–516.

Girard-Lauriault, P.-L., Desjardins, P., Unger, W.E.S., Lippitz, A., Wertheimer, M.R., 2008. Chemical characterisation of nitrogen-rich plasma-polymer films deposited in dielectric barrier discharges at atmospheric pressure. Plasma Processes Polym. 5, 631–644.

Gölander, C.-G., Kiss, E., 1988. Protein adsorption on functionalized and ESCA-characterized polymer films studied by ellipsometry. J. Colloid Interface Sci. 121, 240–253.

Gorbet, M.B., Sefton, M.V., 2004. Biomaterial-associated thrombosis: roles of coagulation factors, complement, platelets and leukocytes. Biomaterials 25, 5681–5703.

Grasserbauer, M., Wilhartitz, P., Stingeder, G., 1983. In-situ trace analysis of materials with SIMS. Mikrochim. Acta 81, 467–492.

Gregoriou, V.G., Rodman, S.E., 2006. Vibrational Spectroscopy of Thin Organic Films. Handbook of Vibrational Spectroscopy. John Wiley & Sons, Ltd.

Griesser, H.J., Kingshott, P., Mcarthur, S.L., Mclean, K.M., Kinsel, G.R., Timmons, R.B., 2004. Surface-MALDI mass spectrometry in biomaterials research. Biomaterials 25, 4861–4875.

Gullekson, C., Lucas, L., Hewitt, K., Kreplak, L., 2011. Surface-sensitive Raman spectroscopy of collagen I fibrils. Biophys. J. 100, 1837–1845.

Hahner, G., 2006. Near edge X-ray absorption fine structure spectroscopy as a tool to probe electronic and structural properties of thin organic films and liquids. Chem. Soc. Rev. 35, 1244–1255.

Haireche, S., Boumeddiene, A., Guittoum, A., El Hdiy, A., Boufelfel, A., 2013. Structural, morphological and electronic study of CVD SnO_2:Sb films. Mater. Chem. Phys. 139, 871–876.

Hariprasad, E., Radhakrishnan, T.P., 2013. In situ fabricated polymer–silver nanocomposite thin film as an inexpensive and efficient substrate for surface-enhanced Raman scattering. Langmuir 29, 13050–13057.

Hartmann, A.J., Lamb, R.N., 1997. X-ray photoemission spectroscopy of thin films. Curr. Opin. Solid State Mater. Sci. 2, 511–516.

Hemraj-Benny, T., Banerjee, S., Sambasivan, S., Balasubramanian, M., Fischer, D.A., Eres, G., Puretzky, A.A., Geohegan, D.B., Lowndes, D.H., Han, W., Misewich, J.A., Wong, S.S., 2006. Near-edge X-ray absorption fine structure spectroscopy as a tool for investigating nanomaterials. Small 2, 26–35.

Höök, F., Kasemo, B., Nylander, T., Fant, C., Sott, K., Elwing, H., 2001. Variations in coupled water, viscoelastic properties, and film thickness of a Mefp-1 protein film during adsorption and cross-linking: a quartz crystal microbalance with dissipation monitoring, ellipsometry, and surface plasmon resonance study. Anal. Chem. 73, 5796–5804.

Huang, N., Yang, P., Leng, Y.X., Chen, J.Y., Sun, H., Wang, J., Wang, G.J., Ding, P.D., Xi, T.F., Leng, Y., 2003. Hemocompatibility of titanium oxide films. Biomaterials 24, 2177–2187.

Hunt, R.D., Mitchell, M.L., Dluhy, R.A., 1989. The interfacial structure of phospholipid monolayer films: an infrared reflectance study. J. Mol. Struct. 214, 93–109.

Icdd. 2014. http://www.icdd.com/ [Accessed 12 September 2014] [Online].

Idla, K., Johansson, L.S., Campbell, J.M., Inganäs, O., 2000. XPS and SIMS study: adhesion of polypyrrole film on titanium. Surf. Interface Anal. 30, 557–560.

Izumi, F., Young, R., 1993. In: Young, R.A. (Ed.), The Rietveld Method. Oxford University Press, Oxford, pp. 236–253.

Jablonski, A., Zemek, J., 2009. Overlayer thickness determination by XPS using the multiline approach. Surf. Interface Anal. 41, 193–204.

Jeynes, C., Barradas, N.P., Szilágyi, E., 2012. Accurate determination of quantity of material in thin films by Rutherford backscattering spectrometry. Anal. Chem. 84, 6061–6069.

Joong Kim, K., Park, K.T., Lee, J.W., 2006. Thickness measurement of SiO_2 films thinner than 1 nm by X-ray photoelectron spectroscopy. Thin Solid Films 500, 356–359.

Kimura, K., 2006. Rutherford Backscattering Spectroscopy. Encyclopedia of Analytical Chemistry. John Wiley & Sons, Ltd.

Kingshott, P., St John, H.A.W., Chatelier, R.C., Griesser, H.J., 2000. Matrix-assisted laser desorption ionization mass spectrometry detection of proteins adsorbed in vivo onto contact lenses. J. Biomed. Mater. Res. 49, 36–42.

Kneipp, K., Kneipp, H., Itzkan, I., Dasari, R.R., Feld, M.S., 1999. Ultrasensitive chemical analysis by Raman spectroscopy. Chem. Rev. 99, 2957–2976.

Kneipp, K., Kneipp, H., Itzkan, I., Dasari, R.R., Feld, M.S., 2002. Surface-enhanced Raman scattering and biophysics. J. Phys. Condens. Matter 14, R597.

Lamberti, W., 2005. Imaging secondary ion mass spectrometry. In: Yao, N., Wang, Z. (Eds.), Handbook of Microscopy for Nanotechnology. Springer, US.

Lane, D.J.R., Richardson, D.R., 2011. William Hunter and radioiodination: revolutions in the labelling of proteins with radionuclides of iodine. Biochem. J. 2011, c1–4.

Latour, R.A., 2008. Biomaterials: Protein–Surface Interactions. Encyclopedia of Biomaterials and Biomedical Engineering. Taylor & Francis.

Léonard, D., Chevolot, Y., Bucher, O., Sigrist, H., Mathieu, H.J., 1998. Part 1. *N*-(*m*-(3-(trifluoromethyl)diazirine-3-yl)phenyl)-4-maleimido-butyramide (MAD) on silicon, silicon nitride and diamond. Surf. Interface Anal. 26, 783–792.

Li, G., Yang, P., Qin, W., Maitz, M.F., Zhou, S., Huang, N., 2011. The effect of coimmobilizing heparin and fibronectin on titanium on hemocompatibility and endothelialization. Biomaterials 32, 4691–4703.

Liao, K., Du, X., 2009. In situ IRRAS studies of NH stretching bands and molecular structures of the monolayers of amphiphiles containing amide and amine units at the air–water interface. J. Phys. Chem. B 113, 1396–1403.

Maechling-Strasser, C., Dejardin, P., Galin, J.C., Schmitt, A., 1989. Preadsorption of polymers on glass and silica to reduce fibrinogen adsorption. J. Biomed. Mater. Res. 23, 1385–1393.

Mao, C., Qiu, Y., Sang, H., Mei, H., Zhu, A., Shen, J., Lin, S., 2004. Various approaches to modify biomaterial surfaces for improving hemocompatibility. Adv. Colloid Interface Sci. 110, 5–17.

Martins, M.C.L., Wang, D., Ji, J., Feng, L., Barbosa, M.A., 2003. Albumin and fibrinogen adsorption on PU–PHEMA surfaces. Biomaterials 24, 2067–2076.

Martins, M.C., Sousa, S.R., Antunes, J.C., Barbosa, M.A., 2012. Protein adsorption characterization. Methods Mol. Biol. 811, 141–161.

Marx, K.A., 2003. Quartz crystal microbalance: a useful tool for studying thin polymer films and complex biomolecular systems at the solution–surface interface. Biomacromolecules 4, 1099–1120.

Meiners, F., Plettenberg, I., Witt, J., Vaske, B., Lesch, A., Brand, I., Wittstock, G., 2013. Local control of protein binding and cell adhesion by patterned organic thin films. Anal. Bioanal. Chem. 405, 3673–3691.

Mendelsohn, R., Mao, G., Flach, C.R., 2010. Infrared reflection–absorption spectroscopy: principles and applications to lipid–protein interaction in Langmuir films. Biochim. Biophys. Acta 1798, 788–800.

Mohai, M., Bertóti, I., 2004. Calculation of overlayer thickness on curved surfaces based on XPS intensities. Surf. Interface Anal. 36, 805–808.

Mora, M.F., Wehmeyer, J.L., Synowicki, R., Garcia, C.D., 2009. Investigating Protein Adsorption via Spectroscopic Ellipsometry, pp. 19–41.

Moskovits, M., 2005. Surface-enhanced Raman spectroscopy: a brief retrospective. J. Raman Spectrosc. 36, 485–496.

Moskovits, M., 2006. Surface-enhanced Raman spectroscopy: a brief perspective. In: Kneipp, K., Moskovits, M., Kneipp, H. (Eds.), Surface-Enhanced Raman Scattering. Springer Berlin Heidelberg.

Mura, S., Greppi, G., Innocenzi, P., Piccinini, M., Figus, C., Marongiu, M.L., Guo, C., Irudayaraj, J., 2013. Nanostructured thin films as surface-enhanced Raman scattering substrates. J. Raman Spectrosc. 44, 35−40.

Nan, H., Ping, Y., Xuan, C., Yongxang, L., Xiaolan, Z., Guangjun, C., Zihong, Z., Feng, Z., Yuanru, C., Xianghuai, L., Tingfei, X., 1998. Blood compatibility of amorphous TiO films synthesized by ion beam enhanced deposition. Biomaterials 19, 771−776.

Nilsson, U., Nilsson, B., 1982. Analogous antigenic alterations elicited in C3 by physiologic binding and by denaturation in the presence of sodium dodecyl sulfate. J. Immunol. 129, 2594−2597.

Oleschuk, R.D., Mccomb, M.E., Chow, A., Ens, W., Standing, K.G., Perreault, H., Marois, Y., King, M., 2000. Characterization of plasma proteins adsorbed onto biomaterials by MALDI-TOFMS. Biomaterials 21, 1701−1710.

Opila, R.L., Eng Jr., J., 2002. Thin films and interfaces in microelectronics: composition and chemistry as function of depth. Prog. Surf. Sci. 69, 125−163.

Oran, U., Swaraj, S., Lippitz, A., Unger, W.E.S., 2006. Surface analysis of plasma deposited polymer films, 7. Plasma Processes Polym. 3, 288−298.

Orendorff, C.J., Gole, A., Sau, T.K., Murphy, C.J., 2005. Surface-enhanced Raman spectroscopy of self-assembled monolayers: sandwich architecture and nanoparticle shape dependence. Anal. Chem. 77, 3261−3266.

Oswald, S., Zier, M., Reiche, R., Wetzig, K., 2006. Angle-resolved XPS: a critical evaluation for various applications. Surf. Interface Anal. 38, 590−594.

Paschoal, A.L., Vanâncio, E.C., Canale, L.D.C.F., Silva, O.L.D., Huerta-Vilca, D., Motheo, A.D.J., 2003. Metallic biomaterials TiN-coated: corrosion analysis and biocompatibility. Artif. Organs 27, 461−464.

Pérez-Luna, V.H., Hooper, K.A., Kohn, J., Ratner, B.D., 1997. Surface characterization of tyrosine-derived polycarbonates. J. Appl. Polym. Sci. 63, 1467−1479.

Perrière, J., 1987. Rutherford backscattering spectrometry. Vacuum 37, 429−432.

Petrovykh, D.Y., Kimura-Suda, H., Tarlov, M.J., Whitman, L.J., 2003. Quantitative characterization of DNA films by X-ray photoelectron spectroscopy. Langmuir 20, 429−440.

Popat, K.C., Mor, G., Grimes, C.A., Desai, T.A., 2004. Surface modification of nanoporous alumina surfaces with poly(ethylene glycol). Langmuir 20, 8035−8041.

Ramin, M.L.A., Le Bourdon, G.N.L., Daugey, N., Bennetau, B., Vellutini, L., Buffeteau, T., 2011. PM-IRRAS investigation of self-assembled monolayers grafted onto SiO_2/Au substrates. Langmuir 27, 6076−6084.

Ratner, B.D., Castner, D.G., 2009. Electron Spectroscopy for Chemical Analysis. Surface Analysis − The Principal Techniques. John Wiley & Sons, Ltd.

Ratner, B.D., Hoffman, A.S., Schoen, F.J., Lemons, J.E., 1997. Biomaterials Science: An Introduction to Materials in Medicine. Elsevier.

Ratner, B.D., 1995. Advances in the analysis of surfaces of biomedical interest. Surf. Interface Anal. 23, 521−528.

Reviakine, I., Johannsmann, D., Richter, R.P., 2011. Hearing what you cannot see and visualizing what you hear: interpreting quartz crystal microbalance data from solvated interfaces. Anal. Chem. 83, 8838−8848.

Rodahl, M., Höök, F., Krozer, A., Brzezinski, P., Kasemo, B., 1995. Quartz crystal microbalance setup for frequency and Q-factor measurements in gaseous and liquid environments. Rev. Sci. Instrum. 66, 3924.

Rodriguez-Llorente, S., Aroca, R., Duff, J., 1998. Vibrational spectra and thin solid films of a bi(propylperylenediimide). J. Mater. Chem. 8, 2175−2179.

Schnabel, W., 2014. Infrared Radiation. Polymers and Electromagnetic Radiation. Wiley-VCH Verlag GmbH & Co. KGaA.

Shapiro, A., Vinuela, E., Maizel, J., 1967. Molecular weight estimation of polypeptide chains by electrophoresis in SDS-PAGE. Biochem. Biophys. Res. Commun. 28, 815−820.

Singhal, J., Ray, A., 2002. Synthesis of blood compatible polyamide block copolymers. Biomaterials 23, 1139−1145.

Suggs, L.J., West, J.L., Mikos, A.G., 1999. Platelet adhesion on a bioresorbable poly(propylene fumarate-*co*-ethylene glycol) copolymer. Biomaterials 20, 683−690.

Theeten, J.B., 1981. Ellipsometry in thin film analysis. Ann. Rev. Mater. Sci. 11, 97−122.

Tompkins, H., Irene, E.A., 2005. Handbook of Ellipsometry. William Andrew.

Ueda, K., Narushima, T., Goto, T., Katsube, T., Nakagawa, H., Kawamura, H., Taira, M., 2007. Evaluation of calcium phosphate coating films on titanium fabricated using RF magnetron sputtering. Mater. Trans. 48, 307−312.

Unsworth, L.D., Sheardown, H., Brash, J.L., 2005. Polyethylene oxide surfaces of variable chain density by chemisorption of PEO-thiol on gold: adsorption of proteins from plasma studied by radiolabelling and immunoblotting. Biomaterials 26, 5927−5933.

USDHHS, 2013. Use of International Standard ISO-10993, "Biological Evaluation of Medical Devices Part 1: Evaluation and Testing".

Van Der Marel, C., Yildirim, M., Stapert, H.R., 2005. Multilayer approach to the quantitative analysis of X-ray photoelectron spectroscopy results: applications to ultrathin SiO_2 on Si and to self-assembled monolayers on gold. J. Vac. Sci. Technol. A 23, 1456−1470.

Vanderah, D.J., Gates, R.S., Silin, V., Zeiger, D.N., Woodward, J.T., Meuse, C.W., Valincius, G., Nickel, B., 2003. Isostructural self-assembled monolayers. 1. Octadecyl 1-thiaoligo(ethylene oxides). Langmuir 19, 2612−2620.

Vickerman, J.C., Briggs, D., 2013. ToF: SIMS: Surface Analysis by Mass Spectrometry. IM Publications LLP.

Voinova, M.V., Rodahl, M., Jonson, M., Kasemo, B., 1999. Viscoelastic acoustic response of layered polymer films at fluid-solid interfaces: continuum mechanics approach. Phys. Scr. 59, 391.

Wagner, M.S., 2004. Molecular depth profiling of multilayer polymer films using time-of-flight secondary ion mass spectrometry. Anal. Chem. 77, 911−922.

Wang, S.-F., Li, X., Agapov, R.L., Wesdemiotis, C., Foster, M.D., 2012. Probing surface concentration of cyclic/linear blend films using surface layer MALDI-TOF mass spectrometry. ACS Macro Lett. 1, 1024−1027.

Wang, W., Murthy, N.S., Kuzmenko, I., Anderson, N.A., Vaknin, D., 2013. Structure of biodegradable films at aqueous surfaces: X-ray diffraction and spectroscopy studies of polylactides and tyrosine-derived polycarbonates. Langmuir 29, 11420−11430.

Weber, K., Osborn, M., 1969. The reliability of molecular weight determinations by dodecyl sulfate-polyacrylamide gel electrophoresis. J. Biol. Chem. 244, 4406−4412.

Williams, R., 2010. Surface Modification of Biomaterials: Methods Analysis and Applications. Elsevier.

Wilson, R., Elliott, J., Dowker, S., 1999. Rietveld refinement of the crystallographic structure of human dental enamel apatites. Am. Mineral. 84, 1406−1414.

Zorn, S., Martin, N., Gerlach, A., Schreiber, F., 2010. Real-time PMIRRAS studies of in situ growth of $C_{11}Eg_6OMe$ on gold and immersion effects. Phys. Chem. Chem. Phys. 12, 8985−8990.

This page intentionally left blank

Mechanical behavior and properties of thin films for biomedical applications

6

A.H. Choi, B. Ben-Nissan
University of Technology, Sydney, NSW, Australia

A. Bendavid
Commonwealth Scientific and Industrial Research Organisation, Lindfield, NSW, Australia

B. Latella
Commonwealth Scientific and Industrial Research Organisation, Perth, WA, Australia

6.1 Introduction

During the past three decades, the use of coatings has emerged as one of the leading strategies for surface modification of biomaterials and metallic implants. Depending on their applications, different biomedical and dental devices will require coating materials with different designs, functions, and properties. For these reasons, accurate measurement techniques are needed to determine the mechanical properties of these coatings because they can differ markedly from the bulk material. In particular, better and more reliable techniques are needed to measure the adhesion strength and hardness of coatings quantitatively as well as the fracture toughness at the coating−substrate interface (Ben-Nissan et al., 2013).

Measurements from nanoindentation and microscratch tests are essential tools for characterizing coating properties at the submicron level. Improved understanding of the mechanical properties and failure processes from these tests combined with other appropriate characterization methods will assist in acquiring materials information of coatings. Moreover, theoretical modeling approaches such as finite element analysis (FEA) are vital to the progress of understanding thin film−substrate interfacial behavior, which may result in the better design and selection of thin film and substrate materials.

All coatings in dental and orthopedic implant applications are subjected to a range of external stresses and loads so that the strength and fracture resistance of the coating and the combined effect of the coating−substrate properties to mechanical deformation are vital. Clearly, fracture and de-adhesion can expose the substrate to accelerated corrosion and wear, and the coating debris may provoke a negative response within human tissue. Consequently, it is important that these coatings maintain their integrity when subjected to concentrated and repeated applied loads. Gaining in-depth knowledge of the coating's susceptibility to deformation, fracture, and delamination is

Thin Film Coatings for Biomaterials and Biomedical Applications. http://dx.doi.org/10.1016/B978-1-78242-453-6.00006-7

important in both scientific terms and in clinical applications. The aim of this chapter is to provide a brief background of some of the most widely used test methods for measuring mechanical properties and adhesion performance of coatings and thin films used in biomedical applications.

6.2 Stresses in thin films

It is important to determine stresses in thin films in relation to mechanical stability as a result of the deposition process and the temperatures involved. The stress developed in a film is made up of three components. The first component is intrinsic, which is the result of factors such as deposition, structure, and mode of growth; the second is the result of the mismatch in thermal expansion between film and substrate; and the third is related to externally applied stresses (Lepienski et al., 2004). Once the values of intrinsic stress ($\sigma_{(\text{intrinsic})}$), thermal stress ($\sigma_{(\text{thermal})}$), and externally applied stress ($\sigma_{(\text{external})}$) are determined, the stress developed within a film can be calculated using the following equation:

$$\sigma_{\text{f}} = \sigma_{(\text{intrinsic})} + \sigma_{(\text{thermal})} + \sigma_{(\text{external})} \quad [6.1]$$

In 1909, Stoney proposed a formula that describes the relationship between the change in the curvature radius of a coated and uncoated substrate and the corresponding stress in the layer. Using Stoney's equation, the stress (intrinsic + thermal) in the coating can be calculated with no prior knowledge of the coating properties, but information such as the thickness of the coating and the substrate and Young's modulus and Poisson's ratio of the substrate are needed:

$$\sigma = \frac{1}{6}\left[\frac{1}{R_{\text{f}}} - \frac{1}{R_{\text{i}}}\right] \frac{E_{\text{s}}}{(1 - \nu_{\text{s}})} \frac{t_{\text{s}}^2}{t_{\text{f}}} \quad [6.2]$$

where R_{i} and R_{f} are the radius of curvature before and after coating, respectively; E_{s}, ν_{s}, and t_{s} are the Young's modulus, Poisson's ratio, and the thickness of the substrate; and t_{f} is the thickness of the coating.

The radius (R) can be calculated given the assumption that the length (L) of the substrate is much greater than the final bow (B) using the following equation:

$$R = \frac{L^2}{8B} \quad [6.3]$$

Measurements can be taken in situ during thermal treatment or deposition using optical means such as interferometry or the deflection method with a cantilever beam and a low-power laser. Similarly, elastic strain in films can be determined from changes in crystal lattice d-spacing using X-ray diffraction, from which the stress can be calculated given knowledge of the Young's modulus and strain-free lattice spacing, which may be unknown in many cases (Tsui et al., 1998).

6.3 Adhesion of thin films

The magnitude of adhesive forces that occur as the thin film is applied to the substrate and during drying or firing will depend on the nature of the film and the substrate surface. These adhesive forces can be generally classified as either primary interatomic bonds (ionic and covalent bonds) or secondary bonding (van der Waals bonding) (William and Callister, 1994; Kendall, 2001).

Primary interatomic bonds provide much higher adhesion than do the secondary bonds because the latter are based on much weaker physical forces characterized by hydrogen bonds or dispersion forces. Hydrogen bonds typically arise on polar materials surfaces, whereas all surfaces give rise to interfacial dispersion forces.

Chemical bonding through diffusion, electrostatic attraction, or mechanical interlocking between the coating and the substrate may perhaps be the forces holding the two bodies together. A combination of one or more of these proposed mechanisms may be involved, depending on the physics and chemistry that both the substrate surface and the coating used (Kendall, 2001).

6.3.1 Adhesion based on chemical bond theory

Chemical bonding is expected to be the most durable and the strongest, and it is often possible to form covalent bonds across the interface of the substrate and coating. However, a requirement for this type of bonding is the presence of mutually reactive chemical groups bounded firmly to the coating and the substrate surface.

Under appropriate conditions, the formation of chemical bonds with the substrate material is also possible for some surfaces that contain various chemical functional groups, such as previously coated surfaces, composites, and some plastics (Lee, 1991).

6.3.2 Adhesion based on diffusion theory

Depending on the curing conditions and material properties, atoms will diffuse across the interface to varying extents when two phases of coating and a substrate achieve molecular contact by wetting. The phenomenon is a two-stage process: Wetting is followed by interdiffusion of an element across the interface to establish a chemical bond (Lee, 1991; Kendall, 2001).

6.3.3 Adhesion based on electrostatic theory

It is possible that electrostatic forces are formed at the coating−substrate interface in the form of an electrical double layer. Both coating and substrate surfaces possess residual electric charges that are dispersed throughout the system. Interaction between these electric charges could account for some adhesion of the coating (Lee, 1991; Kendall, 2001).

6.3.4 Adhesion based on mechanical theory

This mechanism of coating action takes place when the coating penetrates the surface of a substrate material containing crevices, voids, pores, and scratches.

This coating is then said to have a mechanical keying or interlocking behavior depending on the substrate's roughness. A number of surface analytical techniques have revealed that the coating can doubtless penetrate into complex tunnel-shaped cracks and undercutting that provide mechanical attachment upon setting or firing (Kendall, 2001).

The interfacial area between the substrate and the coating is influenced by the surface roughness and the force holding the coating onto the substrate is related to the actual interfacial contact area. As a result, the adhesion of a coating can be increased by increasing the surface area.

An increase in surface area can be achieved through surface roughening by means of various mechanical abrasion approaches. Greater surface roughness is advantageous only when the coating completely penetrates into all irregularities on the surface. Failure to penetrate completely will generate voids between the coating and the substrate and will result in a reduction of coating-to-interface contact compared with the corresponding geometric area.

Care must be exercised to avoid sharp and deep profiles even though adhesion is improved by surface roughening in general. The formation of nonuniform films is allowed by these types of profiles, which acts as stress points that tend to decrease the durability of the coating by weakening the adhesion (Lee, 1991). Shrinkage, uneven depths, and three-dimensional changes produce little unrelieved stress as long as the films are fluid. Substantial stresses are accumulated and retained in the final film as viscosity and film stiffness increase and as film adhesion to the substrate develops.

6.3.5 Interfacial adhesion between thin film and substrate

The interfacial adhesion of a coating−substrate system is of vital importance to the performance and reliability of medical products. The work of adhesion (W_A) describes the energy required during fracture of a coating−substrate interface and is calculated using the surface energies of the coating (γ_c) and substrate (γ_s) and at the interface (γ_{cs}):

$$W_A = \gamma_c + \gamma_s - \gamma_{cs} \quad [6.4]$$

This is the same as Griffith fracture, in which the work of adhesion is identical to the fracture resistance of the interface (Lawn, 1993). However, the work of adhesion does not account for roughness, bridging ligaments, asperity contacts, and plastic deformation (Lane, 2003).

For this reason, the practical work of adhesion (W_{prac}) then becomes a more valid measure of adhesion and can be calculated based on the energy spent in plastic deformation of the coating (U_c) and the substrate (U_s). The practical work of adhesion is referred to as the interfacial toughness or strain energy release rate:

$$W_{prac} = W_A + U_C + U_S \quad [6.5]$$

6.3.6 Effects of wettability and surface energetics on adhesion

A new interface is formed when two dissimilar materials are brought into intimate contact at the expense of the two free surfaces. The strength of the bond that forms between the coating and the substrate is determined by the nature of the interaction at the interface. The extent of these interactions is greatly determined by the wettability of one phase by the other. A criterion necessary for adhesion is wetting. Only with the presence of effective wetting between the substrate and the coating can the mechanisms of adhesion previously discussed become operational.

The wetting of a surface can be described in thermodynamic terms. Important parameters that could have an effect on adhesion development and the interfacial bond include the surface energetics of both the solid coating and the substrate as well as the surface tension of the coating in its liquid state (Lee, 1991; Kendall, 2001). The spreading coefficient, which is related to the surface tension, defines the capability of a liquid to wet and spread on a solid. The surface tension of both substances (liquid and solid) will determine whether a given coating will wet a solid surface.

The contact angle determines the degree to which a solid surface is being wetted by a liquid coating. The liquid spreads freely over the surface when the contact angle is zero and is said to wet it completely. Complete wetting takes place when the molecular attraction between the solid molecules and the liquid is greater than that between similar liquid molecules.

In the case of coatings that are applied in the liquid state, the viscosity of the coating phase is also of great importance. For this reason, wetting may be considered as intimate contact between a substrate and a coating. In addition to initial wetting, it is critical for intimate bonding and wetting to remain intact after the coating has been applied for adequate adhesion between the coating and the substrate.

6.4 Mechanical and adhesion testing methods of thin films

With ever-increasing demands imposed by the use of coated implants and devices for dental, orthopedic, and maxillofacial applications, robust and reliable techniques are required for their mechanical characterization. There have been significant advancements in the techniques and equipment capable of extracting the adhesion behavior and mechanical properties of thin films, particularly with the increasing trend toward deposition of nanometer-thick films on smaller devices.

6.4.1 Three- and four-point bending tests

Three- and four-point bending methods have been used to evaluate interfacial fracture energy quantitatively and to characterize the interfacial fracture between dissimilar materials and films on substrates.

The four-point bending method requires a simple bend bar of the coated substrate with a notch machined in the coated layer (Fig. 6.1). The four-point bend delamination

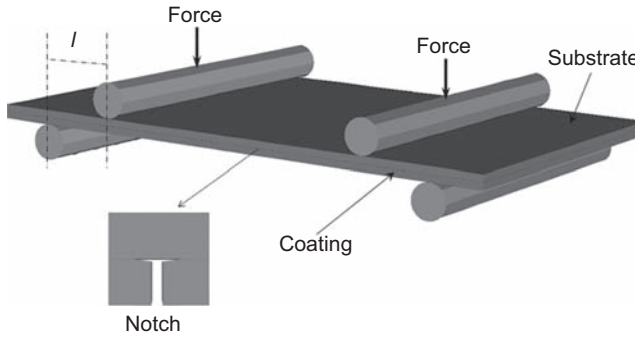

Figure 6.1 Schematic diagram of a four-point bending test.

test was first developed by Charalambides et al. (1989) to study biomaterial interfaces, and it has since been used in many other areas including biomaterials research to measure the mixed-mode fracture energy of numerous coating−substrate systems (Evans et al., 1990; Kuper et al., 1997; Dauskardt et al., 1998; Hofinger et al., 1998; Suansuwan and Swain, 2003; Birringer et al., 2011). The advantage of four-point bending is that the interface fracture energy is independent of the crack length as long as the crack tip is not in close proximity to the precrack or the loading points.

When the specimen is loaded, a crack is initiated from the notch and propagates to the interface as the bending moment increases. For a sufficiently weak interface bond, the crack deflects and propagates symmetrically along the interface at a constant load. The interfacial fracture energy (γ) can be determined using:

$$\gamma = \frac{21P_c^2 l^2\left(1 - v_s^2\right)}{16E_s b^2 h^3} \qquad [6.6]$$

where b is the width of the beam or specimen, h is the total thickness, l is the moment arm or the distance between inner and outer loading lines, P_c is the plateau or critical load for stable crack propagation, and v_s and E_s are the Poisson's ratio and Young's modulus, respectively, of the substrate material.

Similarly, the three-point bend method uses the same type of notched bending specimen as described and has also shown to provide an adequate means to determine the interfacial fracture energy of thin films (Latella and Ignat, 2012). The method relies on cracks generated along the interface from the notch using a simple energy balance for the system before cracking and debonding and the critical moment when the crack deflects into and along the interface.

6.4.2 Bulge and blister testing

Applicable only to pore- and defect-free coatings, a gas or a fluid is used during bulge and blister testing to pressurize the coating−substrate system through a hole in the substrate. With an interferometer or optical microscopy, the height of the resulting

hemispherical bulge in the film is measured. Information on elastic, plastic, and time-dependent deformation can be obtained from the pressure and deflection height.

The pressure is increased until the film starts to debond from the substrate during blister testing. The interfacial energy (γ) can be derived from the critical pressure for debonding using the following equation (Bennet et al., 1974):

$$\gamma = \frac{\rho^2\left(3 - v_f^2\right)r^4}{16E_f t_f^3} \qquad [6.7]$$

where ρ is the applied pressure; r is the radius of the hole; and E_f, v_f, and t_f are the Young's modulus, Poisson's ratio, and the thickness of the film, respectively.

6.4.3 Instrumented nanoindentation technique

Considered the method of choice and starting point by many researchers in the biomedical field for determining the mechanical properties of implants and coatings, instrumented nanoindentation also provides a comprehensive assessment of the elastic–plastic response from the loading and unloading curves based on the coating–substrate combination (for example, soft/hard and rigid/compliant coating on a soft/hard and rigid/compliant substrate).

Nanoindentation is considered a simple and effective way to obtain meaningful values of coating hardness and Young's modulus on the micro- and nanoscales. To obtain the best possible results during nanoindentation, key requirements are sample preparation, calibration of equipment and corrections for thermal drift, initial penetration, frame compliance, indenter tip shape, and penetration depth (Field and Swain, 1993, 1995; Gan et al., 1996; Fischer-Cripps, 2002).

During nanoindentation testing, a set load in the millinewton range is applied to the indenter in contact with the specimen (Fig. 6.2). The penetration depth in the

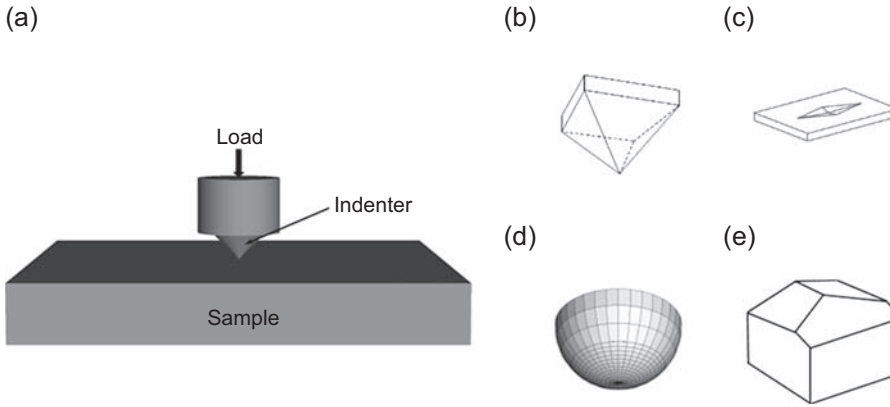

Figure 6.2 Schematic diagram of a nanoindentation test (a) and commonly used indenter type: (b) Vickers indenter; (c) elongated diamond-shaped indent formed on the sample by Knoop indenter; (d) spherical indenter; and (e) Berkovich indenter.

nanometer range is recorded as the load is applied. At maximum load, the area of contact is determined by the depth of the impression and the known angle or radius of the indenter. The result is a load–displacement curve that yields contact pressure or hardness and Young's modulus from the shape of the unloading curve using software based on the model and indenter type (pointed, ie, Berkovich, Vickers, Knoop, or spherical) (see Fig. 6.2(b)–(e)) (Field and Swain, 1995).

Similarly, different types of loading and unloading approaches can be used to extract desired properties as a function of penetration depth (Gan et al., 1996; Gan and Ben-Nissan, 1997; Fischer-Cripps, 2002). The application of nanoindentation as suggested by Field and Swain (1993, 1995) can also be used to determine coating adhesion and residual stress from the load at which delamination occurs (taken from the pop-in that corresponds to a plateau or discontinuity in the load–displacement curve).

The original analysis using microindentation (a technique also valid for nanoindentation) as a method to measure adhesion was performed by Marshall and Evans (1984) and later by Rossington et al. (1984), in which a section of a coating above a delaminating crack induced by indentation was treated as a rigidly clamped disk. The release rate of strain energy obtained consists of three contributing energies:

$$G = \frac{h\sigma_I^2\left(1-\nu_C^2\right)}{2E_C} + (1-\alpha)\frac{h\sigma_r^2(1-\nu_C)}{E_C} - (1-\alpha)\frac{h(\sigma_I-\sigma_B)^2(1-\nu_C)}{2E_C} \quad [6.8]$$

Major disadvantages of using this approach in measuring coating adhesion are that well-adhered or ductile coatings may plastically deform around the indent so that no delamination occurs and the thickness of the coating restricts the indentation load applied (Lane, 2003). Deformation and cracking of the substrate will take place when the indent load is too large, causing the test to become invalid. To overcome such issues, the superlayer indentation technique has been developed, consisting of a hard superlayer deposited on top of the coating, requiring only the plastic indentation depth from nanoindentation and the measurement of debond radius using microscopy (Kriese et al., 1999).

Furthermore, the depth of indentation should not be greater than one-tenth or 10% of the thickness of the coating that is being tested. In general, it is observed that the effect of the substrate is insignificant when the penetration depth is less than 10% of the coating thickness (Sun et al., 1995; Fischer-Cripps, 2002; Chen et al., 2007). This issue is extremely important for coating–substrate systems with submicron- or nanometer-thick coatings, because the indentation results could become inaccurate if the penetration depth is greater than 10% of the coating thickness. This is because the results are strongly affected by the mechanical properties of the substrate and the coating, since they both have a part in supporting the indenter load (Fischer-Cripps, 2002). This problem can be resolved by limiting the amount of force applied to the indenter during testing of nanometer-thick coatings.

By indenting on or near the coating–substrate interface, it is also possible to investigate interfaces and examining the crack deflection and propagation processes (Lardner et al., 1990; Chicot et al., 1996; Latella et al., 2002; Saied et al., 2011). From such studies, important information about interfacial bonding on a localized scale can be obtained from the crack behavior.

Pioneered by Lawn (1998), an area of research that has affected the dental field uses spherical indenters to identify important fracture and deformation damage modes in layered structures and coating−substrate systems such as plasma-sprayed coatings (Pajares et al., 1996) and dental ceramics (Lawn et al., 2001). Coupled with observations, fracture mechanics provide a basis for evaluating the key conditions that control the type of damage and failure mechanisms that predominate, which is important for biomaterials design. Haq et al. (2010) reported an extension of this type of technique to examine damage modes at the microscopic level using spherical nanoindentation and high-resolution microscopy.

Their ability to be used exclusively to study adhesion on a small length scale or in localized regions is the significant characteristic of current instrumented nanoindentation testing systems. The nanoscale measurement and control of load and displacement means that nanoindenters can function in a number of modes by simple modifications to the loading system to carry out tests such as bending, blister, scratching, and pullout (Fischer-Cripps, 2002). The explosion of research in this area is particularly relevant to the field of biology with work on hydroxyapatite (HAp) coatings, which have received considerable attention in the coating implant area (Paital and Dahotre, 2009; Gross et al., 2010; Roest et al., 2011), dental studies (He and Swain, 2009; Lawn et al., 2010), and bone studies (Bembey et al., 2006).

Special attention is required when selecting the correct indenter tip. Sharp indenters such as the Berkovich tip indenter have been used by most researchers to measure the hardness and Young's modulus. However, the assumption of the transition from elastic to plastic behavior of the material is not permissible with a sharp-tipped indenter because these indenters create a nominally constant plastic strain impression. With a spherical tip, on the other hand, the depth of penetration increases as the contact stress increases; therefore, the response of the elastic to plastic transition and the contact stress−strain property of a material can be determined (He and Swain, 2007).

6.4.4 Microtensile testing

In microtensile testing, the coated substrate in the shape of a tensile coupon is uniaxially strained in a universal mechanical testing device (Fig. 6.3) and the surface can be viewed in a scanning electron microscope or with an optical microscope (Agrawal and Raj, 1989, 1990; Ignat, 1996; Latella et al., 2007; Roest et al., 2011). Typically, brittle

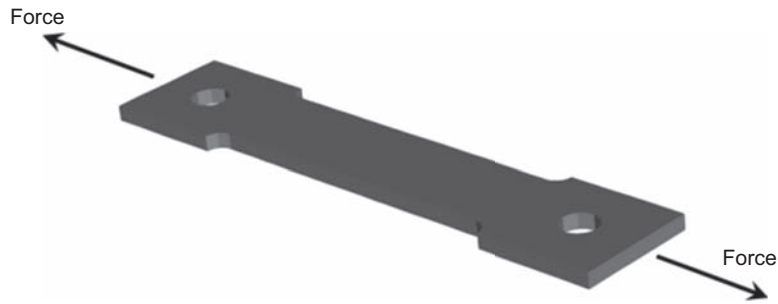

Figure 6.3 Schematic of a coated tensile test specimen pulled during microtensile testing.

coatings on ductile substrates generate parallel cracks perpendicular to the tensile axis when uniaxially stressed. These cracks increase in number with additional elongation, leading to a decrease in crack spacing. These cracks can also be accompanied by significant delamination of the coating.

Microtensile testing is ideal for determining properties of thin films on a variety of ductile substrates. Tensile testing of thin films in this configuration is advantageous in that the stress field is uniform along the gauge length of the sample and relatively small specimens can be used. Evolution in cracking and debonding during loading can be observed using microscopy to gain useful qualitative insights into cracking and de-adhesion susceptibility. However, for quantitative analysis, Young's modulus and the residual stress of the coating are required using other means, such as from curvature measurements and nanoindentation when analyzing the behavior of coatings (Latella et al., 2006).

The coating strength, interfacial shear stress, and interface energy can be calculated using fracture mechanics (Hu and Evans, 1989). The instant of first cracking in the film when a substrate is strained in tension is given by a strain, ε_{cr}. The critical stress for cracking (σ_{cr}) is determined using the Young's modulus of the coating (E_c), taking into account the effect of the residual stress (σ_r). The residual stress is a result of the difference in thermal expansion coefficient of the coating and substrate and during the drying and firing of coatings:

$$\sigma_{cr} = \varepsilon_{cr} E_c + \sigma_r \qquad [6.9]$$

Using the thickness of the coating (h) and the average crack spacing (λ), the interfacial shear stress (τ) can then be determined (Agrawal and Raj, 1989):

$$\tau = \frac{\sigma_{cr} \pi h}{1.5\lambda} \qquad [6.10]$$

The fracture toughness (K_{IC}) of the coating (Ignat, 1996) can be calculated considering the function of the elastic contrast between the coating and substrate ($F(\alpha_D)$) (Beuth and Klingbeil, 1996) and the yield stress of the substrate (σ_Y) obtained experimentally:

$$K_{IC} = \left(\sigma_{cr}^2 h \left[\pi F(\alpha_D) + \frac{\sigma_{cr}}{\sqrt{3}\sigma_Y} \right] \right)^{1/2} \qquad [6.11]$$

Adhesion of the coating to the substrate is determined by measuring the strain (ε_i) at which buckling or detachment of the coating is first observed. When delamination of the coating occurs, the apparent interfacial fracture energy or the steady-state strain energy release rate (γ_i) for a phase angle of ≈ 50 degree (Hutchinson and Suo, 1991) is given by:

$$\gamma_i = \frac{1}{2} E_c h \varepsilon_i^2 \qquad [6.12]$$

An important mechanical property for consideration in assessing the durability of a biomedical material is toughness, which is defined as the ability of a material to absorb energy during deformation up to the point of fracture, typically measured in terms of fracture toughness (Swain and Mencik, 1994; Saha and Nix, 2002; Zhang and Zhang, 2012).

6.4.5 Tensile pull-off and shear testing

The adhesive or bonding strength of the coating layer to the metallic substrate is determined in tensile pull-off testing through the application of a tensile load normal to the interface of the coating on the substrate (Cheng et al., 2009). A structural adhesive is used to glue-coated test specimens with a general diameter of 25 mm to uncoated coupons. A tensile stress is applied to separate the coating and the substrate from which the adhesive strength is determined, which is the maximum load over the coated area (Fig. 6.4(a)). The test is normally carried out on at least five coated coupons from which the average adhesion strength is calculated.

The shear test method (Fig. 6.4(b)) uses a similar approach, but the load is applied to the bonded coating layer parallel to the interface (Wei et al., 1999). The test depends on the use of a sufficiently strong bonding agent to remove the coating from the substrate with an applied shear stress.

Attention must be paid to overcome problems of these techniques, which are related to the uniformity of strength and application of the adhesive and pulling the coating parallel or perpendicular to the interface without misalignment issues. In particular, the adhesive may diffuse through the coating if it is porous, resulting in misleading strength values. Another issue is the need to ascertain adhesive failure over cohesive failure by visual means after testing.

6.4.6 Scratch testing

Undoubtedly, the most popular and widely used technique for assessing the adhesion strength of coating−substrate systems (Benjamin and Weaver, 1960; Laugier, 1981, 1984; Burnett and Rickerby, 1987; Bull and Berasetegui, 2006), scratch testing

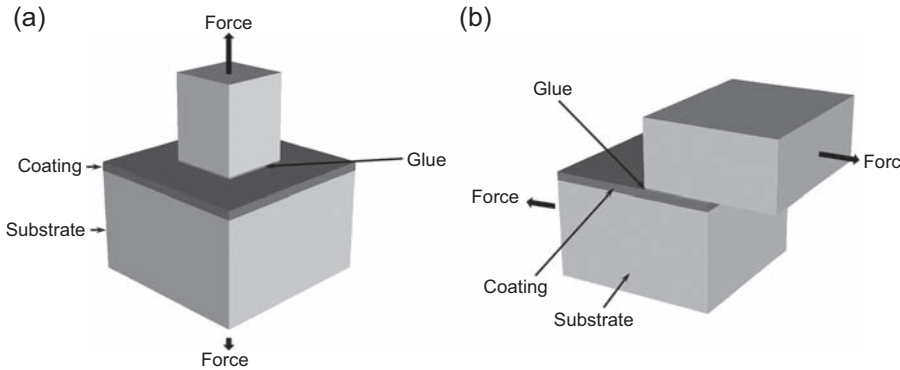

Figure 6.4 Schematic illustrations of (a) the tensile test and (b) the shear test.

consists of using a hard metal or diamond spherical tipped indenter (typically with a radius of 200 μm) to apply an increasing load on the coating surface continuously while the sample is displaced at a constant velocity. Scratching of the surface results in increasing elastic and plastic deformation until extensive spalling of the coating from the substrate occurs at some critical load (L_c). In general, the critical load is determined by acoustic emission, friction force measurements, or optical microscopy.

The practical work of adhesion (W_{prac}) for a coating on substrate system (Burnett and Rickerby, 1987, 1988; Bull et al., 1988) can be calculated by measuring the critical load (L_c), given the information regarding the thickness (h) and the Young's modulus (E) of the coating as well as the contact radius (a) using the following equation:

$$W_{prac} = \left(\frac{L_c}{\pi a^2}\right)^2 \frac{2h}{E} \quad [6.13]$$

However, this equation does not take into consideration the residual stress in the coating. In similar studies by Laugier (1984) for purely elastic coatings on stiff substrates, the practical work of adhesion is given by:

$$W_{prac} = \frac{\sigma^2 h}{2E} \quad [6.14]$$

where σ is a function in the coating that is determined using the residual stress (σ_r) and the applied stress (σ_{appl}), employing the following equation:

$$\sigma = \sigma_r + \sigma_{appl} \quad [6.15]$$

The residual stress in the coating is accounted for, but the model is not entirely valid to describe the stresses when some plastic deformation occurs. These key studies were further developed to take into account the elastic stress distribution and residual stress in the coating, which resulted in an improved equation for determining the strain energy release rate (Hutchinson and Suo, 1991; Venkataraman et al., 1993):

$$G = \left[\frac{(1-\nu^2)\sigma_r^2 h}{2E}\right] + \sum\left[\frac{(1-\nu^2)\overline{\tau}_{ij}^2 h}{2\mu} + \frac{(1-\nu^2)\overline{\sigma}_{ij}^2 h}{2E}\right] \quad [6.16]$$

where σ_r is the residual stress, τ_{ij} and σ_{ij} are the average elastic shear and normal stresses in the delaminated coating, and μ is the shear modulus of the coating.

Generally, scratch testing needs to be approached with caution as a result of the complex stress states involved and the broad array of damage processes that can occur. Likewise, other factors to be considered that can affect the test results include scratching speed, tip shape, environment, loading rate, and coating−substrate properties such as the thickness of the coating, hardness, and roughness.

6.5 Adhesion and mechanical properties of thin films: examples

Over the years, the use of coatings such as HAp for implants and prostheses has gone from being a rarity to being an absolute necessity. A number of excellent studies on adhesion and mechanical properties have been carried out on a range of coatings; major ones include HAp, diamond-like carbon (DLC), titanium nitride, titanium oxide, and nickel-titanium (Ben-Nissan et al., 2013). Listed below are some studies carried out on pure HAp and DLC thin films.

6.5.1 Hydroxyapatite coatings

Although the most popular technique for the deposition of HAp coatings is thermal plasma spraying, the adhesion of plasma-sprayed HAp coatings has been a major concern for cementless hip, knee, and dental prostheses, and it has been the focus of numerous investigations over the past decade (Laonapakul et al., 2012; Gadow et al., 2010; Guipont et al., 2010; Dey et al., 2009; Yang et al., 2009; Yang and Lui, 2007; Oh et al., 2005; Yang et al., 2003; Lin and Berndt, 1994). Furthermore, it is vital to gain insight into the mechanical behavior of plasma-sprayed HAp coatings to overcome problems such as mechanical disintegration associated with the technique (Ben-Nissan and Choi, 2006; Choi and Ben-Nissan, 2007; Saber-Samandari et al., 2014; Hasan et al., 2014).

The adhesion of thermally sprayed coatings involves the integrity of the coating–substrate interface, crack population, residual stresses, and the distribution and size of the pores. Numerous factors can influence the adhesion strength, some of which are related to spray variables such as spray parameters, substrate preparation, and powder characteristics, along with post-heat treatment processes (Dey et al., 2009; Yang et al., 2009; Yang and Lui, 2007). In addition to spray variables, studies have been conducted to ascertain how different deposition processes such as high-velocity flame spraying and solution and suspension thermal spraying affect the adhesion and mechanical strength of the coatings (Gross and Saber-Samandari, 2009; Gadow et al., 2010).

In an attempt to measure the interfacial strength of HAp, Guipont et al. (2010) developed a specific adhesion testing procedure referred to as the Laser Shock Adhesion Test, applied to plasma-sprayed HAp coatings without complicated preparations and fixtures. They observed that a rough surface can significantly improve the bond strength of coatings. However, a thin TiO_2 layer on a smooth Ti-6Al-4V substrate can also have a major influence on adhesion owing to strong chemical adhesion.

6.5.1.1 Properties of sol-gel-derived thin films

The sol-gel technique is a preferred thin film fabrication method because of the relative ease of production and the inexpensive equipment used. Advantages of the process are based on its ability to form a physically and chemically pure and uniform coating over complex geometric shapes and the potential to deliver exceptional mechanical properties.

Significant research has gone into determining factors that could enhance the adhesion of sol-gel-derived coatings. It has been suggested that the use of a TiO_2 interlayer may enhance the adhesion of HAp coating to titanium substrates (Kim et al., 2004; Lee et al., 2009; Roest et al., 2011). The heat treatment temperature is also a key factor that affects the mechanical behavior of coatings. Aksakal and Hanyaloglu (2008) examined the relationship between bonding stress and the treatment temperatures and found that the hardness and bonding strength were optimized after treatment at 750°C.

Alkali treatment introduced by Kokubo et al. (1992) is another approach used to stabilize the coating and improve bonding strength. Balakrishnan et al. (2007) noticed that higher bond strength was achieved on NaOH-treated substrate surfaces. They postulated that the higher bonding strength on NaOH-treated samples could be attributed to factors such as the formation of a thin sodium titanium oxide layer and the high surface roughness.

6.5.2 Diamond-like carbon thin films

Early investigations of DLC coatings were plagued with problems such as decohesion and high compressive stress. To overcome the issue of coating delamination, the use of interlayers such as silicon-based materials was investigated to improve adhesion between DLC and metallic substrates (Bonetti et al., 2006).

Researchers have also focused on improving the mechanical properties of DLC coatings through optimizing deposition processing parameters. Tabbal et al. (1999) discovered that the hardness and elastic modulus both increased with laser intensity used in the deposition process and the observed variations in the hardness and elastic modulus correlated well with variations in the sp^3 content of the DLC coatings. A similar trend was observed in a later study by Leng et al. (2003), in which the hardness of the pulsed vacuum arc plasma-deposited films decreased with an increase in argon flow during deposition. This corresponds to the decrease in sp^3-bonded carbon atoms with increasing argon flow. Sahoo et al. (2010) investigated variations in the hardness of microwave plasma chemical vapor deposited films grown under different processing conditions and suggested that even higher values of hardness (6−16 GPa using nanoindentation) could be achieved when films were grown under optimized process conditions, in which the structure would be predominantly nanocrystalline sp^3 clusters with minimal sp^2 fraction. Ouchabane et al. (2010) noticed in their study that both the hardness and Young's modulus of the plasma-enhanced chemical vapor deposited film decreased as the negative bias voltage increased. They claimed that the observed decrease was probably attributable to the decrease in sp^3C−C bonds through transformation into sp^2 and sp^3C−H bonds under more energetic species contributing to the film growth, and that such microstructure weakens the rigidity of DLC films.

6.6 Finite element examination of thin films

In the 1970s, the finite element method (FEM) was comprehensively applied in engineering and in orthopedic biomechanics to calculate stresses and deformation

in human bones during functional loading and in the design and analysis of implants. Moreover, it has also been used in conjunction with nanoindentation to investigate different types of tissue other than bone, such as dental hard tissue, and to evaluate the biomechanical properties of nanocoatings on implants and devices.

6.6.1 Basics of finite element analysis

In simple terms, FEA takes the physical model that describes the problem and subdivides it into a suitable set of smaller elements of finite dimensions. Once these smaller finite elements combine, they form the mesh model of the investigated structure (Fig. 6.5).

Each element can adopt a specific geometric shape. By combining the actual geometry of the element and its structural and material properties, we can establish equilibrium relations between the external forces acting on the element and the resulting displacements occurring at its corner points or nodes. These equations are most conveniently written in matrix form for use in a computer algorithm.

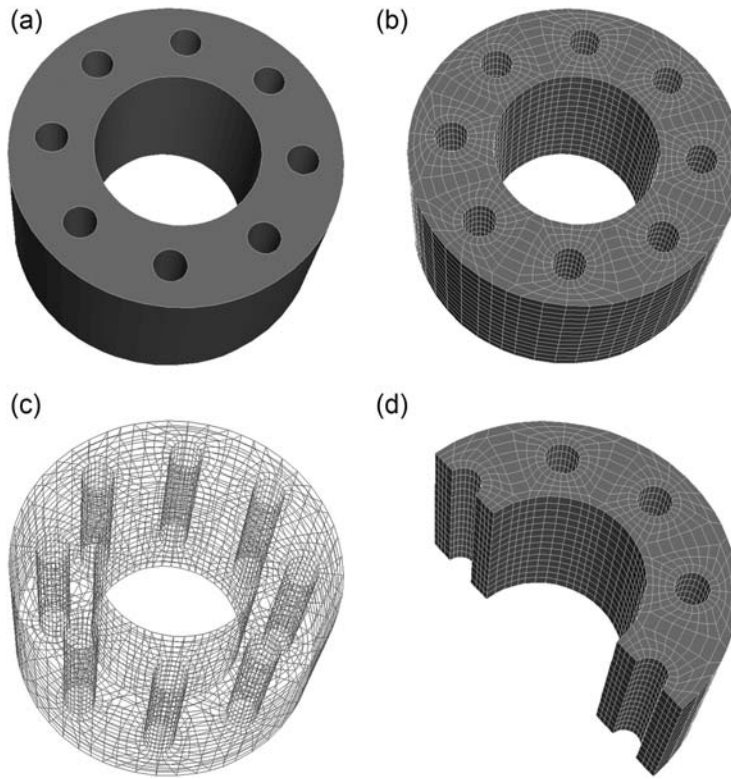

Figure 6.5 Schematic of a reaction vessel. (a) Solid model; (b) finite element mesh; (c) wire frame model; and (d) a cross-sectional view of (b).

The predictive accuracy of FEA is influenced by a number of factors such as the geometric detail of the object to be modeled and analyzed, the applied boundary conditions, functional loading, and material properties. The assignment of proper material properties to an FEA model is a necessary step to ensure predictive accuracy. Stress and strain in a structure are derived based on the material properties.

The capability of FEA lies in its versatility because it can be used to solve a number of physical problems. The model of the problem can contain random sizes and shapes, loads, and support conditions. This great versatility is also enclosed within a single computer program. Another attractive feature of FEA is the close physical similarity between the actual structure and its FEA model (Fig. 6.5). The model is not simply an abstraction. This seems especially true in structural mechanics and may account for the FEM having its origins there.

On the other hand, FEM also has disadvantages. FEA requires that care be taken during the formation of the wire frame model (Fig. 6.5(c)), because mesh volumes should be created to provide a reasonable geometric aspect ratio and behavior for the derived elements. Another option is to manipulate the geometry by dividing contoured curves into smaller ones, thus creating more detailed mesh volumes. However, this option is feasible only in regions with complex shapes or anticipated high gradients of material deformation.

6.6.2 Nonlinear analysis

In FEA, a problem is nonlinear if the force−displacement relationship depends on the current state of the displacement, force, and stress−strain relations. Nonlinearity in a problem can be classed as material nonlinearity, geometric nonlinearity, and bound conditions.

A material is called nonlinear if stresses and strains are related by a strain-dependent matrix instead of a matrix of constants. Thus, the computational difficulty is that equilibrium equations must be written using materials properties that depend on strains, but strains are not known in advance. Plastic flow is often a cause of material nonlinearity.

Geometric nonlinearity occurs if the relationships of strains and displacements are nonlinear with the stresses and forces. This can lead to changes in structural behavior and loss of structural stability. Examples of geometric nonlinearity include buckling and large displacement problems.

Boundary condition can cause nonlinearity if they vary with displacement of the structure. Boundary condition is the load and the resistance to the deformation induced by the loads that represent the effects of the surrounding environment on the model. Many of these nonlinear boundary conditions have a discontinuous character, which makes them some of the most severe nonlinearities in mechanics. Examples are frictional slip effects and contact between two bodies, such as an indenter and a coating.

The main difference between linear and nonlinear FEA lies in the solution of the algebraic equations. Nonlinear analysis is usually more complex and expensive than linear analysis. Nonlinear problems generally require an iterative incremental solution strategy to ensure that equilibrium is satisfied at the end of each step. Unlike linear problems, nonlinear results are not always unique.

6.6.3 Finite element analysis and indentation

FEA has been widely adopted to simulate the elastic and plastic deformations beneath a pointed indenter in nanoindentation tests (Fig. 6.6). A number of advantages are offered by FEA, including a reduction in the experimental time. To date, large-scale commercial codes are available for FEA software that provide a simulation environment for different indenter tips, films, and substrates. Gaining an understanding of the deformation and fracture as well as improving the mechanical characteristics of thin film/coating−substrate system can be achieved by combining FEA and experimental data on indentation.

A new approach to simulating the response during nanoindentation tests of materials with nonlinear behavior using artificial neural networks was proposed by Haj-Ali et al. (2008). They described variables such as indentation deflection, material parameters, and resisting force that are continuously inputted and outputted by the neural networks. Various neural network models such as dimensionless input/output variables are generated and trained with discrete finite element simulations with different nonlinear material parameters and geometries. Only the monotonic loading part of the load−displacement indentation response was used to create the trained neural network models, which is a departure from classical indentation simulations in which the unloading portion is used to determine the stiffness and hardness in general.

Indentations with spherical indenter have been extensively investigated using FEA. Gan et al. (1996) and Gan and Ben-Nissan (1997) investigated the stresses and deformation in sol-gel-derived zirconia films coated on stainless steel under spherical indentation using FEA. Weppelmann and Swain (1996) simulated the deformation and fracture behavior of thin hard films deposited on softer substrates in an effort to examine the stresses responsible for the first fracture event of the film. Thomsen et al. (1998) examined the mechanisms of crack formation during micro- and macro-indentation of DLC coatings on elastic−plastic substrates. The simulations were used to predict the onset of cracking and the fracture mechanisms taking place. Vlachos et al. (2001) investigated the critical ratio of coating thickness to the indentation depth up to which the substrate properties have a negligible effect on the force versus indentation depth curve, and thus on the determined mechanical properties of the coating.

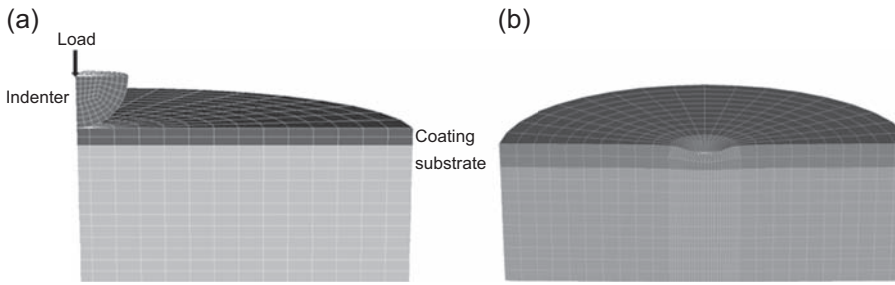

Figure 6.6 Schematic representation of a three-dimensional FEA nanoindentation model. (a) The load is applied to the top of the indenter that is resting on the surface of the coating. The base of the substrate is fixed to prevent movement during simulation; (b) deformation of the nanocoatings at the conclusion of the nanoindentation simulation.

The indentation confidence depth was determined to be a function of the coating to substrate yield strength ratio for three different substrate configurations. Tilbrook et al. (2007) incorporated microstructural failure mechanisms into finite element simulations of nanoindentation of TiN thin films on elastic−plastic substrates. Intergranular sliding that occurs as a result of the columnar grain structure is incorporated into the model via anisotropic property definitions and nodal coupling.

In addition to spherical indentation, various authors conducted studies using conical indenters such as Vickers and Berkovich. Wang and Bangert (1993) studied the Vickers indentation process on the general behavior of bulk and thin film samples using three-dimensional FEA. Two representative systems were analyzed: a soft coating on a hard substrate and a hard coating on a soft substrate. Olaf and Scheer (1993) examined the effect of various parameters such as the geometry and the geometrical imperfections of indenters, friction between indenter and specimen, material properties, coating thickness, and interface properties on indentation using two-dimensional as well as three-dimensional models. Sun et al. (1995) and Panich and Sun (2004) simulated the nanoindentation process of a hard coating on a softer substrate as well as soft coating on hard substrates to examine the influence of the yield strength ratio of the coating and substrate and the indenter tip radius in the critical indentation depth. Knapp et al. (1999) developed a procedure based on FEM of nanoindentation data to determine the mechanical properties of thin films independently of the properties of the underlying substrates. They claimed these procedures accurately deduce properties such as yield strength, Young's modulus, and hardness from indentations as deep as 50% or more of the film's thickness.

Cai and Bangert (1995) examined the relationship between the mechanical properties of both film and substrate on the shape and size of the plastic deformed zone using a wedge-shaped indenter relative to the ratio of penetration depth to film thickness. They found that the general rule not to exceed 10−20% of the film thickness in indentation experiments to obtain a true film hardness value was not a universal law. On the contrary, an investigation by Lichinchi et al. (1998) revealed that the presence of the substrate affected the hardness measurement for relative indentation depths greater than about 15% of the film thickness, and the general criterion that the film should not be penetrated more than 10−20% of its thickness is still acceptable for hard films such as TiN on soft substrates.

FEA has also been used to study interface adhesion between thin film and substrate under indentation. Liu et al. (2007) examined the interface delamination and buckling of thin film subjected to microwedge indentation. In their model, the interface adjoining the thin film and substrate is assumed to be the only site where cracking can occur. A traction−separation law with interface strength and interface energy as two major parameters was introduced to simulate the adhesive and failure behaviors of the interface between the film and the substrate.

6.6.4 Finite element analysis and adhesion testing

In addition to indentation simulations, researchers have investigated the use of FEA to simulate the adhesion and debonding of thin films and coatings. Sauer and Mergel

(2014) developed a nonlinear beam formulation that also incorporated adhesion by body forces and adhesion by surface tractions in an effort to describe the adhesion and debonding of thin films. The new beam formulation was validated both against analytical peeling models and existing two- and three-dimensional solid FE models.

A computational−experimental approach was used by Hopkins et al. (2013) to determine the characteristic interface properties for a polymeric coating bonded to stainless steel. To simulate the bond interaction between the coating and substrate, a user-defined subroutine was used to implement the cohesive zone model. Each simulation consisted of a positioning step in which the polymer was lifted from 0° lying flat along the substrate to 90° directly above the first bonded node of the interface and a pulling step that displaces the polymer arm upward at 90° to the substrate.

An accurate closed-form analytical solution for the strain energy release rate for a thin rectangular film loaded by a central line force using the pull-off test was derived by Sun et al. (2004) in the presence of a tensile residual stress. The theoretical constitutive relation and the strain energy release rate agreed well with two-dimensional nonlinear FEA for the entire deformation regime ranging from the bending plate to the stretching membrane. Later, Sun and Dillard (2010) investigated interfacial delamination for the pull-off test of a thin film strip debonded from a stiff substrate. The strain energy rates of all three modes along the debond front were considered and calculated to examine the mixed fracture modes for the entire deformation regime from the bending plate to the stretching membrane.

6.7 Concluding remarks

The mechanical properties of biomaterial thin films depend strongly on factors such as the deposition process and the microstructure of the deposited film. Accurate techniques are needed to measure the properties of these films because their properties such as hardness and Young's modulus can be different from the equivalent bulk material and the underlying substrate on which they are deposited. It is essential to have tools such as scratching and nanoindentation available for the characterization of submicron coating properties.

New approaches to determine the interfacial adhesion of thin films quantitatively on substrates with complex shapes are being developed. More nanoscale measurement techniques will be needed to cater to the next generation of medical devices with typical micro- and macroscale interfacial adhesion. Furthermore, additional information on the mechanical properties of ultrathin films under various conditions may be revealed by in situ nanomechanical characterization techniques. Other indirect techniques such as atomic force imaging, acoustic emission sensing, and electrical contact resistance may be used in conjunction with the techniques described in this chapter to examine the mechanical properties of biomedical thin films. In-depth understanding of coating deformation and fracture processes using these types of mechanical tests will assist in obtaining valuable information as well as identifying their limitations.

The modification of surfaces using thin film deposition has become a valuable tool for research aimed at understanding how surface properties on the chemical and structural level influence interactions between film material and biosystems, which is a major issue in biomedical materials research. In addition to biological factors, bone−implant interactions are affected by functionally applied multiaxial forces and biomechanics. Gains in fundamental knowledge about biological systems can be accomplished only with appropriate nanoscale mechanical properties of biogenic structures and the influence of nanostructures and nanoscale loading on these biological systems.

Our motivation to determine and measure the mechanical properties of thin films is crucial as developments in ultrathin nanoscale structures and devices continue to grow at an alarming rate. We can envisage and expect that surface modifications aimed at controlling tissue responses will create new opportunities for the development of more durable and functional implants as greater understanding and designs are achieved.

References

Agrawal, D.C., Raj, R., 1989. Measurement of the ultimate shear-strength of a metal ceramic interface. Acta Metall. 37, 1265−1270.

Agrawal, D.C., Raj, R., 1990. Ultimate shear strengths of copper silica and nickel silica interfaces. Mater. Sci. Eng. A 126, 125−131.

Aksakal, B., Hanyaloglu, C., 2008. Bioceramic dip-coating on Ti-6Al-4V and 316L SS implant materials. J. Mater. Sci. Mater. Med. 19, 2097−2104.

Balakrishnan, A., Lee, B.C., Kim, T.N., Panigrahi, B.B., 2007. Hydroxyapatite coatings on NaOH treated Ti-6Al-4V alloy using sol−gel precursor. Mater. Sci. Technol. 23, 1005−1007.

Bembey, A., Oyen, M., Bushby, A., Boyde, A., 2006. Viscoelastic properties of bone as a function of hydration state determined by nanoindentation. Philos. Mag. 86, 5691−5703.

Ben-Nissan, B., Choi, A.H., 2006. Sol−gel production of bioactive nanocoatings for medical applications. Part 1: an introduction. Nanomedicine 1, 311−319.

Ben-Nissan, B., Choi, A.H., Bendavid, A., 2013. Mechanical properties of inorganic biomedical thin films and their corresponding testing methods. Surf. Coat. Technol. 233, 39−48.

Benjamin, P., Weaver, C., 1960. Measurement of adhesion of thin films. Proc. R. Soc. Lond. A 254, 163−176.

Bennet, S.J., Devries, K.L., Williams, M.L., 1974. Adhesive fracture mechanics. Int. J. Fract. 10, 33−43.

Beuth, J.L., Klingbeil, N.W., 1996. Cracking of thin films bonded to elastic-plastic substrates. J. Mech. Phys. Solids 44, 1411−1428.

Birringer, R.P., Chidester, P.J., Dauskardt, R.H., 2011. High yield four-point bend thin film adhesion testing techniques. Eng. Fract. Mech. 78, 2390−2398.

Bonetti, L.F., Capote, G., Santos, L.V., Corat, E.J., Trava-Airoldi, V.J., 2006. Adhesion studies of diamond-like carbon films deposited on Ti6Al4V substrate with a silicon interlayer. Thin Solid Films 515, 375−379.

Bull, S., Berasetegui, E., 2006. An overview of the potential of quantitative coating adhesion measurement by scratch testing. Tribol. Int. 39, 99−114.

Bull, S.J., Rickerby, D.S., Matthews, A., Leyland, A., Pace, A.R., Valli, J., 1988. The use of scratch adhesion testing for the determination of interfacial adhesion − the importance of frictional drag. Surf. Coat. Technol. 36, 503−517.

Burnett, P.J., Rickerby, D.S., 1987. The relationship between hardness and scratch adhesion. Thin Solid Films 154, 403−416.

Burnett, P.J., Rickerby, D.S., 1988. The scratch adhesion test: an elastic-plastic indentation analysis. Thin Solid Films 157, 233−254.

Cai, X., Bangert, H., 1995. Hardness measurements of thin films-determining the critical ratio of depth to thickness using FEM. Thin Solid Films 264, 59−71.

Charalambides, P.G., Lund, J., Evans, A.G., McMeeking, R.M., 1989. A test specimen for determining the fracture resistance of biomaterial interfaces. J. Appl. Mech. 56, 77−82.

Chen, S.H., Liu, L., Wang, T.C., 2007. Small scale, grain size and substrate effects in nano-indentation experiment of film-substrate systems. Int. J. Solid Struct. 44, 4492−4504.

Cheng, K., Ren, C.B., Weng, W.J., Du, P.Y., Shen, G., Han, G.R., Zhang, S., 2009. Bonding strength of fluoridated hydroxyapatite coatings: a comparative study on pull-out and scratch analysis. Thin Solid Films 517, 5361−5364.

Chicot, D., Demarecaux, P., Lesage, J., 1996. Apparent interface toughness of substrate and coating couples from indentation tests. Thin Solid Films 283, 151−157.

Choi, A.H., Ben-Nissan, B., 2007. Sol−gel production of bioactive nanocoatings for medical applications. Part II: current research and development. Nanomedicine 2, 51−61.

Dauskardt, R.H., Lane, M., Ma, Q., 1998. Adhesion and debonding of multi-layer thin film structures. Eng. Fract. Mech. 61, 141−162.

Dey, A., Mukhopadhyay, A.K., Gangadharan, S., Sinha, M.K., Basu, D., 2009. Characterization of microplasma sprayed hydroxyapatite coating. J. Therm. Spray Technol. 18, 578−592.

Evans, A.G., Rühle, M., Dalgleish, B.J., Charalambides, P.G., 1990. The fracture energy of biomaterial interfaces. Mater. Sci. Eng. A 126, 53−64.

Field, J.S., Swain, M.V., 1993. A simple predictive model for spherical indentation. J. Mater. Res. 8, 297−306.

Field, J.S., Swain, M.V., 1995. Determining the mechanical properties of small volumes of material from submicrometer spherical indentations. J. Mater. Res. 10, 101−112.

Fischer-Cripps, A.C., 2002. Introduction to Nanoindentation. Springer, New York.

Gadow, R., Killinger, A., Stiegler, N., 2010. Hydroxyapatite coatings for biomedical applications deposited by different thermal spray techniques. Surf. Coat. Technol. 205, 1157−1164.

Gan, L., Ben-Nissan, B., 1997. The effect of mechanical properties of thin films on nano-indentation data: finite element analysis. Comput. Mater. Sci. 8, 273−281.

Gan, L., Ben-Nissan, B., Ben-David, A., 1996. Modelling and finite element analysis of ultra-microhardness indentation of thin films. Thin Solid Films 290-291, 362−366.

Gross, K.A., Saber-Samandari, S., 2009. Revealing mechanical properties of a suspension plasma sprayed coating with nanoindentation. Surf. Coat. Technol. 203, 2995−2999.

Gross, K.A., Saber-Samandari, S., Heemann, K.S., 2010. Evaluation of commercial implants with nanoindentation defines future development needs for hydroxyapatite coatings. J. Biomed. Mater. Res. B 93, 1−8.

Guipont, V., Jeandin, M., Bansard, S., Khor, K.A., Nivard, M., Berthe, L., Cuq-Lelandais, J.P., Boustie, M., 2010. Bond strength determination of hydroxyapatite coatings on Ti-6Al-4V substrates using the LAser Shock Adhesion Test (LASAT). J. Biomed. Mater. Res. A 95, 1096−1104.

Haj-Ali, R., Kim, H.K., Koh, S.W., Saxena, A., Tummala, R., 2008. Nonlinear constitutive models from nanoindentation tests using artificial neural networks. Int. J. Plast. 24, 371−396.

Haq, A., Munroe, P., Hoffman, M., Martin, P., Bendavid, A., 2010. Effect of coating thickness on the deformation behavior of diamond-like carbon-silicon system. Thin Solid Films 518, 2021−2028.

Hasan, M.F., Wang, J., Berndt, C., 2014. Evaluation of the mechanical properties of plasma sprayed hydroxyapatite coatings. Appl. Surf. Sci. 303, 155−162.

He, L.H., Swain, M.V., 2007. Nanoindentation derived stress-strain properties of dental materials. Dent. Mater. 23, 814−821.

He, L., Swain, M., 2009. Nanoindentation creep behavior of human enamel. J. Biomed. Mater. Res. A 91, 352−359.

Hofinger, I., Oechsner, M., Bahr, H.A., Swain, M.V., 1998. Modified four-point bending specimen for determining the interfacial fracture energy for thin, brittle layers. Int. J. Fract. 92, 213−220.

Hopkins, C., McHugh, P.E., O'Dowd, N.P., Rochev, Y., McGarry, J.P., 2013. A combined computational and experimental methodology to determine the adhesion properties of stent polymer coatings. Comput. Mater. Sci. 80, 104−112.

Hu, M.S., Evans, A.G., 1989. The cracking and decohesion of thin films on ductile substrates. Acta Metall. 37, 917−925.

Hutchinson, J.W., Suo, Z., 1991. Mixed-mode cracking in layered structures. Adv. Appl. Mech. 29, 64.

Ignat, M., 1996. Mechanical response of multilayers submitted to in-situ experiments. Key Eng. Mater. 116-117, 279−290.

Kendall, K., 2001. Molecular Adhesion and Its Applications. Kluwer Academic/Plenum Publishers, New York.

Kim, H.W., Koh, Y.H., Li, L.H., Lee, S., Kim, H.E., 2004. Hydroxyapatite coating on titanium substrate with titania buffer layer processed by sol−gel method. Biomaterials 25, 2533−2538.

Knapp, J.A., Follstaedt, D.M., Myers, S.M., Barbour, J.C., Friedmann, T.A., 1999. Finite-element modeling of nanoindentation. J. Appl. Phys. 85, 1460−1474.

Kokubo, T., Kushitani, H., Ohtsuki, C., Sakka, S., Yamamuro, T., 1992. Chemical reaction of bioactive glass and glass-ceramics with a simulated body fluid. J. Mater. Sci. Mater. Med. 3, 79−83.

Kriese, M.D., Gerberich, W.W., Moody, N.R., 1999. Quantitative adhesion measures of multilayer films: Part I. Indentation mechanics. J. Mater. Res. 14, 3007−3018.

Kuper, A., Clissold, R., Martin, P.J., Swain, M.V., 1997. A comparative assessment of three approaches for ranking the adhesion of TiN coatings onto two steels. Thin Solid Films 308-309, 329−333.

Lane, M., 2003. Interface fracture. Ann. Rev. Mater. Res. 33, 29−54.

Laonapakul, T., Nimkerdphol, A.R., Otsuka, Y., Mutoh, Y., 2012. Failure behavior of plasma-sprayed HAp coating on commercially pure titanium substrate in simulated body fluid (SBF) under bending load. J. Mech. Behav. Biomed. Mater. 15, 153−166.

Lardner, T.J., Ritter, J.E., Shiao, M.L., Lin, M.R., 1990. Behavior of indentation cracks near free surfaces and interfaces. Int. J. Fract. 44, 133−143.

Latella, B.A., Ignat, M., 2012. Interface fracture surface energy of sol−gel bonded silicon wafers by three-point bending. J. Mater. Sci. Mater. Electron. 23, 8−13.

Latella, B.A., Nicholls, T.W., Cassidy, D.J., Barbe, C.J., Triani, G., 2002. Evaluation of interfacial toughness and bond strength of sandwiched silicon structures. Thin Solid Films 411, 247−255.

Latella, B.A., Gan, B.K., Davies, K.E., Mckenzie, D.R., Mcculloch, D.G., 2006. Titanium nitride/vanadium nitride alloy coatings: mechanical properties and adhesion characteristics. Surf Coat Technol 200, 3605−3611.

Latella, B.A., Triani, G., Zhang, Z., Short, K.T., Bartlett, J.R., Ignat, M., 2007. Enhanced adhesion of atomic layer deposited titania on polycarbonate substrates. Thin Solid Films 515, 3138−3145.

Laugier, M.T., 1981. The development of the scratch test technique for the determination of the adhesion of coatings. Thin Solid Films 76, 289−294.

Laugier, M.T., 1984. An energy approach to the adhesion of coatings using the scratch test. Thin Solid Films 117, 243−249.

Lawn, B.R., 1993. Fracture of Brittle Solids. Cambridge University Press, Cambridge.

Lawn, B.R., 1998. Indentation of ceramics with spheres: a century after hertz. J. Am. Ceram. Soc. 81, 1977−1994.

Lawn, B.R., Deng, Y., Thompson, V.P., 2001. Use of contact testing in the characterization and design of all-ceramic crownlike layer structures: a review. J. Prosthet. Dent. 86, 495−510.

Lawn, B.R., Lee, J., Chai, H., Clarke, D., Ruhle, M., Zok, F., 2010. Teeth: among nature's most durable biocomposites. Ann. Rev. Mater. Res. 40, 55−75.

Lee, L.H., 1991. Fundamentals of Adhesion. Plenum Press, New York.

Lee, H.U., Jeong, Y.S., Park, S.Y., Jeong, S.Y., Kim, H.G., Cho, C.R., 2009. Surface properties and cell response of fluoridated hydroxyapatite/TiO_2 coated on Ti substrate. Curr. Appl. Phys. 9, 528−533.

Leng, X.Y., Chen, J.Y., Yang, P., Sun, H., Wan, G.J., Huang, N., 2003. Mechanical properties and platelet adhesion behavior of diamond-like carbon films synthesized by pulsed vacuum arc plasma deposition. Surf. Sci. 531, 177−184.

Lepienski, C.M., Pharr, G.M., Park, Y.J., Watkins, T.R., Misra, A., Zhang, X., 2004. Factors limiting the measurement of residual stresses in thin films by nanoindentation. Thin Solid Films 447, 215−257.

Lichinchi, M., Lenardi, C., Haupt, J., Vitali, R., 1998. Simulation of Berkovich nanoindentation experiments on thin films using finite element method. Thin Solid Films 312, 240−248.

Lin, C.K., Berndt, C.C., 1994. Measurement and analysis of adhesion strength for thermally sprayed coatings. J. Therm. Spray Technol. 3, 75−104.

Liu, P., Zhang, Y.W., Zeng, K.Y., Lu, C., Lam, K.Y., 2007. Finite element analysis of interface delamination and buckling in thin film systems by wedge indentation. Eng. Fract. Mech. 74, 1118−1125.

Marshall, D.B., Evans, A.G., 1984. Measurement of adherence of residually stressed thin films by indentation. I. Mechanics of interface delamination. J. Appl. Phys. 56, 2632−2638.

Oh, I.K., Nomura, N., Chiba, A., Murayama, Y., Masahashi, N., Lee, B.T., Hanada, S., 2005. Microstructures and bond strengths of plasma-sprayed hydroxyapatite coatings on porous titanium substrates. J. Mater. Sci. Mater. Med. 16, 635−640.

Olaf, J.M., Scheer, C., 1993. Finite-element analysis of indentation experiments in surfaces and surface-coated materials. Comput. Mater. Sci. 1, 276−282.

Ouchabane, M., Salah, H., Herrmann, M., Tabet, N., Henda, K., Touchrift, B., Kechouane, M., 2010. Influence of bias voltage on the structure and deposition mechanism of diamond-like carbon films produced by RF (13.56 MHz) CH_4 plasma. Phys. Status Solidi A 207, 2311−2318.

Paital, S.R., Dahotre, N.B., 2009. Calcium phosphate coatings for bio-implant applications: materials, performance factors, and methodologies. Mater. Sci. Eng. R 66, 1−70.

Panich, N., Sun, Y., 2004. Effect of penetration depth on indentation response of soft coatings on hard substrates: a finite element analysis. Surf. Coat. Technol. 182, 342−350.

Pajares, A., Wei, L., Lawn, B.R., Padture, N.P., Berndt, C.C., 1996. Mechanical characterization of plasma-sprayed ceramic coatings on metal substrates by contact testing. Mater. Sci. Eng. A 208, 158−165.

Roest, R., Latella, B.A., Heness, G., Ben-Nissan, B., 2011. Adhesion of sol−gel derived hydroxyapatite nanocoatings on anodized pure titanium and titanium (Ti6Al4V) alloy substrates. Surf. Coat. Technol. 205, 3520−3529.

Rossington, C., Evans, A.G., Marshall, D.B., Khuri-Yakub, B.T., 1984. Measurements of adherence of residually stressed thin films by indentation. II. Experiments with ZnO/Si. J. Appl. Phys. 56, 2639−2644.

Saber-Samandari, S., Alamara, K., Saber-Samandari, S., 2014. Calcium phosphate coatings: morphology, micro-structure and mechanical properties. Ceram. Int. 40, 563−572.

Saha, R., Nix, W.D., 2002. Effects of the substrate on the determination of thin film mechanical properties by nanoindentation. Acta Mater. 50, 23−38.

Sahoo, S., Pradhan, S.S., Bhavanasi, V., Pradhan, S.K., 2010. Structural and mechanical characterization of diamond like carbon films grown by microwave plasma CVD. Surf. Coat. Technol. 204, 2817−2821.

Saied, M.A., Lloyd, I.K., Haller, W.K., Lawn, B.R., 2011. Joining dental ceramic layers with glass. Dent. Mater. 27, 1011−1016.

Sauer, R.A., Mergel, J.C., 2014. A geometrically exact finite beam element formulation for thin film adhesion and debonding. Finite Elem. Anal. Des. 86, 120−135.

Stoney, G.G., 1909. The tension of metallic films deposited by electrolysis. Proc. R. Soc. Lond. 82, 172−175.

Suansuwan, N., Swain, M.V., 2003. Adhesion of porcelain to titanium and a titanium alloy. J. Dent. 31, 509−518.

Sun, Y., Bell, T., Zheng, S., 1995. Finite-element analysis of the critical ratio of coating thickness to indentation depth for coating property measurements by nanoindentation. Thin Solid Films 258, 198−204.

Sun, Z., Dillard, D.A., 2010. Three-dimensional finite element analysis of fracture modes for the pull-off test of a thin film from a stiff substrate. Thin Solid Films 518, 3837−3843.

Sun, Z., Wan, K.T., Dillard, D.A., 2004. A theoretical and numerical study of thin film delamination using the pull-off test. Int. J. Solid Struct. 41, 717−730.

Swain, M.V., Mencik, J., 1994. Mechanical property characterization of thin-films using spherical tipped indenters. Thin Solid Films 253, 204−211.

Tabbal, M., Merel, P., Chaker, M., El Khakani, M.A., Herbert, E.G., Lucas, B.N., O'Hern, M.E., 1999. Synthesis of diamond-like-carbon coatings by pulsed laser deposition: optimization of process parameters. Surf. Coat. Technol. 116, 452−455.

Thomsen, N.B., Fischer-Cripps, A.C., Swain, M.V., 1998. Crack formation mechanisms during micro and macro indentation of diamond-like carbon coatings on elastic-plastic substrates. Thin Solid Films 332, 180−184.

Tilbrook, M.T., Paton, D.J., Xie, Z.H., Hoffman, M., 2007. Microstructural effects on indentation failure mechanisms in TiN coatings: finite element simulations. Acta Mater. 55, 2489−2501.

Tsui, Y.C., Doyle, C., Clyne, T.W., 1998. Plasma sprayed hydroxyapatite coatings on titanium substrates Part 1: mechanical properties and residual stress levels. Biomaterials 19, 2015−2029.

Venkataraman, S.K., Kohlstedt, D.L., Gerberich, W.W., 1993. Metal ceramic interfacial fracture-resistance using the continuous microscratch technique. Thin Solid Films 223, 269−275.

Vlachos, D.E., Markopoulos, Y.P., Kostopoulos, V., 2001. 3-D modelling of nanoindentation experiment on a coating-substrate system. Comput. Mech. 27, 138−144.

Wang, H.F., Bangert, H., 1993. Three-dimensional finite element simulation of Vickers indentation on coated systems. Mater. Sci. Eng. A 163, 43−50.

Wei, M., Ruys, A.J., Swain, M.V., Kim, S.H., Milthorpe, B.K., Sorrell, C.C., 1999. Interfacial bond strength of electrophoretically deposited hydroxyapatite coatings on metals. J. Mater. Sci. Mater. Med. 10, 401−409.

Wepplemann, E., Swain, M.V., 1996. Investigation of the stresses and stress intensity factors responsible for fracture of thin protective films during ultra-micro indentation tests with spherical indenters. Thin Solid Films 286, 111−121.

William, D., Callister, J., 1994. Materials Science and Engineering, third ed. John Wiley and Sons, New York.

Yang, C.W., Lui, T.S., 2007. Effect of crystallization on the bonding strength and failures of plasma-sprayed hydroxyapatite. Mater. Trans. 48, 211−218.

Yang, S., Man, H.C., Xing, W., Zheng, X.B., 2009. Adhesion strength of plasma-sprayed hydroxyapatite coatings on laser gas-nitrided pure titanium. Surf. Coat. Technol. 203, 3116−3122.

Yang, Y.C., Chang, E., Lee, S.Y., 2003. Mechanical properties and Young's modulus of plasma-sprayed hydroxyapatite coating on Ti substrate in simulated body fluid. J. Biomed. Mater. Res. 67A, 886−899.

Zhang, S., Zhang, X., 2012. Toughness evaluation of hard coatings and thin films. Thin Solid Films 520, 2375−2389.

This page intentionally left blank

Thin film coatings and the biological interface

7

J. Chen
Newcastle University, Newcastle upon Tyne, United Kingdom

7.1 Introduction

Biomaterial surface design is critical for controlling cell–material interactions, which will consequently determine the success of tissue engineering and biomedical implants. Depending on the actual applications, polymer, metallic, or ceramics materials may be selected for biomedical engineering. Polymer-based materials have been used for knee replacement[1–5] and scaffold materials[6–12] for soft tissue regeneration. Metallic materials such as Ti (and its alloys)[13,14] and Mg alloys[15–17] are typically used for load-bearing implants (eg, orthopaedic and dental implants). Ceramic materials such as bioglass have been used as scaffold materials for bone regeneration.[18–20] Other materials such as carbon nanotubes have found applications as implanted biosensors.[21]

Depending on the applications of these materials, protein adsorption and subsequent cell adhesion behaviour can be advantages or disadvantages. For implant and scaffold materials, protein adsorption and cell adhesion at the material surface are desirable to promote tissue–material integration. For example, metals or metal alloys meet many of the biomechanical requirements for orthopaedic implants, but interfacial bonding between the metallic surface and surrounding bone is often poor and may lead to failure of the device.[22–25] Therefore, various commercial coatings have applied to the metallic implant to enhance osteointegration of the bone, thus alleviating implant–tissue interface loosening-induced device failure.[26,27] Bacterial–implant adhesion is unwanted because it may lead to biofilm formation and cause infection, which would significantly affect implant success.[28–33] Therefore, it is essential to apply appropriate coatings for the desired mammalian cellular functions and inhibition of bacterial adhesion and formation of biofilm.

In this chapter, various materials that can be used as coatings for biomedical implants are discussed. Key techniques to produce these coatings are briefly explained, followed by discussions about the mechanisms of cell–material interactions. Then, typical examples are provided to illustrate how the surface properties of coatings affect cell–material interactions. Finally, challenges and future trends in developing new coatings for long-term clinical success are discussed.

Thin Film Coatings for Biomaterials and Biomedical Applications. http://dx.doi.org/10.1016/B978-1-78242-453-6.00007-9

7.2 Materials and technologies

7.2.1 Organic coatings

Organic coatings are appealing to biomedical engineering because they have great chemical versatility that can be implemented at the biological surface. These coatings have mechanical properties that are similar to soft biological tissues and can promote desirable mammalian cell−material interactions. Typical polymer coatings include poly(ethylene glycol)-based polymers,[34,35] zwitterionic polymers,[36,37] hyperbranched polymers with hydrophilic groups[38] such as oligosaccharide surfactant polymers,[39] and oligomaltose surfactant polymers,[40] polyelectrolyte multilayers,[41] polyurethane coatings,[42,43] paracyclophane derivative-based coatings,[44] poly(allylamine hydrochloride),[45−47] poly(DL-lactide-*co*-glycolide),[48] and various extracellular matrix (ECM) components (eg, collagen[49]). In addition to promoting mammalian cell−material interactions, some organic coatings such as polyethylene oxide coatings have demonstrated good antifouling properties.[50]

The relative ease of fabrication is another reason for the extensive application of organic coatings. There are a few techniques to apply such organic coatings to medical devices. Typical techniques such as dip-coating, spray-coating, and spin-coating are briefly explained as follows.

Dip-coating: Pull the substrate from the solution of the coating material after it is immersed in the solution for a while, leaving a thin layer of the solution on the substrate surface. After the solvent evaporates, a thin layer of the polymer forms.
Spray-coating: Polymer powder is injected into a heat source and transported to a preheated substrate. It has the ability to apply polymer coatings onto a wide variety of materials.
Spin-coating: Polymer is dissolved in a volatile solvent and the solution is spun. Spin-coating is the preferred method for applying thin, uniform films to flat substrates.
Layer-by-layer: Films are formed by depositing alternating layers of oppositely charged materials with wash steps in between. This can be accomplished using various techniques such as immersion, spin, spray, electromagnetism, and fluidics.
Self-assembled monolayers (SAMs): Organic molecules are molecular assemblies formed spontaneously on surfaces by adsorption and are organized into more or less large ordered domains.[51]
Chemical vapour deposition: Solid film is formed on a substrate as the result of the reaction of vapour-phase chemical reactants, which is a widely used material-processing technology.

7.2.2 Inorganic coatings

There are various inorganic coatings used for biomedical engineering. These include calcium phosphate (CaP)-based bioceramics,[52−54] titanium oxide layers (or nanotubes),[55−58] and carbon-based coatings (eg, diamond-like carbon, carbon nanotubes, graphene coating).[59−62] These coatings can promote cell−material interactions and subsequent tissue regeneration. Titanium oxide coatings also enable implants to have better corrosion resistance.[55−58]

Among these inorganic coatings, CaP-based bioceramic coatings are one of the most common inorganic coatings for implant materials.[63] Such coatings can be produced by plasma-spraying,[64] thermal-spraying,[65] sputter-coating,[66] pulsed laser deposition,[67] sol-gel dip-coating,[68] electrophoretic deposition,[69] hot isostatic pressing[70] and ion beam-assisted deposition.[71,72] To improve adhesion between the CaP layer and the implant, anodic plasma-chemical treatment has been developed, which enables the formation of a porous oxide layer incorporating CaP directly into the oxide.[73,74] Detailed discussions about the applications of typical CaP ceramic coatings in biomedical implants will be provided in Section 7.4.

In many cases, it is particularly useful to combine organic and inorganic coatings with metal particles to enhance the antibacterial functions. For example, silver has been widely applied as an antibacterial coating for various commercially available products such as vascular and urinary catheters and other medical devices. However, the toxicity of the silver released into the environment and the relatively high cost are key issues limiting the applications of silver.[75]

7.3 Cell–material interactions

Material surface characteristics are important for cell–material surface interactions. Three types of cell–material surface interactions can be defined,[76] as illustrated in Fig. 7.1, which is based on the concept proposed in Ref. 76. The first one is nonfouling interactions, in which case cells fail to interact with the material surface.[76] This type of interaction is preferred for various biomedical applications such as artificial blood vessels and valves, artificial heart devices, catheters and blood preservation bags.[76] The second type of interactions is passive adhesion, in which case interfacial response is controlled by physicochemical interactions between the material surface, adsorbed proteins and adhering cells.[76] Surfaces in this category inhibit cellular metabolic changes. The adherent cells remain intact and are readily detached from these surfaces with little damage.[77] The third is bioactive cell adhesion, in which cells activate

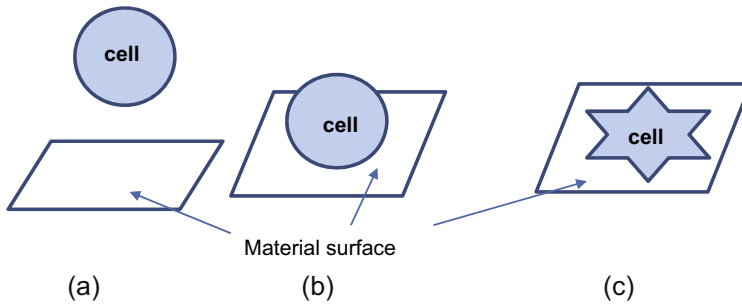

Figure 7.1 Schematic of three types of cell–material surface interactions: (a) nonadsorption interactions; (b) passive adhesion interactions; (c) active adhesion interactions.

receptor-mediated processes, change their morphology and trigger signalling processes for attachment-dependent phenotypes.[76]

Bacterial infection also represents a serious complication for various biomedical implants. Therefore, when discussing cell−material interactions, both mammalian cell−material interactions and bacterial−material interactions should be included.

Fundamentally, active interactions between cells and materials always involve direct interactions between cells and a preabsorbed layer of extracellular biomolecules.[78] Such a principle applies to both mammalian cells and bacteria cells.[78−81] For example, mammalian cells bind to titanium and its alloys by adhesive molecules such as vitronectin and fibronectin.[78,82] When it comes to bacteria, usually bacterial cells bind to the conditioning layer on the material surface. Anything that may be present in the bulk fluid settles on the material surface owing to gravitational force or flow; it may become part of a conditioning layer.[83] For both preabsorbed layers that promote mammalian cells and bacterial adhesion to the material surface, they will be affected by the surface properties of the underlying materials in a given environment. Therefore, this chapter will shed light on how various surface properties of biomaterials may affect the activities of mammalian cells and bacterial adhesion.

7.4 Primitive examples

This section focuses on surface coatings and design for orthopaedic and dental implants. For implanted materials, both mammalian cell−material and bacterial cell−material interactions are important. For the former, active cell−material adhesion is preferred because it may promote tissue integration with the implant or scaffold materials. For the latter, nonadhesion is preferred because bacterial attachment may lead to infection.

Both mammalian cell−material interactions and bacterial adhesion are affected by various chemical and physical factors on the material surface. These factors include the surface biochemistry, surface charge, surface hydrophobicity, surface roughness/topography, surface porosity, surface crystallinity and surface stiffness. All of these will be discussed as follows.

7.4.1 Biochemical interactions

To promote mammalian cell−material interactions, chemical and biochemical surface modifications of the materials can be used. These include inducing immobilized ECM proteins on the implant surfaces and applying CaP[63] and so on.

For example, hydroxyapatite (HA), a typical CaP, is an osteoconductive material that has been shown to promote osteoblast adhesion,[84−91] and which has been widely used as a coating for orthopaedic and dental implants. However, the loss of HA coating owing to delamination[69,92] leads to micromotion of the implant and increased fretting and wear debris particles, which may cause failure of the implant. Therefore, it has been proposed to combine HA (a relatively insoluble calcium ceramic) and tricalcium

phosphate (a more soluble counterpart).[93] Such a biphasic CaP (BCP) would increase interfacial bonding, reducing the risk of micromotion of the implant.[93,94] In addition, BCP coatings further improve osteogenic differentiation of mesenchymal stem cells (MSC) and bone formation.[95–100] However, the orthopaedic implants may develop bacterial infection, which may lead to implant loosening after joint arthroplasty. Therefore, it is essential to improve the coatings further by introducing antiinfective properties. To tackle this, silver particles can be loaded onto CaP coatings to impart antimicrobial properties to metallic substrates.[101,102] It has been demonstrated that HA coatings loaded with silver particles have shown antimicrobial activity for various bacterial cells such as *Staphylococcus aureus* and *Escherichia coli*.[101–105] The antimicrobial mechanism of silver is that it disrupts bacterial membranes and binds to bacterial deoxyribonucleic acid and to the sulphhydryl groups of metabolic enzymes in the bacterial electron transport chain, which disables bacterial replication and key metabolic processes.[101,102] In addition, such silver-containing HA coatings on titanium have been found to inhibit bacterial adhesion and growth effectively without compromising the activities of osteoblasts and epithelial cells.[104,107] These silver coatings can easily be applied by physical vapour deposition and immersion ion implantation.[104,108] In addition, other coatings such as titanium dioxide layers can promote osteointegration[109–112] and reduce bacterial infection,[109,113,114] and can be used as a beneficial coating for implants.

7.4.2 Biophysical interactions

7.4.2.1 Surface charge

A lot of work has been done on how surface charge affects neural cells.[115–117] However, there has been limited work on how the surface charge of biomaterials affects MSC osteogenesis.[118,119] For example, polarized ferroelectric crystal lithium niobate wafers with differently charged surfaces have been used to examine the surface charge effects on the cellular responses of MSCs. Studies revealed that the positively charged wafer surface enhances MSCs osteogenic differentiation.[118] Also, positively charged gold nanoparticles showed higher cellular uptake for human bone marrow–derived MSCs (hMSCs).[119] Different surface charges of gold nanoparticles did not inhibit the osteogenic differentiation of hMSCs, but gold nanoparticles functionalized by the –COOH group reduced alkaline phosphatase (ALP) activity and matrix mineralization in hMSCs, promoted cell proliferation and inhibited ECM development.[119]

Surface charge is important for bacteria adherence to the material surface, and it affects subsequent biofilm formation. Most bacterial cells are negatively charged. Therefore, in general, a positively charged surface is more prone to bacterial adhesion and a negatively charged surface is more resistant to bacterial adhesion.[82] A number of cationic surfaces, such as quaternary ammonium compounds,[120] cationic peptides,[121] chitosan,[122] cationic proteins such as lysozyme[123] and antibiotics,[124] have been found to be antibacterial. Among these, chitosan has been used as a biocompatible scaffold in a range of tissue engineering applications.[125–127] Its antimicrobial properties are mainly the result of positively charged amino groups on the chitosan backbone that

bind to negatively charged bacterial membranes, inducing membrane leakage.[125–127] Therefore, chitosan can be used as a good biological interface for MSCs and osteoblast cells, which could promote cell function and discriminate against bacterial colonization.

7.4.2.2 Surface hydrophobicity

The surface hydrophobicity effect of mammalian cells has been less explored compared with other material surface features. For example, the hydrophobicity of the material surface has been found to affect the adhesion, spreading, proliferation and osteogenic differentiation of MSCs of human and mouse origin.[128] When the $-OH/-CH_3$ mixed SAMs with water contact angles of 40–70 degrees, the adhesion of hMSCs reaches maximum,[128] whereas SAMs with water contact angles of 70–90 degrees are an optimized surface for mouse bone marrow MSCs (mMSCs).[128] Mixed SAMs with a water contact angle of 20–70 degrees promote the spreading of both hMSCs and mMSCs. Proliferation of both hMSCs and mMSCs was most favoured on hydrophilic SAMs with a water contact angle around 70 degrees.[128] In general, a moderate hydrophilic surface (with a contact angle of 40–90 degrees for hMSCs and 70 degrees for mMSCs) promoted osteogenic differentiation in the presence of biological stimuli.[128] Other work reported that hydrophilic surfaces of various polymers affected MSC differentiation[129,130] and adhesion.[131] For instance, the hydrophilicity of poly(epsilon-caprolactone) (PCL) can enable selective differentiation of MSCs into neural cells.[129,130] The alteration of PCL hydrophobicity can be achieved by oxygen plasma treatment[129] and by applying the hydrophobic retinoic acid molecules.[130]

For bacteria cells, it is well known that the hydrophobicity of substratum surfaces significantly influences bacterial adhesion.[132–138] In general, by tuning the surface hydrophobicity, bacterial adhesion can be either enhanced or inhibited, depending on the hydrophobicity of the bacterial species.[139,140] For example, the number of adherent hydrophobic *Streptococcus sanguinis* cells on saliva-coated pure titanium and titanium alloy (Ti-6Al-4V) was twofold higher than that of hydrophilic *Streptococcus constellatus* cells.[141] An increase in apatite hydrophobicity caused the zeta potential of enamel to be more negative and reduced the adhesion of *Streptococcus mitis* but not for *Streptococcus oralis* and *S. sanguinis*.[142] This is because of the difference in the surface properties of bacterial cells, which includes hydrophobicity, zeta potential and the abundance of proteins at surface.[142] In principle, superhydrophobic surfaces may potentially prevent bacterial adhesion and colonization.[143] The advent of the synthetic superhydrophobic surfaces was inspired by the lotus leaf, which is superhydrophobic (with a water contact angle above 150 degrees) and self-cleaning owing to the low surface energy of waxes and the dense microprotrusions and nanopillars on the surface.[144] Based on Cassie–Baxter model, for a heterogeneous surface with microscale and nanoscale patterns, air is trapped in the grooves between surface features, which prevents wetting.[145] Based on such a principle, many superhydrophobic material surfaces have been designed.[143,146] In addition, superhydrophilic surfaces are nonfouling owing to the formation of a dense layer of water molecules, which weakens

the interaction between the cell surface and substratum material and thus reduces cell adhesion.[140,147] Guided by this principle, many nonfouling materials have been developed. These include zwitterionic polymers, neutral molecules with a positive and a negative electrical charge in close proximity, which have demonstrated superhydrophilicity properties and reduced fouling caused by proteins and bacteria.[147] Further evidence has shown that zwitterionic polymers could inhibit oral bacterial adhesion on human teeth by up to 70%.[148]

7.4.2.3 Surface roughness and topography

Cell–biomaterial interactions in tissue engineering are influenced not only by topographical features comparable to cell size (1–100 μm)[149–150] but also by nanoscale details of the biomaterial surface.[151–155] For example, it has demonstrated that surface roughness affects both osteoblast adhesion and differentiation.[152,153,156–158] Osteoblast-like cells grown on rough titanium surfaces (average surface roughness [Ra] of 4–7 μm) show reduced proliferation and enhanced osteogenic differentiation with upregulation of ALP activity and the osteogenic differentiation marker osteocalcin.[152,153,156–158]

Various implants in clinical practice have micropits on the surface. The surface features can be engineered through techniques such as grit blasting, acid etching and plasma spraying.[159] These microtextured implants have demonstrated enhanced osteointegration compared with smooth implants by in vivo tests.[151,160] In addition, mammalian cells (eg, MSCs, osteoblasts) can detect, interact and respond to nanotopographical features in vitro (see Ref. 159). To create surface patterns, techniques can be used including screen printing,[161–163] soft lithography,[164] nanoimprint lithography/embossing,[165,166] laser ablation,[167] three-dimensional printing[168–170] and photopatterning.[171–174]

Nanoscale architecture is defined by a feature or grain size less than 100 nm. This architecture affects the roughness, surface area and surface energy of the material and can thus enhance osteoblast contact signalling.[175–177] Nanophase titanium surfaces, typically with a grain size below 100 nm, have been shown to be more effective in promoting osteoblast adhesion and proliferation compared with microtextured surfaces (typically with a grain size above 1 μm).[178–182] The in vivo rabbit tibial model has shown that titanium dioxide nanotubes significantly enhance bone bonding compared with surface with microscale architecture.[183,184] In addition, titanium dioxide nanotubes demonstrated antibacterial properties.[185] Other work showed that nano-titania and nano-HA surfaces support bone ongrowth.[186–190] A similar roughness-dependent cell response has been found for organic surface coatings such as collagen type I, vitronectin and fibronectin.[106,154]

However, nanotextured surfaces without an underlying microstructure may not have good osteointegration. For example, when purely nanostructured surfaces were implanted into rat femurs, there was a period of bony ingrowth into the nanoarchitecture.[185] However, the implant–bone interface was weak and was disrupted by the gross motion of the rat.[185] When nanoscale architecture was combined with the underlying microstructure, there was significant improvement in both bone matrix

mineralization and implant fixation strength.[185] Other work suggested that the combination of titanium dioxide nanotube coatings with underlying microstructure surfaces could further enhance osteogenesis compared with a nanoscale or microscale surface alone.[159]

For bacterial cells, the irregularities of a surface promote bacterial adhesion and biofilm formation whereas ultrasmooth surfaces may not favour bacterial adhesion and biofilm deposition, as found in both experimental work[191] and computational modelling.[192] This is possibly because a rough surface has a greater surface area and the crevices in the roughened surfaces may provide more favourable sites for colonization[193] as well as a decrease in the energy barrier for bacteria to be deposited onto the material surface.[192] Moreover, how the grooves in the surface affect bacterial adhesion depends on the grooves' size.[191] Widths of the grooves between 10 and 40 μm displayed no effect on bacterial adhesion, which suggests that bacteria preferentially adhere to irregularities comparable to their size so that the bacterial surface contact area may be maximized.[191] If the grooves or scratches on the surface are too small for the bacterium to fit, it would reduce the contact area and the binding between the bacteria and the material surface.[194] Moreover, it has been shown that an increase in Ra on stainless steel from 0.04 to 0.30 μm increased bacterial adhesion strength more than a larger increase in surface roughness from 0.04 to 0.96 μm for unpolished stainless steel.[195]

7.4.2.4 Surface porosity

Surface porosity affects interactions between osteoblast cells and biomaterials by allowing direct ingrowth of osteogenic cells into the implant, thus strengthening the bone−implant interface.[196] Much work has been done on the effect of pore morphology and dimension on osteoblast differentiation and osteointegration. Scaffolds with interconnected pores usually enhance bony ingrowth compared with those with closed pores.[197] This is because improved ingrowth of vasculature enables better delivery of osteoprogenitors to the scaffold bulk.[197,198] Furthermore, it has been proposed that pores must be sufficiently large for vascular infiltration without compromising the mechanical properties of the coating.[197] Porous CaPs with increased micropores (pores < 10 μm) are more osteoinductive than their nonporous counterparts.[199]

However, surface porosity increases surface contact area, which may also promote the bacterial adhesion and bacterial colonization at the material surface.[200–203] This would jeopardize implant fixation. For example, in vitro staphylococcal adhesion and biofilm formation on porous pure Ti and Ti-6Al-4V alloy coatings has been found to be significantly higher than their dense counterparts.[200] The effect of a porous surface on bacterial adherence and bacteria colonization is mainly because porous surfaces usually increase surface roughness and hydrophobicity. These open surface pores often are colonized with large bacterial colonies.[200] To eliminate such bacteria colonization, micro-arc oxidation of H_3PO_4 solution with HA and $CaCl_2$ additions has been proposed to modify the pore surface of Ti coating by applying a TiO_2 layer containing calcium and phosphate ions.[200]

7.4.2.5 Surface crystallinity

There has been only a small amount of work on the effect of surface crystallinity on mammalian cells. For example, Overgaard et al. inserted two HA-coated implants with crystallinities of 50% (HA 50%) and 75% (HA 75%) into the medial femoral condyles of the knees of dogs.[204] They found that the implant−tissue interface strength of HA 50% reached a peak within 16 weeks, and it took much longer for the HA 70% to reach similar peak strength. In addition, HA 50% also promoted more bony ingrowth, which replaced the resorbed HA coating. In summary, the increased crystallinity of HA coating appears to slow resorption of HA and decrease bone ingrowth.[204]

Modifying the crystalline structure of the surface layer may also affect bacterial adhesion. For example, Del Curto adopted the approach of combined anodization and heat treatment to convert amorphous titanium oxide to a TiO_2 crystalline layer enriched with anatase phase.[205] Two typical cell lines, MG63 human osteoblastic-like cells and L9292 murine fibroblasts, and three typical *Streptococcus* species have been examined to study how these cells interact with an amorphous and crystalline TiO_2 layer. Such an anatase-rich TiO_2 layer significantly reduced bacterial attachment without affecting the host cells' metabolic activities.[205] Compared with other forms of TiO_2, anatase phase has a larger band gap, which increases the surface redox potentials and prolongs the carrier lifetime.[206] The valence band hole oxidizes water to form hydroxyl radicals that oxide cells.[207] This may be attributed to the inhibition of bacterial adhesion.

7.4.2.6 Surface stiffness

A lot of work has been done regarding how surface mechanical properties regulate the activities of mammalian cells.[209–212] The mechanical property discussed in the literature usually refers to the stiffness of the materials. For example, MSCs and many other cells spread on stiff materials and retain a nearly spherical shape on very soft materials.[211,213] It has been demonstrated that MSCs are more likely to differentiate to soft tissue phenotypes when cultured on a soft matrix and to hard tissue phenotypes when cultured on a stiff matrix.[214] Similar observations were found for many biopolymers. However, it was shown that MSCs spread on polydimethylsiloxane (PDMS) despite varied stiffness.[81] Also, MSC differentiation was unaffected by the stiffness of PDMS. Chen et al. suggested that the viscoelastic properties and surface adhesion of the PDMS could contribute to cell−material interaction.[215]

The surface stiffness-dependent behaviour of bacteria has been less explored compared with that of mammalian cells. Using polyelectrolyte multilayer thin films composed of poly(allylamine hydrochloride) and poly(acrylic acid) as model materials, Lichter et al.[208] found that the adhesion of *Staphylococcus epidermidis* is positively correlated with the stiffness of this material with a varied Young's modulus from 0.8 to 80 MPa, independent of surface roughness and charge density. Other photo-cross-linkable polyelectrolyte films made from poly(L-lysine) (PLL) and hyaluronan derivative modified with photo-reactive vinylbenzyl groups (HAVB) have also been examined.[216] The adhesion and growth of two model bacteria, *E. coli* and *Lactococcus lactis*, were examined on the softer (non-cross-linked) and stiffer

(cross-linked) polyelectrolyte films. The gram-negative bacteria *E. coli* exhibited more rapid growth on the softer films compared with the stiffer ones. However, the gram-positive bacteria *L. lactis* grew slowly on both films independently of their stiffness. Therefore, the photo-cross-linked (PLL/HAVB) films are interesting coatings for tissue engineering because they resist bacterial colonization and promote the growth of mammalian cells.

Song and Ren[217] further revealed that bacterial cells are able to sense and respond to material stiffness. For example, *E. coli* RP437 and *Pseudomonas aeruginosa* PAO1 have been used as model strains to investigate early-stage biofilm formation on PDMS surfaces with varied stiffness. An inverse correlation between cell adhesion and the stiffness of PDMS was found for both species. The cells attached on relatively stiffer PDMS (with higher cross-linking density) were significantly smaller than those on relatively soft substrate.[217] In addition, the bacterial cells on the stiffer PDMS were more resistant to antibiotics.[217] In summary, surface stiffness affects both bacterial adhesion and the physiology of the attached bacterial cells.

7.5 Challenges and future trends

For inorganic coatings (usually ceramic coatings) for implant materials, their biological properties and mechanical properties need to be further improved for desired applications. The biological properties can be enhanced by adding osteoinductive molecules such as growth factors[218] and creating micro-nanoscale features for the coatings and the underlying implant materials. Strengthening the mechanical properties, typically for interface binding, can be achieved by combining different coatings (eg, TiO_2 layers incorporating CaP) with the enabling techniques such as anodic plasma-chemical treatment. In addition, the creation of a porous structure and inducing appropriate crystallinity may promote bony ingrowth and thus increase implant fixation.

In addition to supporting the desired biological functions of mammalian cells and the subsequent tissue−implant integration, the coatings should be capable of resisting bacteria colonization at the biological interface. The key challenges are that bacterial and host cells both may positively respond to similar surface features. For example, osteoblasts and bacteria both prefer surfaces with higher surface energy (hydrophilic), roughness and nanoscale architecture.[224] In such a case, the competitive mechanisms of mammalian cell−material interactions and bacterial adhesion can be described by the 'race to the surface' theory.[83] This means that whichever cell type, osteogenic or bacterial, first reaches the implant surface determines whether the biofilm may develop or not.[83]

To inhibit bacterial adhesion and colonization, silver particle can be a good addition to surface coatings on the implant materials owing to its antibacterial properties for a wide range of gram-negative and gram-positive bacterial cells, to its long-lasting antibacterial effect and to its being less prone to the development of resistance.[219] However, the Ag particle may induce long-term tissue toxicity, which is a concern.

Therefore, future trends are likely to adopt a physical-based approach without involving biochemistry. It has been discovered that the dense nanopillars on cicada wings can kill bacteria such as *P. aeruginosa*.[220] Such nanopillars enable membrane rupture in multiple sites and tear the bacteria apart.[220] Inspired by this, the so-called black silicon, a synthetic silicon-based nanomaterial with high-aspect ratio nanoprotrusions, has been fabricated to mimic surface nanoarray nanopillars on cicada wings.[221,222] These nanostructures can be produced by a reactive-ion etching technique. Both nanopillars on cicada wings and black silicon are highly bactericidal against all tested gram-negative and gram-positive bacteria.[221] Estimated bacterial average killing rates by black silicon are 450,000 cells per minute per square centimeter.[221] When adopting such a nanostructure, potential rupture of mammalian cell membranes should be avoided. Brush-like and pocket-like titanium nanowires have been fabricated that are capable of discriminating bacterial from mammalian cells and further enhancing the cellular functions of mammalian cells.[219]

A similar nanostructure-based principle could be applied to soft organic coatings. For example, self-assembly topology enabling a netlike architectural mimetic of native extracellular matrices has been found to enhance mammalian cell attachment and proliferation and resist bacterial colonization.[223] For such soft inorganic materials, a mechanical rupturing mechanism is unlikely to be applicable. Instead, modulations of mammalian and bacterial cell adhesion by microscale to nanoscale structures are more likely to be attributed to different cell sizes between the mammalian and bacterial cells.

Therefore, the future trend will be to combine appropriate coating materials with surface nanostructures to promote desired mammalian cellular functions and resist bacterial adhesion and colonization. Such a strategy can also be extended to a wide range of biomedical engineering.

Acknowledgements

This work was funded by the Engineering and Physical Sciences Research Council, entitled ‘A New Frontier in Design: The Simulation of Open Engineered Biological Systems’ (EP/K039083/1) and by the Medical Research Council Confidence in Concept (CiC) Fund. Dr. Maria Katsikogianni at University of Bradford is acknowledged for useful discussions.

References

1. Senatov FS, et al. UHMWPE-based nanocomposite as a material for damaged cartilage replacement. *Mater Sci Eng C Mater Biol Appl* 2015;**48**:566−71.
2. Tozzi S, et al. The effects of contact area and applied load on the morphology of in vitro worn ultra-high molecular weight knee prostheses: a micro-Raman and gravimetric study. *J Raman Spectrosc* 2014;**45**(9):781−7.
3. Affatato S, et al. Quantification of wear rates and plastic deformation on mobile unicompartmental UHMWPE tibial knee inserts. *Tribol Lett* 2013;**52**(1):57−65.

4. Pokorny D, Slouf M, Fulin P. Current knowledge on the effect of technology and sterilization on the structure, properties and longevity of UHMWPE in total joint replacement. *Acta Chir Orthop Traumatol Cech* 2012;**79**(3):213−21.
5. Slouf M, et al. Ultrahigh molecular weight polyethylene for total joint replacements with longer lifetime. *Chem Listy* 2013;**107**(10):783−90.
6. Hannink G, et al. Effect of load on the repair of osteochondral defects using a porous polymer scaffold. *J Biomed Mater Res B Appl Biomater* 2012;**100**(8):2082−9.
7. Mary SA, Dev VRG. Electrospun herbal nanofibrous wound dressings for skin tissue engineering. *J Text Inst* 2015;**106**(8):886−95.
8. Oktay B, et al. Fabrication of collagen immobilized electrospun poly(vinyl alcohol) scaffolds. *Polym Adv Technol* 2015;**26**(8):978−87.
9. Jensen T, et al. Biomimetic and synthetic esophageal tissue engineering. *Biomaterials* 2015;**57**:133−41.
10. Jiang T, et al. Electrospinning of polymer nanofibers for tissue regeneration. *Prog Polym Sci* 2015;**46**:1−24.
11. Koetting MC, et al. Stimulus-responsive hydrogels: theory, modern advances, and applications. *Mater Sci Eng R Rep* 2015;**93**:1−49.
12. Mukundan S, et al. Nanofibrous composite scaffolds of poly(ester amides) with tunable physicochemical and degradation properties. *Eur Polym J* 2015;**68**:21−35.
13. Cheng M, et al. Calcium plasma implanted titanium surface with hierarchical microstructure for improving the bone formation. *ACS Appl Mater Interfaces* 2015;**7**(23):13053−61.
14. Ozan S, et al. Development of Ti-Nb-Zr alloys with high elastic admissible strain for temporary orthopedic devices. *Acta Biomater* 2015;**20**:176−87.
15. Chaya A, et al. In vivo study of magnesium plate and screw degradation and bone fracture healing. *Acta Biomater* 2015;**18**:262−9.
16. Iskandar ME, et al. Nanostructured calcium phosphate coatings on magnesium alloys: characterization and cytocompatibility with mesenchymal stem cells. *J Mater Sci Mater Med* 2015;**26**(5).
17. Razavi M, et al. In vivo biocompatibility of Mg implants surface modified by nanostructured merwinite/PEO. *J Mater Sci Mater Med* 2015;**26**(5).
18. Aniket, et al. Early osteoblast responses to orthopedic implants: synergy of surface roughness and chemistry of bioactive ceramic coating. *J Biomed Mater Res A* 2015; **103**(6):1961−73.
19. Ardeshirylajimi A, et al. Enhanced osteoconductivity of polyethersulphone nanofibres loaded with bioactive glass nanoparticles in in vitro and in vivo models. *Cell Prolif* 2015; **48**(4):455−64.
20. Lin K, et al. Degradation and silicon excretion of the calcium silicate bioactive ceramics during bone regeneration using rabbit femur defect model. *J Mater Sci Mater Med* 2015; **26**(6):197.
21. Ziegler KJ. Developing implantable optical biosensors. *Trends Biotechnol* 2005;**23**(9): 440−4.
22. Urban RM, et al. The bone-implant interface of femoral stems with non-circumferential porous coating − a study of specimens retrieved at autopsy. *J Bone Jt Surg Am* 1996; **78**(7):1068−81.
23. Long M, Rack HJ. Titanium alloys in total joint replacement − a materials science perspective. *Biomaterials* 1998;**19**(18):1621−39.
24. Bobyn JD, et al. The susceptibility of smooth implant surfaces to periimplant fibrosis and migration of polyethylene wear debris. *Clin Orthop Relat Res* 1995;**311**: 21−39.

25. Cook SD, Thomas KA, Haddad RJ. Histologic analysis of retrieved human porous-coated total joint components. *Clin Orthop Relat Res* 1988;**234**:90−101.
26. Kitsugi T, et al. Bone-bonding behavior of plasma-sprayed coatings of Bioglass(R), AW-glass ceramic, and tricalcium phosphate on titanium alloy. *J Biomed Mater Res* 1996;**30**(2):261−9.
27. Kitsugi T, et al. Bone bonding behavior of titanium and its alloys when coated with titanium oxide (TiO_2) and titanium silicate (Ti_5Si_3). *J Biomed Mater Res* 1996;**32**(2):149−56.
28. Cats-Baril W, et al. International consensus on periprosthetic joint infection: description of the consensus process. *Clin Orthop Relat Res*® 2013;**471**(12):4065−75.
29. Lentino JR. Prosthetic joint infections: bane of orthopedists, challenge for infectious disease specialists. *Clin Infect Dis* 2003;**36**(9):1157−61.
30. Zmistowski B, et al. Periprosthetic joint infection increases the risk of one-year mortality. *J Bone Jt Surg* 2013;**95**(24):2177−84.
31. Dale H, et al. Increasing risk of revision due to deep infection after hip arthroplasty: a study on 97,344 primary total hip replacements in the Norwegian Arthroplasty Register from 1987 to 2007. *Acta Orthop* 2009;**80**(6):639−45.
32. Dale H, et al. Infection after primary hip arthroplasty: a comparison of 3 Norwegian health registers. *Acta Orthop* 2011;**82**(6):646−54.
33. Dale H, et al. Increasing risk of prosthetic joint infection after total hip arthroplasty: 2,778 revisions due to infection after 432,168 primary THAs in the Nordic Arthroplasty Register Association (NARA). *Acta Orthop* 2012;**83**(5):449−58.
34. Chapman RG, et al. Polymeric thin films that resist the adsorption of proteins and the adhesion of bacteria. *Langmuir* 2001;**17**(4):1225−33.
35. Drachuk I, et al. Silk macromolecules with amino acid poly(ethylene glycol) grafts for controlling layer-by-layer encapsulation and aggregation of recombinant bacterial cells. *ACS Nano* 2015;**9**(2):1219−35.
36. Hayward JA, Chapman D. Biomembrane surfaces as models for polymer design − the potential for hemocompatibility. *Biomaterials* 1984;**5**(3):135−42.
37. Chen SF, et al. Strong resistance of phosphorylcholine self-assembled monolayers to protein adsorption: insights into nonfouling properties of zwitterionic materials. *J Am Chem Soc* 2005;**127**(41):14473−8.
38. Perrino C, et al. A biomimetic alternative to poly(ethylene glycol) as an antifouling coating: resistance to nonspecific protein adsorption of poly(L-lysine)-graft-dextran. *Langmuir* 2008;**24**(16):8850−6.
39. Holland NB, et al. Biomimetic engineering of non-adhesive glycocalyx-like surfaces using oligosaccharide surfactant polymers. *Nature* 1998;**392**(6678):799−801.
40. Ruegsegger MA, Marchant RE. Reduced protein adsorption and platelet adhesion by controlled variation of oligomaltose surfactant polymer coatings. *Student Research Award in the Doctoral Degree Candidate Category, 27th Annual Meeting of the Society for Biomaterials, St. Paul, MN, April 24−29, 2001. J Biomed Mater Res* 2001;**56**(2): 159−167.
41. Ladam G, et al. Protein interactions with polyelectrolyte multilayers: interactions between human serum albumin and polystyrene sulfonate/polyallylamine multilayers. *Biomacromolecules* 2000;**1**(4):674−87.
42. Yao C, et al. Surface modification and antibacterial activity of electrospun polyurethane fibrous membranes with quaternary ammonium moieties. *J Membr Sci* 2008;**320**(1−2): 259−67.
43. Chen J-P, Chiang Y. Bioactive electrospun silver nanoparticles-containing polyurethane nanofibers as wound dressings. *J Nanosci Nanotechnol* 2010;**10**(11):7560−4.

44. Elkasabi Y, et al. Towards multipotent coatings: chemical vapor deposition and bio-functionalization of carbonyl-substituted copolymers. *Macromol Rapid Commun* 2008; **29**(11):855−70.
45. Yang SY, Mendelsohn JD, Rubner MF. New class of ultrathin, highly cell-adhesion-resistant polyelectrolyte multilayers with micropatterning capabilities. *Biomacromolecules* 2003;**4**(4):987−94.
46. Olenych SG, et al. Fibronectin and cell attachment to cell and protein resistant polyelectrolyte surfaces. *Biomacromolecules* 2005;**6**(6):3252−8.
47. Tsai W-B, Chen Y-H, Chien H-W. Collaborative cell-resistant properties of polyelectrolyte multilayer films and surface PEGylation on reducing cell adhesion to cytophilic surfaces. *J Biomater Sci Polym Ed* 2009;**20**(11):1611−28.
48. Karp JM, Shoichet MS, Davies JE. Bone formation on two-dimensional (DL-lactide-*co*-glycolide) (PLGA) films and three-dimensional PLGA tissue engineering scaffolds in vitro. *J Biomed Mater Res A* 2003;**64**(2):388−96.
49. Muller R, et al. Surface engineering of stainless steel materials by covalent collagen immobilization to improve implant biocompatibility. *Biomaterials* 2005;**26**(34):6962−72.
50. Cima LG. Polymer substrates for controlled biological interactions. *J Cell Biochem* 1994;**56**(2):155−61.
51. Madou M. *Fundamentals of microfabrication: the science of miniaturization*. CRC; 2002.
52. Arul KT, et al. Novel ultraviolet emitting low energy nitrogen ion implanted magnesium ion incorporated nanocrystalline calcium phosphate. *Mater Lett* 2015;**153**:182−5.
53. Ko C-L, et al. Characterization of the aspects of osteoprogenitor cell interactions with physical tetracalcium phosphate anchorage on titanium implant surfaces. *Mater Sci Eng C Mater Biol Appl* 2015;**49**:7−13.
54. Supova M. Substituted hydroxyapatites for biomedical applications: a review. *Ceram Int* 2015;**41**(8):9203−31.
55. Bahl S, et al. Enhancing the mechanical and biological performance of a metallic biomaterial for orthopedic applications through changes in the surface oxide layer by nanocrystalline surface modification. *Nanoscale* 2015;**7**(17):7704−16.
56. Ohtsu N, Yokoi K, Saito A. Fabrication of a visible-light-responsive photocatalytic antibacterial coating on titanium through anodic oxidation in a nitrate/ethylene glycol electrolyte. *Surf Coat Technol* 2015;**262**:97−102.
57. Teker D, et al. Characteristics of multi-layer coating formed on commercially pure titanium for biomedical applications. *Mater Sci Eng C Mater Biol Appl* 2015;**48**:579−85.
58. Xu G, et al. Fabrication of tantalum oxide layers onto titanium substrates for improved corrosion resistance and cytocompatibility. *Surf Coat Technol* 2015;**272**:58−65.
59. Kaur J, Kumari A. Exigency for fusion of graphene and carbon nanotube with biomaterials. *Toxicol Environ Chem* 2014;**96**(5):699−721.
60. Wehling J, et al. Bactericidal activity of partially oxidized nanodiamonds. *ACS Nano* 2014;**8**(6):6475−83.
61. Passeri D, et al. Biomedical applications of nanodiamonds: an overview. *J Nanosci Nanotechnol* 2015;**15**(2):972−88.
62. Prodana M, et al. A new complex ceramic coating with carbon nano-tubes, hydroxyapatite and TiO_2 nanotubes on Ti surface for biomedical applications. *Ceram Int* 2015; **41**(5):6318−25.
63. Campbell AA. Bioceramics for implant coatings. *Mater Today* 2003;**11**:27−31.
64. Bunker BC, et al. Ceramic thin-film formation on functionalized interfaces through biomimetic processing. *Science* 1994;**264**(5155):48−55.

65. Sarao TPS, Sidhu HS, Singh H. Characterization and in vitro corrosion investigations of thermal sprayed hydroxyapatite and hydroxyapatite-titania coatings on Ti Alloy. *Metall Mater Trans A* 2012;**43**(11):4365−76.
66. Surmeneva MA, et al. Effect of silicate doping on the structure and mechanical properties of thin nanostructured RF magnetron sputter-deposited hydroxyapatite films. *Surf Coat Technol* 2015;**275**:176−84.
67. Mroz W, et al. In vivo implantation of porous titanium alloy implants coated with magnesium-doped octacalcium phosphate and hydroxyapatite thin films using pulsed laser depostion. *J Biomed Mater Res B Appl Biomater* 2015;**103**(1):151−8.
68. Haddow DB, James PF, Van Noort R. Sol−gel derived calcium phosphate coatings for biomedical applications. *J Sol−Gel Sci Technol* 1998;**13**(1−3):261−5.
69. Mohseni E, Zalnezhad E, Bushroa AR. Comparative investigation on the adhesion of hydroxyapatite coating on Ti-6Al-4V implant: a review paper. *Int J Adhes Adhes* 2014; **48**:238−57.
70. Wang Y, Khor KA, Cheang P. Thermal spraying of functionally graded bioceramic coatings. In: Sudarshan TS, Khor KA, Jeandin M, editors. *Surface modification technologies X, ed*; 1997. p. 925−33.
71. Blalock T, Bai X, Rabiei A. A study on microstructure and properties of calcium phosphate coatings processed using ion beam assisted deposition on heated substrates. *Surf Coat Technol* 2007;**201**(12):5850−8.
72. Bai X, et al. Deposition and investigation of functionally graded calcium phosphate coatings on titanium. *Acta Biomater* 2009;**5**(9):3563−72.
73. Frauchiger VM, et al. Anodic plasma-chemical treatment of CP titanium surfaces for biomedical applications. *Biomaterials* 2004;**25**(4):593−606.
74. Schlegel P, et al. An in vivo evaluation of the biocompatibility of anodic plasma chemical (APC) treatment of titanium with calcium phosphate. *J Biomed Mater Res B Appl Biomater* 2009;**90**(1):26−34.
75. Chopra I. The increasing use of silver-based products as antimicrobial agents: a useful development or a cause for concern? *J Antimicrob Chemother* 2007;**59**(4): 587−90.
76. Kikuchi A, Okano T. Nanostructured designs of biomedical materials: applications of cell sheet engineering to functional regenerative tissues and organs. *J Control Release* 2005;**101**(1−3):69−84.
77. Ito E, et al. Active platelet movements on hydrophobic/hydrophilic microdomain-structured surfaces. *J Biomed Mater Res* 1998;**42**(1):148−55.
78. Degasne I, et al. Effects of roughness, fibronectin and vitronectin on attachment, spreading, and proliferation of human osteoblast-like cells (Saos-2) on titanium surfaces. *Calcif Tissue Int* 1999;**64**(6):499−507.
79. Heilmann C, et al. Molecular basis of intercellular adhesion in the biofilm-forming *Staphylococcus epidermidis*. *Mol Microbiol* 1996;**20**(5):1083−91.
80. O'Toole G, Kaplan HB, Kolter R. Biofilm formation as microbial development. *Annu Rev Microbiol* 2000;**54**(1):49−79.
81. Trappmann B, et al. Extracellular-matrix tethering regulates stem-cell fate. *Nat Mater* 2012;**11**(7):642−9.
82. Yang YZ, Cavin R, Ong JL. Protein adsorption on titanium surfaces and their effect on osteoblast attachment. *J Biomed Mater Res A* 2003;**67**(1):344−9.
83. Subbiahdoss G, et al. Microbial biofilm growth vs. tissue integration: "the race for the surface" experimentally studied. *Acta Biomater* 2009;**5**(5):1399−404.

84. Fan X, et al. Effects of the surface modification of poly(amino acid)/hydroxyapatite/calcium sulfate biocomposites on the adhesion and proliferation of osteoblast-like cells. *J Appl Polym Sci* 2015;**132**(33).
85. Soriano-Souza CA, et al. Chlorhexidine-loaded hydroxyapatite microspheres as an antimicrobial delivery system and its effect on in vivo osteo-conductive properties. *J Mater Sci Mater Med* 2015;**26**(4).
86. Rong Z, et al. Enhanced bioactivity of osteoblast-like cells on poly(lactic acid)/poly(methyl methacrylate)/nano-hydroxyapatite scaffolds for bone tissue engineering. *Fibers Polym* 2015;**16**(2):245−53.
87. Xie JW, Baumann MJ, McCabe LR. Osteoblasts respond to hydroxyapatite surfaces with immediate changes in gene expression. *J Biomed Mater Res A* 2004;**71**(1):108−17.
88. Mello A, et al. Osteoblast proliferation on hydroxyapatite thin coatings produced by right angle magnetron sputtering. *Biomed Mater* 2007;**2**(2):67−77.
89. Shu R, et al. Hydroxyapatite accelerates differentiation and suppresses growth of MC3T3-E1 osteoblasts. *J Biomed Mater Res A* 2003;**67**(4):1196−204.
90. Chang BS, et al. Osteoconduction at porous hydroxyapatite with various pore configurations. *Biomaterials* 2000;**21**(12):1291−8.
91. He J, et al. Collagen-infiltrated porous hydroxyapatite coating and its osteogenic properties: in vitro and in vivo study. *J Biomed Mater Res A* 2012;**100**(7):1706−15.
92. Le Guehennec L, et al. Surface treatments of titanium dental implants for rapid osseointegration. *Dent Mater* 2007;**23**(7):844−54.
93. Dorozhkin SV. Biphasic, triphasic and multiphasic calcium orthophosphates. *Acta Biomater* 2012;**8**(3):963−77.
94. Wongwitwichot P, et al. Comparison of TCP and TCP/HA hybrid scaffolds for osteoconductive activity. *Open Biomed Eng J* 2010;**4**:279−85.
95. Frayssinet P, et al. Osseointegration of macroporous calcium-phosphate ceramics having a different chemical-composition. *Biomaterials* 1993;**14**(6):423−9.
96. Goyenvalle E, et al. Osteointegration of femoral stem prostheses with a bilayered calcium phosphate coating. *Biomaterials* 2006;**27**(7):1119−28.
97. Yuan H, et al. A comparison of bone formation in biphasic calcium phosphate (BCP) and hydroxyapatite (HA) implanted in muscle and bone of dogs at different time periods. *J Biomed Mater Res A* 2006;**78**(1):139−47.
98. Develioglu H, et al. Assessment of the effect of a biphasic ceramic on bone response in a rat calvarial defect model. *J Biomed Mater Res A* 2006;**77**(3):627−31.
99. Yuan H, et al. Cross-species comparison of ectopic bone formation in biphasic calcium phosphate (BCP) and hydroxyapatite (HA) scaffolds. *Tissue Eng* 2006;**12**(6):1607−15.
100. Zhu XD, et al. Bovine serum albumin adsorption on hydroxyapatite and biphasic calcium phosphate and the correlation with zeta potentials and wettability. In: Nakamura T, Yamashita K, Neo M, editors. *Bioceramics 18, Pts 1 and 2*; 2006. p. 73−6.
101. Chung RJ, et al. Anti-microbial hydroxyapatite particles synthesized by a sol−gel route. *J Sol−Gel Sci Technol* 2005;**33**(2):229−39.
102. Dubnika A, et al. Impact of sintering temperature on the phase composition and antibacterial properties of silver-doped hydroxyapatite. *Pure Appl Chem* 2013;**85**(2):453−62.
103. Rameshbabu N, et al. Antibacterial nanosized silver substituted hydroxyapatite: synthesis and characterization. *J Biomed Mater Res A* 2007;**80**(3):581−91.
104. Chen W, et al. In vitro anti-bacterial and biological properties of magnetron co-sputtered silver-containing hydroxyapatite coating. *Biomaterials* 2006;**27**(32):5512−7.

105. Shirkhanzadeh M, Azadegan M, Liu GQ. Bioactive delivery systems for the slow-release of antibiotics − incorporation of Ag^{+} ions into micro-porous hydroxyapatite coatings. *Mater Lett* 1995;**24**(1−3):7−12.
106. Park JE, et al. Effects of a carbon nanotube-collagen coating on a titanium surface on osteoblast growth. *Appl Surf Sci* 2014;**292**:828−36.
107. Zhang W, et al. Ag and Ag/N(2) plasma modification of polyethylene for the enhancement of antibacterial properties and cell growth/proliferation. *Acta Biomater* 2008;**4**(6):2028−36.
108. Ewald A, et al. Antimicrobial titanium/silver PVD coatings on titanium. *Biomed Eng Online* 2006;**5**.
109. Yue C, et al. Simultaneous interaction of bacteria and tissue cells with photocatalytically activated, anodized titanium surfaces. *Biomaterials* 2014;**35**(9):2580−7.
110. Tunesi M, et al. Mesenchymal stem cell differentiation on electrochemically modified titanium: an optimized approach for biomedical applications. *J Appl Biomater Funct Mater* 2013;**11**(1):9−17.
111. Battiston GA, et al. Dental implants of complex form coated by nanostructered TiO_2 thin films via MOCVD. In: Uskokovic DP, et al., editors. *Trends in advanced materials and processes*; 2000. p. 151−7.
112. Zhang YM, et al. Surface analyses of micro-arc oxidized and hydrothermally treated titanium and effect on osteoblast behavior. *J Biomed Mater Res A* 2004;**68**(2):383−91.
113. Haenle M, et al. An extended spectrum bactericidal titanium dioxide (TiO_2) coating for metallic implants: in vitro effectiveness against MRSA and mechanical properties. *J Mater Sci Mater Med* 2011;**22**(2):381−7.
114. Nimittrakoolchai O-U, Supothina S. Bactericidal activity and UV-filtering property of TiO_2-based photocatalysts coated on curtain fabrics. *Res Chem Intermed* 2009;**35**(3): 271−80.
115. Aregueta-Robles UA, et al. Organic electrode coatings for next-generation neural interfaces. *Front Neuroeng* 2014;**7**:15.
116. Hu X, et al. Charge-tunable autoclaved silk-tropoelastin protein alloys that control neuron cell responses. *Adv Funct Mater* 2013;**23**(31):3875−84.
117. Zhang Q, et al. Synthesis of amphiphilic reduced graphene oxide with an enhanced charge injection capacity for electrical stimulation of neural cells. *J Mater Chem B* 2014; **2**(27):4331−7.
118. Li J, et al. Surface charge regulation of osteogenic differentiation of mesenchymal stem cell on polarized ferroelectric crystal substrate. *Adv Healthc Mater* 2015;**4**(7):998−1003.
119. Li JEJ, Kawazoe N, Chen G. Gold nanoparticles with different charge and moiety induce differential cell response on mesenchymal stem cell osteogenesis. *Biomaterials* 2015;**54**: 226−36.
120. Tiller JC, et al. Designing surfaces that kill bacteria on contact. *Proc Natl Acad Sci USA* 2001;**98**(11):5981−5.
121. Thierry B, et al. Reactive epoxy-functionalized thin films by a pulsed plasma polymerization process. *Langmuir* 2008;**24**(18):10187−95.
122. Joerger RD, et al. Antimicrobial activity of chitosan attached to ethylene copolymer films. *Packag Technol Sci* 2009;**22**(3):125−38.
123. Conte A, et al. Antimicrobial activity of immobilized lysozyme on plasma-treated polyethylene films. *J Food Prot*® 2008;**71**(1):119−25.
124. Aumsuwan N, Heinhorst S, Urban MW. The effectiveness of antibiotic activity of penicillin attached to expanded poly(tetrafluoroethylene) (ePTFE) surfaces: a quantitative assessment. *Biomacromolecules* 2007;**8**(11):3525−30.

125. Shi CM, et al. Therapeutic potential of chitosan and its derivatives in regenerative medicine. *J Surg Res* 2006;**133**(2):185−92.
126. Chiono V, et al. Layer-by-layer coating of photoactive polymers for biomedical applications. In: *2009 9th IEEE conference on nanotechnology (IEEE-NANO)*; 2009. p. 798−801.
127. Jayakumar R, et al. Novel carboxymethyl derivatives of chitin and chitosan materials and their biomedical applications. *Prog Mater Sci* 2010;**55**(7):675−709.
128. Hao L, et al. Directing the fate of human and mouse mesenchymal stem cells by hydroxyl-methyl mixed self-assembled monolayers with varying wettability. *J Mater Chem B* 2014;**2**(30):4794−801.
129. Jahani H, et al. Controlled surface morphology and hydrophilicity of polycaprolactone toward selective differentiation of mesenchymal stem cells to neural like cells. *J Biomed Mater Res A* 2015;**103**(5):1875−81.
130. Teo BKK, Tan G-DS, Yim EKF. The synergistic effect of nanotopography and sustained dual release of hydrophobic and hydrophilic neurotrophic factors on human mesenchymal stem cell neuronal lineage commitment. *Tissue Eng A* 2014;**20**(15−16): 2151−61.
131. Viswanathan P, et al. Controlling surface topology and functionality of electrospun fibers on the nanoscale using amphiphilic block copolymers to direct mesenchymal progenitor cell adhesion. *Biomacromolecules* 2015;**16**(1):66−75.
132. Biniarz P, et al. The lipopeptides pseudofactin II and surfactin effectively decrease *Candida albicans* adhesion and hydrophobicity. *Antonie Van Leeuwenhoek* 2015; **108**(2):343−53.
133. Di Ciccio P, et al. Biofilm formation by *Staphylococcus aureus* on food contact surfaces: relationship with temperature and cell surface hydrophobicity. *Food Control* 2015;**50**: 930−6.
134. Pimentel-Filho NDJ, et al. Bovicin HC5 and nisin reduce *Staphylococcus aureus* adhesion to polystyrene and change the hydrophobicity profile and Gibbs free energy of adhesion. *Int J Food Microbiol* 2014;**190**:1−8.
135. Fernandes PE, et al. Influence of the hydrophobicity and surface roughness of mangoes and tomatoes on the adhesion of *Salmonella enterica* serovar Typhimurium and evaluation of cleaning procedures using surfactin. *Food Control* 2014;**41**:21−6.
136. Yang Y, et al. Influence of poly(ethylene oxide)-based copolymer on protein adsorption and bacterial adhesion on stainless steel: modulation by surface hydrophobicity. *Bioelectrochemistry* 2014;**97**:127−36.
137. Busscher HJ, Norde W, Van der Mei HC. Specific molecular recognition and nonspecific contributions to bacterial interaction forces. *Appl Environ Microbiol* 2008;**74**(9): 2559−64.
138. Nobbs AH, Lamont RJ, Jenkinson HF. *Streptococcus* adherence and colonization. *Microbiol Mol Biol Rev* 2009;**73**(3):407−50.
139. Quirynen M, Bollen CML. The influence of surface-roughness and surface-free energy on supragingival and subgingival plaque-formation in man − a review of the literature. *J Clin Periodontol* 1995;**22**(1):1−14.
140. Song F, Koo H, Ren D. Effects of material properties on bacterial adhesion and biofilm formation. *J Dent Res* 2015;**94**(8):1027−34.
141. Mabboux F, et al. Surface free energy and bacterial retention to saliva-coated dental implant materials − an in vitro study. *Colloids Surf B Biointerfaces* 2004;**39**(4): 199−205.

142. Hu XL, et al. Thermal treatments modulate bacterial adhesion to dental enamel. *J Dent Res* 2011;**90**(12):1451−6.
143. Zhang X, Wang L, Levanen E. Superhydrophobic surfaces for the reduction of bacterial adhesion. *RSC Adv* 2013;**3**(30):12003−20.
144. Neinhuis C, Barthlott W. Characterization and distribution of water-repellent, self-cleaning plant surfaces. *Ann Bot* 1997;**79**(6):667−77.
145. Marmur A. Wetting on hydrophobic rough surfaces: to be heterogeneous or not to be? *Langmuir* 2003;**19**(20):8343−8.
146. Feng L, et al. Super-hydrophobic surfaces: from natural to artificial. *Adv Mater* 2002; **14**(24):1857−60.
147. Mi L, Jiang S. Integrated antimicrobial and nonfouling zwitterionic polymers. *Angew Chem Int Ed* 2014;**53**(7):1746−54.
148. Venault A, et al. Bacterial resistance control on mineral surfaces of hydroxyapatite and human teeth via surface charge-driven antifouling coatings. *ACS Appl Mater Interfaces* 2014;**6**(5):3201−10.
149. Lossdorfer S, et al. Microrough implant surface topographies increase osteogenesis by reducing osteoclast formation and activity. *J Biomed Mater Res A* 2004;**70**(3):361−9.
150. Gittens RA, et al. Implant osseointegration and the role of microroughness and nanostructures: lessons for spine implants. *Acta Biomater* 2014;**10**(8):3363−71.
151. Diniz MG, et al. Surface topography modulates the osteogenesis in human bone marrow cell cultures grown on titanium samples prepared by a combination of mechanical and acid treatments. *J Mater Sci Mater Med* 2002;**13**(4):421−32.
152. Batzer R, et al. Prostaglandins mediate the effects of titanium surface roughness on MG63 osteoblast-like cells and alter cell responsiveness to 1 alpha,25-(OH)(2)D(3). *J Biomed Mater Res* 1998;**41**(3):489−96.
153. Boyan BD, et al. Titanium surface roughness alters responsiveness of MG63 osteoblast-like cells to 1 alpha,25-(OH)(2)D-3. *J Biomed Mater Res* 1998;**39**(1):77−85.
154. Feinberg AW, et al. Systematic variation of microtopography, surface chemistry and elastic modulus and the state dependent effect on endothelial cell alignment. *J Biomed Mater Res A* 2008;**86**(2):522−34.
155. Senaratne W, et al. Functionalized surface arrays for spatial targeting of immune cell signaling. *J Am Chem Soc* 2006;**128**(17):5594−5.
156. Liu R, et al. Surface characteristics and cell adhesion: a comparative study of four commercial dental implants. *J Prosthodont* 2013;**22**(8):641−51.
157. Schwartz Z, et al. Implant surface characteristics modulate differentiation behavior of cells in the osteoblastic lineage. *Adv Dent Res* 1999;**13**:38−48.
158. Olivares-Navarrete R, et al. Direct and indirect effects of microstructured titanium substrates on the induction of mesenchymal stem cell differentiation towards the osteoblast lineage. *Biomaterials* 2010;**31**(10):2728−35.
159. Zhang BGX, et al. Bioactive coatings for orthopaedic implants-recent trends in development of implant coatings. *Int J Mol Sci* 2014;**15**(7):11878−921.
160. Zhou R, et al. Synergistic effects of surface chemistry and topologic structure from modified microarc oxidation coatings on Ti implants for improving osseointegration. *ACS Appl Mater Interfaces* 2015;**7**(16):8932−41.
161. Eshkeiti A, et al. Screen printing of multilayered hybrid printed circuit boards on different substrates. *IEEE Trans Compon Packag Manuf Technol* 2015;**5**(3):415−21.
162. Qiu Y, et al. Screen-printed ultrasonic 2-D matrix array transducers for microparticle manipulation. *Ultrasonics* 2015;**62**:136−46.

163. Patel N, et al. Printing patterns of biospecifically-adsorbed protein. *J Biomater Sci Polym Ed* 2000;**11**(3):319−31.
164. Zheng W, Zhang W, Jiang X. Precise control of cell adhesion by combination of surface chemistry and soft lithography. *Adv Healthc Mater* 2013;**2**(1):95−108.
165. Schulte VA, et al. A hydrophobic perfluoropolyether elastomer as a patternable biomaterial for cell culture and tissue engineering. *Biomaterials* 2010;**31**(33):8583−95.
166. Sun Y, et al. Conformal nanopatterning of extracellular matrix proteins onto topographically complex surfaces. *Nat Methods* 2015;**12**(2):134−U168.
167. Lim YC, et al. Micropatterning and characterization of electrospun poly(epsilon-caprolactone)/gelatin nanofiber tissue scaffolds by femtosecond laser ablation for tissue engineering applications. *Biotechnol Bioeng* 2011;**108**(1):116−26.
168. Li Y-Y, Li L-T, Li B. Direct write printing of three-dimensional ZrO_2 biological scaffolds. *Mater Des* 2015;**72**:16−20.
169. Shirazi SFS, et al. A review on powder-based additive manufacturing for tissue engineering: selective laser sintering and inkjet 3D printing. *Sci Technol Adv Mater* 2015; **16**(3).
170. Zhang X, Zhang Y. Tissue engineering applications of three-dimensional bioprinting. *Cell Biochem Biophys* 2015;**72**(3):777−82.
171. Chan V, et al. Three-dimensional photopatterning of hydrogels using stereolithography for long-term cell encapsulation. *Lab Chip* 2010;**10**(16):2062−70.
172. Gramlich WM, Kim IL, Burdick JA. Synthesis and orthogonal photopatterning of hyaluronic acid hydrogels with thiol-norbornene chemistry. *Biomaterials* 2013;**34**(38): 9803−11.
173. Mosiewicz KA, et al. In situ cell manipulation through enzymatic hydrogel photopatterning. *Nat Mater* 2013;**12**(11):1071−7.
174. Alsop AT, et al. Photopatterning of vascular endothelial growth factor within collagen-glycosaminoglycan scaffolds can induce a spatially confined response in human umbilical vein endothelial cells. *Acta Biomater* 2014;**10**(11):4715−22.
175. Nikkhah M, et al. Engineering microscale topographies to control the cell-substrate interface. *Biomaterials* 2012;**33**(21):5230−46.
176. Ross AM, et al. Physical aspects of cell culture substrates: topography, roughness, and elasticity. *Small* 2012;**8**(3):336−55.
177. Cassidy JW, et al. Osteogenic lineage restriction by osteoprogenitors cultured on nanometric grooved surfaces: the role of focal adhesion maturation. *Acta Biomater* 2014; **10**(2):651−60.
178. Misra RDK, et al. Biological significance of nanograined/ultrafine-grained structures: interaction with fibroblasts. *Acta Biomater* 2010;**6**(8):3339−48.
179. Han P, et al. Improved osteoblast proliferation, differentiation and mineralization on nanophase Ti6Al4V. *Chin Med J* 2011;**124**(2):273−9.
180. Huang R, Lu S, Han Y. Role of grain size in the regulation of osteoblast response to Ti-25Nb-3Mo-3Zr-2Sn alloy. *Colloids Surf B Biointerfaces* 2013;**111**:232−41.
181. Evis Z, Sato M, Webster TJ. Increased osteoblast adhesion on nanograined hydroxyapatite and partially stabilized zirconia composites. *J Biomed Mater Res A* 2006;**78**(3): 500−7.
182. Misra RDK, et al. Cellular response of preosteoblasts to nanograined/ultrafine-grained structures. *Acta Biomater* 2009;**5**(5):1455−67.
183. Bjursten LM, et al. Titanium dioxide nanotubes enhance bone bonding in vivo. *J Biomed Mater Res A* 2010;**92**(3):1218−24.

184. Oh S, et al. Stem cell fate dictated solely by altered nanotube dimension. *Proc Natl Acad Sci USA* 2009;**106**(7):2130−5.
185. Ferraris S, et al. Antibacterial and bioactive nanostructured titanium surfaces for bone integration. *Appl Surf Sci* 2014;**311**:279−91.
186. Brammer KS, et al. Improved bone-forming functionality on diameter-controlled TiO_2 nanotube surface. *Acta Biomater* 2009;**5**(8):3215−23.
187. Kavitha K, et al. Optimization of nano-titania and titania-chitosan nanocomposite to enhance biocompatibility. *Curr Nanosci* 2013;**9**(3):308−17.
188. Li Z, et al. Hydroxyapatite additive influenced the bioactivity of bioactive nano-titania ceramics and new bone-forming capacity (vol. 14, pg 1145, 2012). *J Nanopart Res* 2013;**15**(3).
189. Li L, et al. Preparation and cell infiltration of lotus-type porous nano-hydroxyapatite/polyurethane scaffold for bone tissue regeneration. *Mater Lett* 2015;**149**:25−8.
190. D'Elia NL, et al. Nano-hydroxyapatite for use in bone tissue repair. *Bone* 2015;**71**:260.
191. Scheuerman TR, Camper AK, Hamilton MA. Effects of substratum topography on bacterial adhesion. *J Colloid Interface Sci* 1998;**208**(1):23−33.
192. Ammar Y, Swailes D, Bridgens B, Chen J. Influence of surface roughness on initial formation of biofilm. *Surface Coating & Technology* 2015;**284**:410−6.
193. Katsikogianni M, et al. Adhesion of slime producing *Staphylococcus epidermidis* strains to PVC and diamond-like carbon/silver/fluorinated coatings. *J Mater Sci Mater Med* 2006;**17**(8):679−89.
194. Edwards KJ, Rutenberg AD. Microbial response to surface microtopography: the role of metabolism in localized mineral dissolution. *Chem Geol* 2001;**180**(1):19−32.
195. Boyd RD, et al. Use of the atomic force microscope to determine the effect of substratum surface topography on bacterial adhesion. *Langmuir* 2002;**18**(6):2343−6.
196. Ryan G, Pandit A, Apatsidis DP. Fabrication methods of porous metals for use in orthopaedic applications. *Biomaterials* 2006;**27**(13):2651−70.
197. Gittens RA, et al. Differential responses of osteoblast lineage cells to nanotopographically-modified, microroughened titanium-aluminum-vanadium alloy surfaces. *Biomaterials* 2012;**33**(35):8986−94.
198. Wei G, Ma PX. Nanostructured biomaterials for regeneration. *Adv Funct Mater* 2008; **18**(22):3568−82.
199. Levengood SKL, et al. The effect of BMP-2 on micro- and macroscale osteointegration of biphasic calcium phosphate scaffolds with multiscale porosity. *Acta Biomater* 2010; **6**(8):3283−91.
200. Braem A, et al. Staphylococcal biofilm growth on smooth and porous titanium coatings for biomedical applications. *J Biomed Mater Res A* 2014;**102**(1):215−24.
201. Kinnari TJ, et al. Influence of surface porosity and pH on bacterial adherence to hydroxyapatite and biphasic calcium phosphate bloceramics. *J Med Microbiol* 2009; **58**(1):132−7.
202. An YH, Friedman RJ. Concise review of mechanisms of bacterial adhesion to biomaterial surfaces. *J Biomed Mater Res* 1998;**43**:338−48.
203. Katsikogianni M, Missirlis YF. Concise review of mechanisms of bacterial adhesion to biomaterials and of techniques used in estimating bacteria-material interactions. *Eur Cells Mater* 2004;**8**:37−57.
204. Overgaard S, et al. The influence of crystallinity of the hydroxyapatite coating on the fixation of implants − mechanical and histomorphometric results. *J Bone Jt Surg Br* 1999;**81**(4):725−31.

205. Del Curto B, et al. Decreased bacterial adhesion to surface-treated titanium. *Int J Artif Organs* 2005;**28**(7):718−30.
206. Sumita T, et al. Photo-induced surface charge separation of highly oriented TiO_2 anatase and rutile thin films. *Appl Surf Sci* 2002;**200**(1−4):21−6.
207. Mills A, LeHunte S. An overview of semiconductor photocatalysis. *J Photochem Photobiol A Chem* 1997;**108**(1):1−35.
208. Lichter JA, Thompson MT, Delgadillo M, Nishikawa T, Rubner MF, Van Vliet KJ. Substrata Mechanical Stiffness Can Regulate Adhesion of Viable Bacteria, Biomacromolecules 2008;**9**:1571−8.
209. Burdick JA, Vunjak-Novakovic G. Engineered microenvironments for controlled stem cell differentiation. *Tissue Eng A* 2009;**15**(2):205−19.
210. Chen J, et al. Cell mechanics, structure, and function are regulated by the stiffness of the three-dimensional microenvironment. *Biophys J* 2012;**103**(6):1188−97.
211. Chen J. Nanobiomechanics of living cells: a review. *Interface Focus* 2014;**4**(2).
212. Eroshenko N, et al. Effect of substrate stiffness on early human embryonic stem cell differentiation. *J Biol Eng* 2013;**7**(1).
213. Lee J, et al. Directing stem cell fate on hydrogel substrates by controlling cell geometry, matrix mechanics and adhesion ligand composition. *Biomaterials* 2013;**34**(33):8140−8.
214. Engler AJ, et al. Matrix elasticity directs stem cell lineage specification. *Cell* 2006; **126**(4):677−89.
215. Chen J, Wright KE, Birch MA. Nanoscale viscoelastic properties and adhesion of polydimethylsiloxane for tissue engineering. *Acta Mech Sin* 2014;**30**(1):2−6.
216. Saha N, et al. Influence of polyelectrolyte film stiffness on bacterial growth. *Biomacromolecules* 2013;**14**(2):520−8.
217. Song F, Ren D. Stiffness of cross-linked poly(dimethylsiloxane) affects bacterial adhesion and antibiotic susceptibility of attached cells. *Langmuir* 2014;**30**(34): 10354−62.
218. Goodman SB, et al. The future of biologic coatings for orthopaedic implants. *Biomaterials* 2013;**34**(13):3174−83.
219. Diu T, et al. Cicada-inspired cell-instructive nanopatterned arrays. *Sci Rep* 2014;**4**.
220. Ivanova EP, et al. Natural bactericidal surfaces: mechanical rupture of *Pseudomonas aeruginosa* cells by cicada wings. *Small* 2012;**8**(16):2489−94.
221. Ivanova EP, et al. Bactericidal activity of black silicon. *Nat Commun* 2013;**4**.
222. Pham VTH, et al. Nanotopography as a trigger for the microscale, autogenous and passive lysis of erythrocytes. *J Mater Chem B* 2014;**2**(19):2819−26.
223. Faruqui N, et al. Differentially instructive extracellular protein micro-nets. *J Am Chem Soc* 2014;**136**(22):7889−98.
224. Lim JY, Shaughnessy MC, Zhou Z, Noh H, Vogler EA, Donahue HJ. Surface energy effects on osteoblast spatial growth and mineralization. *Biomaterials* 2008;**29**:1776−84.

Part Three

Functional thin films for biomedical applications

This page intentionally left blank

Thin films for tissue engineering applications

8

M. Mozafari
Materials and Energy Research Center (MERC), Tehran, Iran

A. Ramedani
Sharif University of Technology, Tehran, Iran

Y.N. Zhang
University of Toronto, Toronto, ON, Canada

D.K. Mills
Louisiana Tech University, Ruston, LA, United States

8.1 Introduction

Modern surface science has been under development since the late 1960s. Surfaces, interfaces and thin films are planar structures that occur on the boundary of materials or at the junction or interface between two different media. In the late 20th century, the design of thin solid films at the molecular level attracted much attention because of its potential applications in the biological and medical fields. Many studies showed that the modification of surfaces could have an important role in cell and tissue response. In addition, applying thin films has been widely recognized as a promising approach in modifying the surface properties of a biomaterial. Studies have attracted focus on hard tissues and stiff biomaterials (high Young's modulus); however, less attention has been directed toward the field of soft tissues and viscoelastic biomaterials. Furthermore, the significance of thin films in biology and biomaterials research has rapidly increased in recent decades.

Thin films are at the core of many important technologies that have essential roles. Thin films can be applied onto different surfaces with respect to their physicochemical characteristics such as wettability, reactivity, conductivity and corrosion properties. Thin films can be deposited onto different surfaces using a variety of mechanisms including solvent casting, spraying, coating, covalent conjugation, surface-initiated polymerization and self-assembly (ie, electrostatic interactions, hydrogen bonding). These thin films have been produced using a wide variety of biomaterials, including both natural and synthetic materials with diverse architectures and properties. The unique ability of thin films to control various physicochemical characteristics supports the application of this strategy for tissue engineering applications. Thin film components, methods and conditions must be nontoxic and should not affect cellular functions in the body. Thin films are now being applied for osseointegration in terms

Thin Film Coatings for Biomaterials and Biomedical Applications. http://dx.doi.org/10.1016/B978-1-78242-453-6.00008-0

of dental and orthopaedic implants, biodegradable scaffolds and biomimetic materials in the field of tissue engineering and biomedical industries. This chapter describes the fundamentals of thin film process for tissue engineering, including thin film manufacturing, surface modification and molecular engineering. It summarizes current research results in thin film techniques for both soft and hard tissues. This chapter also highlights many pitfalls that researchers may want to consider in future studies. In addition, the use of surface modification methods for study of skeletal and dental tissues is highlighted. Difficulties in using different methods are also discussed in detail.

8.2 Thin film coating technologies for tissue engineering applications

8.2.1 Spin-coating

The spin-coating process has been widely used to deposit uniform thin films on flat substrates. Spin-coating includes four basic steps: deposition, spin-up, spin-off and evaporation.[1,2] The steps involve in this method are summarized in Fig. 8.1. In this technique, an excess of liquid is initially deposited onto the surface, followed by slow rotation. In the spin-up stage, centrifugal force is generated by rotating the substrate, resulting in the liquid flowing radially outward. The centrifugal force can be manipulated to achieve different film thickness on the substrates. In the spin-off stage, the excess liquid flows to the perimeter of the substrate and departs as droplets. The rate of excess liquid removal by spin-off process becomes slower as the film gets thinner. In the fourth stage, evaporation becomes the primary mechanism of thinning.[3] This spin-coating method is capable of coating intraluminal stents, synthetic grafts and stent coverings. In this technique, different therapeutic agents can be mixed with the polymeric matrix to form different therapeutic compositions. There are many studies describing the use of thin film biodegradable coatings for tissue engineering using a variety of biomaterials, methods and techniques.

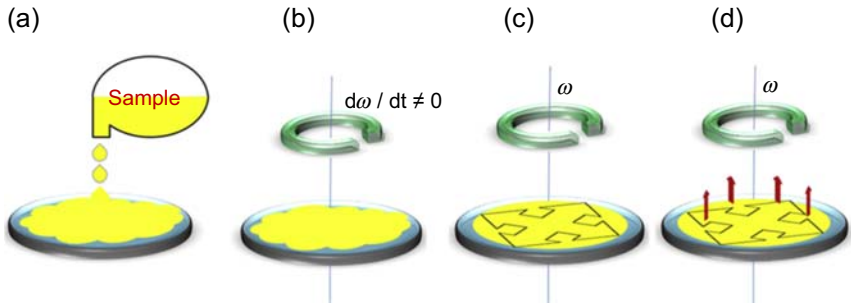

Figure 8.1 Stages of the spin-coating process. (a) Dispensation, (b) Acceleration, (c) Flow dominated, (d) Evaporation dominated.

In the past few years, bioactive thin film coatings have been of great interest owing to the improvement in bone-bonding performance on metallic implants. Mozafari et al.[4] reported the synthesis of bioactive glass−zirconium titanate composite thin films by a solgel spin-coating method. They showed that uniform, multilayer thin films could be successfully obtained through optimization of the process variables and the application of carboxymethyl cellulose as a dispersing agent. They stated that the thickness and roughness of the surface coatings could increase nonlinearly with an increase in the number of the layers, as shown in Fig. 8.2.

The most essential factor in determining the biocompatibility of metallic implants is their corrosion resistance. The same group reported that bioactive glass−zirconium titanate composite thin films could significantly improve the corrosion resistance of metallic implants, as realized by an increase in the corrosion potential and a decrease in the corrosion current density.[5] Fig. 8.3 indicates the electrochemical potentiodynamic polarization curves of the uncoated and coated samples. Also, Table 8.1 summarizes the related electrochemical parameters. As can be seen, the corrosion behaviour of the coated samples signifies notable differences compared with that of the uncoated substrate, whereas the number of thin film layers has no marked influence on the corrosion behaviour of the coated samples. It is an important achievement that the substrate exhibits no passivity, although 316L stainless steel is essentially an active−passive alloy. This is attributed to the considerable concentration of chloride in simulated body fluid (SBF) under the naturally aerated condition, which encourages localised corrosion such as pitting and avoids passivation. It is known that the in vivo corrosion resistance of metallic implants is frequently higher than that under in vitro conditions, owing to the inhibiting effect of organic species such as proteins. However, thin film deposition encourages the stainless-steel substrate polarized in the SBF to be passive. In addition, the coatings advantageously increase the corrosion potential and decrease the corrosion current density of the substrate, which indicates an improvement in corrosion resistance. Thus, it can be concluded that the thin films can act as a physical protective barrier to retard electrolyte access to the metal surface and thereby electrochemical processes. It is expected that this new class of nanocomposite thin films, comprising the bioactive and inert components, will not only enhance bioactivity and biocompatibility but also protect the surface of biomedical implants against wear and corrosion in the body.

8.2.2 Layer-by-layer assembly

In the second half of the 20th century, scientists have been attracted to the design of thin solid films at the molecular level because of their potential for application in the fields of biology and medicine. Two techniques dominated research in this area: Langmuir−Blodgett deposition[6,7] and self-assembled monolayers (SAMs). However, several intrinsic disadvantages of both methods limit their applications in the field of biology. For Langmuir−Blodgett deposition, the problems are the expensive instrumentation and time-consuming process for preparing the films. In addition, limited types of biomolecules can be embedded in the film (Langmuir−Blodgett deposition requires the assembly components to be amphiphilic). For SAMs, because of their

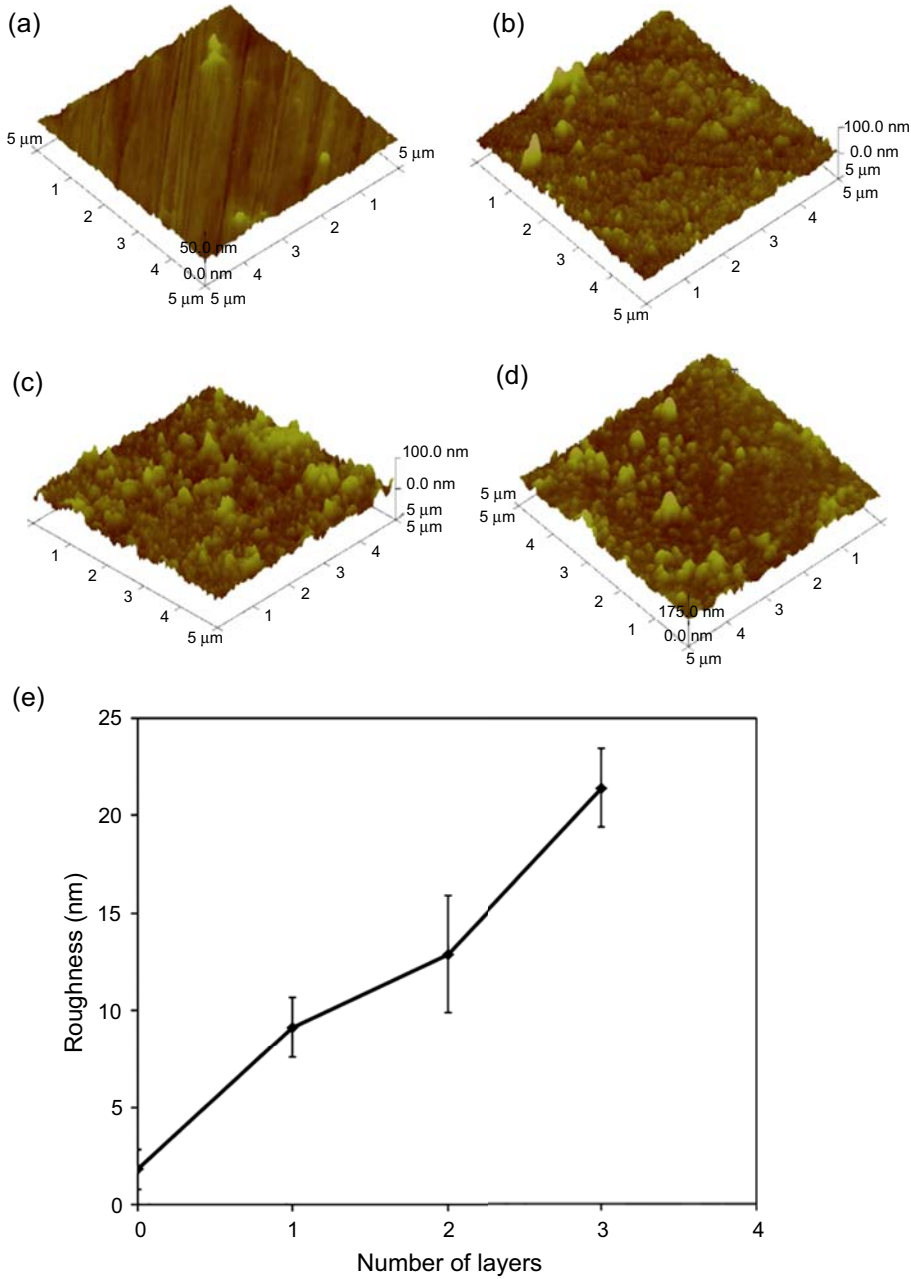

Figure 8.2 Three-dimensional atomic force microscopy images of the surface of (a) uncoated, (b) single-layered, (c) double-layered, and (d) triple-layered coated samples, (e) roughness values of the deposited films.[4]

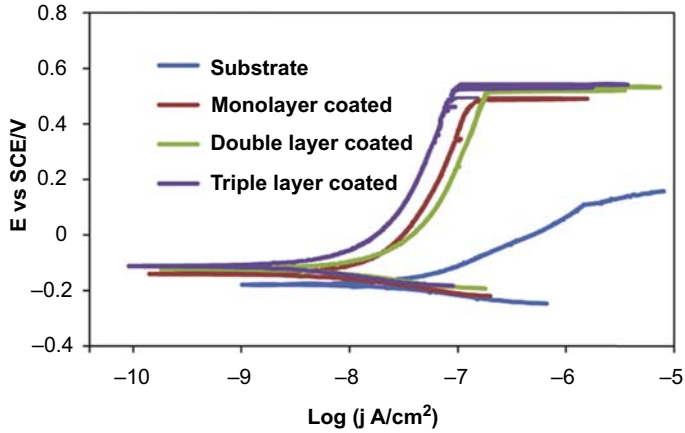

Figure 8.3 Anodic potentiodynamic polarization curves of the samples.[5]

Table 8.1 Corrosion potential (E_{corr}), corrosion current density (j_{corr}), passive current density (j_p), and breakdown potential (E_b). Note that the uncoated sample shows no typical passivity[5]

Sample	E_{corr} (mV(SCE))	j_{corr} (A/cm^2)	j_p (A/cm^2)	E_b (mV(SCE))
Uncoated	−192	4.8×10^{-8}	–	–
Monolayer	−130	1.1×10^{-8}	1.3×10^{-7}	485
Double layer	−114	9.4×10^{-9}	7.9×10^{-8}	518
Triple layer	−105	8.8×10^{-9}	5.1×10^{-8}	531

monolayer nature, a small amount of biological components can be loaded into the thin films. In addition, because SAMs are fabricated only by the adsorption of thiols onto noble metal surfaces or by silanes onto silica surfaces, a limited number of substrate types are applicable with this technique. This strategy is also limited because of the low stability of films under ambient and physiological conditions. An alternative to Langmuir–Blodgett deposition and SAMs is layer-by-layer (LbL) assembly.[8]

LbL deposition is a thin film fabrication technique in which films are formed by depositing alternating layers of oppositely charged materials. Wash steps are added between the different depositing layers. The first implementation of this LbL deposition technique was mentioned in a research by Kirkl and Iler.[9,12] They carried it out in 1966 using microparticles.[10] The method was later revitalized by Decher by the discovery of its applicability to a wide range of polyelectrolytes.[11]

It is known that LbL assembly is a prevalent method for coating substrates with functional thin films. After early studies that reported multilayer assembly,[9,12] it has only been in the past two decades that the field has grown significantly.[13] Generally, LbL assembly is a cyclical process in which a charged material is adsorbed onto a

substrate, and after washing, an oppositely charged material is adsorbed on top of the first layer. This constitutes a single bilayer with a thickness generally on the order of nanometres, and the deposition process can then be repeated until a multilayer film of desired thickness or function has been assembled.[13] For certain applications, the substrate can then be removed, forming macroscopic films such as membranes,[14] or forming microscopic or nanoscopic films such as hollow capsules.[15,16]

In addition to widely used electrostatic interactions for the formation of thin films, other molecular interactions such as covalent, hydrogen bonding and host−guest interactions are currently well established for LbL formation. Furthermore, to achieve different applications, diverse materials such as polymers, nanoparticles, suprastructures, proteins, lipids and nucleic acids can be incorporated into the film.[17] The simplicity, versatility and nanoscale control of the LbL assembly makes this technology to be one of the most widely used technologies for coating both planar and particulate substrates in a diverse range of fields including optics, energy, catalysis, separations and biomedicine (Fig. 8.4(a)).[10] The widespread use of LbL assembly in fields with different standard tools and procedures and the processing requirement of using different corresponded substrates has led to the development of a number of LbL assembly technologies that can be widely applied to porous membranes, particles and biological matters. Examples include dipping,[9] dewetting,[18] roll-to-roll,[19] centrifugation,[20] creaming,[21] calculated saturation,[22] immobilization,[23] spinning,[24] high gravity,[25] spraying,[26] atomization,[27] electrodeposition,[28] magnetic assembly,[29] electrocoupling,[30] filtration,[31] fluidics[32] and fluidized beds.[33] These different methods have often been treated as black boxes, in which the main focus has been on what materials are used (the input) to assemble the thin films (the output), with little focus on the actual assembly method. However, there is now growing realization that the assembly method not only determines the process properties (such as the time, scalability and manual intervention) but also directly affects the physicochemical properties of the films (such as the thickness, homogeneity and interlayer and intralayer film organization), with both sets of properties linked to application-specific performance (Fig. 8.4(b)).[10] The basis of LbL assembly is the sequential exposure of a substrate to the materials that will compose the multilayer films. Assembly technologies used to assemble such films form five distinct categories: (1) immersive, (2) spin, (3) spray, (4) electromagnetic and (5) fluidic assembly (Fig. 8.5).[10] These assembly technologies affect both the process properties and the resultant material properties; therefore, careful choice of the assembly method can be crucial for successful application of the assembled thin films. Furthermore, two main themes can be identified for current developments in assembly technologies: The first is moving away from random diffusion-driven kinetics for layer deposition, and the second is the advancement from manual assembly toward automated systems.

In addition to conventional ways of making LbL assembly, a novel technique to introduce free amino groups onto polyester scaffolds via aminolyzing the ester groups with diamine has been developed.[34] Positively charged chitosan was then deposited onto the aminolyzed poly(L-lactic acid) (PLLA) membrane surface using poly(styrene sulfonate) sodium salt (PSS) as a negatively charged polyelectrolyte through LbL assembly. The LbL deposition process of PSS and chitosan was investigated by

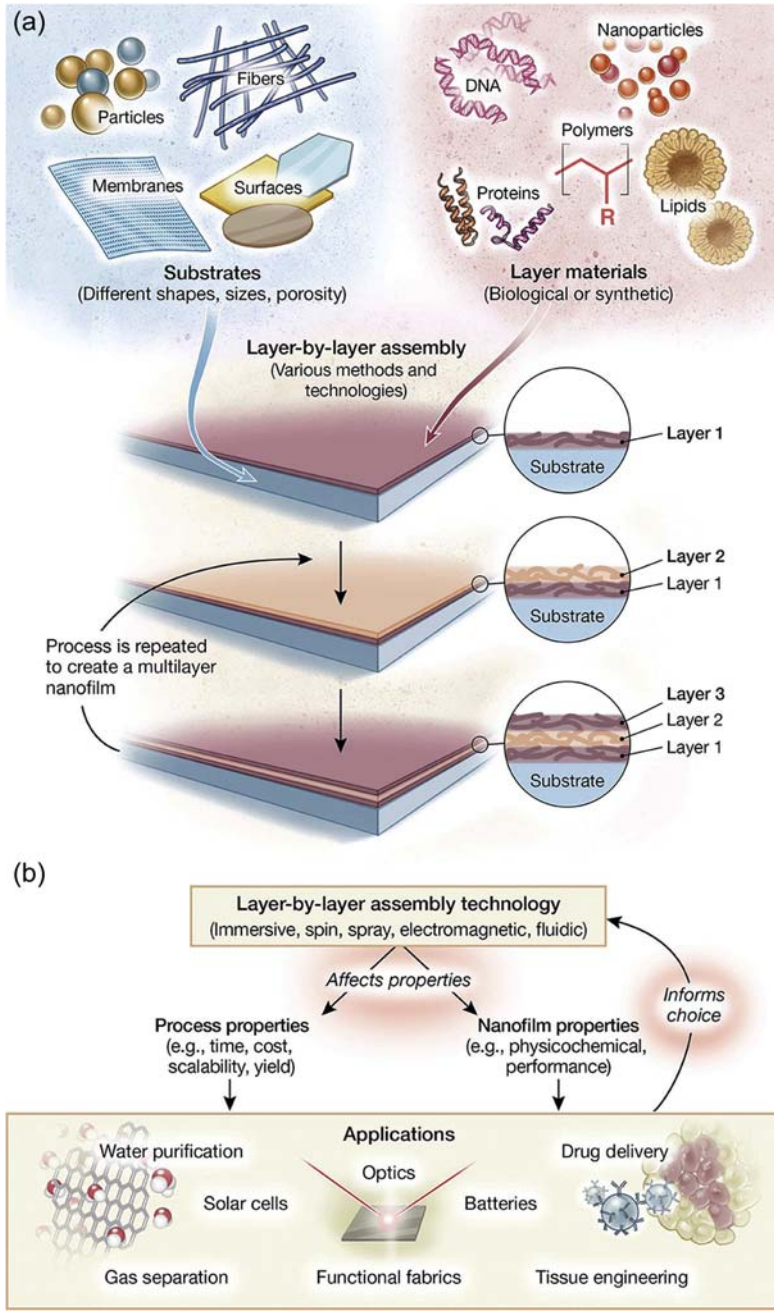

Figure 8.4 Versatility of LbL assembly. (a) Schematic overview of LbL assembly; (b) an overview showing that assembly technology influences film and process properties as well as application areas.[10]

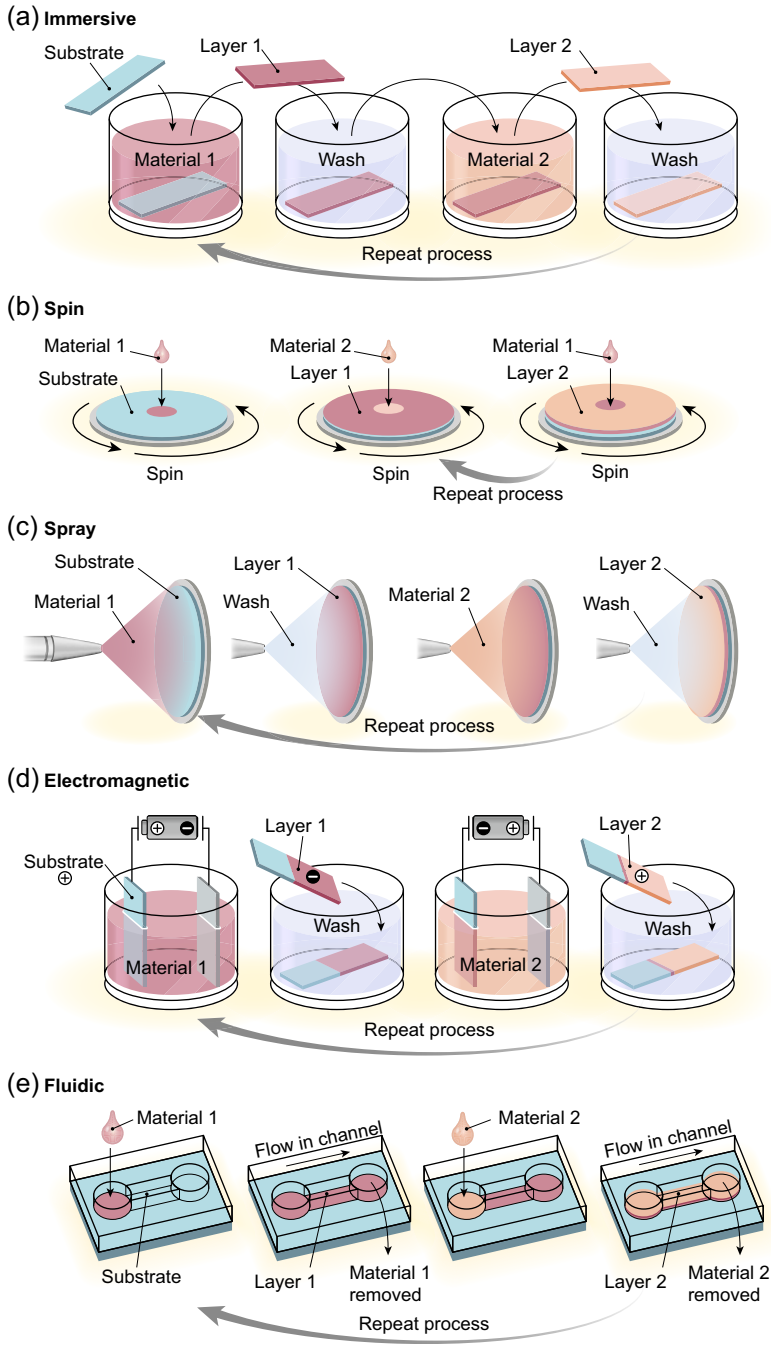

Figure 8.5 Layer-by-layer assembly technologies. (a–e) Schematics of the five major technology categories for LbL assembly.[10]

ultraviolet−visible absorbance spectroscopy, energy transfer by fluorescence spectroscopy and advancing contact angle measurements. The existing coated chitosan on PLLA obviously improved the cytocompatibility of PLLA to human endothelial cells. In addition, different outermost layer structures were studied. The PLLA membranes assembled with three or five bilayers of PSS/chitosan with chitosan as the outermost layer had better cell attachment, activity, spreading and proliferation than those with one bilayer of PSS/chitosan or the control PLLA. The endothelial cells also showed elongated morphology with abundant cytoplasm, which indicated that good spreading on the materials occurred. A confluent cell layer was reached after culturing 4 days. Endothelial cells secreting von Willebrand factor were measured and the endothelial function on the PLLA was confirmed, indicating that good biocompatibility of the PLLA was achieved after LbL assembly.[34]

8.2.3 Dip-coating technology

The physics of dip-coating has been extensively reviewed by Scriven.[35] The researcher divided the batch dip-coating process into five stages: (1) immersion, (2) startup, (3) deposition, (4) drainage and (5) evaporation (Fig. 8.6). With volatile solvents such as alcohol, evaporation normally accompanies startup, deposition and drainage.

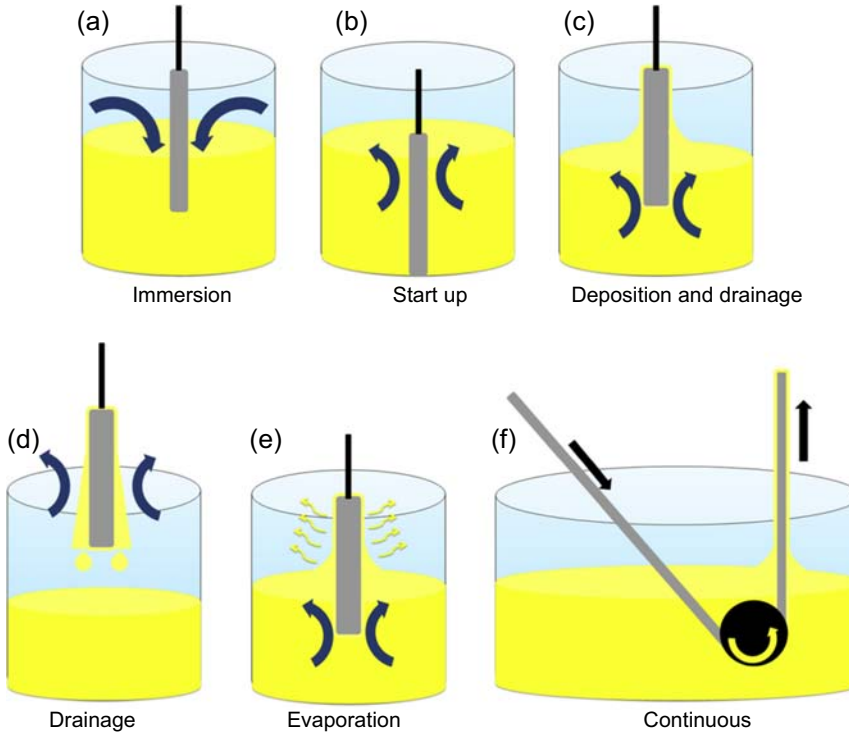

Figure 8.6 Stages of dip-coating process: (a−e) batch; (f) continuous.

The continuous dip-coating process is simpler because it separates immersion from the other stages, essentially eliminates startup, hides drainage in the deposited film and restricts evaporation to the deposition stage. As in dip-coating, evaporation may occur throughout the process. The thickness of the film in the deposition region (Fig. 8.6) is controlled by competition among as many as six forces.[3] The first is the viscous drag upward on the liquid by the moving substrate, force of gravity, resultant force of surface tension in the concave curved meniscus, the inertial force of the boundary layer liquid arriving at the deposition region, the surface tension gradient and disjoining or conjoining pressure (important for films with less than 1 μm thickness).

8.2.3.1 Hydroxyapatite dip-coating

Titanium (Ti) and Ti-based alloys are widely used in dental and orthopaedic implants because of their excellent biocompatibility.[36] However, bone ingrowth and implant fixation and tissue–material integration properties need to be improved to shorten the implant–tissue osseointegration time.[37] Therefore, significant effort in research has been carried out to improve the physical and chemical properties of the surface structure of Ti and its alloys.[38–40] Among the different proposed solutions, hydroxyapatite (HA) (Ca_{10} $[PO_4]_6[OH]_2$) coatings on Ti substrates have attracted much attention over the past few years.[41–43] The excellent biocompatibility of HA is the result of its chemical and biological similarities to human hard tissues.[44] Studies of HA coatings on Ti implants have revealed good fixation to the host bones and an increased amount of bone ingrowth into implants in vivo.[45] In addition to HA, fluorapatite (FA) ($Ca_{10}[PO_4]_6F_2$) coatings have also attracted considerable attention in areas that require long-term chemical and mechanical stability for the thin film layer.[46] Compared with HA, pure FA has a lower biodegradation rate and a similar level of biocompatibility. These important properties demonstrate behaviour for FA as a promising candidate for the fixation of bone and bone ingrowth.[47,48] Moreover, a fluor-hydroxyapatite (FHA) ($Ca_{10}[PO_4]_6[OH,F]_2$) solid solution with HA can be formed on FA to replace the F^- with OH.[49] In reality, F^- itself can prevent dental caries in bacterial and acidic environments, which enhances its application in the dental restoration field.[49,50] In addition, F^- can further promote the mineralization and crystallization of calcium phosphate in the process of bone formation.[51]

To date, most HA and FHA coatings are obtained using plasma-spraying techniques.[41,42] However, poor adherence to the substrate, chemical inhomogeneity and high porosity are the major problems of using the plasma-spraying process. Most of these problems result from the excessively high fabrication temperature.[41,42] In comparison, dip-coating technology offers many advantages including high chemical homogeneity, a fine grain structure, and the low crystallization temperature of the resultant coating. This technology is economically feasible and technically simple to perform.[52,53] Because of these advantages, dip-coating methods have been reported to be widely used for fabricating HA and FHA thin films for tissue engineering applications. In addition, combined with the dip-coating technique, the solgel approach was used to deposit HA and FHA films on Ti substrates. The biological performance of these thin films indicated excellent dissolution behaviour and in vitro cell response.[54]

8.2.3.2 Magnetic scaffolds

In past years, bioengineered scaffolds have been used in bone graft replacement combined with a variety of bioagents. Nevertheless, a problem with using these conventional scaffolds is reloading the scaffold with bioagents after implantation. A conceptually novel solution is magnetic scaffolds. Magnetic scaffolds can attract and take up growth factors and stem cells, or other bioagents can bind to the magnetic particles using a magnetic drive. In a research study, Bock et al.[55] reported on their success in developing a simple and inexpensive technique to transform standard commercial scaffolds made of HA and collagen into magnetic scaffolds. They prepared the scaffolds by dip-coating them in aqueous ferrofluids containing iron oxide nanoparticles coated with various biopolymers. After dip-coating, the nanoparticles were integrated into the structure of the scaffolds. The scaffolds' magnetization values were 15 emu/g at 10 kOe. These values are suitable for generating magnetic gradients, enabling magnetic guiding in the vicinity and inside the scaffold. The magnetic scaffolds maintain their specific porosity and shape and do not experience structural damage during the dip-coating process. According to this study, the magnetic scaffolds did not release magnetic particles under a constant flow of SBF over 8 days. Furthermore, the biocompatibility of the magnetic scaffolds was supported by in vitro adhesion and proliferation of human bone marrow stem cells on the scaffolds. Therefore, this new type of magnetic scaffold is a promising candidate for tissue engineering applications.[55]

In bone tissue engineering, the complete histomorphological and biological maturation of tissues is only achieved if angiogenesis is permanently stimulated by various angiogenic proteins such as growth factors, leading to vascular ingrowth from surrounding tissues in the vicinity of the scaffold.[56,57] During the bone healing process, reestablishing the complete functionality of damaged tissues usually takes longer regeneration times. The temporal control of the tissue regeneration process is important to allow optimal clinical outcomes in the tissue−biomaterial system, and it involves different agents at different times.[58,59] However, in bone graft substitution, such temporal control cannot be achieved with traditional scaffold approaches, in which growth factors are usually seeded in the scaffold before implantation.[60,61]

In some cases, preloading techniques reduce the delivery of localized, controllable, and long-term biochemical stimuli, thus impairing the tissue regeneration potential in the scaffold.[60,62] A controlled delivery that mimics endogenous growth factor production therefore remains a serious issue in the use of conventional scaffolds in tissue engineering.[63−65] This problem has been addressed by fabricating these conceptually new types of bone graft substitutes, which are able to attract and take up the growth factors or other bioagents via a driving magnetic force.[66−69]

In addition, studies have shown that these nanoparticles with biocompatible coatings do not have cytotoxic effects on cell development either in vitro or in vivo,[70] and some magnetic nanoparticles coated with arginylglycylaspartic acid peptides showed excellent biocompatibility in contact with osteoblasts.[71] It was also shown that the change in the magnetic properties of magnetic nanoparticles in the presence of a magnetic field had no influence on cellular toxicity.[72] This suggests that the

magnetization of standard HA−collagen composite scaffolds with magnetic nanoparticles has no adverse effects on cell viability and development. Therefore, magnetic nanoparticles with biocompatible coatings were chosen to magnetize conventional scaffolds and maintain the initial biocompatibility properties of both materials. To reach this objective, an innovative magnetization technique was developed consisting of infilling the nanoparticles in the scaffolds by a simple process of dip-coating in ferrofluid, which is not damaging to biological matter.[55]

8.2.3.3 Bioactive glass−ceramics and biodegradable materials

Biodegradable metals have attracted much attention in the field of biomedical implants owing to their advantages over nonbiodegradable metals such as stainless steel and titanium-based alloys.[73] In particular, magnesium alloys have shown great potential for applications in bone tissue repairing[74] because of their remarkable physical and mechanical properties, such as an elastic modulus similar to human bone,[75] high specific strength and low density. However, magnesium alloys are highly susceptible to corrosion in the biological environment, which could lead to sudden failure of the implants in long-term service.[76] Therefore, an effective approach of surface modification with inorganic coating materials is applied to retard the biodegradation of magnesium alloys.[77] The solgel technique, which offers controlled composition and morphology, high adhesion with metallic substrate, low processing temperature and enhanced bioactivity and so forth, is adoptive to produce ecofriendly anticorrosion coatings.[78] Several investigations have been reported into protecting magnesium alloys with inorganic coating by a combination of solgel and dip-coating techniques.

Bioglass 45S5, a commercially available inorganic material, possesses excellent bioactivity, favourable biocompatibility and controllable biodegradability.[79] The material also exhibits strong interfacial bonding with bone in living organisms and facilitates integration of osseous tissue with the implant, which could promote bone regeneration and has been used clinically as a hard tissue-regenerative biomaterial in orthopaedic surgery. In a research study, Huang et al.[80] reported an improvement in corrosion resistance and bioactivity using mesoporous 45S5 bioactive glass−ceramic (45S5 MBGC) thin films on AZ31 magnesium alloy by dip-coating and the evaporation-induced self-assembly process. Nonmesoporous 45S5 bioactive glass−ceramic (45S5 BGC) thin films were also prepared for comparative investigation. The results of that investigation showed that 45S5 MBGC thin films were crack-free and uniform with a larger special surface area and pore volume and better surface wettability in contrast to 45S5 BGC coatings. In addition, 45S5 MBGC coatings showed good adhesion strength to the AZ31 substrate owing to the chemical bonding interface. Investigation tests in SBF revealed that the pitting corrosion potential and polarization resistance of AZ31 substrate were improved by the 45S5 MBGC coatings. Furthermore, the anticorrosion property decreased the corrosion current density. Consequently, the 45S5 MBGC-coated magnesium alloys had potential for use as biodegradable biomedical implant material.[80] The 45S5 MBGC coatings were more hydrophilic than 45S5 BGC coatings and had more desirable adhesion strength to the AZ31 substrate for chemical bonding in the interface. The electrochemical impedance spectroscopy (EIS) and

potentiodynamic polarization tests verified that 45S5 MBGC coatings can greatly improve the pitting corrosion potential and corrosion resistance of magnesium alloys. Therefore, 45S5 MBGC coatings are a potential material for the development of anticorrosion and bioactivity in magnesium alloys.[80]

To date, research efforts regarding protective thin films have primarily focused on compact textures.[81,82] In fact, studies have confirmed that mesoporous thin films could confer corrosion protection for magnesium alloys. Furthermore, a mesoporous structure is beneficial to the integrity of the outer surface. This mesoporous structure could effectively release stress in the thin film and ameliorate the mismatch between the substrate and coating; thus, crack-free thin films can be successfully prepared. In addition, studies have reported that mesoporous thin films can easily induce apatite formation and have high bone-forming ability owing to the enhancement of cell activity and protein adsorption.[83]

8.2.4 Biomimetic approach

In most cases, bone defects filled with biocompatible materials are encapsulated by fibrous tissue separated from the surrounding bones. It is known that various types of ceramics bond to living bone without forming fibrous tissues around them. Hydroxyapatite, bioactive glass, and glass–ceramic A-W including apatite and wollastonite ($CaO \cdot SiO_2$) are frequently used as bone-restorative materials for clinical applications.[84] Although these biomaterials have excellent mechanical strength, they cannot be used confidently under high load-bearing conditions such as femoral and tibia bones. This phenomenon occurs for two main reasons: their low fracture toughness and their high elastic modulus with respect to human cortical bone.

It is known for various kinds of glasses and glass-ceramics that the essential requirement for them to bond to living bone is the formation of a biologically active bonelike apatite layer on their surfaces in the body.[85] This bonelike apatite layer can be reproduced on their surfaces as a thin film.[86] The mechanism of bonelike apatite formation on their surfaces is associated with their surface chemistry. These findings enable us to form apatite thin films even on surfaces of metals and organic polymers through the biomimetic approach.

All known kinds of bioactive materials bond to living bone through an apatite layer that is formed on their surfaces in the living body. The apatite layer can be reproduced on their surfaces in acellular SBF with ion concentrations nearly equal to those of human blood plasma[87] and are identified as a thin film of carbonate-containing HA with small crystallites and defective structures similar to apatite in natural bone.[88] The mechanism of biomimetic apatite formation on the surfaces of bioactive glass and glass–ceramics in the living body is explained as follows.[89] Calcium release from them increases ionic activity in the surrounding fluid, and hydrated silica on their surfaces provides apatite nucleation sites. After the formation of apatite nuclei, they grow by consuming calcium and phosphate ions, because the body fluid is supersaturated with these ions.[90] These findings provide a biomimetic method for forming a bonelike apatite thin film on different substrates.[91] Simple oxide gels with compositions such as TiO_2, ZrO_2, Nb_2O_5 and Ta_2O_5 also form an apatite thin film coating

on their surfaces in SBF.[91] This shows that even metallic materials based on Ti, Zr, Nb and/or Ta can form apatite layers on their surfaces in the living body and bond to living bone through apatite layers when their surfaces are slightly modified (Fig. 8.7).

In the past few decades, many methods such as physical machining and controlled oxidation have been used to improve the in vivo osseointegration of titanium-based implants. Calcium phosphate—based thin films such as HA have been used frequently on orthopaedic implants. As a new concept in tissue engineering, it has been suggested that HA has distinct luminescence properties allowing rapid identification of phase distribution of biomimetic apatite thin films. In a research study, Sepahvandi et al.[93] reported that the photoluminescence property can be used in the characterization and early detection of biomimetic bonelike apatite formation on the surface of alkaline-treated titanium implants (in SBF solution).

According to their state-of-the-art research, the researchers concluded that the photoluminescence emission peak did not have a significant shift to shorter or higher wavelengths, and the photoluminescence intensity increased as the exposure time increased. This research proved that the observed inherent photoluminescence of biomimetic apatite thin films can be of specific interest for histological probing and bone remodelling monitoring. In that study, the formation of apatite thin film on the surface of implants was confirmed by energy-dispersive X-ray spectroscopy (EDX) analysis, so the appearance of apatite formation after immersion in SBF solution was established by EDX, as shown in Fig. 8.8(a). As can be seen, the EDX spectrum shows the peaks of Ti, Al and V elements related to the titanium implant, and the peaks of P, Ca and C correspond to the newly formed biomimetic apatite thin film. Also, according to the Ca and P peaks of the EDX graph, the Ca—P molar ratio was calculated to be in the range of 2.6, which could be related to nonstoichiometric hydroxy-carbonate apatite.[94,95] In addition, Fig. 8.8(b) shows a scanning electron micrograph of the cross section of the implant after immersion in SBF solution, indicating that the newly formed biomimetic apatite thickness of the specimens is less than 5 μm and also homogeneous and uniform.

8.2.5 Electrophoretic deposition

Electrophoretic deposition (EPD) was discovered in 1808 by the Russian scientist Ruess; it was first used in a practical application in 1933 to deposit thoria particles on a platinum cathode.[96] EPD is a low-cost, flexible and non—line-of-sight coating process which can be used to deposit uniform thin films on substrates of complex shape or surface morphology. Furthermore, EPD can produce thin films of a wide range of thicknesses, from nano to micron, with a high degree of control over thickness and morphology.[97] As for many other ceramic coating techniques, EPD-coated implants need a subsequent densification stage to sinter the thin film. Wei et al.[98] reported a nano particulate dual-coating approach to deposit HA nanoparticles on the surface of metallic substrates through EPD. They also studied the interfacial bond strength of the prepared thin films. Hamagami et al.[99] fabricated highly ordered macroporous apatite thin films onto titanium by EPD. Unfortunately, such coatings deposited by electrophoretic technique have the major drawback of poor adhesion and the need for posttreatment

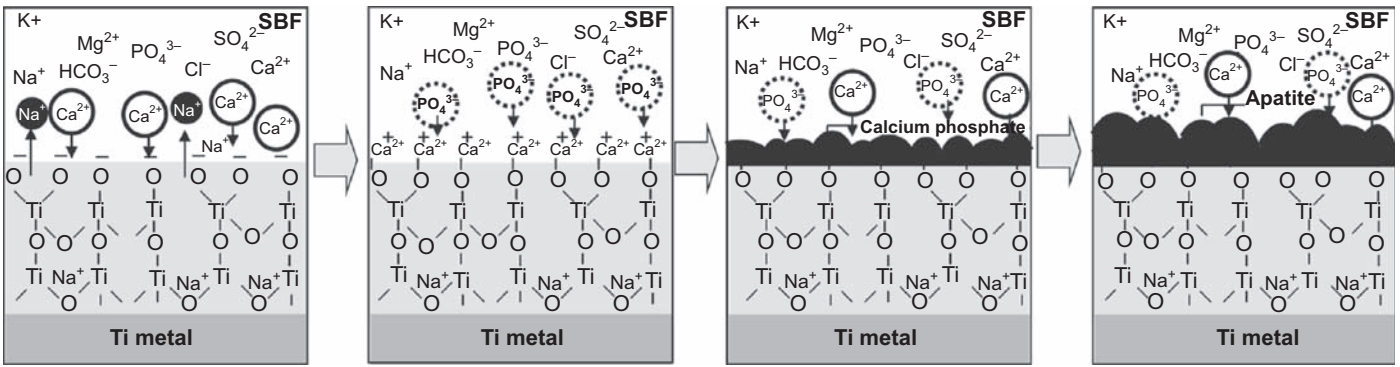

Figure 8.7 Process of apatite formation in simulated body fluid (SBF) on Ti metal subjected to acid NaOH and heat treatment.[92]

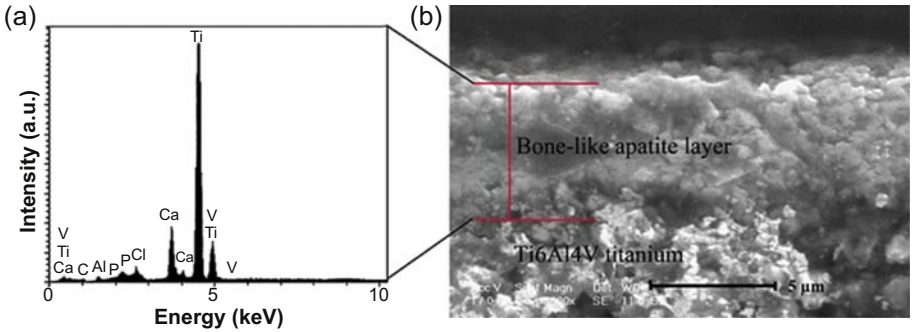

Figure 8.8 (a) Energy-dispersive X-ray pattern and (b) scanning electron micrograph of the cross-section of newly formed biomimetic apatite thin film after 7 days immersion in SBF.[93]

to improve adhesion. The difference in thermal expansion can also cause cracks to generate on the surface of coated layers or at the interface between the thin films and substrates during cooling after sintering.[98] Therefore, relatively low sintering temperatures are desirable for HA-coated systems. Studies have also demonstrated that well-dispersed particles are necessary to produce densely packed thin films because aggregates form loosely bound structures with low green densities and poor sintering behaviour.[100,101] Therefore, it is highly desirable to produce stable suspensions containing fine HA particles. As previously pointed out, the choice of a suitable medium is important for EPD. In fact, EPD is a material processing technique based on the movement of charged particles in liquid suspension and their deposition on a substrate acting as an electrode in the EPD cell, showed in Fig. 8.9. This processing technique is increasingly being considered for the production of nanostructured coatings and layers on a variety of substrates for numerous applications, including wear and oxidation resistance, bioactive coatings for biomedical implants and devices as well as functional coatings for photocatalytic, electronic, magnetic and related applications.

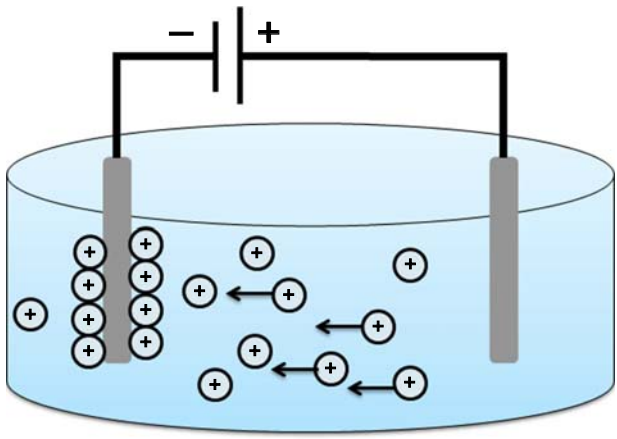

Figure 8.9 Two electrodes for electrodepositing showing positively charged particles in suspension migrating toward the negative electrode.

Carbon nanotubes (CNTs) have been the subject of extensive research over the past 10 years.[102] Because of their impressive structural, electrical and mechanical properties as well as their small size and mass, they have become one of the most promising materials for future development and have opened up a new era in the field of biomaterials science.[102,103] In recent years, considerably effort has been devoted to applying CNTs in the biological and medical fields.[104] Available data suggest that CNT-containing materials may be optimal for tissue engineering applications. This is not only because of their ability to simulate dimensions of proteins that comprise native tissue but also because of their higher reactivity for interactions involved in the cell attachment mechanism.

In a research study, Boccaccini et al.[105] investigated the thin films of highly porous Bioglass-based scaffolds with multiwalled CNT (MCNTs). They fabricated foamlike Bioglass scaffolds by EPD and deposited homogeneous layers of CNT throughout the scaffolds' porous structure. Optimal experimental conditions were determined to be an applied voltage of 15 V and deposition time of 20 min, using a concentrated aqueous suspension of CNT with the addition of a surfactant and iodine. The scaffolds' porous structure remained invariant after the CNT coating. The incorporation of CNTs induced a nanostructured internal surface of the pores that was thought to be beneficial for osteoblast cell attachment and proliferation. Bioactivity of the scaffolds was assessed by immersion studies in SBF for up to 2 weeks and the subsequent determination of HA formation. The presence of CNTs can enhance the bioactive behaviour of the scaffolds because CNTs can serve as a template for the ordered formation of nanostructured HA layers, which does not occur on uncoated Bioglass surfaces.

Several studies have been carried out on the interaction between CNTs and a variety of cells including osteoblasts and have focused on the biocompatibility of CNTs.[106,107] These studies suggest the possibility of using CNTs as an alternative material to treat bone pathologies in combination with bone cells, with the potential for enhanced osteoblast proliferation and bone formation. In addition, next-generation scaffolds could incorporate further functionalities to enhance neotissue formation. For instance, an electric field is known to stimulate the healing of various tissues. In the case of bone regeneration and fracture healing, the use of an electric field is based on the observation that when a bone is subjected to mechanical stresses, deformation of bone is normally accompanied by an electrical signal bearing the strain characteristics. Therefore, a conductive scaffold, eg, incorporating CNT, can potentially be used to stimulate cell growth and tissue regeneration by facilitating physioelectrical signal transfer.

A review of previous work on the EPD of CNT was published.[108] That article showed that EPD is a convenient method to manipulate CNTs and produce reliable CNTs assemblies and layers on planar substrates. For example, Du et al.[109] deposited CNT on metallic substrates by EPD using ethanol−acetone mixed suspensions. Further studies were carried out by Thomas et al.[110] in which homogeneous deposition of CNT assemblies using aqueous suspensions was accomplished on stainless-steel substrates. Incorporation of CNTs into the scaffolds also has a number of special advantages, such as that it encourages cell adhesion and proliferation by inducing nanotopography, it provides a crack-inhibiting mechanism on the scaffold surfaces and it

confers biosensing (electrical conduction) properties while maintaining bioactivity and the interconnected porous network of the scaffold. Moreover, the addition of CNTs to a biocompatible matrix has further advantages for multifunctional (smart) scaffolds because CNT can be used for targeted delivery of growth factors or drugs. In brief, EPD is a technique for the development of complex CNT−ceramic nanocomposite layers and coatings of high structural homogeneity and reproducible properties for tissue engineering.[108,111]

8.2.6 Chemical vapour deposition

In the past few decades, it has been demonstrated that many types of materials can be deposited as films at pressures below 1 atm using chemical vapour deposition (CVD) processes.[112] This is a promising technology for a wide range of biomaterials in the field of tissue engineering because of the great combination of superior properties including hardness, fracture toughness, the low friction coefficient, high chemical resistance and a variety of possible coating substrates. It has been frequently reported that the biocompatibility of CVD surfaces is similar to that of bare titanium implant surfaces. A study[113] demonstrated that thin films of diamond-like carbon containing up to 22 atm% silicon (DLC-Si) deposited onto silicon substrates by low-frequency pulsed direct current plasma-activated CVD (PACVD) showed exceptional characteristics compared with untreated samples. That study showed that biocompatibility tests using MG-63 osteoblast-like cell cultures indicated homogeneous and optimal tissue integration for both the DLC and the DLC-Si surfaces. The pulsed PACVD technique has been shown to produce biocompatible DLC and DLC-Si coatings with potential for tissue engineering applications. Fig. 8.10 represents a schematic of basic process steps during CVD.

In other research activities, CVD polymerization offers several advantages compared with other solvent-based coating processes.[114] First, CVD coatings are conformal, which allows for the easy and uniform modification of nonplanar substrate geometries. Second, although the activation step (which takes place away from the substrate) requires high temperatures, the substrates can be maintained at a controlled temperature (typically room temperature) or below. Third, impurities associated with the use of solvents, initiators or plasticizers can be precluded. Several examples of CVD-based polymer coatings have been reported. Frank and coworkers[115] used CVD to prepare polypeptide chains that are grafted onto a surface. Gleason and coworkers have shown through various examples[116] that even if the monomer of interest does not contain an initiator, polymerization initiators can be introduced together with the monomer through basic process modification. In cases in which hot filaments within the deposition chamber were used for initiation, radical polymerizations often yielded conformal thin films.

8.2.7 Pulsed laser deposition

The pulsed laser deposition (PLD) technique has been used to deposit crystalline HA thin films on titanium substrates.[117,118] The structure and properties of HA thin films

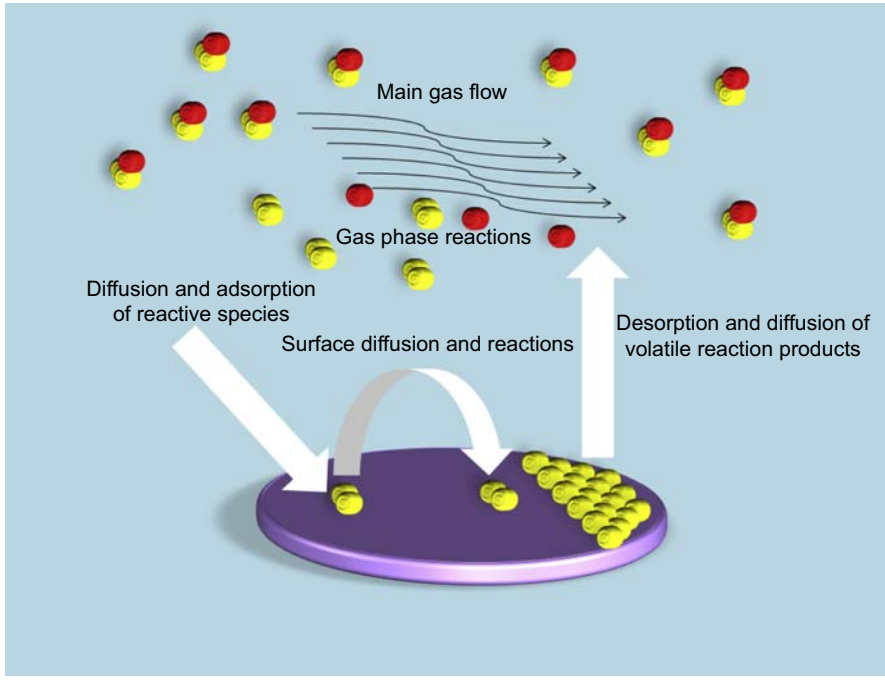

Figure 8.10 Schematic representation of basic process steps during chemical vapour deposition (CVD).

using PLD technique can be tuned with different laser deposition parameters. As an excellent technique for tissue engineering applications, Wang et al.[118] showed that PLD process did not induce a large amount of calcium phosphate phases other than apatite. The process did not also change the behaviour of hydroxyl or phosphate functional groups. In addition, microscopic observations revealed that HA thin films consisted of numerous essentially spheroidal particles of different sizes during solidification, whereas the lateral morphology indicated that columnar and dome-shaped structures both existed in the film. The adhesion strength of the thin film, mostly in the range 30–40 MPa, was closely related to the fractography of the tested sample. The fractured surfaces with higher bond strengths were usually accompanied by a higher degree of deformation and coating–substrate debonding, whereas the fracture of samples with lower bond strengths occurred more frequently within the HA thin films in a more brittle manner.

In addition, two newly developed techniques, matrix-assisted pulsed laser evaporation (MAPLE) and MAPLE direct write (MDW), were suggested to deposit biomaterials thin films. MAPLE involves dissolving the biomaterial in a volatile solvent, freezing for the creation of a solid target and evaporating the target for deposition of the solute inside a vacuum system (using a low-fluorescence pulsed laser). Using shadow masks such as dots or arrays, pattern features with small length scales can be deposited using compound materials on numerous types of substrates.

In comparison, MDW uses a pulsed laser to transfer the target material directly from a ribbon to a substrate, in which the patterns with a spatial resolution can be written directly. Furthermore, pulsed laser ablation has been used to develop improved surface conformation on tissue engineering scaffolds. The in vitro and in vivo biocompatibility of an HA thin film deposited on titanium web (TW) scaffolds was studied.[119] In that study, HA thin films were deposited onto the surface using a pulsed laser operating at a rate of 10 Hz followed by annealing at 380 °C for 1 h. The presence of HA not only along the surface but also in the TW inner region was confirmed by the elementary mapping of calcium, phosphorous and titanium. Finally, the X-ray diffraction (XRD) patterns showed that crystalline HA coated the entire surface of TW scaffolds, indicating the high potential of that technique for tissue engineering applications.

8.2.8 Solgel technique

The use of thin film coatings is one of the most efficient surface modification approaches to improve the performance of metallic implants. Among the various methods used to prepare thin films, solgel deposition has many advantages, such as high homogeneity and simplicity for full coverage of complex structures.[120,121] Generally, solgel-derived thin films are classified into two categories: inorganic oxide and organic−inorganic hybrid thin films. The latter has been developed to overcome the drawbacks of the former, especially brittleness and the need for relatively high-temperature treatment (sintering) after deposition, by introducing an organic component into the inorganic network.[122] According to the literature, organic−inorganic hybrid thin films can better improve the corrosion resistance of metallic implants compared with inorganic thin films[122]; however, the adhesion of inorganic thin films to metallic substrates is better than that of organic−inorganic thin films.[123] In a similar situation, Fedrizzi et al.[124] found that the anticorrosion performance of polyester organic thin films on low-carbon steel improved owing to pretreatment of the substrate by applying an inorganic zirconia coating, which enhanced the film's adhesion to the substrate.

In a research study, Salahinejad et al.[125] investigated a new double-layer solgel thin film coating to improve the corrosion resistance of medical-grade stainless steel in an SBF solution. One effective way to overcome some of the drawbacks of oxide coatings for the corrosion protection of metal surfaces is to incorporate an organic component into the inorganic network, although commonly, film adhesion is disadvantageously affected. In that work, for the first time, by exploiting both inorganic and organic−inorganic coatings, a new double-layer thin film composed of $ZrTiO_4$ as the bottom layer and $ZrTiO_4$−PMMA as the top layer was deposited on a medical-grade stainless-steel substrate via solgel spin-coating. According to potentiodynamic polarization experiments in SBF, the substrate coated with this hybrid thin film exhibited superior corrosion resistance compared with the same substrate coated with purely inorganic $ZrTiO_4$ films.

In a comparable study, Naghib et al.[126] investigated the bioactivation of a 304 stainless-steel surface through 45S5 Bioglass coatings for biomedical applications.

The ability of 45S5 Bioglass to form a bond to living bone tissue and stimulate bone–cell proliferation may be different for melt- and solgel-derived samples. In that research, the differences in corrosion resistance, bioactivity and physical properties between the melt- and solgel-derived 45S5 Bioglass coated on the surface of austenitic 304 stainless steel as a dental and orthopaedic metallic implant were studied. The morphologies of different coated samples were investigated by scanning electron microscopy. Then, electrochemical measurements were performed and compared with uncoated samples. To investigate the bioactivity and surface reactivity of the coated samples, the researchers monitored the samples in SBF solution in vitro and examined their microstructures and electrochemical properties in detail. Immediately after immersion in SBF, reactions occurred on the surface of the coated samples, and the obtained results from XRD and Fourier transform infrared spectroscopy analyses showed typical characteristic peaks of HA crystals. In addition, the coated samples showed enhanced corrosion resistance and bioactivity compared with the uncoated ones. The solgel-derived coated sample had higher corrosion resistance and formed the HA layer more quickly, qualities that are useful for dental and orthopaedic metallic implants.

8.3 Novel innovative strategies for tissue engineering purposes

Studies have reported a novel coating approach to deposit crack-free and nanostructured HA thin films on Ti6Al4V alloys with an Al_2O_3 buffer layer for tissue engineering purposes.[127] In this novel method, the Al_2O_3 buffer layer was deposited by plasma-spraying whereas the HA top layer was applied by dip-coating. The XRD and Raman reflections of alumina buffer layer showed α- to γ-Al_2O_3 phase transformation and the fractographic analysis of the sample revealed the formation of columnar grains in well-melted splats. Surprisingly, the bonding strength between Al_2O_3 coating and Ti6Al4V substrate was estimated to be about 40 MPa. In addition, the microscopic images showed that the HA top layer homogeneously enveloped the troughs and crests of the underneath rough ($R_a = 2.91$-μm) Al_2O_3 surface. It is believed that this novel coating approach to preparing thin films might be useful for rapid cement-less fixations in critical situations for longer periods of time.

In another innovative approach, Kim et al.[128] suggested that nanocrystalline HA thin films can be formed at the surface of Ti by single-step microarc oxidation method using Ca^{2+} and P^{5+} ion-containing electrolytes. They reported that the HA films were 10–25 μm thick and showed strong crystallinity dependence on the $CaCl_2$ concentration in the electrolytes. Also, the formation of an amorphous $CaTiO_3$ interlayer was identified as existing between the HA film and Ti substrates. In contrast to previous research, using K_2HPO_4 for the electrolytes could allow formation of a crystalline HA layer. It is suggested as the most probable mechanism for the HA formation that the high-density hydroxyl groups of $TiO(OH)_2$, formed by the reactions between the amorphous $CaTiO_3$ interlayer and the H^+ ions from the dissolution of the KH_2PO_4,

can have a key role in the nucleation and crystal growth of HA films by attracting Ca^{2+} and P^{5+} ions in the electrolytes. Undoubtedly, this basic research shed light on the creation of the most effective coating thin films by controlling the nucleation and crystal growth of HA on the surface of tissue engineering implants.

Plasma-enhanced CVD (PECVD) for the deposition of nanostructures composed of diphenylalanine has shown promising advantages over conventional methods. This is a solvent-free approach that allows sublimation of the peptide to form dense, uniform arrays of peptide nanostructures on a variety of substrates. The PECVD-deposited D-diphenylalanine nanostructures have a range of chemical and physical properties depending on the specific discharge parameters used during the deposition process.

This technology has been used to deposit two different fluorocarbon precursors (octofluoropropane and hexafluoropropylene oxide) on polycaprolactone scaffolds. These two coating systems were chosen with intention of modifying the scaffold surfaces to be bio-nonreactive while maintaining the desirable bulk properties of the scaffold. Microscopic observations confirmed that fluorocarbon film deposition yielded conformal rather than blanket coatings as the porous scaffold structure was maintained after plasma treatment. The treated scaffolds seeded with human dermal fibroblasts demonstrated that the cells do not attach after 72 h and that the scaffolds are not cytotoxic to the cells. This work demonstrates that conformal fluorocarbon coatings can be deposited on three-dimensional (3D) polymeric scaffolds using PECVD to fabricate 3D bio-nonreactive materials for advanced applications in tissue engineering.

8.4 Conclusion

It is known that biomaterials interact with biological systems through their surfaces. Biocompatibility is a crucial property to minimize unwanted and undesirable responses and permit the surface of the biomaterial to integrate with the host tissues. Therefore, organic and inorganic thin films have attracted much attention because of the following properties: versatility, biocompatibility, biodegradability and integration with tissues. These coated materials can have properties similar to hard and soft tissues, including Young's modulus, fracture stress, elasticity and hardness. To achieve thin film formation for biomedical applications, spin-coating, LbL assembly, dip-coating, EPD, CVD, PLD and the solgel process can be used, as summarized in this chapter. Chemical grafting of molecules onto the surface of biomaterials has also been achieved with such coating technologies as one of the most important advances in the field of tissue engineering. Among different techniques, multilayer thin film coatings based on LbL assembly provides precise control over the physicochemical characteristics of biomaterials on different surfaces. This new type of thin films has the potential to be considered as grafts with new properties to attract drug carriers as the next generation of functional thin films. Furthermore, in vitro and in vivo investigations should be performed to study the biocompatibility and osteoinductivity of these biomaterials. In addition, a suitable biodegradability rate is a

necessary property for the development of tissue engineering implants for enhanced regeneration and must be matched with the rate of neotissue formation. Furthermore, solgel process has been widely used to prepare thin film oxide layers with improved surface characteristics. These thin biocompatible and biodegradable films with an optimized composition and structure on the surface of metallic implants can significantly improve implant integration. It is believed that a combination of these novel coating technologies can effectively solve problems associated with the rapid fixation of implants into natural tissues as well as biocompatibility for longer periods of time in the human body.

References

1. Scriven LE. Better ceramics through chemistry III: symposium. In: *Materials research society symposium proceedings*; 1988. p. 717−29.
2. Bornside DE, Macosko CW, Scriven LEJ. On the modeling of spin coating. *Imaging Tech* 1987;**13**:122.
3. Rahaman MN. *Ceramic processing and sintering*. 2nd ed. (New York): Marcel Dekker; 2003.
4. Mozafari M, Salahinejad E, Shabafrooz V, Yazdimamaghani M, Vashaee D, Tayebi L. Multilayer bioactive glass/zirconium titanate thin films in bone tissue engineering and regenerative dentistry. *Int J Nanomedicine* 2013;**8**:1665−72.
5. Mozafari M, Salahinejad E, Sharifi-Asl S, Macdonald DD, Vashaee D, Tayebi L. Innovative surface modification of orthopaedic implants with positive effects on wettability and in vitro anticorrosion performance. *Surf Eng* 2014;**30**(9):688−92.
6. Picart C, Caruso F, Voegel J-C, editors. *Layer-by-layer films for biomedical applications*. 1st ed. Wiley-VCH; 2014.
7. McCullough DH, Regen SL. Don't forget Langmuir−Blodgett films. *Chem Commun (Camb)* 2004;(24):2787−91.
8. Tang Z, Wang Y, Podsiadlo P, Kotov NA. Biomedical applications of layer-by-layer assembly: from biomimetics to tissue engineering. *Adv Mater* 2006;**18**(24):3203−24.
9. Iler RK. Multilayers of colloidal particles. *J Colloid Interface Sci* 1966;**21**(6):569−94.
10. Richardson JJ, Bjornmalm M, Caruso F. Technology-driven layer-by-layer assembly of nanofilms. *Science* 2015;**348**(6233):aaa2491.
11. Decher G, Hong JD, Schmitt J. Buildup of ultrathin multilayer films by a self-assembly process: III. Consecutively alternating adsorption of anionic and cationic polyelectrolytes on charged surfaces. *Thin Solid Films* 1992;**210**−**211**:831−5.
12. Kirkland JJ. Porous thin-layer modified glass bead supports for gas liquid chromatography. *Anal Chem* 1965;**37**(12):1458−61.
13. Decher G. Fuzzy nanoassemblies: toward layered polymeric multicomposites. *Science* 1997;**277**(5330):1232−7.
14. Ott P, Trenkenschuh K, Gensel J, Fery A, Laschewsky A. Free-standing membranes via covalent cross-linking of polyelectrolyte multilayers with complementary reactivity. *Langmuir* 2010;**26**(23):18182−8.
15. Kleinke H, Finckh EW, Tremel W. Ta4BTe8: tantalum telluride cluster chains with encapsulated boron atoms. *Angew Chem Int Ed* 1999;**38**(13/14):2054−7.

16. Caruso F. Nanoengineering of inorganic and hybrid hollow spheres by colloidal templating. *Science* 1998;**282**(5391):1111−4.
17. Zhang X, Chen H, Zhang H. Layer-by-layer assembly: from conventional to unconventional methods. *Chem Commun* 2007;(14):1395−405.
18. Shim BS, Podsiadlo P, Lilly DG, Agarwal A, Lee J, Tang Z, et al. Nanostructured thin films made by dewetting method of layer-by-layer assembly. *Nano Lett* 2007;**7**(11): 3266−73.
19. Fujimoto K, Fujita S, Ding B, Shiratori S. Fabrication of layer-by-layer self-Assembly films using roll-to-roll process. *Jpn J Appl Phys Part 2 Lett* 2005;**44**(1−7).
20. Donath E, Walther D, Shilov VN, Knippel E, Budde A, Lowack K, et al. Nonlinear hairy layer theory of electrophoretic fingerprinting applied to consecutive layer by layer polyelectrolyte adsorption onto charged polystyrene latex particles. *Langmuir* 1997; **13**(20):5294−305.
21. Grigoriev DO, Bukreeva T, Möhwald H, Shchukin DG. New method for fabrication of loaded micro- and nanocontainers: emulsion encapsulation by polyelectrolyte layer-by-layer deposition on the liquid core. *Langmuir* 2008;**24**(3):999−1004.
22. Hoogeveen NG, Stuart MAC, Fleer GJ, Böhmer MR. Formation and stability of multilayers of polyelectrolytes. *Langmuir* 1996;**12**(15):3675−81.
23. Richardson JJ, Ejima H, Lörcher SL, Liang K, Senn P, Cui J, et al. Preparation of nano- and microcapsules by electrophoretic polymer assembly. *Angew Chem Int Ed* 2013; **52**(25):6455−8.
24. Thomas IM. Single-layer TiO(2) and multilayer TiO(2)−SiO(2) optical coatings prepared from colloidal suspensions. *Appl Opt* 1987;**26**(21):4688−91.
25. Ma L, Cheng M, Jia G, Wang Y, An Q, Zeng X, et al. Layer-by-layer self-assembly under high gravity field. *Langmuir* 2012;**28**(25):9849−56.
26. Schlenoff JB, Dubas ST, Farhat T. Sprayed polyelectrolyte multilayers. *Langmuir* 2000; **16**(26):9968−9.
27. Qi A, Chan P, Ho J, Rajapaksa A, Friend J, Yeo L. Template-free synthesis and encapsulation technique for layer-by-layer polymer nanocarrier fabrication. *ACS Nano* 2011;**5**(12):9583−91.
28. Sun J, Gao M, Feldmann J. Electric field directed layer-by-layer assembly of highly fluorescent CdTe nanoparticles. *J Nanosci Nanotechnol* 2001;**1**(2):133−6.
29. Hong X, Li J, Wang M, Xu J, Guo W, Li J, et al. Fabrication of magnetic luminescent nanocomposites by a layer-by-layer self-assembly approach. *Chem Mater* 2004;**16**(21): 4022−7.
30. Rydzek G, Thomann JS, Ben Ameur N, Jierry L, Mésini P, Ponche A, et al. Polymer multilayer films obtained by electrochemically catalyzed click chemistry. *Langmuir* 2010;**26**(4):2816−24.
31. Voigt A, Lichtenfeld H, Sukhorukov GB, Zastrow H, Donath E, Ba H, et al. Membrane filtration for microencapsulation and microcapsules fabrication by layer-by-layer polyelectrolyte adsorption. *Ind Eng Chem Res* 1999;**38**:4037−43.
32. Picart C, Lavalle P, Hubert P, Cuisinier FJG, Decher G, Schaaf P, et al. Buildup mechanism for poly(L-lysine)/hyaluronic acid films onto a solid surface. *Langmuir* 2001; **17**(23):7414−24.
33. Richardson JJ, Teng D, Björnmalm M, Gunawan ST, Guo J, Cui J, et al. Fluidized bed layer-by-layer microcapsule formation. *Langmuir* 2014.
34. Zhu Y, Gao C, He T, Liu X, Shen J. Layer-by-layer assembly to modify poly(L-lactic acid) surface toward improving its cytocompatibility to human endothelial cells. *Biomacromolecules* 2003;**4**(2):446−52.

35. Scriven LE. Physics and applications of dip coating and spin coating. *MRS Proc* 1988;**121**.
36. Adell R, Lekholm U, Rockler B, Brånemark PI. A 15-year study of osseointegrated implants in the treatment of the edentulous jaw. *Int J Oral Surg* 1981;**10**(6): 387−416.
37. Kumar G, Narayan B. Osseointegrated titanium implants: requirements for ensuring a long-lasting, direct bone-to-implant anchorage in man. In: Banaszkiewicz PA, Kader DF, editors. *Classic papers in orthopaedics*. (London): Springer; 2014. p. 507−9.
38. Nanci A, Wuest JD, Peru L, Brunet P, Sharma V, Zalzal S, et al. Chemical modification of titanium surfaces for covalent attachment of biological molecules. *J Biomed Mater Res* 1998;**40**(2):324−35.
39. Block MS, Finger IM, Fontenot MG, Kent JN. Loaded hydroxylapatite-coated and grit-blasted titanium implants in dogs. *Int J Oral Maxillofac Implants* 1989;**4**(3): 219−25.
40. Ratner BD. New ideas in biomaterials science−a path to engineered biomaterials. *J Biomed Mater Res* 1993;**27**(7):837−50.
41. Lucas LC, Lacefield WR, Ong JL, Whitehead RY. Calcium phosphate coatings for medical and dental implants. *Colloids Surf A Physicochem Eng Aspects* 1993;**77**(2): 141−7.
42. Ducheyne P, Cuckler JM. Bioactive ceramic prosthetic coatings. *Clin Orthop Relat Res* 1992;(276):102−14.
43. Lacefield WR. Hydroxylapatite coatings. In: Hench L, Wilson J, editors. *An introduction to bioceramics*. (USA): World Scientific; 1993. p. 223−38.
44. Hench LL. Bioceramics: from concept to clinic. *J Am Ceram Soc* 1991;**74**(7):1487−510.
45. McPherson EJ, Dorr LD, Gruen TA, Saberi MT. Hydroxyapatite-coated proximal ingrowth femoral stems. A matched pair control study. *Clin Orthop Relat Res* 1995; (315):223−30.
46. Heling I, Heindel R, Merin B. Calcium-fluorapatite. A new material for bone implants. *J Oral Implantol* 1981;**9**(4):548−55.
47. Ślósarczyk A, Stobierska E, Paszkiewicz Z, Gawlicki M. Calcium phosphate materials prepared from precipitates with various calcium: phosphorus molar ratios. *J Am Ceram Soc* 1996;**79**(10):2539−44.
48. Overgaard S, Lind M, Glerup H, Grundvig S, Bünger C, Søballe K. Hydroxyapatite and fluorapatite coatings for fixation of weight loaded implants. *Clin Orthop Relat Res* 1997; (336):286−96.
49. Posner AS. The mineral of bone. *Clin Orthop Relat Res* 1985;(200):87−99.
50. Moreno EC, Kresak M, Zahradnik RT. Fluoridated hydroxyapatite solubility and caries formation. *Nature* 1974;**247**(5435):64−5.
51. LeGeros RZ, Silverstone LM, Daculsi G, Kerebel LM. In vitro caries-like lesion formation in F-containing tooth enamel. *J Dent Res* 1983;**62**(2):138−44.
52. Weng W, Baptista JL. Sol−gel derived porous hydroxyapatite coatings. *J Mater Sci Mater Med* 1998;**9**(3):159−63.
53. Liu DM, Yang Q, Troczynski T, Tseng WJ. Structural evolution of sol−gel-derived hydroxyapatite. *Biomaterials* 2002;**23**(7):1679−87.
54. Kim HW, Kim HE, Knowles JC. Fluor-hydroxyapatite sol−gel coating on titanium substrate for hard tissue implants. *Biomaterials* 2004;**25**(17):3351−8.
55. Bock N, Riminucci A, Dionigi C, Russo A, Tampieri A, Landi E, et al. A novel route in bone tissue engineering: magnetic biomimetic scaffolds. *Acta Biomater* 2010;**6**(3): 786−96.

56. Glowacki J. Angiogenesis in fracture repair. *Clin Orthop Relat Res* 1998;(355 Suppl.): S82−9.
57. Whitaker MJ, Quirk RA, Howdle SM, Shakesheff KM. Growth factor release from tissue engineering scaffolds. *J Pharm Pharmacol* 2001;**53**(11):1427−37.
58. Causa F, Netti PA, Ambrosio L. A multi-functional scaffold for tissue regeneration: the need to engineer a tissue analogue. *Biomaterials* 2007;**28**(34):5093−9.
59. Milkiewicz M, Ispanovic E, Doyle JL, Haas TL. Regulators of angiogenesis and strategies for their therapeutic manipulation. *Int J Biochem Cell Biol* 2006;**38**(3): 333−57.
60. Laschke MW, Harder Y, Amon M, Martin I, Farhadi J, Ring A, et al. Angiogenesis in tissue engineering: breathing life into constructed tissue substitutes. *Tissue Eng* 2006; **12**(8):2093−104.
61. Rose FRAJ, Oreffo ROC. Bone tissue engineering: hope vs hype. *Biochem Biophys Res Commun* 2002;**292**(1):1−7.
62. Shimizu K, Ito A, Honda H. Enhanced cell-seeding into 3D porous scaffolds by use of magnetite nanoparticles. *J Biomed Mater Res Part B Appl Biomater* 2006;**77**(2): 265−72.
63. Lode A, Reinstorf A, Bernhardt A, Wolf-Brandstetter C, König U, Gelinsky M. Heparin modification of calcium phosphate bone cements for VEGF functionalization. *J Biomed Mater Res Part A* 2008;**86**(3):749−59.
64. Patel ZS, Young S, Tabata Y, Jansen JA, Wong MEK, Mikos AG. Dual delivery of an angiogenic and an osteogenic growth factor for bone regeneration in a critical size defect model. *Bone* 2008;**43**(5):931−40.
65. Schicker M, Seitz H, Drosse I, Seitz S, Mutschler W. Biomaterials as scaffold for bone tissue engineering. *Eur J Trauma* 2006;**32**(2):114−24.
66. Muthana M, Scott SD, Farrow N, Morrow F, Murdoch C, Grubb S, et al. A novel magnetic approach to enhance the efficacy of cell-based gene therapies. *Gene Ther* 2008; **15**(12):902−10.
67. Barry SE. Challenges in the development of magnetic particles for therapeutic applications. *Int J Hyperth* 2008;**24**(6):451−66.
68. Arruebo M, Fernández-Pacheco R, Ibarra MR, Santamaría J. Magnetic nanoparticles for drug delivery. *Nano Today* 2007;**2**(3):22−32.
69. Ito A, Shinkai M, Honda H, Kobayashi T. Medical application of functionalized magnetic nanoparticles. *J Biosci Bioeng* 2005;**100**(1):1−11.
70. Butoescu N, Seemayer CA, Foti M, Jordan O, Doelker E. Dexamethasone-containing PLGA superparamagnetic microparticles as carriers for the local treatment of arthritis. *Biomaterials* 2009;**30**(9):1772−80.
71. Hughes S, Dobson J, El Haj AJ. Magnetic targeting of mechanosensors in bone cells for tissue engineering applications. *J Biomech* 2007;**40**(Suppl. 1).
72. Dobson J. Remote control of cellular behaviour with magnetic nanoparticles. *Nat Nanotechnol* 2008;**3**(3):139−43.
73. Shi P, Ng WF, Wong MH, Cheng FT. Improvement of corrosion resistance of pure magnesium in Hanks' solution by microarc oxidation with sol−gel TiO_2 sealing. *J Alloys Compd* 2009;**469**(1−2):286−92.
74. Yang JX, Jiao YP, Cui FZ, Lee IS, Yin QS, Zhang Y. Modification of degradation behavior of magnesium alloy by IBAD coating of calcium phosphate. *Surf Coat Technol* 2008;**202**(22−23):5733−6.
75. Shadanbaz S, Dias GJ. Calcium phosphate coatings on magnesium alloys for biomedical applications: a review. *Acta Biomater* 2012;**8**(1):20−30.

76. Carboneras M, Hernández LS, del Valle JA, García-Alonso MC, Escudero ML. Corrosion protection of different environmentally friendly coatings on powder metallurgy magnesium. *J Alloys Compd* 2010;**496**(1−2):442−8.
77. Wang J, Tang J, Zhang P, Li Y, Wang J, Lai Y, et al. Surface modification of magnesium alloys developed for bioabsorbable orthopedic implants: a general review. *J Biomed Mater Res Part B Appl Biomater* 2012;**100 B**(6):1691−701.
78. Wang H, Akid R, Gobara M. Scratch-resistant anticorrosion sol−gel coating for the protection of AZ31 magnesium alloy via a low temperature sol−gel route. *Corros Sci* 2010;**52**(8):2565−70.
79. Chen Q-Z, Li Y, Jin L-Y, Quinn JMW, Komesaroff PA. A new sol−gel process for producing Na(2)O-containing bioactive glass ceramics. *Acta Biomater* 2010;**6**(10): 4143−53.
80. Huang K, Cai S, Xu G, Ye X, Dou Y, Ren M, et al. Preparation and characterization of mesoporous 45S5 bioactive glass-ceramic coatings on magnesium alloy for corrosion protection. *J Alloys Compd* 2013;**580**:290−7.
81. Hu J, Zhang C, Cui B, Bai K, Guan S, Wang L, et al. In vitro degradation of AZ31 magnesium alloy coated with nano TiO_2 film by sol−gel method. *Appl Surf Sci* 2011; **257**(21):8772−7.
82. Song YW, Shan DY, Han EH. High corrosion resistance of electroless composite plating coatings on AZ91D magnesium alloys. *Electrochim Acta* 2008;**53**(5):2135−43.
83. Wang X, Li X, Onuma K, Ito A, Sogo Y, Kosuge K, et al. Mesoporous bioactive glass coatings on stainless steel for enhanced cell activity, cytoskeletal organization and AsMg immobilization. *J Mater Chem* 2010;**20**(31):6437.
84. Hench LL, Anderson O. Bioactive glasses. In: Hench LL, Wilson J, editors. *An introduction to bioceramics*. (Singapore): World Scientific; 1993. p. 41−62.
85. Kokubo T, Yamaguchi S. Biomimetic surface modification of metallic biomaterials. In: *Surface coating and modification of metallic biomaterials*; 2015. p. 219−46.
86. Kokubo T, Kushitani H, Sakka S, Kitsugi T, Yamamuro T. Solutions able to reproduce in vivo surface-structure changes in bioactive glass-ceramic A-W3. *J Biomed Mater Res* 1990;**24**(6):721−34.
87. Ohtsuki C, Aoki Y, Kokubo T, Bando Y, Neo M, Nakamura T. Transmission electron microscopic observation of glass-ceramic A-W and apatite layer formed on its surface in a simulated body fluid. *J Ceram Soc Jpn* 1995;**103**(1197):449−54.
88. Kokubo T, Ito S, Huang ZT, Hayashi T, Sakka S, Kitsugi T, et al. Ca,P-rich layer formed on high-strength bioactive glass-ceramic A-W. *J Biomed Mater Res* 1990;**24**(3):331−43.
89. Ohtsuki C, Kokubo T, Yamamuro T. Mechanism of apatite formation on $CaOSiO_2P_2O_5$ glasses in a simulated body fluid. *J Non-Cryst Solids* 1992;**143**:84−92.
90. Sawhney AS, Pathak CP, van Rensburg JJ, Dunn RC, Hubbell JA. Optimization of photopolymerized bioerodible hydrogel properties for adhesion prevention. *J Biomed Mater Res* 1994;**28**(7):831−8.
91. Kokubo T, Takadama H. How useful is SBF in predicting in vivo bone bioactivity? *Biomaterials* 2006;**27**(15):2907−15.
92. Kim H-M, Himeno T, Kawashita M, Lee J-H, Kokubo T, Nakamura T. Surface potential change in bioactive titanium metal during the process of apatite formation in simulated body fluid. *J Biomed Mater Res A* 2003;**67**(4):1305−9.
93. Sepahvandi A, Moztarzadeh F, Mozafari M, Ghaffari M, Raee N. Photoluminescence in the characterization and early detection of biomimetic bone-like apatite formation on the surface of alkaline-treated titanium implant: state of the art. *Colloids Surf B Biointerfaces* 2011;**86**(2):390−6.

94. Mozafari M, Moztarzadeh F. Controllable synthesis, characterization and optical properties of colloidal PbS/gelatin core-shell nanocrystals. *J Colloid Interface Sci* 2010; **351**(2):442−8.
95. Mozafari M, Moztarzadeh F, Tahriri M. Green synthesis and characterisation of spherical PbS luminescent micro- and nanoparticles via wet chemical technique. *Adv Appl Ceram* 2011;**110**(1):30−4.
96. Corni I, Ryan MP, Boccaccini AR. Electrophoretic deposition: from traditional ceramics to nanotechnology. *J Eur Ceram Soc* 2008;**28**(7):1353−67.
97. Ducheyne P, Van Raemdonck W, Heughebaert JC, Heughebaert M. Structural analysis of hydroxyapatite coatings on titanium. *Biomaterials* 1986;**7**(2):97−103.
98. Wei M, Ruys AJ, Swain MV, Kim SH, Milthorpe BK, Sorrell CC. Interfacial bond strength of electrophoretically deposited hydroxyapatite coatings on metals. *J Mater Sci Mater Med* 1999;**10**(7):401−9.
99. Hamagami J, Ato Y, Kanamura K. Fabrication of highly ordered macroporous apatite coating onto titanium by electrophoretic deposition method. *Solid State Ionics* 2004; **172**(1−4):331−4.
100. Zhitomirsky I, Gal-Or L. Formation of hollow fibers by electrophoretic deposition. *Mater Lett* 1999;**38**(1):10−7.
101. Ma J, Wang C, Peng KW. Electrophoretic deposition of porous hydroxyapatite scaffold. *Biomaterials* 2003;**24**(20):3505−10.
102. Harris PJF. *Carbon nanotubes and related structures: new materials for the 21st century*. New York: Cambridge University Press; 1999.
103. de Heer WA. Nanotubes and the pursuit of applications. *MRS Bull* 2004;**29**(04):281−5.
104. Sinha N, Yeow JTW. Carbon nanotubes for biomedical applications. *IEEE Trans Nanobioscience* 2005;**4**(2):180−95.
105. Boccaccini AR, Chicatun F, Cho J, Bretcanu O, Roether JA, Novak S, et al. Carbon nanotube coatings on bioglass-based tissue engineering scaffolds. *Adv Funct Mater* 2007;**17**(15):2815−22.
106. MacDonald RA, Laurenzi BF, Viswanathan G, Ajayan PM, Stegemann JP. Collagen-carbon nanotube composite materials as scaffolds in tissue engineering. *J Biomed Mater Res Part A* 2005;**74**(3):489−96.
107. Boccaccini AR, Zhitomirsky I. Application of electrophoretic and electrolytic deposition techniques in ceramics processing − Part 2. *InterCeram Int Ceram Rev* 2005;**54**(4): 242−6.
108. Boccaccini AR, Cho J, Roether JA, Thomas BJC, Jane Minay E, Shaffer MSP. Electrophoretic deposition of carbon nanotubes. *Carbon* 2006;**44**(15):3149−60.
109. Du C, Yeh J, Pan N. Carbon nanotube thin films with ordered structures. *J Mater Chem* 2005;**15**(5):548.
110. Thomas BJC, Boccaccini AR, Shaffer MSP. Multi-walled carbon nanotube coatings using electrophoretic deposition (EPD). *J Am Ceram Soc* 2005;**88**(4):980−2.
111. Boccaccini AR, Cho J, Subhani T, Kaya C, Kaya F. Electrophoretic deposition of carbon nanotube-ceramic nanocomposites. *J Eur Ceram Soc* 2010;**30**(5):1115−29.
112. Roy RK, Lee K-R. Biomedical applications of diamond-like carbon coatings: a review. *J Biomed Mater Res B Appl Biomater* 2007;**83**(1):72−84.
113. Bendavid A, Martin PJ, Comte C, Preston EW, Haq AJ, Magdon Ismail FS, et al. The mechanical and biocompatibility properties of DLC-Si films prepared by pulsed DC plasma activated chemical vapor deposition. *Diam Relat Mater* 2007;**16**(8):1616−22.

114. Elkasabi Y, Yoshida M, Nandivada H, Chen HY, Lahann J. Towards multipotent coatings: chemical vapor deposition and biofunctionalization of carbonyl-substituted copolymers. *Macromol Rapid Commun* 2008;**29**(11):855−70.
115. Lee NH, Frank CW. Surface-initiated vapor polymerization of various α-amino acids. *Langmuir* 2003;**19**(4):1295−303.
116. Martin TP, Gleason KK. Combinatorial initiated CVD for polymeric thin films. *Chem Vap Depos* 2006;**12**(11):685−91.
117. Rajesh P, Muraleedharan CV, Komath M, Varma H. Pulsed laser deposition of hydroxyapatite on titanium substrate with titania interlayer. *J Mater Sci Mater Med* 2011; **22**(3):497−505.
118. Wang CK, Chern Lin JH, Ju CP, Ong HC, Chang RPH. Structural characterization of pulsed laser-deposited hydroxyapatite film on titanium substrate. *Biomaterials* 1997; **18**(20):1331−8.
119. Hontsu S, Hashimoto Y, Yoshikawa Y, Kusunoki M, Nishikawa H, Ametani A. Fabrication of hydroxyl apatite coating titanium web scaffold using pulsed laser deposition method. *J Hard Tissue Biol* 2012;**21**(2):181−8.
120. Wang D, Chen C, Liu X, Lei T. Effects of sol−gel processing parameters on the phases and microstructures of HA films. *Colloids Surf B Biointerfaces* 2007;**57**(2):237−42.
121. Zarzycki J. Past and present of sol−gel science and technology. *J Sol−Gel Sci Technol* 1997;**8**(1−3):17−22.
122. Wang D, Bierwagen GP. Sol−gel coatings on metals for corrosion protection. *Prog Org Coat* 2009;**64**(4):327−38.
123. Messaddeq SH, Pulcinelli SH, Santilli CV, Guastaldi AC, Messaddeq Y. Microstructure and corrosion resistance of inorganic−organic (ZrO_2−PMMA) hybrid coating on stainless steel. *J Non Cryst Solids* 1999;**247**:164−70.
124. Fedrizzi L, Rodriguez F, Rossi S, Deflorian F, Di Maggio R. The use of electrochemical techniques to study the corrosion behaviour of organic coatings on steel pretreated with sol−gel zirconia films. *Electrochimica Acta* 2001;**46**(24−25):3715−24.
125. Salahinejad E, Hadianfard MJ, Macdonald DD, Mozafari M, Vashaee D, Tayebi L. A new double-layer sol−gel coating to improve the corrosion resistance of a medical-grade stainless steel in a simulated body fluid. *Mater Lett* 2013;**97**:162−5.
126. Naghib SM, Ansari M, Pedram A, Moztarzadeh F, Feizpour A, Mozafari M. Bioactivation of 304 stainless steel surface through 45S5 bioglass coating for biomedical applications. *Int J Electrochem Sci* 2012;**7**(4):2890.
127. Khalid M, Mujahid M, Khan AN, Rawat RS. Dip coating of nano hydroxyapatite on titanium alloy with plasma assisted γ-alumina buffer layer: a novel coating approach. *J Mater Sci Technol* 2013;**29**(6):557−64.
128. Kim MS, Ryu JJ, Sung YM. One-step approach for nano-crystalline hydroxyapatite coating on titanium via micro-arc oxidation. *Electrochem Commun* 2007;**9**(8):1886−91.

This page intentionally left blank

Thin film coatings for stem cell technologies

9

T. Fernandez, N. Rogers, J.D. Whittle
University of South Australia, Adelaide, SA, Australia

9.1 Introduction

Progress in the field of biomaterials design and development has been rapid in recent times, with increasingly elegant materials at the interface of synthetic and biological systems being developed. Biomaterials form a cornerstone in the tissue engineering, regenerative medicine and drug delivery systems of the future. These materials hold the potential to mimic aspects of the complex biochemical and biophysical extracellular environments of various tissues and organ systems. Currently, engineered biomaterials are able to facilitate processes surrounding tissue morphogenesis and regeneration both in vitro and in vivo.

Since the 1960s, surface modification has been used to enable cells to be cultured on normally inhospitable plastic. The marketing of plasma-treated polystyrene microplates, flasks, roller bottles and dishes has allowed cell culture to be carried out quickly and cheaply on disposable base materials, avoiding the need to culture in glass (in vitro) and reducing the possibility of cross-contamination. More recently, the challenges associated with the culture of primary and pluripotent cells and a focus on the reduction or elimination of animal-derived products in cell culture have stimulated the development of novel surface-coated cell culture products.

In this chapter, the fundamental processes contributing to successful cell culture are reviewed, and a number of different approaches to engineering novel surfaces are described. The major challenges are discussed in the context of ongoing research efforts in this field.

9.2 Thin film coatings for culture of normal cells

Among factors required for the in vitro cultivation of cells and tissues, optimal temperature, pH and osmolality, as well as a suitable growth medium and substrate for cell attachment are among the most critical. Cell culture media are composed of a mixture of nutrients including amino acids, glucose, salts and vitamins required for the survival and growth of cells. Fetal bovine serum (FBS) is a commonly used supplement in cell culture media and provides a variety of hormones, growth factors and other nutrients important for stimulating cell growth and division [1]. Also, proteins in FBS act as binding proteins for growth factors and contain extracellular matrix (ECM)

Thin Film Coatings for Biomaterials and Biomedical Applications. http://dx.doi.org/10.1016/B978-1-78242-453-6.00009-2

components such as fibronectin, which adsorb onto cell culture surfaces, thus aiding in cell attachment and spreading [2].

The term 'in vitro,' used to describe the cultivation of plant, animal and human cells under laboratory conditions, is derived from the Latin word for glass, *vitrum*. Historically, glass and polystyrene have been the most common substrates for supporting cell growth for research and clinical purposes. Among the first recorded artificial cultivation of cells, Wilhelm Roux, a German zoologist in 1885, reported the successful maintenance of cells from chicken embryos in flat glass plates. Over the past 40 years of routine laboratory eukaryotic cell culture, glass and polystyrene are among the most frequently used materials in most cell biology studies from developmental biology to the creation of novel pharmaceutical products.

Cell lines (immortalized cell populations derived from human tissues) represent the most frequently used type of cultures in the biomedical research setting. Because of their relative homogeneity and ability to be passaged multiple times while maintaining genomic stability, cell lines are among the most reproducible platforms for a wide variety of research operations. Primary cell cultures (isolated directly from human or animal donors with no genetic modifications) are more frequently being chosen by investigators to study cellular biology, because these cells are thought to generate more physiologically relevant data compared with genetically manipulated cell lines. However, these cells have a limited lifespan and are more sensitive to culture conditions such as the media type, cell culture ware used and cell plating density. Overall, cell cultures and their by-products, including immunobiologicals, anticancer agents and synthetic proteins, form a considerable part of the biotechnology market for commercial, research and clinical applications.

Rapidly emerging clinical applications for cell-based therapies and an increasing demand for reliable and reproducible high-yield cell culture systems for research drive the evolution of improved biomaterials for in vitro cell culture. Through the advancement of these materials, it was observed that interactions between cells and the interface of biomaterials form the cornerstone of the regulation of cellular behaviours. From the synthesis of biomolecules and cell division to the activation of complex intracellular networks, surface properties of a material that mirror aspects of the ECM in vivo as closely as possible significantly improve the viability and cellular physiology of resulting cultures.

9.2.1 Cell adhesion

The adhesion of cells to a substrate or surface occurs via cell adhesion molecules, or adhesins, which are proteins mostly from the integrin, selectin and cadherin families (Table 9.1). The attachment of cells to the extracellular milieu and each other is critical for maintaining the architectural integrity of tissues, and on a cellular level, for regulating and stimulating a variety of signalling networks and cellular processes. Besides providing anchorage, cell adhesion is also vital for migration, signalling polarity and differentiation status, as well as promoting growth and viability [3].

Table 9.1 Common extracellular matrix (ECM) molecules and their cell surface receptors. Cells bind to ECM molecules via specific amino acid motifs which can be used in vitro to enhance cell adhesion

ECM molecule	Amino acid sequence recognized	Cell surface receptor	Biological processes	References
Fibronectin	RGD	Integrins α5β1, α2β1	Wound healing, carcinoma development, embryogenesis	[5]
	KQAGDV	Integrin αvβ3		
	REDV	Integrin α4β1		
Vitronectin	RGD	Integrin αvβ3	Haemostasis, angiogenesis, immune defence, tissue repair	[6]
	KQAGDV			
Elastin	VGVAPG	Elastin-binding protein	Maintaining elasticity in vascular smooth muscle cells	[7]
Collagen	DGEA	Integrins α1β1, α2β1	Wound healing, tissue regeneration	[8]
	GFOGER			
Laminin	IKVAV	Integrins α6β1, α7β1	Embryonic development, tissue regeneration	[9]
Heparin	KRSR	Selectins, integrin Mac-1	Anticoagulation, osteoblast differentiation	[10]

In vitro, cells recognize and attach to artificial surfaces via a layer of adsorbed proteins. Molecules such as fibronectin, vitronectin, collagen and laminin from the cell culture media spontaneously form a film on the surface of the cell culture vessel. In turn, receptors on the cell surface recognize specific amino acid sequences present on these ECM molecules and bind to these active sites. The homogeneity and quantity of adsorbed proteins, together with the accessibility of active binding sites to the cell receptors, affect the degree of cell adhesion to a surface. These characteristics of the adsorbed protein layer are in turn influenced by the physical and chemical properties of the surface material [4]. Roughness, surface charge, hydrophilicity and chemical functionalities are all determining factors in the level of cell attachment to a surface. The adsorption of proteins occurs much faster than the migration of cells onto a foreign

surface; hence the initial adsorbed protein layer is thought to be a primary determinant of the rate of cell adhesion.

With regard to wettability, highly hydrophobic surfaces with contact angles approaching 100 degree tend to adsorb high levels of albumin [11]. Despite being able to adsorb a variety of proteins to the surface, adhesion molecules on hydrophobic surfaces often adopt orientations and conformations that are not easily accessible to integrins and other receptors. Water contact angles of about 40−70 degree have previously been reported to be optimal for cell adhesion (Fig. 9.1) [11−13]. Upon adsorption, the flexibility of cell attachment proteins to the surface heavily influences active

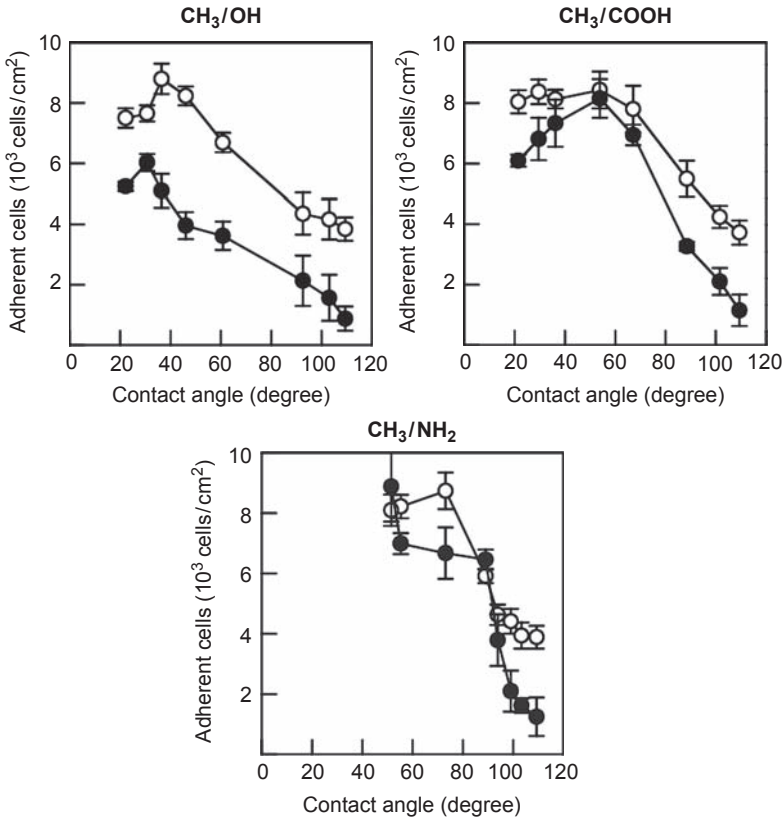

Figure 9.1 Relationship between contact angle and cell adhesion. Human umbilical vein endothelial cells (*open circles*) and HeLa cells (*closed circles*) were allowed to attach to self-assembled monolayers (SAMs) carrying methyl (CH_3), hydroxyl (OH), carboxylic acid (COOH), or amino (NH_2) terminal functional groups mixed with two kinds of alkane thiols (CH_3/OH, CH_3/COOH and CH_3/NH_2) for 1 h. A clear trend showing increasing cell adhesion with decreasing contact angle was observed for all SAMs.
Reproduced with permission from Arima Y, Iwata H. Effect of wettability and surface functional groups on protein adsorption and cell adhesion using well-defined mixed self-assembled monolayers. Biomaterials 2007;28:3074−82 (Elsevier).

spatial recognition and reorganization by cells coming into contact with a surface [14]. Conversely, however, optimal cell adhesion and spreading (depending on the cell type) also requires a sufficiently rigid adhesion substrate; overly elastic and flexible substrates are unable to facilitate adequate cell anchorage [15].

Broadly, chemical functional groups, their overall charge, roughness and the wettability of a surface have fundamental roles in determining their favourability for cell attachment, spreading and proliferation [11,16,17].

Improving surfaces by thin film coating using techniques such as nitrogen-containing plasma-grafted groups [18,19], plasma-deposited fluoropolymers [20] and polyethylene oxide-like coatings [21] have been widely studied. Generally, oxygen-containing groups such as hydroxyl, carbonyl and carboxyls are more favourable to cellular attachment and proliferation. This is in part because of ionic interactions with proteins in the cell culture media, thus forming a layer which promotes cell adherence. The growth of various cell types on plasma polymer-modified surfaces has been investigated. For instance, keratinocyte attachment was found to be enhanced in surfaces containing higher proportions of carboxylic acid groups in acrylic acid plasma-polymerized substrates [22]. Oxygen-functionalized surfaces were also found to promote attachment on osteoblast cells [23]. The density of deposited carbonyl groups has been shown to strongly influence the growth of aortic endothelial cells [24].

Laser-assisted patterning of polystyrene is a technique which enables the grafting of functional groups onto surfaces using UV photons. Laser patterning using short wavelengths has been shown to enhance wettability and protein adsorption, hence improving the biocompatibility of polystyrene for cell culture [25].

The roughness and topography of a surface are also known to contribute to variations in cell attachment and physiology. Titanium, for instance, used widely for dental and orthopaedic purposes, has been found to elicit different cellular responses based on its surface roughness, which ultimately contribute to the tissue properties of cells cultured on the titanium surface [26,27]. Besides the initial cell attachment, surface roughness has been reported to affect collagen synthesis [28] as well as the secretion of prostaglandin E_2 and transforming growth factor β [29]. Interestingly, electrical stimulation has also been demonstrated to affect the degree of protein absorption, in particular fibronectin, to artificial surfaces [30]. This property was harnessed to enhance the attachment of neural cells on stimulated polymer polypyrrole (PPy), with potential uses in the treatment of peripheral nerve damage [30]. On the other hand, some studies have shown that surfaces composed of chemicals such as tri(sarcosine), *N*-acetylpiperazine, permethylated sorbitol, hexamethylphosphoramide and phosphoryl choline, known to resist protein adsorption, have no correlation to the degree of cell attachment [31].

Alterations to the physicochemical characteristics of a material's surface can have a significant impact on the resultant biology of cells seeded upon it. As discussed previously, one of the main underlying principles of this phenomenon can be attributed to differences in the adsorption of proteins onto a surface, namely cell adhesion-mediating molecules, which are strongly influenced by the polarity, charge, wettability and topography of a particular surface [4]. Thus, surface modification techniques are employed to optimize the properties of the interface between a material and

cells while leaving the base substrate material properties unchanged. The most commonly used ways to enhance a surface for the cultivation of cells involve plasma treatment, plasma polymerization and irradiation with UV light or ions. This step can be followed by adding bioactive molecules such as oligopeptides or amino acids, which are functionalized onto the modified surface to promote specific cellular responses.

Plasma, or a state of ionized gas, was described by Irving Langmuir in 1928 in his experiments using electrified gases in vacuum tubes. Under laboratory conditions, plasma is most often generated using an electrical discharge. Treatment of a material under plasma conditions can induce changes in the elemental composition of the surface, such that properties such as hydrophilicity and bioactivity can be modified. For example, the treatment of polystyrene (the most commonly used material for routine cell culture vessels) using oxygen plasmas introduces hydroxyl functionalities to the surface, hence improving wettability and cell colonization. This technique is becoming an increasingly popular method to improve and develop materials both for cell culture and a variety of other biomedical engineering applications.

The process of plasma polymerization, defined as the formation of polymeric materials under the influence of plasma, involves the relatively uniform deposition of organic compounds onto a surface [32]. The advantages of plasma polymerization as a technique to modify the surface of materials via the deposition of these pinhole-free thin films have been recognized, resulting in the rapid advancement of plasma technology and processes [33]. These include its widespread application in the biomedical and water purification sectors, as well as in the creation of protective and conductive coatings and membranes [34]. The surface chemistry of resultant plasma polymers can be altered by parameters including the flow rate of the monomer, temperature, power, frequency and the type of plasma reactor used [35,36]. For the purpose of manufacturing materials for biomedical research and clinical applications, there are advantages of plasma polymerization to modify surface properties:

1. The bulk properties of the substrate are unaffected. Thus, only the uppermost surface layer can be modified independent of the physical or chemical properties of the underlying materials, which include metals, ceramics and polymers.
2. By changing specific plasma reaction parameters, functional groups can be introduced onto a surface.
3. Plasma polymerization deposits a relatively uniform, cross-linked and pinhole-free film over the substrate. These can be monitored for reproducibility using plasma diagnostic devices.
4. The reaction involves a simple, dry, relatively economical, one-step procedure.
5. Plasma processing can sterilize surfaces and can be scaled up for a variety of industrial production applications relatively more easily.
6. Masking techniques for surface patterning (described in later sections) can be achieved using plasma polymerization techniques [37].

9.2.2 Amine-functionalized surfaces for cell culture

Ammonia plasma discharges and amine-containing organic monomers have been employed to introduce amine functional groups onto surfaces, thus creating favourable

surfaces for biomedical applications. The generation of amine-functionalized surfaces, together with the immobilization of the glycosaminoglycan heparin, has been performed to create in vitro environments for the culture of osteoblasts [38,39], endothelial cells [40] and neurons [41,42]. Unsaturated monomers such as allylamine are preferred over saturated propargylamine to generate amine-functionalized surfaces, owing to the relatively lower energy levels required to perform the polymerization reaction and the higher retention of primary amines in the polymer [43].

These amine-functionalized surfaces are thought to enhance the attachment and viability of cells by increasing the hydrophilicity and adsorption of proteins, such as fibrinogen [44]. Using allylamine as a monomer, the resultant plasma films on poly(ethylene terephthalate) (PET) were shown to enhance fibrinogen adsorption significantly, thus activating integrin receptor-extracellular adhesion protein systems [45]. Increasing the nitrogen content of surfaces has also been shown to correlate positively with the attachment of endothelial cells and fibroblasts, indicating that the introduction of amide groups promotes cell attachment to a surface [19]. Besides fibrinogen, other bioactive proteins such as bone morphogenetic protein-4 (BMP4) have been successfully immobilized onto allylamine plasma-polymerized surfaces [46].

9.2.3 Acid-functionalized surfaces for cell culture

Optimization of the surface chemistry of biomaterials for cell culture also heavily depends on the cell type. In vitro investigations have revealed that certain cell types show improved attachment and growth rate with an increasing negative surface charge composed of acid groups. A good example of this is the elevated Schwann cell adhesion observed on poly-L-lactide microfibres with plasma-polymerized acrylic acid film deposited onto the fibre surfaces [47]. Low concentrations of carboxylic acid groups introduced onto surfaces via plasma polymerization were also shown to improve human keratinocyte attachment significantly onto surfaces [22,23,48]. These surfaces represent a considerable improvement to the current reference standard of keratinocyte cell cultures, which owing to their complex biology normally require a feeder cell layer of irradiated mouse fibroblasts to support their growth in vitro [49]. Indeed, the potential to isolate and expand autologous keratinocyte populations from patients for skin grafting applications without the use xenogenic factors in the culture conditions is highly advantageous for minimizing inherent risks [50].

Oxygen-functionalized surfaces have also been successful in improving the attachment of osteoblast-like cells [23,51]. Besides improved attachment and proliferation rates, increasing the surface energy of ultrahigh molecular weight polyethylene improved in vitro mineralization and matrix deposition in these cells (Fig. 9.2) [51]. Grafting to incorporate acrylic acid onto PET films has also been used to immobilize collagen for the culture of bladder smooth muscle cells [52,53]. The culture of urothelial and smooth muscle cells for engineering bladder tissue has been a challenging exercise owing to the requirement of serum-containing media factors and issues relating to appropriate substrate biomaterials for successful transplantation [54,55]. Hence, in the future the incorporation of acid-functionalized surface groups onto

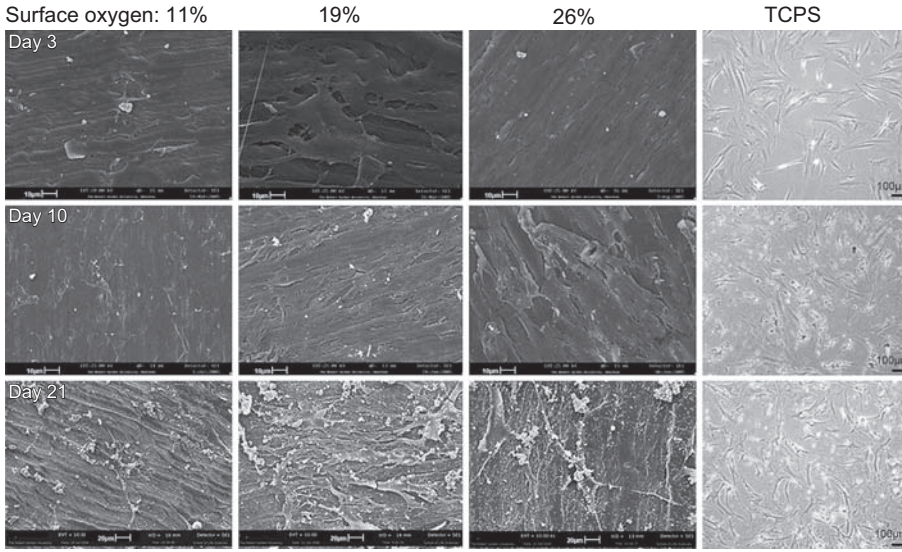

Figure 9.2 Oxygen-functionalized surfaces improve the attachment and culture of osteoblast-like cells in vitro. Scanning electron microscopy showing human primary osteoblast-like cells (isolated from femoral heads) cultured on ultrahigh molecular weight polyethylene (UHMWP) surfaces with increasing surface oxygen concentration and tissue culture polystyrene (TCPS). UV/ozone-treated UHMWP samples showed elevated cell densities of osteoblast-like cells and cell morphologies which paralleled those observed in vivo. Individual scale bars are shown on the SEM images of 10 and 20 μm, and for the optical microscope images (TCPS) the scale bar indicates 100 μm.
Reprinted with permission from Poulsson AH, Mitchell SA, Davidson MR, Johnstone AJ, Emmison N, Bradley RH. Attachment of human primary osteoblast cells to modified polyethylene surfaces. Langmuir 2009;25:3718−27 (American Chemical Society).

improved biomaterials may aid in the growth of these cells for downstream bladder reconstruction.

The type and distribution of oxygen-containing functional groups which contribute to protein adsorption (and subsequent cellular attachment) on the hydrated surface have yet to be categorically defined. Hydroxyl groups (at an optimal concentration of 2000 OH groups per 1×10^{-11} cm^2) have been reported to promote cell attachment onto surfaces, whereas high surface densities of hydroxyl and carboxyl groups inhibit cellular adhesion [56]. More recent work demonstrates that integrin binding and the formation of cellular focal adhesions follow the pattern $OH > NH_2 > COOH > CH_3$ in terms of surface functional groups [57,58].

9.2.4 RGD−ligand surface integration

The integration of specific structural motifs, in particular RGD (R = arginine; G = glycine; D = aspartic acid) cell adhesion ligands, is yet another technique for modifying biomaterials to enhance cellular compatibility [59]. Massia and Hubbell described the covalent linking of the αvβ3 integrin adhesion ligand RGD onto normally poorly cell-adhesive glass substrates which improved the attachment of

human fibroblasts [60]. It was observed that the spacing distance between ligands strongly correlated with the degree of fibroblast attachment; a 400-nm interligand spacing improved adhesive properties [60]. This, in turn, led to other studies into the conjugation of RGD ligands onto two-dimensional (2D) surfaces to enhance their functionality for cell culture. Cellular responses such as attachment and migration are specific to the surface densities and binding affinities to these ligands [61]. Moreover, the activation of specific intracellular signalling pathways is influenced by the spatial distribution of RGD ligands as well as the colocalization of synergistic ligands [62]. A spacing of 4 nm between RGD and the synergy site Pro-His-Ser-Arg-Asn, for example, has been shown to enhance metabolic activity and alkaline phosphatase production in osteoblasts while diminishing ECM production [63].

The dynamics of cell spreading, migration and adhesion, which are closely linked cellular processes, have been studied in the context of RGD nanopatterning [64]. Ligand functionalization and spacing are important parameters in designing nanopatterned surfaces, which together influence the expression of focal adhesion and stress fibres, particularly in fibroblasts (Fig. 9.3) [64,65]. Stable linking of RGD ligands to

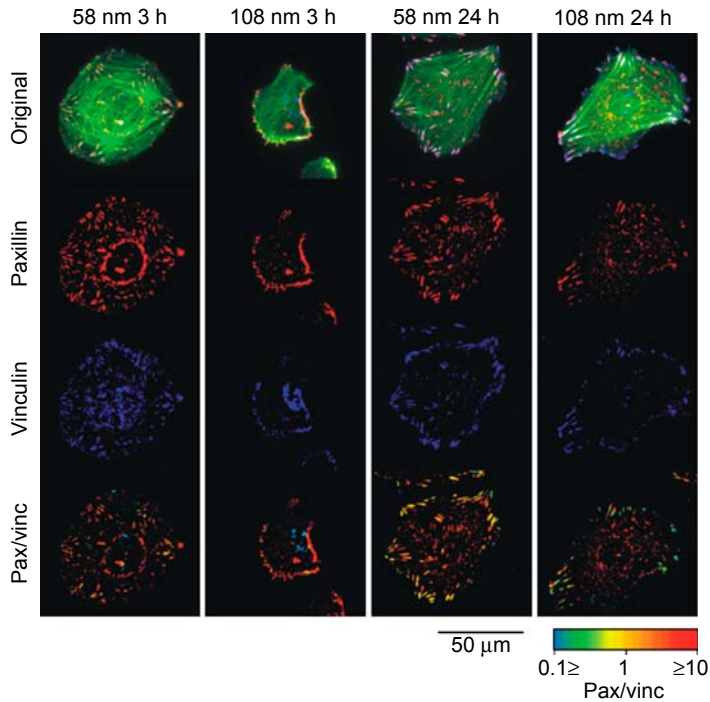

Figure 9.3 Distribution of focal adhesion proteins on RGD nanopatterned surfaces. Embryonic rat fibroblasts were seeded onto nanopatterned surfaces with either a 58- or 108-nm separation distance between RGD ligands. The localization of focal adhesion proteins vinculin and paxillin were visualized using immunofluorescence at 3 and 24 h post-seeding. Cells seeded on the 58-nm nanopatterned surfaces showed significantly higher degrees of cell spreading compared with those on the 108-nm surfaces. Actin filaments in the fibroblasts were stained using an immunofluorescent phalloidin stain [64].

the substrate of choice is another requirement for efficient cell attachment, such that the ligands are able to withstand contractile forces exerted by cells during the formation of focal adhesions [66]. These forces are strong enough to redistribute or internalize weakly linked integrin ligands, which can then lead to either the formation of weak fibrillar adhesions or nonattachment of cells [67,68]. Stable linking of RGD peptides to polymer substrates is often achieved via functional groups such as hydroxyl, carboxyl or amino groups, which can be introduced onto the surface via blending, copolymerization, chemical or physical treatments [69].

Such cell-recognition ligands are favoured over other techniques that rely on protein adsorption to enhance cell attachment, for numerous reasons. First, proteins such as fibronectin and vitronectin present in cell culture media are often sourced from animal serum, which is expensive and unsuitable for many clinical applications. In addition, these proteins are subject to proteolytic degradation and pH variation and need to be replenished during culture [70]. Moreover, only a proportion of adsorbed proteins on surface are in the correct conformation and stochastic orientation to facilitate cell attachment properly [71,72]. Hence, the modification of surfaces on a nanoscale via the immobilization of small immobilized peptides may be favourable over other surface modification techniques to improve biocompatibility. These peptides can be packed at relatively high densities onto surfaces and are relatively more stable and resistant to sterilization, pH changes, heat treatment and proteins compared with proteins [59]. Nevertheless, the control over ligand patterning and the colocalization of multiple motifs remain challenges in biomaterial design and synthesis and await further advancements in the field of nanoscale surface engineering.

9.2.5 Patterned surfaces and grafted bioactive molecules

Binding bioactive species onto surfaces can also be enhanced by introducing free radicals, double bonds and chemical functionalized groups through ion, plasma or UV treatment of materials [73–75]. Indeed, various amino acids, oligopeptides, enzymes and receptors have been introduced to surfaces using these techniques [76]. For example, the growth and viability of fibroblasts were found to improve after the grafting of amino acids such as glycine, alanine or leucine onto polymers pretreated under argon plasma conditions [77].

Microfabrication techniques to introduce specific patterns of cells onto surfaces have immense potential as a platform for culturing cells for research and other applications. Using methods such as photolithography, microcontact printing and microfluidic channel patterning, these micropatterns can be used to study aspects of cell surface interactions with various biomaterials [78]. Such systems have been used, for example, in the study of the correlation between cell shape and function. Hepatocyte cell shape was observed to influence growth and protein secretion [79] whereas endothelial cell spreading was shown to control cell survival and death [80]. These technologies are being used in the development of cell-based biochips for high-throughput drug screening [81].

Surface-grafted temperature sensitive polymers are another method employed to control cell adhesion [82,83]. Poly(*N*-isopropyl acrylamide) (PIPA Am) exhibits a fully expanded chain conformation at temperatures below 32°C and a collapsed, compact conformation at higher temperatures. Hence, above this temperature, the surface exhibits cell attachment properties similar to those of tissue culture polystyrene. By grafting PIPA Am onto surfaces, various cell types including hepatocytes, endothelial cells, macrophages and endothelial cells have been successfully cultured [84,85]. A major advantage of this technique is that upon lowering of the temperature below 32°C, PIPA Am-grafted surfaces rapidly hydrate and become nonadhesive to cells, thus spontaneously lifting cultured monolayers without the need for enzymatic digestion via trypsin [86]. By designing surface properties on a molecular level, emerging biomaterials with properties sensitive to pH, chemicals and light are also currently being developed, with a wide variety of applications in the field of in vitro cell and tissue cultivation [87].

9.2.6 Self-assembled monolayers for cell culture

SAMs of organosilanes are another method for tailoring surface properties on a molecular scale to study interactions at the cell surface interface [88]. Long-chained alkane thiols adsorbed onto gold, for instance, allow the chemical composition of a surface to be controlled through the patterning of functional groups. This allows fundamental mechanistic studies on the process of protein adsorption and cell adhesion to be performed in vitro. The immobilization of various proteins to a surface via their covalent coupling to SAMs has been achieved, which in turn have been used to cultivate adhesion-dependant mammalian cells [89,90]. Amine, hydroxyl, carboxyl and methyl groups incorporated into SAMs, for example, can be used to tailor the hydrophilicity and roughness of a surface, hence creating a means to characterize cell attachment and spreading. This has been applied to studies such as those performed by Faucheux et al., which found that the deposition of fibronectin, spreading, attachment and growth of human fibroblasts was stronger on SAMs incorporating NH_2 and COOH functional groups [91]. Conversely, hydrophobic methyl-terminated alkane thiol SAMs on gold surfaces were unfavourable to the formation of focal adhesions and spreading by fibroblasts [92].

9.3 Thin film coatings for culture of stem cells

9.3.1 Stem cells

Stem cells are defined as a population of cells with the ability to perpetuate and develop into organ-specific tissues through the processes of self-renewal and differentiation. These cells can be of embryonic, fetal or adult (somatic) in origin and have a fundamental role from embryogenesis to the physiological turnover of tissues in adulthood. Because of their ability to replicate and create specialized progeny, they are the most versatile and important source for new cells to regenerate tissues during disease, injury or aging.

It is unsurprising, therefore, that interest in the potential and involvement of stem cells in human health and disease has been mounting over a long time. Over 130 years ago, German pathologist Cohnheim conducted a series of experiments using dyes to monitor the origin of cells involved in the wound-healing process in animals [93]. From his observations, he theorized that collagen-depositing fibroblasts within the wound site were derived from the bone marrow. From these early observations, Friedenstein and colleagues were among the first to report the culture and differentiation of multipotent bone marrow cells isolated from mice under in vitro conditions in the late 1970s [94]. In this study, cells demonstrated the ability to differentiate into a variety of cell types, including osteoblasts, chondrocytes, adipocytes and myoblasts. Since these early breakthroughs, stem cells have been regarded as the future of regenerative medicine, cell therapies and drug discovery, as well as an experimental platform for better understanding human disease and development.

9.3.2 Embryonic stem cells

Derived from the inner cell mass of approximately 3.5-day-old blastocysts, human embryonic stem cell (hESC) populations contain all of the cells required for embryonic growth and development [95]. This group of cells represents the first source of human pluripotent cells that can differentiate to generate any cell type. During the maturation phase of the embryo, hESCs rapidly lose their characteristic pluripotency as they divide and differentiate. When maintained under specific conditions in vitro, this unique property of hESCs empowers researchers with a vast array of cell biology research applications. The self-renewing nature of hESCs can be harnessed using cell culture techniques to maintain and expand pure undifferentiated hESC populations over long periods of time. Importantly, these cells are able to retain normal karyotypes through continued subculture, unlike many routinely used transformed cell lines. However, this immense potential for hESC in the study of human health and disease has been associated with controversy and heavy governmental regulation because of ethical considerations associated with the use of human embryos [96].

9.3.3 Induced pluripotent stem cells

Induced pluripotent stem cells (iPSCs) share the characteristics of embryonic stem cells but originate through the introduction of specific protein-encoding genes into somatic cells such as fibroblasts from skin [97]. Genetic reprogramming via the incorporation of *OCT4*, *SOX2*, *NANOG* and *LIN28* can be introduced into the patients' own somatic cells to form iPSCs, thus generating tissues without the risk of immune rejection [98,99].

9.3.4 Somatic stem cells

Because of the short lifespan of blood cells, it is unsurprising that bone marrow is a rich source of haematopoietic stem cells which form progenitors for erythrocytes, lymphocytes, granulocytes, platelets and monocytes. Interestingly, human mesenchymal

stem cells (hMSCs) capable of differentiating into osteoblasts [100], chondrocytes [101] and even myoblasts [102] have also been found to reside in bone marrow. The connective tissue of bones and muscles, liver, spleen and fetal blood are also known to be repositories for hMSC populations, which have the ability to form adipocytes, skin and muscle tissue, for example, as well as tendon and ligaments [103,104]. Adult or somatic stem cells have also been reported to reside in the stem cell niche of brain, skeletal muscle, skin, dental, cardiac, gut, liver, ovarian and testicular tissues. In the 1990s, multipotent stem cells were isolated from the subventricular of mice brains, with the capacity to differentiate into oligodendrocytes, neurons and astrocytes in vitro [105,106]. These cells are central to the process of neurogenesis in adult brains and are the focus of intense investigation in the development of diseases such as multiple sclerosis, Parkinson disease and stroke [107]. Constant renewal of the epithelial lining of the digestive tract is facilitated by epithelial stem cells, which through proliferation and differentiation give rise to ongoing populations of absorptive cells, goblet cells, Paneth cells and enteroendocrine cells [108].

Akin to the gastrointestinal tract, the skin requires repair and renewal throughout adult life. Accordingly, the skin contains progenitor cells which aid in the replacement of the epidermis as well as hair follicles. Deep within the hair follicle, stem cells reside in a niche known as the bulge. Besides being stimulated during the hair cycle, these stem cells provide a reservoir for proliferative cells during wound repair [109].

9.3.5 Isolation and in vitro culture of stem cells

Interest into the application of hESCs in human cell therapy began mounting upon the successful isolation and cultivation of these cells in vitro [110]. The establishment of hESC lines involves the mechanical dissociation and disaggregation of inner cell masses or blastocysts. Cells are normally cultured on a feeder layer of mitotically inactivated mouse fibroblasts on tissue culture-treated polystyrene [111]. Feeder layers of cells derived from human tissues such as fetal muscle or skin and the fallopian tubes can also maintain hESCs in an undifferentiated state. Leukaemia inhibitory factor (LIF) has been identified as one of the feeder cell-derived molecules responsible for maintaining hESCs in a pluripotent state [112]. Indeed, studies have shown that LIF supplementation can be used as an alternative to feeder cells for hESC culture [113].

Isolated via aspiration from bone marrow, hMSCs can be purified using size separation [114] or positive selection [115]. Similarly, hMSCs are cultured on a feeder layer of mouse fibroblasts, and once established can be transferred to gelatinized tissue culture surfaces [116]. After about 15−25 population doublings, stem cells cultured using these routine techniques undergo a process of replicative senescence [117]. Upon removal of specific factors that maintain the pluripotency of stem cells, differentiation into the derivatives of the embryonic germ layers (ectoderm, mesoderm and endoderm) occurs. Inducing this differentiation process in vitro involves the culture of hESCs on stromal cells [118] or ECM proteins [119] or allowing aggregates of hESCs to form 3D embryoid bodies [120].

The potential for the ex vivo creation of tissues and organs for transplantation into patients using stem cell culture has been at the forefront of stem cell research. Indeed,

stem cell-based therapies have been addressed by the Food and Drug Administration to map a framework of regulation and legislation for their use clinically [121]. However, major safety considerations exist for the use of stem cells cultured in vitro for clinical use owing to the routine methods commonly used for cell culture. These include the use of animal-derived products such as bovine serum and murine fibroblast feeder cells. Thus there is a constant risk of the transmission of diseases via viruses and prions, for example, as well as the potential for immune reactions to xenogenic antigens from these animal-derived culture components. Other limitations include the fact that long-term culture of hMSCs often results in a heterogeneous population of cells with a limited capacity for replication, karyotype instability and diminished differentiation potential [122]. Emerging research has, however, demonstrated the potential for the long-term culture and maintenance of hMSCs in xenogenic feeder cell-free conditions with minimal phenotypic and functional changes [116]. Molecules such as BMP4 have also been used as supplements in stem cell culture in the absence of fetal calf serum [123].

9.4 Challenges

Because of the limitations associated with traditional methods for stem cell cultivation, there is a need for novel technologies to facilitate large-scale, cost-effective and reproducible stem cell culture using xeno-free, defined components. Several commercially available, chemically defined culture media for stem cell culture are available [124]. These incorporate ECM components such as laminin, collagen type IV and heparan sulphate to promote adhesion and a variety of growth factors to stimulate cell growth and proliferation [125].

Coupled with the use of synthetic, scalable surfaces, defined media to support stem cell cultivation will be valuable for both cell therapies and research purposes. Chemical moieties present on the cell culture substrate determine its surface properties, such as roughness, wettability and charge, which in turn have an effect on its biological activity. Thus far, synthetic surfaces for stem cell growth have been reported to support hESC self-renewal, albeit at relatively high seeding densities [126,127]. Clonal growth from single hESCs, however, has not been achieved on synthetic substrates alone, a process which is required in the study of gene targeting in pluripotent stem cells [128]. Nonetheless, high-throughput engineering methods are being employed to uncover surface substrates most likely to support and stimulate pluripotent stem cell culture under defined conditions [129].

9.5 Understanding stem cell interactions with extracellular matrix molecules

In mapping the complex molecular regulators involved in maintaining the stem cell niche, various biomaterial approaches have been adopted to identify cellular behaviour

on specific ECM molecules. Robotic spotting is a high-throughput technique used to screen for combinations and concentrations of ECM elements required to induce specific cellular responses [130−132].

The technique of silane modification on glass substrates results in the production of defined and organized substrates with specific surface chemistries and energies [133,134]. For instance, polydimethylsiloxane-coated slides have been used to spot ECM and signalling molecules including cadherin, laminin and JAG1 [132]. Indeed, specific combinations of these ECM factors were found to enhance the differentiation of mammary progenitor cells into myoepithelial and luminal epithelial cells.

9.6 Surface treatments to enhance biocompatibility for stem cell culture

The surface of a biomaterial represents the first point of interactions between proteins and cells in in vitro and in vivo systems, and thus is critical to facilitating cellular attachment and downstream biochemical responses. Most biological responses depend heavily on high-affinity binding between cell surface receptors to ligands on surfaces. In the case of many biomaterials used in cell culture, for example, proteins from culture media rapidly adsorb onto the culture surface, thus enhancing biocompatibility. Hydrophobic and cationic surfaces tend to have higher protein adsorption rates, with most proteins bearing a net negative charge. The functionality of the protein, however, is influenced by the folding and overall structure upon adsorption to a surface. Studies on the relationship between surface chemistry and protein adsorption, along with the responses of differentiated cells cultured on these surfaces, have been described [135−137].

Synthetic peptides that contain the RGD integrin recognition sequence can mimic the ECM, facilitating cellular attachment to a surface and cellular signalling [138]. By incorporating these bioactive molecules onto synthetic surfaces, this will also allow the adsorption of other proteins such as growth factors to be degraded by endogenous proteases for cellular remodelling and thus release peptide fragments or other molecules to support cell growth [139].

The CRGDC cyclic RGD peptide has been shown to have a strong affinity to $\alpha v\beta 3$, $\alpha v\beta 5$ and $\alpha 5\beta 1$ integrins, hence enhancing attachment [140]. To study its application to hESC culture, this cyclic RGD peptide sequence was conjugated to amine-modified tissue culture plates with a bifunctional linker, which reacts with an amine on the culture substrate and thiol of the peptide [141]. These surfaces were shown to support hESC adhesion and the expression of pluripotency markers when cultured in defined cell culture media. Nanopatterning of RGD sequences is another factor that has been demonstrated to affect stem cell adhesion, proliferation and differentiation [142,143]. The density of the RGD sequence is known to regulate the efficiency of cell attachment as well as the activation of integrin receptors [144]. Not surprisingly, therefore, RGD nanopatterns on nonfouling poly(ethylene glycol) (PEG) hydrogel were shown to have a significant effect on mesenchymal stem cell (MSC) behaviour and adipogenic and osteogenic differentiation potential [142].

New technologies are emerging allowing for surface modifications of biomimetic materials which allow the immobilization of specific biological moieties while preventing nonspecific protein adsorption and cell adhesion. PEG is often used in these materials owing to its protein and cell adhesion-resistant properties [145,146]. Surface modification using ethylene oxide and propylene oxide terminated by a reactive isocyanate group (Star PEG) onto glass surfaces has been used to tailor specific regions for hMSC adhesion and proliferation [147]. This study demonstrated that by controlling the amount of immobilized-RGD sequences in the PEG network, adherent cell numbers on the substrate can be regulated.

PPy is a conductive polymer with several biomedical applications owing to its good biocompatibility and the ability of cells to attach, differentiate and proliferate on its surface [148,149]. In one study, the attachment, proliferation and differentiation of rat MSCs on PPy surfaces was shown to be comparable to those of regular tissue culture plastic surfaces [150]. The synthesis of PPy involves either electrochemical or chemical polymerization, with the admicellar polymerization technique enabling the uniform deposition of thin PPy films from a few to 100 nm thick [151]. Moreover, the attachment of cells to the PPy surface can be improved, for example, via the adsorption of fibronectin or the incorporation of Arg-Gly-Asp (RGD)-containing peptides [152]. Immobilization of the glycosaminoglycans heparin and hyaluronic acid on PPy surfaces was also shown to maintain bone marrow-derived MSC cultures and to induce differentiation successfully into mature osteoblasts [153].

Poly(dimethylsiloxane) (PDMS) has been investigated for use as a biomaterial with various applications [154]. Properties of PDMS, such as its ability to be moulded easily into submicrometer designs as well as to control surface roughness and elastic modulus, biocompatibility and stability, have made it desirable for the fabrication of biomedical devices [155]. However, a major drawback of PDMS is the high hydrophobicity of its surface, thus decreasing surface wettability and cell adherence [156]. Plasma and biosurfactant treatment as well as protein adsorption have been shown to enhance cell attachment to PDMS surfaces [157,158]. A study showed that the chemical modification of PDMS with (3-aminopropyl)triethoxy silane and gluteraldehyde, followed by the immobilization of ECM proteins such as collagen I and fibronectin greatly enhanced hMSC attachment and proliferation on PDMS [159].

Acrylates are commonly used as a biomaterial because of their capacity for control during the fabrication process, which can allow for the incorporation of bioactive components on their surface [160,161]. By taking advantage of this chemical property, biologically active peptides from the active domains of vitronectin, fibronectin, laminin and sialoprotein have been conjugated onto acrylate surfaces for stem cell culture [127]. These synthetic peptide−acrylate surfaces were observed to maintain the capacity for hESC self-renewal and differentiation while maintaining their multipotent properties. Peptide−acrylate surfaces are available commercially for hESC culture (Corning Synthemax surfaces) and have shown promising results in terms of large-scale hESC culture and their differentiation into cardiomyocytes and insulin-producing cells [127,162].

Acrylate surfaces have also been employed for microarray studies aimed at discovering optimal surface chemistries required for stem cell cultivation [129,163,164].

Using such unbiased, high-throughput approaches, 25 acrylate-based polymers were used to create 576 combinations of arrays to identify specific combinations that influenced embryonic stem cell attachment, proliferation and differentiation on a nanolitre scale [163].

The surfaces of many commercially available polymers for the manufacture of cell culture surfaces are hydrophobic. However, the bioactivity and hydrophilicity of these surfaces can be improved using methods such as glow discharge gas plasma or dielectric barrier discharges to enrich the polymeric surface with amine groups [165,166]. Protonated amine groups are more optimal owing to their localized positive charge, which can attach negatively charged biomolecules at physiological pH [167]. Theoretically, amine groups covalently couple proteins in aqueous conditions, hence immobilizing biomolecules required for the attachment and proliferation of cells [168].

Surface modification of polymers using glow discharge plasma treatment in ammonia gas is a technique used to create substrates for hMSC culture [168]. Currently, a drawback associated with the tissue engineering of cartilage tissue using hMSCs is the production of collagen type X, a chondrocyte hypertrophy marker indicating endochondral ossification [169]. In this study, hMSCs cultured on plasma-functionalized nylon-6 and polypropylene were demonstrated to show some promise in terms of generating cartilage tissue [168].

The most commonly used and widely available surface for cell culture is tissue culture polystyrene or glass. This rigid 2D plane on which cells are cultivated is vastly different from the in vivo situation in which cells reside in the ECM, surrounded by anchored molecules which direct cell physiology. Not surprisingly, therefore, various cellular processes such as the expression of receptors and transcriptional factors, migration and apoptosis have been shown to differ significantly in cells cultured on synthetic 2D surfaces [170]. Although 2D culture systems have their place as a simplified platform to study stem cell biology, ultimately a shift towards 3D culture environments will be required to recapitulate in vivo stem cell niches more closely.

The value of hESCs as potential cell therapies lies in their characteristic pluripotency, thus enabling the regeneration, in theory, of any human tissue or organ. However, this property of hESCs also creates a challenge for their large-scale, reproducible and reliable in vitro cultivation in an undifferentiated state [171]. Ultimately this is a requirement for the therapeutic application of hESCs. However, implantation of undifferentiated hESCs in vivo can lead to teratoma formation or the spontaneous differentiation into multiple disorganized tissue types [172]. Hence a delicate balance needs to be maintained to guide the differentiation of hESCs into their required lineage on demand before implantation using sophisticated culture techniques and materials [173].

9.7 Future trends

The properties of biomaterials for cell culture can be selectively modified to enhance cellular behaviour such as attachment, growth, proliferation and the activation of various intracellular signalling networks. This can be achieved by tailoring physical

and chemical properties at the cell−material interface. The deposition of ultrathin films via techniques such as plasma polymerization or by nanopatterning can be used to control the adsorption of bioactive molecules such as ECM proteins onto materials for cell culture. Upon recognition by cell surface receptors, this adsorbed protein layer directly facilitates the attachment and growth of cells on a surface. Enhancing biocompatibility of various materials allows for their application not only as biomedical devices and surgical tools but also as elegant platforms to study the biological mechanisms involved in the interactions of cells with their microenvironment. Surface modifications of biomaterials allows tissue engineers to synthesize important aspects of the ECM milieu more accurately without altering the bulk attributes of substrate materials. Moreover, these techniques can be employed in the design of cell-based assays and culture systems which minimize the requirement for animal-based by-products such as bovine serum. Conceivably, ongoing collaborations among materials scientists, cell biologists, plasma physicists, clinicians and bioengineers can create the next generation of designer biomaterials tailor-made for the rapidly increasing applications of these materials in medicine and research.

References

[1] Kerbel R, Blakeslee D. Rapid adsorption of a foetal calf serum component by mammalian cells in culture. A potential source of artifacts in studies of antisera to cell-specific antigens. Immunology 1976;31:881.
[2] Kragh-Hansen U. Molecular aspects of ligand binding to serum albumin. Pharmacol Rev 1981;33:17−53.
[3] Ruoslahti E, Pierschbacher MD. New perspectives in cell adhesion: RGD and integrins. Science 1987;238:491−7.
[4] Tang L, Wu Y, Timmons RB. Fibrinogen adsorption and host tissue responses to plasma functionalized surfaces. J Biomed Mater Res 1998;42:156−63.
[5] Couchman JR, Austria MR, Woods A. Fibronectin-cell interactions. J Invest Dermatol 1990;94:7S−14S.
[6] Preissner KT. Structure and biological role of vitronectin. Annu Rev Cell Biol 1991;7: 275−310.
[7] Duca L, Floquet N, Alix AJ, Haye B, Debelle L. Elastin as a matrikine. Crit Rev Oncol Hematol 2004;49:235−44.
[8] Leitinger B, Hohenester E. Mammalian collagen receptors. Matrix Biol 2007;26: 146−55.
[9] Belkin AM, Stepp MA. Integrins as receptors for laminins. Microsc Res Tech 2000;51: 280−301.
[10] Barzu T, Van Rijn JL, Petitou M, Molho P, Tobelem G, Caen JP. Endothelial binding sites for heparin. Specificity and role in heparin neutralization. Biochem J 1986;238: 847−54.
[11] Arima Y, Iwata H. Effect of wettability and surface functional groups on protein adsorption and cell adhesion using well-defined mixed self-assembled monolayers. Biomaterials 2007;28:3074−82.
[12] van Wachem PB, Beugeling T, Feijen J, Bantjes A, Detmers JP, van Aken WG. Interaction of cultured human endothelial cells with polymeric surfaces of different wettabilities. Biomaterials 1985;6:403−8.

[13] Lee JH, Lee JW, Khang G, Lee HB. Interaction of cells on chargeable functional group gradient surfaces. Biomaterials 1997;18:351−8.
[14] Ostuni E, Yan L, Whitesides GM. The interaction of proteins and cells with self-assembled monolayers of alkanethiolates on gold and silver. Colloids Surf B 1999; 15:3−30.
[15] Yeung T, Georges PC, Flanagan LA, Marg B, Ortiz M, Funaki M, et al. Effects of substrate stiffness on cell morphology, cytoskeletal structure, and adhesion. Cell Motil Cytoskelet 2005;60:24−34.
[16] Lampin M, Warocquier-Clérout R, Legris C, Degrange M, Sigot-Luizard M. Correlation between substratum roughness and wettability, cell adhesion, and cell migration. J Biomed Mater Res 1997;36:99−108.
[17] Kasemo B, Lausmaa J. Biomaterial and implant surfaces: a surface science approach. Int J Oral Maxillofac Implants 1988;3.
[18] Detomaso L, Gristina R, Senesi GS, d'Agostino R, Favia P. Stable plasma-deposited acrylic acid surfaces for cell culture applications. Biomaterials 2005;26:3831−41.
[19] Griesser HJ, Chatelier RC, Gengenbach TR, Johnson G, Steele JG. Growth of human cells on plasma polymers: putative role of amine and amide groups. J Biomater Sci Polym Ed 1994;5:531−54.
[20] Masurovsky EB, Bunge RP. Fluoroplastic coverslips for long-term nerve tissue culture. Stain Technol 1968;43:161−5.
[21] Ratner BD. Plasma deposition for biomedical applications: a brief review. J Biomater Sci Polym Ed 1993;4:3−11.
[22] France R, Short R, Dawson R. Attachment of human keratinocytes to plasma co-polymers of acrylic acid/octa-1,7-diene and allyl amine/octa-1,7-diene. J Mater Chem 1998;8:37−42.
[23] Daw R, Candan S, Beck AJ, Devlin AJ, Brook IM, MacNeil S, et al. Plasma copolymer surfaces of acrylic acid/1,7 octadiene: surface characterisation and the attachment of ROS 17/2.8 osteoblast-like cells. Biomaterials 1998;19:1717−25.
[24] Ertel SI, Chilkoti A, Horbetti TA, Ratner BD. Endothelial cell growth on oxygen-containing films deposited by radio-frequency plasmas: the role of surface carbonyl groups. J Biomater Sci Polym Ed 1992;3:163−83.
[25] Pfleging W, Bruns M, Welle A, Wilson S. Laser-assisted modification of polystyrene surfaces for cell culture applications. Appl Surf Sci 2007;253:9177−84.
[26] Deligianni DD, Katsala N, Ladas S, Sotiropoulou D, Amedee J, Missirlis YF. Effect of surface roughness of the titanium alloy Ti−6Al−4V on human bone marrow cell response and on protein adsorption. Biomaterials 2001;22:1241−51.
[27] Ong JL, Prince CW, Raikar GN, Lucas LC. Effect of surface topography of titanium on surface chemistry and cellular response. Implant Dent 1996;5:83−8.
[28] Martin JY, Schwartz Z, Hummert TW, Schraub DM, Simpson J, Lankford Jr J, et al. Effect of titanium surface roughness on proliferation, differentiation, and protein synthesis of human osteoblast-like cells (MG63). J Biomed Mater Res 1995;29:389−401.
[29] Lincks J, Boyan BD, Blanchard CR, Lohmann CH, Liu Y, Cochran DL, et al. Response of MG63 osteoblast-like cells to titanium and titanium alloy is dependent on surface roughness and composition. Biomaterials 1998;19:2219−32.
[30] Kotwal A, Schmidt CE. Electrical stimulation alters protein adsorption and nerve cell interactions with electrically conducting biomaterials. Biomaterials 2001;22:1055−64.
[31] Ostuni E, Chapman RG, Liang MN, Meluleni G, Pier G, Ingber DE, et al. Self-assembled monolayers that resist the adsorption of proteins and the adhesion of bacterial and mammalian cells. Langmuir 2001;17:6336−43.

[32] Yasuda H. Glow discharge polymerization. J Polym Sci Macromol Rev 1981;16: 199−293.
[33] Inagaki N, Yasuda H. Adhesion of glow discharge polymers to metals and polymers. J Appl Polym Sci 1981;26:3333−41.
[34] Akhavan B, Jarvis K, Majewski P. Hydrophobic plasma polymer coated silica particles for petroleum hydrocarbon removal. ACS Appl Mater Interfaces 2013;5:8563−71.
[35] Yasuda H, Hirotsu T. Critical evaluation of conditions of plasma polymerization. J Polym Sci Polym Chem Ed 1978;16:743−59.
[36] Yasuda H. Plasma polymerization. Academic Press; 1985.
[37] Inagaki N. Plasma surface modification and plasma polymerization. CRC Press; 1996.
[38] Kim SE, Song S-H, Yun YP, Choi B-J, Kwon IK, Bae MS, et al. The effect of immobilization of heparin and bone morphogenic protein-2 (BMP-2) to titanium surfaces on inflammation and osteoblast function. Biomaterials 2011;32:366−73.
[39] Rezania A, Healy KE. Biomimetic peptide surfaces that regulate adhesion, spreading, cytoskeletal organization, and mineralization of the matrix deposited by osteoblast-like cells. Biotechnol Prog 1999;15:19−32.
[40] Genové E, Shen C, Zhang S, Semino CE. The effect of functionalized self-assembling peptide scaffolds on human aortic endothelial cell function. Biomaterials 2005;26: 3341−51.
[41] Saneinejad S, Shoichet MS. Patterned glass surfaces direct cell adhesion and process outgrowth of primary neurons of the central nervous system. J Biomed Mater Res 1998; 42:13−9.
[42] Harsch A, Calderon J, Timmons RB, Gross GW. Pulsed plasma deposition of allylamine on polysiloxane: a stable surface for neuronal cell adhesion. J Neurosci Methods 2000;98:135−44.
[43] Fally F, Doneux C, Riga J, Verbist JJ. Quantification of the functional groups present at the surface of plasma polymers deposited from propylamine, allylamine, and propargylamine. J Appl Polym Sci 1995;56:597−614.
[44] Malmsten M, Muller D, Lassen B. Sequential adsorption of human serum albumin (HSA), immunoglobulin G (IgG), and fibrinogen (Fgn) at HMDSO plasma polymer surfaces. J Colloid Interface Sci 1997;193:88−95.
[45] Chinn J, Ratner B, Horbett T. Adsorption of baboon fibrinogen and the adhesion of platelets to a thin film polymer deposited by radio-frequency glow discharge of allylamine. Biomaterials 1992;13:322−32.
[46] Puleo DA, Kissling RA, Sheu MS. A technique to immobilize bioactive proteins, including bone morphogenetic protein-4 (BMP-4), on titanium alloy. Biomaterials 2002;23:2079−87.
[47] Murray-Dunning C, McArthur SL, Sun T, McKean R, Ryan AJ, Haycock JW. Three-dimensional alignment of Schwann cells using hydrolysable microfiber scaffolds: strategies for peripheral nerve repair. Methods Mol Biol 2011;695:155−66.
[48] Haddow D, France R, Short R, MacNeil S, Dawson R, Leggett G, et al. Comparison of proliferation and growth of human keratinocytes on plasma copolymers of acrylic acid/1,7-octadiene and self-assembled monolayers. J Biomed Mater Res 1999;47: 379−87.
[49] Rheinwatd JG, Green H. Serial cultivation of strains of human epidermal keratinocytes: the formation keratinizing colonies from single cell is. Cell 1975;6:331−43.
[50] Shipley GD, Pittelkow MR. Control of growth and differentiation in vitro of human keratinocytes cultured in serum-free medium. Arch Dermatol 1987;123:1541a−4a.

[51] Poulsson AH, Mitchell SA, Davidson MR, Johnstone AJ, Emmison N, Bradley RH. Attachment of human primary osteoblast cells to modified polyethylene surfaces. Langmuir 2009;25:3718−27.
[52] Bisson I, Kosinski M, Ruault S, Gupta B, Hilborn J, Wurm F, et al. Acrylic acid grafting and collagen immobilization on poly(ethylene terephthalate) surfaces for adherence and growth of human bladder smooth muscle cells. Biomaterials 2002;23:3149−58.
[53] Gupta B, Plummer C, Bisson I, Frey P, Hilborn J. Plasma-induced graft polymerization of acrylic acid onto poly(ethylene terephthalate) films: characterization and human smooth muscle cell growth on grafted films. Biomaterials 2002;23:863−71.
[54] Elbahnasy AM, Shalhav A, Hoenig DM, Figenshau R, Clayman RV. Bladder wall substitution with synthetic and non-intestinal organic materials. J Urol 1998;159: 628−37.
[55] Wilson C, Leopard J, Cheresh D, Nakamura R. Extracellular matrix and integrin composition of the normal bladder wall. World J Urol 1996;14:S30−7.
[56] Curtis A, Forrester J, Clark P. Substrate hydroxylation and cell adhesion. J Cell Sci 1986;86:9−24.
[57] Keselowsky BG, Collard DM, Garcıa AJ. Surface chemistry modulates focal adhesion composition and signaling through changes in integrin binding. Biomaterials 2004;25: 5947−54.
[58] Curran J, Pu F, Chen R, Hunt J. The use of dynamic surface chemistries to control MSC isolation and function. Biomaterials 2011;32:4753−60.
[59] Hersel U, Dahmen C, Kessler H. RGD modified polymers: biomaterials for stimulated cell adhesion and beyond. Biomaterials 2003;24:4385−415.
[60] Massia SP, Hubbell JA. An RGD spacing of 440 nm is sufficient for integrin alpha V beta 3-mediated fibroblast spreading and 140 nm for focal contact and stress fiber formation. J Cell Biol 1991;114:1089−100.
[61] Palecek SP, Loftus JC, Ginsberg MH, Lauffenburger DA, Horwitz AF. Integrin-ligand binding properties govern cell migration speed through cell-substratum adhesiveness. Nature 1997;385:537−40.
[62] Cukierman E, Pankov R, Stevens DR, Yamada KM. Taking cell-matrix adhesions to the third dimension. Science 2001;294:1708−12.
[63] Benoit DS, Anseth KS. The effect on osteoblast function of colocalized RGD and PHSRN epitopes on PEG surfaces. Biomaterials 2005;26:5209−20.
[64] Cavalcanti-Adam EA, Volberg T, Micoulet A, Kessler H, Geiger B, Spatz JP. Cell spreading and focal adhesion dynamics are regulated by spacing of integrin ligands. Biophys J 2007;92:2964−74.
[65] Pelham RJ, Wang Y-L. Cell locomotion and focal adhesions are regulated by the mechanical properties of the substrate. Biol Bull 1998:348−50.
[66] Choquet D, Felsenfeld DP, Sheetz MP. Extracellular matrix rigidity causes strengthening of integrin−cytoskeleton linkages. Cell 1997;88:39−48.
[67] Grinnell F. Focal adhesion sites and the removal of substratum-bound fibronectin. J Cell Biol 1986;103:2697−706.
[68] Memmo LM, McKeown-Longo P. The alphavbeta5 integrin functions as an endocytic receptor for vitronectin. J Cell Sci 1998;111:425−33.
[69] Neff JA, Tresco P, Caldwell K. Surface modification for controlled studies of cell−ligand interactions. Biomaterials 1999;20:2377−93.
[70] Ito Y, Kajihara M, Imanishi Y. Materials for enhancing cell adhesion by immobilization of cell-adhesive peptide. J Biomed Mater Res 1991;25:1325−37.

[71] Elbert DL, Hubbell JA. Conjugate addition reactions combined with free-radical cross-linking for the design of materials for tissue engineering. Biomacromolecules 2001;2:430−41.

[72] Lhoest JB, Detrait E, Van Den Bosch De Aguilar P, Bertrand P. Fibronectin adsorption, conformation, and orientation on polystyrene substrates studied by radiolabeling, XPS, and ToF SIMS. J Biomed Mater Res 1998;41:95−103.

[73] Heitz J, Švorčík V, Bačáková L, Ročková K, Ratajova E, Gumpenberger T, et al. Cell adhesion on polytetrafluoroethylene modified by UV-irradiation in an ammonia atmosphere. J Biomed Mater Res A 2003;67:130−7.

[74] Bačáková L, Walachová K, Švorčík V, Hnatowicz V. Adhesion and proliferation of rat vascular smooth muscle cells (VSMC) on polyethylene implanted with O^+ and C^+ ions. J Biomater Sci Polym Ed 2001;12:817−34.

[75] Bačáková L, Mareš V, Grazia Bottone M, Pellicciari C, Lisá V, Švorčík V. Fluorine ion-implanted polystyrene improves growth and viability of vascular smooth muscle cells in culture. J Biomed Mater Res 2000;49:369−79.

[76] Marchand-Brynaert J, Detrait E, Noiset O, Boxus T, Schneider Y-J, Remacle C. Biological evaluation of RGD peptidomimetics, designed for the covalent derivatization of cell culture substrata, as potential promotors of cellular adhesion. Biomaterials 1999; 20:1773−82.

[77] Švorčık V, Ročková K, Ratajova E, Heitz J, Huber N, Bäuerle D, et al. Cell proliferation on UV-excimer lamp modified and grafted polytetrafluoroethylene. Nucl Instrum Methods Phys Res Sect B 2004;217:307−13.

[78] Kleinfeld D, Kahler KH, Hockberger PE. Controlled outgrowth of dissociated neurons on patterned substrates. J Neurosci 1988;8:4098−120.

[79] Singhvi R, Kumar A, Lopez GP, Stephanopoulos GN, Wang D, Whitesides GM, et al. Engineering cell shape and function. Science 1994;264:696−8.

[80] Chen CS, Mrksich M, Huang S, Whitesides GM, Ingber DE. Geometric control of cell life and death. Science 1997;276:1425−8.

[81] Mitchell P. Microfluidics−downsizing large-scale biology. Nat Biotechnol 2001;19: 717−21.

[82] Okano T, Yamada N, Sakai H, Sakurai Y. A novel recovery system for cultured cells using plasma-treated polystyrene dishes grafted with poly(*N*-isopropylacrylamide). J Biomed Mater Res 1993;27:1243−51.

[83] Yamato M, Konno C, Utsumi M, Kikuchi A, Okano T. Thermally responsive polymer-grafted surfaces facilitate patterned cell seeding and co-culture. Biomaterials 2002;23:561−7.

[84] Shimizu T, Yamato M, Kikuchi A, Okano T. Two-dimensional manipulation of cardiac myocyte sheets utilizing temperature-responsive culture dishes augments the pulsatile amplitude. Tissue Eng 2001;7:141−51.

[85] Ebara M, Yamato M, Aoyagi T, Kikuchi A, Sakai K, Okano T. Temperature-responsive cell culture surfaces enable "on-off" affinity control between cell integrins and RGDS ligands. Biomacromolecules 2004;5:505−10.

[86] Uchida K, Sakai K, Ito E, Hyeong Kwon O, Kikuchi A, Yamato M, et al. Temperature-dependent modulation of blood platelet movement and morphology on poly(*N*-isopropylacrylamide)-grafted surfaces. Biomaterials 2000;21:923−9.

[87] Jeong B, Gutowska A. Lessons from nature: stimuli-responsive polymers and their biomedical applications. Trends Biotechnol 2002;20:305−11.

[88] Mrksich M, Whitesides GM. Using self-assembled monolayers to understand the interactions of man-made surfaces with proteins and cells. Annu Rev Biophys Biomol Struct 1996;25:55–78.
[89] Hong HG, Jiang M, Sligar SG, Bohn PW. Cysteine-specific surface tethering of genetically engineered cytochromes for fabrication of metalloprotein nanostructures. Langmuir 1994;10:153–8.
[90] Lopez GP, Albers MW, Schreiber SL, Carroll R, Peralta E, Whitesides GM. Convenient methods for patterning the adhesion of mammalian cells to surfaces using self-assembled monolayers of alkanethiolates on gold. J Am Chem Soc 1993;115: 5877–8.
[91] Faucheux N, Schweiss R, Lützow K, Werner C, Groth T. Self-assembled monolayers with different terminating groups as model substrates for cell adhesion studies. Biomaterials 2004;25:2721–30.
[92] McClary KB, Ugarova T, Grainger DW. Modulating fibroblast adhesion, spreading, and proliferation using self-assembled monolayer films of alkylthiolates on gold. J Biomed Mater Res 2000;50:428–39.
[93] Prockop DJ. Marrow stromal cells as stem cells for nonhematopoietic tissues. Science 1997;276:71–4.
[94] Friedenstein AJ, Gorskaja JF, Kulagina NN. Fibroblast precursors in normal and irradiated mouse hematopoietic organs. Exp Hematol 1976;4:267–74.
[95] Martin GR. Isolation of a pluripotent cell line from early mouse embryos cultured in medium conditioned by teratocarcinoma stem cells. Proc Natl Acad Sci USA 1981;78: 7634–8.
[96] de Wert G, Mummery C. Human embryonic stem cells: research, ethics and policy. Hum Reprod 2003;18:672–82.
[97] Takahashi K, Yamanaka S. Induction of pluripotent stem cells from mouse embryonic and adult fibroblast cultures by defined factors. Cell 2006;126:663–76.
[98] Yu J, Vodyanik MA, Smuga-Otto K, Antosiewicz-Bourget J, Frane JL, Tian S, et al. Induced pluripotent stem cell lines derived from human somatic cells. Science 2007; 318:1917–20.
[99] Okita K, Ichisaka T, Yamanaka S. Generation of germline-competent induced pluripotent stem cells. Nature 2007;448:313–7.
[100] Ashton BA, Abdullah F, Cave J, Williamson M, Sykes BC, Couch M, et al. Characterization of cells with high alkaline phosphatase activity derived from human bone and marrow: preliminary assessment of their osteogenicity. Bone 1985;6:313–9.
[101] Keating A, Horsfall W, Hawley RG, Toneguzzo F. Effect of different promoters on expression of genes introduced into hematopoietic and marrow stromal cells by electroporation. Exp Hematol 1990;18:99–102.
[102] LaBarge MA, Blau HM. Biological progression from adult bone marrow to mononucleate muscle stem cell to multinucleate muscle fiber in response to injury. Cell 2002; 111:589–601.
[103] Caplan AI. Mesenchymal stem cells. J Orthop Res 1991;9:641–50.
[104] in 't Anker PS, Noort WA, Scherjon SA, Kleijburg-van der Keur C, Kruisselbrink AB, van Bezooijen RL, et al. Mesenchymal stem cells in human second-trimester bone marrow, liver, lung, and spleen exhibit a similar immunophenotype but a heterogeneous multilineage differentiation potential. Haematologica 2003;88:845–52.
[105] Temple S. Division and differentiation of isolated CNS blast cells in microculture. Nature 1989;340:471–3.

[106] Reynolds BA, Weiss S. Generation of neurons and astrocytes from isolated cells of the adult mammalian central nervous system. Science 1992;255:1707−10.
[107] Paspala SA, Murthy TV, Mahaboob VS, Habeeb MA. Pluripotent stem cells − a review of the current status in neural regeneration. Neurol India 2011;59:558−65.
[108] Barker N, van de Wetering M, Clevers H. The intestinal stem cell. Genes Dev 2008;22: 1856−64.
[109] Blanpain C, Fuchs E. Epidermal stem cells of the skin. Annu Rev Cell Dev Biol 2006; 22:339−73.
[110] Thomson JA, Itskovitz-Eldor J, Shapiro SS, Waknitz MA, Swiergiel JJ, Marshall VS, et al. Embryonic stem cell lines derived from human blastocysts. Science 1998;282: 1145−7.
[111] Evans MJ, Kaufman MH. Establishment in culture of pluripotential cells from mouse embryos. Nature 1981;292:154−6.
[112] Smith AG, Heath JK, Donaldson DD, Wong GG, Moreau J, Stahl M, et al. Inhibition of pluripotential embryonic stem cell differentiation by purified polypeptides. Nature 1988;336:688−90.
[113] Williams RL, Hilton DJ, Pease S, Willson TA, Stewart CL, Gearing DP, et al. Myeloid leukaemia inhibitory factor maintains the developmental potential of embryonic stem cells. Nature 1988;336:684−7.
[114] Hung SC, Chen NJ, Hsieh SL, Li H, Ma HL, Lo WH. Isolation and characterization of size-sieved stem cells from human bone marrow. Stem Cells 2002;20:249−58.
[115] Nadri S, Soleimani M, Hosseni RH, Massumi M, Atashi A, Izadpanah R. An efficient method for isolation of murine bone marrow mesenchymal stem cells. Int J Dev Biol 2007;51:723−9.
[116] Varga N, Vereb Z, Rajnavolgyi E, Nemet K, Uher F, Sarkadi B, et al. Mesenchymal stem cell like (MSCl) cells generated from human embryonic stem cells support pluripotent cell growth. Biochem Biophys Res Commun 2011;414:474−80.
[117] Wagner W, Horn P, Castoldi M, Diehlmann A, Bork S, Saffrich R, et al. Replicative senescence of mesenchymal stem cells: a continuous and organized process. PLoS One 2008;3:e2213.
[118] Nakano T, Kodama H, Honjo T. Generation of lymphohematopoietic cells from embryonic stem cells in culture. Science 1994;265:1098−101.
[119] Nishikawa SI, Nishikawa S, Hirashima M, Matsuyoshi N, Kodama H. Progressive lineage analysis by cell sorting and culture identifies $FLK1^{+}VE\text{-}cadherin^{+}$ cells at a diverging point of endothelial and hemopoietic lineages. Development 1998;125: 1747−57.
[120] Keller GM. In vitro differentiation of embryonic stem cells. Curr Opin Cell Biol 1995;7: 862−9.
[121] Halme DG, Kessler DA. FDA regulation of stem-cell-based therapies. N Engl J Med 2006;355:1730−5.
[122] de Peppo GM, Sjovall P, Lenneras M, Strehl R, Hyllner J, Thomsen P, et al. Osteogenic potential of human mesenchymal stem cells and human embryonic stem cell-derived mesodermal progenitors: a tissue engineering perspective. Tissue Eng A 2010;16: 3413−26.
[123] Ying QL, Nichols J, Chambers I, Smith A. BMP induction of Id proteins suppresses differentiation and sustains embryonic stem cell self-renewal in collaboration with STAT3. Cell 2003;115:281−92.
[124] Chin AC, Padmanabhan J, Oh SK, Choo AB. Defined and serum-free media support undifferentiated human embryonic stem cell growth. Stem Cells Dev 2010;19:753−61.

[125] Xu C, Inokuma MS, Denham J, Golds K, Kundu P, Gold JD, et al. Feeder-free growth of undifferentiated human embryonic stem cells. Nat Biotechnol 2001;19:971−4.
[126] Braam SR, Zeinstra L, Litjens S, Ward-van Oostwaard D, van den Brink S, van Laake L, et al. Recombinant vitronectin is a functionally defined substrate that supports human embryonic stem cell self-renewal via alphavbeta5 integrin. Stem Cells 2008;26: 2257−65.
[127] Melkoumian Z, Weber JL, Weber DM, Fadeev AG, Zhou Y, Dolley-Sonneville P, et al. Synthetic peptide-acrylate surfaces for long-term self-renewal and cardiomyocyte differentiation of human embryonic stem cells. Nat Biotechnol 2010;28:606−10.
[128] Hockemeyer D, Soldner F, Beard C, Gao Q, Mitalipova M, DeKelver RC, et al. Efficient targeting of expressed and silent genes in human ESCs and iPSCs using zinc-finger nucleases. Nat Biotechnol 2009;27:851−7.
[129] Mei Y, Saha K, Bogatyrev SR, Yang J, Hook AL, Kalcioglu ZI, et al. Combinatorial development of biomaterials for clonal growth of human pluripotent stem cells. Nat Mater 2010;9:768−78.
[130] Flaim CJ, Chien S, Bhatia SN. An extracellular matrix microarray for probing cellular differentiation. Nat Methods 2005;2:119−25.
[131] Soen Y, Mori A, Palmer TD, Brown PO. Exploring the regulation of human neural precursor cell differentiation using arrays of signaling microenvironments. Mol Syst Biol 2006;2:37.
[132] LaBarge MA, Nelson CM, Villadsen R, Fridriksdottir A, Ruth JR, Stampfer MR, et al. Human mammary progenitor cell fate decisions are products of interactions with combinatorial microenvironments. Integr Biol (Camb) 2009;1:70−9.
[133] Seo JH, Shin DS, Mukundan P, Revzin A. Attachment of hydrogel microstructures and proteins to glass via thiol-terminated silanes. Colloids Surf B 2012;98:1−6.
[134] Chaki NK, Vijayamohanan K. Self-assembled monolayers as a tunable platform for biosensor applications. Biosens Bioelectron 2002;17:1−12.
[135] Keselowsky BG, Collard DM, Garcia AJ. Surface chemistry modulates fibronectin conformation and directs integrin binding and specificity to control cell adhesion. J Biomed Mater Res A 2003;66:247−59.
[136] Keselowsky BG, Garcia AJ. Quantitative methods for analysis of integrin binding and focal adhesion formation on biomaterial surfaces. Biomaterials 2005;26:413−8.
[137] Lan MA, Gersbach CA, Michael KE, Keselowsky BG, Garcia AJ. Myoblast proliferation and differentiation on fibronectin-coated self assembled monolayers presenting different surface chemistries. Biomaterials 2005;26:4523−31.
[138] Ruoslahti E. The RGD story: a personal account. Matrix Biol 2003;22:459−65.
[139] Bellis SL. Advantages of RGD peptides for directing cell association with biomaterials. Biomaterials 2011;32:4205−10.
[140] Koivunen E, Wang B, Ruoslahti E. Phage libraries displaying cyclic peptides with different ring sizes: ligand specificities of the RGD-directed integrins. Biotechnol (NY) 1995;13:265−70.
[141] Kolhar P, Kotamraju VR, Hikita ST, Clegg DO, Ruoslahti E. Synthetic surfaces for human embryonic stem cell culture. J Biotechnol 2010;146:143−6.
[142] Wang X, Ye K, Li Z, Yan C, Ding J. Adhesion, proliferation, and differentiation of mesenchymal stem cells on RGD nanopatterns of varied nanospacings. Organogenesis 2013;9.
[143] Wang X, Yan C, Ye K, He Y, Li Z, Ding J. Effect of RGD nanospacing on differentiation of stem cells. Biomaterials 2013;34:2865−74.

[144] Arnold M, Cavalcanti-Adam EA, Glass R, Blummel J, Eck W, Kantlehner M, et al. Activation of integrin function by nanopatterned adhesive interfaces. Chemphyschem 2004;5:383−8.
[145] Zhao X, Harris JM. Novel degradable poly(ethylene glycol) hydrogels for controlled release of protein. J Pharm Sci 1998;87:1450−8.
[146] Roberts MJ, Harris JM. Attachment of degradable poly(ethylene glycol) to proteins has the potential to increase therapeutic efficacy. J Pharm Sci 1998;87:1440−5.
[147] Groll J, Fiedler J, Engelhard E, Ameringer T, Tugulu S, Klok HA, et al. A novel star PEG-derived surface coating for specific cell adhesion. J Biomed Mater Res A 2005;74: 607−17.
[148] Yuan W, O'Rear EA, Cho G, Funkhouser GP, Glatzhofer DT. Thin polypyrrole films formed on mica and alumina with and without surfactant present: characterization by scanning probe and optical microscopy. Thin Solid Films 2001;385.
[149] Aoki T, Tanino M, Sanui K, Ogata N, Kumakura K, Okano T, et al. Culture of mammalian cells on polypyrrole-coated ITO as a biocompatible electrode. Synth Met 1995;71.
[150] Castano H, O'Rear EA, McFetridge PS, Sikavitsas VI. Polypyrrole thin films formed by admicellar polymerization support the osteogenic differentiation of mesenchymal stem cells. Macromol Biosci 2004;4:785−94.
[151] Funkhouser GP, Arevalo MP, Glatzhofer DT, O'Rear EA. Solubilization and adsolubilization of pyrrole by sodium dodecyl sulfate: polypyrrole formation on alumina surfaces. Langmuir 1995;11:1443−7.
[152] Shastri VR, Schmidt CE, Kim T-H, Vacanti JP, Langer R. Polypyrrole − a potential candidate for stimulated nerve regeneration. MRS Online Proc Libr 1995;414.
[153] Serra Moreno J, Sabbieti MG, Agas D, Marchetti L, Panero S. Polysaccharides immobilized in polypyrrole matrices are able to induce osteogenic differentiation in mouse mesenchymal stem cells. J Tissue Eng Regen Med 2012;8.
[154] Fu J, Wang YK, Yang MT, Desai RA, Yu X, Liu Z, et al. Mechanical regulation of cell function with geometrically modulated elastomeric substrates. Nat Methods 2010;7: 733−6.
[155] Sunyer R, Jin AJ, Nossal R, Sackett DL. Fabrication of hydrogels with steep stiffness gradients for studying cell mechanical response. PLoS One 2012;7:e46107.
[156] Lee JN, Jiang X, Ryan D, Whitesides GM. Compatibility of mammalian cells on surfaces of poly(dimethylsiloxane). Langmuir 2004;20:11684−91.
[157] Pinto S, Alves P, Santos AC, Matos CM, Oliveiros B, Goncalves S, et al. Poly(dimethyl siloxane) surface modification with biosurfactants isolated from probiotic strains. J Biomed Mater Res A 2011;98:535−43.
[158] Pinto S, Alves P, Matos CM, Santos AC, Rodrigues LR, Teixeira JA, et al. Poly(dimethyl siloxane) surface modification by low pressure plasma to improve its characteristics towards biomedical applications. Colloids Surf B 2010;81:20−6.
[159] Kuddannaya S, Chuah YJ, Lee MH, Menon NV, Kang Y, Zhang Y. Surface chemical modification of poly(dimethylsiloxane) for the enhanced adhesion and proliferation of mesenchymal stem cells. ACS Appl Mater Interfaces 2013;5:9777−84.
[160] Muthukrishnan S, Nitschke M, Gramm S, Özyürek Z, Voit B, Werner C, et al. Immobilized hyperbranched glycoacrylate films as bioactive supports. Macromol Biosci 2006;6:658−66.
[161] Francesch L, Garreta E, Balcells M, Edelman ER, Borrós S. Fabrication of bioactive surfaces by plasma polymerization techniques using a novel acrylate-derived monomer. Plasma Process Polym 2005;2:605−11.

[162] Lin PY, Hung SH, Yang YC, Liao LC, Hsieh YC, Yen HJ, et al. A synthetic peptide-acrylate surface for production of insulin-producing cells from human embryonic stem cells. Stem Cells Dev 2014;23:372−9.
[163] Anderson DG, Levenberg S, Langer R. Nanoliter-scale synthesis of arrayed biomaterials and application to human embryonic stem cells. Nat Biotech 2004;22:863−6.
[164] Saha K, Mei Y, Reisterer CM, Pyzocha NK, Yang J, Muffat J, et al. Surface-engineered substrates for improved human pluripotent stem cell culture under fully defined conditions. Proc Natl Acad Sci 2011;108:18714−9.
[165] Bullett NA, Bullett DP, Truica-Marasescu F-E, Lerouge S, Mwale F, Wertheimer MR. Polymer surface micropatterning by plasma and VUV-photochemical modification for controlled cell culture. Appl Surf Sci 2004;235:395−405.
[166] Meyer-Plath AA, Schroder K, Finke B, Ohl A. Current trends in biomaterial surface functionalization − nitrogen-containing plasma assisted processes with enhanced selectivity. Vacuum 2003;71:391−406.
[167] Guimond S, Wertheimer MR. Surface degradation and hydrophobic recovery of polyolefins treated by air corona and nitrogen atmospheric pressure glow discharge. J Appl Polym Sci 2004;94:1291−303.
[168] Nelea V, Luo L, Demers CN, Antoniou J, Petit A, Lerouge S, et al. Selective inhibition of type X collagen expression in human mesenchymal stem cell differentiation on polymer substrates surface-modified by glow discharge plasma. J Biomed Mater Res A 2005;75:216−23.
[169] Mwale F, Billinghurst C, Wu W, Alini M, Webber C, Reiner A, et al. Selective assembly and remodelling of collagens II and IX associated with expression of the chondrocyte hypertrophic phenotype. Dev Dyn 2000;218:648−62.
[170] Haycock JW. 3D cell culture: a review of current approaches and techniques. Methods Mol Biol 2011;695:1−15.
[171] Li Y, Kniss DA, Lasky LC, Yang ST. Culturing and differentiation of murine embryonic stem cells in a three-dimensional fibrous matrix. Cytotechnology 2003;41:23−35.
[172] Mitjavila-Garcia MT, Simonin C, Peschanski M. Embryonic stem cells: meeting the needs for cell therapy. Adv Drug Deliv Rev 2005;57:1935−43.
[173] Dawson E, Mapili G, Erickson K, Taqvi S, Roy K. Biomaterials for stem cell differentiation. Adv Drug Deliv Rev 2008;60:215−28.

This page intentionally left blank

Uniform, adhesive, and low cytotoxic films accelerating bacterial reduction in the dark and under visible light

10

S. Rtimi, C. Pulgarin, J. Kiwi
Ecole Polytechnique Fédérale de Lausanne, EPFL-SB-ISIC-GPAO, Lausanne, Switzerland

10.1 Introduction

As a result of hospital infections caused by the increased resistance of bacterial strands to antibiotics inducing infections for which they are not effective, such as methicillin-resistant *Staphylococcus aureus* (MRSA), *Pseudomonas aeruginosa*, and certain strands of *Escherichia coli*, there is a need to develop new robust antibacterial films.[1–9] These films should reduce or abate pathogenic bacteria resistant to synthetic antibiotics when administered for a long time. The films should have fast bacterial reduction kinetics, be uniform, adhese to the support, and have low cytotoxicity. That is the focus of this study addressing silver (Ag)-nitride/oxynitride bacterial inactivation films. Nitrides/oxynitrides have been shown to be resistant composites and have no or extremely low cytotoxic activity.

Silver has been used as antibacterial on cotton and artificial fibers such as polyester, polyamide, and wound pads, thin polymer films such as polyethylene. Silver biocide surfaces are the strongest growth segment in medical and health-care applications. The silver ion-release kinetics[10,11] over extended operational times and low cytotoxicity (biocompatibility) determine its effective use when deposited onto antibacterial surfaces.[12–15] The nanoparticles of Ag exhibit bacterial and fungicidal properties. They can accumulate on the cell wall of bacteria and release Ag ions that penetrate into cells through the wall porins owing to their small size.[16,17]

Solgel commercial methods are used to prepare TiO_2 and Ag thin films on heat-resistant substrates. However, the thickness of these solgel-deposited films is not reproducible, they are not mechanically stable, and they have low adhesion because they can be wiped off by a cloth or thumb.[18] Colloid deposition on substrates requires temperatures of a few hundred degrees centigrade for adequate adherence to the selected substrate, which will not work on low thermal-resistant substrates such as the polyester used in this study. Photo-switching processes by finely divided dispersed Ag 2 nm in size have been reported relating the hydrophobic Ag initial surface kinetics when the surfaces changed to superhydrophilic under light concomitant to *E. coli* and *S. aureus* inactivation. In this way, the contact angle (CA) and surface energy were followed during the light-induced and dark reversible process after bacterial disinfection.[19]

Thin Film Coatings for Biomaterials and Biomedical Applications. http://dx.doi.org/10.1016/B978-1-78242-453-6.00010-9

To cover heat-resistant surfaces with uniform thin films, chemical vapor deposition (CVD) has been used, in which materials are heated in vacuum until they decompose. The released atoms or species condense on the substrate whose surface has a lower temperature mainly on heat-resistant materials. The disadvantages of CVD deposition are high investment costs, the high temperatures needed precluding film deposition on textiles such as polyester, and the amount of heat used that require costly cooling systems. Silver films from 6 to 50 nm have been reported to lead to bacterial inactivation under ultraviolet (UV)/visible light irradiation. Using CVD, Ag films have been deposited by Page et al.,[20,21] Foster et al.,[22] Dunlop et al.,[23] and Yates et al.[24]

More recently, our laboratory has used sputtering methods to deposit thin metal or oxides (by reactive sputtering) on non-heat-resistant substrates such as textiles or polymer-like polyethylene at temperatures less than 150°C. Direct current (DC) magnetron sputtering and pulsed direct current (DCP) magnetron sputtering[25] and high-power impulse magnetron sputtering[26,27] have been used to graft Ag−metal/oxide nanoparticulate uniform adhesive films onto a variety of textile fabrics. Bacterial reduction by Ag textiles in the dark and under light has been reported.[25−27]

Antimicrobial Ag/Ag_2O sputtered films showing effective bacterial reduction on textiles have been reported as assessed by transmission electron microscopy (TEM) and X-ray electron spectroscopy (XPS).[28] The magnetron sputtering processes lead to $Ag/AgO/Ag_2O$ because traces of H_2O_v on the magnetron chamber decompose at pressures of 10^{-5}, generating O_2 in the Ar vacuum-swept cavity.

In principle, Ag hospital textiles should be able to reduce or eliminate the contamination of public hospitals from *E. coli* and MRSA. The levels found for these bacteria in many United Kingdom hospitals are higher than those allowed for hospital rooms. For example, the contamination of 10^5 colony-forming units (CFU)/cm^2 was observed in a diabetic wound dressing. However, in the vicinity of the patient, a microbial density of about 10^2 CFU/cm^2 was found. The use of Ag textiles as described should be sufficient to decrease the room bacterial concentration significantly, because we do not deal with a high bacterial concentration to start with.[1−3] Sputtering Ag textiles research is warranted because it aims to reduce or eliminate Ag leaching during textile washings[29] and to keep meaningful Ag disinfection performance. The speciation of heavy metals like Ag from reaching natural waters through furtive emissions is a recurrent problem owing to increasing amounts of Ag being used in different industrial processes. This is why we have focused work on the sputtering of Ag textile surfaces,[30] which considerably reduces the leaching of Ag deposited by solgel methods on wound pads and disinfecting fabrics.[31,32] This is significant in the case of cotton and other hydrophilic textiles used in medical facilities because by the large uptake of water, they are able to provide an effective brewing medium for bacterial colonization.[33]

Silver-nitrides/oxynitrides were sputtered stepwise or concomitant with Ag in the magnetron chamber and showed resistance, adhesion to the support, and uniformity of deposition. P. Kelly[34−36] reported the use of sputtered nitrides for many industrial applications. Bacterial reduction in the dark and under daylight/actinic light was reported using colored nitrides/oxynitrides.

In the current work, we focused on the following Ag-nitrides and oxynitrides: (1) Ag-TiN/TiON,[37,38] (2) Ag-ZrN/ZrON,[39,40] and (3) Ag-TaN/TaON.[41,42] Acceleration of the bacterial reduction kinetics at the solid−air interface was explored stepwise in these studies as the guiding objective of this work. The objective was to design and produce films showing fast bacterial reduction concomitant with low cytotoxicity as reported in a few cases for nitrides.[7,8,34−36] Why use nitride/oxynitride layers to bind metal/oxides to textile or polymer substrates?

As the nitride/oxynitride layer nucleates, these layers promote bonding of the sputtered metal/metal-oxide atoms on the template by coalescence without the formation of grain boundaries. In this way, the sputtered cluster size closely duplicates the support microstructure. A highly coherent film lattice with intimate bonding develops between the nitride/oxynitride and the substrate.[43,44] Nitride layers have been reported to lead to the production of smooth, adhesive, and quality films when nucleating metal/oxides.[45] In many cases, the continuous film shows epitaxial growth.[46] The large-scale epitaxy attained in some cases translates into strong adhesion of the nitrides/oxynitrides to the substrate. The critical size for the metal clusters sputtered was observed to vary in the presence or absence of a nitride sublayer compared with the case when the metal was sputtered by itself. In the latter case, the metal atoms bind to other metal atoms or clusters rather than to the substrate and to grow into a compact cluster of atoms but not necessarily to be crystallographic.[47]

We have used a high-power magnetron sputtering source to provide a high density of charges (e^-/m^3) compared with DC and DCP-sputtering.[48] Concomitantly, a higher ionization percentage was attained for the sputtered metal(s).[49] This results from the larger applied power to drive the plasma away from the target confinement extending the ionization volume.[50]

Pathogenic bacteria, fungi, and viruses are able to survive in any environment under minimal life-supporting conditions owing to their ability to form biofilms, which are microorganism aggregates adhering to each other and to the surface. Biofilms are regarded as the most common mode of bacterial growth and stabilization.[51] They are resistant to detergents, disinfectants, and antibiotics and transmit about 80% of all microbial infections, which make them a primary health concern.

Biofilms are usual vehicles to transmit hospital-acquired infections and community-acquired infections. Once they are fully matured, they spread pathogens such as bacteria and fungi to the environment from dry surfaces, where they remain active for long times. These biofilms are found in hospital walls, floors, and medical devices such as catheters, surgical equipment, oximeters, and bedding. Multiple and sequential contacts with hospital gadgets transfer bacterial infections.[52] Therefore, Ag and Ag-nitrides/oxynitride coatings should preclude the formation of bacterial biofilms. Nitrides/oxynitrides have the advantage of absorbing light in the visible spectrum (>400 nm). This is an advantage over TiO_2, which has to be doped to be fairly active, extending the absorption spectrum beyond the UVA range (320−400 nm).[23,53,54] This is an important aspect for the applications of these films because hospital indoor lighting does not emit light in the UV region, Visible light absorption by Ag-plasmons was reported by K. Vasilev[55] and S. Pillai[56]

for the effect of visible light improving bacterial-reducing performance of TiO_2 and other semiconductors, metals, and oxides.

The deposition of metals such as Ag, Au, Pt, and Pd on TiO_2 has been shown to partially preclude the e^-/h^+ recombination under daylight irradiation, increasing TiO_2 charge separation.[9] Interfacial photo-induced electron transfer by metals/oxide on the TiO_2 surface has been addressed in relation to solar light environmental applications. There is a critical need to develop photocatalytic materials driven by solar irradiation with innovative structures able to disinfect the environment with faster kinetics. Robust coatings with long operational lifetimes are needed, as suggested in this study focusing on Ag-visible light−absorbing nitrides/oxynitrides.[57]

The film community of pathogens in a biofilm at the solid−air interface has a protecting layer complicating the testing and analysis of biofilm deposits.[58,59] Attached microorganisms do not necessarily lead to biofilm formation. If food is made unavailable to these surface biofilms by cleaning or disinfection, further growth of these pathogens can be avoided.[60,61]

The methodological approach used in this study addressed (1) evaluation of the bacterial reduction kinetics, (2) cyclic operational stability of the catalytic/photocatalytic surface during the bacterial reduction process, (3) detailed surface characterization, and (4) the amount of leaching of Ag nanoparticles. This was followed by ion-coupled plasma mass spectrometry (ICP-MS) during repetitive disinfection cycles.

10.2 Results and discussion: design, magnetron sputtering, evaluation of bacterial reduction, and surface layer characterization

10.2.1 Ti-nitride Ag surfaces active in bacterial inactivation in the dark and under light (Ag-TiN)

The Ag-TiN was DC-sputtered on polyester, as shown schematically by Fig. 10.1. The sputtering details have been previously reported from our laboratory.[25−27] To avoid environmental Ag-contamination introduced into the environment by Ag-loaded bactericide surfaces, TiN were sputtered films on polyester and evaluated during the bacterial inactivation kinetics. Titanium was sputtered in the plasma chamber in an N_2 atmosphere depositing TiN films loaded on polyester fibers. These films have absorption in visible range between 330 and 800 nm as detected by Diffuse reflectance spectroscopy (DRS) and shown in Fig. 10.2. A TiN layer of 50 nm sputtered for 3 min under low intensity/actinic visible light led to inactivation of 99.99% of bacteria within 120 min.[37]

XPS measurements were carried out on an AXIS NOVA photoelectron spectrometer (Kratos Analytical, Manchester, UK). The surface atomic concentration was determined from peak areas using sensitivity factors.[62,63] Spectrum background was subtracted according to Shirley.[64] The XPS peaks of the Ti species were analyzed by spectra deconvolution software (CasaXPS-Vision 2, Kratos Analytical, UK).

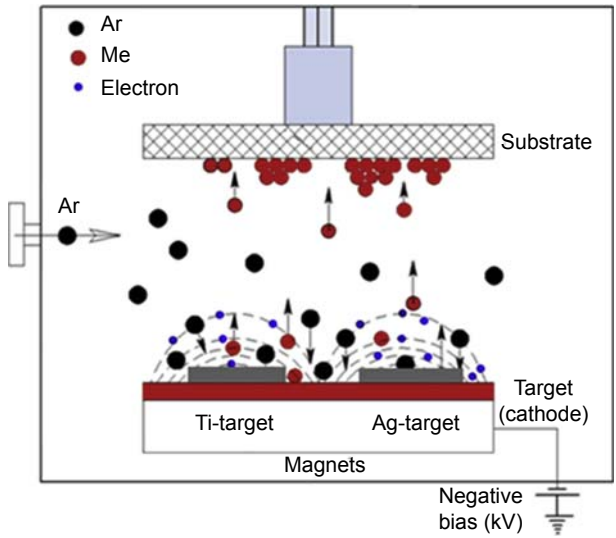

Figure 10.1 Schematic representation of the two-target direct current magnetron sputtering chamber.
Baghriche O, Sanjines R, Ruales C, Pulgarin C, Stolitchnov I, Zertal A, Kiwi J. Ag-surfaces sputtered by DC and pulsed DC-magnetron sputtering effective in bacterial inactivation: testing and characterization. *Surf Coat Technol* 2012;**206**:2410−16.

The formation of TiO_2 can be understood in terms of how the partial oxidation of TiN takes place in the presence of an oxygen source owing to the residual H_2O vapor in the sputtering chamber at the residual pressure $Pr = 10^{-4}$ Pa. This pressure is representative of about 10^{15} molecules/cm^2 of H_2O and this water monolayer is sufficient to generate O-radicals and partial oxidation of TiN film. In addition, the films oxidize after sputtering is over when exposed to air and also during the sterilization process when autoclaving at 121°C.

Fig. 10.3 presents TiO_2 ($Ti2p_{3/2}$ doublet) for polyester when sputtering TiN for 3 min. The peaks in Fig. 10.3(a) assigned to TiN and Ti_2O_3 (Ti^{3+} in the net sense) have been deconvoluted and TiN shows a peak at 455.62 eV, the Ti^{3+} doublet at 456.22 eV, and the Ti^{4+} doublet at 458.43 eV. Fig. 10.3(b) presents the XPS deconvoluted spectra for the TiN sample at the end of the bacterial inactivation process (120 min). The TiO_2 ($Ti2p_{3/2}$ doublet) BE shifted to 459.01 eV. Peak shifts of 0.2 eV or greater reflect changes in the oxidation states of Ti^{4+}/Ti^{3+} during bacterial inactivation. The shift of the Ti_2O_3/Ti^{3+} doublet to 457.13 eV at 120 min reflects an increase in the reduced Ti^{3+}-species at the end of the bacterial inactivation. The surface atomic concentration of the fastest TiN (3-min) sample at time 0 was determined by XPS as O1s 10.2%, Ti2p 44.7%, N1s 3.5%, and C1s 22.31%.

Titanium nitride-Ag films on polyester induce photocatalytic and catalytic inactivation of *E. coli*[37]; the bacterial reduction kinetics is shown in Fig. 10.4. For TiN-Ag samples, a 3 log10 bacterial reduction was attained within about 15 min, as shown

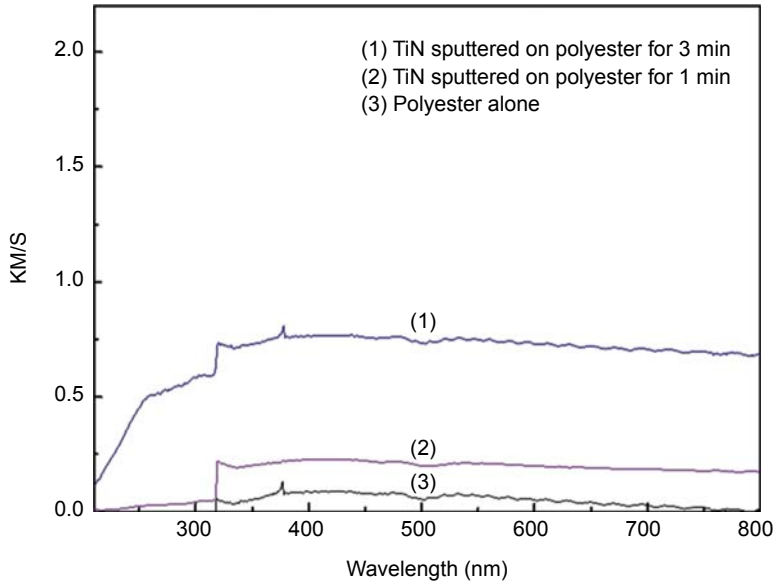

Figure 10.2 Diffuse reflectance spectroscopy of TiN-polyester for sputtering times shown in Fig. 10.10.
Rtimi S, Baghriche O, Sanjines R, Pulgarin C, Ben-Simon M, Lavanchy, J-C. et al. Photocatalysis/catalysis by TiN/TiN-Ag surfaces efficient in bacterial inactivation under visible light. *Appl Catal B* 2012;**123**−**24**:306−315.

in the inset in Fig. 10.4. The TiN and TiN-Ag thin films were sputtered onto polyester heated at less than 130°C using two confocal magnetron sputtering systems. The polyester samples were 2 × 2 cm in size. Before deposition of the films, the residual pressure P_r in the sputtering chamber was typically $P_r \leq 10^{-4}$ Pa. The substrate-to-target distance was fixed at 10 cm. The TiN thin films were deposited by reactive DC-magnetron sputtering (DC) using a 5-cm diameter Ti-target at 99.99% (Kurt J. Lesker, East Sussex, UK) in an $Ar + N_2$ atmosphere. The total working pressure $P_T = (P_{Ar} + P_{N2})$ was fixed at 0.5 Pa and the $P_{N2}/P_T = 4.5\%$.

Fig. 10.4 shows the bacterial inactivation of *E. coli* for TiN-Ag films. The deposition time of TiN under layer film was fixed at 3 min whereas the deposited amount of Ag was tuned by changing the deposition time from 10 to 30 s. A 15-min irradiation period led to a 3 $\log_{10}$ reduction (99.9%) of the initial *E. coli* concentration, as shown in the inset. Complete bacterial inactivation was observed within about 60−90 min, in agreement with work reported on nitride-induced bacterial inactivation and biocompatibility issues.[65,66] Darker gray Ag was observed on the polyester with increasing sputtering time. Dark gray corresponds to the Ag_2O-Ag° with a band gap (b_g) of 0.7−1.0 eV and an absorption edge of about 1000 nm.

Fig. 10.5 shows the release of ions from polyester samples sputtered with Ag, TiN-Ag, and TiN. For Ag-sputtered samples up to the eighth cycle, the level of Ag release was 6 and 8 parts per billion (ppb)/cm^2. In the case of TiN-Ag samples, Ag release was

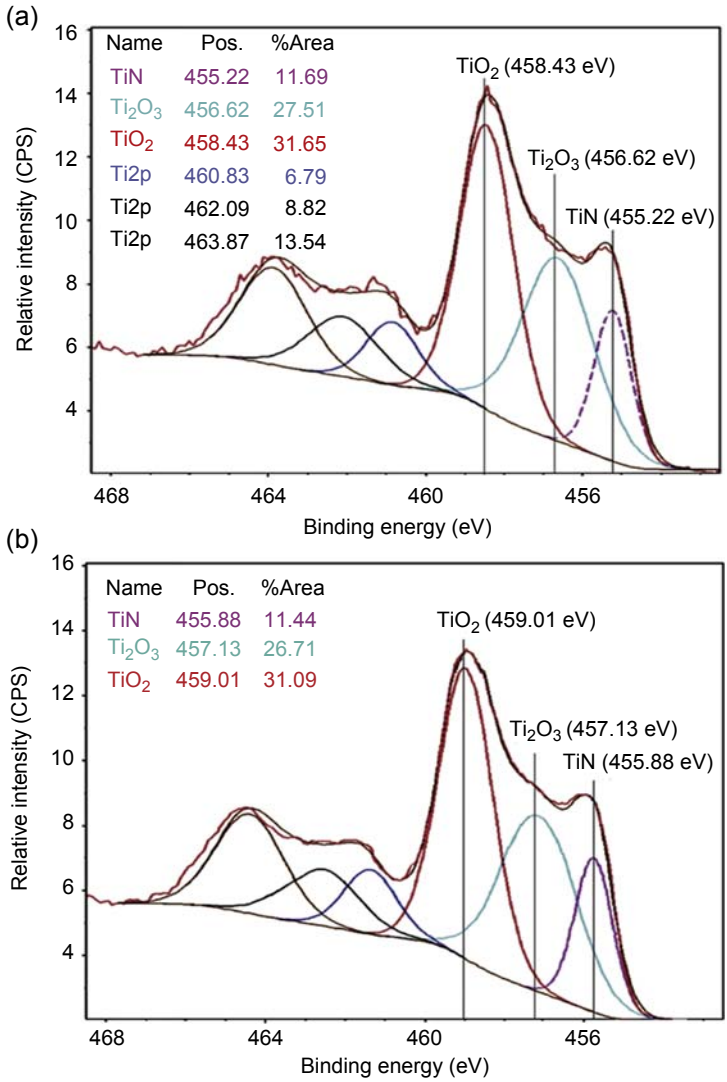

Figure 10.3 X-ray photoelectron spectroscopy of TiN (3 min) in contact with bacteria for 3 s: (a) time = 0 min and (b) time 120 min, showing the shift in deconvoluted peaks after bacterial inactivation.
Rtimi S, Baghriche O, Sanjines R, Pulgarin C, Ben-Simon M, Lavanchy, J-C. et al. Photocatalysis/catalysis by TiN/TiN-Ag surfaces efficient in bacterial inactivation under visible light. *Appl Catal B* 2012;**123−24**:306−315.

observed to decrease with the number of cycles to 5 ppb/cm^2. Ag ions on the Ag nanoparticles were formed by oxidation of Ag on the polyester in contact with reaction media. Release of Ag ions greater than 0.1 ppb has been shown to have a significant antimicrobial effect and higher Ag ions greater than 35 ppb can be toxic to human

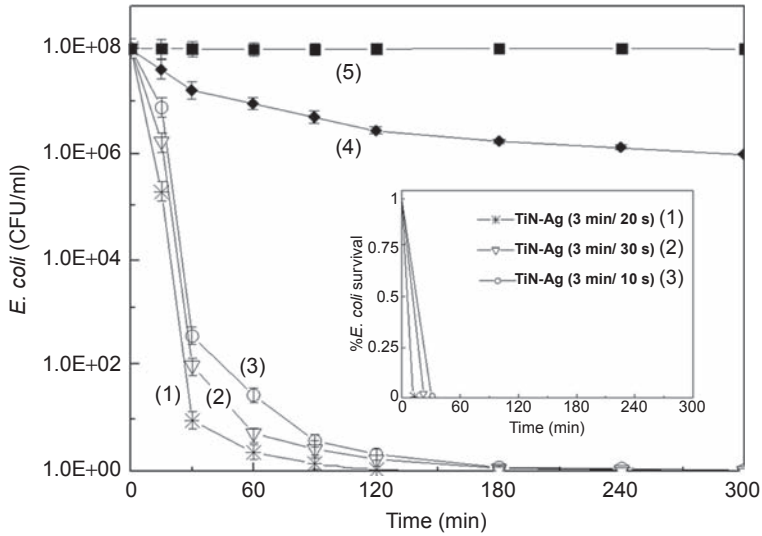

Figure 10.4 *Escherichia coli* survival on TiN-Ag polyester sputtered for different times under light irradiation. Traces (1) TiN-Ag 3 min/20 s; (2) TiN-Ag 3 min/30 s; (3) TiN-Ag 3 min/10 s; (4) TiN-Ag 3 min/20 s in dark and (5) polyester alone. Inset shows the time for bacterial reduction of 3 log10.
Rtimi S, Baghriche O, Sanjines R, Pulgarin C, Ben-Simon M, Lavanchy, J-C. et al. Photocatalysis/catalysis by TiN/TiN-Ag surfaces efficient in bacterial inactivation under visible light. *Appl Catal B* 2012;**123**−**24**:306−315.

cells.[1] The TiN-polyester samples maintained a release of about 14 ppb/cm^2 of Ti ions (Fig. 10.5). The excellent biocompatibility of TiN has been well documented in biomedical applications.[65] Bactericidal kinetics concomitant with low cytotoxicity are two essential requirements for bactericide surfaces commonly referred to as the oligodynamic effect.[1]

10.2.2 Ti-oxynitride Ag surfaces active in bacterial inactivation in the dark and under light (Ag-TiON)

Silver is a low cytotoxic bactericide agent at low concentrations.[67] However, when washing Ag-sputtered textiles, Ag leaches out of the textile surface and becomes an undesirable environmental problem.[29] Exposure data regarding Ag's furtive leaching and its possible toxicity is lacking.[68] *Escherichia coli* inactivation of TiON layers under visible light avoids environmental Ag leaching of Ag-based disinfecting materials, which moved us to explore the bactericidal properties of Ag-TiN.[37]

There has been interest in preparing TiON films with intermediate behavior between metallic TiN and insulating TiO_2. These films are used as interconnectors in the electrical industry.[24] Nitrides are currently being explored for biomedical applications such as implants owing to their biocompatibility and long-term corrosion

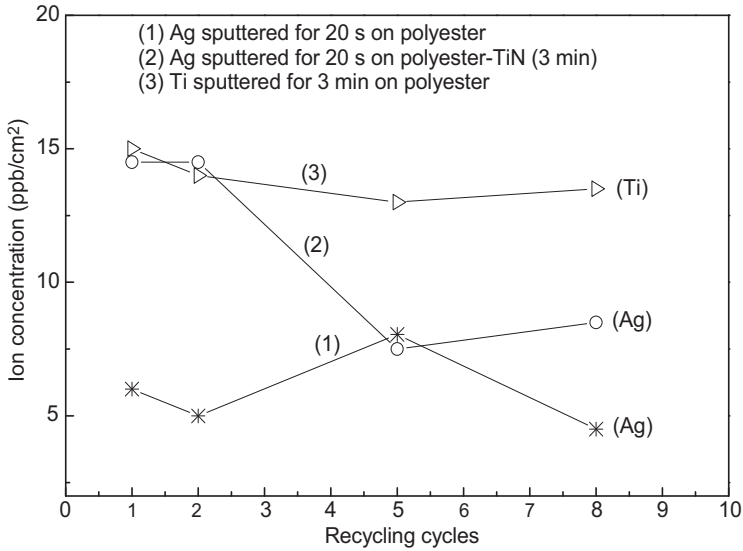

Figure 10.5 Ion-coupled plasma spectrometry determination of Ag ions and Ti ions released during the recycling of (a) sample sputtered with Ag for 30 s (trace 1), (b) TiN-Ag (3 min 20 s) sputtered sample, and (c) TiN sputtered sample for 3 min (trace 3).
Rtimi S, Baghriche O, Sanjines R, Pulgarin C, Ben-Simon M, Lavanchy, J-C. et al. Photocatalysis/catalysis by TiN/TiN-Ag surfaces efficient in bacterial inactivation under visible light. *Appl Catal B* 2012;**123−24**:306−315.

resistance.[69] N-doped titanium oxide films have been reported to improve the visible absorption range of TiO_2 because N-atoms occupy the O-atom sites in the TiO_2 lattice, forming Ti−O−N bonds, red shifting TiO_2 light absorption.[70,71]

Before sputtering the films, the residual pressure P_r in the sputtering chamber was $P_r \leq 10^{-4}$ Pa. The substrate target distance varied between 8.5 and 11 cm, but for most runs the distance was kept at about 11 cm. The TiON thin films were deposited by reactive DC-magnetron sputtering (DC) in an $Ar + N_2 + O_2$ gas flow from a 5-cm-diameter Ti target 99.99% pure (Kurt J. Lesker, East Sussex, UK). The sputtering current on the Ti target was set at 280 mA at a power of 128 W (U −518 V). Direct current magnetron sputtering was used to sputter Ag and was operated at 50 kHz with 15% reversed voltage. The sputtering current was set at 280 mA with U −500 V, 75 V reverse voltage (15% of 500 V), and a power of 140 W.

The substrate used for the sputtered films was polyester with excellent durability during long-term operation, good abrasion resistance, fiber appearance retention, elasticity, stress recovery, and resiliency. The polyester used corresponds to EMPA test cloth sample No. 407. It is a polyester Dacron polyethylene-terephthalate, type 54 spun, plain weave ISO 105-F04.

The colors of the TiON samples sputtered for 4 min are shown in Fig. 10.6, row A. The colors are seen to be a function of the O_2/N_2 ratio. The collective oscillations of the electron plasmons in the TiON show a darker color for a higher ratio of O_2/N_2.

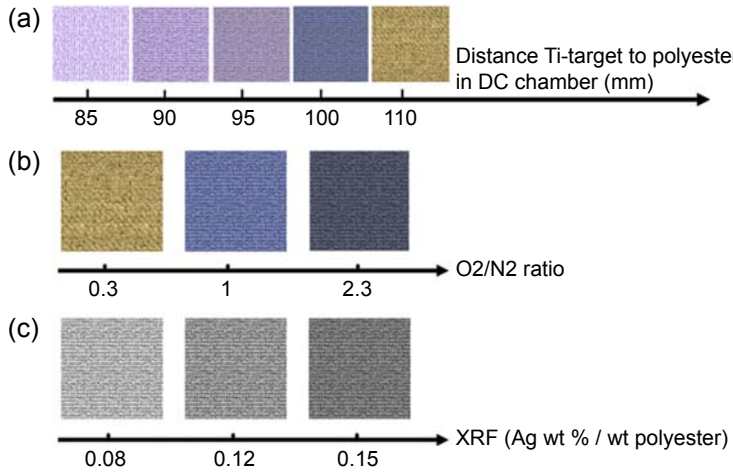

Figure 10.6 Visual presentation of the samples of sputtered TiON and Ag-TiON textiles within 4 min: (A) color variation as a function of the distance of the Ti target and the polyester sample, (B) color variation as a function of O_2-N_2 ratio for TiON samples, (C) color variation of Ag-TiON samples with different Ag wt%/wt polyester.
Rtimi Sami Baghriche, Oualid Sanjines, Rosendo Pulgarin, Cesar Ben-Simon, Michael Lavanchy, Jean-Claude et al. TiON and TiON-Ag sputtered textile showing antibacterial activity induced by simulated-solar-light. *J Photochem Photobiol A* 2013;**256**:52−63.

The visible light photocatalysis mediated by TiON has been suggested to require a certain ratio of N_2/O_2.[30,72] The color results from the N-doping of the TiO_2-lattice inducing interstitial N-doping in the TiO_2 accompanied by the formation of O vacancies and leads to charge transfer states responsible for TiON absorption in the visible region. A higher content of O_2 has been reported to increase the biocompatibility of the TiON samples.[50] The samples TiON 4 min were sputtered with Ag for 20−40 s in Fig. 10.6, row B and became darker for TiON samples sputtered for longer times. The wt% Ag/wt polyester of the TiON-Ag samples sputtering Ag for 20, 30, and 40 s are shown in Fig. 10.6, row C The color darkening is the result of the increased amount of Ag deposited at longer sputtering times.

Fig. 10.7 shows the bacterial inactivation of *E. coli* by TiON-Ag films. The TiON layers were sputtered for 4 min and Ag sputtering was applied sequentially up to 40 s. Slight bacterial inactivation was observed in the dark (Fig. 10.7, trace 5) possibly owing to adsorption of *E. coli* on the polyester, because Ag ions are shown in this study to be produced under light irradiation on Ag-TiON films. The bacterial inactivation kinetics increased as the Ag-sputtering time increased from 10 to 30 s, attaining a maximum at 30 s owing to the known bactericidal properties of Ag. The inactivation kinetics fell at 40 s, possibly because of the formation of larger Ag clusters hindering electron injection from Ag/Ag_2O into TiO_2. The Ag clusters were not necessarily crystalline and darkened the polyester samples as a function of sputtering time. The *E. coli* survival on Ag sputtered directly on the polyester fabric led to longer inactivation

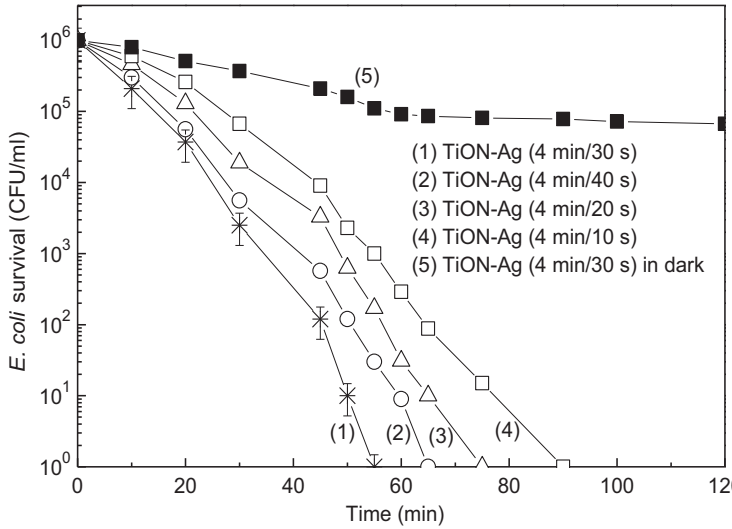

Figure 10.7 *Escherichia coli* survival on Ag-TiON sputtered on polyester for different Ag deposition times on TiON layers. The light source is an Osram lamp L18W/827 (4 mW/cm^2, 400−700 nm). Reactive gas flow composition: Ar 90%:N_2 5%:O_2 5% and total $P = 0.5$ Pa. Rtimi Sami Baghriche, Oualid Sanjines, Rosendo Pulgarin, Cesar Ben-Simon, Michael Lavanchy, Jean-Claude et al. TiON and TiON-Ag sputtered textile showing antibacterial activity induced by simulated-solar-light. *J Photochem Photobiol A* 2013;**256**:52−63.

times of 1 $\log_{10}$, 2 $\log_{10}$, and 3 $\log_{10}$ for sputtering times of 10, 20, and 30 s (data not shown). The 6 $\log_{10}$ bacterial inactivation time of 55 min shown in Fig. 10.7 for TiON-Ag (4 min 30 s) samples was possible because the TiON smooth thin layer on the polyester merged without forming boundaries with the polyester.[44]

The TEM of Ag-TiON is shown in Fig. 10.8(a). On the left side, a dark continuous coating of TiON-Ag (4 min 30 s) is observed on the polyester fiber. The right image with a larger magnification of 100 nm shows the immiscibility of the Ag-dark coating and the TiON coating gray layers. The Ag particles have sizes between 20 and 40 nm within a TiON-Ag layer with a width of 70 ± 10 nm. Ag/Ag_2O particles of 20−40 nm will not permeate a bacterial cell wall having protein porin pores with a diameter of 1.1−1.5 nm.[16,17] This confirms once more that Ag bacterial inactivation goes by Ag ions with sizes less than 1 nm and not Ag nanoparticulates. Fig. 10.8(b) shows the image of a TiON-Ag (4 min 30 s) sample in bright field (BF). The immiscibility of the Ag and Ti on the sample surface is readily seen at the current beam position.

Fig. 10.9 presents the release of Ti and Ag up to the eighth cycling during bacterial inactivation runs. The results for samples of TiON, TiON-Ag, and Ag are shown in Fig. 10.9. Fig. 10.9, trace 1 shows the slow release of Ti up to the eighth cycling from the TiON 4-min sample. Trace 2 shows the Ag ion release starting at a level of 6 ppb/cm^2 for Ag-TiON (4 min 30 s) sample and reaching about 5 ppb/cm^2 on the eighth cycle. Silver ions are formed by oxidation of Ag on the polyester in the reaction media. Silver ions with a concentration greater than 0.1 ppb have significant

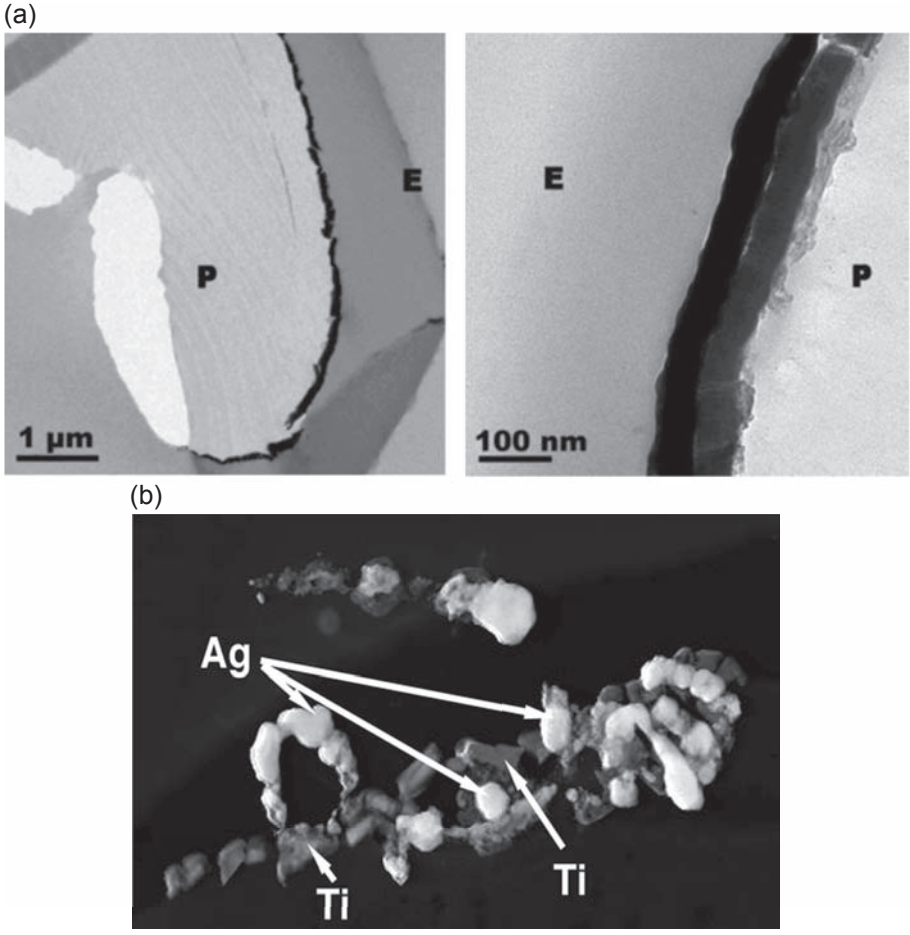

Figure 10.8 (a) Left side: TEM of Ag-TiON-Ag (4 min 30 s) DC-sputtered sample showing continuity of the sputtered layer around the polyester fiber. Right side: The same sample with larger magnification of the darker continuous Ag layers being immiscible with the gray TiON layer. (P: polyester and E: epoxide). (b) Transmission electron microscopy image of Ag-TiON (4 min 30 s) in BF mode, showing the nonmiscibility of Ag- and Ti-sputtered layers. Rtimi Sami Baghriche, Oualid Sanjines, Rosendo Pulgarin, Cesar Ben-Simon, Michael Lavanchy, Jean-Claude et al. TiON and TiON-Ag sputtered textile showing antibacterial activity induced by simulated-solar-light. *J Photochem Photobiol A* 2013;**256**:52−63.

antimicrobial activity. Higher Ag ion concentrations more than 35 ppb can be toxic to human cells.[50,69] The level of Ag released by Ag polyester in Fig. 10.9 reached on the eighth cycle a level similar to the Ag released by the Ag-TiON-Ag (4 min 30 s) samples. Biocompatibility of TiON has been well documented in biomedical applications.[26,35] The Ag-TiON fast inactivation kinetics and concomitant low cytotoxicity are two essential requirements for potential practical application of these antibacterial surfaces.

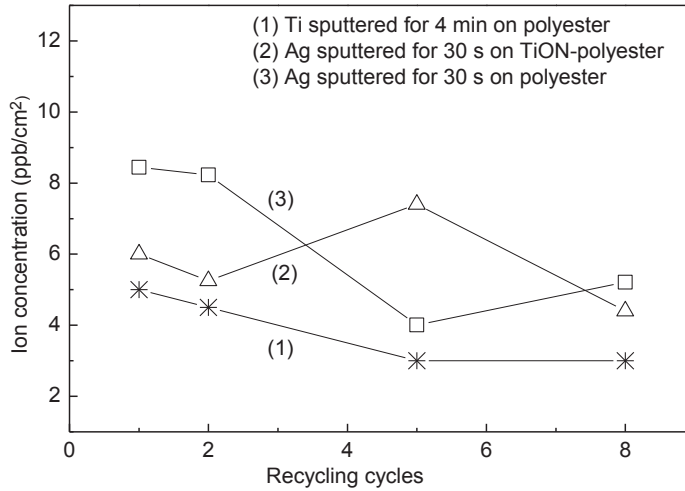

Figure 10.9 Ion-coupled plasma spectrometry determination of Ag ions and Ti ions released during the recycling of (1) TiON sputtered 4 min on polyester, (2) Ag-TiON (4 min 30 s) polyester sample, and (3) a sample of Ag-polyester sputtered 30 s.
Rtimi Sami Baghriche, Oualid Sanjines, Rosendo Pulgarin, Cesar Ben-Simon, Michael Lavanchy, Jean-Claude et al. TiON and TiON-Ag sputtered textile showing antibacterial activity induced by simulated-solar-light. *J Photochem Photobiol A* 2013;**256**:52−63.

The mechanism of bacterial inactivation for the TiON-Ag film is suggested by the scheme in Fig. 10.10. Silver oxide is formed on the film surface when Ag films enter into contact with air (O_2) and H_2O (vapor). The AgOH decomposes spontaneously to Ag_2O (Eq. [10.1]):

$$2AgOH \rightarrow Ag_2O + H_2O \quad (pk = 2.87) \qquad [10.1]$$

This Ag_2O is stable at pH 6−7, at which the bacterial inactivation of *E. coli* proceeds. Light irradiation photoactivates Ag_2O with $1.46 < bg < 2.25$ eV,[73] as noted in Eq. [10.2]:

$$Ag_2O + light \rightarrow Ag_2O\ h^+ + Ag_2O\ e^- \qquad [10.2]$$

For the Ag_2O/TiO_2 transfer of charges, we have to consider the position of the energy bands of Ag_2O and TiO_2. Under visible light irradiation, the transfer of charge from Ag_2O to TiO_2 is thermodynamically favorable because the position of the Ag_2O conduction band (cb) at 1.3 eV NHE at pH 0 and the vb of Ag_2O +0.2 eV NHE at pH 0[74] lies above the TiO_2 cb at −0.1 V versus NHE and the vb at +3.2 V. Under light, an interfacial charge transfer process (IFCT) may take place between Ag_2O and TiON/TiO_2.[75] The Ag_2O cb transfers electrons to the TiO_2 cb in an energetic favorable process, which will hinder the electron−hole recombination in Ag_2O. We suggest that the transfer of Ag_2O electrons to O_2 resulting from this increased charge separation has an important role in the photocatalytic activity leading to bacterial inactivation.

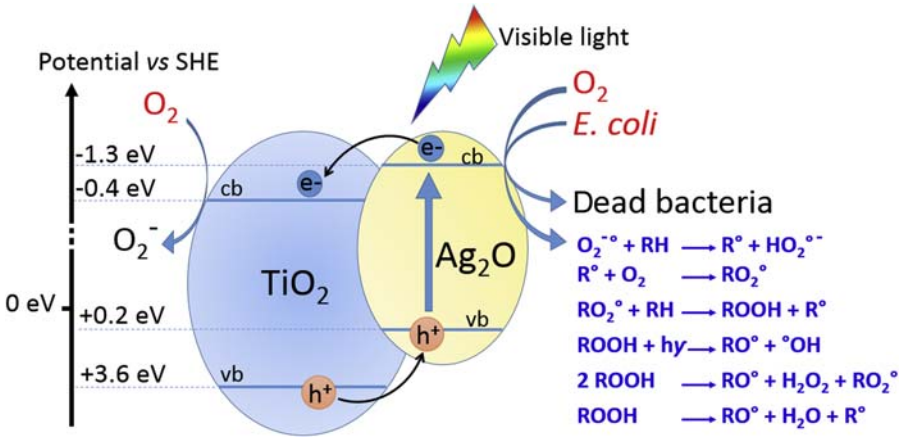

Figure 10.10 Interfacial charge transfer mechanism for TiO_2-Ag_2O.
Rtimi Sami Baghriche, Oualid Sanjines, Rosendo Pulgarin, Cesar Ben-Simon, Michael Lavanchy, Jean-Claude et al. TiON and TiON-Ag sputtered textile showing antibacterial activity induced by simulated-solar-light. *J Photochem Photobiol A* 2013;**256**:52−63.

We suggest a mechanism in which the Ag_2O in Eq. [10.1] reacts:

$$Ag_2O^- \rightarrow 2Ag^\circ + {}^1\!/\!_2O_2{}^- \qquad [10.3]$$

The O_2 in Eq. [10.3] would promote at later stages reactions[5,6] producing highly oxidative radicals, whereas the h^+ in Eq. [10.2] reacts with H_2O, as noted in Eq. [10.4]. This reaction runs parallel to Eq. [10.5], generating OH^o radicals or other highly reactive oxidative radicals by way of the Ag_2Ovb h^+ (Eq. [10.2]):

$$h^+ + H_2O \rightarrow OH^\circ + H^+ \qquad [10.4]$$

$$2e^- + 2H_2O + O_2 \rightarrow 2OH^\circ + 2OH^- \qquad [10.5]$$

10.2.3 Zr nitride Ag surfaces active in bacterial inactivation in the dark and under light (Ag-ZrN)

Reports have described some Ag-based transition metal nitride (TmN) nanocomposites such as Ag-ZrN[76,77] that are effective in biological applications consisting of biphased nanocomposites with separated Ag and cubic fcc-TmN nanocrystallites. This is the result of the nonmiscibility of Ag atoms in the fcc-TmN phase caused by the higher Ag-nitridation energy compared with the TmN formation energy. We have co-sputtered Ag-ZrN on polyester[39] correlating to the sputtered Ag-ZrN surfaces in the dark and under light to the amount of Ag- and Zr-sputtered with the antibacterial

kinetics, the absorption in the visible range, and optimized the Ag-ZrN deposition time of 20 s to attain the fastest bacterial reduction kinetics, as will be show in the text below.

The polyester alone in Fig. 10.11, image (a), shows no color in the absence of Ag-ZrN. A light gray appears in sample (b), indicative of Ag clusters or nanoparticles deposited at 50 mA for 10 s; (c) this sample shows a darker gray metallic Ag color sputtering 2 s at 300 mA; and finally, (d) this image shows a dark mostly Ag deposit on the Ag-ZrN-polyester sputtered for 20 s at 300 mA. The Ag atoms diffuse anisotropically on the polyester surface and the migration or aggregation of the Ag particles is driven by the sputtering energy leading to thermodynamically stable agglomerates.[39]

Fig. 10.12 shows the faster inactivation kinetics attained by Ag-ZrN surfaces sputtering at 300 mA. Fig. 10.12 shows an *E. coli* inactivation time of 1.5 h on Ag-ZrN

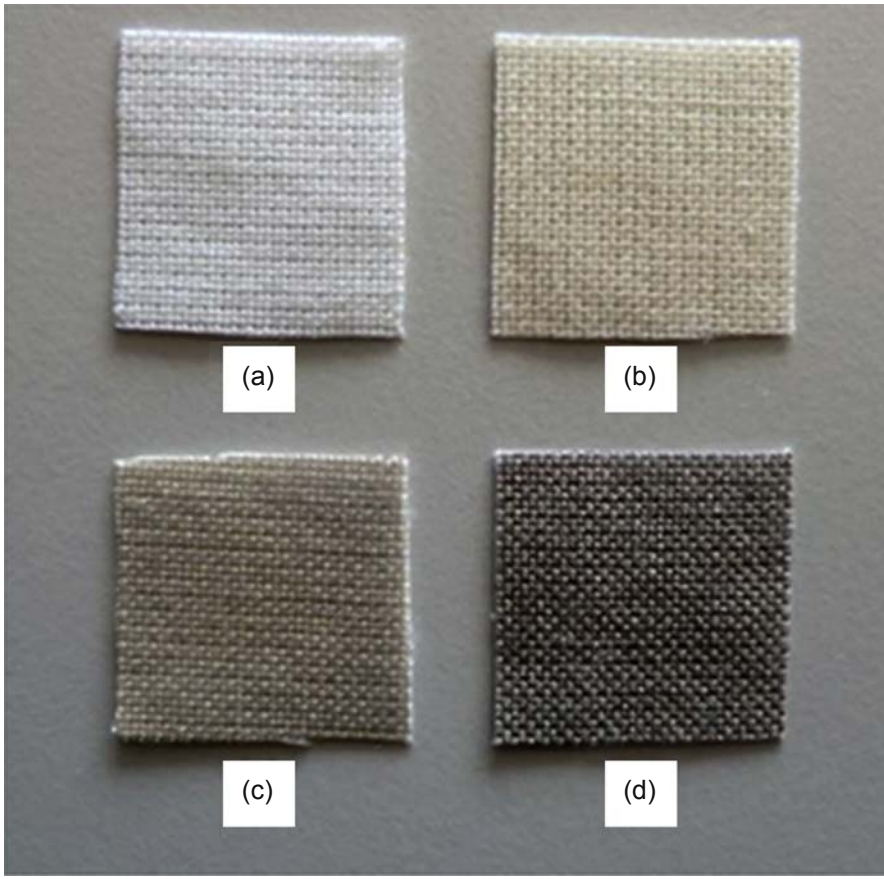

Figure 10.11 Visual appearance of Ag-ZrN polyester DC-sputtered under different experimental conditions: (a) polyester alone, (b) AgZr-N films 10 s at 50 mA, (c) AgZr-N films 2 s at 300 mA, and (d) AgZr-N films 20 s at 300 mA.
Baghriche O, Kiwi J, Pulgarin C, Sanjinés R. Antibacterial Ag-ZrN surfaces promoted by Zr and deposited by reactive pulsed magnetron sputtering. *J Photochem Photobiol A* 2012;**229**:39−45.

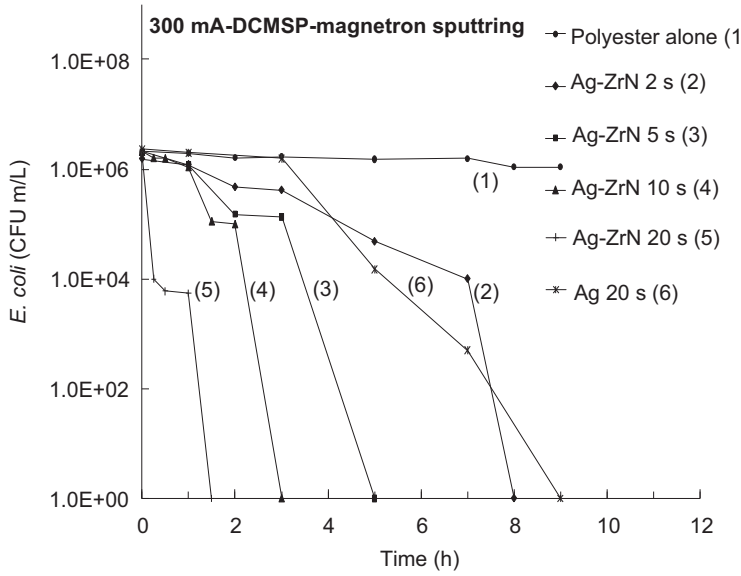

Figure 10.12 *Escherichia coli* inactivation on co-sputtered direct current magnetron sputtering (pulsed) at different times using simultaneously an Ag and Zr target in Ar-10% N_2 0.5 Pa atm. Current: 300 mA.
Baghriche O, Kiwi J, Pulgarin C, Sanjinés R. Antibacterial Ag-ZrN surfaces promoted by Zr and deposited by reactive pulsed magnetron sputtering. *J Photochem Photobiol A* 2012;**229**: 39−45.

polyester sputtered for 20 s. Fig. 10.12, trace 5 shows that *E. coli* inactivation is a complex process and does not proceed smoothly in the timescale. This sample had the optimal ratio of Ag loading/Ag cluster size exposing the highest amount of Ag sites. Silver sputtered alone as a control experiment induced *E. coli* inactivation within about 9 h. This shows the favorable effect of the Ag-ZrN co-sputtered composite surface. Fig. 10.13 shows that for samples sputtered above 20 s, the *E. coli* inactivation kinetics became larger compared with samples sputtered for 20 s. The Ag agglomerates became larger but the catalytic activity per exposed atom decreased. For sputtering below 20 s, there was not enough Ag on the polyester to mediate fast *E. coli* inactivation. We suggest that the reactive oxygen species of *E. coli* involved interaction with Ag^+/Ag° species:

$$Ag^\circ + O_2 \rightarrow Ag^+ + O_2{}^{\bullet -} \quad [10.6]$$

$$Ag^+ + O_2{}^{\bullet -} \rightarrow Ag^\circ + O_2 \quad [10.7]$$

10.2.4 Zr oxynitride Ag surfaces active in bacterial inactivation in the dark and under light (Ag-ZrON)

This study carried out in our laboratory (EPFL, Lausanne, Switzerland) addressed the acceleration of bacterial reduction kinetics by Ag-ZrON relative to the bacterial

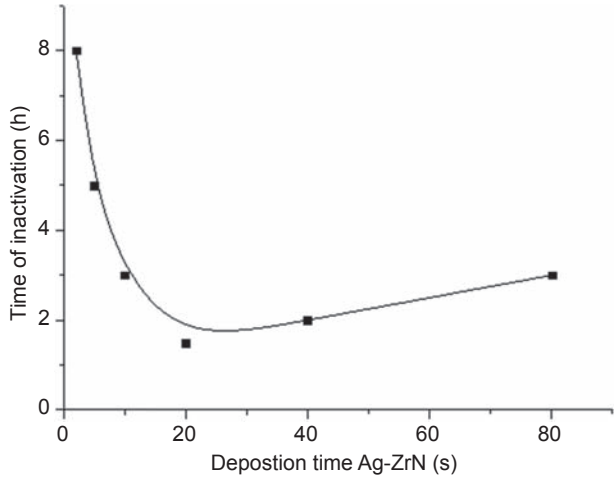

Figure 10.13 Inactivation time of *E. coli* on Ag-ZrN polyester as a function of the deposition time by DCMSP sputtered at 300 mA.
Baghriche O, Kiwi J, Pulgarin C, Sanjinés R. Antibacterial Ag-ZrN surfaces promoted by Zr and deposited by reactive pulsed magnetron sputtering. *J Photochem Photobiol A* 2012;**229**: 39–45.

reduction found for ZrON–samples.[40] To correlate the catalyst microstructure with the bacterial reduction kinetics, the sputtering of Zr and Ag on polyester was carried out in a sequential and co-sputtering mode; the results are shown in Fig. 10.14.

In the sputtering chamber, the pressure was set to 0.1 Pa and the substrate-to-target distance was 10 cm. Before deposition of the films, the residual pressure in the sputtering chamber was Pr $\leq 10^{-4}$ Pa. The 2-in-diameter or 5-cm Zr cathode was obtained from Lesker Corp (Hastings, East Sussex, UK). During the deposition of ZrNO on the polyester, we determined the most appropriate gas composition to be 5% N_2:5% O_2: 90% Ar. We varied the percent gas flow of N_2 and O_2, maintaining the flow of Ar at a fixed value. The gas composition of 5% N_2:5% O_2:90% Ar allowed us to prepare ZrNO-Ag coating sputtering for 90 s leading to the shortest time to attain total loss of bacterial cultivability (40 min), as shown in Fig. 10.14(c). Fig. 10.14(a) shows ZrNO-sputtered polyester samples under low-intensity actinic light (4 mW/cm^2). Within 150 min, bacterial reduction was observed from 10^6 CFU/mL to undetected bacteria.

Fig. 10.14(a), trace 1 includes the statistical analysis of the data for the bacterial reduction of *E. coli.* No regrowth was observed after the first inactivation cycle for ZrNO and ZrNO-Ag samples. Fig. 10.14(b) shows the bacterial inactivation of *E. coli* by ZrNO-Ag samples under low-intensity actinic light. Within about 115 min, complete bacterial reduction was observed. Fig. 10.14(c) shows that ZrNO-Ag co-sputtered for 90 s on polyester led to a 6 $\log_{10}$ bacterial reduction within 45 min. The co-sputtered Ag-ZrON for 90 s led to the complete loss of cultivability within 40–45 min (Fig. 10.14(c), trace 1). This time was much shorter than to the time needed by the sequentially sputtered ZrNO (90 s)-Ag (10 s) sample shown in Fig. 10.1(b).

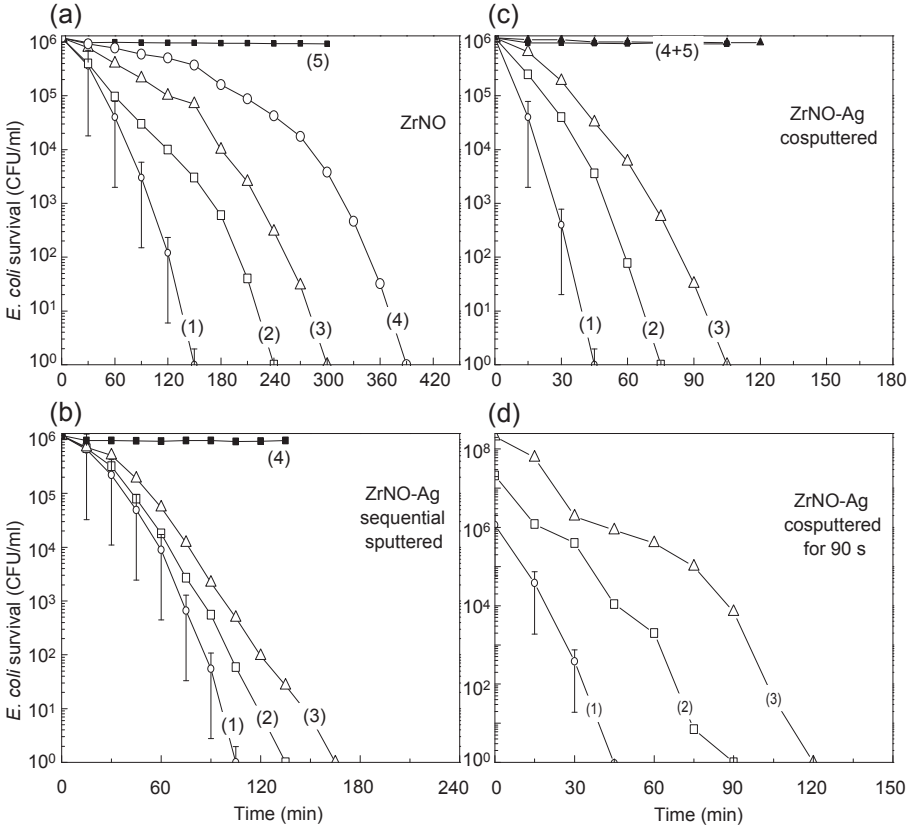

Figure 10.14 a) *Escherichia coli* inactivation by ZrNO as a function of time for (1) Zr sputtered for 90 s on polyester; (2) Zr sputtered for 150 s; (3) Zr sputtered for 60 s; and (4) Zr sputtered for 40 s (samples were irradiated with an Osram Lumilux 18/827 actinic lamp); and (5) Zr sputtered for 90 s on polyester but in dark bacterial inactivation runs. (b) Zr sputtered on polyester for 90 s followed by Ag deposition for (1) Ag 10 s; (2) Ag 20 s; (3) Ag 40 s (under Osram Lumilux 18/827 actinic lamp irradiation); and (4) Zr sputtered on polyester for 90 s but in dark bacterial inactivation runs. (c) ZrNO-Ag co-sputtered on polyester for (1) 90 s; (2) 60 s; and (3) 150 s (Osram Lumilux 18/827 actinic lamp irradiation); and (4) Zr sputtered on polyester for 90 s but in dark bacterial inactivation runs. (d) Effect of initial concentration on inactivation kinetics of *E. coli* inactivation on a co-sputtered ZrNO-Ag (90 s) sample under Osram Lumilux 18/827 actinic lamp irradiation.
Baghriche O, Kiwi J, Pulgarin C, Sanjinés R. Antibacterial Ag-ZrN surfaces promoted by Zr and deposited by reactive pulsed magnetron sputtering. *J Photochem Photobiol A* 2012;**229**: 39−45.

The polyester fabrics were sterilized by autoclaving at 121°C for 2 h. The 20-μL aliquots with an initial concentration of 10^6 CFU/mL in a solution of NaCl/KCl at pH 7 were placed on coated and uncoated (control) polyester fabric. The samples were placed on Petri dishes provided with a lid to prevent evaporation. After each determination, the fabric was transferred into a sterile 2-mL Eppendorf tube containing

1 mL autoclaved NaCl/KCl saline solution. This solution was subsequently mixed thoroughly using a Vortex for 3 min. Serial dilutions were made in NaCl/KCl solution. A 100-μL sample of each dilution was pipetted onto a nutrient agar plate and spread over the plate using standard plate method. The polyester is a microporous substrate and distributes the inoculum evenly on the ZrNO, Ag-ZrON films without needing an adsorption stage. Well-dispersed nonheterogeneous contact is established between the sample and the bacterial solution.

Fig. 10.15 shows reuse of the co-sputtered Ag-ZrON (90 s) sample during *E. coli* bacterial inactivation. After eight cycles, the samples kept their initial performance. The discontinuity in the abscissa shows nonsequential kinetics for the fourth and eighth cycles with conservation of the initial bacterial reduction kinetics within 40−45 min. The surface atomic percent concentration of elements in the ZrNO-Ag (90 s) sputtered samples after being contacted for 3 s with bacteria were O1s 8.8%, N1s 2.3%, C1s 54.9%, Zr3d 2.8%, and Ag3d 35.4%. These percentages varied less than 10% during the 40-min reaction, leading to total bacterial loss of cultivability. Therefore, the rapid destruction of fragments resulting from bacterial decomposition during photocatalysis allows conservation of the initial bacterial inactivation kinetics, as shown in Fig. 10.15. The band gap for ZrO_2 nanoparticles is about 3.2 eV.[78−79] Defects in their structure have been reported to have a role in the ZrO_2 donor to acceptor electron transfer reactions.[80] The sputtering of Zr in O_2/N_2 atmosphere led to the formation of ZrO_2.

Fig. 10.16 presents the TEM of a co-sputtered ZrNO-Ag (90 s) polyester sample. On the left side, the Zr and Ag are shown to be immiscible on the polyester fibers. The right side of Fig. 10.16 shows the Zr and Ag nanoparticles contrasted by high

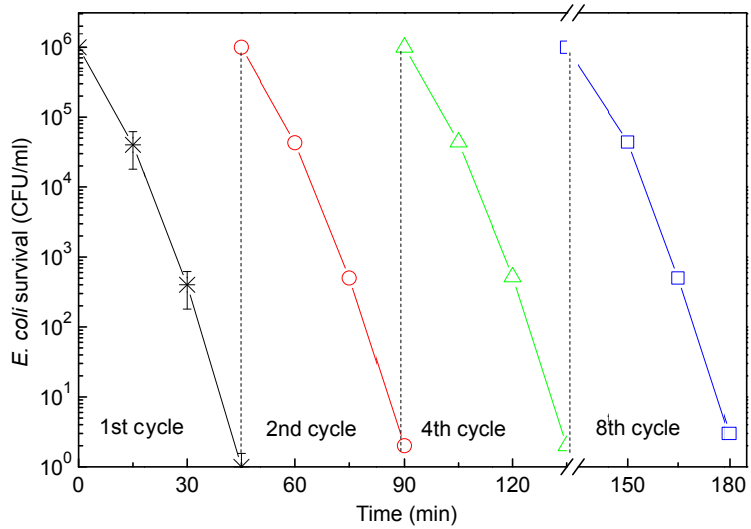

Figure 10.15 Cycling of ZrNO-Ag (90 s) samples leading to total bacterial inactivation under Osram Lumilux 18W/827 (400−700 nm) irradiation.
Baghriche O, Kiwi J, Pulgarin C, Sanjinés R. Antibacterial Ag-ZrN surfaces promoted by Zr and deposited by reactive pulsed magnetron sputtering. *J Photochem Photobiol A* 2012;**229**: 39−45.

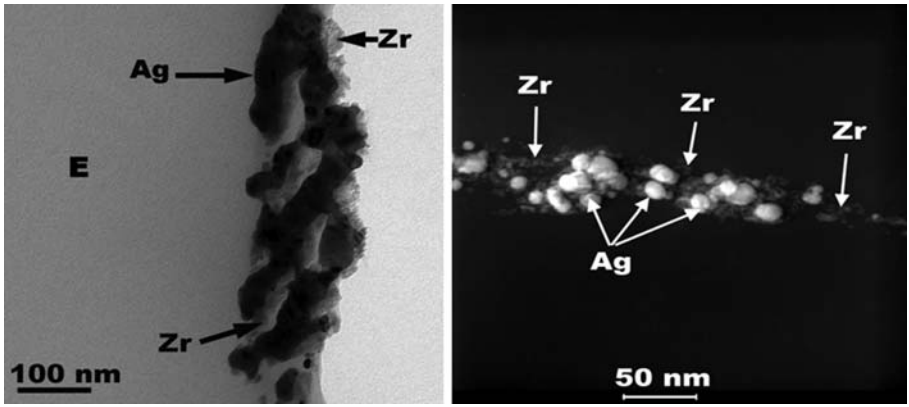

Figure 10.16 Left side: Transmission electron microscopy image of a co-sputtered ZrON-Ag (90 s) sample (amplification 28 k) Right: The same sample in HAADF representation. Baghriche O, Kiwi J, Pulgarin C, Sanjinés R. Antibacterial Ag-ZrN surfaces promoted by Zr and deposited by reactive pulsed magnetron sputtering. *J Photochem Photobiol A* 2012;**229**: 39−45.

angular annular dark field (HAADF). The sizes of the ZrO_2 and Ag nanoparticles were 80−130 and 8−15 nm, respectively. Because of their size, Ag nanoparticles are not able to penetrate to the bacteria core through bacterial porins with diameters of 1−1.1 nm.[16,17] Only Ag ions diffuse through bacterial porins, leading to deoxyribonucleic acid damage, and finally to bacterial inactivation.[28]

10.2.5 Ta-nitride Ag surfaces active in bacterial inactivation in the dark and under light (Ag-TaN)

Because the current chapter focuses on Ag-TiN and Ag-ZrN polyester surfaces active in bacterial reduction in the dark and under light irradiation, we will address the investigation of the polyester−Ag-TaN-mediated bacterial reduction kinetics. Here, we report the polyester-TaN, and polyester-Ag-TaN bacterial reduction kinetics, the characterization of surface properties by surface science techniques of the polyester−Ag-TaN, and the changes induced in the polyester−Ag-TaN surface during redox catalysis during bacterial interaction and reduction by XPS.[41]

Fig. 10.17 shows the *E. coli* reduction kinetics when Ta was sputtered onto polyester in an $Ar + N_2$ (0.5 Pa) atmosphere for different times on polyester in the dark and under light. Fig. 10.17 reveals the semiconductor behavior of the Ta sputtered on polyester. The TaN-polyester sample sputtered for 2 min and irradiated by an L18W/827 Lumilux/Osram led to complete bacterial reduction within 120 min (Fig. 10.17, trace 7).

The formation of Ta_2O_5 may be related to the following: (1) the partial oxidation of TaN in the presence of oxygen generated by residual H_2O vapor in the magnetron chamber at residual pressure $Pr = 10^{-4}$ Pa. This pressure is equivalent to 10^{15} molecules/cm^2 s; and sufficient O-radicals are available to induce partial

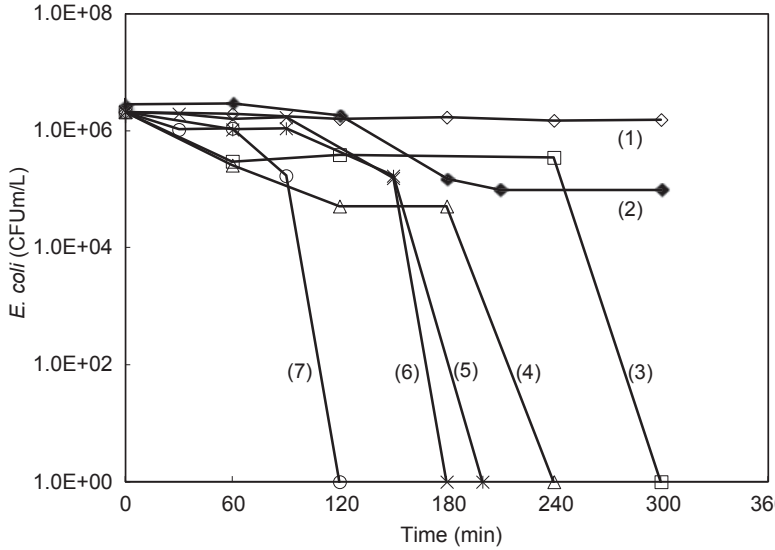

Figure 10.17 *Escherichia coli* survival on polyester−TaN samples in the dark and under light: (1) polyester alone, (2) sputtered for 2 min in the dark, (3) sputtered for 0.5 min under light, (4) sputtered for 1 min under light, (5) sputtered for 8 min under light (6) sputtered for 4 min under light, and (7) sputtered for 2 min under light. Irradiation source L18W/827 Lumilux/Osram (4 mW/cm^2).
Baghriche O, Rtimi S, Zertal A, Pulgarin C, Sanjinés R, Kiwi J. Accelerated bacterial reduction on Ag−TaN compared with Ag−ZrN and Ag−TiN surfaces. *App Cat B: Environ* 2015; **174**−**175**:376−82.

oxidation of TaN films; (2) the films can also oxidize after deposition when exposed to air and during the sterilization process (autoclaving at 121°C). Fig. 10.17 shows the bacterial reduction kinetics accelerated with sputtering time from 0.5 to 2 min (Fig. 10.17, traces 3, 4, and 7). Fig. 10.17, traces 5 and 6 sputtered for 8 and 4 min, respectively, show slower bacterial inactivation kinetics compared with trace 7 (2 min). This is because of the increase in layer thickness leading to bulk inward diffusion of the charge carriers.[80] These charge carriers are responsible for electrostatic attraction between the TaN film and bacteria.

Fig. 10.18 shows the faster bacterial reduction of *E. coli* for Ag-TaN polyester under L18W/827 Lumilux/Osram lamp irradiation. It is readily seen that polyester alone has no bactericide action and that the *E. coli* inactivation kinetics becomes faster at longer co-sputtering times of Ta and Ag up to 120 s, leading to complete bacterial reduction within 20 min. Sputtering times above 20 s led to a slower bacterial reduction kinetics. For a sample sputtered for 120 s (Fig. 10.18, trace 4), the bacterial reduction of *E. coli* became longer compared with samples sputtered for 20 s (Fig. 10.18, trace 7). The size of the Ag clusters increased with the sputtering time, leading to Ag agglomeration, but the catalytic activity per exposed atom consequently decreased owing to Ag agglomeration.

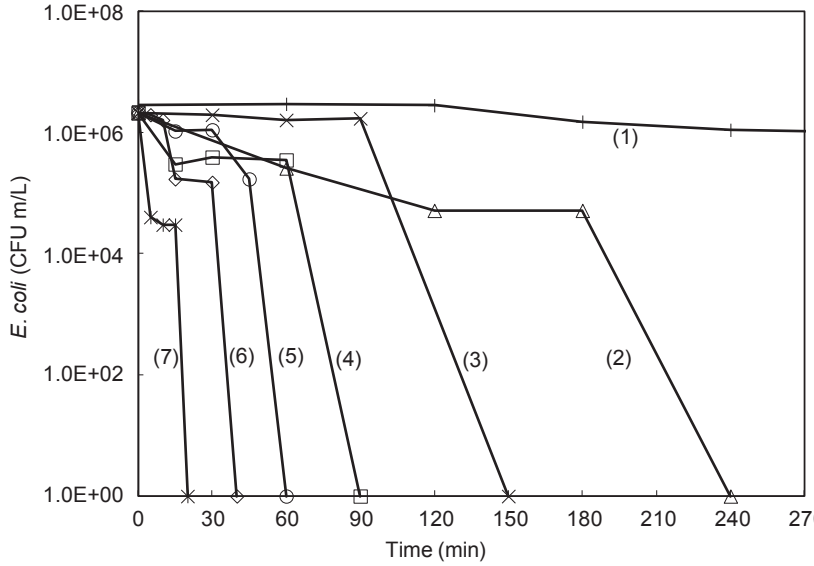

Figure 10.18 *Escherichia coli* bacterial reduction on polyester−Ag-TaN sputtered for times: (1) polyester alone, (2) for 5 s, (3) for 10 s, (7) for 20 s, (6) for 40 s, (5) for 60 s, and (4) for 120 s. Irradiation source L18W/827 Lumilux/Osram (4 mW/cm^2).
Baghriche O, Rtimi S, Zertal A, Pulgarin C, Sanjinés R, Kiwi J. Accelerated bacterial reduction on Ag−TaN compared with Ag−ZrN and Ag−TiN surfaces. *App Cat B: Environ* 2015; **174−175**:376−82.

Fig. 10.19 presents the bacterial inactivation kinetics mediated by Ag-TaN (20 s) as a function of the applied light dose. It is readily seen that the bacterial inactivation kinetics depends on the light dose applied in the reactor cavity. This reveals the semiconductor character of the nanocomposite Ag-TaN. In the presence of oxygen, the Ag-TaN becomes Ta_2O_5-Ag_2O. The oxygen comes from the decomposition of H_2O (vapor) left in the magnetron sputtering chamber (Fig. 10.10) and when the composite catalyst is exposed to air. An interfacial transfer charge mechanism applies for the charge injection under light irradiation, similar to the case of Ag-TiON composites shown previously in Fig. 10.10. The inset in Fig. 10.19 shows the spectral distribution of the light source used.

Fig. 10.20 presents the release of Ag from polyester/Ag (160 s) and polyester/Ag-TaN (20 s). For the polyester/Ag samples up to the eighth cycle, the level of Ag release drops from 8 to about 4 ppb/cm^2, and for the Ag-TaN (20 s) sample, Ag release drops from 4 to about 1 ppb/cm^2. TaN sputtered on polyester will therefore improve the biocompatibility level of Ag because the disinfection process occurs at a lower Ag release level. The TaN is known for its excellent biocompatibility, which makes Ag-TaN an important material in biorelated applications.[79,80] This feature makes polyester−Ag-TaN important to biochemical applications in implants because of nitride TaN-proven biocompatibility concomitant with observed accelerated bacterial

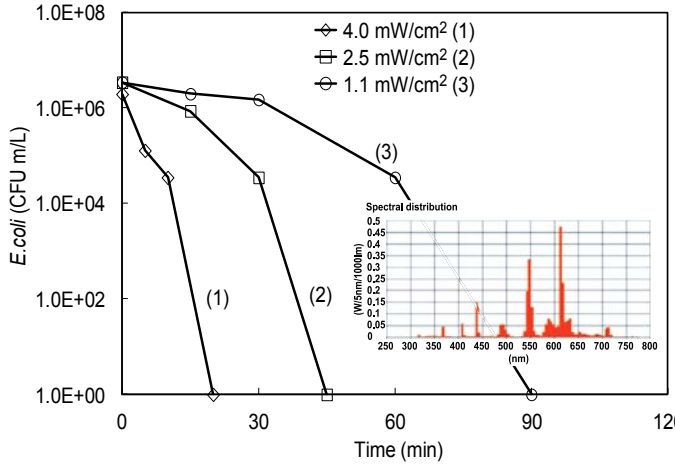

Figure 10.19 *Escherichia coli* bacterial reduction kinetics on polyester−Ag-TaN co-sputtered for 20 s on polyester as a function of the applied light dose. Irradiation source L18W/827 Lumilux/Osram (4 mW/cm^2) lamp.
Baghriche O, Rtimi S, Zertal A, Pulgarin C, Sanjinés R, Kiwi J. Accelerated bacterial reduction on Ag−TaN compared with Ag−ZrN and Ag−TiN surfaces. *App Cat B: Environ* 2015; **174**−**175**:376−82.

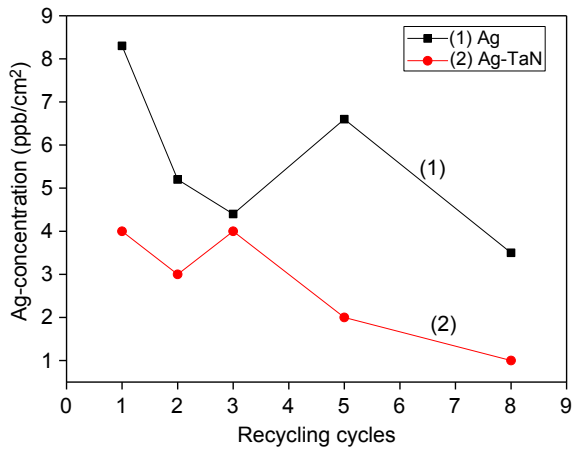

Figure 10.20 (a) Ion-coupled plasma spectrometry determination of Ag ions released during recycling of (1) polyester−Ag sputtered for 160 s and (2) polyester−Ag-TaN co-sputtered for 20 s.
Baghriche O, Rtimi S, Zertal A, Pulgarin C, Sanjinés R, Kiwi J. Accelerated bacterial reduction on Ag−TaN compared with Ag−ZrN and Ag−TiN surfaces. *App Cat B: Environ* 2015; **174**−**175**:376−82.

reduction (Fig. 10.18). Silver ions were released by oxidation of Ag nanoparticles in the reaction media during the bacterial reduction process. The release of Ag ions greater than 0.1 ppb has been reported to induce an antimicrobial effect. At levels higher than 35 ppb, Ag nanoparticles become cytotoxic to human (mammalian) cells.[81–82] The identification of Ag ions during the bacterial reduction time is addressed below by XPS.

The XPS of the polyester/Ag-TaN when Ag was sputtered for 20 s is shown in Figs. 10.21 and 10.22 for Ag°/Ag^{+} and Ag°/Ag^{2+} peaks, respectively. In air, the uptake of oxygen and film aging led to Ag_2O (Ag^{+}) and AgO (Ag^{2+}) phases, as shown in Figs. 10.21 and 10.22. In both cases, it is interesting that the Ag° fully crystallized metal state signal persisted along the Ag ionic/oxide states. The electrostatic correction for the Ag signals was carried out according to Shirley.[63] Fig. 10.21 shows at time 0 the $Ag3d_{5/2}$ doublet with Ag° at 367.6 eV and the Ag^{+} doublet at 368.2 eV. After 20 min bacterial inactivation, the Ag° doublet shifted to 368.8 eV and a new Ag^{2+} doublet appeared at 368.8 eV. The Ag signals were observed at the topmost polyester layers. This is evidence for the intervention of Ag interfacial Ag during bacterial reduction. The XPS BE shift greater than 0.2 eV is considered reasonable evidence for the appearance of new ionic species and provides evidence for redox catalysis occurring on the polyester–Ag-TaN during bacterial reduction. The mechanism for the interaction between the polyester–Ag-TaN and bacteria is similar to that reported previously for Ag–TiON bacterial reduction.[37]

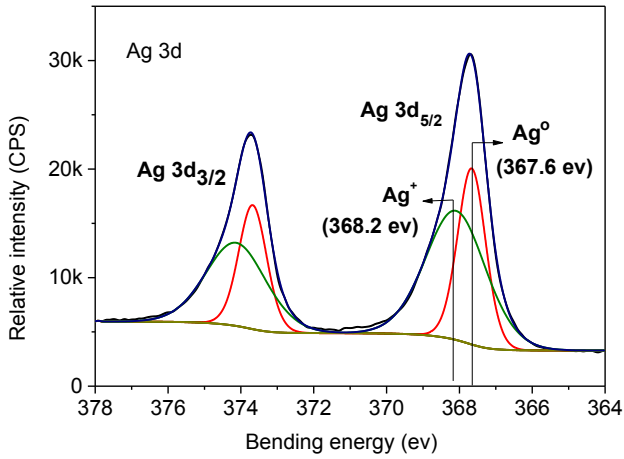

Figure 10.21 X-ray electron spectroscopy image of Ag3d5/2 doublet at time 0 on polyester–Ag-TaN sputtered for 160 s.
Baghriche O, Rtimi S, Zertal A, Pulgarin C, Sanjinés R, Kiwi J. Accelerated bacterial reduction on Ag–TaN compared with Ag–ZrN and Ag–TiN surfaces. *App Cat B: Environ* 2015; **174–175**:376–82.

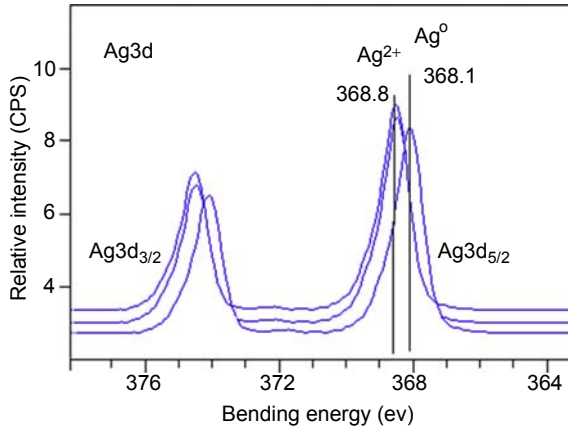

Figure 10.22 X-ray electron spectroscopy image of Ag3d5/2 doublet for polyester−Ag-TaN sputtered for 20 s after 20 min bacterial reduction under an L18W/827 Lumilux/Osram (4 mW/cm^2) irradiation source.
Baghriche O, Rtimi S, Zertal A, Pulgarin C, Sanjinés R, Kiwi J. Accelerated bacterial reduction on Ag−TaN compared with Ag−ZrN and Ag−TiN surfaces. *App Cat B: Environ* 2015; **174**−**175**:376−82.

10.2.6 Ta-oxynitride Ag surfaces active in bacterial inactivation in the dark and under light (Ag-TaON)

Continuing with our search for Ag-nitride systems with the most favorable kinetics for bacterial reduction, we sputtered polyester−Ag-TaN on polyester[42]; the most important results are shown in the subsequent discussion.

Fig. 10.23 displays the results for the thickness calibration of sputtered TaN, TaON, Ag, and co-sputtered TaON−Ag layers on the polyester. The fastest bacterial inactivation kinetics was observed for co-sputtered TaON-Ag layers for 2 min and attained coatings about 130 nm thick. This is equivalent to 650 layers. Assuming each layer is 10^{15} atoms/cm^2, a deposition rate of about 5.4×10^{15} atoms/cm^2 s can be estimated.[44] Work in our laboratory showed faster bacterial inactivation of *E. coli* on Ag films sputtered by DCP compared with DC-sputtered Ag films. The results obtained for bacterial reduction show that thin Ag-TaON thicknesses below 50 nm were not to be effective in inducing fast bacterial inactivation kinetics.

Fig. 10.24 present *E. coli* bacterial results on TaN, Ag-TaN and TaON, and Ag-TaON films. The effects of the light dose and bacterial reduction by Ag sputtered on polyester by itself are considered. Bacterial inactivation becomes faster for increasing TaN-sputtering times. Fig. 10.24(a) shows that sputtering TaN for 120 s inactivated bacteria within 300 min. Fig. 10.24(a), trace 5 shows that in the dark there was no bacterial inactivation on Ag-TaN polyester. Ag-TaN showed faster bacterial inactivation compared with TaN films and inactivated *E. coli* within 120 min for a 120-s co-sputtered sample. Fig. 10.24(a), trace 3 shows bacterial inactivation for Ag-TaN−Ag-surfaces co-sputtered for 60 s. Because the *E. coli* inactivation time

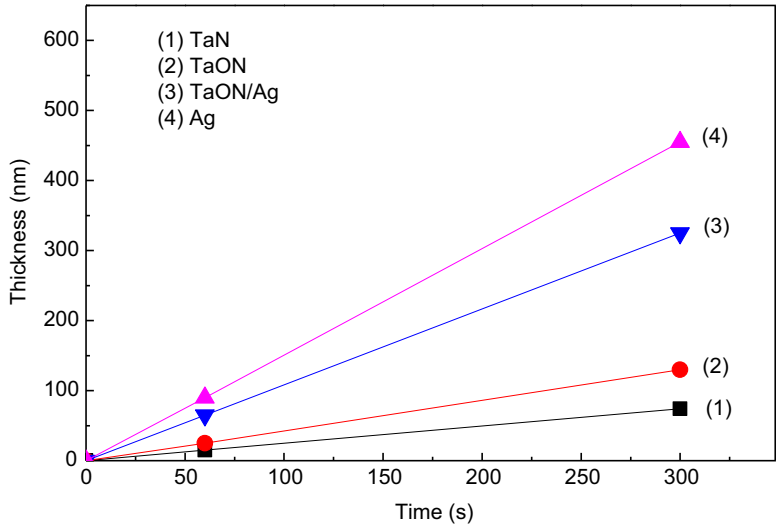

Figure 10.23 Thickness calibration of TaN, TaON, Ag-TaON, and Ag layers on Si-wafers as a function of sputtering time.
Rtimi S, Pulgarin C, Houas A, Sanjines R, Lavanchy J-C, Kiwi J. Coupling of narrow and wide band-gap semiconductors on uniform films in bacterial disinfection under low intensity visible light: implications of the interfacial charge transfer (IFTC). *J Hazard Mater* 2013;**260**: 860–868.

for samples sputtered for 120 s became shorter, a 60-s sputtering time did not deposit sufficient Ag-TaN layers or allow full light absorption of the incident visible light.

Fig. 10.24(b) shows the bacterial inactivation kinetics on Ag-TaON polyester under an O_2-N_2-Ar atmosphere. A 6 $\log_{10}$ (99.99%) reduction in bacterial concentration was observed within about 40 min for the Ag-TaON co-sputtered sample for 120 s. Sequential sputtering of Ta and Ag led to slower bacterial inactivation than the co-sputtered samples, as shown in Fig. 10.24(b), trace 4.

The faster bacterial reduction kinetics reported in Fig. 10.24(b) compared with Fig. 10.24(a) can be rationalized considering that reactive sputtering in the presence of O_2 introduces the TaN ionic metal-oxygen species in a matrix of covalent metal–nitrogen bonds.[83] The polarity introduced by these metal-oxygen species results from van der Waals forces composed of permanent dipoles, induced dipoles, and hydrogen bonds. The surface energy of the Ag-TaON surface (Fig. 10.24(b)) is higher than that available on the Ag-TaN (Fig. 10.24(a)) surface because of the presence of ionic Ag-O metal-oxygen species. Fig. 10.24(c) shows that Ag sputtered on polyester did not lead to complete bacterial inactivation even after 6 h of irradiation. Fig. 10.24(d) shows that TaON samples sputtered on polyester for 120 s inactivated bacteria within 90 min. This was two times longer than the time required by Ag-TaON because of an interfacial charge transfer between Ag and TaON.

Fig. 10.25(a) shows an atomic force microscopy (AFM) image for a sputtered polyester–TaON (120 s) sample showing nonuniform TaON grains with sizes of

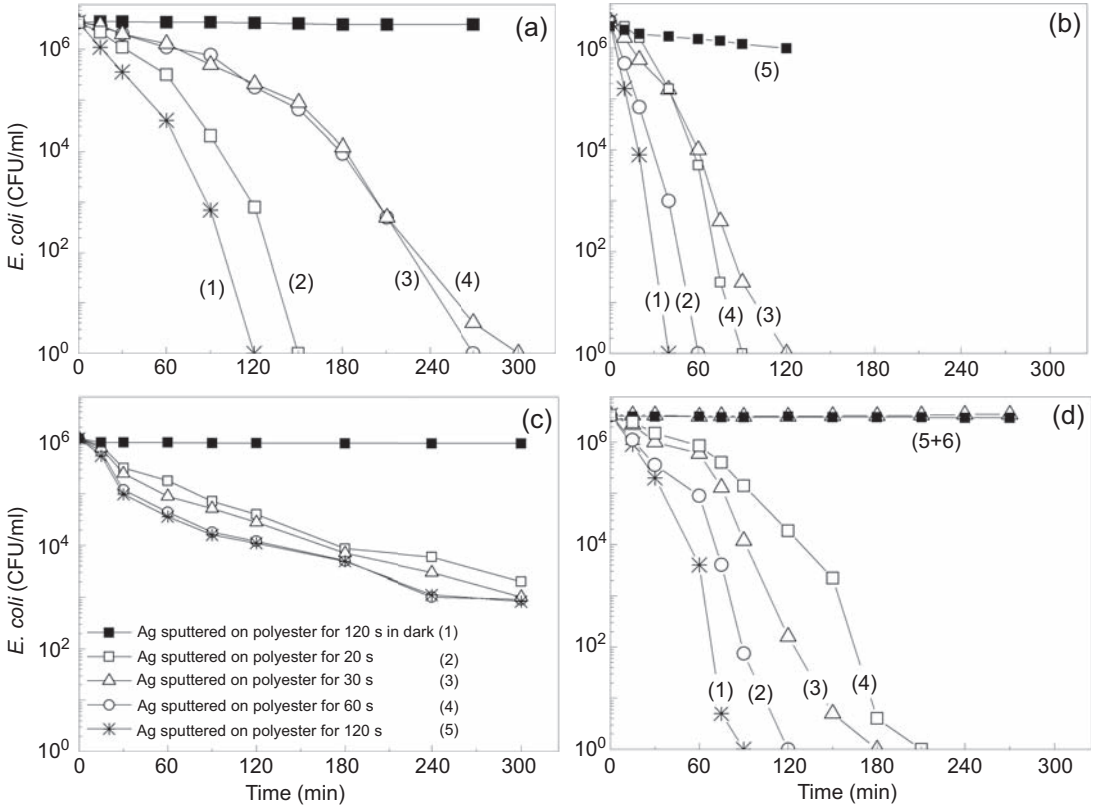

Figure 10.24 *Escherichia coli* bacterial inactivation on TaN, Ag-TaN, TaON, and Ag-TaON sputtered on polyester for different times and irradiated with Osram Lumilux light (400−700 nm) with an output of 4 mW/cm^2. (a)(1) Ag-TaN co-sputtered for 120 s, (2) for 150 s, (3) for 60 s, (4) TaN sputtered for 120 s and (5) Ag-TaN co-sputtered for 120 s in dark. (b)(1) Ag-TaON co-sputtered for 120 s, (2) for 150 s, (3) for 60 s, (4) TaON/Ag sequential sputtered for 120 s TaON/40 s Ag and (5) Ag-TaON co-sputtered for 120 s in dark runs. (c) Ag sputtered on polyester for different times and irradiated with Osram Lumilux light. (d)(1) TaON for 120 s, (2) TaON for 150 s, (3) TaON for 60 s, (4) TaON for 20 s, (5) TaON sputtered on polyester for 120 s in the dark, and (6) polyester alone irradiated with Osram Lumilux light.

Rtimi S, Pulgarin C, Houas A, Sanjines R, Lavanchy J-C, Kiwi J. Coupling of narrow and wide band-gap semiconductors on uniform films in bacterial disinfection under low intensity visible light: implications of the interfacial charge transfer (IFTC). *J Hazard Mater* 2013;**260**:860−868.

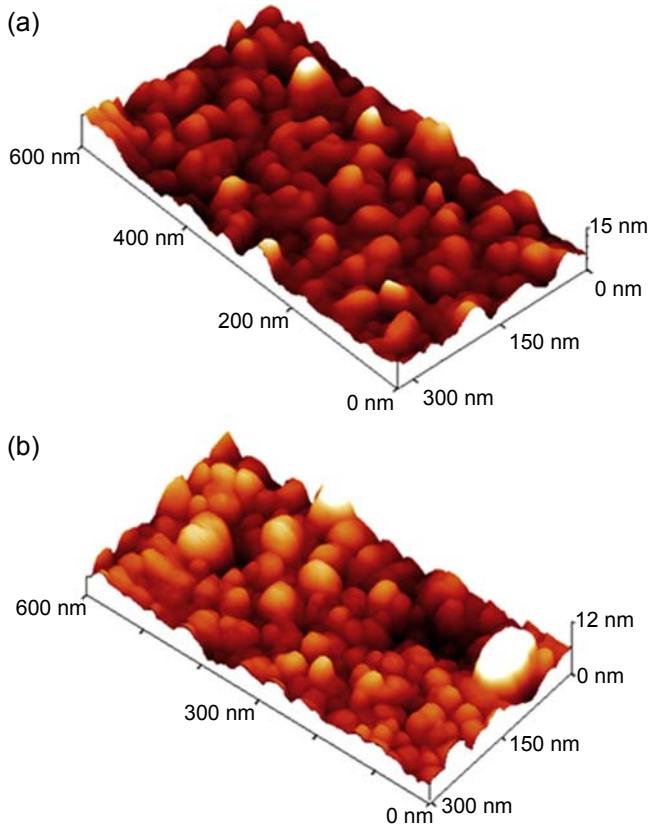

Figure 10.25 Atomic force microscopy image for polyester samples: (a) sputtered with TaON for 120 s and (b) co-sputtered Ag-TaON for 120 s.
Rtimi S, Pulgarin C, Houas A, Sanjines R, Lavanchy J-C, Kiwi J. Coupling of narrow and wide band-gap semiconductors on uniform films in bacterial disinfection under low intensity visible light: implications of the interfacial charge transfer (IFTC). *J Hazard Mater* 2013;**260**: 860−868.

40−60 nm. Fig. 10.25(b) shows the AFM image for a co-sputtered Ag-TaON (120 s) sample with grain sizes of 70−100 nm. The root mean square roughness for the samples TaON and TaON-Ag were 2.2 and 2.7 nm, respectively. An increase in roughness led to a higher CA, reducing the polarity and total surface energy.[84] Increased sample roughness allows for better adhesion of Ag ions, leading to bacterial inactivation (see the XPS section).

The CAs with TaON and Ag-TaON polyester as a function of time after bacterial inactivation are shown in Figs. 10.26(a) and (b). The TaON sample after 2 s shows a CA of 80 degrees, and after 6 s, of 12 degrees. The water droplet disappeared after 10 s. This means that the TaON sample surface becomes completely hydrophilic after 10 s and eliminated any hydrophobic residues left by bacterial inactivation.

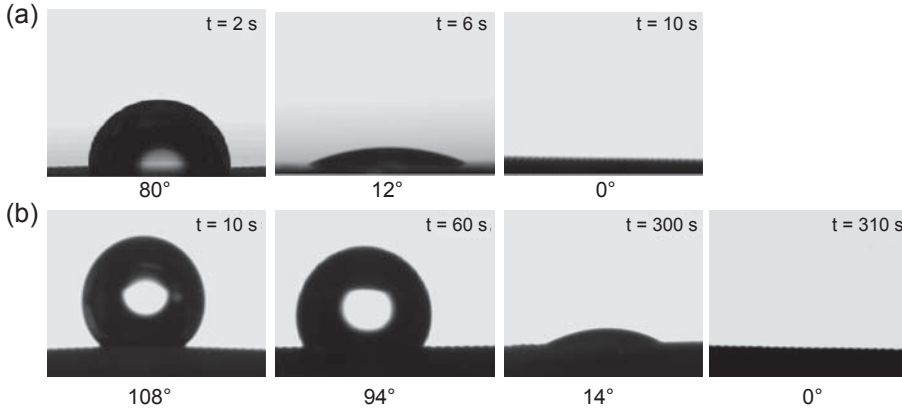

Figure 10.26 Contact angle water droplets as a function of contact time for (a) TaON sputtered on polyester for 120 s and (b) Ag-TaON co-sputtered on polyester for 120 s.
Rtimi S, Pulgarin C, Houas A, Sanjines R, Lavanchy J-C, Kiwi J. Coupling of narrow and wide band-gap semiconductors on uniform films in bacterial disinfection under low intensity visible light: implications of the interfacial charge transfer (IFTC). *J Hazard Mater* 2013;**260**: 860−868.

A water droplet on the polyester alone was observed to disappear by contact with the fabric. Although polyester is hydrophobic, it has a high amount of void areas and porosity promoting water penetration throughout the polyester microstructure. Sputtering TaON decreases the void areas, allowing water penetration and concomitantly increasing the sample hydrophobicity. The amount of O_2 has a role in the CA of the surface. Studies on nitrides/oxynitrides have reported that O_2 photoadsorption introduces highly polar and electronegative groups compared with N_2 changing the electronegativity and electron density of nitrides.[85]

Fig. 10.26(b) shows the CA of the water droplet on the surface of co-sputtered TaON-Ag-polyester samples. A slower decrease in the CA with time was observed for TaON. The CA varied from an initial value of 108 degrees at 10 s to 14 degrees within 300 s and disappeared after 310 s. The surface energy of Ta_2O_5 controls the surface CA.[86] The addition of Ag increases the hydrophobicity in the Ag-TaON surface, leading to longer water absorption times, as shown in Fig. 10.26(b).

The photo-induced interfacial charge transfer from the Ag layers to the TaON layers under visible light irradiation is considered, knowing that (1) the narrow band semiconductor Ag_2O absorption goes up to 880 nm, and (2) the wide band semiconductor Ta_2O_5 absorbs UV light less than 310 nm (Fig. 10.27), which suggests the mechanism for electron injection for charge transfer from Ag_2O into Ta_2O_5. This mechanism considers the potential energy of the semiconductor bands.[84] Silver layers exposed to air water vapor lead to the formation of surface AgOH. The AgOH decomposes spontaneously to Ag_2O (Eq. [10.1]), as mentioned before when discussing the results found for the Ag-TiON photocatalysis. Fig. 10.27 shows that electron injection from Ag_2O to the Ta_2O_5 is thermodynamically favorable. The

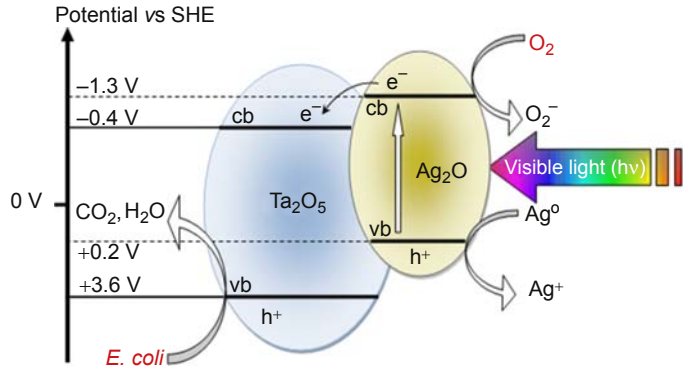

Figure 10.27 Scheme for photo-induced interfacial charge transfer from Ag_2O to Ta_2O_5 under visible light irradiation.
Rtimi S, Pulgarin C, Houas A, Sanjines R, Lavanchy J-C, Kiwi J. Coupling of narrow and wide band-gap semiconductors on uniform films in bacterial disinfection under low intensity visible light: implications of the interfacial charge transfer (IFTC). *J Hazard Mater* 2013;**260**: 860−868.

Ag_2O (cb) is positioned at −1.3 eV NHE and lies above the Ta_2O_5 (cb) at 0.4 eV NHE. The potential 1.7 eV difference provides a considerable driving force inducing a fast electron injection from Ag_2O into Ta_2O_5. Because of the magnitude of this driving potential, the Ag_2O transfers electrons to the Ta_2O_5 cb, hindering the e^-/h^+ recombination in Ag_2O. The values for the potentials for the cb for both semiconductors are only indicative, because in quantum size nanoparticles, band energy shifts have been reported to higher potentials.[73] The reductive character in the quantum-size Ag_2O particles proceeds at a higher energy level than −1.3 eV NHE. The potential energy of the h^+ at the valence band (vb) of Ta_2O_5 (3.6 eV) becomes more positive than the standard reduction potential of HO^o/HO^- of about 1.9 eV. The vb holes h^+ will oxidize the Ta_2O_5 surface-OH to OH^o and this radical subsequently oxidizes *E. coli* in Fig. 10.27. The IFCT charge transfer would be favored by the close contact between Ag and Ta particles co-sputtered on an Ag-TaON (120 s) sample. The higher activity of the coupled semiconductors may be also result from a higher density of defects in their crystallite structure.[87]

The recycling of the co-sputtered TaON/Ag (120 s) sample up to the fifth cycle is seen in Fig. 10.28. The recycling proceeds with no significant loss in activity because the bacterial inactivation time remained the same. The sample was thoroughly washed after each recycling experiment. Reuse of the co-sputtered samples was possible because total bacterial destruction was attained at each cycle. Total destruction of the bacterial residues enables stable sample recycling owing to sample self-cleaning under light irradiation leading to the destruction of the bacterial reduction residues. The N- and C-bacterial residues did not accumulate on the polyester, and rapid catalytic destruction of these elements occurs on the photocatalyst surface. Adventitious hydrocarbons spontaneously adsorb from the air onto the film surface, whereas the O, Ta, N, and Ag percent surface concentration remained stable.[42] Further proof of

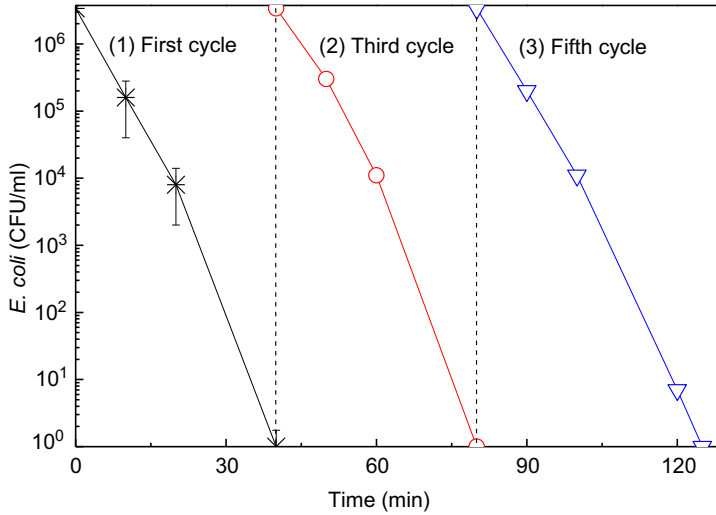

Figure 10.28 Recycling of Ag-TaON (120 s) during five-cycle *E. coli* bacterial inactivation: (1) first cycle, (2): third cycle, and (3) fifth cycle.
Rtimi S, Pulgarin C, Houas A, Sanjines R, Lavanchy J-C, Kiwi J. Coupling of narrow and wide band-gap semiconductors on uniform films in bacterial disinfection under low intensity visible light: implications of the interfacial charge transfer (IFTC). *J Hazard Mater* 2013;**260**: 860–868.

surface self-cleaning is provided by the CA shown in Fig. 10.26(b). That the CA vanishes after 310 s indicates that no hydrophobic compounds remained on the sample surface after the bacterial inactivation cycle.

10.3 Conclusions and future outlook

In this review, we have addressed the deposition of thin uniform adhesive films able to reduce bacteria in the dark and under light within acceptable times and able to work in a repetitive fashion. These films consisted of Ag-nitrides of TiN, ZrN, and TaN. The nitrides were selected for their chemical stability, inertness, and low or nonexistent cytotoxicity.

This chapter presents the design, sputtering (synthesis), bacterial evaluation, and surface characterization of Ag-nitride films on cotton and polyester fabrics. Film preparation was optimized for the most suitable inactivation kinetics of *E. coli* taken as a standard probe, because disinfection kinetics is a major parameter to consider for the potential application of these films in textiles, thin polymer films, glass structures, walls, and metal plates. The approach taken was to seek the systematic, detailed, and comprehensive investigation of a nitride that would be kinetically fast during bacterial reduction. Ag-TaN was found to be a faster Ag-nitride compared with Ag-ZrN and Ag-TiN, respectively, in that order.

In coming years, despite the progress made in this area in the last decade, improvements will be needed in the synthesis of high-quality functionalized nitrides using a more sophisticated approach to prepare nanoparticulate films. Moreover, synthesis and surface engineering of nitrides nanoparticles will be developed involving more complex chemical, physical, and surface functionalization. This may involve innovative composite chemical phases. The improved stability of films will be a common objective to be addressed followed by work on how to translate laboratory findings into large-scale industrial synthesis.

Future work in this area must focus on research on toxicity and may address environmental pollution materials and meta-materials in two- and three-dimensional objects. These same objects may be useful in disinfecting pathogens that can survive for long times in the form of surface biofilms. Biofilms are currently the most common and dangerous way to spread highly infectious pathogens into the environment in pubic places and health-care facilities. New products developed from research in this area could be of interest for industrial applications.

Acknowledgments

We thank the EPFL and Swiss National Science Foundation (SNF) Project (200021-143283/1) for financial support and CIME-EPFL for microscopy experiments. We also thank the COST Action MP1101 and MP1106 for interactive discussions during the course of this study.

References

1. Thüringer Surface and Biomaterials Kolloquium. 13−15 September 2011. Zeulenroda. Germany.
2. Dancer S. The role of the environmental cleaning in the control of hospital acquired infections. *J Hosp Infect* 2009;**73**:378−86.
3. Kramer A, Schwebke I, Kampf G. How long do nosocomial pathogens persist in on inanimate surfaces? *BMC Infect Dis* 2006;**6**:137−46.
4. Noimark S, Dunnill CW, Wilson M, Parkin IP. The role of surfaces in catheter-associated infections. *Chem Soc Revs* 2009;**38**:3435−48.
5. Page K, Wilson M, Parkin IP. Antimicrobial surfaces and their potential in reducing the role of the inanimate environment in the incidence of hospital-acquired infections. *J Mater Chem* 2009;**19**:3819−31.
6. Robin S, Soulimane M, Levelle S. 'Interactions of biofilm−forming bacteria with abiotic surfaces' RSC Nanoscience and Nanotechnology No 21. In: Tofail S, editor. *Biological interacations with surface charge in biomaterials*. RSC; 2012. p. 122−35. Ch. 9.
7. Foster AH, Ditta BI, Varghese S, Steele S. Photocatalytic disinfection using TiO_2: spectrum and mechanism of antimicrobial acivity. *Appl Microbiol Biotechnol* 2011;**90**:1847−68.
8. Fujishima A, Zhang X, Tryck D. TiO_2 photocatalysis and related surface phenomena. *Surf Sci Rep* 2008;**63**:515−82.
9. Pelaez M, Nolan N, Pillai S, Seery M, Falaras P, Kontos A, et al. A review on the visible light active TiO_2 photocatalysis for environmental applications. *Appl Catal B* 2012;**125**:331−49.

10. Liu J, Sonshine D, Shervani S, Hurt D. Controlled release of biologically active Ag from Ag-surfaces. *ACS Nano* 2010;**4**:6903−13.
11. Fox C, Modak M. Antibacterial silver-sulfadiazine. *Antimicrob Agents Chemother* 1974; **5**:582−8.
12. Klasen JH. A historical review of the use if silver in the treatment of burns. Renewed interest for silver. *Burns* 2000;**26**:131−8.
13. Ashrani PV, Mun GL, Hande PM, Valyaveettil S. Cytotoxicity and genotoxicity of Ag-nanoparticles in human cells. *ACS Nano* 2009;**3**:279−90.
14. Holt K, Bard JA. Interaction of Ag^{+} ions with the respiratory chain of *E. coli*: an electrochemical and scanning electrochemical microscopy study of the antimicrobial mechanism of micromolar Ag-ions. *Biochemistry* 2005;**44**:13214−23.
15. Sondi L, Sondi S. Silver nanoparticles as antimicrobial agents: a case study on *E. coli* as a model Gram negative bacteria. *J Coll Interface Sci* 2004;**275**:177−82.
16. Nikaido H. Porins and specific diffusion channels in bacterial outer membranes. *J Biol Chem* 1994;**269**:3905−9.
17. Li X, Nikaido H, Williams K. Silver resistant mutants of *E. coli* display active efflux of Ag-ions and are deficient in porins. *J Bacteriol* 1997;**179**:6127−32.
18. Zhang L, Dillert R, Bahnemann D, Vormoor M. Photo-induced hydrophilicity and self-cleaning: models and reality. *Energy Environ Sci* 2012;**5**:7491−507.
19. Gunawan C, Teoh W, Marquis CP, Lifia J, Amal R. Reversible antimicrobial photo-switching in nanosilver. *Small* 2009;**5**:341−4.
20. Page C, Wilson M, Mordan N, Chrzanowski W, Knowles P, Parkin PI. Study of the adhesion of *Staphylococcus aureus* to coated glass substrates. *J Mater Sci* 2010;**46**:6355−63.
21. Page K, Palgrave R, Parkin PI, Wilson M, Savin S, Chadwick A. Titania and silver titania composite films on glass-potent antimicrobial coatings. *J Mater Chem* 2007;**17**:95−104.
22. Foster AH, Sheel P, Sheel DW, Evans P, Varghese S, Rutschke N, et al. Antimicrobial activity of titania/silver and titania/copper films prepared by CVD. *J Photochem Photobiol A* 2010;**216**:283−9.
23. Dunlop PSM, Sheeran CP, Byrne MJA, McMahon SA, Boyle AM, McGuigan KG. Inactivation of clinically relevant pathogens by photocatalytic coatings. *J Photochem Photobiol A* 2010;**216**:303−10.
24. Yates HM, Brook LA, Ditta IB, Evans P, Foster AH, Sheel WD, et al. Photo-induced self−cleaning and biocidal behaviour of titania and copper oxide multilayers. *J Photochem Photobiol A* 2008;**197**:197−2008.
25. Baghriche O, Sanjines R, Ruales C, Pulgarin C, Stolitchnov I, Zertal A, Kiwi J. Ag-surfaces sputtered by DC and pulsed DC-magnetron sputtering effective in bacterial inactivation: testing and characterization. *Surf Coat Technol* 2012;**206**:2410−6.
26. Baghriche O, Ehiasarian A, Kusiak-Nejman E, Morawski A, Pulgarin C, Sanjines R, et al. Advantages of high power impulse magnetron sputtering (HIPIMS) of silver for improved *E. coli* inactivation. *Thin Solid Films* 2012;**520**:3567−73.
27. Baghriche O, Ehiasarian A, Kusiak-Nejman E, Morawski A, Pulgarin C, Sanjines R, et al. High power impulse magnetron sputtering (HIPIMS) and traditional pulsed sputtering (DCMSP) Ag-surfaces leading to *E. coli* inactivation. *J Photochem Photobiol A* 2012;**227**:11−7.
28. Mejía I-M, Restrepo GJ, Marín M, Sanjines R, Pulgarín C, Mielczarski J, et al. Magnetron-sputtered Ag-modified cotton textiles active in the inactivation of airborne bacteria. *Appl Mater Interfaces* 2010;**2**:230−5.
29. Geranio L, Heuberger M, Nowack E. The behavior of silver nano textiles during washing. *Environ Sci Technol* 2009;**43**:8113−8.

30. Rtimi S, Baghriche O, Pulgarin C, Arutiun E, Bandorf R, Kiwi J. Comparison of the performance HIPIMS sputtered Ag- and Cu-surfaces leading to accelerated bacterial inactivation in the dark. *Surf Coat Technol* 2014;**250**:14−20.
31. Yuranova T, Rincon A, Bozzi A, Parra S, Pulgarin C, Albers P, et al. Antibacterial textiles prepared by RF-plasma and Vacuum-UV mediated deposition of silver. *J Photochem Photobiol A* 2003;**161**:27−33.
32. Yuranova T, Rincon A, Pulgarin C, Laub D, Xanthopoulos X, Mathieu H-J, et al. Performance and characterization of Ag-cotton and Ag/TiO_2 loaded textiles during the abatement of *E. coli*. *J Photochem Photobiol A* 2006;**81**:363−9.
33. Daoud WA. *Self-cleaning materials and surface*. UK: Woodhead Pub. Co; 2013.
34. Kelly P, Li H, Benson P, Whitehead K, Verran J, Arnell R, et al. Comparison of the tribological and antimicrobial properties of CrN/Ag, ZrN/Ag, TiN/Ag, and TiN/Cu nanocomposite coatings. *Surf Coat Technol* 2010;**205**:1606−10 and references therein.
35. Kelly P, Li H, Whitehead K, Verran J, Arnell R, Iordanova I. A study of the antimicrobial and tribological properties of TiN/Ag nanocomposite coatings. *Surf Coat Technol* 2009; **204**:1137−41.
36. Ratova M, West TG, Kelly JP. Optimisation of HIPIMS photocatalytic titania coatings for low temperature deposition. *Surf Coat Technol* 2014;**250**:7−13.
37. Rtimi S, Baghriche O, Sanjines R, Pulgarin C, Ben-Simon M, Lavanchy J-C, et al. Photocatalysis/catalysis by TiN/TiN-Ag surfaces efficient in bacterial inactivation under visible light. *Appl Catal B* 2012;**123−24**:306−15.
38. Rtimi Sami, Baghriche Oualid, Sanjines Rosendo, Pulgarin Cesar, Ben-Simon Michael, Lavanchy Jean-Claude, et al. TiON and TiON-Ag sputtered textile showing antibacterial activity induced by simulated-solar-light. *J Photochem Photobiol A* 2013;**256**:52−63.
39. Baghriche O, Kiwi J, Pulgarin C, Sanjinés R. Antibacterial Ag-ZrN surfaces promoted by Zr and deposited by reactive pulsed magnetron sputtering. *J Photochem Photobiol A* 2012; **229**:39−45.
40. Rtimi S, Pascu M, Sanjines R, Pulgarin C, Ben-Simon M, Lavanchy J-C, et al. ZrNO and ZrNO-Ag co-sputtered surfaces leading to bacterial inactivation under actinic light. Evidence for the oligodynamic effect. *Appl Cat B* 2013;**138-9**:113−21.
41. Baghriche O, Rtimi S, Zertal A, Pulgarin C, Sanjinés R, Kiwi J. Accelerated bacterial reduction on Ag−TaN compared with Ag−ZrN and Ag−TiN surfaces. *App Cat B: Environ* 2015;**174−175**:376−82.
42. Rtimi S, Pulgarin C, Houas A, Sanjines R, Lavanchy J-C, Kiwi J. Coupling of narrow and wide band-gap semiconductors on uniform films in bacterial disinfection under low intensity visible light: implications of the interfacial charge transfer (IFTC). *J Hazard Mater* 2013;**260**:860−8.
43. Ehiasarian A, Münz DS, Hultman L, Hemersson U, Petrov I. Highpower magnetron sputtered CrNx films. *Surf Coat Technol* 2003;**163−164**:267−72.
44. Mathews J. *Epitaxial growth part B*. IBM Thomas Watson Research Center. New York: Academic Press; 1975. p. 382−436.
45. Ehiasarian A. High-power impulse magnetron sputtering and its applications. *Pure Appl Chem* 2010;**82**:1247−58.
46. Kelly JP, Arnell DR. Magnetron sputtering. A review of recent developments and applications. *Vacuum* 2000;**56**:159−72.
47. Burcalova K, Hecimovic A, Ehiasarian P. Ion energy distributions and efficiency of sputtering process in HIPIMS system. *J Phys D Appl Phys* 2008;**41**:115306.
48. Ehiasarian A, Gonzalvo AY, Whitmore DT. Plasma process, time resolved studies of the high power impulse magnetron discharge in mixed Ar and N-atmosphere. *Polym* 2007;**4**:5309−13.

49. Sarakinos J, Alami J, Konstantinidis S. High power pulsed magnetron sputtering: a review on scientific and engineering state of the art. *Surf Coat Technol* 2010;**204**: 1661−84.
50. Lin J, Moore W, Sproul B, Mishra N, Wang J. The structure and properties of Cr-nitride coatings deposited using DC, pulsed DC and modulated pulse power magnetron sputtering. *Surf Coat Technol* 2010;**204**:2230−9.
51. Ch. 9. In: Tofail S, editor. *Biological interactions with surface charge biomaterials*. Robin S, Soulimane T, Lavelle S, editors. *Interactions of biofilm forming bacteria with abiotic surfaces RSC Nanoscience*, **21**; 2012. p. 122−35.
52. Hoffman P. In: *Photocatalytic and superhydrophilic surfaces workshop' PSS. 2013. Manchester Museum*; December 12/13, 2013. p. 7. IP1.
53. Hamilton JWJ, Byrne JA, Dunlop PS. Evaluating the mechanism of visible light activity for N,F-TiO2 using photoelectrochemistry. *J Phys Chem C* 2014;**118**:12206−15.
54. Liu G, Han C, Pelaez M, Dunlop MSP, Byrne AJ, Diounysiou DD. Synthesis, characterization and photocatalytic evaluation of visible light activated C-doped TiO_2 nanoparticles. *Nanotechnology* 2012;**23**:294003.
55. Vasilev K, Cook J, Griesser H. Antibacterial surfaces for biomedical devices. *Expert Rev Med Devices* 2009;**6**:553−67.
56. Seery MK, George R, Floris P, Pillai SC. Silver doped titanium dioxide nanomaterials for enhanced visible light photolysis. *J Photochem Photobiol A* 2007;**189**:258−63.
57. Banerjee S, Pillai S, Falaras P, O'Shea K, Byrne JA, Dionysiou D. New insight into the mechanism of visible light photocatalysis. *J Phys Chem Lett* 2014:2543−54.
58. Allen NS, Edge M, Verran J, Stratton M, Maltby J, Bygott C. Photocatalytic titania based surfaces: environmental benefits. *Polym Degrad Stab* 2008;**93**:1632−46.
59. Caballero L, Whitehead KA, Allen NS, Verran J. Inactivation of *Escherichia coli* on immobilized TiO_2 using fluorescent light. *J Photochem Photobiol A Chem* 2009;**202**:92−8.
60. Francolini I, Donelli G. Prevention and control of biofilm based medical device related infections. *FEMS Immunol Med Microbiol* 2010;**59**:227−38.
61. Ewald A, Glükermann S, Thull R, Gbureck U. Antimicrobial titanium/silver PVD coating in titanium. *Biochem Eng* 2006;**5**:22−32.
62. Wagner CD, Riggs WM, Davis EL, Müllenberg, editors. *Handbook of x-ray photoelectron spectroscopy*. Minnesota: Perkin-Elmer Corporation Physical Electronics Division; 1979.
63. Shirley D. Corrections of electrostatic charged species in XSP-spectroscopy. *Phys Rev* 1972;**B5**:4709−16.
64. Nogier J, Delamar M, Ruiz P, Gratzel M, Thampi R, Kiwi J. X-Ray photoelectron spectroscopy of TiO_2/V_2O_5. *Catal Today* 1994;**20**:109−23.
65. Rtimi S, Baghriche O, Pulgarin C, Sanjines R, Kiwi J. New evidence for sputtered TiN-surfaces able to inactivate bacteria under visible light. *RSC Adv* 2012;**2**:8591−5.
66. Wisbey A, Gregson J, Tuke M. Application of PVD TiN coating to Cr-Mo based surgical implants. *Biomaterials* 1987;**8**:9477−80.
67. Thiel J, Pakstis L, Buzby S, Raffi M, Ni C, Pochan DJ, et al. Antibacterial properties of silver-doped titania. *Small* 2007;**3**:799−803.
68. Benn T, Westerhoff P. Nanoparticle silver released into water from commercially available sock fabrics. *Environ Sci Technol* 2008;**42**:133−9.
69. Probst J, Gbureck R, Thull R. Binary nitride and oxynitride PVD coatings on titanium for biomedical applications. *Surf Coat Technol* 2007;**148**:226−33.
70. Wan L, Li J, Feng J, Sun F, Mao Z. Improved optical response and photocatalysis for N-doped titanium oxide films prepared by oxidation of TiN. *Appl Surf Sci* 2007;**253**: 4764−7.

71. Lee S, Yamasue S, Okumura H, Ishihara K. Effect of oxygen and nitrogen concentration of nitrogen doped TiOx film as photocatalyst prepared by reactive sputtering. *Appl Cat A* 2009;**371**:179−90.
72. Park H, Kim H, Kim J, Lee J, Hahn J, Gu M, et al. Silver-ion mediated reactive oxygen species generation affecting bactericide activity. *Water Res* 2009;**43**:1027−32.
73. Ida Y, Watase T, Shinagawa M, Watabanbe M, Chigane M, Inaba A, et al. Direct electrodeposition of 1.46 eV band-gap silver (I) oxide semiconductor films by electro-generated acid. *Chem Mater* 2000;**20**:1254−6.
74. Yuand J, Ran R. Some optical properties of silver peroxide (AgO) and silver oxide (Ag_2O) films produced by chemical-bath deposition. *Energy Environ Sci* 2011;**4**:1364−71.
75. Irie H, Miura S, Kamiya K, Hashimoto K. Efficient visible light-sensitive photocatalysts: grafting Cu(II) ions onto TiO_2 and WO_3 photocatalysts. *Chem Phys Lett* 2008;**457**:202−5.
76. Liu CP, Hsieh HJ, Li C, Chang KY, Yang CC. Dissolution of Cu nanoparticles and antibacterial behaviors of TaN-nanocomposite thin films. *Thin Solid Films* 2009;**517**: 4956−60.
77. Hsieh HJ, Tseng CC, Chang KY, Chang YS, Wu W. Antibacterial behavior of TaN-Ag nanocomposite thin films with and without annealing. *Surf Coat Technol* 2008;**202**: 5586−9.
78. Emeline A, Kateva G, Rudakova V, Ryabchuk N, Serpone N. Spectroscopic and photoluminescence studies of a wide band gap insulating material: powdered and colloidal ZrO_2 sols. *Langmuir* 1998;**14**:5011−22.
79. Sayama K, Arakawa H. Photocatalytic decomposition of water and photocatalytic reduction of CO_2 over ZrO_2 catalyst. *J Phys Chem* 1993;**97**:531−3.
80. Jeyachandran Y, Narayandass S. The effect of titanium nitride coatings on bacterial adhesion. *Trends BiomaterArtif Organs* 2009;**24**:90−3.
81. Geetha C, Sebareeswaran A, Mohanan P. Preclinical evaluation of TiN and TiN coated Ti-materials. *Toxic Mech Methods* 2012;**22**:144−50.
82. Bondarenko O, Juganson K, Ivask A, Kasemets K, Mortimer M, Kahru A. Toxicity of Ag, Cuo and ZnO nanoparticles to selected environmental relevant test organisms and mammalian cells in vitro: a critical review. *Arch Toxic* 2013;**87**:1181−2000.
83. Creutz C, Brunschwig B,S, Sutin N. Interfacial charge transfer absorption: application to metal-molecule assemblies. *Chem Phys* 2006;**324**:244−58.
84. Chun W, Ishikawa S, Fujisawa H, Takata T, Kondo N, Hara M, et al. Conduction and Valence band positions of Ta_2O_5, TaON, and Ta3N5 by UPS and Electrochemical methods. *J Phys Chem B* 2003;**107**:1798−803.
85. Mohamed H, Bahneman D. The role of electron transfer in photocatalysis: fact and fictions. *Appl Cat B* 2012;**128**:91−104.
86. Biedermann G, Sillen G. Studies on the hydrolysis of metal-ions. Part 30. A critical survey of the solubility equilibria of Ag_2O. *Acta Chem Scand* 1960;**14**:07−17.
87. Nozik A. In: *A photo-effects at the semiconductor electrolyte interface*. *ACS Symposium Series*, **140**. Washington. USA: Amer. Chem. Soc; 1960.

DLC thin films for implantable medical devices

11

T.I.T. Okpalugo, A.A. Ogwu
University of the West of Scotland, Paisley, Scotland, United Kingdom

11.1 Introduction

There is currently a growing need to implant medical devices into the human body to achieve improved healthcare conditions. Areas of application include artificial heart valves, catheters, stents, guide wires, hip joints, intraocular lens, dental implants and biosensors. Most current biomaterial implants are not completely biocompatible, haemocompatible or noncytotoxic. Many potential implant materials have to be investigated for cellular protein and human deoxyribonucleic acid interactions (Narayan, 2005; Hasebe et al., 2007; Prodan, 2010). The implants can trigger a number of inflammatory responses and thrombogenic reactions (Ogwu et al., 2008; Okpalugo et al., 2004, 2006, 2008) and life-threatening coating failure (Ogwu et al., 2003). Platelet aggregation and thromboembolism are usually avoided through lifelong treatment with anticoagulants. This situation has led to the need to apply haemocompatible and biocompatible coatings to improve the performance of biomedical implant materials. This chapter is based on one of the most promising coatings identified for this purpose to date, ie, diamond-like carbon (DLC). Love et al. (2013) highlighted the potential of DLC films as coatings for implant materials.

11.2 Materials and technologies

Diamond and graphite are two crystalline allotropes of carbon. Both have similar thermodynamic stability ($\Delta G = 0.04$ eV at 300 K) although separated by a large kinetic barrier (Robertson, 1992). The large varieties of noncrystalline carbons and hydrocarbons that exist can be classified in terms of their atom density, hydrogen content and their sp^3-sp^2 carbon contents relative to diamond, graphite and hydrocarbon polymers (Angus, 1987; Angus and Hayman, 1988). DLC was first deposited by Aisenberg and Chabot in 1971. Today, different forms of plasma-enhanced chemical vapour deposition (PECVD) methods are used for the deposition of DLC. Among PECVD methods, parallel plate radiofrequency (RF) reactor systems are the most common type employed. PECVD is commonly used to produce hydrogenated DLC (hydrogenated amorphous carbon, a-C:H) with high film thickness uniformity (Ohja, 1982) and coating continuity over a large substrate area (Catherine, 1991).

Thin Film Coatings for Biomaterials and Biomedical Applications. http://dx.doi.org/10.1016/B978-1-78242-453-6.00011-0

The filtered cathodic vacuum arc (FCVA) method of DLC deposition has the potential to produce very hard films (Gupta and Bhushan, 1995; Shi et al., 1997) and hydrogen-free DLC (Fallon et al., 1993; Chhowalla et al., 1995; Shi et al., 1997). However, the macroparticle filters in FCVA used to prevent particle contamination (Anders et al., 1994; McKenzie et al., 1997) in the film limits the film thickness uniformity on large area substrates and the repeatability of the deposition. Thus, although hydrogenated DLCs (a-C:H) produced by PECVD are not as mechanically hard as the nonhydrogenated DLCs (ta-C) produced by FCVA, the improved tribochemical properties offered by a-C:H lead to improved wear resistance in hard−disk interface, for example. If sufficient vapour pressure is applied to any hydrocarbon, it can be used for DLC film deposition in a PECVD chamber. Commonly, acetylene is used. Other precursors include benzene, butane, cyclohexane, ethane, ethylene, hexane, isopropane, methane, pentane, propane and propylene. In this study, acetylene was used as a precursor gas and tetramethylsilane vapour for silicon incorporation. Gaseous nitrogen was used for postdeposition N_2 doping of DLC.

11.3 Major challenges to using diamond-like carbon for implantable medical devices: cellular and blood interactions

11.3.1 The biocompatibility and haemocompatibility of DLC and Si-DLC

In this subsection, the biocompatibility and haemocompatibility of DLC and Si-DLC as reported in the literature are reviewed under specific interaction with various cells for possible differences in particular cell behaviour. We also take into consideration whether the cells used for the test are human or animal cells and whether the test is carried out in vitro, ex vivo and/or in vivo. These tests can equally be categorized under cell counting to estimate the number of cells (cell adhesion and/or cell aggregation for platelets) and assays to determine the level of enzymes from the cells. An additional category is the interaction of DLC with plasma proteins and with blood cells in haemocompatibility tests. Some cells that exist in the blood when used for toxicity tests or examined for cellular proliferation on the biomaterial are actually a test of biocompatibility rather than haemocompatibility, although almost all haemocompatibility tests may be used equally to assess the degree of biocompatibility. Biocompatibility tests may not be used to assess haemocompatibility.

11.3.1.1 Species differences

1. The dog model is relatively inexpensive and convenient but it may lack relevance to humans.
2. The baboon model is relatively expensive and unavailable but it is relevant to humans.
3. Similarity of platelet function, the concentration and activity of clotting factors, and the haematocrit should be the primary determinants for deciding which species are most relevant to humans.

11.3.1.2 Cell specificity

Different cells perform different functions, and thus their interactions with the same biomaterial may differ. Specific biomaterial–cellular interactions can be compared with those of another cell line if the cell type, origin and function are similar.

11.3.2 Definitions and general aspects of biocompatibility

Biocompatibility can be defined as 'the ability of a material to perform with an appropriate host-response in a specific application' (William, 1989). Four components of biocompatibility have been identified:

1. The initial events that take place at the interface, mainly including the adsorption of constituents of tissue fluids onto the material surface (Andrade, 1988);
2. Changes in the material as a result of its presence in the tissues, usually described under the headings of corrosion or degradation (William, 1985);
3. The effects that the material have on the tissue, the local host-response (William, 1987a);
4. The sequelae of the interfacial reaction that are seen systematically or at some remote sites (William, 1981).

Possible tests useful for evaluation of biocompatibility are listed below.

11.3.2.1 Toxicity evaluation of polymers for biomedical applications (Peppas, 1982)

LEVEL I
- Initial screening and quality control of polymers
- Agar overlay response of materials
- Agar overlay response of materials extracts
- Inhibition of cell growth by water extracts of materials
- Intradermal irritation test for materials extract and leachable components

LEVEL II
- Initial evaluation of novel biomaterial
- Tissue culture test on materials
- Tissue culture test on materials extracts
- Cell growth in contact with test materials
- Haemolytic activity test
- Intramuscular implantation of material
- Test of osmotic fragility of erythrocytes
- In vitro mutagenicity test
- Test of material extracts by perfusion of isolated rabbit heart

11.3.3 Diamond-like carbon interaction with specific cells in vitro

When a cell comes into contact with a biomaterial, the degree of interaction can generally be taken as adsorption, contact, attachment and/or spreading, as illustrated in Fig 11.1.

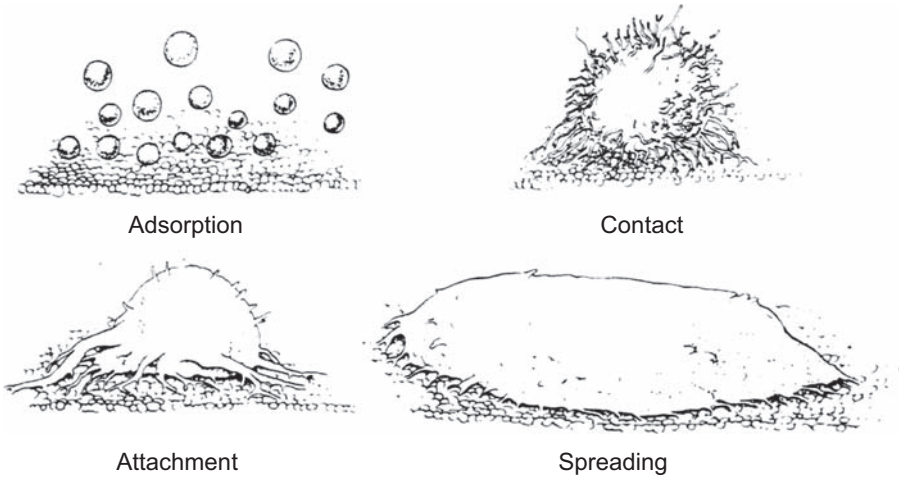

Figure 11.1 Various degrees of cellular–biomaterial interaction (Grinnell, 1976; 1978).

For activated platelets, five stages of spreading can be described according to the increasing degrees of activation (Goodman et al., 1984):

1. Round or discoid with no pseudopodia
2. Dendritic, early pseudopodia with no flattening
3. Spread-dendritic, intermediate pseudopodia with one or more flattened pseudopodia, but with no spreading of the cell body
4. Spreading, late pseudopodia with the cell body beginning to spread
5. Fully spread morphology; the cell is well-spread with no distinct pseudopodia.

11.3.3.1 Diamond-like carbon interactions with fibroblasts in vitro

The body's connective tissues can be classified as connective tissue proper (subdivided into loose and dense connective tissue proper), fluid connective tissues (subdivided into blood and lymph) and supporting connective tissues (subdivided into the cartilage and the bone). Fibroblasts are the most abundant permanent residents of the connective tissue proper and are the only cells always present in it. Fibroblasts secrete hyaluronans (a polysaccharide derivative) and proteins, both of which interact in the extracellular fluid to form proteoglycans that make ground substances viscous. They also secrete protein subunits that interact to form large extracellular fibres that could create loose/open framework or densely packed framework.

Human fibroblasts

Dowling et al. (1997) carried out a cell adhesion test on a DLC (obtained by saddle beam deposition) partially coated, 2.8-cm-diameter, stainless-steel disc using

human fibroblast cell line and reported very good cell adhesion and good spreading of the cells on the coated as well as the uncoated surfaces of the disc.

Allen et al. (1994) tested DLC-coated polystyrene (coating obtained by the low-temperature dual ion beam technique using a saddle field source) and control uncoated polystyrene tissue culture plates with primary cultured human synovial fibroblast and reported that there was no statistically significant difference in cell growth on both samples. The lactate dehydrogenase (LDH) assay of the fibroblasts also indicated that DLC caused no significant level of cell toxicity compared with the uncoated samples (Allen et al., 1994).

Mouse fibroblasts

Hauert et al. (1997) examined the interaction of mouse fibroblast (3T3 cell line) with a-C:H:Si (0.2 atm% to 22.5 atm% silicon addition) obtained with PACVD system and reported that the cells proliferated well on the coated culture dishes and that no influence such as a toxic effect was observed from the Si-C bonds present on the surface to the growth and proliferation of the cells after 2 days of incubation. Hauert et al. (1997) concluded that the toxic effect described by Allen et al. (1995) was caused by bulk Si-C bonds not present in the a-C:H:Si thin film.

McColl et al. (1993) and Parker et al. (1993, 1994) studied the interaction of DLC with 3T3-1 mouse fibroblasts in vitro. The 3T3-1 cell viability in inserts in Millicell-PCF membrane with DLC and without it were determined in their study by trypan blue dye exclusion; the researchers reported that the cells grew well in both the control membrane inserts and the DLC-coated sample, which implies that DLC is not cytotoxic to growing 3T3-1 cells.

After exposing mouse fibroblasts (C3H10T1/2 cell line) to DLC-coated, 24-well culture plates obtained by saddle field source (using acetylene, butane or propane source gas) over 7 days, Thomson et al. (1991) reported that there was no significant difference in the release of LDH in any of the coated samples and the uncoated control sample. Also, their photomicrographic morphological examination confirmed that there was no cellular damage to the coated samples compared with the uncoated control samples (Thomson et al., 1991).

Murine fibroblast

Dowling et al. (1997) conducted a cytotoxicity study using murine fibroblast to examine DLC-coated alloy, a titanium alloy and a plastic sample using scanning electron microscopy (SEM) after 6-, 24- and 48-h incubation periods. According to Dowling et al. (1997), good cell morphology, adhesion, density and spreading were observed on both the DLC-coated alloy and the plastic, but the titanium alloy surface exhibited much cell death; thus, the DLC coating acts as a barrier between the titanium alloy and the murine fibroblast cell line and demonstrates a low level of cytotoxicity.

11.3.3.2 Diamond-like carbon interaction with osteoblasts in vitro

Osteoblasts are bone-forming cells and have a major role in mineralization leading to osseointegration of a prosthesis.

Allen et al., 2001 investigated the effect of DLC coatings (obtained by fast-atom bombardment from a hexane precursor) deposited on polystyrene 24-well tissue culture plates on two osteoblast-like cell lines cultured on uncoated and DLC-coated plates for up to 72 h, by measuring the production of three osteoblast-specific marker proteins: alkaline phosphatase, osteocalcin and type I collagen. According to Allen et al. (2001), there was no evidence that the presence of the DLC coating had an adverse effect on any of these measured parameters, which are indicative of metabolic processes in these osteoblast-like musculoskeletal system cells.

Schroeder et al. (2000) evaluated a new surface coating for bone-related implants by combining the hardness and inertness of a-C:H (DLC, obtained by a combination of RF plasma and DC magnetron sputtering deposition techniques) films with the biological acceptance of titanium. They incorporated different amounts of titanium (7−24 atm%) into a-C:H films by a combined RF and magnetron sputtering setup. Their X-ray photoelectron spectroscopy of air-exposed a-C:H/titanium (a-C:H/Ti) films revealed that the films were composed of TiO_2 and TiC embedded in and connected to an a-C:H matrix. They performed cell culture tests using primary adult rat bone marrow cell cultures to determine effects on cell number and on osteoblast and osteoclast differentiation. According to Schroeder et al. (2000), addition of titanium to the carbon matrix leads to cellular reactions such as increased proliferation and reduced osteoclast-like cell activity, whereas these reactions were not seen on pure a-C:H films and on glass control samples. Thus, they concluded that a-C:H/Ti could be a valuable coating for bone implants, by supporting bone cell proliferation while reducing osteoclast-like cell activation (Schroeder et al., 2000).

Du et al. (1998) reported, based on their study of the interaction between osteoblasts (isolated from 4-day-old Wistar rats) and DLC as well as carbon nitride (CN) thin films (obtained by ion beam−assisted deposition (IBAD) technique), that the osteoblasts attach, spread and proliferate on both DLC and CN sample surfaces without apparent impairment of cell physiology.

Allen et al. (1994) also reported that DLCs interact well with human ‘osteoblast-like’ cell line SaOS-2. When they compared the growth of human osteoblasts in both the DLC-coated and uncoated polystyrene plates, they found a similar level of growth observed in both samples, and the osteoblasts adhered well to the DLC samples and produced extensive filopodia when viewed under the scanning electron microscope (Allen et al., 1998). The LDH assay of the osteoblast-like cells also indicated that DLC caused no significant level of cell lysis or toxicity compared with the uncoated samples (Allen et al., 1994).

11.3.3.3 Diamond-like carbon interaction with kidney cells in vitro

Human embryonic kidney cells

Lu et al. (1993) observed the interaction of DLC (obtained by IBAD) with human embryonic kidney (HEK-293) cells using a haemocytometer for cell counting and trypan blue dye exclusion to assess HEK-293 cell viability in DLC-coated P-35 dishes. According to Lu et al. (1993), HEK-293 cells grew well; there was no delayed attachment to the DLC-coated dishes compared with the control, and both the cells growing in the DLC-coated and control dishes had a cell viability of 60% on the first day of incubation that increased to greater than 90% on the second day of incubation.

Baby hamster kidney cells

Evans et al. (1991) examined the interaction of DLC obtained using a saddle field source and baby hamster kidney cells and reported good cell adhesion on the coated surfaces, indicating good cell compatibility.

Mutagenicity evaluation of diamond-like carbon

Dowling et al. (1997) performed a mutagenicity test (Ames test) on DLC coatings on stainless-steel samples coated on both sides and uncoated samples using five strains of *Salmonella typhimurium* bacteria (TA-98, TA-100, TA-1535, TA-1537 and TA-102) with and without metabolic activation in accordance with the method originally reported by Ames et al. (1975). According to Dowling et al. (1997), neither the DLC and the stainless-steel samples were mutagenic because they induced no significant increase in the number of revertants of the five strains of *S. typhimurium* tested.

11.3.4 Haemocompatibility of diamond-like carbon

11.3.4.1 The blood

The blood is a fluid connective tissue with a matrix called plasma. Plasma proteins are in solution unlike the other connective tissues that occur in insoluble forms like fibres; thus, proteins in solution in the plasma make the plasma slightly denser than water. The blood is composed of plasma (46–63%) and formed elements (37–54%). The plasma is composed of water (92%), plasma proteins (7%) and other solutes (1%). The formed elements of blood are composed of red blood cells (RBCs) (99.9%), and the remaining 0.1% is platelets and white blood cells (WBCs). The water dissolves and transports organic and inorganic molecules, formed elements and heat from one part of the body to the other. The plasma proteins are composed of albumins (60%), globulins (35%), transport ions, hormones, and lipids, which have an immune function, fibrinogen (4%) and regulatory proteins (<1%: enzymes, proenzymes and hormones). Other solutes of blood are composed of electrolytes (major ones are Na^+, K^+, Ca^{2+}, Mg^{2+},

Cl^-, HCO_3^-, HPO_4^{2-} and SO_4^{2-}), organic nutrients (lipids:fatty acids, cholesterol, glycerides; carbohydrates, mainly glucose; and amino acids) and organic wastes (eg, urea, uric acid, creatinine, bilirubin, ammonium ions). Albumin is the major contributor to the osmotic pressure of plasma and transport lipids and steroid hormones. Fibrinogen is an essential component of the blood-clotting system that can be converted to insoluble fibrin (Martini, 2001).

11.3.4.2 Definitions and general aspects of haemocompatibility

Following the considerations of the Macromolecule Division of the International Union of Pure and Applied Chemistry, the European Society for Biomaterials Consensus Conference suggested that the definition of blood compatibility should take into account the following (William, 1987b):

- activation of the blood coagulation system at the blood−material interface;
- the response of the immune system induced after blood−material contact;
- other tissue responses that appear as consequences of blood−material contact.

At the conference, they proposed defining four properties characteristic of the biomaterial's blood compatibility:

- Thrombogenicity
- Antithrombogenicity
- Complement activation ability
- Complement inhibition ability

An understanding of the process of coagulation occurring during injury to the blood vessel wall such as a cut may give some background on the events that may apply to the blood−material interaction. The process of haemostasis, the cessation of bleeding and establishment of a framework for tissue repair, consists of three phases: vascular, platelet and coagulation, all of which occur in a chain reaction. The vascular and platelet phases occur within a few seconds after the injury, but the coagulation phase does not start until 30 s or more after the vessel wall has been damaged. When the blood vessel wall is cut in an injury, for example, contraction of the vessel's smooth muscle is triggered locally (vascular spasm), which decreases the diameter of the vessel wall. This vascular spasm and constriction help to stop the loss of blood and last for about 30 min, a period known as the vascular phase. During this phase, changes occur in the local vessel endothelium: Endothelial cells contract and expose the underlying basement membrane to the bloodstream; endothelial cells begin releasing chemical factors and local hormones (eg, adenosine diphosphate (ADP), tissue factor, prostacyclin, endothelin); and then the endothelial cell membranes become 'sticky'. Platelets then begin to attach to the sticky endothelial surfaces, the basement membrane and the exposed collagen fibres. This attachment marks the start of the platelet phase of the haemostasis: platelet adhesion, activation, platelet aggregation and the formation of a platelet plug. Platelet aggregation begins within 15 s after an injury occurs. As the platelets arrive at the injury site, they become activated, change shape, become spherical and develop cytoplasmic processes that extend towards adjacent

platelets. The platelets begin releasing ADP (which stimulates platelet aggregation and further secretion from the platelets), thromboxane A2 and serotonin (which stimulate vascular spasm), clotting factors, platelet-derived growth factor (PDGF) (a peptide that promotes vessel repair) and calcium ions (required for platelet aggregation and by several steps in clotting process). The platelet phase proceeds rapidly because the ADP, thromboxane and calcium ions that each arriving platelet releases stimulate further platelet aggregation. Finally, the blood coagulation occurring during the coagulation phase involves a complex sequence of steps that leads to the conversion of circulating fibrinogen into the insoluble protein fibrin, forming a growing network that covers the surface of the platelet plug (Martini, 2001). Listed below are various hypotheses proposed for blood–biomaterial interactions by several authors.

Interfacial blood–biomaterial interactions: some 'conventional wisdom' and some 'unresolved hypotheses' (adapted partly from Hoffman, 1982; Vroman, 1977; NHLBI Guidelines 1980):

General hypothesis

The overall process of in vivo thrombogenesis, thromboembolization and subsequent endothelialization on a foreign surface are dominated by surface properties rather than haemodynamics (or by haemodynamics rather than by surface properties).

Material

1. A material with a critical surface tension of about 25 dyn/cm will have a low thrombogenic potential.
2. A small negative surface charge lowers material thrombogenicity.
3. High-water-content materials have a low thrombogenic potential owing to the lowered free energy of the hydrated interface.
4. High-water-content materials may continually expose a fresh foreign interface, leading to a high thrombogenic potential; however, they also tend to exhibit low thrombo-adherence owing to their low interfacial free energy.
5. H-bonding group in a surface leads to strong interactions with biological species and therefore endows a surface with a high thrombogenic potential.
6. A surface with a high apolar/polar ratio is desirable for low thrombogenic potential.
7. Thrombus is nucleated in regions of the surface where a specific spatial distribution of specific chemical (electrostatic) groups is present.
8. Flexible (as opposed to stiff) polymer chain ends and loops in the material interface lower the thrombogenic potential of the foreign surface.

Material and haemodynamics

1. Thrombi will always be generated at surface imperfections because of flow disturbances, surface compositional differences and/or trapped gas bubbles.
2. Smooth surfaces in arterial flow conditions may release thromboemboli before they grow too large to be dangerous. (Corollary: high shear rates can detach thromboemboli before they have grown too large.)
3. Certain rough and textured surfaces may form and retain fibrin and thrombus, leading to a 'passivated' surface.

Haemodynamic

1. Thrombi will always be generated in regions of low flow or flow separation.
2. Low shear rates can lead to regional accumulation of activated protein coagulation factors and subsequent thrombogenesis on a nearby surface.
3. High shear rates can be destructive to blood cells (eg, shear rates can initiate platelet activation and lead to thrombogenesis).
4. In a tubular flow field, the platelets tend to accumulate preferentially near the wall and the red cells near the central core. (Corollary: the red cells enhance the rate of collision of platelets with the wall.)

Erythrocytes and leucocytes

1. The role of leucocytes in thrombogenesis may be related to their ability to recognize a particular biomaterial surface as 'foreign' after certain proteins and/or platelets have adhered to that surface.
2. RBCs may have only a minor role in the thrombogenic process.

Blood cells and protein surface tensions

1. Surface tensions of cells and proteins can be measured by a variety of techniques.
2. Surface tension of cells and proteins are relatively high; they tend to be hydrophilic in their natural state (Neumann et al., 1983).

Heparinized surfaces and drugs

1. The natural endothelium is nonthrombogenic because endothelial cells produce the powerful antiplatelet aggregation agent prostacyclin (PGI_2).
2. There may be synergistic interaction between specific drug therapies and specific biomaterials such that reduced drug regimens may be indicated combined with the use of specific biomaterials in devices or implants.
3. Heparinized surfaces must leach heparin to be nonthrombogenic. (General corollary: 'immobilized' antithrombogenic drugs are ineffective unless they leach into the flowing blood.)
4. Heparinized surfaces that bind antithrombin III do not need to leach heparin to be nonthrombogenic.

Calcification

1. Calcification may be initiated at points of high mechanical strain in a foreign material (such as blood pump diaphragm).
2. Calcification in foreign materials is a biological process; γ-carboxyl glutamic acid is a necessary amino acid in one key protein involved in this process.

Surface charges

1. Under normal conditions, the blood vessel wall and blood cells are negatively charged (potentials across the blood vessel wall were measured using Ag-AgCl reference electrodes; under normal conditions, the inner electrode was negative with respect to the outer electrode) (Srinivasan and Sawyer, 1970).
2. Injury to the blood vessel wall reduces the magnitude of the negative charge density and often even causes a reversal in the sign of the surface charge (injury is generally accompanied by thrombus formation) (Sawyer and Pate 1953).

3. A decrease in pH reduces the negative charge density of the blood vessel wall and of blood cells. The isoelectric point occurs at about pH 4.7 (Sawyer and Srinavasan, 1967). (The pH of the electrolyte has a significant effect on the surface charge of the blood vessel walls. At about pH 4.7 the blood vessel wall has zero surface charge, and below this pH the blood vessel wall is positively charged.)
4. Antithrombogenic drugs increase the magnitude of the negative charge density, whereas thrombogenic drugs have the opposite effect and in many cases even reverse its signs (electrophoresis measurements conducted on RBCs and WBCs in the presence and absence of antithrombogenic and coagulant drugs show similar actions of these drugs on both blood cells and the blood vessel wall) (Srinivasan and Sawyer, 1969).
5. Positively charged prosthetic materials are thrombogenic whereas negatively charged surfaces tend to be nonthrombogenic; the higher and more uniform the negative charge density, the better is the chance of the material being nonthrombogenic (Martin et al., 1968). (Tubes of various metals were implanted in the canine thoracic aorta or the canine thoracic inferior vena cava. Metals that have negative standard electrode potential tended to function longer in dogs than those that registered positive potential. With insulator materials using streaming potential to determine surface charge characteristics and using untreated chemically treated and electrically treated Teflon tubes, the more negative the surface, the more useful the material.)

11.3.4.3 Diamond-like carbon interaction with specific cells and proteins in vitro

Bruck pointed to the importance of species-related haematological differences in experimental animals in the proper assessment of biomaterials for human use. He pointed out that 'the terms "biocompatibility" and "haemocompatibility" are often used inaccurately to denote the performance of biomaterials based on single or few in-vitro tests; these tests frequently ignoring considerations of haemo-rheological parameters, damages to the reticulo-endothelial system, and haematological species-related differences' (Bruck, 1977).

DLC deposited on stainless-steel and titanium alloys used for components of artificial heart valves has been found to be biologically and mechanically capable of improving their performance (McHargue, 1991). Devlin et al. (1997) showed improvements to carbon−carbon composite prostheses with DLC coating.

11.3.4.4 Diamond-like carbon interaction with endothelial cells

Endothelium is nature's haemocompatible surface, and the performance of any biomaterial designed to be haemocompatible must be compared with that of the endothelium (Gordon, 1986). Endothelial haemocompatibility can be considered according to three areas: the interaction between the endothelium and circulating cells (mainly platelets and leucocytes − close interactions between erythrocytes and endothelium are rare); the modulation of coagulation and fibrinolysis by endothelium; and other activities that affect the circulating blood or the vascular wall. Under normal circumstances, platelets do not interact with the endothelial cells − that is, platelet adhesion to the vessel wall and the formation of platelet aggregates do not normally take place except when required for haemostasis. Hence, the surface of endothelial cells does not

promote platelet attachment (Gordon, 1986). The formation of platelet aggregates in close proximity to the endothelium is also rendered difficult by PGI_2, a powerful inhibitor of platelet aggregation secreted by the endothelial cells. Prostacyclin can be secreted by endothelial cells in culture as well as by isolated vascular tissue (Moncada and Vane, 1982). The vascular endothelium is now known to be a dynamic regulator of haemostasis and thrombosis, with the endothelial cells having multiple and active (rather than passive) roles in haemostasis and thrombosis (Gimbrone, 1986; Gimbrone, 1987). Many functions of endothelial cells appear to be antithrombotic in nature. Several of the 'natural anticoagulant mechanisms', including heparin-antithrombin, protein C-thrombo-modulin and tissue plasminogen activator, are endothelial-associated. Among proteins on the endothelial surface is antithrombin III (Chan and Chan, 1981), which catalyses the inactivation of thrombin by heparin. Endothelial cells also have heparin sulphate and dermatan sulphate (glycosaminoglycan) on their surfaces (Busch et al., 1979), which are known to have anticoagulant activity. On the other hand, endothelial cells also appear capable of active prothrombotic behaviour under some extreme conditions of anticoagulation, because endothelial cells synthesize adhesive cofactors such as von Willebrand factor (Jaffe, 1982), fibronectin and thrombospondin (Mosher et al., 1982). Endothelial cells is now known to have crucial roles in a large number of physiological and pathological processes (Folkman and Haudenschild, 1980; Tonnesen et al., 1984; Kubota et al., 1988; Pauli and Lee, 1988; Picker et al., 1989; Pober, 1988; Berg et al., 1989; Rice and Bevilacqua, 1989; Springer, 1990; Hynes, 1992). Most of these physiopathologic events take place at the microvasculature (capillary beds), which constitutes the vast majority of the human vascular compartment. Thus, it becomes vital to conduct haemocompatibility studies using microvascular endothelial cells. This is also vital because not all endothelial cells are alike. Endothelial cells derived from the microvascular structures of specific tissues differ significantly from large-vessel endothelial cells (Folkman et al., 1979; Keegan et al., 1982; Charo et al., 1984; Gerritsen, 1987; Fujimoto and Singer, 1988; Kubota et al., 1988). The study of human microvascular endothelial cells has been limited because these cells are difficult to isolate in pure culture, are fastidious in their in vitro growth requirements and have a very short lifespan, undergoing senescence at passages 8–10. Ades et al. (1992) overcame these problems by transfecting and immortalizing human dermal microvascular endothelial cells (HMECs). These cells, termed CDC/EU.HMEC-1 (HMEC-1), retain the characteristics of ordinary endothelial cells (HMEC) and can be passaged up to 95 times; they grow to densities three to seven times higher than ordinary HMEC and require much less stringent growth medium (Ades et al., 1992). HMEC-1 is just like ordinary endothelial cells and exhibits typical cobblestone (or polyhedral) morphology when grown in a monolayer culture.

Van Wachem et al. (1985) reported that in their investigation of the in vitro interaction of human endothelial cells (HEC) and polymers with different wettabilities in culture, optimal adhesion of HEC generally occurred onto moderately wettable polymers. Within a series of cellulose type of polymers, cell adhesion increased with increasing contact angle of the polymer surfaces (van Wachem et al., 1985). Moderately wettable polymers may exhibit a serum and/or cellular protein adsorption

pattern that is favourable for growth of HEC (van Wachem et al., 1985). Van Wachem et al. (1989) reported that moderately wettable tissue culture poly(ethylene terephthalate) (TCPETP), with a contact angle of 44° as measured by captive bubble technique, is a better surface for adhesion and proliferation of HEC than hydrophobic poly(ethylene terephthalate) (PETP), with a contact angle of 65°. This suggests that vascular prostheses with a TCPETP-like surface will perform better in vivo than prostheses made of PETP (van Wachem et al., 1989).

11.3.4.5 Diamond-like carbon interaction with platelets

Platelets are small, granulated bodies 2−4 μm in diameter. They are round to spindle-shaped cytoplasmic fragments containing enzymes and pre-enzymes but no nucleus. There are about 300,000/μL platelets in the circulating blood and they normally have a half life of about 4 days. Membranes of platelets contain receptors for collagen, vessel wall von Willebrand factor and fibrinogen. When a blood vessel wall is severed, platelets adhere to the exposed collagen, laminin and von Willebrand factor in the wall via integrins. Unlike platelet aggregation, this process of platelet adhesion does not require platelet metabolic activity (Ganong, 1995). However, binding of platelets to collagen initiates platelet activation (this can also be induced by ADP or thrombin). The activated platelets change shape, put out pseudopodia and discharge granules that attract other platelets to stick to other platelets, a process known as platelet aggregation. The cytoplasm of platelets contains actin, myosin, glycogen, lysosomes and two kinds of granules (dense granules and α-granules) that may be released after platelets are activated. The dense granules contain nonprotein substances (includes serotonin, ADP and other adenine nucleotides) that are secreted in response to platelet activation and the α-granules contain secreted proteins other than hydrolases in lysosomes, which include clotting factors and PDGF. Released platelet granules generate inflammatory response to injury; the WBCs (leucocytes) are attracted by selectins and bind to integrins on endothelial cells, leading to their extravasation through the blood vessel walls (Ganong, 1995).

Platelet adhesion hypothesis

1. Platelets adhesion on a foreign surface is a necessary precursor to platelet aggregation on that surface.
2. High platelet adhesion on a foreign surface is bad.
3. In vitro platelet adhesion is related directly to in vivo thrombus formation and embolization on foreign surfaces.
4. Platelets adhere with different strengths on different sites.
5. Platelet adhesion and release reactions at foreign interfaces occur when specific platelet membrane receptor sites ‘recognize’ specific groups on the foreign surface. (Corollary: platelet adhesion is not a random process.)
6. Some platelet release factors (eg, serotonin and ADP from dense granules) enhance platelet aggregation on foreign surfaces, whereas the roles of others (platelet factor IV with its heparin-neutralizing activity and β-thymoglobulin from α-granules) remain to be clarified.

Chen et al. (2002) varied acetylene to argon flow ratios in the DLC obtained with plasma immersion ion implantation deposition technique. According to Chen et al., the blood compatibility of DLC depends on the sp^3 to sp^2 ratio rather than absolute sp^3 or sp^2 content and blood compatibility becomes worse with a larger sp^3 to sp^2 ratio (Chen et al., 2002).

Krishnan et al. (2002) performed a quantitative analysis of I-125 radio-labelled platelets to examine platelet adhesion (using radioscintigraphy) on titanium and DLC-coated titanium and showed that DLC-coated titanium exhibited lower platelet adhesion compared with uncoated titanium.

Cui and Li (2000) also studied platelet interaction with DLC-coated polymethylmethacrylate (PMMA) intraocular lenses and uncoated PMMA intraoccular lenses (IOLs). Their result showed that DLC-coated PMMA-IOLs had lower platelet adhesion compared with the uncoated sample (Cui and Li, 2000).

Gutensohn et al. (2000a,b) studied the interaction of stents coated on both inner and outer surfaces with DLC (obtained by plasma-induced cold deposition) and human platelets. In their study they used DLC to achieve a uniform protective coating to reduce the release of metal ion, platelet activation and thrombogenicity. Cytometric flow analyses revealed a significantly higher increase in mean channel fluorescence intensity for platelet activation-dependent antigens CD62p and CD63 in uncoated stents compared with DLC-coated stents ($p < 0.05$). Patients undergoing coronary angioplasty and stenting procedures are known to be at higher risk for reocclusion and restenosis of vessel when platelets express increased numbers of activation-dependent antigens (Gawaz et al., 1996; Inoue et al., 1996). Of all of the antigens they analysed, P-selectin (GMP-140) seemed to have a key role and appeared to be most closely associated with an increase in thrombotic risk (Gawaz et al., 1996; Inoue et al., 1996). Using atomic adsorption spectrophotometry and inductively coupled plasma mass spectrometry analyses, they showed that there was a significant release of metallic ions in the uncoated stents compared with DLC-coated stents. As a consequence of reduced metal ion release owing to DLC coating, platelet activation was significantly lower in DLC-coated stents compared with the uncoated stents under otherwise identical experimental conditions (Gutensohn et al., 2000a,b).

Alanazi et al. (2000) evaluated the interaction of polycarbonate-coated DLC (obtained with CVD under varied deposition conditions), segmented polyurethane (usually used to fabricate medical devices including artificial hearts) and an amphiphilic block copolymer composed of 2-hydroxyethylmethacrylate (HEMA) and styrene (St) (HEMA/St; an excellent nonthrombogenic polymer was used as a negative control) with platelets in whole human blood. They used the parallel plate flow chamber and epifluorescent video microscopy (EVM) using whole human blood containing mepacrine-labelled platelets perfuse at a wall shear rate of 100 s^{-1} at 1-min intervals for 20 min. In their assessment of the optical penetration of their EVM system and the activation and adhesion of platelets, they concluded that the activation of platelets on PC-DLC compared with the other biomaterials was minimal, surface roughness before and after the coating was applied to blood-contacting devices was insignificant (16−23 nm), the contact angle improved after DLC coating, the contact angle and chemical composition were independent of

film thickness, defects in DLC films may have been caused by elevated substrate and blood compatibility depended on deposition conditions (Alanazi et al., 2000).

Jones et al. (1999) studied the interaction between rabbit platelets and components of a Ti−TiN−TiC−DLC multilayer system. They adopted an interlayer approach to achieve adequate adhesion between DLC coatings deposited by plasma-assisted CVD and titanium substrate. The substrate, interlayers and DLC were assessed for haemocompatibility and thrombogenicity using a dynamic blood method and interactions with rabbit blood platelets, respectively. The adhesion, activation and morphology of the platelets were determined by stereological techniques using SEM. The coatings produced no significant haemolytic effect compared with the medical-grade polystyrene control. In contrast to the DLC coating, all of the interlayers showed a slight tendency towards thrombus formation during the later stages of incubation (Jones et al., 1999).

Dion et al. (1993) evaluated the in vitro platelet retention of the new prosthetic heart valve that was designed by FII Company and Pr. Baudet, composed of Ti6Al4V titanium alloy coated with DLC (obtained by CVD). The retention and adhesion of platelets was evaluated by analyzing radioactivity on the exposed wall of test or control tubes through which a blood cell suspension containing ^{111}In-labelled platelets had circulated. Their results showed that on DLC/Ti6Al4V, platelets adhered twice the amount that they did on the reference material (a silicone medical-grade elastomer the behaviour of which in contact with blood is the same as that observed with the National Institutes of Health-recommended polydimethyl siloxane) (Dion et al., 1993).

11.3.4.6 *Diamond-like carbon interaction with blood cells that are not involved with the clotting process*

Going strictly by the definition of haemocompatibility, apart from endothelial cells and platelets that are directly involved in the process of thrombosis and antithrombosis, although they are present in the blood, the other blood cells can be used to assess only biocompatibility instead of haemocompatibility because they are not directly involved in thrombus formation and/or prevention of thrombus formation. Thus, the interaction of DLC with other blood cells such as neutrophils, lymphocytes, monocytes and erythrocytes (RBCs) can only give an indication of biocompatibility and not really ‘haemocompatibility’.

11.3.4.7 *Diamond-like carbon interaction with erythrocytes (RBCs)*

Higson et al. (1995a,b) examined biocompatibility and substrate diffusion limiting properties for a range of DLC (obtained from a saddle field source) coated porous polycarbonate membranes (nominal pore size of 0.01 μm) and haemodialysis membranes in whole blood. According to Higson et al. (1995a,b), after 30-min exposure to unstirred whole blood, the uncoated polycarbonate showed RBCs (and possibly other blood cells) adherent to the membrane surface, whereas in the DLC-coated membranes there was much reduced surface adherence of RBCs and proteins, although some

deposition of amorphous materials occurred. They also found that glucose sensors employing DLC-coated outer covering membranes were found to have experienced smaller losses of response after exposure to whole blood (Higson et al., 1995a,b).

Dion et al. (1993) also evaluated the in vitro RBC retention of the new prosthetic heart valve that designed by FII Company and Pr. Baudet, which is composed of Ti6Al4V titanium alloy coated with DLC (obtained by CVD). The retention/adhesion of RBC was evaluated by analyzing radioactivity on the exposed wall of test or control tubes through which a blood cell suspension containing ^{99m}Tc-labelled RBCs had circulated. According to Dion et al. (1993) the red cell retention, which may have resulted from either poor rinsing or morphological irregularities, led to greater platelet retention; that mechanical entrapment accounted for only 0.07% of red cell retention for silicone and 0.08% for DLC/Ti6Al4V.

11.3.4.8 *Diamond-like carbon interaction with human haematopoietic myeloblasts in vitro*

Haematopoietic myeloblasts are young blast cells derived from progenitor cells in the bone marrow responsible for generating new WBC-granulocytes (neutrophils, basophils and eosinophils).

ML-1 Cells

ML-1 human haematopoietic myeloblasts were used in the study of Lu et al. (1993) to assess the biocompatibility of DLC. Using the haemocytometer for cell counting and trypan blue dye exclusion to determine cell viability, Lu et al. (1993) found that ML-1 cells cultured in DLC-coated P-35 dishes proliferated well compared with ML-1 cells growing in uncoated control dishes, and there was no sign indicating cellular differentiation occurring among ML-1 cells growing on the DLC-coating dishes.

11.3.4.9 *Diamond-like carbon interactions with granulocytes (neutrophils, basophils or eosinophils) in vitro*

Granulocytes are WBCs containing granules (granules can be acidic, basic or neutral, thereby giving rise to different types of granulocytes, neutrophils, basophils and eosinophils) which are also responsible for combating infections. Neutrophils and eosinophils are also called microphages.

Neutrophils (polymorphonuclear leucocytes or polymorphs)

Neutrophils are the most abundant WBC, numbering an average of 4150 cells/μL (50−70% of the total number of WBCs). They are round cells with a lobed nucleus (usually two to five lobes) that may resemble a string of beads and cytoplasm containing large pale inclusions. Their granules are neutral and difficult to stain with either acidic or basic dyes. Their function is phagocytic, engulfing pathogens or debris in tissues and releasing cytotoxic enzymes and chemicals (lysosomal enzymes and bactericidal compounds). They measure about 12 μm in diameter

and are the first of the WBCs to arrive at an injury site. High neutrophil adhesion produce negative effect on tissue biocompatibility, as this is indicative of high tissue inflammation.

Based on their study of neutral granulocyte−neutrophil interaction with DLC (obtained by IBAD technique) coated PMMA IOLs, Li et al. (1999) reported that DLC-coated PMMA IOLs exhibit lower neutrophil adhesion compared with uncoated PMMA IOLs.

Eosinophils (acidophils)

Eosinophils are another type of granulocyte with cytoplasms that contains large granules that generally stain bright red with a red dye eosin, and can also stain with other acid dyes, hence also known as acidophils. The size of eosinophils is similar to that of neutrophils (about 12 μm). Eosinophils have bilobed nucleus and make up approximately 2−4% of the WBC population. They are phagocytic and engulf antibody-coated or marked foreign substances. Their primary mode of attack is the exocytosis of toxic compounds, including nitric oxide, and cytotoxic enzymes, onto the surface of their targets. They are attracted to site of injury and so an increase in their number may indicate inflammation, allergy, etc.

Basophils

Basophils are another type of granulocytes with numerous granules that stain darkly with basic dyes. They measure 8−10 μm in diameter and make up only about 1% of WBCs. Basophils migrate to injury sites and cross the capillary endothelium to accumulate in the damaged tissue, where they discharge granules that contain histamine (dilates blood vessels) and heparin (prevents clotting). They enhance local inflammation at the sites of injury and other chemicals that attract eosinophils and other basophils to the area of injury.

11.3.4.10 Diamond-like carbon interaction with monocytes (macrophages) in vitro

Monocytes also fall into the WBC category primarily produced in bone marrow. The monocytes are 'agranular-leucocytes' (agranulocytes); that is, they lack abundant, deeply stained granules, although they also contain vesicles and lysosomes that are much smaller compared with those of the granulocytes. They are very large cells (about 15 μm in diameter, nearly about two times the diameter of RBCs) with a kidney bean−shaped nucleus and abundant pale cytoplasm. They constitute about 2−8% of the population of circulating WBCs. Monocytes move from flowing blood to the tissues after 1−2 days. When monocytes enter the tissue, they become known as macrophages and are responsible for fighting foreign bodies or pathogen and debris by engulfing and inactivating and digesting them in a process known as phagocytosis. They are aggressive phagocytes, often attempting to engulf debris as large as or larger than their size. When activated, they release chemicals that attract and stimulate neutrophils, monocytes and other phagocytic cells, as well as fibroblasts

to the region of injury. The fibroblasts then begin producing scar tissue that walls off the injured area.

Linder et al. (2002) studied the adhesion, cytoarchitecture and activation of primary human monocytes and their differentiated derivatives, macrophages, on DLC (obtained by RF PACVD using a methane—helium mixture: 1.5 vol %/98.5 vol %) coated glass coverslips using immunofluorescence. According to Linder et al. (2002), the adhesion of primary monocytes to a DLC-coated coverslip is slightly but not significantly enhanced compared with uncoated coverslips, whereas the actin and microtubule cytoskeletons of mature macrophages show normal development. The activation status of macrophages, as judged by polarization of the cell body, was not affected by growth on a DLC surface; thus, DLC shows good indication for biocompatibility to blood monocytes in vitro. It is therefore unlikely that contact with a DLC-coated surface in the human body would cause the cells to elicit an inflammatory reaction (Linder et al., 2002).

Allen et al. (1994) reported that DLC-coated polystyrene (coating obtained by the low-temperature dual ion beam technique using a saddle field source) culture plates produced good macrophage (murine macrophage cell line, IC-21) cell proliferation with a statistically significant faster growth rate (observed at the 48- and 72-h time points) compared with uncoated polystyrene, and with no evidence of cytoplasmic vacuolation, membrane damage or excessive macrophage cell death. Their LDH assay also indicated that no significant increase in LDH release from cells grown on DLC-coated surfaces compared with cells grown on control surfaces. Thus, DLC caused no significant level of cell toxicity compared with the uncoated samples (Allen et al., 1994).

By measuring the level of lysosomal enzymes *N*-acetyl-D-glucosaminidase released (enzyme is usually released as part of inflammatory reaction) in cell culture medium by macrophages (mouse peritoneal macrophage) after the cells interacted with DLC, Thompson et al. (1991) reported no significant difference in the amount of enzyme detected in the DLC-coated samples (using a saddle field source and different source gases: acetylene, butane or propane) compared with the uncoated control tissue culture sample (24-well tissue culture plates). This implies that DLC is not cytotoxic and may not have elicited an inflammatory reaction. This was also corroborated by their LDH assay, which indicated that there was no statistically significant different level of LDH detected for the DLC-coated samples compared with the uncoated samples.

11.3.4.11 Diamond-like carbon interaction with lymphocytes

Lymphocytes are also 'agranular-leucocytes' (agranulocytes) lacking abundant and deeply stained granules. In a blood smear, they are seen as a thin halo of cytoplasm around a relatively large nucleus. In diameter, they are slightly larger than RBCs. Lymphocytes account for 20—30% of the WBC population of blood. Some lymphocytes are in circulation (a small percentage) whereas others are in various tissues, organs and lymphatic system. Three classes of lymphocytes exist in the circulating blood: the T cells (responsible for cell-mediated immunity), the B cells (responsible for humoral immunity) and the natural killer (NK) cells (responsible for immune

surveillance; they are important for preventing cancer, and are sometimes known as large granular lymphocytes).

11.3.4.12 Diamond-like carbon interaction with plasma proteins and cell adhesion proteins/molecules

Dion et al. (1993) examined labelled albumin plasma protein adhesion on DLC-coated Ti6Al4V and silicone elastomer and reported that DLC can adhere more to albumin than to medical-grade elastomer.

Nonadhesive/adhesive protein ratios: albumin/fibrinogen ratios

Platelet adhesion depends on the albumin/fibrinogen ratio: The higher the albumin/fibrinogen ratio, the lower the number of adhering platelets, and hence the less risk of platelet aggregation and of thromboembolism. The albumin/fibrinogen ratio for DLC is 1.24, and it is 0.76 for silicone elastomer (Dion et al., 1993). According to Dion et al. (1993) these two ratios allow us to consider that platelet adhesion would be weaker on DLC than on silicone elastomer, but in fact the opposite occurred, which they thought could be explained by the large dispersion of results in the percentage of platelets retained owing to the device concept itself.

Cui and Li (2000) also studied the adhesion of plasma proteins on DLC-coated, CN-coated PMMA and uncoated PMMA using radioactive targeted proteins. They reported an albumin/fibrinogen ratio of 1.008 for DLC, 0.49 for CN and 0.39 for PMMA (Cui and Li, 2000).

11.3.4.13 In vivo studies on the biocompatibility and haemocompatibility of diamond-like carbon

Allen et al. (2001) implanted DLC-coated cobalt-chromium cylinders in intramuscular locations in rats and in transcortical sites in sheep. Their histological analysis of specimens retrieved 90 days after surgery showed that the DLC-coated specimens were well tolerated in both sites (Allen et al., 2001).

Fournier et al. (2001) showed from their clinical and angiographic data that the hydrogenated silicon carbide coating of the Tenax coronary stent may indeed have a beneficial role in patient outcome, and should therefore be evaluated by prospective clinical trials. They implanted the prostheses (231 Tenax stents) in 206 patients (62 ± 5 years) in patients' left anterior descending (51%) and right coronary arteries (36%). Their results showed that revascularization was complete in 70% and elective in 80%, and implantation was direct in 25% of the patients, and that the procedure was successful in all lesions, reducing stenosis from $62 \pm 16\%$ to $16 \pm 10\%$ and increasing the minimal luminal diameter from 0.81 ± 0.40 to 2.61 ± 0.59 mm. Also, thrombolysis in myocardial infarction grade flow was reduced in 30% but normalized after the stent in all but one patient. They also reported that the incidence of cardiac events was minimal: There was one patient whose one acute thrombosis (0.5%) resolved by a new angioplasty and one patient with non-Q myocardial infarction (0.5%); and finally

at the 6-month clinical follow-up, 10% of patients had symptoms of angina greater than class II (Fournier et al., 2001).

De Scheerder et al. (2000) investigated in vivo bio-interaction with one particular class of modified DLC coatings: diamond-like nanocomposite coatings (DLN) (or Dylyn, Bekaert, Kortrijk, Belgium). Coated or uncoated stents were randomly implanted in two coronary arteries of 20 pigs so that each group contained 13 stented arteries. Pigs underwent a control angiogram at 6 weeks and were then killed. The researchers performed a quantitative coronary analysis before and immediately after stent implantation, and at 6 weeks using the semiautomated Polytron 1000 system (Siemens, Erlangen, Germany). They also performed a morphometry using a computerized morphometric program and their angiographic analysis showed similar baseline selected arteries and poststenting diameters. At 6-week follow-up, they discovered no significant difference in minimal stent diameter and their histopathological investigation revealed a similar injury score in the three groups. According to De Scheerder et al. (2000), inflammatory reactions increased significantly in the DLN-DLC coating group, thrombus formation decreased significantly in both coated stent groups and neointimal hyperplasia decreased in both coated stent groups; however, the difference with the uncoated stents was not statistically significant and area stenosis was lower in the DLN-coated stent group than in the control group ($41 \pm 17\%$ vs $54 \pm 15\%$; $p = 0.06$). In their conclusion, they indicated that the diamond-like nanocomposite stent coatings are compatible, resulting in decreased thrombogenicity and decreased neointimal hyperplasia, and that covering this coating with another DLC resulted in an increased inflammatory reaction and no additional advantage compared with the single-layer diamond-like nanocomposite coating (De Scheerder et al., 2000).

Tran et al. (1999) reviewed the mechanical heart valve's (MHV) thrombogenicity and pointed out that the application of surface modification technology to reduce the incidence of thrombus formation on MHV is a novel undertaking requiring collaboration within the bioengineering and cardiothoracic surgery fields. From reviewing results of recent and past investigations, and their own preliminary study with DLC coating and plasma or glow discharge treatment (GDT) of MHV, they identified and discussed several potentially beneficial effects that may reduce the extent of valve-related thrombogenesis by surface modification: DLC and GDT may affect the surfaces of MHV in many ways, including cleaning of organic and inorganic debris, generating reactive and functional groups on the surface layers without affecting their bulk properties, and making the surfaces more adherent to endothelial cells and albumin and less adherent to platelets; therefore, these different effects of surface modification, separately or combined, may transform the surfaces of MHV to be more thromboresistant in the vascular system (Tran et al., 1999).

Dowling et al. (1997) implanted two DLC-coated and uncoated stainless-steel cylinders into both cortical bone (femur) and muscle (femoral quadriceps) sites of six adult (> 40 kg) sheep for 4 weeks (three sheep), and the rest for 12 weeks. According to Dowling et al. (1997), after explantation of the implants and pathological/histological examination of the implanted cylinders, no macroscopic adverse effect was observed on both the bone and the muscles of the sheep.

Yang et al. (1996b) examined in vivo interactions of discs coated with TiN, DLC (deposited on SS316L disc using PVD) and of pyrolytic carbon (PyC) films implanted into the descending aorta of anaesthesized sheep (six animals) for 2 h. They evaluated the three different samples simultaneously in each animal. After explantation, they examined the thrombus-free area on the disc with close-up photography and planimetry, and the test surfaces with SEM. Yang et al. (1996b) found that there were many leucocytes adherent, activated and spread onto PyC and DLC, but on TiN the erythrocytes were mainly adherent.

11.4 Examples

11.4.1 Medical implant and biomedical applications of diamond-like carbon

DLC is chemically inert and impermeable to liquids. Therefore, it could protect biological implants against corrosion and serve as a diffusion barrier. DLC films are considered for use as coatings of metallic as well as polymeric biocomponents to improve their compatibility with body fluids (Lettington, 1991; Evans et al., 1991; Grill, 1999). The potential biomedical application of DLC and modified DLC includes surgical prostheses of various kinds: intracoronary stents (Gutensohn et al., 2000a,b) and prosthetic heart valves (Zheng et al., 1991; Dion et al., 1993; Yang et al., 1996a,b; Jones et al., 2000). The new prosthetic heart valve designed by FII Company and Pr. Baudet is composed of a Ti6Al4V titanium alloy coated with DLC (Dion et al., 1993). When artificial heart organ polymers used to make heart organs are compared with DLC-coated polymers, these polymers seem to show higher complement activation compared with their DLC counterpart (polycarbonate substrates coated with DLC, PC-DLC compared with Tecoflex, polyurethane) (Alanazi et al., 2000). DLC and modified DLC can be used in blood-contacting devices (eg, rotary blood pump) (Alanazi et al., 2000).

In orthopaedics, DLC can be used as coatings for orthopaedic pins (Lettington, 1991) and coatings in hip implants (eg, femoral heads) (Maizza et al., 1999; Dowling et al., 1997; Veli-Matti Tiainen, 2001). DLC can reduce the wear of the polyethylene cup by a factor of 10−600 when used on metal implants to form a DLC-on-DLC sliding surface. The wear (and the amount of particles causing a foreign body reaction) is 10^5−10^6 lower than metal-on-metal pairs. The corrosion of a DLC-coated metal implant can be 100,000 times lower than in an uncoated one. DLC can diminish bone cement wear by a factor of 500, which can improve bone cement to implant bonding (Butter and Lettington, 1995; Dowling et al., 1997; Veli-Matti Tiainen, 2001).

In urological dialysis (haemodialysis), DLC-coated microporous polycarbonate and DLC-coated dialysis membranes showed that DLC imparted enhanced enzyme electrode performance (Higson and Vadgama, 1995a; 1995b). DLC has also been reported to do well in both organ (Du et al., 1998) and cell culture (Cui and Li, 2000) compared with materials conventionally used for this purpose. DLC can also be used as an active barrier against attack by microorganisms and against biodeterioration of advanced

technological devices operating in closed spaces of satellites, aircraft, and submarines, for example (Ivanov-Omskii et al., 2000), and as good protectors against environmental pollutants and atmospheric waste (Dyuzhev et al., 1996). In addition, nanocrystallite copper-modified DLC has been reported to have a fungicidal effect (Ivanov-Omskii et al., 1996).

11.5 Future trends

11.5.1 Diamond-like carbon in prostheses (orthopaedic)

Santra et al (2012), Van Recum (1999) and Dearnaley et al. (2005) reported on the performance of DLC in orthopaedic applications, such as coatings on hip, knee and joint implants subjected to friction and wear. Typically, when polyethylene is used in these applications, estimates are put at around 10^{10} particulates per year. These particulates are phagocytized, leading to osteolysis, granulomatosis lesions and bone resorption, finally resulting in aseptic loosening and pain in patients. Sheeja et al. (2005) and Lappalainen (2005) reported reduced wear rates on Co-Cr hip implants when coated with DLC, which has led to a reduction in the potential for reactions causing aseptic loosening.

11.5.2 Diamond-like carbon in surgical devices (laparoscopy)

Jones et al. (2010) reported investigating the use of a DLC coating in minimally invasive keyhole surgery. They reported investigating the effect of coating an aluminium alloy-based support for lightweight laparoscopic assist equipment. A lightweight material is required for surgical devices requiring retraction, which gives aluminium a considerable advantage over stainless steel. They reported improved performance during surgical processes such as cholecystectomy (gall bladder removal), and in exploratory techniques for the diagnosis of cancer, when this device was coated with DLC. They conducted diffusion barrier studies by immersing their RF PECVD-coated aluminium substrates in an aggressive sodium hydroxide solution. They investigated for the presence of aluminium in the solute by atomic absorption spectroscopy. Sharma et al. (2009) and Crapper et al. (1976) previously suggested that aluminium leads to the enhancement of neurodegeneration and is a potential risk factor in Alzheimer disease. However, reports by Foncin et al. (1987), Verstraeten et al. (2008) and Iregen et al. (2001), based on studies conducted on metal workers exposed to high levels of aluminium, indicated that even when such workers exhibited high levels of aluminium in their blood and urine, this did not necessarily result in a detrimental effect on their neurobehavioural performance. The prospect of an adverse risk when aluminium is used in minimally invasive surgical devices seems to justify the need to coat these devices with DLC or similar coatings to reduce possible adverse reactions and improve biocompatibility and haemocompatibility. The preliminary investigation by Jones et al. (2010) showed promise when silicon-modified DLC

was used to coat aluminium-based laparoscopic equipment based on reported initial clinical trials.

11.5.3 Surface-functionalized drug eluting stents

Okamoto et al. (2008) considered the potential for using DLC coatings to replace polymers in drug eluting stents to overcome the challenge of adhesion between the polymer and the metal stent. They investigated the potential of overcoming this challenge by using silicon-doped DLC coatings that have the additional advantage of supporting surface functionalization through carbon bonding. They reported applying their silicon-doped DLC films on drug eluting stents as coatings with improved adhesion to the metal stents. Nitta et al. (2008) further demonstrated the possibility of attaching amino and carboxyl groups onto DLC surfaces by plasma treatment. They reported zeta potential measurements indicating a negatively charged DLC surface when carboxyl groups are on the DLC surface and a positively charged surface when an amino group is on the coated surface.

References

Ades, E.W., Candal, F.J., Swerlick, R.A., George, V.G., Summers, Susan, Bosse, D.C., Lawley, T.J., 1992. J. Invest. Dermatol. 99, 683–690.
Aisenberg, S., Chabot, R., 1971. J. Appl. Phys. 42, 2953.
Alanazi, A., Nojiri, C., Noguchi, T., et al., 2000. ASAIO J. 46 (4), 440–443.
Allen, M., Butter, R., Chandra, L., Lettington, A., Rushton, N., 1995. Biomed. Mater. Eng. 5 (3), 151–159.
Allen, M., Law, F.C., Rushton, N., 1994. Clin. Mater. 17, 1–10.
Allen, M., Myer, B., Rushton, N., 1998. Diam. Rel. Mater. 7, 482–485.
Allen, M., Myer, B., Rushton, N., May 1, 2001. J. Biomed. Mater. Res. 58 (3), 319–328.
Ames, B.N., McCann, J., Yamasaki, E., 1975. Mutat. Res. 31, 347–367.
Anders, S., Anders, A., Brown, I., 1994. J. Appl. Phys. 75 (10), 4894–4899.
Andrade, J.D. (Ed.), 1988. Surface and Interfacial Aspect of Biomedical Polymers. Protein Adsorption, vol. 2. Plenum, New York.
Angus, J.C., Hayman, C.C., 1988. Science 241, 913.
Angus, J.C., 1987. Proc. Eur. MRS 17, 179.
Berg, E.L., Goldstein, L.A., Jutila, M.A., Nakache, M., Picker, L.J., Streeter, P.R., Wu, N.W., Zhou, D., Butcher, E.C., 1989. Immunol. Rev. 108, 1–18.
Bruck, S.D., 1977. Biomat. Med. Dev. Art. Org. 5 (1).
Busch, C., Ljungman, C., Heldin, C.-M., Waskson, E., Obrink, B., 1979. Surface properties of cultured endothelial cells. Haemost. 8, 142–148.
Butter, R.S., Lettington, A.H., 1995. DLC for biomedical applications (Reviews). J. Chem. Vapour Depos. 3, 182–192.
Catherine, Y., 1991. In: Clausing, R.E., Horton, L.L., Angus, J.C., Koidl, P. (Eds.), Diamond and Diamond like Films and Coatings, NATO-ASI series B: Physics, vol. 266. Plenum Pub, New York, ISBN 0-306-44004-0, pp. 193–227.

Chan, T.K., Chan, V., 1981. Antithrombin III, the major modulator of intravascular coagulation is synthesised by human endothelial cells. Thromb. Haemost. 46, 504–506.
Charo, I., Karasek, M.A., Davison, P.M., Goldstein, I.M., 1984. J. Clin. Invest. 74, 914–919.
Chen, J.Y., Wang, L.P., Fu, K.Y., Huang, N., Leng, Y., Leng, Y.X., Yang, P., Wang, J., Wan, G.J., Sun, H., Tian, X.B., Chu, P.K., 2002. Surf. Coat. Technol. 156, 289–294.
Chhowalla, M., Weiler, M., Davis, C.A., Kleinsorge, B., Amaratunga, G.A.J., 1995. Appl. Phys. Lett. 67 (7), 894–896.
Crapper, D.R., Krishnan, S.S., Quittkat, S., 1976. Brain 99, 67.
Cui, F.Z., Li, D.J., 2000. Surf. Coat. Technol. 131, 481–487.
De Scheerder, I., Szilard, M., Yanming, H., Ping, X.B., Verbeken, E., Neerinck, D., Demeyere, E., Coppens, W., Van de Werf, F., August 2000. J. Invasive Cardiol. 12 (8), 389–394.
Dearnaley, et al., 2005. Surf. Coat. Technol. 190, 231.
Devlin, D., et al., 1997. In: Simons, B. (Ed.), ASME International Mechanical Engineering Congress and Exposition, Proceeding. ASME, Bioengineering Division, Fairfield, NJ, USA, p. 265.
Dion, I., Roques, X., Baquey, C., Baudet, E., Basse Cathalinat, B., More, N., Spring 1993. Biomed. Mater. Eng. 3, 51–55.
Dowling, D.P., Kola, P.V., Donnelly, K., Kelly, T.C., Brumitt, K., Lloyd, L., Eloy, R., Therin, M., Weill, N., 1997. Diam. Rel. Mater. 6, 390–393.
Du, C., Su, X.W., Cui, F.Z., Zhu, X.D., 1998. Biomaterials 19, 651–658.
Dyuzhev, G.A., Ivanov-Omskii, V.I., Kuznetsova, E.K., Rumyantsev, V.D., et al., 1996. Mol. Mater. 8, 103–106.
Evans, A.C., Franks, J., Revell, P.J., 1991. Surf. Coat. Technol. 47, 662–667.
Fallon, P.J., Veerasamy, V.S., Davis, C.A., Robertson, J., Amaratunga, J.A., Wilne, W.I., Koskinen, J., 1993. Phys. Rev. B 48 (7), 4777.
Folkman, J., Haudenschild, C., 1980. Angiogenesis in vitro. Nature 288, 551–556.
Folkman, J., Haudenschild, C., Zetter, B.R., 1979. Proc. Natl. Acad. Sci. U.S.A. 76, 5217–5221.
Foncin, J.F., et al., 1987. Nature 326, 136.
Fournier, J.A., Calabuig, J., Merchán, A., Augé, J.M., Melgares, R., Colman, T., Martín De Dios, R., Insag, L., Santos, I., May 2001. Revista Espanola de Cardiologia 54 (5), 567–572.
Fujimoto, T., Singer, S.J., 1988. J. Histochem. Cytochem. 36, 1309–1317.
Ganong, W.F., 1995. Review of Medical Physiology, seventeenth ed. Appleton & Lange.
Gawaz, M., Neumann, F.J., Ott, I., May, A., Schomig, A., 1996. Circulation 94, 279–285.
Gerritsen, M.E., 1987. Biochem. Pharmacol. 36, 2701–2711.
Gimbrone Jr., M.A., 1986. In: Gimbrone Jr., M.A. (Ed.), Vascular Endothelium in Hemostasis and Thrombosis. Churchill Livingstone, Edinburgh, pp. 1–13.
Gimbrone Jr., M.A., 1987. Ann. N. Y. Acad. Sci. 516, 5–11.
Goodman, S.L., Lelah, M.D., Lambrecht, L.K., Cooper, S.L., Albrecht, R.M., 1984. Scanning Electron Microsc. 1, 279.
Gordon, J.L., 1986. In: Cazenave, J.P., Davies, J.A., Kazatchkine, M.D., van Aken, W.G. (Eds.), Blood-surface Interactions: Biological Principles Underlying Haemocompatibility with Artificial Materials. Elsevier Science Publishers (Biomedical Division), p. 5.
Grill, A., 1999. Diam. Relat. Mater. 8, 428.
Grinnell, F., 1976. In: Marchesi, V.T. (Ed.), Membranes and Neoplasia: New Approaches and Strategies. Alan R. Liss, Inc., New York, USA, p. 227.
Grinnell, F., 1978. Int. Rev. Cytol. 53, 65.

Gupta, B.K., Bhushan, B., 1995. Wear 190, 110−122.
Gutensohn, K., Beythien, C., Bau, J., Fenner, T., Grewe, P., Koester, R., Padmanaban, K., Kuehnl, P., 2000a. Thrombosis Research 99, 577−585.
Gutensohn, K., Beythien, C., Koester, R., Bau, J., Fenner, T., Grewe, P., Padmanaban, K., Schaefer, P., Kuehnl, P., 2000b. Infusionstherapie und Transfusionmedizin 27 (4), 200−206.
Hasebe, T., et al., 2007. Recent advances in DLC films in medical and food-packaging fields. New Diam. Front. Carbon Technol. 17 (6), 263−279.
Hauert, R., Muller, U., Francz, G., Birchler, F., Schroeder, A., Mayer, J., Wintermantel, E., 1997. Thin Solid Films 308-309, 191−194.
Higson, S.P.J., Vadgama, Pankaj M., 1995a. Analytica Chemica Acta 300, 77−83.
Higson, S.P.J., Vadgama, Pankaj M., 1995b. Biosens. Bioelectron. 10 (5), 8.
Hoffman, A.S., 1982. Adv. Chem. Ser. 199, 3.
Hynes, R., 1992. Cell 69, 11−25.
Inoue, T., Sakai, Y., Fujito, T., Hoshi, K., Hayashi, T., Takayanagi, K., Morooka, S., Sohma, R., 1996. Circulation 94, 1518−1523.
Iregen, A., et al., 2001. Occup. Environ. Med. 58, 458.
Ivanov-Omskii, V.I., Tolmatchev, A.V., Yastrebov, S.G., 1996. Phil. Mag. B 73 (4), 715−722.
Ivanov-Omskii, V.I., Panina, L.K., Yastrebov, S.G., 2000. Carbon 38, 495−499.
Jaffe, E.A., 1982. Synthesis of factor VIII by endothelial cells. Ann. N. Y. Acad. Sci. 401, 163−170.
Jones, M.I., McColl, I.R., Grant, D.M., Parker, K.G., Parker, T.L., 1999. Diam. Relat. Mater. 8, 457−462.
Jones, M.I., McColl, I.R., Grant, D.M., Parker, K.G., Parker, T.L., 2000. J.Biomed. Mater. Res. 52 (2), 413−421.
Jones, B.J., et al., 2010. Diam. Relat. Mater. 19, 685.
Keegan, A., Hill, C., Kumar, S., Phillips, P., Schof, A., Weiss, J., 1982. Cell Sci. 55, 261−276.
Krishnan, L.K., Varghese, N., Muraleedharan, C.V., Bhuvaneshwar, G.S., Derangere, F., Sampeur, Y., Suryanarayanan, R., 2002. Biomol. Eng. 1−3.
Kubota, Y., Kleinman, H.K., Martin, G.R., Lawley, T.J.;J., 1988. Cell Biol. 107, 1589−1598.
Lappalainen, R., 2005. In: International Conference on Metallurgical Coatings and Thin Films, San Diego, California, USA.
Lettington, A.H., 1991. Applications of diamond films and related materials. In: Tzeng, Y., et al. (Eds.), Materials Science Monographs, 73. Elsevier, New York, p. 703.
Li, D.J., Cui, F.Z., Gu, H.Q., 1999. J. Adhes. Sci. Technol. 13, 169.
Linder, Stefan, Pinkowski, Wolfhard, Aepfelbacher, Martin, 2002. Biomaterials 23, 767−773.
Love, C.V., Cook, R.B., Harvey, T.J., Dearnley, P.A., Wood, R.J.K., 2013. Tribology Int. 63, 141−150.
Lu, L., Jones, M.W., Wu, R.L.C., 1993. Biomed. Mater. Eng. 3, 223.
Maizza, G., Saracco, G., Abe, Y., 1999. In: Vincenzini, P. (Ed.), Advances in Science and Technology, 9th Cimetec-World Forum on New Materials, Faenza, pp. 75−82.
Martin, J.G., Afshar, A., Kaplitt, M.J., Chopra, P.S., Srinivasan, S., Sawyer, P.N., 1968. Implantation studies with some non-metallic prostheses. Trans. Amer. Soc. Artif. Int. Organs 14, 78−81.
Martini, F.C., 2001. Fundamentals of Anatomy and Physiology, fifth ed. Prentice Hall, New Jersey, USA.
McColl, I.R., Grant, D.M., Green, S.M., et al., 1993. Diam. Rel. Mater. 3, 83.
McHargue, C.J., 1991. In: Tzeng, Y., et al. (Eds.), Applications of Diamond Films and Related Materials., Materials Science Monographs. Elsevier, New York, p. 113.

McKenzie, D.R., Yin, Y., Gerstener, E.G., Bilek, M.M.M., 1997. IEEE Transaction Plasma Sci. 25 (4), 653−659.
Moncada, S., Vane, J.R., 1982. The role of prostaglandins in platelet-vessel wall interactions. In: Nossel, H.L., Vogel, H.J. (Eds.), Pathobiology of Endothelial Cells. New York Academic Press, pp. 253−285.
Mosher, D.F., Doyle, M.J., Jaffe, E.A., 1982. Secretion and synthesis of thrombospondin by cultured human endothelial cells. J. Cell Biol. 93, 343−348.
Narayan, R.J., 2005. Mater. Sci. Eng. C 25 (3), 405−416.
Neumann, A.W., Absolom, D.R., Francis, D.W., Omenyi, S.N., Spelt, J.K., Policova, Z., Thomson, C., Zingg, W., van Oss, C.J., 1983. Ann. N.Y. Acad. Sci. 416, 276.
NHLBI (USA) Guidelines, 1980.
Nitta, Y., Okamoto, K., Nakatani, T., Hoshi, H., et al., 2008. Diam. Relat. Mater. 17, 1972−1976.
Ogwu, A.A., Coyle, T., Okpalugo, T.I.T., Kearney, P., Maguire, P.D., McLaughlin, J.A., 2003. Acta Materialia 51 (12), 3455−3465.
Ogwu, A.A., Okpalugo, T.I.T., Ali, N., Maguire, P.D., McLaughlin, J.A., 2008. J. Biomed. Mater. Res. Part B: Appl. Biomater. 85B (1), 105−113.
Ohja, S.M., 1982. Phys. Thin Films 237.
Okamoto, K., et al., 2008. Surf. Coat. Technol. 202, 5750−5752.
Okpalugo, T.I.T., Ogwu, A.A., Maguire, P., McLaughlin, J., 2004. Biomaterials 25 (3), 239−245.
Okpalugo, T.I.T., Ogwu, A.A., Maguire, P.D., McLaughlin, J.A., McCullough, R.W., 2006. J. Biomed. Mater. Res. Part B: Appl. Biomater. 78B (2), 222−229.
Okpalugo, T.I.T., Ogwu, A.A., McCullough, R.W., Ahmed, W., 2008. J. Biomed. Mater. Res. Part B: Appl. Biomater. 85B (1), 188−195.
Parker, T.L., Parker, K.L., McColl, I.R., Grant, D.M., Wood, J.V., 1993. Diam. Relat. Mater. 93, 118.
Parker, T.L., Parker, K.L., McColl, I.R., Grant, D.M., Wood, J.V., 1994. Diam. Relat. Mater. 3, 1120−1123.
Pauli, B., Lee, C., 1988. Lab Invest. 58, 379−387.
Peppas, N.A., 1982. Advances in Chemistry Series, 199. American Chemical Society, p. 466.
Picker, L.J., Nakache, M., Butcher, E.C., 1989. Monoclonal antibodies to human lymphocyte homing receptors define a novel class of adhesion molecules on diverse cell types. J. Cell Biol. 109 (2), 927−937.
Pober, J., 1988. Am. J. Pathol. 133, 426−433.
Prodan, M., 2010. Biotechnol. Lett. 15 (3), 109−116.
Rice, G.E., Bevilacqua, M.P., 1989. Science 246, 1303−1306.
Robertson, J., 1992. Surf. Coat. Technol. 50, 185−203.
Santra, T.S., et al., 2012. In: Islam, N. (Ed.), DLC and DLN Thin Films for NEMS Applications. In-Tech, ISBN 978-953-51-0306-6.
Sawyer, P.N., Pate, J.W., 1953. Am. J.Physiol 175, 113.
Sawyer, P.N., Srinavasan, S., 1967. Am. J. Surg. 114, 42.
Schroeder, A., Francz, Gilbert, Bruinink, Arend, Hauert, Roland, Mayer, Joerg, Wintermantel, Erich, 2000. Biomaterials 21, 449−456.
Sharma, D., Seth, P., Hussein, E., 2009. Biogerontology 10, 489.
Sheeja, D., et al., 2005. Surf. Coat. Technol. 190, 231.
Shi, X., Flynn, D., Tay, B.K., Prawer, S., Nugent, K.W., Silva, S.R.P., Lifshitz, Y., Milne, W.I., 1997. Phil. Mag. B 76 (3), 351−361.
Springer, T., 1990. Nature 346, 425−433.

Srinivasan, S., Sawyer, P.N., 1969. JAAMI 3, 116.
Srinivasan, S., Sawyer, P.N., 1970. J. Colloid Interface Sci. 32 (3), 456.
Thomson, L.A., Law, F.C., Rushton, N., Franks, J., 1991. Biomaterials 12, 37−40.
Tiainen, Veli-Matti, 2001. Diam. Rel. Mater. 10, 153−160.
Tonnesen, M.G., Smedly, L.A., Henson, P.M., 1984. J. Clin. Invest. 74, 1581−1592.
Tran, H.S., Puc, M.M., Hewitt, C.W., Soll, D.B., Marra, S.W., Simonetti, V.A., Cilley, J.H., DelRossi, A.J., May − June 1999. J. Invest. Surg. Off. J. Acad. Surg. Res. 12 (3), 133−140.
Van Recum, 1999. In: Van Recum, A.F. (Ed.), Handbook of Biomaterials evaluation. Taylor and Francis 1999.
Van Wachem, P.B., Schakenraad, J.M., Feijen, J., Beugeling, T., van Aken, W.G., Blaauw, E.H., Nieuwenhuis, P., Molenaar, I., 1989. Biomaterials 10, 532−539.
Van Wachem, P.B., Beugeling, T., Feijen, J., Bantjes, A., Detmers, J.P., van Aken, W.G., 1985. Biomaterials 6, 403−408.
Verstraeten, S., Aimo, L., Cheiza, P., 2008. Arch. Toxicol. 82, 789.
Vroman, L., 1977. In Vroman, L. and Leonard, E.F. (Eds), Ann. N. Y. Acad. Sci. 283, 65.
William, D.F., 1981. Systemic Aspects of Biocompatibility, vol. 1 & 2. CRC Press, Boca Raton.
William, D.F., 1985. Physiological and microbiological corrosion. CRC Crit. Rev. Biocompat. 1, 1−30.
William, D.F., 1987a. Tissue-biomaterial interactions. J. Material Sci. 21, 3421.
William, D.F. (Ed.), 1987b. Definitions in Biomaterials. Elsevier.
Williams, D.F., 1989. J. Biomed. Eng. 11, 185.
Yang, Y., Franzen, S.F., 1996a. C.L Olin. J. Heart Valves Dis. 5, 532−537.
Yang, Y., Franzen, S.F., Olin, C.L., 1996b. Cells Mater. 6 (4), 339−354.
Zheng, C., Ran, J., Yin, G., Lei, W., 1991. In: Tzeng, Y., et al. (Eds.), Applications of Diamond Films and Related Materials, Materials Science Monographs, vol.73. Elsevier, New York, p. 711.

This page intentionally left blank

Index

'*Note*: Page numbers followed by "f" indicate figures and "t" indicate tables.'

Coatings have been historically used by scientists to improve the properties and biological responses of the material–host interface. Thin films in particular are becoming more widely used and researched as an alternative to traditional sprayed coatings because they have been shown to have a more uniform structure and therefore greater stability in vivo.

Thin Film Coatings for Biomaterials and Biomedical Applications provides readers with a comprehensive guide to these thin film coatings and their application in the biomaterials field. Chapters in the first section discuss the fundamentals of thin films for biomedical applications. Part two looks at the special properties of thin films whereas the final set of chapters reviews functional thin films for biomedical applications.

Professor Griesser is Director of the Mawson Institute and has a longstanding international reputation particularly for his research on biomaterials interfaces. He is a physical chemist by training and has applied this background to interdisciplinary research in various fields, particularly surface science, the analysis and modification of polymer surfaces, thin film deposition, biomaterials, and adhesion.

ELSEVIER
WP
WOODHEAD PUBLISHING
An imprint of Elsevier • elsevier.com

ISBN 978-1-78242-453-6
9 781782 424536